# Middle Atmosphere Program

## HANDBOOK FOR MAP VOLUME 9

Edited by
S.A. Bowhill
Belva Edwards

ICSU

International Council of Scientific Unions

SCOSTEP

Scientific Committee on Solar-Terrestrial Physics
K. D. Cole, President
J. G. Roederer, Vice President
C. H. Liu, Scientific Secretary

## MAP ORGANIZATION

### MIDDLE ATMOSPHERE PROGRAM STEERING COMMITTEE

S. A. Bowhill, SCOSTEP, Chairman
K. Labitzke, COSPAR, Vice Chairman
C. H. Liu, SCOSTEP, Secretary

R. D. Bojkov, WMO
A. D. Danilov, COSPAR
J. C. Gille, COSPAR
A. H. Manson, SCOSTEP
I. Hirota, IUGG/IAMAP
J. W. King, URSI
L. R. Megill, IUGG/IAGA
T. Nagata, SCAR
R. G. Roper, IAMAP
P. C. Simon, IAU
J. Taubenheim, IUGG/IAGA
T. E. VanZandt, URSI
M. Wada, IUPAP

### MAP STANDING COMMITTEES

Data-Management -- G. Hartmann and I. Hirota, Co-Chairmen
Dynamics Calendar -- T. E. VanZandt, Chairman
Publications -- C. F. Sechrist, Jr., Chairman

### MAP STUDY GROUPS

MSG-5 Ions and Aerosols, F. Arnold and M. P. McCormick, Co-Chairmen
MSG-6 Scientific Aspects of an International Equatorial Observatory, S. Kato, Chairman
MSG-7 Penetration of Solar Radiation into the Atmosphere, J. E. Frederick, Chairman
MSG-8 Atmospheric Chemistry, G. Witt, Chairman
MSG-9 Measurement of Middle Atmosphere Parameters by Long Duration Balloon Flights, J. E. Blamont, Chairman

### APPROVED MAP PROJECTS

| | Coordinator | | Coordinator |
|---|---|---|---|
| AMA: | T. Hirasawa | GOSSA: | M. P. McCormick |
| ATMAP: | J. M. Forbes | GRATMAP: | M. A. Geller |
| CAMP: | G. Witt | MAE: | N. C. Maynard |
| CLIMAT: | J. M. Russell | MSTRAC: | B. B. Balsley and S. K. Avery |
| DYNAMICS: | K. Labitzke | OZMAP: | D. F. Heath |
| GLOBMET: | R. G. Roper | SSIM: | P. C. Simon |
| GLOBUS: | D. Offermann | WINE: | U. von Zahn |

### MAP REGIONAL CONSULTATIVE GROUP

Europe: M. L. Chanin, Chairman

# Middle Atmosphere Program

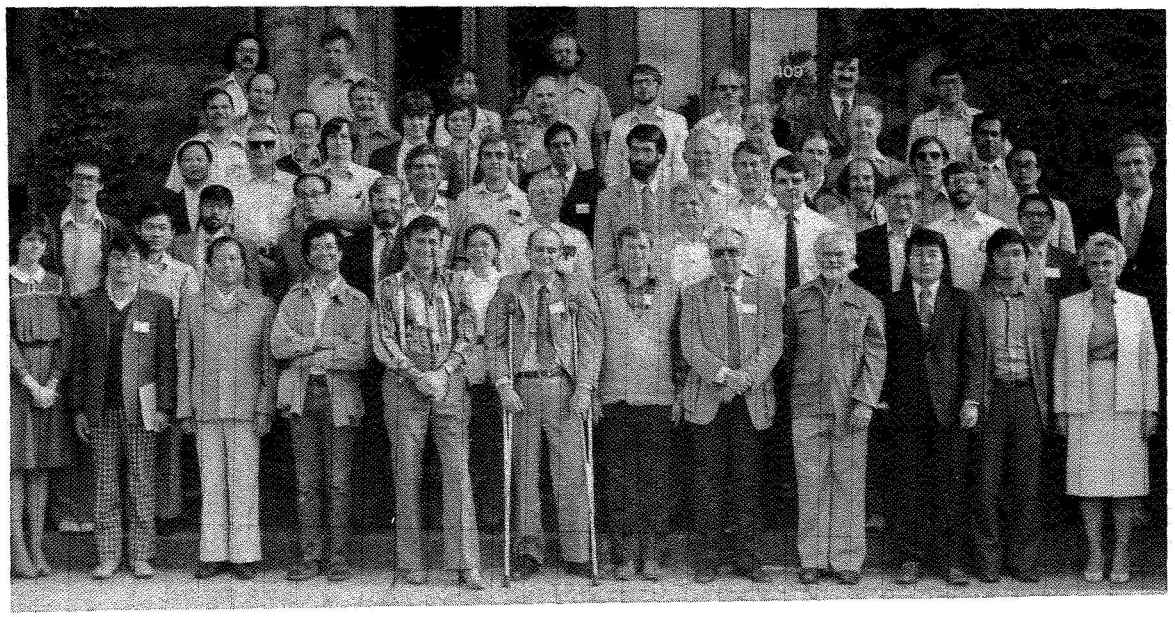

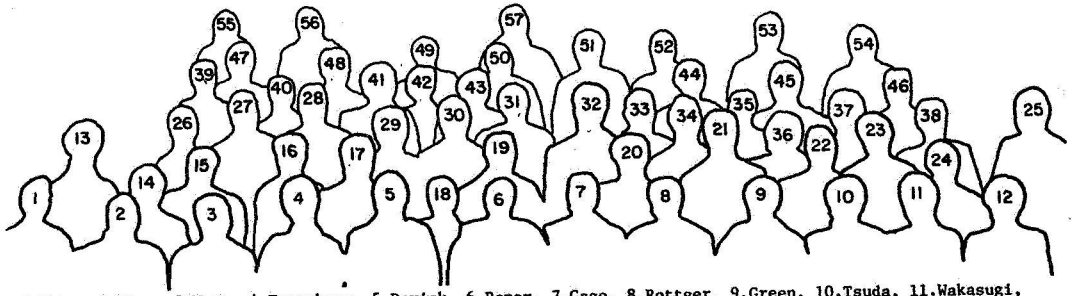


1.Ware, 2.Chao, 3.Wang, 4.Tetenbaum, 5.Doviak, 6.Roper, 7.Gage, 8.Rottger, 9.Green, 10.Tsuda, 11.Wakasugi, 12.Edwards, 13.Stitt, 14.Y.H.Chen, 15.Rastogi, 16.Yu, 17.Wickwar, 18.Zhang, 19.Staggs, 20.Peters, 21.Forbes, 22.VanZandt, 23.Mathews, 24.Liu, 25.Bowhill, 26.F.Chen, 27.Mueller, 28.Watkins, 29.Woodman, 30.Farley, 31.Lagos, 32.Fairall, 33.Ecklund, 34.Riddle, 35.Hocking, 36.Geller, 37.Cornish, 38.Kuo, 39.Swartz, 40.Glass, 41.Larsen, 42.Avery, 43.Sasamori, 44.Carter, 45.Hall, 46.Koshy, 47.Crochet, 48.Balsley, 49.Meek, 50.Strauch, 51.Clark, 52.Royrvik, 53.Brosnahan, 54.Ying, 55.Ierkic, 26.Schmidt, 57.Sulzer.

M I D D L E

A T M O S P H E R E

P R O G R A M

HANDBOOK FOR MAP

VOLUME 9

Papers presented at the
URSI/SCOSTEP Workshop on
Technical Aspects of MST Radar
May 23-27, 1983
Urbana, Illinois 61801

Edited by

S. A. Bowhill
Belva Edwards

December 1983

Published for the ICSU Scientific Committee on Solar-Terrestrial Physics (SCOSTEP) with financial assistance in part from UNESCO Subvention 1981-1983 DG/7.6.2/Sub. 13 (SC) and in part from the National Aeronautics and Space Administration Contract NASW 3805.

Copies available from SCOSTEP Secretariat, University of Illinois, 1406 W. Green Street, Urbana, Illinois 61801

# FOREWORD

The term "Mesosphere-Stratosphere-Troposphere Radar" was invented to describe the use of a high-power radar transmitter (typically 1 MW) together with a large vertically, or near vertically, pointing antenna to study the dynamics and structure of the atmosphere from about 10 to 100 km, using the very weak coherently scattered radiation returned from small-scale irregularities in refractive index. Many interesting and important scientific results obtained with this technique have been published in the scientific literature (typically in the Journal of Geophysical Research, Radio Science, and the Journal of Atmospheric and Terrestrial Physics), but until recently there had been no forum for the exchange of information of a more technical nature.

A workshop was organized by Drs. S. Kato and I. Hirota in May 1982, on the subject of Equatorial Middle Atmosphere Measurements and Middle Atmosphere Radars, sponsored by SCOSTEP, COSPAR, IAGA, IAMAP and URSI. A summary of this workshop appears in Handbook for MAP Vol. 7, pp. 102-148. One session of the workshop, on radar techniques, revealed a substantial number of unresolved questions which seemed to be worth pursuing in a separate workshop.

The First URSI/SCOSTEP Workshop on Technical Aspects of MST Radar was therefore organized, and was held on May 23-27, 1983; this volume contains the papers presented at that meeting. The response to the Call for Papers was substantial, amounting to 108 papers from 10 different countries; the vast majority of these papers have never before appeared in print.

The discussions at the Workshop involved nine major topics, each of which was in the charge of a convener, who prepared an introductory review. Each also prepared a separate contribution (or modified the original contribution) based on the papers presented and the discussion that ensued.

Each major topic was in turn divided into subtopics with one person responsible for preparing a paper and leading the discussion. A number of contributed papers were also furnished under many of the topics.

It is hoped that this volume will be helpful both to scientists who use MST radar results, so that they may understand the capabilities and limitations of the technique; and also to scientists and engineers worldwide who may be interested in designing and constructing an MST radar of their own.

My co-organizer, C. H. Liu, and I would like to express our thanks to the sponsoring organizations, to the topic conveners, and to the subtopic discussion leaders for a most interesting and stimulating week of technical discussions. We would also like to extend our thanks to Mrs. Belva Edwards, Chairman of the Local Organizing Committee, and to the staff and students of the Aeronomy Laboratory of the University of Illinois for their invaluable help.

S. A. Bowhill

WORKSHOP ON TECHNICAL ASPECTS OF MST RADAR
May 23-27, 1983

TABLE OF CONTENTS

# 1. METEOROLOGICAL AND DYNAMICAL REQUIREMENTS FOR MST RADAR NETWORKS (Keynote Paper)

R. G. Roper

Department of Geophysical Sciences
Georgia Institute of Technology
Atlanta, GA 30332

While the ST radar is an ideal tool for operational wind profiling, it is highly doubtful that it will replace the radiosonde, even when coupled with microwave detectors capable of measuring temperature and humidity profiles (Larsen, 1.1-A this volume). There is a possibility that low-VHF radars may be able to produce temperature profiles. ST radars are most useful for studying jet stream dynamics, tropopause height, passage of fronts, atmospheric stability, wave motions, and vertical velocities. Their major advantage is that continuous real-time wind data are available over a height range extending well into the lower stratosphere. The reliability of these systems is such that they can operate virtually unattended.

An excellent example of an ST synoptic/mesoscale network consisting of both attended and unattended sites is located in Colorado (PROFS - Prototype Regional Observing Forecasting Service; see Strauch, this volume p. 325). Wind profiles are available from this net by telephone dial-in (terminal and modem required!). Each individual profiler in this net costs out at less than $100K.

While the global view of planetary waves is best determined from satellite observations, the interaction of gravity waves with mean motion has been recognized as playing an important part in the general circulation. ST radars can contribute significantly to our understanding of these interactions.

The measurement of wind profiles at low levels, such as produced by ST radars, are of importance to MAP, since waves propagate vertically and can be the source of turbulence at much higher altitudes.

The higher powered MST radar produces data with a better signal-to-noise ratio at lower altitudes, and pushes the useful return height range into the upper stratosphere, with mesospheric and lower thermospheric echoes becoming evident. However, the region between roughly 40 and 60 km remains inaccessible, and mesospheric returns are far from being continuous. This intermittency in the method is of consequence in the measurement of all scales larger than gravity wave/turbulence scales (periods more than a few hours at most). Limitations in the measurement of tidal amplitudes and phases are addressed in detail by Forbes (this volume p. 22).

MST radars are realizing their potential as scientific tools, particularly in the detailed study of short-period phenomena -- gravity waves and turbulence in particular. Their future use in mesoscale monitoring is primarily governed by economic considerations -- for example, it has been suggested that the optimum siting for real-time readout of wind profiles for aviation use would be on a 100 km grid. While it appears that a synoptic network is not feasible at this stage, the siting of at least one or two more MST radars in equatorial latitudes perhaps on the Pacific island of Nauru, between the Japanese MU radar, and the MST radar being developed in Australia, and on Canton Island, midway between Nauru and Jicamarca, would contribute significantly to our knowledge of meridional circulation throughout the middle atmosphere, give further insight into the role of equatorial Kelvin waves, and help in resolving some of the gaps in our understanding of the atmospheric tides.

One should not lose sight of the fact that the MST radar is not the only tool for ground-based studies of the middle atmosphere. Whenever possible, complementary techniques should be employed at the same site, and the already existing network of radio meteor wind and partial reflection drift stations should be utilized as effectively as possible in coordinated observations of atmospheric dynamics.

QUESTIONS NOT ANSWERED

1. Do models exist which can absorb high resolution wind profile data into a forecasting scheme?

2. Can ST radars resolve vertical motion at jet stream perturbation scales?

PROPOSED EXPERIMENTS

1. Wind speed/turbulence correlations are higher than mean shear/turbulence correlations for radars located near hills/mountains. These correlations should also be determined by a radar located in flat terrain (e.g. Urbana).

2. The measurement of ageostrophy in stratospheric winds can be determined by comparison between actual wind profiles (ST measurements) and satellite derived winds.

3. Upcoming satellites will measure middle atmosphere winds directly. The "ground truth" provided by MST radars will be invaluable in the initial interpretation of these results.

# 1.1A THE MST RADAR TECHNIQUE: REQUIREMENTS FOR OPERATIONAL WEATHER FORECASTING

M. F. Larsen

School of Electrical Engineering
Cornell University
Ithaca, NY 14853

## INTRODUCTION

Recent interest in improving our ability to make mesoscale forecasts has been the result of improving observational technology and theoretical understanding of mesoscale motions. There is a feeling that the accuracy of forecasts for spatial scales of less than 1000 km and time scales of less than 12 hours can be improved significantly if our resources are applied to the problem in an intensive effort over the next decade. Since the most dangerous and damaging types of weather occur at these scales, there are major advantages to be gained if such a program is successful. The interest in improving short-term forecasting is evident in the series of papers resulting from the International IAMAP Symposium on Nowcasting (BROWNING, 1982), the paper on the long-term goals of NOAA as presented by SCHMIDT (1983) at the Fifth Symposium on Meteorological Observations and Instrumentation, and the two handbooks published by the UCAR Committee on the National STORM (Stormscale Operational and Research Meteorology) Program (UCAR, 1982; ANTHES, 1983). The conclusion of all of these publications is that the technology at the present time is sufficiently developed, both in terms of new observing systems and the computing power to handle the observations, to warrant an intensive effort to improve stormscale forecasting.

The National STORM Program handbooks (UCAR, 1982, ANTHES, 1983) are excellent source books on the general problem of short term forecasting. The first handbook summarizes the need for this type of forecasting and the framework for achieving the desired improvements. The second handbook gives a detailed assessment of our capabilities and understanding at the present and the areas of research most in need of attention. Questions that will have to be addressed deal with the type of observing system or systems that will be used to generate data compatible with the scales of motion being discussed and the way the data will be used operationally. HOOKE (1983) summarized the situation as follows:

> "Within the next several years, operational meteorology will be facing some crucial decisions regarding measurement systems. The most obvious and important example is the determination of winds. A variety of remote sensing techniques have been used experimentally to measure wind direction and speed in clear air. There is substantial need for an integrated effort to determine which of these techniques is most promising by testing alternative methods in the field. This will be a necessary prelude to the procurement and deployment of a next-generation wind sensing system."

In this review I will attempt to provide an assessment of the extent to which the so-called MST radar technique fulfills the requirements for an operational mesoscale observing network, and I will delineate the extent to which improvements in various types of forecasting could be expected if such a network is put into operation.

## CHARACTERISTICS AND CAPABILITIES OF THE RADAR TECHNIQUE

The MST radar measures the vertical profile of horizontal winds based either on the Doppler shift of the signal backscattered from turbulent variations in the refractive index or from the cross correlation between the signals re-

ceived at a set of three spaced antennas. The technique has been described in detail by WOODMAN and GUILLEN (1974), GAGE and BALSLEY (1978), BALSLEY and GAGE (1980), and ROTTGER (1980) among others. Details and advantages of various specific measurement techniques are discussed in much greater detail in other papers in this volume.

I will concentrate on VHF radars that use a fixed dipole array and are capable of measuring the vertical profile of the horizontal winds as a minimum. Some MST radars operating at shorter wavelengths have fully steerable dishes. An example is the 23-cm radar formerly located at Chatanika, Alaska, and now located in Sondre Stromfjord, Greenland. I will not consider such radars here since they are in the same category as the existing weather radar network if upgraded to provide Doppler capability.

The radar's ability to provide wind profiles is something that is duplicated by the standard rawinsonde. However, the radar wind measurements have many advantages, particularly if the mesoscale is of interest. The radar wind profiles can be measured as often as desired down to the imposed equipment limitation of a few minutes. There are no expendables involved except for the power used to run the radar equipment. Also, the radar measures the wind profiled immediately above the radar. During periods of high winds, the rawinsonde can drift as much as 100 km during its ascent. Such an error can be a major one if the scales of motion of interest are of the order of a few hundred kilometers. Finally, a large part of the cost of running a radiosonde station has always been the salaries of the personnel. Since the radar measurements are easily automated, adding VHF Doppler radars to the network would only increase the required extra manpower by a small fraction of the number of personnel needed if an equal number of new radiosonde stations were established. The success of such an approach is already evidenced by the Poker Flat MST Radar which has been operating unattended since 1979.

However, the comparison between the radiosonde and the radar is not really the most appropriate. The possibility of establishing a mesoscale radiosonde observing network has never been considered very seriously since the cost is prohibitive. Most likely the competition will come from satellites or some other ground-based remote sensing system such as sodars or lidars. The primary advantage of the radar over the acoustic sounder is the height range covered and the insensitivity of the former to various forms of noise. A very complete review of the capabilities of the acoustic sounding technique is given by BROWN and HALL (1978). The lidar is competitive with the radar in terms of the height range covered and the time and, certainly, the height resolution, but the lidar is seriously hampered when there is precipitation or fog or simply when it is overcast (STRAUCH and COHEN, 1972). The lidar provides information on atmospheric density and humidity, but the radar provides data on the height of the tropopause and other temperature structure such as inversions and fronts. Further comparison between the advantages of the two techniques is needed, although the main drawback of the lidar for operational applications appears to be the limitations of the technique when used in the presence of clouds.

The satellite has a number of advantages over the radar. Primarily it provides vast areal coverage in relatively short periods of time. Since a very large source of error for large-scale forecasting is due to a lack of data in sparsely populated regions, underdeveloped areas, and the oceans, satellite measurements appear to be the best hope for improving large-scale observations. The radars do not immediately offer any hope for providing data in data-sparse regions. The height and time resolution, and the height range covered by the radar is significantly better than that of the satellite, but the lack of spatial coverage of the radar measurement is still one of the limitations of the technique.

So far, I have compared the advantages and disadvantages of the various techniques. It is clear that the radar by itself cannot replace the other types of measurements, but it can provide a relatively inexpensive solution to the problem of upgrading the observing network to provide mesoscale resolution. Meteorological radars already exist and provide important information for the forecaster. Half-hourly satellite photos are an important input to the forecast process and satellite measurements of temperature and winds are providing data for areas where no information could be obtained otherwise, albeit with less than desirable height resolution. However, the VHF radars can fill the gaps that exist in the present radiosonde network. It has been shown by HOKE and ANTHES (1976), DALEY and PURI (1980), and DALEY (1980) among others that when small scales of motion are of interest, the wind information is more important than pressure and temperature information. Therefore, the fact that the radar only measures the winds, and not also pressure and temperature, should not necessarily be viewed as a compromise of the technique when it is used for mesoscale observations. I will discuss this point in more detail later.

## REQUIREMENTS FOR AN OPERATIONAL SYSTEM

Although the topic of the Workshop is the MST (Mesosphere-Stratosphere-Troposphere) radar, the ability to measure winds in the troposphere, stratosphere, and mesosphere is not required of the systems used for mesoscale weather forecasting. A simple "Model T" Radar would be sufficient. With thanks to Henry Ford, such a radar should be simple to mass produce, low cost, and dependable in operation. The reductions in antenna size and transmitter power gained by reducing the design specifications of the system could reduce the cost of the system by as much as a factor of ten when compared to an MST system. That is a crude estimate but probably not unrealistic.

Discussions about the applicability of the radar wind measurements to operational weather forecasting have generally centered on applications to large-scale forecasting with improved spatial resolution so that mesoscale phenomena can be resolved. Of course, it is important that this aspect of the radar technique should be discussed, and that may be how the systems are ultimately applied. However, there are intermediate applications for such systems that would allow the radars to be phased into the large-scale observing network with possible significant forecast improvements at each intermediate step. There are a number of very localized phenomena that lead to severe weather that a small network of VHF radars could be useful in forecasting.

Applications that come to mind include the following. A network of between 3 and 6 radars distributed around the Great Lakes could be used for operational forecasting of lake-effect snows. Typically, the snows are generated by directional changes in the mesoscale flow patterns and eventually mesoscale circulations develop in response to the heating effects of the lakes (ZIPSER, 1983). It should be possible to detect these small-scale circulation changes with a network of radars. More study would be needed to determine the real usefulness of such a system for forecasting this very specific local phenomena.

A second application would involve use of a system of radars as a forecast tool for the severe Colorado wind storms that occur every year in the lee of the Rocky Mountains (LILLY and ZIPSER, 1972; KLEMP and LILLY, 1975). Since a cloudy or precipitating atmosphere is not necessarily associated with this phenomena, a scanning weather radar, even one with Doppler capability, is not particularly useful for forecasting this type of event. Actually, the necessary network may already exist in the form of the PROFS (Prototype Regional Observing and Forecasting System) network of wind profilers operated by the Wave Propagation Laboratory of NOAA (STRAUCH et al., 1982).

Another application of a small-scale system of Model T radars is for studies of the sea breeze in the Florida peninsula. The sea breeze develops in response to the diurnal heating cycle and the temperature differences between land and sea. The vertical circulation that develops acts as a modulator of the convective activity over the land and over the ocean (LHERMITTE and GILET, 1975; ATKINSON, 1981). The resulting thunderstorms can be very severe and may involve large shears, heavy rainfall rates, hail, and turbulence that can be a hazard to local aviation. A scanning weather radar can be used to detect the developing cells, but since the lifetime of a single cell is from 30 to 45 minutes, only a short-term warning can be issued. Clear air wind measurements may be capable of detecting the buildup of the conditions leading to intense convection.

The possible applications of the radar systems for local forecasting just named are only a few of the possibilities. The important point is that a small number of the radar systems can be installed to provide improved forecasting of specific local phenomena. Confidence in the systems and operational experience would be gained before making a commitment to use the radars on a network-wide basis.

Another area in which the radars can be applied for forecasting purposes relates to pollutant dispersion. Most of the models used to estimate dispersion of pollutants are based on the Gaussian plume models (HANNA et al., 1982). The two major input parameters are an atmospheric stability index derived from the radiosonde temperature profile and the wind at the height of the center of the plume. A major problem is the significant diurnal variation in the winds that cannot be resolved by the rawinsonde measurements made once every 12 hours (DRAXLER, 1983). Only a small system that could measure the winds up to a height of a few kilometers would be needed to improve the wind information data base significantly. Other locations that could benefit from such a system would be airports where the primary hazard is from clear air turbulence and downdrafts that affect aircraft during takeoff and landings. Again only measurements within the boundary layer or a little higher would be required. There are no doubt other possibilities.

## PREVIOUS WORK

Very little work has been done to date dealing directly with applicability of the radars to the forecasting problem. BALSLEY and GAGE (1982) have discused considerations for implementation of an operational radar system including antenna size needed, most favorable frequency ranges, and the type of power needed. CARLSON and SUNDARARAMAN (1982) have made a preliminary case showing that a few percent of the annual fuel consumption of the airlines could be saved if data from a wind measuring radar network was available for flight planning purposes. They indicate that a detailed study has to be made to determine if their rough calculations of potential savings are correct. However, the savings that they envision would be enough to justify the cost of a radar network within the first year.

FUKAO et al. (1982) have made a detailed comparison of rawinsonde data from San Juan, Puerto Rico and wind profiles measured with the Arecibo 430 MHz radar. Twenty-six separate days from August and September of 1977 were involved in the study. The comparison indicated a difference of 4.9 m/s in the upper troposphere and a difference of 3.3 m/s in the lower stratosphere. The difference in the lower stratosphere could be explained by the experimental error in the rawinsonde measurement, but the larger difference in the upper troposphere was apparently due to spatial variations over the 80 km distance separating the two sites.

LARSEN (1983) investigated the effect of high frequency meteorological noise on the representativeness of the radar wind data. If one is interested in

using the data for input to a numerical model that can resolve synoptic and mesoscale motions down to scales of a few hundred kilometers, any motions with smaller scales are effectively just noise or an error in the measurement. The radar wind measurements from the Poker Flat MST radar were compared to the rawinsonde measurements from Fairbanks, Alaska, and both were compared to the geostrophic wind calculated by applying an objective analysis scheme to the standard radiosonde data from five nearby stations. By averaging the high time resolution radar data over intervals of several hours, the high frequency oscillations could be filtered out. The comparison showed that the radar and rawinsonde data agreed to within 2-3 m/s when the radar data were averaged over 12 hours or more, and that the difference between the radar winds and the geostrophic winds was about the same as the difference between the rawinsonde winds and the geostrophic wind. The two independent wind measurements were most similar, and both differed from the geostrophic wind by 1.5-2.0 m/s more than they differed from each other. The results indicate that it is crucial that the data should be averaged in some way if it is used as input to a numerical model. The errors decrease as the averaging interval is increased. Therefore, the acceptable error for a given model will have to be determined in order to know how to process the radar data.

LARSEN and ROTTGER (1983) have shown that a VHF radar can detect the location of frontal boundary surfaces as enhancements of the radar reflectivity. When coupled to the measurements of the horizontal and vertical wind components, such information would be of value in forecasting the development and position of fronts since such small-scale features are not resolved by the synoptic observing system or in operational numerical forecast models.

GREEN et al. (1978) showed the ability of the radar to detect changes in the jet stream height and intensity in real time, as well as gravity wave activity and vertical velocities associated with the jet stream. Turbulence intensity and location can also be determined along with the rate of turbulent dissipation (GAGE et al., 1978). The results are intriguing, and more work needs to be done in this area. One very interesting aspect of their study is that radar measurements may be used in the future to provide real-time inputs for the parameterization schemes used in numerical models. All processes in a numerical model with spatial scales smaller than the models grid spacing are parameterized. Such things as the vertical fluxes of heat and momentum due to convection and the loss of energy to subgrid scales are included in the parameterizations. The schemes used usually depend in some way on the physical quantities calculated by the model, but the high time resolution measurements of the radar, along with the vertical velocity measurements (e.g., ECKLUND et al., 1982), may provide valuable information on the actual magnitude of these various quantities as a function of time and location.

The most detailed investigation of the applicability of the radar technique to mesoscale forecasting is being undertaken by the Wave Propagation Laboratory of NOAA using their Profiler system (STRAUCH, 1981; STRAUCH et al., 1982). The Profiler uses several microwave radiometers to measure the temperature and humidity profile. A set of three Doppler radars distributed in a triangular network around Boulder, Colorado is used to resolve mesoscale features in the local winds. The system is dedicated to the problem of mesoscale forecasting. Except for results dealing with the measurement capabilities of the system and the corresponding accuracies, few results are available to date. However, the Profiler should provide a good assessment of potential improvements in mesoscale forecasting that can be realized with such a system.

## OPTIMAL SPECIFICATION OF INITIAL DATA

Much of the discussion about using the MST systems operationally has focused on the WPL Profiler which uses a clear air radar for wind profiling. How-

ever, the system was designed to test the possibility of replacing the standard National Weather Service radiosonde. To this end, microwave radiometers are used to provide profiles of the temperature and humidity, though to date the achievable height resolution has been less than that of the radiosonde. It remains to be seen whether the difference is significant.

There is little doubt that the thermodynamic and moisture information is valuable, but in this case we should question whether the extra cost would be justified on a network-wide basis. The radiometers are by far the most expensive part of the system. The cost ratio between the Model T radar discussed here and the microwave system may be as great as 1 to 5 for an operational system. The estimated cost of a Profiler system has been given as approximately $500,000 (M. T. Decker, personal communication). CARLSON and SUNDARARAMAN (1982) estimate that a tropospheric wind profiling system, without the radiometers, could be built for 10% of that sum or less.

Will the wind information be useful in and of itself? The answer apparently is yes. Studies by RUTHERFORD and ASSELIN (1972), WILLIAMSON and DICKINSON (1972), HOKE and ANTHES (1976), DALEY and PURI (1980), DALEY (1980), and BUBE and GHIL (1982) indicate that at small scales the wind information is by far the most important. Small scales in this case are defined by a horizontal scale related to the Rossby radius of deformation. The various studies have used either analytic models or numerical models that characterize the dynamics of the atmosphere and considered the problem of how new information is assimilated into the model. The winds and the thermodynamic variables have been given as initial conditions singly and in combination. Updating the calculated fields with the pressure fields would eventually cause an adjustment to the input data, but the adjustment time would be long. However, the wind information is readily absorbed with a minimum of wave noise being generated. The pressure field then adjusts to reflect the changes in the wind field so that a complete set of information relevant to the small-scale motions is obtained even though only the wind fields are used as input. There seems to be agreement that wind information is more important for scales less than 1000-2000 km. At large scales the reverse is true, and the thermodynamic information is more important.

The physical reason for this effect is associated with the process known as geostropic adjustment and first described by ROSSBY (1938). The crucial parameter in the problem is the Rossby radius of deformation given by the ratio of the speed of sound, or the propagation velocity of gravity waves of the appropriate scale, to the Coriolis parameter (BLUMEN, 1972). At scales much larger than the Rossby radius, the wind field will adjust to balance a perturbed pressure field. For scales smaller than the Rossby radius, the pressure field adjusts to balance the wind field. Therefore, the smaller the scale of motion that is of interest, the more useful is the wind information. Since the mesoscale lies in the range of spatial scales where the wind information is most useful, there may be a significant improvement in our ability to forecast for this scale even if only the wind fields are measured. SHAPIRO et al. (1983) also discussed the importance of wind information at small scales, and they indicate that improved spatial resolution may be obtained from the measurements of a single radar if the data are used to extrapolate quantities along air parcel trajectories.

## CONCLUSION

This article was meant to suggest a number of possible applications for the MST radar technique in operational weather forecasting. The results to date have shown that there is great promise for the technique as part of the standard observing network once it is resolved to increase the resolution to include mesoscale motions. In reality, very little work has been done to date relating

to the forecast improvements that actually can be achieved with an operational wind profiling system. Forecast improvements due to a network of radars should be investigated both theoretically and experimentally. The possibility of using the radar data to refine some of the parameterization schemes used in forecast modeling should also be investigated. Finally, the applications of the radar systems to forecasting area-specific phenomena should be examined in the near future.

ACKNOWLEDGEMENTS

The author was supported by the Air Force Office of Scientific Research while writing this paper under grant AFOSR-83-0100.

REFERENCES

Anthes, R. A. (1983), The National STORM Program: Scientific and Technological Bases and Major Objectives, University Corporation for Atmospheric Research, Boulder, Colorado.

Atkinson, B. W. (1981), Meso-scale Atmospheric Circulations, Academic Press, New York.

Balsley, B. B. and K. S. Gage (1980), The MST radar technique: Potential for middle atmospheric studies, Pure Appl. Geophys., 118, 452-493.

Balsley, B. B. and K. S. Gage (1982), On the use of radars for operational wind profiling, Bull. Amer. Meteor. Soc., 63, 1009-1018.

Blumen, W. (1972), Geostrophic adjustment, Rev. Geophys. Space Phys., 10, 485-528.

Brown, E. H. and F. F. Hall, Jr. (1978), Advances in atmospheric acoustics, Rev. Geophys. Space Phys., 16, 47-110.

Browning, K. A. (ed.) (1982), Nowcasting, Academic Press, New York.

Bube, K. P. and M. Ghil (1982), Assimilation of asynoptic data and the initialization problem, in Dynamic Meteorology: Data Assimilation Methods, L. Bengtsson, M. Ghil and H. Kallen, eds., Applied Mathematical Sciences Series, 36, Springer-Verlag, New York.

Carlson, H. C., Jr. and N. Sundararaman (1982), Real-time jetstream tracking: National benefit from an ST radar network for measuring atmospheric motions, Bull. Amer. Meteor. Soc., 63, 1019-1026.

Daley, R. (1980), On the optimal specification of the initial state for deterministic forecasting, Mon. Wea. Rev., 108, 1719-1735.

Daley, R. and K. Puri (1980), Four-dimensional data assimilation and the slow manifold, Mon. Wea. Rev., 108, 85-99, 1980.

Draxler, R. R. (1983), Variability in winds and temperatures from sequential rawinsonde ascents, Preprint volume, Fifth Symposium on Meteorological Observations and Instrumentation, April 11-15, 1983, Toronto, Ont., Can., AMS, Boston, Mass.

Ecklund, W. L., K. S. Gage, B. B. Balsley, R. G. Strauch and J. L. Green (1982), Vertical wind variability observed by VHF radar in the lee of the Colorado Rockies, Mon. Wea. Rev., 110, 1451-1457.

Fukao, S., T. Sato, N. Yamasaki, R. M. Harper and S. Kato (1982), Winds measured by a UHF Doppler radar and rawinsondes: Comparisons made on twenty-six days (August-September 1977) at Arecibo, Puerto Rico, J. Appl. Met., 21, 1357-1363.

Gage, K. S. and B. B. Balsley (1978), Doppler radar probing of the clear atmosphere, Bull. Amer. Meteor. Soc., 58, 1074-1093.

Gage, K. S., J. L. Green and T. E. VanZandt (1978), Application of the VHF pulsed Doppler radar to cloud physics research, Preprint volume, Conference on Cloud Physics and Atmospheric Electricity, July 31-August 4, 1978, Issaquah, Washington, AMS, Boston, Mass.

Green, J. L., K. S. Gage and T. E. VanZandt (1978), Three dimensional observations of a jet stream using a VHF Doppler radar, Preprint volume, 18th Conference on Radar Meteorology, March 28-31, Atlanta, Georgia, AMS, Boston, Mass.

Hanna, S. R., G. A. Briggs and R. P. Hosker, Jr. (1982), Atmospheric Diffusion National Technical Information Service, Springfield, Virginia.

Hoke, J. E. and R. A. Anthes (1976), The initialization of numerical models by a dynamic-initialization technique, Mon. Wea. Rev., 104, 1551-1556.

Hooke, W. (1983), Observation and data assimilation: Present status and future research-and-development opportunities, in The National STORM Program: Scientific and Technological Bases and Major Objectives, R. A. Anthes (ed.), University Corporation for Atmospheric Research, Boulder, Colorado.

Klemp, J. B. and D. K. Lilly (1983), The dynamics of wave-induced downslope winds, J. Atmos. Sci., 32, 320-339.

Larsen, M. F. (1983), Can a VHF Doppler radar provide synoptic wind data?: A comparison of 30 days of radar and radiosonde data, Mon. Wea. Rev., in press

Larsen, M. F. and J. Rottger (1982), VHF and UHF Doppler radars as tools for synoptic research, Bull. Amer. Meteor. Soc., 63, 996-1008.

Lhermitte, J. S. and M. Gilet (1975), Dual-Doppler radar observation and study of sea-breeze convective storm development, J. Appl. Met., 14, 1346-1361.

Lilly, D. K. and E. J. Zipser (1972), The front range windstorm of 11 January 1972 - A meteorological narrative, Weatherwise, 25, 56-63.

Rossby, C.-G. (1938), On the mutual adjustment of pressure and velocity distributions in certain simple current systems, 2, J. Mar. Res., 1, 239-263.

Rottger, J. (1980), Structure and dynamics of the stratosphere and mesosphere revealed by VHF radar investigations, Pure Appl. Geophys., 118, 494-527.

Rutherford, I. D. and R. Asselin (1972), Adjustment of the wind field to geopotential data in a primitive equations model, J. Atmos. Sci., 29, 1059-1063.

Schmidt, H. (1983), NOAA's long-term goals, Preprint volume, Fifth Symposium on Meteorological Observations and Instrumentation, April 11-15, 1983, Toronto, Ont. Can., AMS, Boston, Mass.

Shapiro, M. A., D. C. Hogg and C. G. Little (1983), The wave propagation laboratory profiler system and its applications, Preprint volume, Fifth Symposium on Meteorological Observations and Instrumentation, April 11-15, 1983, Toronto, Ont., Can. AMS, Boston, Mass.

Strauch, R. G. (1981), Radar measurement of tropospheric wind profiles, Preprint volume, 20th Conference on Radar Meteorology, Nov. 30-Dec. 3, 1981, Boston, Mass., AMS, Boston, Mass.

Strauch, R. G. and A. Cohen (1972), Atmospheric remote sensing with laser radar, in Remote Sensing of the Troposphere, V. E. Derr (ed.), U. S. Government Printing Office, Washington, DC.

Strauch, R. G., M. T. Decker and D. C. Hogg (1982), An automatic profiler of the troposphere, Preprint volume, 20th Aerospace Sciences Meeting, Jan. 11-14, 1982, Orlando, Florida, AIAA, New York, NY.

UCAR (1982), The National STORM Program: Framework for a Plan, University Corporation for Atmospheric Research, Boulder, Colorado.

Williamson, D. L. and R. E. Dickinson (1972), Periodic updating of meteorological variables, J. Atmos. Sci., 29, 190-193.

Woodman, R. F. and A. Guillen (1974), Radar observations of winds and turbulence in the stratosphere and mesosphere, J. Atmos. Sci., 31, 493-505.

Zipser, E. (1983), Nowcasting and very-short-range forecasting, in The National STORM Program: Scientific and Technological Bases and Major Objectives, R. A. Anthes (ed.), University Corporation for Atmospheric Research, Boulder, Colorado.

# 1.2A JET STREAM RELATED OBSERVATIONS BY MST RADARS

K. S. Gage

Aeronomy Laboratory
National Oceanic and Atmospheric Administration
Boulder, CO 80303

## ABSTRACT

This paper presents an overview of the jet stream and its observation by MST radar. The climatology and synoptic and mesoscale structure of jet streams is briefly reviewed. MST radar observations of jet stream winds, and associated waves and turbulence are then considered. The possibility of using a network of ST radars to track jet stream winds in near real-time is explored.

## INTRODUCTION

The jet stream is one of the most important and prominent features evident on upper level synoptic maps. Meteorological investigations of the jet stream have a long history dating back to early upper-level balloon observations. Actually, there are a multiplicity of jet stream phenomenon that have been observed in different regions of the atmosphere. For example, low-level jets are important in the dynamics of the planetary boundary layer (BONNER, 1968) and the Polar night jet plays a central role in the dynamics of the middle atmosphere (GELLER, 1979). The principal jet streams which have been studied by meteorologists are those which are evident at midlatitudes at tropopause heights: namely, the subtropical jet and the Polar front jet.

This survey is concerned primarily with MST/ST radar observations related to midlatitude jet streams. Before reviewing some of the jet stream-related observations the synoptic and mesoscale structure of jet streams will be briefly reviewed. The radar observations which follow are concerned with mean horizontal wind, vertical wind and concurrent measurements of turbulence and waves.

## CLIMATOLOGICAL AND LARGE-SCALE FEATURES OF JET STREAMS

Synoptic scale analyses of jet stream structure can be found in REITER (1963), and PALMEN and NEWTON (1969) etc. Basically the jet streams are found in the baroclinic zones which are associated with the tropopause breaks as shown in Figure 1. DEFANT and TABA (1957) drew attention to this relationship by pointing out that there are three major latitude bands with different tropopause heights: The tropical tropopause (16-17 km) extending to about 40N, the mid-latitude tropopause (10-12 km in the winter) ranging from about 30N to 60N and the polar tropopause (8-10 km, in the winter) north of 60N. Accordingly, the subtropical jet is found at about 12 km (200 mb) near latitude 30N and the polar front jet is found at about 9 km (300 mb) in the range 40-60 N.

The location of the jet stream varies greatly from day to day. The meandering of the jet stream follows the planetary waves and shows varying degrees of structure. At times the jet stream winds flow primarily, zonally, i.e., west to east. More often wave disturbances are evident and pronounced troughs and ridges are present. Such day-to-day variations are known to play an important role in the dynamics of tropospheric storms which give us our weather.

The jet streams are, of course, more pronounced during the winter season when meridional temperature gradients are most intense. The mean axis of the subtropical jet stream in the Northern Hemisphere is shown in Figure 2. Also shown in this figure is the principal range of the polar front jet stream. Both

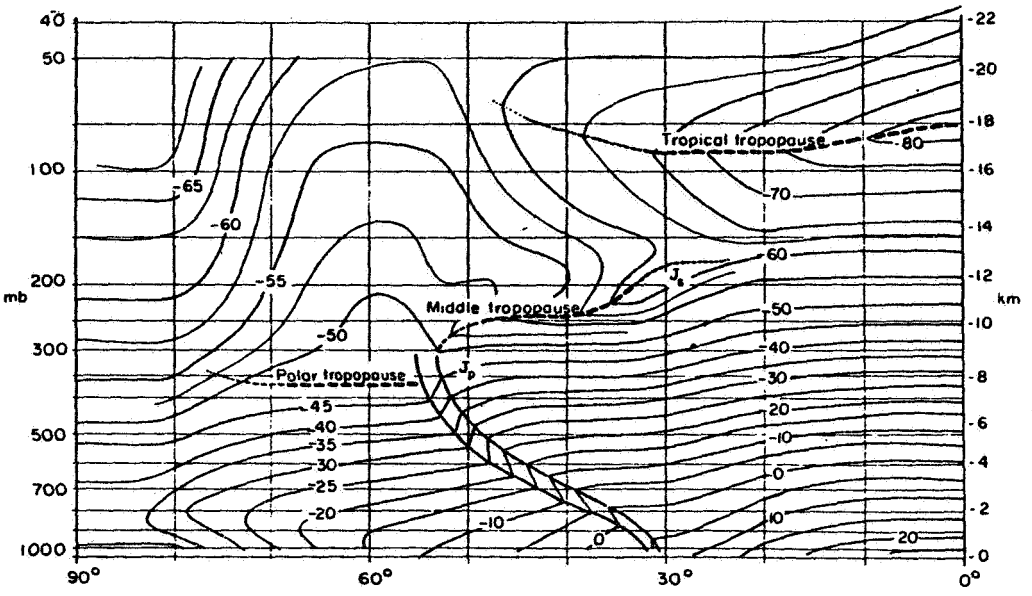


Figure 1. Meridional cross section showing mean conditions around the Northern Hemisphere on Jan. 1, 1956. $J_p$ and $J_s$ denote locations of the polar front and subtropical jet streams. Isotherms in degrees celsius (after DEFANT and TABA, 1957).

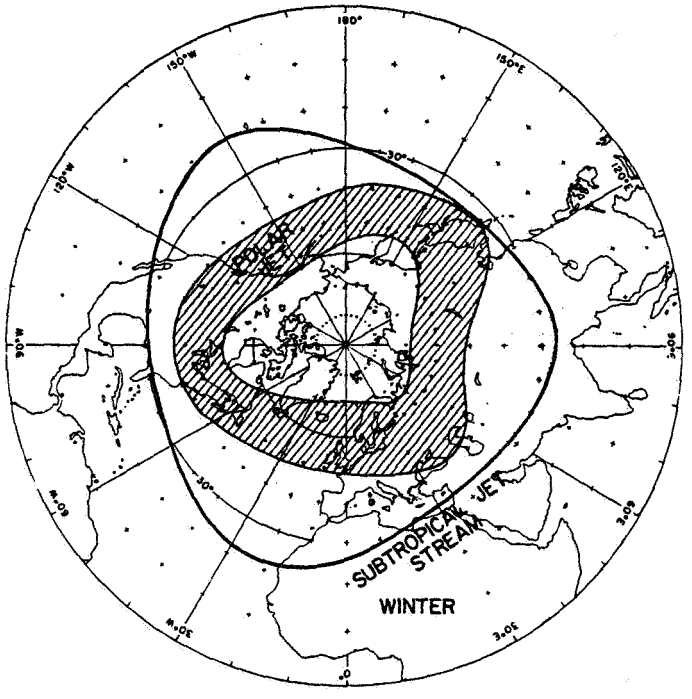


Figure 2. Mean axis of subtropical jet stream during winter, and area (shaded) of principal activity of polar-front jet stream (after RIEHL, 1962).

jet streams show a pattern distorted by standing planetary waves. There is an out-of-phase relation between the troughs and ridges in the two jet streams. For example, Japan and the eastern United States are located at longitudes where the two jet streams come together. As a consequence jet streams in these locations are particularly strong.

## MESOSCALE STRUCTURE OF JET STREAMS

While jet streams can be resolved on upper level synoptic maps, they possess considerable mesoscale structure which cannot be resolved. Continuous MST/ST radar observations from a single station have been used to infer some of this structure (GREEN et al., 1978; LARSEN and ROTTGER, 1982; and SHAPIRO et al., 1983). Nevertheless, most of our knowledge of the mesoscale structure of jet streams has been derived from careful analysis of data collected by research aircraft (SHAPIRO, 1974, 1978).

A typical cross section across a polar-front jet stream is reproduced in Figure 3a. This schematic cross section shows the relationship of the jet stream winds to the locations of the tropopause and the upper level frontal zone. If the jet stream is zonal (west-east), the maximum winds are found just below the tropopause and just south of the upper level front. Strong wind shear is concentrated in the polar front beneath the jet stream.

The MST radar (at lower VHF) observes enhanced reflectivity at vertical incidence from stable regions of the atmosphere (GAGE and GREEN, 1978, 1979; and ROTTGER and LIU, 1978). As a consequence, it is possible to resolve the tropopause and frontal structure associated with jet streams from continuous MST radar observations. This capability is shown most clearly in Figure 3b reproduced from LARSEN and ROTTGER (1982). Wind measurements, of course, can be made simultaneously.

One of the important features associated with the polar-front jet stream is the occurrence of stratospheric intrusions. These have been studied extensively (see, e.g., DANIELSEN, 1968; and REITER, 1975) as an important mechanism for the exchange for chemical constituents between the stratosphere and troposphere. Basically, the upper level fronts which protrude into the troposphere contain stratospheric ozone, etc. and provide a locus for turbulent mixing of tropospheric and stratospheric constituents (SHAPIRO, 1980). These stratospheric intrusions are visible to the MST radar as evidenced by Figure 3.

Recently, considerable attention has been focused on ageostrophic circulations associated with jet streaks (SECHRIST and WHITTAKER, 1979; UCCELLINI and JOHNSON, 1979; SHAPIRO 1981; and SHAPIRO and KENNEDY, 1981). Jet streaks are regions of local wind maxima which can often be seen to propagate along jet streams. Entrance and exit regions of jet streaks have been shown to possess significant ageostrophic motions resulting from adjustment of the wind to the mass field.

In the entrance region a thermally direct transverse circulation is set up so that warm air rises and cold air sinks. By contrast a thermally indirect transverse circulation is set up in the exit region. SECHRIST and WHITTAKER (1979) consider the implications of propagating jet streaks on the development of cyclonic disturbances in the atmosphere.

While the magnitude of the transverse circulations referred to above may be too small to detect in routine MST radar observations, other ageostrophic motions exist which should easily be observed. UCCELLINI and JOHNSON (1979) describe the ageostrophic winds to be expected in the entrance and exit regions of jet streaks. In the entrance region confluent streamlines and downstreams acceleration of geostrophic wind leads to an ageostrophic component directed

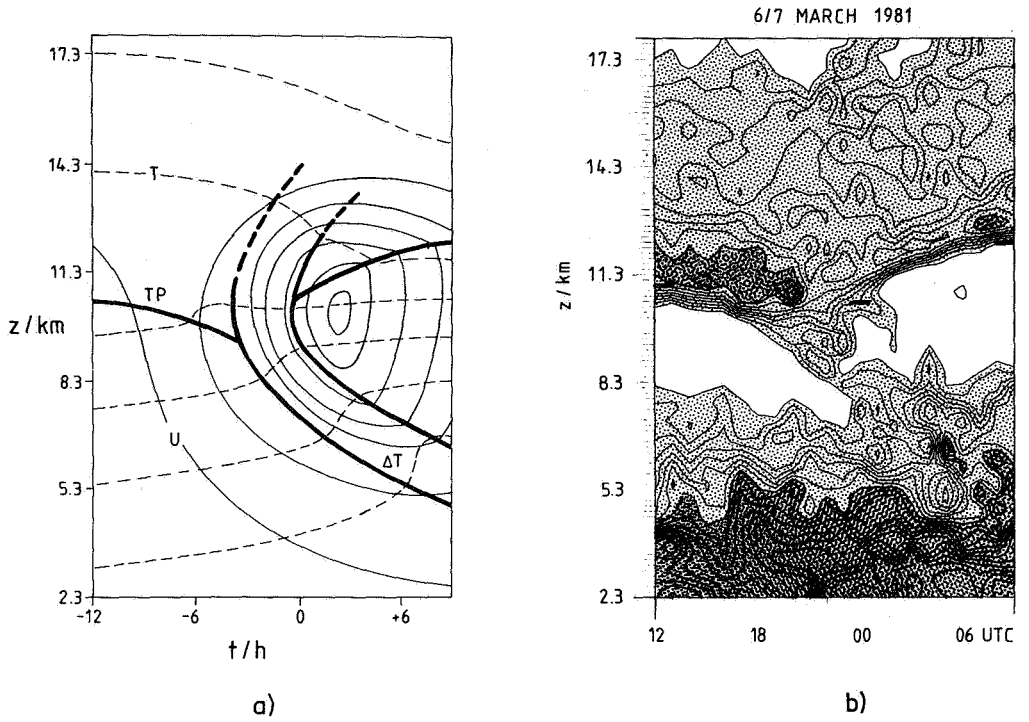


Figure 3. a. Thermal structure and winds near fronts adapted from PALMEN and NEWTON (1969) by LARSEN and ROTTGER (1982). The heavy line labeled TP corresponds to the height of the tropopause. The dashed lines are isotherms, and the solid lines are the isotachs. The jet is located on the warm side of the front just below the tropopause. b. Reflectivity contour plot obtained using the SOUSY radar. Difference between contour lines is 2 dB. Intensity of shading corresponds to intensity of echoes (after LARSEN and ROTTGER, 1982).

toward the cylonic side of the jet streak. In the exit region diffluent streamlines and downstream deceleration of the geostrophic wind leads to an ageostrophic component directed to the anticyclonic side of the jet streak. The magnitude of these ageostrophic winds are expected to be about 10 $ms^{-1}$. SHAPIRO and KENNEDY (1981) report cross-height contour ageostrophic winds as exceeding 20 $ms^{-1}$.

## MST RADAR OBSERVATIONS OF WAVES AND TURBULENCE ASSOCIATED WITH JET STREAMS

MST radars have been used successfully in the past few years to observe waves and turbulence associated with jet streams. These observations include: Kelvin-Helmholtz instabilities, clear air turbulence and gravity waves.

Shear flow instabilities in stratified fluids are commonly referred to as Kelvin-Helmholtz instabilities. For many years fluid dynamicists investigated this class of instabilities using linear stability theory applied to highly idealized models with specified profiles of mean flow and stability (DRAZIN and HOWARD, 1967; and DRAZIN and REID, 1981). With the use of power UHF radars in the 1960s the connection between the occurrence of clear air turbulence and Kelvin-Helmholtz instability was clarified (ATLAS et al., 1970; and DUTTON and PANOFSKY, 1971). With the advent of more powerful VHF and UHF Doppler radars

capable of detailed wind measurements over a broad range of altitudes, it became possible to quantitatively investigate Kelvin-Helmholtz instabilities. For the first time the stability of realistic models simulating observed atmospheric flows were investigated and the results compared to detailed radar observations (VANZANDT et al., 1979; and KLOSTERMEYER and RUSTER, 1980).

An example of the high-frequency velocity fluctuations which can be resolved by an MST radar is contained in Figure 4. This figure shows the filtered radial velocity fluctuations observed by the SOUSY radar during a jet stream passage. The decrease in amplitude and the phase shift evident at the height of generation in the observations has been modelled successfully. In addition to the instability a clear modulation of background turbulence with the phase of the resulting "wave" disturbance has been shown by VANZANDT et al. (1979) and by KLOSTERMEYER and RUSTER (1981).

The occurrence of clear air turbulence in the free atmosphere is thought to be controlled by the magnitude of the Richardson number. If the wind shear is large enough to overcome the stabilizing effect of buoyancy, instabilities arise and turbulence is generated. Under such circumstances the Richardson number should be close to .25. However, the Richardson number depends very much on the vertical scale over which it is calculated. The scale dependence of the Richardson number appears to be a result of the perturbing influence of waves and is consistent with the idea that the occurrence of clear air turbulence is related to <u>both</u> the background wind and temperature fields and the intensity of the background wave field (BRETHERTON, 1969).

The fact that the wave activity varies greatly from day-to-day can be seen in the variability of the vertical wind (ECKLUND et al., 1981, 1982). Figure 5 shows the strong correlation that exists between zonal wind and the intensity of wave activity observed at Platteville, CO in the lee of the Colorado Rockies.

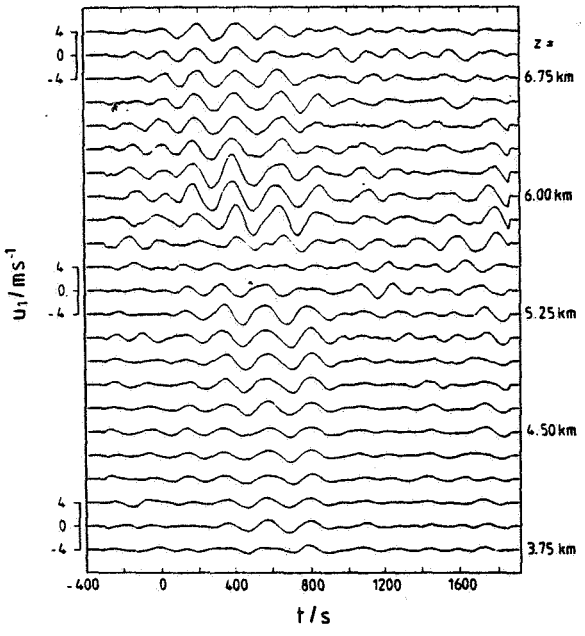


Figure 4. Band-pass-filtered time series of radial velocity observed by the SOUSY radar illustrating Kelvin-Helmholtz instability during a jet stream passage (after KLOSTERMEYER and RUSTER, 1981).

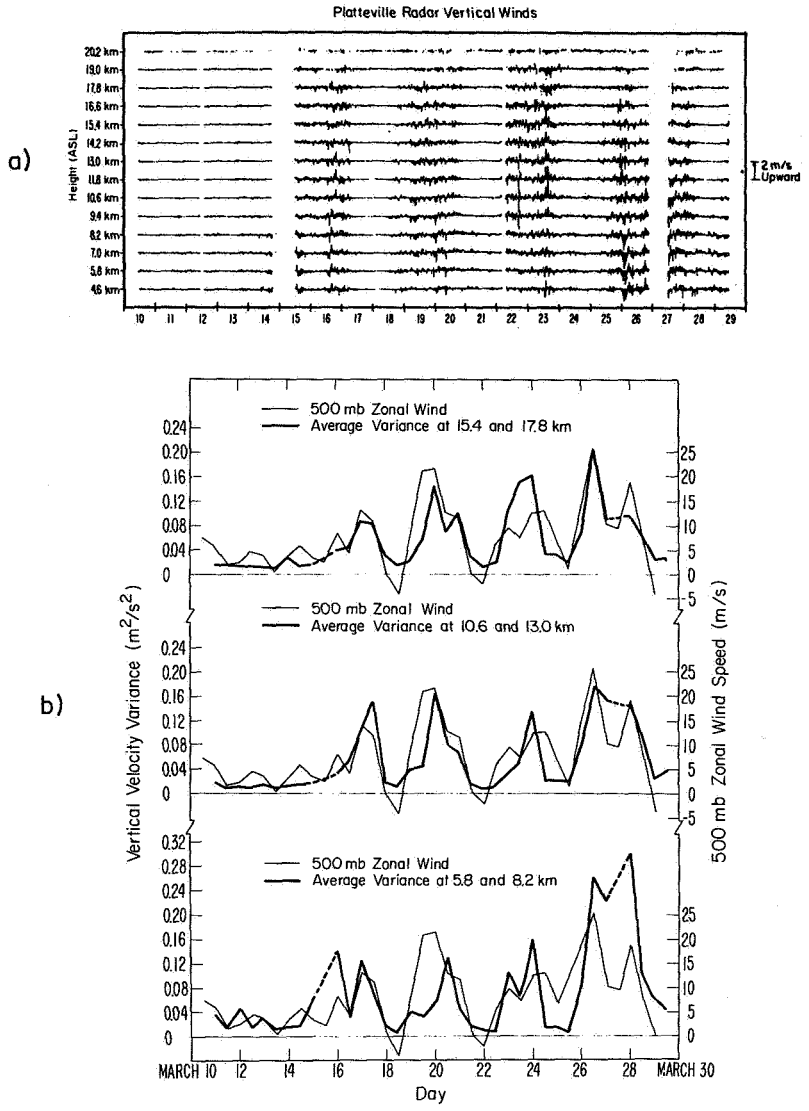


Figure 5. a. Vertical velocities observed by the Platteville radar during March 1981. b. A comparison of the vertical velocity variance shown in a. with the 500 mb zonal wind (after ECKLUND et al., 1982).

While further observations in other locations will be required to determine how much of this variability is due to topography, all indications to date suggest a significant dependence of wave activity on wind speed (NASTROM and GAGE, 1983).

If the occurrence of clear air turbulence depends on both the background wind and stability and the background wave activity, it follows that the magnitude of clear air turbulence should be significantly enhanced under jet stream conditions. This is in accord with common experience that MST radars can see to

higher altitudes during jet stream conditions. Indeed, the analyses of VANZANDT et al. (1978), NASTROM et al. (1981), and SMITH et al. (1983) show a clear relation between the magnitude of $C_n^2$ and jet stream level winds. Following GAGE et al, (1980) it is possible to estimate eddy dissipation rates observations of $C_n^2$. Figure 6 shows the variation of eddy dissipation rates determined in this fashion during a jet stream passage over the Sunset radar in Colorado. These observations reveal a variation of eddy dissipation rates in excess of 3 orders of magnitude. The most intense regions of turbulence are located as expected in the shear zones above and below the jet stream core.

## APPLICATION OF ST RADARS TO JET STREAM NOWCASTING

Considerable interest and attention has been focused recently (CARLSON and SUNDARARAM, 1982) on the potential savings to the aviation industry of having accurate and timely wind information at flight altitudes. The network of rawinsonde sites which currently provide upper level wind data is shown in Figure 7. This network is too sparse and the 12-hour sounding schedule currently in use is inadequate to resolve mesoscale jet stream structure. A network of ST radars constructed on a 100 km grid is illustrated in Figure 8. Such a network could be constructed for less than $100 million. The estimated annual fuel savings to the domestic commercial aviation industry range from 1-3%. Current annual fuel consumption is in the neighborhood of 45 billion liters. At a cost of 25 cents a liter a 1% fuel savings would be sufficient to pay for the construction cost in the first year of operation.

## CONCLUDING REMARKS

Jet stream related observations of MST radars have been summarized. To date these observations have been limited to single stations and mostly to case studies. The uniqueness of the data sets obtained by MST radars lies in their temporal continuity. Temporal continuity enables the inference of spatial structure provided temporal evolution is not too fast. It is clear, however, that the ultimate utility of MST radars for jet stream analysis will be realized only after mesoscale networks of ST radars are in operation.

Mesoscale networks of ST radars may be in operation in the very near future. A small network is nearing completion in Colorado to be used in conjunction with the Prototype Regional Observation and Forecast System (PROFS). As

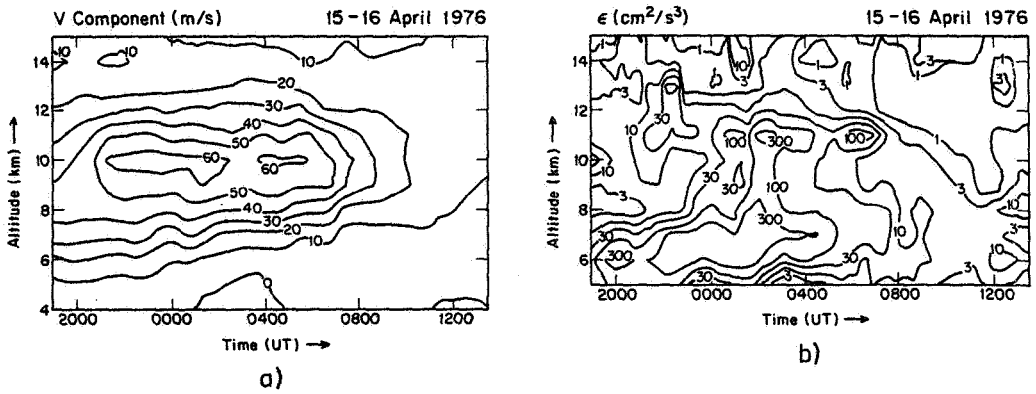


Figure 6. Observations of the Sunset radar during a jet stream passage April 15-16, 1976: a. Time-height contours of south wind v; b. Time-height contours of ε estimated from $C_n^2$ (after GAGE et al., 1980).

Figure 7. Existing upper-air observational network.

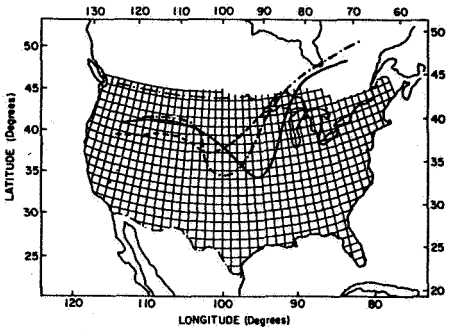


Figure 8. Illustrative network of ST radars for tracking jet stream in real time at a spacing of every 100 km. Also shown are representative locations of the jet stream core at three consecutive 24 hr intervals (after REITER, 1963; CARLSON and SUNDARARAMAN, 1982).

noted earlier, the potential savings to the airline industry of an operational mesoscale network of ST radars may provide the incentive for the realization of much larger networks in the very near future. Finally, the National Weather Service is considering how to implement the wind sensing capabilities of ST radars into their observing system. Clearly, the wind information obtained from dense networks of ST radars should lead to a greatly improved understanding of mesoscale structure of jet streams.

REFERENCES

Atlas, D., J. I. Metcalf, J. H. Richter and E. E. Gossard (1970), The birth of "CAT" and microscale turbulence, J. Atmos. Sci., 27, 903-913.

Balsley, B. B. and K. S. Gage (1982), On the use of radars for operational wind profiling, Bull. Amer. Meteorol. Soc., 63, 1009-1018.

Bonner, W. D. (1968), Climatology of the low-level jet, Mon. Wea. Rev., 96, 833-850.

Bretherton, F. P. (1969), Waves and turbulence in stably stratified fluids, Radio Sci., 4, 1279-1287.

Carlson, H. C. and N. Sundararaman (1982), Real-time jet stream tracking: National benefit from an ST radar network for measuring atmospheric motions, Bull. Amer. Meteorol. Soc., 63, 1019-1026.

Danielsen, E. F. (1968), Stratospheric-tropospheric exchange based on radioactivity, ozone, and potential vorticity, J. Atmos. Sci., 25, 502-518.

Defant, F. and H. Taba (1957), The three-fold structure of the atmosphere and the characteristics of the tropopause, Tellus, 9, 259-274.

Drazin, P. G. and L. N. Howard (1966), Hydrodynamic stability of parallel flow of inviscid fluid, Adv. Appl. Mech., 9, 1-89.

Drazin, P. G. and W. H. Reid (1981), Hydrodynamic Stability, Cambridge University Press, Cambridge, England, 525 pp.

Dutton, J. A. and H. A. Panofsky (1970), Clear air turbulence: A mystery may be unfolding, Science, 167, 937-944.

Ecklund, W. L., D. A. Carter and B. B. Balsley (1979), Continuous measurements of upper atmospheric winds and turbulence using a VHF Doppler radar: Preliminary results, J. Atmos. Terr. Phys., 41, 983-994.

Ecklund, W. L., K. S. Gage and A. C. Riddle (1981), Gravity wave activity in vertical winds observed by the Poker Flat MST radar, Geophys. Res. Lett., 8, 285-288.

Ecklund, W. L., K. S. Gage, B. B. Balsley, R. G. Strauch and J. L. Green (1982), Vertical wind variability observed by VHF radar in the lee of the Colorado Rockies, Mon. Wea. Rev., 110, 1451-1457.

Gage, K. S. and B. B. Balsley (1978), Doppler radar probing of the clear atmosphere, Bull. Amer. Meteorol. Soc., 59, 1074-1093.

Gage, K. S. and J. L. Green (1978), Evidence for specular reflection from monostatic VHF radar observations of the stratosphere, Radio Sci., 13, 991-1001.

Gage, K. S. and W. L. Clark (1978), Mesoscale variability of jet stream winds observed by the Sunset VHF Doppler radar, J. Appl. Meteorol., 17, 1412-1416.

Gage, K. S. and J. L. Green (1979), Tropopause detection by partial specular reflection with very-high-frequency radar, Science, 203, 1238-1240.

Gage, K. S. J. L. Green and T. E. VanZandt (1980), Use of Doppler radar for the measurement of atmospheric turbulence parameters from the intensity of clear air echoes, Radio Sci., 15, 407-416.

Geller, M. A. (1979), Dynamics of the middle atmosphere, J. Atmos. Terr. Phys., 41, 683-705.

Green, J. L., K. S. Gage and T. E. VanZandt (1978), Three-dimensional wind observations of a jet stream using a VHF Doppler radar, Preprint volume, 18th Conf. on Radar Meteorology, Atlanta, GA, March 28-31, pp 184-189.

Klostermeyer, J. and R. Ruster (1981), Further study of a jet stream-generated Kelvin-Helmholtz instability, J. Geophys. Res., 86, 6631-6637.

Larsen, M. F. and J. Rottger (1982), VHF and UHF Doppler radars as tools for synoptic research, Bull. Amer. Meteorol. Soc., 63, 996-1007.

Nastrom, G. D., K. S. Gage and B. B. Balsley (1982), Variability of $C_n^2$ at Poker Flat, Alaska from mesosphere, stratosphere, troposphere (MST) Doppler radar observations, Opt. Eng., 21, 347-351.

Nastrom, G. D. and K. S. Gage (1983), A brief climatology of vertical wind variability as seen by the Poker Flat, Alaska MST radar, submitted to J. Climate and Appl. Meteorol.

Palmen, E. and C. W. Newton (1969), Atmospheric Circulation Systems: Their Structure and Interpretation, Academic Press, New York, 603 pp.

Reiter, E. R. (1963), Jet Stream Meteorology, Univ. of Chicago Press, Chicago, IL, 515 pp.

Reiter, E. R. (1975), Stratospheric-tropospheric exchange processes, Rev. Geophys. Space Phys., 13, 459-474.

Riehl, H. (1962), Jet streams of the atmosphere, Tech. Rep. #32, 117 pp., Dept. of Atmospheric Sciences, Colorado State Univ., Fort Collins, CO.

Rottger, J. and C. H. Liu (1978), Partial reflection and scattering of VHF radar signals from the clear atmosphere, Geophys. Res. Lett., 5, 357-360.

Rottger, J. and G. Schmidt (1981), Characteristics of frontal zones determined from spaced antenna VHF radar observations, Preprint volume, 20th Conf. on Radar Meteorology, Boston, MA, AMS, Boston, pp. 30-37.

Ruster, R. and P. Czechowsky (1980), VHF radar measurements during a jet stream passage, Radio Sci., 15, 363-369.

Sechrist, F. S. and T. M. Whittaker (1979), Evidence of jet streak vertical circulations, Mon. Wea. Rev., 107, 1014-1021.

Shapiro, M. A. (1974), A multiple structured frontal zone-jet stream system revealed by meteorologically instrumented aircraft, Mon. Wea. Rev., 102, 244-253.

Shapiro, M. A. (1978), Further evidence of the mesoscale and turbulent structure of upper level jet stream-frontal zone systems, Mon. Wea. Rev., 106, 1100-1111.

Shapiro, M. A. (1980), Turbulent mixing within tropopause folds as a mechanism for the exchange of chemical constituents between the stratosphere and troposphere, J. Atmos. Sci., 37, 994-1004.

Shapiro, M. A. (1981), Frontogenesis and geostrophically forced secondary circulations in the vicinity of jet stream-frontal zone systems, J. Atmos. Sci., 38, 954-973.

Shapiro, M. A. and P. J. Kennedy (1981), Research aircraft measurements of jet stream geostrophic and ageostrophic winds, J. Atmos. Sci., 38, 2642-2652.

Shapiro, M. A., M. T. Decker and D. Van de Kamp (1983), Time-series measurements through a baroclinic wave, upper-level jet stream and lower-tropospheric front with a ground-based remote sensing meteorological sounder, submitted to Mon. Wea. Rev.

Smith, S. A., G. J. Romick and K. Jayaweera (1983), Poker Flat MST radar observations of shear induced turbulence, J. Geophys. Res., 88, 5265-5217.

Uccellini, L. W. and D.R. Johnson (1979), The coupling of upper and lower tropospheric jet streaks and implications for the development of severe convective storms, Mon. Wea. Rev., 107, 682-703.

VanZandt, T. E., J. L. Green, K. S. Gage and W. L. Clark (1978), Vertical profiles of refractivity turbulence structure constant: Comparison of observations by the Sunset radar with a new theoretical model, Radio Sci., 13, 819-829.

VanZandt, T. E., J. L. Green, W. L. Clark and J. R. Grant (1979), Buoyancy waves in the troposphere: Doppler radar observations and a theoretical model, Geophys. Res. Lett., 6, 429-432.

# 1.3A MST RADAR DETECTION OF MIDDLE ATMOSPHERE TIDES

J. M. Forbes

Department of Physics, Boston College
Chestnut Hill, MA 02167

## SUMMARY

Meteorological and dynamical requirements pertaining to the specification of middle atmosphere tides by the MST radar technique are outlined. Major issues addressed include: (1) the extraction of tidal information from measurements covering a fraction of a day; (2) the ramifications of transient effects ("tidal variability") on the determination and interpretation of tides; (3) required temporal and spatial resolutions and; (4) desired global distributions of of MST radars, so as to complement existing MST, meteor wind, and partial reflection drift radar locations.

Specific conclusions are as follows:

(1) A height resolution of 2 km is considered necessary to resolve all tidal structures that might reasonably be expected throughout the middle atmosphere (10-100 km).

(2) Time resolutions of about 30 minutes in the stratosphere and 5 minutes in the meso-thermosphere are required to determine with acceptable accuracy tidal Fourier components from a single day's measurements. (It is assumed that data above 50 km are available only during daytime for 12 hours.) Alternatively, one to three weeks of data at 30 minute intervals would enable determination of semidiurnal and diurnal components above 50 km to roughly the same accuracy. (These estimates assume nominal values of diurnal and semidiurnal amplitudes and standard deviations relative to the standard deviation of uncorrelated noise in the data, and may require adjustment to reflect actual conditions.)

(3) Nominal accuracies necessary for the delineation of middle atmosphere tidal structures are about 2 m $sec^{-1}$ (.5 m $sec^{-1}$) for altitudes above (below) 60 km.

(4) Since the set-up time for tides is typically several days or more, it is not meaningful to speak of "day-to-day variability" of a tide (which implies a steady-state response at a period exactly a subharmonic of a solar or lunar day). Four-day vector averages are recommended for comparison with models, other data, and delineating the variability of tidal components.

(5) The geographical distribution of radars is an extremely important factor in determining the scientific return of global tidal measurement.

(6) Data base management and standardization of reduction and analysis techniques are extremely important issues with regard to tidal studies, which require coordination and interpretation on a global scale.

## INTRODUCTION

Atmospheric tides, oscillations in meteorological fields at subharmonics of a solar and lunar day, comprise an important component of middle atmosphere dynamics. Solar tidal components observable by MST radars are primarily excited by insolation absorption by $H_2O$ and $O_3$ in the tropospheric and stratomesospheric regions, respectively. Tidal oscillations in the middle atmosphere can to first order be viewed as the superposition of several "quasi-modes" each with somewhat distinguishable and identifiable horizontal structures and vertical wavelengths. The modifier "quasi" is used here to suggest possible devia-

tions from "true" model structures (that is, corresponding to the eigenfunctons of Laplace's tidal equation) due to transient effects or the influence of latitudinally varying background propagation conditions. The specific mixture of these structures, which might be comprised of migrating and non-migrating, vertically propagating and evanescent, and symmetric and asymmetric components, determines the global spatial variability of the tidal oscillations.

The purpose of this report is to outline meteorological and dynamical requirements pertaining to the specification of upper atmosphere tides by the MST radar technique. In a report (LINDZEN, 1969) prepared for the Panel on Dynamics and Structure of the Neutral Atmosphere of COSPAR's Working Group II, a group of scientists addressed the problems of measuring tides and gravity waves in the upper atmosphere. HAURWITZ (1964) is referenced extensively in their report. Some of their main points are as follows:

(1) A minimum of five daily rocket ascents, preferably equally spaced in time, are needed to determine diurnal and semidiurnal tidal components at a given station (HAURWITZ, 1964).

(2) Statistical measures of the reliability of tidal measurements, for instance as given by the radius (R) of the probable error circle, should always be provided (HAURWITZ, 1964).

(3) Quoting HAURWITZ (1964), "According to error theory R decreases as $1/\sqrt{N}$ where N is the number of determinations. In order to reduce R to half its value one needs four times as many determinations, that is a four times longer series. In this manner it will be possible to estimate even from a fairly short series, having a large R, how much longer the observation program should be continued".

(4) The question of how many rockets must be deployed in order to measure tides is difficult to answer. It involves a tradeoff between cost and the degree of reliability one is aiming for.

(5) Tides can be associated with rather short vertical wavelengths, as low as 12 km for important diurnal components. A vertical resolution on the order of at least 3 km is needed so as not to smooth out such components.

(6) Meteor radars appear capable of routinely providing economical measurements of tides with good spatial and temporal resolution.

(7) Observations may never be sufficiently extensive to properly define upper atmosphere tidal oscillations. A hybrid approach involving both theory and experiment may be necessary to arrive at a comprehensive delineation of the phenomenon.

(8) Valuable consistency checks on theory can be performed with less data than would be necessary for a complete tidal determination.

The above report emphasizes the role of rocket soundings in detecting upper atmosphere tides, but their points remain valid in the context of radar measurements. Note that they did recognize the potential role that meteor radars could play in the observational study of tides. A shortcoming of the meteor radar technique is that it is restricted to the 80-100 km height range. This deficiency is offset by the global array of meteor radars and partial reflection drift radars that now exist for dynamical studies. The MST radar can in principle provide wind measurements over the 10-100 km height range, and thus add another dimension to the experimental determination of tides.

There have also been significant advances in state of the art modelling as

well as upper atmosphere measurements techniques since the report by Lindzen and his colleagues. In this light the present report defines operational requirements of MST radars necessary to provide useful tidal information, and assesses the overall role of the MST radar technique in the future of tidal studies.

## MEASUREMENTS COVERING A FRACTION OF A DAY

In the mesosphere and lower thermosphere nighttime ionization levels are often so low as to preclude wind measurements by the MST or Thomson scatter radar techniques. The question then arises as to the exact limitations imposed by deriving tidal components from data covering only a fraction of a day. Following a recent treatment by CRARY and FORBES (1983), assume that the data consists of mean, diurnal, and semidiurnal components with a random noise component of standard deviation $\sigma$. Consider a fit function of the form:

$$y(t) = b_o + \sum_{i=1}^{2} b_i \sin\left(\frac{2i\pi}{24} t + \phi_i\right) \qquad (1)$$

and define $\sigma_{bi}$ to be the standard deviations of the fit coefficients. In the case of a full-period (24-hour) fit of the above function it is well known (see, for example, SCHUSTER, 1898) that $\sigma_{bi}$ is given by $\sigma_{b1} = \sigma_{b2} = \frac{2}{\sqrt{N}}\sigma$, where N is the number of points fit. Thus, for this case, a fit to even a small number of data points (i>5) reduces the error in the fit coefficients to below that of the data points. In the case of a partial-period (< 24-hour) fit, however, the errors in the fit coefficients can be large enough, even for relatively small fluctuations, to make the extraction of meaningful results from the data unfeasible. This problem is briefly discussed by CHAPMAN and LINDZEN (1970). In order to illustrate the preceding statements and give a rough estimate of the errors involved in an actual fit, the coefficients $\sigma_{bi}$ were obtained numerically from random data with $\sigma = 1$. It is simple to show that the dependence on $\sigma$ is linear:

$$\sigma_{bi} = f_i(T,N)\sigma \qquad i = 0,1,2 \qquad (2)$$

where T = fit span and N = number of points fit. Figure 1 shows $f_i(T,N)$ for N = T + 1 (hourly data) for T = 7 through T = 20. For large values of T the $f_i(T,N)$ show the expected convergence $f_i(24, 25) = .4$ for i = 1,2. For smaller values of T, however, the various $f_i(T,N)$ show a rapid increase with decreasing T; $f_i(T,N) \approx 1$ ($\sigma_{bi} \approx \sigma$) for T ≈ 15 hours. For T = 12 hours $\sigma_{bi} \approx 3.1\sigma$ and $\sigma_{b2} \approx 1.8\sigma$. Figure 1 also shows $f_i(T,N)$ for N = 4T + 1 (data quarter-hourly). In this case $f_i(24, 97) = .2$ and $f_i(T,N) \approx 1$ for T ≈ 12-14 hours.

Table 1 contains data for T = 12 hours (a half-day's measurements) for various equally spaced time intervals $\tau$ between measurements ($\tau$ (minutes) = 60T/(N-1)). Be aware that $\sigma_{bi}$ or $\sigma_{b2} = \sigma$ is not necessarily a good absolute criterion for acceptability, but is only a relative measure. For a given $\sigma$ reflected in the data, one must choose N and/or T such that the $\sigma_{bi}$'s are acceptable. Let us take a typical example. Suppose we have 12 hours of daytime wind measurements at a given altitude. We bin these data in local time with a time interval ($\tau$) that is as yet unspecified. A Fourier fit to the data is performed and there exists a noise component in the data characterized by some standard deviation, $\sigma$. For the sake of argument, assume $b_1 = 10\sigma$ and $b_2 = 5\sigma$ and that we require $\sigma_{b1}/b1$ and $\sigma_{b2}/b2$ to be $\lesssim .1$. (At 90 km altitude $\sigma$ = 5 m sec$^{-1}$ might be a typical value.) It is evident from Table 1 that these constraints require $\tau \lesssim 5$ minutes. Similarly, for $b_1 = 5\sigma$ and $b_2 = 10\sigma$ we obtain $\tau \lesssim 2$ minutes to measure both the diurnal and semidiurnal components to the desired accuracy. To satisfy only the semidiurnal constraint in this latter

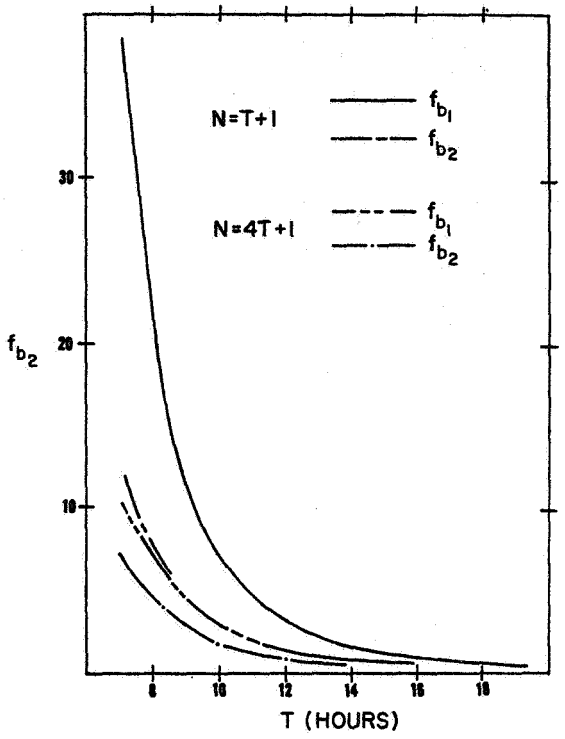


Figure 1. $f_{bi}$ vs T for hourly data (N=T+1) and quarter-hourly data (N=4T+1) where N = number of data points and T = fit span (hours).

example would require $\tau \lesssim 20$ minutes.

Alternatively, we can examine how many days (N) of data for a larger $\tau$ are required to obtain the same accuracies. For $\tau$ = 30 minutes, and the case where $b_1 = 10\sigma$ and $b_2 = 5\sigma$, $\sigma_{b1} = 2.19\sigma$ and $\sigma_{b2} = 1.27\sigma$ for one day's measurement. To obtain $\sigma_{b1} \leq \sigma$ we require $2.19/\sqrt{N_1} = 1$, and for $\sigma_{b2} \leq .5\sigma$ we require $1.27/\sqrt{N_2} = .5$; therefore $N_1 = 4.8$ and $N_2 = 6.5$. To satisfy both constraints we must take the larger of $N_1$ and $N_2$, or $N \approx 7$. Similarly, when $b_1 = 5\sigma$ and and $b_2 = 10\sigma$, $2.19/\sqrt{N_1} = 15$ and $1.27/\sqrt{N_2} = 1$; hence $N_1 = 19.2$ and $N_2 = 1.6$, so that $N \approx 20$.

Table 1. Standard deviations of Fourier components for 12-hour fit span

| | Data Interval ($\tau$, minutes) | | | | |
|---|---|---|---|---|---|
| | (60) | (30) | (15) | (5) | (2) |
| $\sigma_{b1}/\sigma$ | 3.10 | 2.19 | 1.55 | .89 | .57 |
| $\sigma_{b2}/\sigma$ | 1.80 | 1.27 | .90 | .52 | .33 |

It must be emphasized that these results are derived for noise which is uncorrelated over the time interval between data points. Actual data, of course, may or may not reflect this; the above is intended only as a guideline for minimum criterion for reliability.

## VARIABILITY

Observations of atmospheric tides are often characterized as being variable on a day-to-day basis. However, BERNARD (1981) points out that if the intrinsic time ($\tau_s$) to set up stationarity around the earth for a particular mode is greater than a characteristic time scale associated with the variability, then transient effects will exert some influence over the observed 'tidal' behavior. Therefore, it may only be meaningful to refer to the variability of a tide over time scales greater than $\tau_s$. Furthermore, theoretical models should be compared with a steady state or "average" tidal component uncontaminated by transient effects.

As a guide to interpreting observations, BERNARD (1981) has calculated characteristic propagation times ($\tau_p$) around the earth of various pertinent tidal modes (see Table 2). These are obtained from horizontal group velocities ($V_{gH}$, a function of latitude) determined by an "equivalent gravity wave (EGW)" approximation (SPIZZICHINO, 1969; RICHMOND, 1975) wherein the value of $V_{gH}$ is evaluated the latitude ($\theta_o$) where the vertical group velocities of the tidal mode and EGW are equal. These propagation times provide some measure, at least a relative one, of the set-up times ($\tau_s$) for various modes. Note that $\tau_p$ is on the order of ten days for the (2,6) and (1,1) modes, and hence the condition of stationarity may not be frequently realized in practice.

It is difficult to draw specific quantitative information from these estimates. A recent unpublished calculation by Forbes indicates that for $\tau_v \sim$ 3-5 days, distortions of the (1,1) modal shape are typically 15% in amplitude and 1 hour in phase, suggesting that the tabulated values of $\tau_p$ may be too high by more than a factor of two with regard to estimating the onset of "measurable" effects. Given the uncertainties inherent in these estimates, it appears reasonable to say it is meaningful to refer to variations in most tides over periods of over 4 days, whereas variations over shorter time scales may reflect transient effects. To achieve the highest degree of consistency between data sets and provide a meaningful comparison with theoretical models, it is therefore recommended that tidal measurements from MST radars be represented as vector averages of no less than 4 day's observations.

Table 2.*

| Mode | $\theta_o$ (deg) | $V_{gh}$(km $hr^{-1}$) at $\theta_o$ | $\tau_p$ (days) |
|---|---|---|---|
| (2,2) | 35.4 | 662.4 | 2.50 |
| (2,4) | 43.3 | 273.6 | 6.08 |
| (2,6) | 46.4 | 165.6 | 10.1 |
| (1,1) | 21.2 | 140.4 | 11.9 |
| (1,3) | 21.1 | 61.2 | 27.3 |

*After BERNARD (1981). See text for definitions of $\theta_o$, $V_{gh}$, $\tau_p$.

VERTICAL RESOLUTION AND ACCURACY

Vertical wavelengths associated with tidal modes expected to be observable in the mesosphere and lower thermosphere (50-100 km) generally fall in the range 30-70 km. (See FORBES, 1983, for a list of references.) Values as low as 20 km associated with diurnal propagating tides might be found at tropical latitudes (<30°). However, there exists evidence from observations and theoretical models that the superposition of modes, particularly in the 80-100 km region, can cancel and reinforce so as to produce structural features with scales of the order of 10 km.

In the stratosphere, observations (GROVES 1980; FUKAO et al., 1978; and WALLACE and TADD, 1974) are frequently characterized by short vertical wavelengths (~10-20 km), particularly in connection with the diurnal component. KATO et al. (1982) investigated the generation and propagation of tides due to geographically localized sources of excitation, and are able to explain many characteristics of the observed structures, which are apparently non-migrating tidal components. Stratospheric tidal amplitudes are typically much smaller than in the mesosphere, and may reflect transient effects due to variations in source characteristics. Both of these factors suggest that data series of a week or more may be necessary to properly define the stratospheric tidal component, assuming time resolutions of 15-30 minutes and 24 hours of measurements per day.

The above information indicates that a vertical resolution of 2 km throughout the 0-100 km height region would be necessary to resolve all tidal structures that might reasonably be expected. In addition, observations suggest that nominal accuracies necessary for the delineation of middle atmosphere tidal structures are about 2 m $sec^{-1}$ (.5 m $sec^{-1}$) for altitudes above (below) 60 km.

RADAR NETWORKS

Our understanding of middle atmosphere tides can best be improved and tested with simultaneous global measurements, preferably covering a week or more at a time. It is important to span a range of latitudes within a longitude sector, or vice-versa, in order that modes (migrating and non-migrating) be separated. Insofar as it is feasible, the placement of newly proposed MST radars should complement existing MST, meteor wind, and partial reflection drift radar locations. Tidal theory and theoretical simulation models of tides can play an important role in defining the locations and operating requirements of radars so as to derive the optimum scientific return.

Ideal tidal campaigns would include observatories geographically conjugate about the equator and at least one equatorial radar. A MAP Study Group under the direction of Prof. S. Kato is currently examining the scientific aspects of an equatorial radar. Recently, geographically symmetric radars at Kyoto (35°N) and Adelaide (35°S) have delineated strongly asymmetric tidal behavior about the equator in both diurnal and semidiurnal components, between 80 and 100 km altitude (ASO and VINCENT, 1982). For "true" modes (that is, eigenfunctions of Laplace's tidal equation), asymmetric tides are characterized by nonzero N-S velocities and zero E-W velocities at the equator, whereas the reverse is true for symmetric components. A properly placed equatorial radar could, therefore, contribute significantly to the deconvolution of tidal structures in the middle atmosphere.

Tidal observations at the equator could also contribute significantly to other aspects of middle atmosphere dynamics. For instance the gravest symmetric diurnal propagating (1,1) mode is thought to be capable of producing significant turbulence via nonlinear cascade or convective instability mechanisms, and a mean easterly jet (~50 $msec^{-1}$) peaking near 105 km due to momentum deposition in the region where the tide is dissipated (MIYAHARA, 1981). An equatorial

radar would, therefore, also provide the opportunity to observe the important middle atmosphere processes of wave-mean flow interaction and wave/turbulence coupling for a known wave forcing. However, these phenomena primarily occur above 75 km, so that it is imperative that measurements extend as far into the lower thermosphere as possible, preferably above 105 km. Therefore, placement of the radar must avoid possible interference by the equatorial electrojet.

Given the necessity of global coordination, it is important that some consensus be reached concerning the appropriate method of extracting tidal components from data time series, expressing an appropriate 'average' tidal structure for comparison with models, and describing variability about mean monthly or mean seasonal behaviors. In addition, the importance of data exchange and data base management cannot be overemphasized for the global study of tidal phenomena.

## ACKNOWLEDGEMENTS

Preparation of this report was supported by the National Science Foundation under Grant ATM-8113078 to Boston College.

## REFERENCES

Aso, T. and R. A. Vincent (1982), Some direct comparisons of mesospheric winds observed at Kyoto and Adelaide, J. Atmos. Terr. Phys., 44, 278-280.

Bernard, R. (1981),Variability of the semi-diurnal tide in the upper mesosphere, J. Atmos. Terr. Phys., 43, 663-674.

Chapman, S. and R. S. Lindzen (1970), Atmospheric Tides, D. Reidel, Hingham, MA.

Crary, D. J. and J. M. Forbes (1983), On the extraction of tidal information from measurements covering a fraction of a day,Geophys. Res. Lett., in press.

Forbes, J. M. (1983), Middle atmospheric tides,J. Atmos. Terr. Phys.,in press.

Fukao, S., S. Kato, S. Yokoi, R. M. Harper, R. F. Woodman and W. E. Gordon (1978), One full-day radar measurement of lower stratospheric winds over Jicamarca, J. Atmos. Terr. Phys., 40, 1331-1337.

Groves, G. V. (1980), Seasonal and diurnal variations of middle atmosphere winds, Phil. Trans. R. Soc. Long., A296, 19-40.

Haurwitz, B. (1964), Tidal phenomenon in the upper atmosphere, WMO Technical Note 58, World Meteorological Organization, Geneva, Switzerland.

Kato, S., T. Tsuda and F. Watanabe (1982), Thermal excitation of non-migrating tides, J. Atmos. Terr. Phys., 44, 131-146.

Lindzen, R. S. (1969), Data necessary for the detection and description of tides and gravity waves in the upper atmosphere, J. Atmos. Terr. Phys., 31, 449-456.

Miyahara, S. (1981), Zonal mean winds induced by vertically propagating atmospheric tidal waves in the lower thermosphere, J. Met. Soc. Jap., 59, 303.

Richmond, A. D. (1975), Energy relations of atmospheric tides and their significance to approximate methods of solution for tides with dissipative forces, J. Atmos. Sci., 32, 980-987.

Schuster, A. (1898), On the investigation of hidden periodicities with applications to the supposed 26-day period of meteorological phenomena, Terr. Mag., 3, 13-41.

Spizzichino, A. (1969), Etude des interactions entre les differentes composantes du vent dans la haute atmosphère, Ann. Geophysique, 25, 755-771.

Wallace, J. M. and R. F. Tadd (1974), Some further results concerning the vertical structure of atmospheric tidal motions within the lowest 30 km, Mon. Wea. Rev., 102, 795-803.

# 1.4A METEOROLOGICAL AND DYNAMICAL REQUIREMENTS FOR MST RADAR NETWORKS: WAVES

S. K. Avery

CIRES, University of Colorado
Boulder, CO 80309

Studies of wave motions using the MST radar have concentrated on single station time series analyses of gravity waves and tides (for examples see CARTER and BALSLEY, 1982; BALSLEY and CARTER, 1982; ROTTGER, 1980). Since these radars can collect high time resolution data they have the potential to become a significant tool for mesoscale research. In addition, these radars can be operated almost continuously unattended and, consequently, data sets are available for analyzing longer period wave motions such as tides and planetary scale waves. Although we still have much to learn from single station data, the possibilities of new knowledge from a network of radars is exciting.

The scales of wave motions in the atmosphere cover a broad range (see GELLER, 1979 for a review). Consequently the choice of a radar network will depend to a large extent on the types of wave motions that are to be studied. There are many outstanding research problems that would benefit from observations from a MST radar network. In particular, there is a strong need for measurements of gravity wave parameters and equatorial wave motions. Some of the current problems in wave dynamics are discussed below.

Studies of large scale waves have been accomplished through balloon soundings as well as satellite data on a global scale. Supplementary data have been provided by ground-based experiments from single stations and rocket experiments. These techniques have been useful in studying the evolution of stratospheric warmings, the quasi-biennial oscillation, and the semiannual oscillation (HIROTA, 1980; LABITZKE, 1982; HOLTON and TAN, 1982; SMITH 1983). It is important to obtain global coverage when studying large-scale waves. In terms of a radar network this would mean locating two or three stations around a latitude circle at several latitudes. The temporal resolution need only be on the order of hours. Since satellites determine the wind field from a temperature measurement through geostrophy, one of the main contributions that can be made by MST radars is an independent estimate of the winds for these large-scale waves.

Measurements of tidal oscillations also require global observations. Several cooperative observational campaigns have been made amongst meteor radar, partial reflection, and MST radars. From these cooperative observation programs as well as single station data, it has been seen that discrepancies still exist between the latest theories (FORBES, 1982 a,b) and observations in the mesosphere. Most of the tidal information we have is from the upper mesosphere and stratosphere. Tropospheric tides have small amplitudes and therefore require accurate measurements and long data sets to isolate the tidal harmonics. Since the MST radar can operate unattended for long periods, it could provide valuable information about tropospheric tides. Traditionally both theory and observations have dealt with the migrating tides (functions of local time) although recently there has been some theoretical studies of nonmigrating diurnal tides (functions of longitude and local time) by KATO et al. (1982). Kato considered diurnal tides forced by localized heat sources near the equator. These sources generated tidal perturbations having short vertical wavelengths (10 km) in addition to the longer wavelengths associated with classical tides. This may have important implications for observations of tides over a limited height region. The phase variation with height may only determine the smaller wave-length and obscure the longer one. The relative importance of the migrating and and nonmigrating tides needs exploring.

Day-to-day variations in tides have been observed and are not well understood. According to KATO et al. (1982), the amplitudes and phases of the nonmigrating tides vary with time. This may explain some of the variability. Another mechanism to explain tidal variability has been suggested by WALTERSCHEID (1981). In this mechanism, the tidal variability is produced by the interaction of long-period gravity waves with the globally forced tide. To verify this mechanism, simultaneous observations of the tidal structure and gravity wave horizontal and vertical phase speeds are needed. In fact, a determination of the climatology of gravity waves is probably one of the most important measurements needed. The breaking of upward propagating gravity waves and tides and the subsequent generation of turbulence plays an important role in balancing the momentum budget of the mesosphere (LINDZEN, 1981; HOLTON, 1982; MATSUNO, 1982). The partial-reflection experiment in Adelaide, Australia has been used to determine the vertical flux of horizontal momentum during May 1981 (VINCENT and REID, 1983). Vincent and Reid found a mean upward flux of westward momentum which was equivalent to a -20 m/s/day acceleration. There was also significant variations in the flux on the order of hours. This type of measurement is extremely useful and would be desirable at other locations. Since Vincent and Reid's results suggest that most of the momentum is associated with periods less than one hour, the high temporal resolution of the MST would lend itself nicely to this type of measurement. Ideally a gravity wave climatology would also include measurements of periods, wavelengths, and associated phase velocities. The spatial and temporal requirements for obtaining this climatology is discussed by Avery and Carter, p. 247, this volume.

Another important dynamical region in which an MST radar network would be valuable is the equatorial region. There have been very few measurements of short-period waves in this dynamically active region. Satellite and rocket data have shown a semiannual oscillation in the middle atmosphere (HIROTA, 1980). The interaction between midlatitude Rossby waves and Kelvin waves is believed to be the source for driving the semiannual oscillation in the stratosphere and observations support this theory. Recent theoretical modeling by DUNKERTON (1982) suggests that high frequency gravity waves and Kelvin waves are responsible for the mesospheric semiannual oscillation. The large-scale Kelvin waves can be observed in satellite data but the gravity waves will require much higher time resolution data.

Inertial instabilities in the tropical mesosphere should occur due to cross-equatorial shear resulting from the solstice circulation pattern. This has been studied by DUNKERTON (1981) using a simple model. Dunkerton showed that the solstice diabatic circulation produces a much larger cross-equatorial shear than what has been observed. The magnitude of the instability is determined by the magnitude of the eddy diffusion. One of the main questions is whether this is controlled by high frequency gravity waves or whether the inertial waves are self-stabilizing. An MST radar network would be ideally suited to address this problem.

There has been an increased awareness of the potential of a network of ST radars in the use of operational forecasting. While caution must be exercised in using a research instrument for operational applications (BALSLEY and GAGE, 1982), it appears that a national network would be of great value for the commercial aviation industry in providing instantaneous upper level wind measurements (CARLSON and SUNDARARAMAN, 1982). In addition, mesoscale research would be enhanced by observations from an ST network. The evolution of fronts and associated mesoscale phenomena could be more easily tracked. A network of NOAA's Environmental Research Laboratory Profilers is being planned along the Rocky Mountain front range to be used for this type of research and will probably be a test site for the viability of using ST radars in operational

forecasting.

In summary, MST (or ST) radar networks would provide valuable information regarding the wave dynamics of the atmosphere. The high temporal resolution that can be obtained with these radars is essential in order to determine gravity-wave fluctuations. A network is needed to measure the corresponding horizontal wavelengths and phase velocities. Of great scientific interest is the role of the equatorial region in driving circulation patterns. Very few observations are available in the tropics, yet several theories of equatorial instabilities and oscillations have been developed. The MST radar can play a significant role in testing these theories. Finally, operational applications using ST radar networks could also provide information for tropospheric mesoscale research.

REFERENCES

Balsley, B. B. and D. A. Carter (1982), The spectrum of atmospheric velocity at 8 km and 86 km, Geophys. Res. Lett., 9, 465-468.

Balsley, B. B. and K. S. Gage (1982), On the use of radars for operational wind profiling, Bull. Am. Met. Soc., 63, 1009-1018.

Carlson, H. C. and N. Sundararaman (1982), Real time jet stream tracking: National benefit from an ST radar network for measuring atmospheric motions, Bull. Am. Met. Soc., 63, 1019-1026.

Carter, D. A. and B. B. Balsley (1982), The summer windfield between 80 and 92 km observed by the MST radar at Poker Flat, Alaska (65°N), J. Atmos. Sci., 39, 2905-2915.

Dunkerton, T. J. (1981), On the inertial stability of the equatorial middle atmosphere, J. Atmos. Sci., 38, 2354-2364.

Dunkerton, T. J. (1982), Theory of the mesopause semiannual oscillation, J. Atmos. Sci., 39, 2681-2690.

Forbes, J. M. (1982a), Atmospheric tides I. Model description and results for the solar diurnal components, J. Geophys. Res., 87, 5222-5240.

Forbes, J. M. (1982b), Atmospheric tides II. The solar and lunar semidiurnal components, J. Geophys. Res., 87, 5241-5252.

Geller, M. A. (1979), Dynamics of the middle atmosphere, J. Atmos. Terr. Phys., 41, 683-705.

Hirota, I. (1980), Observational evidence of the semiannual oscillation in the tropical middle atmosphere - a review, P. Appl. Geophys., 118, 217-238.

Holton, J. R. (1982), The role of gravity wave induced drag and diffusion in the momentum budget of the mesosphere, J. Atmos. Sci., 39, 791-799.

Holton, J. R. and H.-Ch. Tan (1982), The quasi-biennial oscillation in the northern hemisphere lower stratosphere, J. Met. Soc. Japan, 60, 140-.

Kato, S., T. Tsuda and F. Watanabe (1982), Thermal excitation of non-migrating tides, J. Atmos. Terr. Phys., 44, 131-146.

Labitzke, K. (1982), On the interannual variability of the middle stratosphere during the northern winters, J. Met. Soc. Japan, 60, 124-139.

Lindzen, R. S. (1981), Turbulence and stress owing to gravity waves and tidal breakdown, J. Geophys. Res., 86, 9707-9714.

Matsuno, T. (1982), A quasi one-dimensional model of the middle atmosphere circulation interacting with internal gravity waves, J. Met. Soc. Japan, 60, 215-226.

Rottger, J. (1980), Structure and dynamics of the stratosphere and mesosphere revealed by VHF radar investigations, P. Appl. Geophsy., 118, 494-527.

Smith, A. K. (1983), Observations of wave-wave interactions in the stratosphere, Presented at AMS Fourth Conference on Meteorology of the Upper Atmosphere, Boston.

Vincent, R. A. and I. M. Reid (1983), HF Doppler measurements of mesospheric gravity wave momentum fluxes, submitted to J. Atmos. Sci.

Walterscheid, R. L. (1981), Inertio-gravity wave induced accelerations of mean flows having an imposed periodic component. Implications for tidal observations in the meteor region, J. Geophys. Res., 86, 9698-9706.

# 1.4B RADAR OBSERVATIONS OF INERTIAL PERIOD WAVES IN THE LOWER STRATOSPHERE OVER ARECIBO

C. R. Cornish and M. F. Larsen

School of Electrical Engineering
Cornell University
Ithaca, NY 14853

Several hundred hours of wind velocity measurements made with the Arecibo 430-MHz radar during the past few years have indicated the presence of persistent wave-like structures just above the tropopause (Woodman, private communication). To further investigate these structures, a nearly continuous times series of wind measurements in the upper troposphere and lower stratosphere was made from May 5 to May 12, 1982 at Arecibo. Each of 16 compass points was sampled as the 430-MHz feed was rotated in a velocity azimuth display (VAD) mode at a zenith angle of 15 degrees off-vertical. Using a nonlinear least squares parameter estimation technique described by SATO and WOODMAN (1982), line-of-sight velocities were calculated from Doppler shifts of the received spectra. These velocities have been reduced to zonal and meridional components of the wind vector; the vertical component of the wind vector will be available after further reduction.

Figure 1 is a velocity profile of the meridional wind for the entire 7-day observing period. The sloping line drawn connects points of equal phase; one will note a downward phase progression calculated to be .7 cm/sec. Results of a spectral analysis using a discrete Fourier transform indicate the presence of a periodic event with a period of 35-40 hours for both zonal and meridional wind components in the height range of 12 to 18 km. This measured period is close to the inertial period of 38.8 hours for Arecibo, which is situated at 18 degrees north latitude. Furthermore, the observed wave event exhibits an anticyclonic rotation of velocity with height which is the same variation found by THOMPSON (1978) in his observations of inertial waves in the stratosphere at midlatitudes.

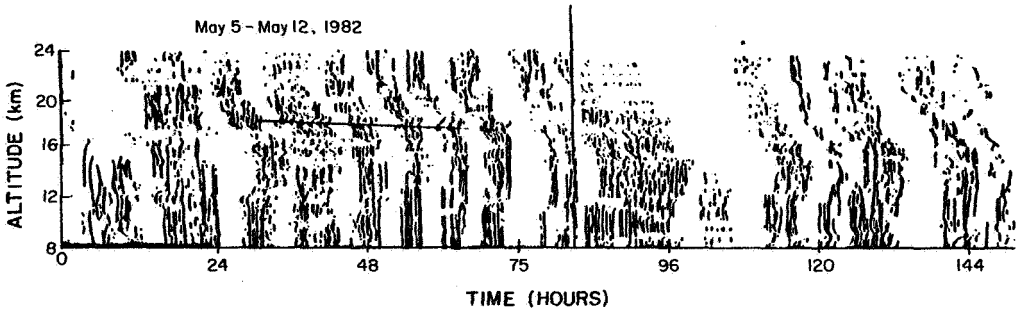


Figure 1. Velocity profile for 7-day observation period for the meridional wind.

## REFERENCES

Sato, T. and R. F. Woodman (1973), Spectral parameter estimation of CAT radar echoes in the presence of fading clutter, Radio Sci., 17, 817-826.

Thompson, R. O. R. Y. (1978), Observation of inertial waves in the stratosphere, Quart. J. R. Met. Soc., 104, 691-698.

# 1.4C BAROCLINIC INSTABILITY IN THE STRATOSPHERE AND MESOSPHERE

K.-S. Zhang and T. Sasamori

Department of Atmospheric Sciences
University of Illinois
Urbana, IL 61801

ABSTRACT

The energy source of stratospheric planetary waves is largely due to vertical propagation from the troposphere, but it is shown in this paper that the stratospheric zonal-mean state which changes with time is not stable against small perturbations, whereby transient perturbation waves may be generated at the expense of the stratospheric zonal-mean available potential energy. This theoretical conclusion is obtained based on the quasi-geostrophic model in spherical coordinates which calculates the characteristic solutions for the basic zonal mean-state changing with time.

(This paper will be published in the Journal of Atmospheric Sciences.)

# 1.4D EQUATORIAL MST RADARS: FURTHER CONSIDERATION

P. Lagos

Instituto Geofisico del Peru
Apartado 3747
Lima 100, Peru

## INTRODUCTION

As an outcome of the Workshop on Equatorial Middle Atmosphere Measurements and Middle Atmosphere Radar held in Estes Park on May 10-12, 1982, the need for a new MST radar in the geographic equatorial region was proposed (KATO and HIROTA, 1982). It was also suggested that such a facility could be established and operated under international cooperation and the MST radar would be one of the activities of the future International Equatorial Observatory.

An equatorial MST radar is needed in equatorial latitudes for the investigation of the dynamics of equatorial waves, precise structure of tides, wave-mean flow interaction processes, MST interactions and other related atmospheric problems. The newly emerging radar techniques for MAP are very promising for detecting and studying shorter wavelength modes such as gravity and acoustic waves.

The equatorial region has unique properties. As the corialis force vanishes at the equator and increases with latitude, waves generated in this region will be trapped. Kelvin waves are such a trapped equatorial waves known to be an important source of westerly momentum in the semiannual oscillation (HIROTA, 1978, 1979; DUNKERTON, 1982). These waves are also believed to be important in the momentum budget of the quasi-biennial oscillation (WALLACE and KOUSKY, 1968). Likewise, Rossby and other equatorial waves must play important roles in the dynamics of the equatorial region and elsewhere.

The purpose of this note is to provide additional justification for establishing the new equatorial MST radar.

## IMPACT OF EQUATORIAL ATMOSPHERE-OCEAN INTERACTION ON CLIMATE

The atmosphere and the ocean form the two most important fluid systems of a large heat engine that controls the fluctuations of our climate. Large-scale ocean-to-atmosphere influence has been put firmly into the forefront of research by the work of BJERKNES (1969) and NAMIAS (1976). In the equatorial region the ocean and the atmosphere are strongly coupled and consequently their interaction is more evident. Anomalous fluctuations in the atmosphere give rise to anomalous fluctuations in the ocean and viceversa. Sea to air heat transfer modulates cumulus convection with resulting release of latent heat of condensation aloft which then alters the large scale air circulation elsewhere through teleconnection mechanisms.

One of the most important examples of air-sea interaction, on time scale of a few years, is the El Nino phenomenon which takes place along the west coast of South America. The collapse of the wind field in the equatorial central Pacific as a cause of the ocean response is well understood (WYRTKI, 1975; O'BRIEN et al., 1981), but the reason for the collapse of the wind field is essentially unknown. Once the El Nino event has been established, the ocean has a large influence in the atmosphere to the extent of changing the climate in the equatorial region and elsewhere. But the mechanism of this ocean-to-atmosphere influence is not well understood. I wish to point out here the important role that the equatorial wave dynamics in the troposphere and stratosphere must play in the teleconnection mechanism. I think that with the availability of a new

network of MST radar stations in the equatorial region many of these unsolved atmospheric problems could be elucidated.

Although previous studies of synoptic-scale wave motion in the equatorial stratosphere based on analysis of radiosonde data (WALLACE and KOUSKY, 1968) and in the equatorial stratosphere and mesosphere using meteorological rocket and satellite observations (HIROTA, 1978, 1979; SALBY et al., 1982) have provided interesting results on Kelvin waves, the radiosonde, rocket and satellite data alone cannot be sufficient to study the full range of equatorial wave dynamics. On the other hand, MST radars operated nearly continuously in the equatorial region can provide synoptically meaningful data for observing long- and short-period equatorial waves.

## FURTHER EVIDENCE OF EQUATORIAL WAVES IN THE TROPOSPHERE AND STRATOSPHERE

In order to test the hypothesis that large anomalous perturbations in the zonal wind in the equatorial central Pacific can give origin to equatorial waves in the atmosphere, in addition to forcing Rossby and Kelvin waves in the ocean, radar measurements for deducing synoptic wind data were set up at Jicamarca for 30 days in November 1982. Daily radiosonde data from Callao (12° 00'S, 77° 07'W) about 50 km from Jicamarca were analyzed for comparison and for inferring the past and subsequent behavior of the atmosphere.

We have first subjectively and objectively analyzed the daily radiosonde data from Callao in the altitude region from ground to about 25 km and for the period October 1982-March 1983. The subjectively analyzed time-height section of zonal wind presents wind fluctuation with periods on the order of 5-15 days. Since the purpose of this note is only to indicate the existence of atmospheric fluctuation similar in structure to Kelvin waves, the analysis and interpretation will be discussed elsewhere. These data were also subjected to power spectrum analysis. Time series were prepared from the daily wind and temperature data at each reported level and the corresponding power spectra for each level were obtained. Peaks near the period of 10 and 15 days are prominent in the curves with the largest values occurring at 2 and 5 km, respectively.

Late in October 1982, when the oceanic and atmospheric conditions were such that the El Nino phenomenon was very likely to occur, a decision was taken to carry out wind measurements using the Jicamarca coherent-scatter technique for a period of 30 days in November 1982 in the 5-25 km height region and in a nearly continuous mode. The purpose was to observe a very intense Kelvin wave with a period of 10-15 days which could be associated with El Nino events as far away as 12° from the equator. Three antenna beams were used and observed for 20 minutes each hour. Figure 1 shows a sample of the east-west component of the wind data for 7, 10, 15 and 20 km altitude and for the period 3-22 November. Comparison of the two sets of data indicates that the radar technique gives more useful information for wave phenomena studies with periods from seconds to a few days. When radar data are averaged for an hour or more, radar measurements have been shown to produce data of a quality that is at least comparable to radiosonde data (BALSLEY and GAGE, 1982; LARSEN and ROTTGER, 1982).

## SCIENTIFIC REQUIREMENTS FOR THE NEW EQUATORIAL MST RADAR

(1) Purpose: Observation of equatorial waves in the MST region.

(2) Location: It is desirable that two new facilities be established within 5° latitude. Possible locations could be either at Christmas Island (2°S, 157.5°W) or Canton Island (2.8°N, 171.7°W) and Talara (4.34°S, 81.15°W) During the IGY, Talara was used as an IGP ionospheric radiosounder.

(3) Height range: MST region.

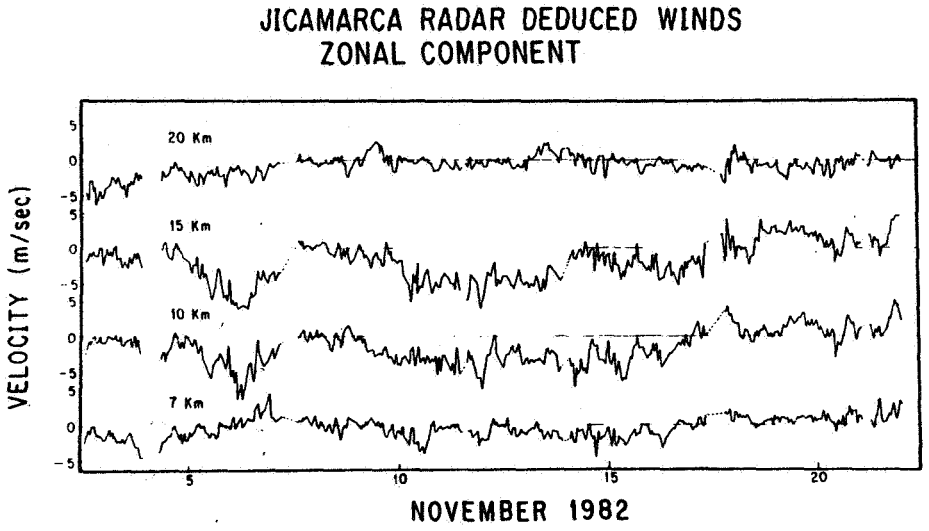


Figure 1

(4) Parameter to be observed: Three components of wind fluctuations.

(5) Height resolution: 500 m.

(6) Time resolution: At least two hours of continuous observation every six hours during 30 days and every three months. With this time resolution, acoustic, gravity, tidal, Rossby, Kelvin waves as well as semiannual, annual, biennial oscillations, can be studied in the equatorial MST region. Table 1 shows the main atmospheric time scale processes. However, an interrupted observation will be desirable.

Table 1

| ATMOSPHERIC TIME SCALE PROCESSES | |
|---|---|
| DAYS | PHYSICAL PROCESSES |
| $10^{-4}$ | Acoustic waves |
| $10^{-3}$ | |
| $10^{-2}$ | Gravity waves |
| $10^{-1}$ | |
| $10^{0}$ | Tidal waves |
| $10^{1}$ | Rossby and Kelvin waves |
| $10^{2}$ | Seasonal cycle, monsoon, semiannual and annual cycle |
| $10^{3}$ | Biennial oscillation El Nino |
| $10^{4}$ | |

## CONCLUSION

The results presented in this note give additional support to the suggestion of the need of equatorial MST radars in order to obtain more information on the nature of equatorial waves in the MST region. Radar-deduced winds such as obtained at Jicamarca for periods of months indicate that with these data the full range of equatorial waves, with time scales of seconds to years, can be studied.

## REFERENCES

Balsley, B. B. and K. S. Gage (1982), Bull. Am. Meteorol. Soc., 63, 1009.

Bjerknes, J. (1969), Monthly Weather Rev., 97, 163.

Dunkerton, T. (1982), J. Atmos. Sci. (to be published).

Hirota, I. (1978), J. Atmos. Sci., 35, 714.

Hirota, I. (1979), J. Atmos. Sci., 36, 217.

Kato, S. and I. Hirota (1982), Handbook for MAP, C. F. Sechrist, Jr., ed., vol. 7, p. 103.

Larsen, M. F. and J. Rottger (1982), Bull. Am. Meteorol. Soc., 63, 996.

Namias, J. (1976), Monthly Weather Rev., 104, 1107.

O'Brien, J. J., A. Busalacchi, and J. Kindle (1981), Resource Management and Environmental Uncertainty, Lesson from Coastal Upwelling Fisheries; M. H. Glantz and J. D. Thompson, eds., Wiley-Interscience, p. 159.

Salby, M. L., D. Hartmann, P. L. Bailey and J. C. Gille (1982), Handbook for MAP, C. F. Sechrist, Jr., ed., vol. 7, p. 119.

Wallace, J. M. and V. B. Kousky (1968), J. Atmos. Sci., 25, 900.

Wyrtki, K. (1975), J. Phys. Oceanog., 5, 572.

# 1.5A THE ECONOMICS OF DATA ACQUISITION COMPUTERS FOR ST AND MST RADARS

B. J. Watkins

Geophysical Institute
University of Alaska
Fairbanks, AK 99701

## INTRODUCTION

The goal of this paper is to present some low cost options for data acquisition computers for ST (stratosphere, troposphere) and MST (mesosphere, stratosphere, troposphere) radars. The particular equipment discussed will reflect choices made by the University of Alaska group but of course many other options exist. We believe the low cost microprocessor and array processor approach presented here has several advantages because of its modularity. An inexpensive system may be configured for a minimum performance ST radar, whereas a multiprocessor and/or a multiarray processor system may be used for a higher performance MST radar. This modularity is important for a network of radars because the initial cost can be minimized while future upgrades will still be possible at minimal expense.

This modularity also aids in lowering the cost of software development because system expansions should require little software changes.

It is assumed in this paper that the functions of the radar computer will be to obtain Doppler spectra in near real-time with some minor analysis such as vector wind determination.

## SYSTEM REQUIREMENTS

The costs for computer and signal processing components depend greatly on the desired radar performance. The height coverage, height resolution, time resolution, Doppler resolution, and number of antenna beam positions all affect the quantity of data to be processed and hence the equipment cost. An ST radar with coarse height resolution (e.g., 1-2 km resolution with about 16 range gates) and poor time resolution (data every few minutes or more) can be purchased for a low cost. A higher spatial and temporal resolution with the capability of height coverage into the mesosphere will require a greater capacity CPU and/or an array processor and have a higher cost.

To simplify the cost comparison, Figure 1 shows possible radar performance specifications and we will estimate the cost for each configuration. For simplicity it is assumed that Doppler spectra will be derived from 64 point FFTs (Fast Fourier Transforms), and that the radar antennas will be directed in three directions for vector wind measurements.

If these radars are to be used only for average wind measurements, then time resolution is likely to be of little significance. Measurements every 2-10 minutes may be adequate. On the other hand, if wave motions are to be distinguished, the sample rate must be fast enough to prevent aliasing. Observed wave periods can be as low as 4-5 minutes in the lower atmosphere. Therefore to make vector measurements of wave motions, a total sampling and analysis time for three antenna directions should be less than about 2 1/2 minutes.

Doppler data are generally obtained in three directions by changing the antenna position if it is physically steerable, or phasing an array. The sequence of data taking and real-time analysis is assumed as follows:

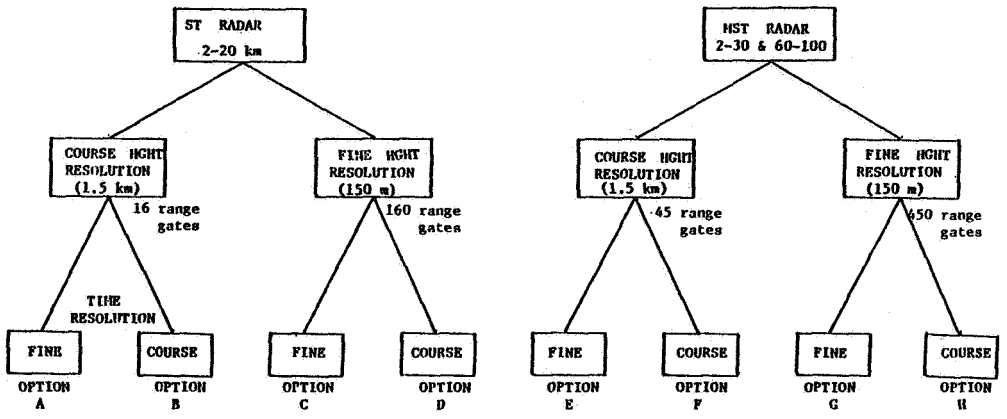


Figure 1. Eight possible radar performance specifications (A--H). For the purposes of this paper, coarse and fine height resolutions are defined as 1.5 km and 150 m, respectively. The time resolution is defined as the total time to determine a vector wind measurement (data from 3 antenna directions); fine resolution is considered $\leq$2.5 minutes and coarse resolution is 2.5--10 minutes.

(1) Select first antenna direction
(2) Transmit $N_p = N_f \cdot N_c$ pulses
where $N_f$ = number of FFT points
$N_c$ = number of coherent integrations.
(3) Sample and store a complex receiver sample at each range, for all $N_p$ pulses.
(4) At the completion of transmitting $N_p$ pulses, the coherent integration process is performed.
(5) At each range a power spectrum of the returned signals is computed using an FFT.
(6) If multiple spectra are to be averaged, steps (2) to (5) above are repeated $N_{AV}$ times. ($N_{AV}$ = number of averaged spectra).
(7) The $N_{AV}$ spectral from each range gate are averaged and finally stored on tape.
(8) A new antenna direction is selected and steps (2) to (7) are repeated.

If phase-coded pulses are used then an additional decoding step is necessary after the coherent integration is performed. This is a minimal task timewise by comparison with other computations so we have neglected it in our timing estimates.

## CHOICE OF COMPUTER

The computer should ideally be the lowest cost unit that will perform the required tasks. However, the exact needs are difficult to define because researchers rarely agree on the mode of operation for radar experiments and frequently place more demands on equipment as time progresses. For example, it is now recognized that high resolution and hence more range gates are desirable for studying turbulence structures. Several ST and MST radars are now upgrading for this higher resolution. Thus, an important specification is expandability.

We have considered many hardware options that would provide the absolute

lowest cost system suitable for a simple ST radar that may be used in a network and yet be expandable to a high performance MST radar.

The University of Alaska group has chosen a microcomputer that uses a Motorola 68000 microprocessor in conjunction with two low cost array processors (APs). While there are many other hardware options available that other researchers may choose, our choice illustrates the modularity concept and the substantially lower cost by comparison with the computers at established radar sites.

The 68000 microprocessor has the advantage of 32-bit internal architecture, and coupled with an array processor provides fast arithmetic capabilities. Each AP ($6,000) can perform one million 32-bit floating-point operations per second; they are made by Sky Computer Corporation. The APs have no memory of their own but share a common memory with the main CPU. This has the advantage of low cost memory, the ability for the AP to access a very large amount of memory (up to 16 M bytes in our case), and minimizing data transfer times.

The microcomputer cost depends greatly on the amount of memory required but should be in the range $5,000 to $15,000. A more detailed costing is given later.

By comparison, presently established radars have computer costs about a factor of ten larger. For example at Millstone Hill and Arecibo, the Harris Computers and Floating-Point System APs have costs far in excess of $100,000. These APs do indeed provide a speed advantage, but as well as their initial high cost, the addition of extra memory is very costly. Even other relatively low price APs that are now available become very costly when any substantial amount of memory is added to them. For example Computer Design and Applications, Inc., sells an AP for about $24,000 with minimum memory, but costs $85,000 with 2 M bytes of memory.

Although many radar experiments, particularly a simple ST radar network, may initially have no need for an AP, it is worthwhile planning for their use so that upgrade costs will be minimized.

## MODULAR APPROACH

To illustrate how a modular approach can be used to assemble computers of different processing capabilities, we present some possible examples including the system now being constructed by the University of Alaska group.

Figure 2 shows the single board computer (made by Omnibyte Corporation) and array processor used. The boards are 7" x 12" and conform to the IEEE Multibus specifications (SNIGIER, 1982; WILSON, 1982). These boards, together with a card cage, power supply and case form the basis of a computer system. Providing there are enough spare slots in the card cage, the system may be expanded by plugging in more memory (up to 15 M bytes), multiple CPUs and multiple APs.

Some examples of various computer configurations are shown in Figure 3. No construction costs are necessary because these boards are commercially available and simply plug together. The University of Alaska system has one CPU, 640 K of memory and two APs operating in parallel.

## DETERMINATION OF REQUIRED PROCESSING POWER

With a given radar specification it is necessary to determine both the time duration to gather the data and the processing time. This total time duration should not be excessive; for example 3 measurements must be made in less than about 2 1/2 minutes to determine waves in the stratosphere. Further, the time

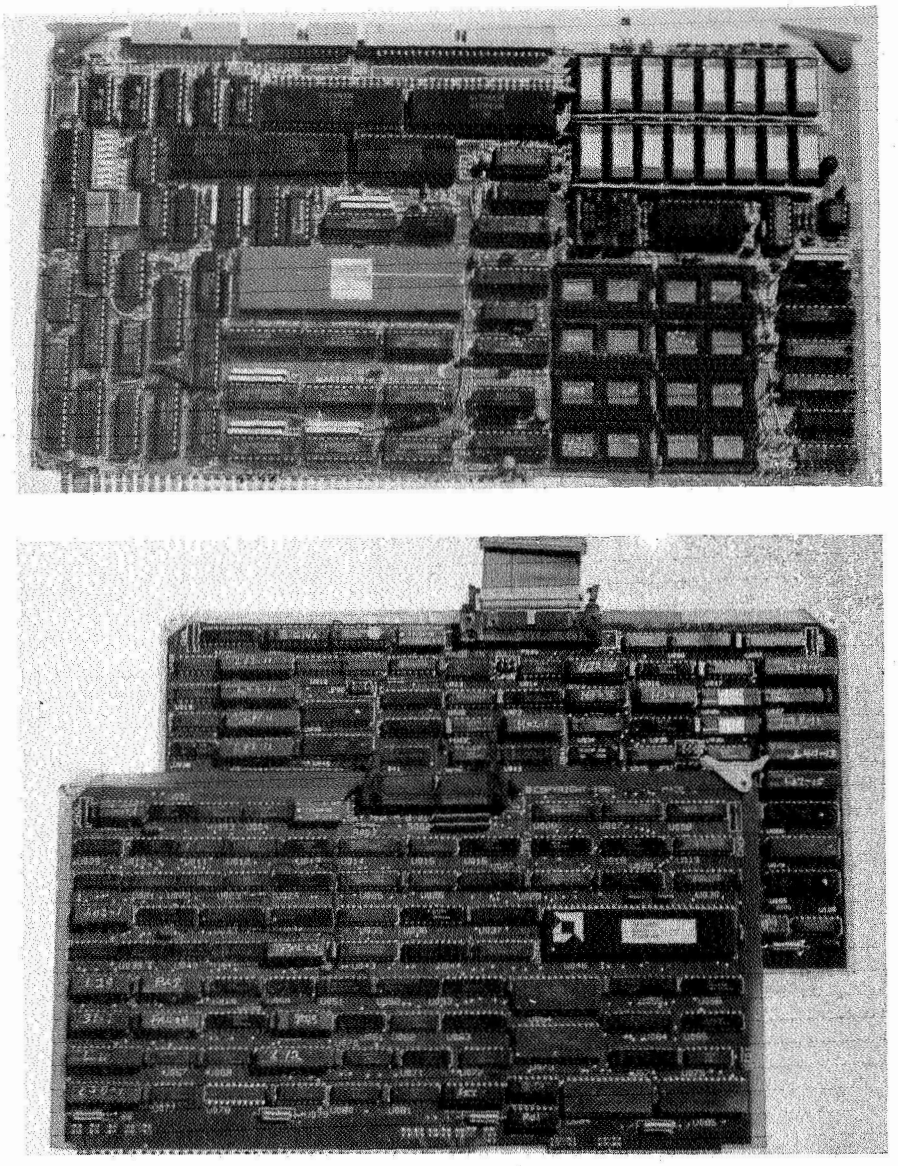

Figure 2. TOP: Single board computer with 128 k of memory, two I/O ports, and two 16-bit parallel I/O ports (cost $2000). BOTTOM: Array processor (two board set, cost $6000).

to process the data should not be large compared to the time required to gather the data. Ideally this processing time should not exceed about 5 - 10% of the time required to take the data. When too much time is wasted processing data instead of sampling, fewer spectra may be integrated in a given time, and hence signal detectability suffers at the upper heights.

The time required to collect samples for three antenna directions, and averaging $N_{AV}$ spectra at each range gate after $N_C$ coherent integrations is given by

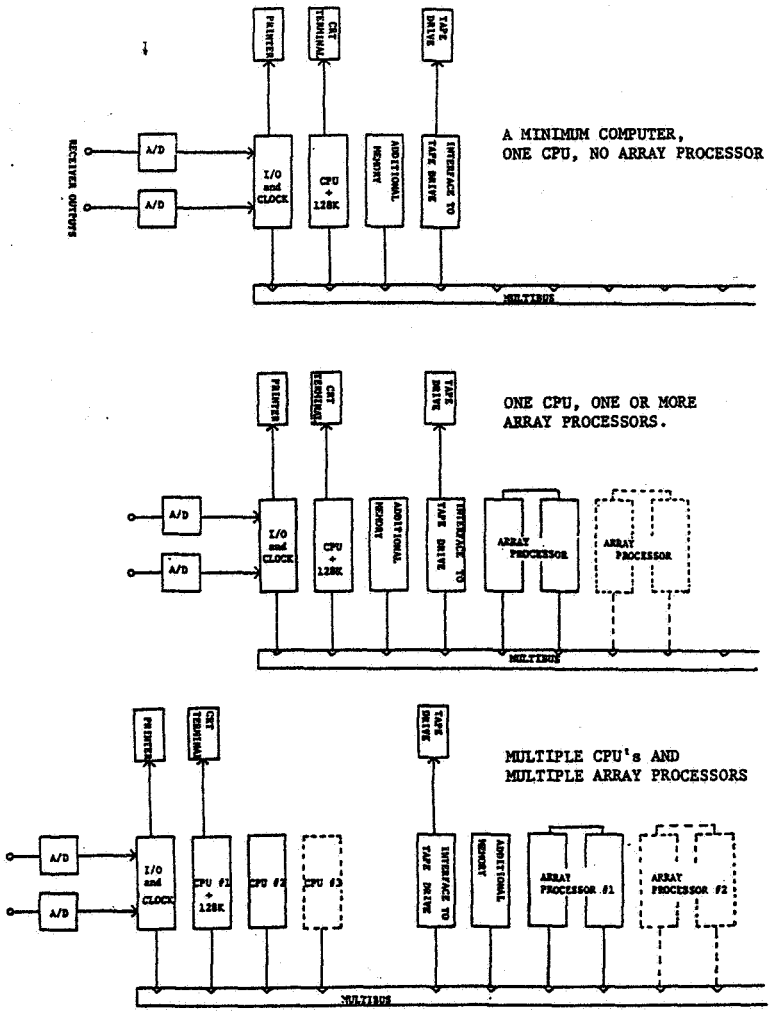


Figure 3. Some possible computer configurations utilizing one or more CPUs and up to four array processors. The University of Alaska has implemented the middle configuration above with two array processors.

$$T_{DATA} = \frac{3 \cdot N_f \cdot N_c \cdot N_{AV}}{PRF} \qquad (1)$$

where PRF = transmitter pulse repetition frequency.

For example if $N_f = 64$, $N_c = 64$, $N_{AV} = 10$, PRF = 1250 Hz then $T_{DATA} = 98$ sec. This value for the PRF is about the maximum possible for an MST radar without range aliasing; it gives a maximum unambiguous range of 120 km. A higher PRF is possible for an ST radar that receives no data from the mesosphere. The values for $N_f$ and $N_c$ are somewhat arbitrary, but together with the PRF and radar wavelength $\lambda$, determine the Doppler resolution $\delta v$ where

$$\delta v = \frac{PRF \cdot \lambda}{2 \cdot N_f \cdot N_c} \text{ m/s} \qquad (2)$$

For a 50 MHz radar ($\lambda$ = 6 m), using the above values yields $\delta v$ = 0/9 m/sec. This should be a usable value as the Poker Flat MST radar has operated with $\delta v$ = 1.3 m/s with excellent results.

The method we have adopted for determining the required computer processing power is to first determine the required radar parameters (e.g., PRF, $N_c$, $N_{AV}$, $N_f$, $\delta\nu$) required to obtain the data with sufficient resolution and signal/noise ratio. The parameters are best estimated from experience and extrapolation from established radars. The values quoted above are typical for the 50 MHz Poker Flat radar although higher values of $N_{AV}$ have been used at Poker Flat.

Next $T_{DATA}$ is calculated; this sets an upper limit to the data processing time. A computer is then selected so that the processing time plus the data-acquisition time is not too large. For example, to detect waves, this total time should be less than ~ 2 1/2 minutes (data in three directions).

The time $T_{PROCESS}$ required to process the data (from 3 antenna directions) is the total time required to perform coherent integration plus the FFTs

$$T_{PROCESS} \approx 3 \cdot N_c \cdot N_{AV} \quad (T_{FLOAT} + T_{SUM}) + 3 \cdot N_g \cdot N_{AV} \cdot T_{FFT}$$

where $N_g$ = number of range gates

$T_{FLOAT}$ = Time for AP to change complex integer array of $N_g$ samples to floating point.

$T_{SUM}$ = Time for AP to sum a complex vector.

$T_{FFT}$ = Time for AP to perform FFT on array of $N_f$ samples.

The minimum amount of memory required by given by:

$$M = 4 \cdot N_f \cdot N_c \cdot N_g \text{ bytes} \qquad (3)$$

The factor 4 comes from the use of 16-bit complex samples.

We have adopted the technique of first acquiring all data before performing any coherent integration. By contrast it is possible to use far less memory by performing the coherent integration pulse by pulse. However, this places constraints on the minimum interpulse period of the transmitter because without a very powerful, and hence costly, computing system it is difficult to perform this integration as well as other required tasks during the interpulse period. It is far more cost effective to use a lesser capacity computer and AP in conjunction with a fairly large memory. In the case where memory requirements become excessive (e.g., Case G on Figure 1 and Table 1) it is then desirable to use a dedicated preprocessor for performing the coherent integration. Such a preprocessor is hard-wired to perform fast additions and may be constructed for about $6,000 (JOHNSTON, 1983).

It should be noted that there are many possible compromises available in establishing a radar's operating parameters. For example, both the data-acquisition time, $T_{DATA}$, and the processing time are affected by the number of averaged spectra $N_{AV}$. If this parameter value is decreased it may be possible to use a computer of lesser capability and cost. However, a lower $N_{AV}$ will

Table 1. Costs for radar options A--H in Figure 1.

| | A | B | C | D | E | F | G | H |
|---|---|---|---|---|---|---|---|---|
| Approx. time to acquire and process data | 103 secs | 600 | 117 | 600 | 108 | 330 | 127 | 380 |
| Costs: CPU board | $2000 | $2000 | $2000 | $2000 | $2000 | $2000 | $2000 | $2000 |
| Memory | $1550 | $1550 | $7750/$1550 | $1550 | $3100 | $1550 | $1550/$21,700 | $1550 |
| Parallel I/O board with clock | $550 | $550 | $550 | $550 | $550 | $550 | $550 | $550 |
| Case, power supply and Multibus rack | $1000 | $1000 | $1000 | $1000 | $1000 | $1000 | $1000 | $1000 |
| Array Processor(s) | $6000 | -- | $12000 | $6000 | $6000 | $6000 | $24,000 | $6000 |
| A/D's and sample-holds | $700 | $700 | $700 | $700 | $700 | $700 | $700 | $700 |
| Hardware Preprocessor | -- | -- | -/$6000 | -- | -- | -- | $6000/- | -- |
| Tape drive + Interface | $5800 | $5800 | $5800 | $5800 | $5800 | $5800 | $5800 | $5800 |
| Printer | $700 | $700 | $700 | $700 | $700 | $700 | $700 | $700 |
| TOTAL COSTS | $18,300 | $12,250 | $30,500/$30,300 | $18,300 | $19,850 | $18,300 | $42,300/$56,450 | $18,300 |

Notes

(1) Radar options C and G have been calculated with and without a hardware preprocessor. Without the preprocessor the memory costs are higher.

(2) For radar option D it has been assumed that data will be acquired and processor by range stepping, i.e. processing 32 range gates at a time. This saves memory but greatly lengthens the total processing time.

(3) The time quoted are for determination of a vector wind measurement, i.e. acquisition and processing times for 3 sequential antenna directions.

decrease the signal detectability and it is likely that data from some upper heights may be lost. Such compromises should be carefully evaluated before deciding on the radar operating parameters.

## COST SUMMARY

Using the method outlined in the previous section, we have evaluated the costs for different radar specifications A - G in Figure 1. A summary is given in Table 1. In addition, the approximate times required to acquire and process data from three antenna directions are given. These times are worst-case values because it has been assumed that during data acquisition the computer is only required to perform the sampling. This reserves some time during the interpulse periods for other tasks such as graphics display, calculation of vector winds, signal/noise ratios, etc.

For the computer configuration B in Table 1 that has no AP, the data-processing time is relatively slow. We estimated the time for floating-point FFTs using the University of Alaska's microcomputer (8 MHz clock). It could be speeded up either by using an integer FFT instead of floating point, or use of an additional simple hardware arithmetic unit, or a CPU with higher clock frequency. The 68000 microprocessor is now available for operation with a 12-MHz clock and a 16-MHz version should be available in future.

It is assumed that some type of hard copy printer (with graphics), and a 9-track tape drive are common to all configurations. In addition, the approximate cost of analog-to-digital converters is included and the Appendix briefly discusses some cost options.

All the costs listed in Table 1 are for a quantity of one. Discounts (15 - 30%) are available for larger quantities that would be purchased for a network of radars.

It should be emphasized that the costs in Table 1 are for hardware only. There may be substantial initial costs for software. A competent programmer may take several months to develop the data-aquisition program. The use of an AP will reduce the software costs because much signal processing software is provided by the AP manufacturer. It is most efficient to develop software using a high-level language, an operating system and disk drives and at the University of Alaska we are doing this with a real-time operating system, a 20 Mb disk drive and the C programming language. The costs for this extra hardware, software and labor should be considered, but for a large network the cost per radar would not be large.

## APPENDIX: ANALOG AND DIGITAL CONVERTERS

The choice of analog-to-digital (A/D) converter resolution may affect the cost of the radar computer. If an 8-bit A/D is chosen the computer will require only half the memory (for storing samples) compared to a 10- or 12-bit data word that is commonly used since data are stored in 8-bit increments. However, the overall dynamic range of the radar will generally be limited by the A/D converter not by the receiver. Unless the radar is sited to substantially reduce ground clutter (e.g., placed in a valley with nearby shielding hills), the dc offset at the receiver output from clutter echoes will be large compared to the noise and signal fluctuations. In practice, a 10- or 12-bit converter is preferred and the calculations in Table 1 have assumed this.

The cost of A/D converters is relatively small. As a cost example in Table 1 we have used a 12-bit 2 $\mu$sec A/D converter made by ILC Data Device Corporation ($150 each) and a Sample/Hold made by Analog Devices ADSHM-SK ($199).

A faster but lower resolution A/D is approximately the same cost, e.g., Analog Devices 10 bits, 1 μsec, MAH-1001 ($219).

REFERENCES

Johnston, P. E. (1983), (at NOAA Aeronomy Laboratory), private communication.

Snigier, P. (1982), Designers guide to the multibus, Digital Design, 52.

Wilson, D. (1982), Multibus: Evolving to meet new system stands, Digital Design, 76.

# 2. INTERPRETATION OF MST RADAR RETURNS FROM CLEAR AIR (Keynote Paper)

C. H. Liu

Department of Electrical Engineering
University of Illinois
Urbana, IL 61801

## INTRODUCTION

The nature of the scattering and reflection mechanisms that give rise to the MST radar echoes from the clear air has been a subject of investigation for many years since the beginning of the experimental observation of tropospheric over-the-horizon propagation of radio waves. The understanding of these mechanisms is essential in the correct interpretation of the data which carry information about winds, waves, turbulence and stability in the atmosphere. There are two main aspects of the problem. The first concerns the nature of the targets the radar sees and their generation mechanisms. The second aspect is the signatures of the radar signals returned from the different targets. Volume scatterings from isotropic or anisotropic turbulence, and partial reflections from horizontally stratified, sharp refractive index gradients are believed to be the main contributors to the radar echoes. In general, it is most likely that combined effects from all these mechanisms produce the observed data. Therefore, it is important to study the signature of the echo signals for these different scatterers under realistic experimental conditions. Questions such as: how the pulse rate, width and coding will affect the returned signal; what are the different features of the complex signal statistics under different scattering and reflection conditions, etc., should be investigated. It is hoped that from these studies, the nature of the targets can be better understood. Then it may be possible to relate them to atmospheric dynamic processes (GAGE and BALSLEY, 1980).

## BASIC THEORY

At the VHF and UHF frequency bands for the MST radars, the atmosphere is almost transparent. The changes of refractive index caused by the inhomogeneous structures are usually very small compared to the ambient values. Under these conditions, the single scattering Booker-Gordon equation for the scattered field can be applied:

$$\vec{E}_s(\vec{r}) = \frac{k^2}{2\pi} \int_{V'} \frac{e^{ik|\vec{r}-\vec{r}'|}}{|\vec{r}-\vec{r}'|} N_1(\vec{r}') \, [\hat{a}_n \times (\vec{E}_0(\vec{r}') \times \hat{a}_n)] \, d\vec{r}' \qquad (1)$$

where the geometry is shown in Figure 1. $\vec{E}_s$ is the scattered field at the receiver, $N_1$ is the inhomogeneous part of the refractive index, $\vec{E}_0$ is the incident field and $\hat{a}_n$ is the unit vector pointing from the scattering volume to the receiver. The formula applies to general types of inhomogeneities which are imbeded in a homogeneous background. For back-scatter geometry, (1) reduces to the familiar expression for plane incident wave

$$\vec{E}_s(\vec{r}) = \frac{k^2 \vec{a} \, e^{ikr}}{2\pi r} \int_{V'} d\vec{r}' \, N_1(\vec{r}') \, e^{-i2k\hat{a}_n \cdot \vec{r}'} \qquad (2)$$

where $\vec{a} = \hat{a} \times (\vec{E}_0 \times \hat{a}_n)$.

This formula has been used in the statistical formulation to study

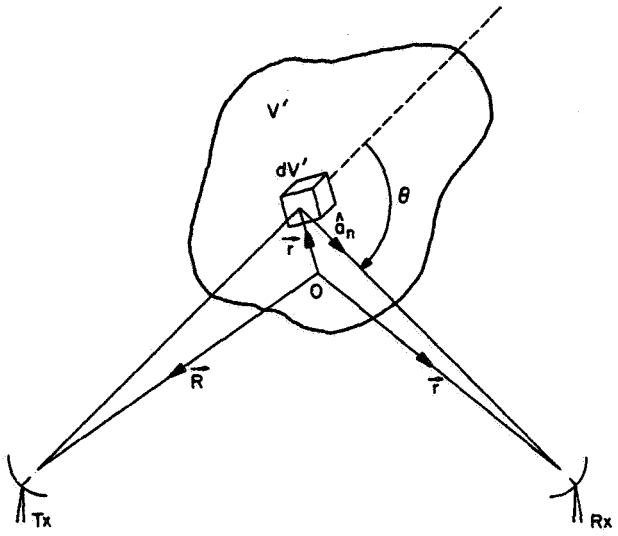


Figure 1.

scattering from turbulence, isotropic or anisotropic, yielding the radar reflectivity

$$\eta_{turb} = 8\pi^2 k^4 S_N(2k\hat{a}_n) \tag{3}$$

where $S_N(\vec{\kappa})$ is the three dimensional power spectrum for the fluctuation of the refractive index, $N_1$. It is worthwhile to point out that the argument of $S_N$ is a vector $2k\,\hat{a}_n$ indicating that the formula can be applied to anisotropic turbulence in general.

Equation (1) can also be used to derive the formula for partial reflection. For this case, the refractive index inhomogeneities form horizontally stratified laminae that extend to horizontal dimensions greater than several Fresnel zone size. For a vertically incident wave, equation (1) can then be integrated first with respect to the horizontal coordinates and yield the expression for a reflected field.

$$E_s(z) = ikE_0\, e^{ikz} \int_L N_1(z')\, e^{-2ikz'}\, dz' \tag{4}$$

From this equation the formula used in partial reflection calculations can be derived

$$E_r(z) = \frac{1}{2} E_0 e^{ikz} \int_L \frac{dN_1}{dz'}\, e^{-2ikz'}\, dz' \tag{5}$$

where the condition that outside the inhomogeneous region L, $N_1$ vanishes has been used. Equation (4) or (5) can be applied for statistical or deterministic analysis of the partial reflection problem. In the statistical approach the

scattered power is proportional to

$$\langle E_s E_s^* \rangle = k^2 E_0^2 \int_{-\Delta r/2}^{\Delta r/2} dz_1 \int_{-\Delta r}^{+\Delta r} d(z_1-z_2) \langle N_1(z_1) N_1(z_2) \rangle e^{-2ik(z_1-z_2)} \quad (6)$$

where the integration limits $-\Delta r/2$ to $\Delta r/2$ correspond to a range gate of width $\Delta r$. In the usual statistical approach, the fluctuating field $N_1(z)$ is assumed to be statistically homogeneous such that $\langle N_1(z_1)N_1(z_2)\rangle$ is a function of $(z_1-z_2)$. If the correlation length $\ell_c$ of $\langle N_1(z_1)N_1(z_2)\rangle$ is much less than the range gate $\Delta r$, then the limits of integration with respect to $(z_1-z_2)$ in equation (6) can be extended to $\pm \infty$ which results in spectral resolution of $N_1$, yielding

$$\langle |E_s|^2 \rangle = k^2 E_0^2 \cdot (\Delta r) \cdot S_N(2k) \quad (7)$$

If, on the other hand, the correlation length $\ell_c$ is not so short as compared to the range gate $\Delta r$, then the $d(z_1-z_2)$ integration will depend on the limits of integration, $\Delta r$ and $\langle |E_s|^2 \rangle$ will not have a strict linear dependence on $\Delta r$. Depending on the correlation function of $N_1$ and the ratio $\Delta r/\ell_c$, the dependence of $\langle |E_s|^2 \rangle$ on $\Delta r$ may vary.

It should be emphasized that it is under the assumption that the linear dimension of the scattering volume is much greater than the correlation length of the turbulence, the scattering process results in the selection of the component of the turbulence spectrum at the Bragg wave number, leading to the results shown in equations (3) and (7). This does not justify in general the pre-selection of that particular Bragg component of the turbulence spectrum alone to represent the refractive index fluctuations in the derivation of the reflectivity formula.

Other complications may arise in the effort to model the scattering process statistically. For example, how much are the results affected if the homogeneity (stationarity) of the scattering region is not strictly satisfied?

SIGNAL STATISTICS

The statistics of the received signal depend on the scattering mechanism. When the returned signal comes from independent scatterers or reflectors of similar strength which are distributed in space in such a way that the rms deviation from the mean position is greater than one wavelength, then the amplitude of the received signal will have the classical Rayleigh distribution. If a dominating specularly reflected component exists in the received signal, the data will exhibit the Rice-Nakagami distribution for the amplitude. Another type of distribution known as the "Hoyt distribution" (BECKMANN, 1962) may result when the phase distribution of the independently scattered/reflected signals is not uniform. This occurs, for example, when the rms deviation from the mean position for the scatterers is less than a wavelength. Examples of these different types of signals are shown in Figures 2 and 3. Numerical simulations can be devised to study these signal statistics. Comparisons between the numerical models with observed data may help us understand more clearly about the various scattering/reflection mechanisms.

Another aspect of signal statistics is the spectral characteristics of the signal. While the classical turbulence theory predicts that the returned power is proportional to the width of the signal power spectrum, the opposite relation has been observed in many occasions (RASTOGI and BOWHILL, 1976; ROTTGER and LIU,

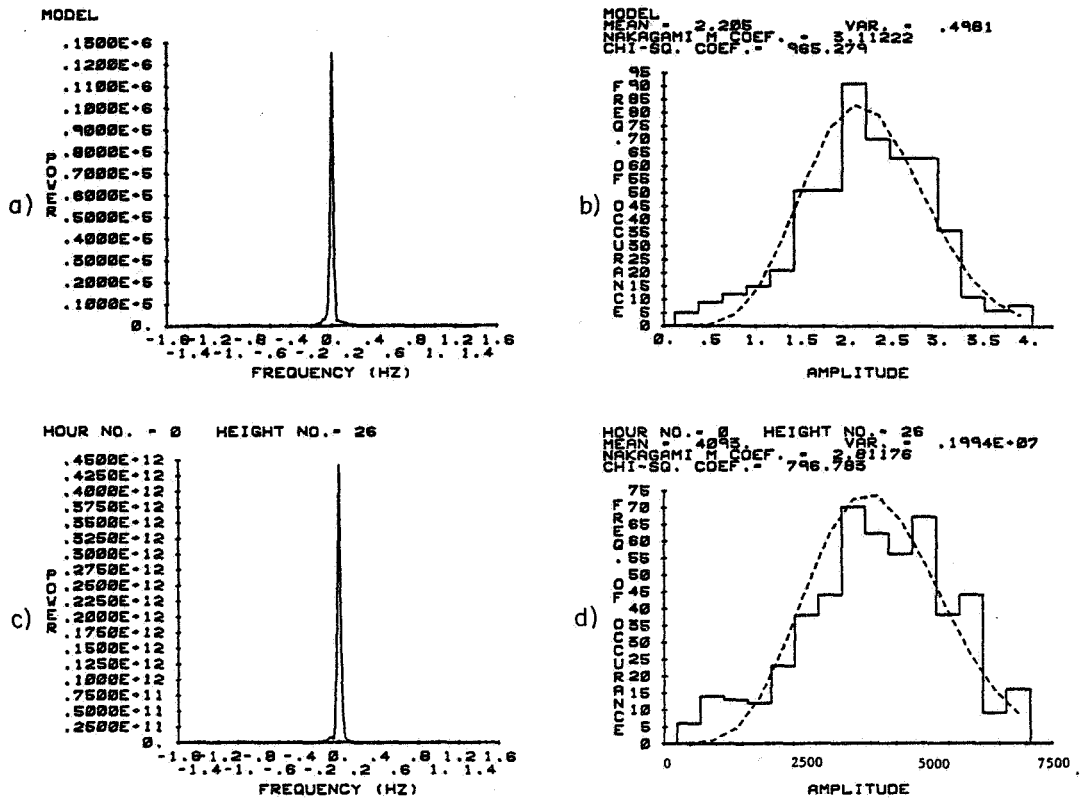


Figure 2. a. Power spectrum of modeled data for specular reflection from a flat layer. b. Histogram of the modeled amplitude data for specular reflection from a flat layer. c. Power spectrum. d. Histogram of the amplitude. Height number 26 corresponds to an actual height of 2.5 km.

1978) in different regions of the atmosphere. Explanations in terms of partial reflection, diffusive scattering etc. have been proposed. However, a satisfactory quantitative explanation of the phenomenon has yet to be developed.

## ORIGIN OF REFRACTIVE INDEX FLUCTUATIONS

Wind shears have been considered as one of the possible sources for generating turbulence. Good correlations have been found between received signal power and measured wind shear in the troposphere and stratosphere. The origin of the horizontally stratified laminae that give rise to enhanced signal return when the radar is operating at the vertical position is not well understood. ROTTGER (1980) suggested that temperature steps separating turbulent layers similar to the situation at oceanic thermocline may be the possible cause. VANZANDT (1982) has shown that experimentally measured power spectra of mesoscale wind fluctuations in the troposphere and lower stratosphere can be modeled by a universal spectrum of buoyancy waves. It will be of interest to investigate how the model extends to smaller scales.

At mesospheric heights, electron-density profiles strongly affect the radar returns. Dynamic effects, such as turbulence and wave activities; as well as solar activities, all can influence the received signal power.

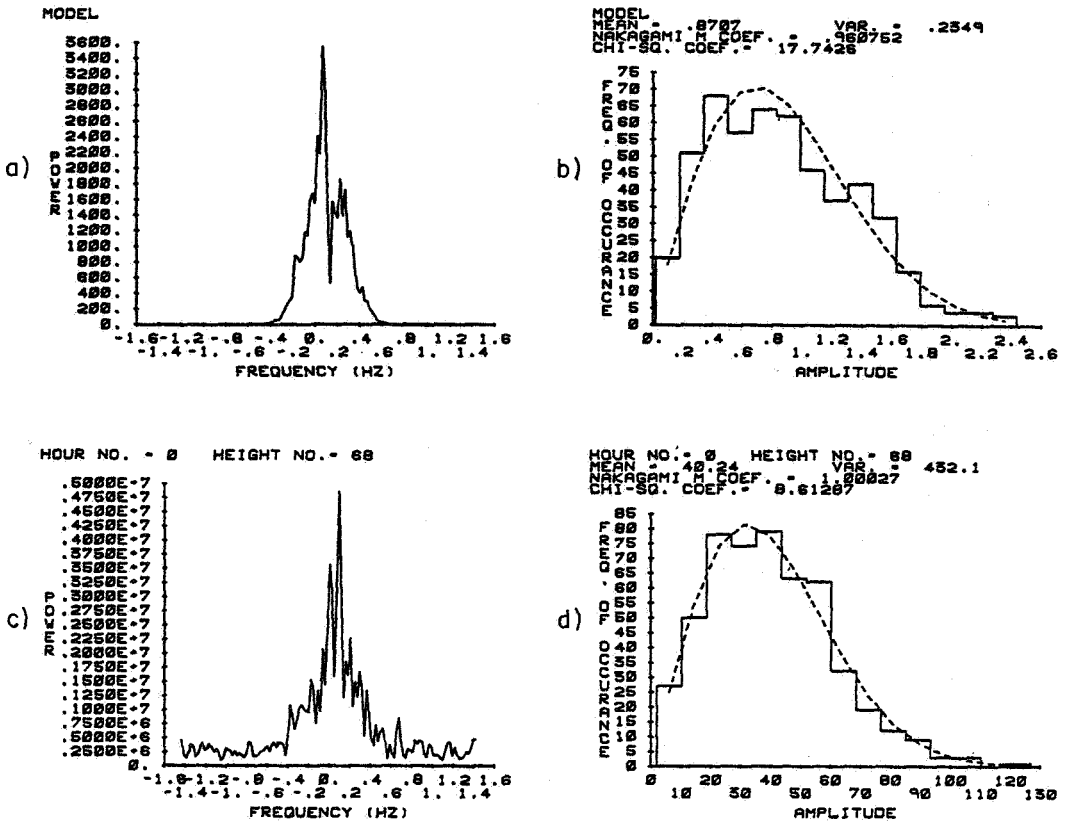


Figure 3. a. Power spectrum of modeled volume scattering data.
b. Histogram of the amplitude for modeled volume scattering data.
c. Power spectrum. d. Histogram of the amplitude.

## RESTRUCTURE OF IRREGULARITIES

Coherent signals of the complex field received at the three receivers in the spaced antenna drift measurements can be used to study the restructuring of the inhomogeneities. The temporal evolutions of the irregularities give rise to change of signal pattern as they drift across the radar beams from the spaced antennas. A number of physical phenomena can be responsible to make the flow non-frozen. For example, the random velocity fluctuations superposed on the mean flow; the diffusion of inhomogeneities; velocity gradient (wind shear) in the scattering volume, etc. To take these factors into account either individually or collectively one needs to examine the space-time structure of the scattering region and model them accordingly. Each model will give rise to a certain radio signal signature which can be compared with experimental data. Hopefully, the physical model and the experimental data can be related following this procedure. The basic starting point is the scattering formulation of Booker-Gordon applied to non-frozen scatterers. Model space-time spectra for non-frozen turbulence can be applied. Both cross-correlation and cross-spectra dispersion analysis should be studied. A clear understanding of the scattering process under the non-frozen condition will help us gain information about the temporal evolution of the irregular structures from the experimental data.

## EFFECTS OF ANTENNA BEAM SIZE

The first order scattering theory as discussed earlier neglects the change of phase in the scattering volume. As the scattering volume increases such that the linear dimension becomes comparable or greater than the Fresnel zone, phase incoherency within the scattering has to be taken into account. Indeed, it turns out that a parameter $P=(kd\ell_c/r)$ plays a role in determining whether the phase incoherence is important or not (LIU and YEH, 1980), where k is the wavenumber corresponding to the radar frequency, d is the linear dimension of the antenna beam, $\ell_c$ is the correlation length of the turbulence and r is the range. For $P\ll 1$, the usual Booker-Gordon formula applies. For $P\gtrsim 1$, the antenna beam width is comparable or larger than the coherent cone of the scattered wave, higher order phase terms in the scatter integral have to be taken into account. These effects should be studied in the general case with the space-time variation of the irregularities also taken into account.

## REFERENCES

Beckmann, P. (1962), NBS J. 60D, 231-240.

Gage, K. S. and B. B. Balsley (1980), Radio Sci., 15, 243-258.

Liu, C. H. and K. C. Yeh (1980), Radio Sci., 15, 277-282.

Rastogi, P. K. and S. A. Bowhill (1980), J. Atmos. Terr. Phys., 38, 449-462.

Rottger, J. (1980), Radio Sci., 15, 259-276.

Rottger, J. and C. H. Liu (1980), Geophys. Res. Lett., 5, 357-360.

VanZandt, T. E. (1982), Geophys. Res. Lett., 9, 575-578.

## SUMMARY

(a) Range Gate Dependence of Specular Echoes

The question of $\Delta R$ vs $(\Delta R)^2$ dependence of specular echoes was resolved during the discussions. More careful and realistic theoretical analyses have led to this conclusion. The main point is that as long as the correlation length of the irregular structure is much shorter than the range gate, $\Delta R$ dependence should be valid in the statistical treatment of the problem. As the range gate is decreased, or other assumptions such as homogeneity of the structure etc. are violated, dependence other than linear on $(\Delta R)$ will arise. Careful experimental results agreed with this conclusion.

(b) Mechanisms for Layered Structures

Two possible mechanisms for generation of the layered structures were discussed. One corresponds to vertical mixing in a local turbulent region due to Kelvin-Helmholz instability. Sharp, step-like gradients will appear at the boundaries of the turbulent regions as the consequence of the mixing. More quantitative study of this mechanism is needed. The other mechanism proposed is that the horizontally stratified laminae of the refractive index may be due to the displacement of low frequency buoyancy waves acting on the background vertical gradient of refractivity. The radar reflectivity based on this model has been estimated. Experimental verfication of the model such as measurements of Fresnel reflectivity as a function of Brunt Vaisala frequency or inertial frequency, the aspect dependence of reflectivity, etc. have been suggested. Certainly the understanding of the generation mechanisms will be one of the

major efforts for the community. For this effort, statistical characterization of Fresnel scattering/reflection structures is important. In particular, the efforts in studying signal statistics of radar returns to determine the statistical nature of scatterers and reflectors, and parameterization of Fresnel returns were discussed.

(c) Mechanism for Maintaining Long Lasting Turbulent Layers

Observations at Arecibo at 15° off zenith direction showed long lasting turbulent layers in the stratosphere. Strong turbulent patches were also observed by the Chatanika radar at 12 km heights for 15° $\sim$ 45° off zenith directions. What are the mechanisms that generate these strong turbulent layers and kept them there?

(d) Spectrum

Several interesting points were discussed. The effect of "diffuse reflection" on "vertical" velocity spectrum has to be considered in data analysis. Beamwidth broadening of the spectrum is important in the measurement of velocity variance. In the lower mesosphere, the signal power is often found to have positive correlation with fading time which is inverse of spectral width. Recent tropospheric low-elevation experiments also showed such positive correlation. This is contrary to the results expected from usual turbulence scattering theory. Some explanations have been suggested. A better knowledge of the structure of the scatterers is needed to interpret the data.

(e) Effects of Pulse Repetition (PRF) Rate, Power ($P_{ph}$) Width ($\tau_p$) and Coding on Signal Detectability

Based on the assumption that the following are constants: antenna area, echo reflectivity, Doppler shift, spectral width, spectral resolution, sampling rate, and incoherent spectral averaging time; the effects of PRF, $P_{ph}$ and $\tau_p$ on the detectability of the radar were discussed.

(f) Clutters from Aircraft and Ground

The problem can be solved during data taking or during data processing. Directional filtering by antenna sidelobe suppression, pulse stuttering, more sampling, etc. can be used during data taking. Temporal filtering, spectra estimation, range filtering, interference filter, notch filter, or selection by signal amplitude distribution or by power limit threshold, etc. can be done during data processing. The problems are discussed more fully in Chapter 8, this volume.

(g) Origin of Mesosphere Refractive Index Fluctuations

Mesospheric echoes are strongly influenced by the electron-density profile in the D region. A sudden increase or even moderate variation by VHF radar signal return usually can be attributed to the enhancement of electron density or electron-density gradient. Observations of the enhancement of radar echo power during solar flare events showed the turbulence to be confined to intermittent layers. Solar control of winter mesospheric echoes at Poker Flat was also observed.

DRAFT RECOMMENDATION FROM DISCUSSION IN TOPIC 2

RECOGNIZING the importance for an accurate characterization of the spectrum of refractive index irregularities for the efforts to understand mechanisms of turbulence generation and to measure with MST radar, winds, turbulence and stability;

**NOTING the spectral sampling capability of steerable, multiple wavelength radars we**

**RECOMMEND that:**

**Multiple frequency radar observations supported by in situ measurements be carried out with existing equipment such as at Arecibo and other radar facilities.**

# 2.1A ON THE MORPHOLOGY OF THE SCATTERING MEDIUM AS SEEN BY MST/ST RADARS

K. S. Gage

Aeronomy Laboratory
National Oceanic and Atmospheric Administration
Boulder, CO 80303

## ABSTRACT

Much can be learned about the morphology of the small-scale structure of the atmosphere from analysis of echoes observed by MST radars. The use of physical models enables a synthesis of diverse observations. Each model contains an implicit assumption about the nature of the irregularity structure of the medium. A comparison is made between the irregularity structure implicit in several models and what is known about the structure of the medium.

## INTRODUCTION

Much has been written in the past five years about the scattering and reflection mechanisms responsible for the echoes observed by MST radar (GAGE and BALSLEY, 1980; ROTTGER, 1980). At UHF it is fairly widely accepted that echoes arise from turbulent irregularities in the radio refractive index. At lower VHF, echoes from stable regions of the atmosphere are very anisotropic and appear to involve Fresnel scattering/reflection as well as turbulent scattering. While the specular nature of these echoes is widely recognized, there is still no consensus as to the detailed mechanism responsible for the echoes.

The occurrence of echoes from the clear atmosphere requires structure in the medium at the scale of half the wavelength of the probing wave. In the case of turbulent scattering this structure is random and presumably associated with active turbulence in the medium. In the case of Fresnel reflection or scattering the medium possesses a coherent structure at least transverse to the probing beam. In both cases the character of the observed echoes reveals much about the structure of the medium. Unfortunately, ambiguities arise when an attempt is made to "work backwards" and infer the structure of the medium from radar observations. To resolve ambiguities and to validate models precise, high-resolution, in situ probing of the medium is required to supplement radar observations.

In this paper I consider the structure of the medium implicit in diverse models for the echoes observed by MST radars. By identifying the implicit structure and comparing it with what is known about the structure of the real atmosphere and what has been learned from radar observations it is possible to judge the reality of some of the proposed mechanisms.

## AN OVERVIEW OF ECHOING MECHANISMS

A diversity of scattering and reflection mechanisms appears to be responsible for the echoes observed by radars operating in the lower VHF. The attempt to understand these mechanisms as they pertain to the MST radar has motiviated a reexamination of the broader literature on radio propagation. Indeed, some of the long standing issues in radio propagation are brought into sharp focus in the attempt to understand the nature of the echoes observed at lower VHF. In the following paragraphs I briefly describe several of the mechanisms:

(a) Isotropic Turbulent Scattering

Turbulent scattering was proposed by BOOKER and GORDON (1950) to explain the over-the-horizon propagation of UHF radio signals in the lower atmosphere. It has also been widely accepted as the mechanism responsible for most of the clear air echoes observed at UHF (HARDY and KATZ, 1969) and the oblique echoes observed at VHF. The mechanism requires active turbulence and gradients of refractive index to produce refractivity turbulence at the scale to which the radar is sensitive (OTTERSTEN, 1969).

(b) Anisotropic Turbulent Scatter

While active turbulence is supposed to be isotropic in the inertial range, at larger scales active turbulence must become anisotropic. For refractivity turbulence all that matters is that the correlation scales which characterize the turbulence be different. For a stable atmosphere this usually means that the correlation distance is much less in the vertical than in the horizontal. The anisotropy in the turbulence field implies an angular dependence in the echo magnitude which resembles the observed variation (GAGE and BALSLEY, 1980; DOVIAK and ZRNIC', 1983).

(c) Fresnel Reflection

Occasions arise, especially in the stable atmosphere, when coherent structure is evident. This coherent structure takes the form of stable laminae which possess coherency over horizontal distances comparable to a Fresnel zone. Reflections from sharp gradients of index of refraction have long been thought to play a role in tropospheric radio propagation (DU CASTEL, 1966). Models of Fresnel reflection are deterministic and usually treat single layers of specific shape. The process of reflection from these layers is often referred to as partial reflection.

(d) Diffuse Reflection

Conceptually, diffuse reflection is pertinent to reflection from a surface which is rough compared to the probing wavelength. The mechanism is discussed by DU CASTEL (1966) as an important component of over-the-horizon tropospheric radio propagation and by ROTTGER (1980) as an important mechanism for lower VHF radar echoes.

(e) Fresnel Scatter

The concept of Fresnel scatter was introduced to account for the volume-filling aspect of the specular echoes observed by VHF radar. As originally proposed, the Fresnel scatter model envisioned a coherent structure along the beam (as well as across the beam) to account for the pulse-width square dependence apparent in early observations. Recent observations, however, more typically show a pulse-width dependence confirming the volume-filling feature but not the coherency assumed along the beam. Fresnel scatter has many of the features of Fresnel reflection and can be thought to be comprised of the incoherent sum of partial reflections from many thin layers. It also has much in common with anisotropic turbulence.

Several of the mechanisms described above are illustrated in Figure 1. Each panel contains a schematic representation of the structure in the profile of radio refractive index along the radar beam. Two profiles are shown to illustrate the extent of coherency across the beam. The left-most panel illustrates a turbulent medium with much irregularity structure but no coherency across the beam. The right-most panel illustrates a few discrete thin layers which extend across the beam as required for Fresnel reflection. The middle

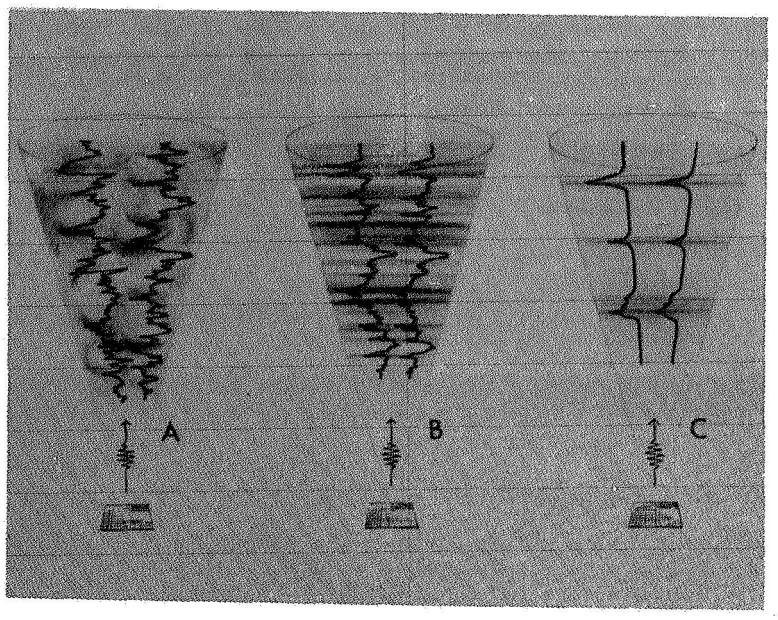


Figure 1. Artist's conception of atmospheric refractivity structure pertinent to i) isotropic turbulence scatter, ii) Fresnel scatter, iii) Fresnel reflection (after GAGE and BALSLEY, 1981).

panel shows a volume-filling irregularity structure which possesses coherency across the beam. This structure is pertinent to Fresnel scatter.

## THE MORPHOLOGY OF TURBULENCE IN THE STABLY STRATIFIED ATMOSPHERE

Turbulence has long been recognized as one of the most important mechanisms for the production of the refractivity structure responsible for over-the-horizon tropospheric radio propagation. In addition, it has been shown to provide a reasonable model for many of the clear air echoes observed by radar (HARDY et al., 1966; KROPFLI et al., 1968; VANZANDT et al., 1978).

The nature of turbulence in the free atmosphere has only recently come into focus. Numerous investigations using aircraft, balloons, and radar to probe the atmosphere have shown the relevance of Kelvin-Helmholtz instability for the production of clear air turbulence. Laboratory experiments (see, e.g., THORPE, 1973) have clearly shown the evolution of shear flow instability in a stably stratified fluid. Theoretical investigations have helped provide a common framework for the interpretation of diverse observational and experimental studies (DRAZIN and REID, 1981). In addition, the role of waves in triggering turbulence has been clarified (BRETHERTON, 1969) and the analogous problem of intermittent turbulence in the ocean has been investigated by WOODS (see, for example, WOODS and WILEY, 1972).

Perhaps the most pronounced feature of radar observations of turbulence in the free atmosphere is the layered structure evident in time-height cross sections of echo magnitude. Figure 2 contains an example of such a cross section as observed by the Arecibo radar (SATO and WOODMAN, 1982). It shows a

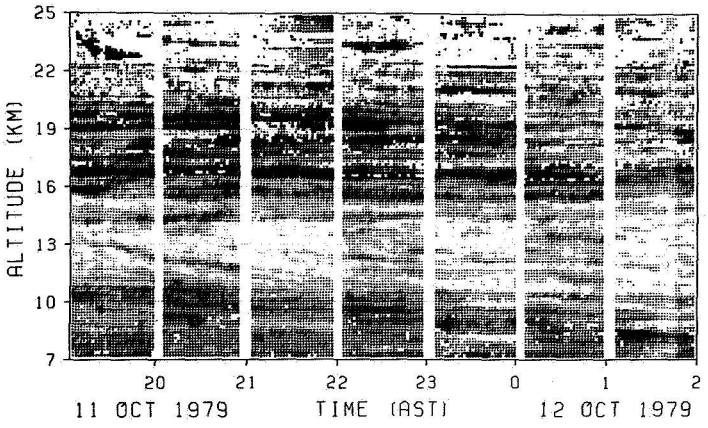


Figure 2. 8-level height-time shade plot for the echo power received by the Arecibo radar. The dynamic range is 32 dB (after SATO and WOODMAN, 1982).

persistent layering on a scale larger than the 150 m range resolution used by the radar. The strong echoes are confined to thin regions in which the Richardson number is small. For example, Figure 3 shows a clear association of strong echoes with strong shear. The fact that the echoes have a wide spectral width confirms that they are due to active turbulence.

CRANE (1980) has summarized the conditions under which turbulence should be observable by a radar of given wavelength. Briefly, the half-wavelength scale to which the radar is sensitive must be larger than the inner scale of turbulence and smaller than the outer scale of turbulence. The inner scale is proportional to $(\nu^3/\bar{\epsilon})^{1/4}$, where $\nu$ is kinematic viscosity and $\bar{\epsilon}$ is the eddy dissipation rate. Since kinematic viscosity increases (as density decreases)

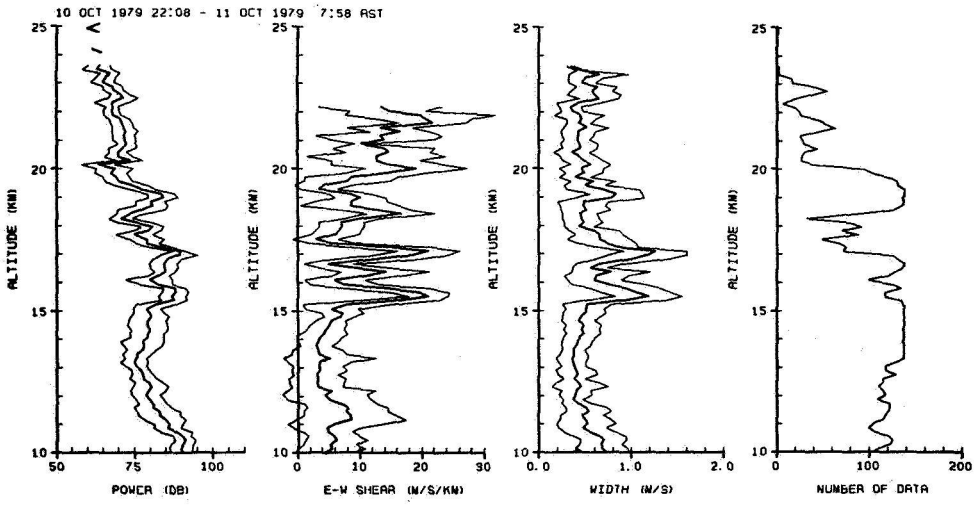


Figure 3. 10-hour mean echo power, E-W component of the wind shear, and the spectral width versus height. The number of good data points used in the average are plotted on the right. Two thin lines around the thick line in each profile indicate the standard deviation from the mean (after SATO and WOODMAN, 1982).

with altitude, the inner scale increases with altitude. At tropopause heights it is close to 1 cm. The outer scale of turbulence is proportional to the buoyancy scale $\bar{\varepsilon}^{1/2}\,\bar{N}^{-3/2}$ where $\bar{N}$ is the Brunt-Vaisala frequency $\bar{N} \equiv (g/\theta\,\partial\theta/\partial z)^{1/2}$. Values of the outer-scale are typically a few tens of meters in the free atmosphere. However, the outer scale can be much less in stable regions where $\bar{N}$ is large and $\bar{\varepsilon}$ is small. To take an extreme example, if $\Delta\theta/\Delta z$ is .1° C/m and $\bar{\varepsilon}$ is $10^{-6}$ $m^2s^{-3}$ the outer scale would be about 10 cm. Regions of active turbulence, on the contrary, are usually associated with small $\bar{N}$ (see, for example, BARAT, 1982) and enhanced $\bar{\varepsilon}$ so that the outer scale will be increased. The outer scale of turbulence has been measured to be a few tens of meters (BARAT, 1982) which is often a small fraction of the turbulent layer thickness.

The creation of layered structure by local regions of Kelvin-Helmholtz instability was discussed by ROTTGER (1981). As illustrated in Figure 4, turbulence acts to concentrate gradients at the boundaries of turbulent layers. Many localized instabilities acting in concert could produce an evolving fine structure of thin regions of turbulence bounded by thin stable layers. It is important to realize, however, that this is not the only mechanism which can produce layered structure. A coherent layered structure can also be produced by large-scale buoyancy-inertia waves. For example, the layered structure evident in Figure 2 is probably associated with such waves.

## THE MORPHOLOGY OF STABLE LAYERS IN THE FREE ATMOSPHERE AND THE SPECULAR ECHOES OBSERVED BY MST/ST RADARS

While the echoes observed by MST/ST radars directed more than 10 degrees or so off vertical are associated with active turbulence, the echoes observed at vertical incidence are associated with stable regions of the atmosphere as shown in Figure 5 (GAGE and GREEN, 1978). Another example of the clear correspondence between echo magnitude at lower VHF and static stability is contained in Figure 6 (LARSEN and ROTTGER, 1982, 1983) which shows an evolutionary pattern of strong stratospheric echoes corresponding to a changing stability structure during the passage of a frontal zone.

The nature of the mechanism responsible for the specular echoes observed at lower VHF has been the subject of continuing controversy. The models which have been proposed to explain these echoes include Fresnel reflection (GAGE and

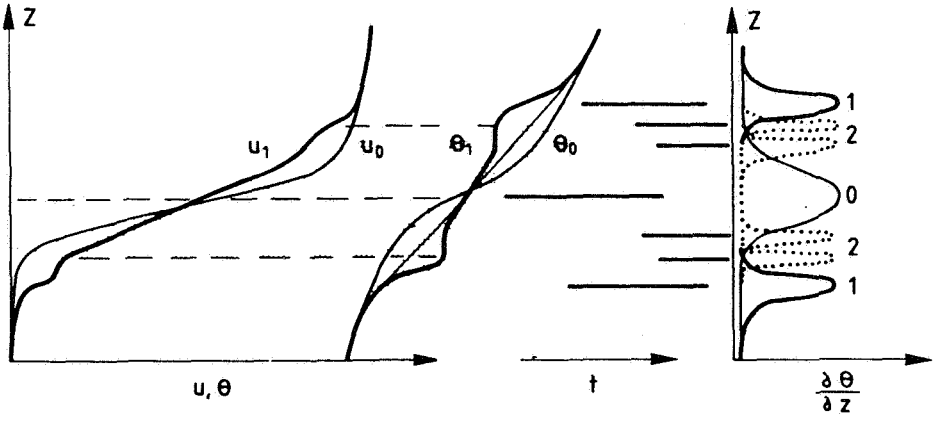


Figure 4. Formation of ensembles of stable layers (sheets) by Kelvin-Helmholtz instability (adapted from PELTIER et al., 1978, by ROTTGER, 1981).

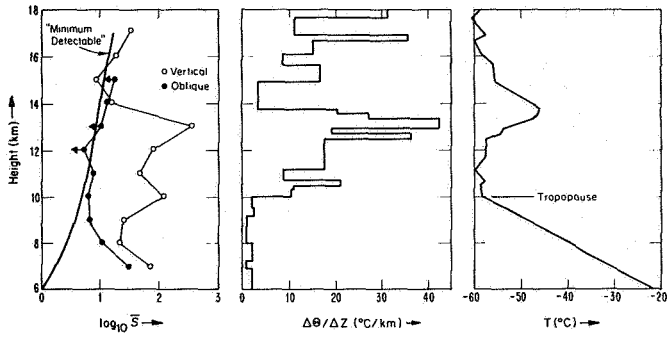


Figure 5. Comparison of the normalized power profiles observed at vertical and oblique incidence by the Sunset radar with stability (after GAGE and GREEN, 1978).

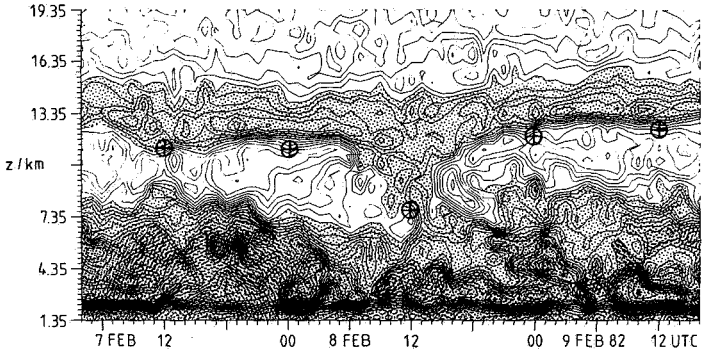


Figure 6a

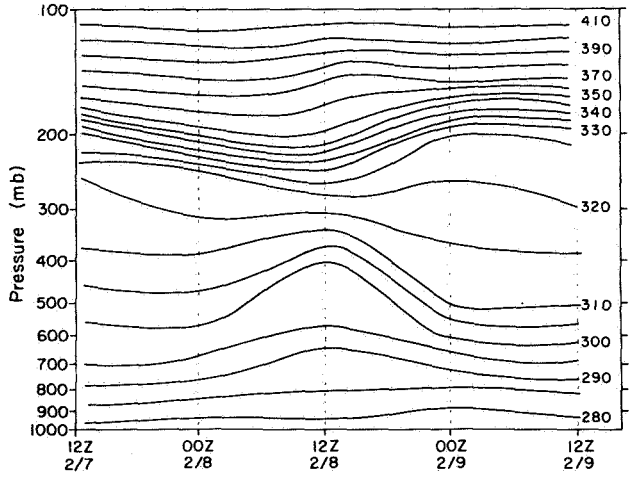


Figure 6b

Figure 6. a. Reflectivity contours observed at vertical incidence for a warm frontal passage by the SOUSY radar during February 1982.
b. Pressure-time cross section of the potential temperature measured by the Hanover radiosonde during the period corresponding to 6a (after LARSEN and ROTTGER, 1982).

GREEN, 1978; ROTTGER and LIU, 1978), diffuse reflection (ROTTGER, 1980), Fresnel scatter (GAGE et al., 1981) and anisotropic turbulent scattering (DOVIAK and ZRNIC', 1983). As discussed earlier, the first two mechanisms involve partial reflections from smooth or rough surfaces while the last two mechanisms involve volume scattering processes.

Fresnel reflection requires a very stable layer which is thin compared to the probing radar wavelength. For example, GAGE and GREEN (1978) estimate that a strong echo would be received from a stable layer of 1-m thickness and .1°C temperature difference located at 12 km. The occurrence of meter-scale microstructure has been reported (METCALF, 1975; METCALF and ATLAS, 1973). Such thin stable layers could be produced by the action of turbulent mixing. Under these circumstances one might anticipate that the echo magnitude would be proportional to the mean stability of the environment in which the thin turbulent layers are imbedded. Their magnitude should also depend on turbulent layer thickness since (everything else being equal) the largest layers will possess the largest temperature differences across them. Since in the most stable regions turbulence must be confined to very thin regions, the two effects mentioned above might be expected to counteract each other.

There is an increasing body of evidence that the backscattered power received at vertical incidence at lower VHF increases with the pulse width of the probing pulse (GREEN and GAGE, 1980; HOCKING and ROTTGER, 1983; GREEN, 1983). This implies a medium filled with refractivity structure. Consequently, any partial-reflection mechanism must be generalized to include the reflection from an aggregate collection of thin layers. Barring some mechanism to space the layers along the beam, random spacing can be assumed and the $\Delta r$-dependence recovered (HOCKING and ROTTGER, 1983).

If the assumption of a coherent structure along the beam is removed from the concept of Fresnel scattering, Fresnel scattering becomes very similar to a volume Fresnel reflection or even anisotropic turbulent scattering. The main difference between volume Fresnel reflection and anisotropic turbulence scattering is that the former consists of gradients concentrated in layers which are thin compared to the radar wavelength while the latter only requires a significant amount of refractivity structure at half the radar wavelength. At this point it should be recognized that the anisotropic turbulence model does not necessarily involve active turbulence. All it requires is an anisotropic distribution of refractivity structure. The issue of when Fresnel scattering is an appropriate description of the scattering process and when anisotropic turbulent scattering is an appropriate description has been addressed recently by DOVIAK and ZRNIC' (1983). These authors show that Fresnel effects do not become important until the transverse correlation length $\rho_t$ of the media exceeds .29 D where D is the diameter of the radar antenna. However, turbulent scattering which fills the antenna beam leads to an $R^{-2}$ range dependence while Fresnel scattering with $\rho_t$ less than a Fresnel zone radius leads to an $R^{-4}$ dependence consistent with the observed range dependence at Poker Flat (BALSLEY and GAGE, 1981), illustrated in Figure 7.

In situ observations of stable atmospheric structure are very sparse. Some insight into the structure of stable layers can be gained from an inspection of routine radiosonde temperature profiles. In such profiles temperatures are specified at mandatory (pre-selected pressures) levels and significant levels. Significant levels are chosen to optimize the agreement between the radiosonde-derived temperature profile and the actual temperature profile. Clearly, the more structure in the actual temperature profile the more significant levels that are required to resolve that structure. Figure 8 contains a histogram of the number of stable layers found in the Fairbanks, Alaska radiosonde soundings between 12 and 14 km during March 1981. Each layer counted was bounded by significant levels above and below. The number of layers is shown as a function

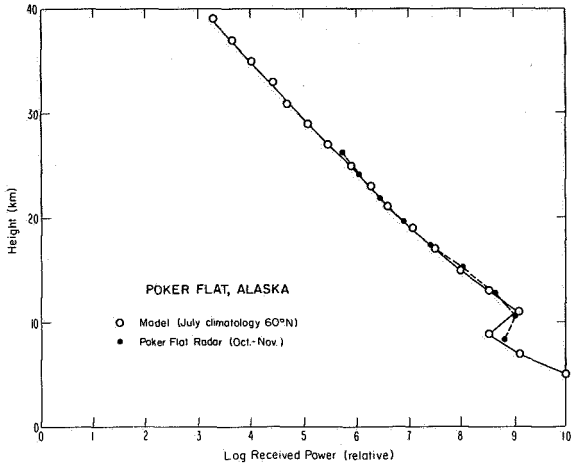


Figure 7. Relative comparison between theoretical and observed backscatter profiles at vertical incidence for the Poker Flat MST radar in Alaska during October-November 1979 (after BALSLEY and GAGE, 1981).

of layer thickness. Note that most layers fall in the range 100 to 500 m. Few layers thicker than 500 m are counted since almost always thick layers are bounded by at least one mandatory level. The distribution of potential temperature gradient with layer thickness is shown in Figure 9. Note the inverse relationship between stability and layer thickness. The most stable layers are very thin. Indeed, the distribution of stability vs. layer thickness can be approximated by $\partial\theta/\partial z \propto 474\Delta z^{-1/2}$.

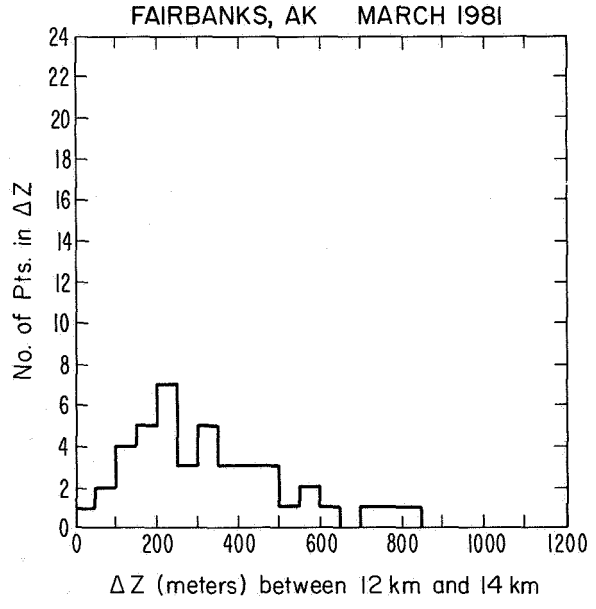


Figure 8. Histograms of occurrence of stable layers between 12 and 14 km versus thickness resolved by the Fairbanks radiosonde for March 1981.

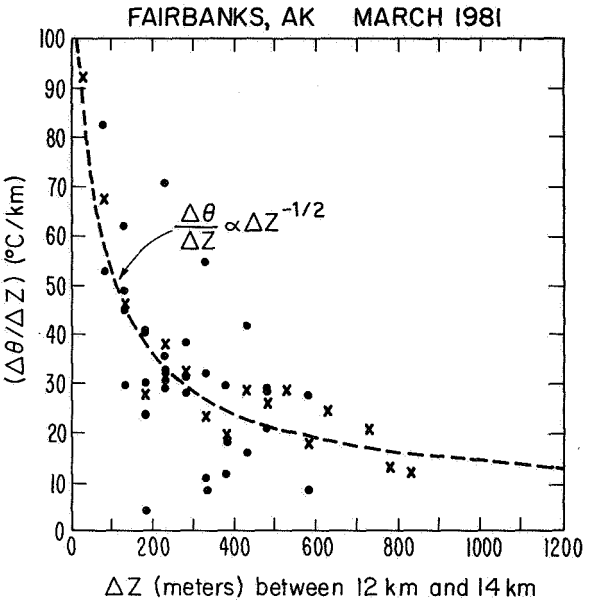


Figure 9. Distribtuion of stability versus layer thicknesses for the stable layers contained in Figure 8. Each dot represents a layer. x's represent the average stability for each bin of layer thicknesses.

The observed dependence of potential temperature gradient upon layer thickness approximates what might be expected for buoyancy waves (VANZANDT, 1982; GARRETT and MUNK, 1979). Indeed, VANZANDT and VINCENT (1983) have argued that buoyancy waves may be used to explain the specular echoes observed by lower VHF radars. Extrapolating the result of Figure 9 to $\Delta z = 3$ m implies a temperature gradient of $\sim .3°/m$ which should be sufficient to cause a strong specular echo. Note that such thin stable layers can be anticipated only within very stable regions (of greater vertical extent) for only then will the outer scale of turbulence be less than a few meters. If the refractivity structure causing the echoes is due to buoyancy waves, the proportionality of echo magnitude to $M^2$ can be explained theoretically (VanZandt, private communication).

## CONCLUDING REMARKS

In this paper I have examined the mechanisms which have been proposed to explain the echoes observed from the clear atmosphere by MST/ST radars. Each has been considered in relation to the atmospheric refractivity structure implicit for its realization. While the echoes observed at oblique incidence are reasonably explained by turbulent scattering, the specular echoes can be explained by several alternative models of atmospheric refractivity structure. A refractivity structure which possesses some transverse coherency but a volume filling random vertical structure seems most likely. Whether the process is better conceptualized as a composite many layered partial reflection process or as a Bragg scattering, anisotropic turbulence process is not yet clear. To resolve this issue will probably require in situ probing of stable layer structure.

REFERENCES

Balsley, B. B. and K. S. Gage (1981), On the vertical incidence VHF backscattered power profile from the stratosphere, Geophys. Res. Lett., 8, 1173-1175.

Barat, J. (1982), Some characteristics of clear-air turbulence in the middle stratosphere, J. Atmos. Sci., 39, 2553-2564.

Booker, H. G. and W. E. Gordon (1950), Theory of radio scattering in the troposphere, Proc. IEEE, 38, 401-412.

Bretherton, F. P. (1969), Waves and turbulence in stably stratified fluids, Radio Sci., 4, 1279-1287.

Crane, R. K. (1980), A review of radar observations of turbulence in the lower stratosphere, Radio Sci., 15, 177-194.

Doviak, R. J. and D. S. Zrnic (1983), Fresnel zone considerations for reflection and scatter from refractive index irregularities, (manuscript in preparation).

Drazin, P. G. and W. H. Reid (1981), Hydrodynamic Stability, Cambridge University Press, Cambridge, England, 525 pp.

du Castel, F. (1966), Tropospheric Radio Wave Propagation Beyond the Horizon, English ed., Pergamon, Oxford, 236 pp.

Gage, K. S. and B. B. Balsley (1980), On the scattering and reflection mechanisms contributing to clear air radar echoes from the troposphere, stratosphere, and mesosphere, Radio Sci., 15, 243-257.

Gage, K. S. and B. B. Balsley (1981), Recent advances in Doppler radar probing of the clear atmosphere, Atmos. Technology, 13, 321.

Gage, K. S., B. B. Balsley and J. L. Green (1981), Fresnel scattering model for the specular echoes observed by VHF radar, Radio Sci., 16, 1447-1453.

Gage, K. S. and J. L. Green (1978), Evidence for specular reflection from monostatic VHF radar observations of the stratosphere, Radio Sci., 13, 991-1001.

Garrett, C. and W. Munk (1979), Internal waves in the ocean, Ann. Rev. Fluid Mech., 11, 339-361.

Green, J. L. (1983), On the range gate dependence of specular echoes, paper 2.1-D, this volume.

Green, J. L. and K. S. Gage (1980), Observations of stable layers in the troposphere and stratosphere using VHF radar, Radio Sci., 15, 395-405.

Hardy, K. R., D. Atlas and K. M. Glover (1966), Multiwavelength backscatter from the clear atmosphere, J. Geophys. Res., 71, 1537-1552.

Hardy, K. R. and I. Katz (1969), Probing the clear atmosphere with high power, high resolution radars, Proc. IEEE, 57, 468-480.

Hocking, W. K. and J. Rottger (1983), Pulse-length dependence of radar signal strengths for Fresnel backscatter, submitted to Radio Sci.

Kropfli, R. A., I. Katz, T. G. Konrad and E. B. Dobson (1968), Simultaneous radar reflectivity measurements and refractive index spectra in the clear atmosphere, Radio Sci., 3, 991-994.

Larsen, M. F. and J. Rottger (1982), VHF and UHF Doppler radars as tools for synoptic research, Bull. Amer. Meteorol. Soc., 63, 996-1007.

Larsen, M. F. and J. Rottger (1983), Comparison of tropopause height and frontal boundary locations based on radar and radiosonde data, Geophys. Res. Lett., 10, 325-328.

Metcalf, J. I. (1975), Microstructure of radio echo layers in the clear atmosphere, J. Atmos. Sci., 32, 362-370.

Metcalf, J. I. and D. Atlas (1973), Microscale ordered motions and atmospheric structure associated with thin echo layers in stably stratified zones, Boundary-Layer Meteor., 4, 7-35.

Ottersten, H. (1969), Atmospheric structure and radar backscattering in clear air, Radio Sci., 4, 1179-1193.

Peltier, W. R., J. Halle and T. L. Clark (1978), The evolution of finite amplitude Kelvin-Helmholtz billows, Geophys. Astrophys. Fluid Dynamics, 10, 53-87.

Rottger, J. (1980), Reflection and scattering of VHF radar signals from atmospheric refractivity structures, Radio Sci., 15, 259-276.

Rottger, J. (1981), The dynamics of stratospheric and mesospheric fine structure investigated with an MST VHF radar, MAP Handbook, 4, 341-350.

Rottger, J. and C. H. Liu (1978), Partial reflection and scattering of VHF radar signals from the clear atmosphere, Geophys. Res. Lett., 5, 357-360.

Sato, T. and R. F. Woodman (1982), Fine altitude resolution observations of stratospheric turbulent layers by the Arecibo 430 MHz radar, J. Atmos. Sci., 39, 2546-2552.

Thorpe, S. A. (1973), Experiments on instability and turbulence in a stratified shear flow, J. Fluid Mech., 61, 731-751.

VanZandt, T. E. (1982), A universal spectrum of buoyancy waves in the atmosphere, Geophys. Res. Lett., 9, 575-578.

VanZandt, T. E., J. L. Green, K. S. Gage and W. L. Clark (1978), Vertical profiles of refractivity turbulence structure constant: Comparison of observations by the Sunset radar with a new theoretical model, Radio Sci., 13, 819-829.

VanZandt, T. E. and R. A. Vincent (1983), Is VHF Fresnel reflectivity due to low frequency buoyancy waves? Workshop on Technical Aspects of MST Radar, May 23-27, Urbana, IL, this volume, pp. 78-80.

Woods, J. D. and R. L. Wiley (1972), Billow turbulence and ocean microstructure, Deep Sea Research, 13, 87-121.

# 2.1B MORPHOLOGY OF THE SCATTERING TARGET - FRESNEL AND TURBULENT MECHANISMS

J. Rottger

EISCAT - Scientific Association
S-981 27 Kiruna, Sweden

Further studies of VHF radar signals from the troposphere and stratosphere revealed not only scattering from isotropic turbulence at scales of half the radar wavelength (typically about 3 m for VHF radars) but also partial or Fresnel reflection or scattering from horizontally stratified temperature discontinuities (e.g., ROTTGER, 1980). Proof for this observation was given by the large spatial and temporal coherence of radar signals. It is recognized that thin structures, particularly in the stratosphere, may be persistent over some ten seconds, which is longer than the coherence time of 3-m scale turbulence in the stratosphere (e.g., WOODMAN and GUILLEN, 1974). The vertical thickness of the structures was estimated to be much thinner than 150 m (ROTTGER and SCHMIDT, 1979). Observations over a longer time period indicate that these fine-scale structures or sheets are clumped together forming patches or ensembles of mostly downward sloping structures.

If one assumes that these fine structures are due to temperature steps or gradients rather than to very thin turbulent layers some evident similarities between the temperature fine structure of the stratosphere and the oceanic thermocline are found (e.g., WOODS, 1968). This is obvious since both the stratosphere and the thermocline are very stable regions due to the increase of potential temperature with height. ROTTGER (1980) proposed to use the same nomenclature as used in oceanography to describe the fine structure detected with vertically beaming VHF radars: the thin, persistent stratifications or laminae are regarded as "sheets" which form thicker "ensembles". Fine-scale measurements of the oceanic temperature profile showed that the sheets are thin interfacial regions separating "turbulent layers". It can be shown that radar echoes are also received from the regions between individual sheets, which are turbulent layers according to observations of the oceanic thermocline. These radar echoes are due to scattering from small-scale turbulence (3-m scale) and are normally much weaker than the echoes from the sheets. Thus, ensembles of sheets at the boundaries of turbulent layers are the typical "turbulence structures" detected by VHF radars.

It shall be stressed here that this model of atmospheric turbulence was already proposed by BOLGIANO (1968). He pointed out that vertical mixing in a turbulent layer tends to equalize the mean temperature profile so that temperature gradients are formed at its boundaries. We regard the temperature gradients as "sheets" being responsible for the enhanced and persistent echo power observed with the VHF radars. Recent theoretical investigations of PELTIER et al. (1978) yield a more detailed description of the temperature profile in a turbulent layer. There is accepted evidence that turbulence in the statically stable atmosphere is caused by Kelvin-Helmholtz instability. The essential condition for the onset of turbulence is that the Richardson number falls below its critical value, which can be due to an increase of wind shear. In Figure 1 the results of PELTIER et al. (1978) are sketched to show how temperature gradients, viz. ensembles of sheets, are formed. The original height profiles of wind velocity u and potential temperature $\theta$ are given by the curve $u_o$ and $\theta_o$. The temperature profile indicates high static stability because the gradient of potential temperature $\partial\theta/\partial z$ is positive. The velocity profile is characterized by a shear which gives rise to Kelvin-Helmholtz

instability and yields a turbulent layer. After a typical growth time of the layer (up to some minutes), the velocity and temperature profiles are given by $u_1$ and $\theta_1$. Consequently, gradients of $\theta$ occur near the top and the bottom of the turbulent layer. These gradients are sheets, according to the above-mentioned definition, which partially reflect VHF radar signals. The splitting of the shear layer ($0 \rightarrow 1 \rightarrow 2 \rightarrow \ldots$) may progress and cause the formation of multiple turbulent layers, i.e., ensembles of sheets at their boundaries. The corresponding time development of the sheets is sketched in the center part of Figure 1 and may be compared with well-known VHF radar observations.

The birth and decay of the sheets depend on the background conditions of static and dynamic stability. Only crude estimates of the lifetime of sheets can be obtained from current radar observations since the turbulence structures are advected with the wind through the radar beam. Typical times of VHF-radar observed sheets range from several seconds to minutes.

We conclude from these definitions and arguments that vertically beaming VHF radars only indirectly detect turbulent layers in the stratosphere, because they are more sensitive to the temperature gradients at the boundaries of the turbulent layers. Consequently some care must be taken in estimating turbulent transport coefficients using the characteristics of VHF radar signals such as echo power and correlation time. Further considerations on these limitations were outlined by ROTTGER (1980). It is interesting to note that recently BARAT (1982) reported about measurements of stratospheric turbulence and temperature profiles which were consistent with the model of Figure 1.

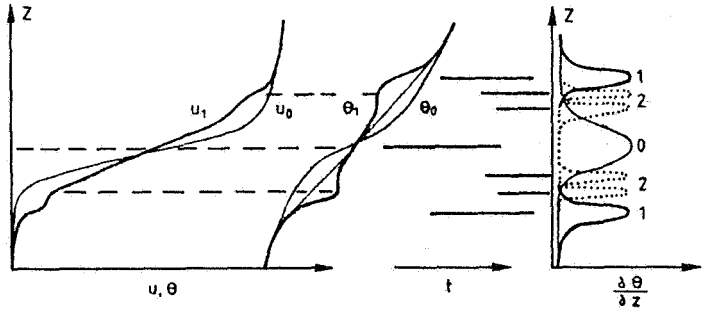


Figure 1. Formation of ensembles of sheets by Kelvin-Helmholtz instability (u and $\theta$ profiles after PELTIER et al., 1978).

REFERENCES

Barat, J. (1982), J. Atmos. Sci., 39, 2553.

Bolgiano, R., Jr. (1968), The general theory of turbulence. Turbulence in the atmosphere, in: Winds and Turbulence in Stratosphere, Mesosphere and Ionosphere (ed. K. Rawer), North-Holland, Amsterdam, 371-400.

Peltier, W. R., J. Halle and T. L. Clark (1978), Geophys. Astrophys. Fluid Dynamics, 10, 53.

Rottger, J. (1980), Radio Sci., 15, 259.

Rottger, J. and G. Schmidt (1979), IEEE Trans. Geosci. Electron. GE-17, 182.

Woodman, R. F. and A. Guillen (1974), J. Atmos. Sci., 31, 493.

Woods, J. D. (1968), Meteorol. Magazine, 97, 65.

Larsen, M. F. and J. Rottger (1983), Comparison of tropopause height and frontal boundary locations based on radar and radiosonde data, Geophys. Res. Lett., 10, 325-328.

Metcalf, J. I. (1975), Microstructure of radio echo layers in the clear atmosphere, J. Atmos. Sci., 32, 362-370.

Metcalf, J. I. and D. Atlas (1973), Microscale ordered motions and atmospheric structure associated with thin echo layers in stably stratified zones, Boundary-Layer Meteor., 4, 7-35.

Ottersten, H. (1969), Atmospheric structure and radar backscattering in clear air, Radio Sci., 4, 1179-1193.

Peltier, W. R., J. Halle and T. L. Clark (1978), The evolution of finite amplitude Kelvin-Helmholtz billows, Geophys. Astrophys. Fluid Dynamics, 10, 53-87.

Rottger, J. (1980), Reflection and scattering of VHF radar signals from atmospheric refractivity structures, Radio Sci., 15, 259-276.

Rottger, J. (1981), The dynamics of stratospheric and mesospheric fine structure investigated with an MST VHF radar, MAP Handbook, 4, 341-350.

Rottger, J. and C. H. Liu (1978), Partial reflection and scattering of VHF radar signals from the clear atmosphere, Geophys. Res. Lett., 5, 357-360.

Sato, T. and R. F. Woodman (1982), Fine altitude resolution observations of stratospheric turbulent layers by the Arecibo 430 MHz radar, J. Atmos. Sci., 39, 2546-2552.

Thorpe, S. A. (1973), Experiments on instability and turbulence in a stratified shear flow, J. Fluid Mech., 61, 731-751.

VanZandt, T. E. (1982), A universal spectrum of buoyancy waves in the atmosphere, Geophys. Res. Lett., 9, 575-578.

VanZandt, T. E., J. L. Green, K. S. Gage and W. L. Clark (1978), Vertical profiles or refractivity turbulence structure constant: Comparison of observations by the Sunset radar with a new theoretical model, Radio Sci., 13, 819-829.

VanZandt, T. E. and R. A. Vincent (1983), Is VHF Fresnel reflectivity due to low frequency buoyancy waves? Paper 2.1 E, this volume.

Woods, J. D. and R. L. Wiley (1972), Billow turbulence and ocean microstructure, Deep Sea Research, 13, 87-121.

# 2.1C COMMENTS ON "FRESNEL SCATTERING"

D. T. Farley

School of Electrical Engineering
Cornell University
Ithaca, NY 14853

In a recent paper GAGE et al. (1981) discuss an echoing mechanism that they call Fresnel scattering. The irregularities responsible for VHF echoes from the troposphere and stratosphere are often highly anisotropic, with the most intense echoes obtained when the radar is pointed vertically. A theory for these echoes is proposed by Gage et al., and this theory predicts that the signal from these 'Fresnel scattering' layers will be proportional to the square of the transmitted pulse length, as long as this length is less than the layer thickness. This is in marked contrast to standard theories of scattering from random media (e.g., BOOKER and GORDON, 1950; BOOKER, 1956), which give a linear relationship between the pulse length and the scattered signal power. (Note that we are referring here to signal strength, not signal-to-noise ratio.) The purpose of this note is to point out that there is a fallacy in the arguments of Gage et al.; the linear relationship is correct. Indeed, many of the usual derivations of scattering theory (e.g., BOOKER, 1956) allow for media fluctuations with arbitrarily anisotropic spatial autocorrelation functions (ACF). Whether the experimental data do or do not sometimes imply a nonlinear relationship is a separate question that will not be dealt with here; we will discuss only the theoretical arguments.

Let us begin with equation (6) of Gage et al., i.e.

$$\rho = \frac{1}{2} \int_{-\Delta r/2}^{\Delta r/2} \frac{dn}{dz} e^{-2ikz} dz \qquad (1)$$

where $\rho$ is the complex voltage reflection coefficient, n is the refractive index averaged over a Fresnel zone in the x-y direction, k is the usual wave number $2\pi/\lambda$, and $\Delta r$ is the transmitted pulse length. The derivation of Gage et al. then assumes a deterministic form for n(z), i.e.,

$$n(z) = (\delta n)_{\lambda/2} \sin(2kz + \phi_{\lambda/2}) \qquad (2)$$

in a layer of thickness L. It is then simple to show that the power reflection coefficient $|\rho|^2$ is proportional to $(\Delta r)^2$ as long as $\Delta r < L$, or $L^2$ if the inequality is reversed. It is almost obvious by inspection of (1) and (2) that this will be the case.

The flaw in the argument is (2), which is not a valid assumption for a random medium. The misconception arises from trying to adapt to this problem theoretical ideas developed for the Radar-Acoustic Sounder System (RASS) (e.g., CLIFFORD and WANG, 1977). In the RASS case (2) is legitimate, because n(z) is forced by the transmitted acoustic wave. For a random medium, however, the fluctuations cannot have a finite amplitude in an infinitesimal region of k-space. There is nothing unique, as far as the medium is concerned, about the radar wavelength, and so the total $\langle|\delta n|^2\rangle$ becomes infinite after integration over any finite range of k-space.

The standard way to handle these calculations is briefly as follows. Since $dn/dz \equiv n'(z)$ is a random variable, we seek the expected value (ensemble average) of $|\rho|^2$, i.e., for a thick layer ($L > \Delta r$)

$$\langle|\rho|^2\rangle = \frac{1}{4}\left\langle \iint_{-\Delta r/2}^{\Delta r/2} dz_1 dz_2 n'(z_1)n'(z_2)\exp[-2ik(z_1 - z_2)]\right\rangle$$

$$= \frac{1}{4}\iint_{-\Delta r/2}^{\Delta r/2} dz_1 dz \langle n'(z_1)n'(z_2)\rangle \exp[-2ik(z_1 - z_2)] \qquad (3)$$

$$\simeq \frac{1}{4}\iint_{-\Delta r/2}^{\Delta r/2} dz_1 \int_{-\infty}^{\infty} dz_3 \langle n'(z_1)n'(z_1 - z_3)\rangle e^{-2ikz_3}$$

where $z_3 = z_1 - z_2$, and the term in brackets is a spatial ACF which is assumed to become small for $|z_3| << \Delta r$ (and therefore we can extend the $z_3$ integration to infinity). The integration in $z_3$ is just the Fourier transform of the spatial ACF of $n'$, i.e., it is the power spectrum of the fluctuations, which we can call $|F(\lambda)|^2$, and we note especially that the $z_3$ integration is clearly independent of $\Delta r$. Hence it is obvious from (3) that $\langle|\rho|^2\rangle$ is proportional to $\Delta r$, not $(\Delta r)^2$.

As one further argument, consider a temporal analogy to this essentially one-dimensional spatial problem. Oblique echoes from a horizontally drifting medium (non-zero wind) are often quite coherent in time (narrow frequency band), certainly more so that we would expect the distribution in altitude of turbulent layers to be. But the (unnormalized) power at the peak frequency changes by a factor of two, not four, when we double or halve the integration time. Compare this with the Fourier analysis of a finite length sine wave. In the latter case the voltage spectrum at the peak will increase linearly with T (and the power at the peak will increase at $T^2$). This is the RASS case. But note also that the peak will become narrower, so that the area under the full power spectrum will increase only linearly.

REFERENCES

Booker, H. G. (1956), A theory of scattering by nonisotropic irregularities with application to radar reflections from the aurora, J. Atmos. Terr. Phys., 8, 204-221.

Booker, H. G. and W. E. Gordon (1950), A theory of radio scattering in the troposphere, Proc. I.R.E., 38, 401-412.

Clifford, S. F. and T.-I. Wang (1977), The range limitation on radar-acoustic sounding systems (RASS) due to atmospheric refractive turbulence, IEEE Trans. Antennas Propag., AP-25, 319-326.

Gage, K. S., B. B. Balsley and J. L. Green (1981), Fresnel scattering model for the specular echoes observed by VHF radar, Radio Sci., 16, 1447-1453.

# 2.1D RANGE GATE DEPENDENCE OF SPECULAR ECHOES

J. L. Green

Aeronomy Laboratory, NOAA
Boulder, CO 80303

Some controversy has surrounded the interpretation of the enhancement of VHF radar echoes at vertical incidence (also known as partial reflections, specular reflections and Fresnel scattering) since they were reported by the Sunset (GAGE and GREEN, 1978) and the SOUSY (ROTTGER and LIU, 1978) radars. There is little doubt as to the observational fact of this enhancement since it has been observed by experimenters using at least eleven MST or ST radars. In addition to the Sunset and SOUSY radars, this result has been obtained in the lower atmosphere at the Platteville (ECKLUND et al., 1979; WESTWATER et al., 1983), Poker Flat (ECKLUND et al., 1980), Jicamarca (FUKAO et al., 1979), Arecibo (ROTTGER et al., 1981) radars as well as the three radars of the ALPEX experiment (BALSLEY et al., 1983). In the upper atmosphere, specular or partial reflections have been observed by VINCENT and BELROSE, 1978 and HOCKING, 1979. These vertical enhancements have been associated with increases in the static stability of the atmosphere (GREEN and GAGE, 1980), with a temperature gradient in the stratosphere (GAGE and GREEN, 1982a), have been used to monitor the height of the tropopause (GAGE and GREEN, 1982b), and have been associated with the passage of fronts (ROTTGER and LARSEN, 1983). This list is but a small part of the publications on this subject.

Since the publication of Fresnel Scattering Model for the Specular Echoes Observed by VHF Radar (GAGE et al., 1981) there has been concern over the prediction of this model that the radar reflectivity should vary as the square of the range gate length, $\Delta R$. A comparison of specular echoes obtained with 300-m and 1-km range gates by the Sunset radar was used to illustrate this assertion.

In another theoretical analysis, HOCKING and ROTTGER (1983) predicted that on average specular reflectivity should be proportional to $\Delta R$, but that it was possible under the right conditions for this ratio to approach $\Delta R^2$.

A special mini-session was held on this subject at the MAP Workshop held at Estes Park, Colorado, May 1983. At that session, I stated that I would soon report on new investigations of the range gate dependence of specular echoes. Several suggestions as to the treatment and interpretation of the data made at that meeting have been incorporated into this report (D. T. Farley, W. K. Hocking, R. L. Woodman and possibly others, private communication by means of unsigned paper table napkins, 1982).

This report of measurements made at the Sunset radar during March and April, 1982 is confined solely to the observed dependence of the radar reflectivity of vertically enhanced echoes. (For further details of the Sunset radar, see Section 5.3 of this volume.)

The Sunset radar was carefully calibrated and characterized for these measurements. The practice of calibrating the received echoes power by comparison with the temperature of the background cosmic noise was abandoned in favor of daily calibrations with a stable noise source. The effective $\Delta R$ and the time response function of each range gate were obtained by direct measurement of the convolution of the transmitted waveform and the range gate filters. The radar reflectivity is presented as the magnitude of the coefficient of reflection, $|\rho|^2$ so that the recorded transmitted power levels could be

incorporated.

It was known from previous experiments that the reflectivity of the vertically enhanced echoes varies with time. Since the radar could only observe with one particular range gate at a time, the range gate lengths were cycled. The data presented here are the median values of the total data set for a particular range resolution and antenna direction observed on a particular day. The observations in most cases were made during a four-hour period centered on the 12 UT NWS rawinsonde launch. Four sizes of $\Delta R$ were used, 150, 300, 1000, and 2400 m. Since the object here is the determination of the exponent of the $\Delta R$ dependence, Figures 1-2 are plotted as altitude vs.

$$\frac{\log (1000\ |\rho|^2)}{\Delta R\ (m)}$$

As suggested at the Estes Park Workshop, the range gate time response was measured. The response of longer range gates were convolved with the $|\rho|^2$ data from shorter range gates to enhance the comparison. This convolution represents an incoherent spatial average (powers summed) while a range gate is a coherent average (voltages summed). In the comparisons shown below, a departure from equality of the responses at different $\Delta R$ sizes is an indication of possible coherence.

Figure 1a is a typical comparison of the 1000 m and 2400 m range gate with a vertical antenna beam. The 1000 m data have been convolved with the 2400 m range gate function to enhance the comparison. In Figure 1b the vertical and the slant (15° from vertical) echoes are compared to show the altitudes with vertical enhancement. Except for perhaps 7 km, Figure 1a shows that indeed the 1000 m and 2400 m echo strengths are related by a $\Delta R$ dependence. This was typical of all the daily comparisons between these two range gates during this observation period.

The results of observations using range gates shorter than 1 km were less consistent. The majority of the comparisons between 300 m and 1 km range gates showed a $\Delta R$ dependence, but about 25-30% showed a $\Delta R^2$ dependence. In a few percent of the observations the 300 m range gate reflectivity was greater than that of the 1 km range gate. This behavior is illustrated in Figure 2a, a comparison of the 300 m and 1000 m range gates with a vertical antenna beam. Again, the data from the shorter range gate have been convolved with the range gate function of the longer. The reflectivities are equal between 6 and 8.5 km altitude, implying a $\Delta R$ dependence. However, between 8.5 and 11 km the reflectivity of the 1 km gate is larger, implying a dependence that approaches a $\Delta R^2$ dependence. Around 12 km the 300 m reflectivities are larger. Between 13 and 15 km a simple $\Delta R$ dependence is again approximately the case. Figure 2c, a comparison of the vertical echoes with the slant echoes, shows a region of strong vertical enhancement between 6 and 14 km.

Figure 2b, a comparison of the 300 m range gate and 150 m range gate convolved with the 300 m gate function, shows the two reflectivities to be related by $\Delta R$. However, over the entire data set from this experiment, the 150 m and 300 m gate length comparison was even less predictable than the 300 m and 1 km gate length comparison.

REFERENCES

Balsley, B. B., M. Crochet, W. L. Ecklund, D. A. Carter, A. C. Riddle and R. Garello (1983), Preliminary observations of vertical atmospheric motions between 3 km and 18 km using three closely-spaced ST radars, preprint, Sixth Symposium on Turbulence and Diffusion, AMS, Boston, MA.

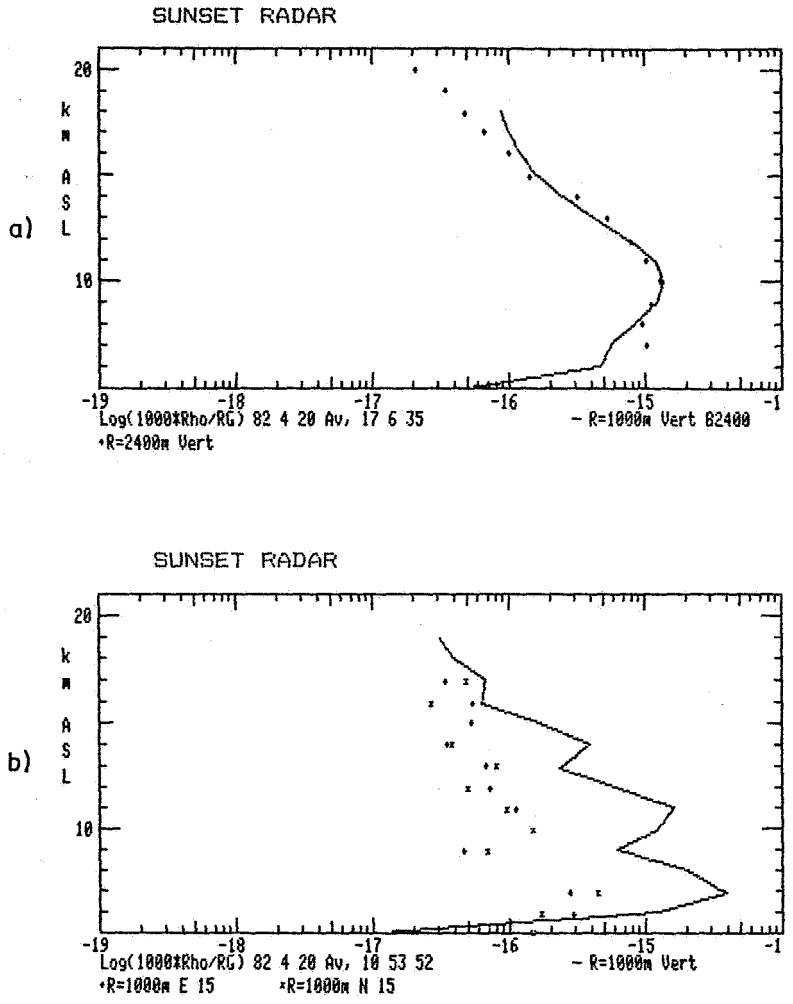


Figure 1. a. Comparison of a 2.4-km range gate and a 1-km range gate convolved with a measured 2.4-km range gate response function. b. Comparison of reflectivity from vertical and slant antenna beam positions with a 1-km range gate.

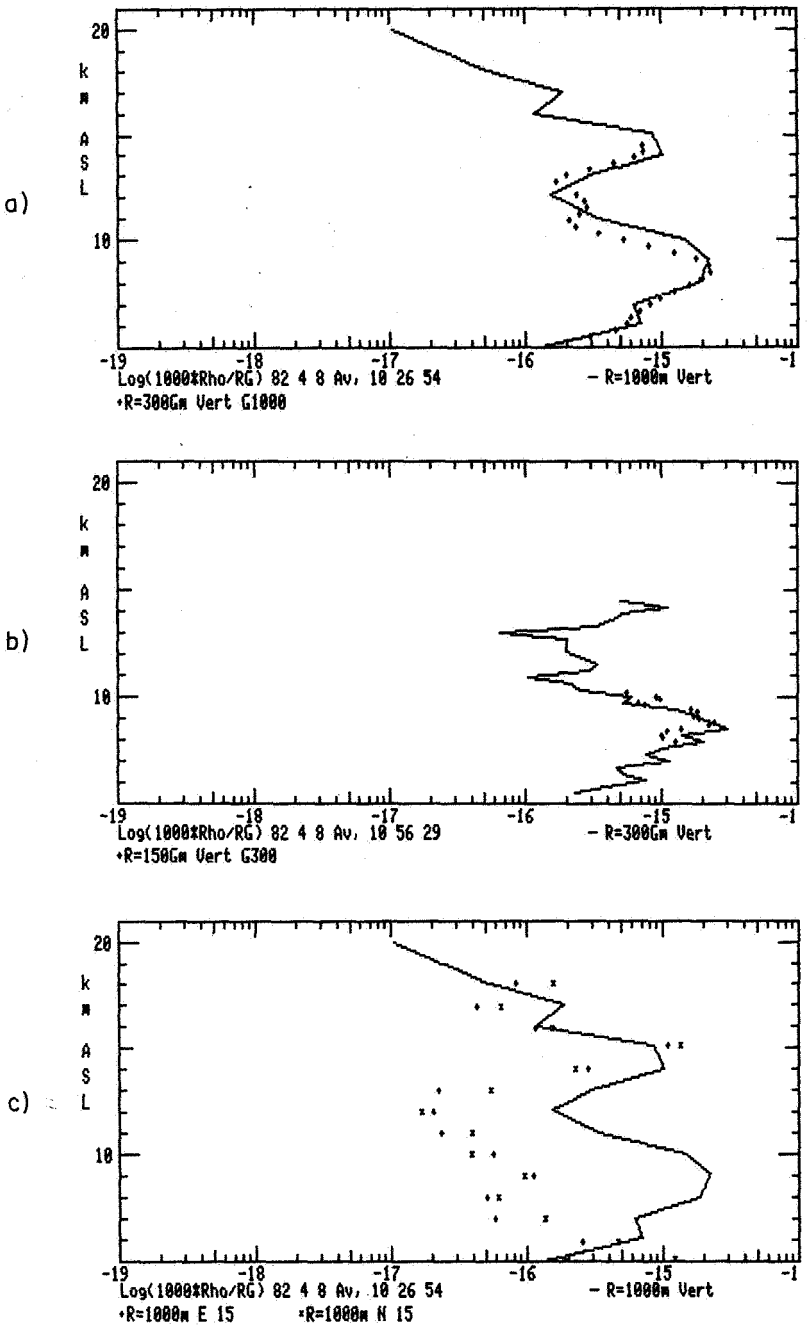


Figure 2. a. Comparison of reflectivity at vertical incidence with a 1-km range gate and a 300-m range gate convolved with a measured 1-km range gate response function. b. Comparison of reflectivity at vertical incidence of a 300-m range gate and a 150-m range gate convolved with a measured 300-m range gate response function. c. Comparison of reflectivity at vertical and slant incidence with a 1-km range gate.

Ecklund, W. L., D. A. Carter, B. B. Balsley (1979), Continuous measurement of upper atmospheric winds and turbulence using a VHF Doppler radar: Preliminary results, J. Atmos. Terr. Phys., 41, 983.

Ecklund, W. L., B. B. Balsley and D. A. Carter (1980), The Poker Flat Radar: Preliminary results between 3-20 km, Preprint, 19th Conf. on Radar Meteorology, AMS, Miami Beach, FL.

Fukao, S., T. Sato, S. Kato, R. M. Harper, R. F. Woodman and W. E. Gordon (1979), Mesospheric winds and waves over Jicamarca on 23-24 May 1974, J. Geophys. Res., 40, 1331.

Gage, K. S. and J. L. Green (1978), Evidence for specular reflection from monostatic VHF radar observations of the stratosphere, Radio Sci., 13, 991-1001.

Gage, K. S. and J. L. Green (1982a), A technique for determining the temperature profile from VHF radar observations, J. Appl. Meteorol., 21, 1146-1149.

Gage, K. S. and J. L. Green (1982b), An objective method for the determination of tropopause height from VHF radar observations, J. Appl. Meteorol., 21, 1159-1163.

Green, J. L. and K. S. Gage (1980), Observations of stable layers in the troposphere and stratosphere using VHF radar, Radio Sci., 15, 395-405.

Hocking, W. K. (1979), Angular and temporal characteristics of partial reflections from the D-region of the ionosphere, J. Geophys. Res., 84, 845-851.

Hocking, W. K. and J. Rottger (1983), Pulse-length dependence of radar signal strengths for Fresnel backscatter, submitted to Radio Sci.

Rottger, J. and C. H. Liu (1978), Partial reflection and scattering of VHF radar signals from the clear atmosphere, Geophys. Res. Lett., 5, 357-360.

Rottger, J., P. Czechowsky and G. Schmidt (1981), First low-power observations of tropospheric, stratospheric and mesospheric winds and turbulence at the Arecibo Observatory, J. Atmos. Terr. Phys., 43, 789-800.

Rottger, J. and M. F. Larsen (1983), Comparison of tropopause height and frontal boundary locations based on radar and radiosonde data, Geophys. Res. Lett., 10, 325-328.

Vincent, R. A. and J. S. Belrose (1978), The angular distribution of radio waves partially reflected from the lower ionosphere, J. Atmos. Terr. Phys., 40, 35-47.

Westwater, E. R., M. T. Decker, A. Zachs and K. S. Gage (1983), Ground-based remote sensing of temperature profiles by a combination of microwave radiometry and radar, J. Climate Appl. Meteorol., 22, 126-133.

## 2.1E IS VHF FRESNEL REFLECTIVITY DUE TO LOW FREQUENCY BUOYANCY WAVES?

T. E. VanZandt and R. A. Vincent*

Aeronomy Laboratory, National Oceanic and Atmospheric Administration, Boulder, CO 80303
*Department of Physics, University of Adelaide, Adelaide, South Australia 5001

VHF radar echoes are greatly enhanced near the zenith relative to other directions. This enhancement must be due to reflection from horizontally stratified laminae of refractive index. In this paper, we suggest that the refractivity laminae are due to the displacements of low frequency buoyancy (internal gravity) waves acting on the background vertical gradient of refractivity.

The radar cross section $\sigma(\underset{\sim}{k})$ is given by (OTTERSTEN, 1969)

$$\sigma(\underset{\sim}{k}) = \frac{\pi}{8} k^4 \quad \Phi\mu(\underset{\sim}{k})$$

where $k = 4\pi/\lambda_{radar}$, $\mu$ is the potential radio refractive index, and $\Phi\mu(\underset{\sim}{k})$ is the spatial power spectral density of $\mu$. If the fluctuations of $\mu$ are due to a spectrum of vertical displacement acting on $\bar{M} = \langle d\mu/dz \rangle$, the background gradient of $\mu$, then

$$\Phi\mu(\underset{\sim}{k}) = \bar{M}^2 E_\zeta (\underset{\sim}{k})$$

where $E_\zeta (\underset{\sim}{k})$ is the spatial power spectrum of vertical displacement. In order for $\sigma(\underset{\sim}{k})$ to be strongly enhanced near the zenith, $E_\zeta (\underset{\sim}{k})$ must also be strongly enhanced.

VANZANDT (1982) has shown that the observed spectra of mesoscale wind fluctuations in the troposphere and lower stratosphere can be modeled by a universal spectrum of buoyancy (internal gravity) waves that is a slight modification of the GARRETT and MUNK (1975) model of oceanic internal gravity waves. Since the observed frequency spectrum is red, the buoyancy wave model of the vertical displacement spectrum is strongly enhanced near the zenith. In other terms, the resulting refractivity irregularities are strongly stratified. The model spectrum is

$$E_\zeta (\underset{\sim}{k}) = \frac{1}{\pi k^4} \left[\frac{9\pi}{16} \left(\frac{n}{k}\right)^{1/2} \frac{E_*}{u_*^{3/2}} \tilde{F}(\theta)\right]$$

where n is the buoyancy (Brunt-Vaisala) frequency, $E_*$ is the normalized energy per unit mass ($E_* \, n \sim 10 \ (m/s)^2$), and $u_*$ is a scale phase velocity ($\sim$6 m/s).

$$\tilde{F}(\theta) = \frac{4}{9\pi\tilde{f}^2} \frac{(\theta/\tilde{f})^2}{((\theta/\tilde{f})^2 + 1)^{7/3}}$$

describes the angular variation normalized so that $\int_0^{2\pi} \int_0^{\infty} \tilde{F}(\theta) \sin\theta \, d\theta \, d\phi = 1$, where $\theta$ is the zenith angle of $\underset{\sim}{k}$, and $\tilde{f} = f/n$, where f is the inertial frequency. $\tilde{F}(\theta)/(4/9\pi\tilde{f}^2) = (\theta/\tilde{f})^2/((\theta/\tilde{f})^2 + 1)^{7/3}$ is plotted in the figure. The maximum lies at $\theta_{max}(°) = (\sqrt{3}/2)\tilde{f} = (\sqrt{3}/2)(\sin(\text{latitude})/120n(\text{rad/s}))$.

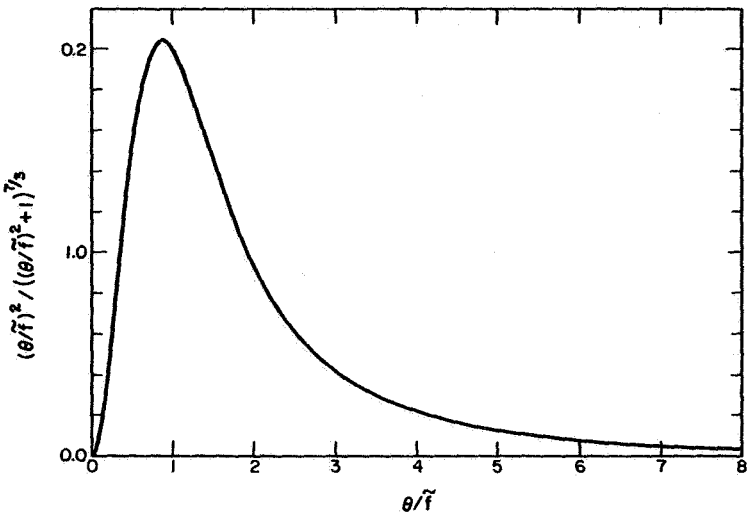


Figure 1. The angular dependence of $\sigma(\underset{\sim}{k})$.

For $n = 1 \times 10^{-2}$ (rad/s) (troposphere) at Arecibo (18.3°), Sunset (40°), and Poker Flat (65°), $\theta_{max} = 0.23°$, 0.46°, and 0.50°, respectively.

With this form of $E_\zeta(\underset{\sim}{k})$

$$\sigma(\underset{\sim}{k}) = \frac{\bar{M}^2}{8}\,[\ ] = \frac{9\pi}{128}\,\bar{M}^2\,\left(\frac{n}{k}\right)^{1/2}\,\frac{E_*}{u_*^{3/2}}\,\tilde{F}(\theta)$$

and the power reflectivity is

$$|\rho|^2 = 4 \iint \sigma(\underset{\sim}{k}))\ g^2(\theta',\phi')\ \sin\theta\ d\theta\ d\phi$$

where $g(\theta',\phi')$ is the normalized antenna gain function. If g is broad compared with F, as it usually is, then near the zenith the integral = 1.

This model can be tested by comparison with measurements of $\sigma(\underset{\sim}{k})$ or $|\rho|^2$ as functions of the parameters. Two reservations must be kept in mind, however. First, it has been assumed implicitly that $E_*$ is a universal constant, independent of latitude, altitude, etc. In fact, $E_*$ could depend on latitude through f and on altitude through the atmospheric density $\rho$, as it should theoretically. Observations so far have been inadequate to describe such variations. Nevertheless, in order to avoid this uncertainty, tests of the model should be made at a given latitude and over a small altitude range.

Second, although the buoyancy wave model fits observed spectra rather well down to vertical scales as small as ~20 m, the limit of the observed spectra, at some scale not much smaller than 20 m the spectrum should start to become increasingly attenuated by K-H instability and eventually by viscosity. Thus, the model can be quantitatively correct only for radar frequencies smaller than about 7.5 MHz (corresponding to 20 m). Unfortunately, the only suitable observations of Fresnel reflectivity are in the attenuated range at frequencies between 40 and 54 MHz ($\lambda_{radar}/2$ between 3.7 and 2.8 m). In this range the observed reflectivity should be much smaller than the model reflectivity and the

dependence of k should be much stronger than $k^{-1/2}$. The dependence on n, $\tilde{f}$, and $\theta$ may also differ from the model.

Nevertheless, comparisons at frequencies between 40 and 54 MHz are of interest. Results so far are: (1) The width of the model angular spectrum convolved with the radar beam is roughly consistent with the observed widths (GREEN et al., 1981; ROTTGER et al., 1981). (2) The model angular width varies inversely with the Brunt-Vaisala frequency, so that the width in the stratosphere should be about 1/2 the width in the troposphere, consistent with observations (ROTTGER et al., 1981). (3) The model dependence on n is given by $\overline{M^2}\ n^{1/2} \propto n^{4.5}$, roughly consistent with observations (GAGE et al., 1981). (4) The model $|\rho|^2$ for $\lambda_{radar} = 7.4$ m is much larger (by a factor of 100) than the reflectivity reported by GAGE et al. (1981), as is to be expected.

These comparisons are satisfactory at the present level of development of the model and the experiments, but further, more critical, tests are clearly needed. Observations with radar half-wavelengths $\gtrsim$ 20 m ($f \lesssim 7.5$ MHz) are clearly needed. The angular variation might be measured by means of an interferometer. In spite of the limitations of the model for half-wavelengths in the lower VHF range, further comparisons should also be made there, since the attenuation of the spectrum may not have first-order effects on the dependence on n, $\tilde{f}$, and $\theta$.

It should be noted that if the model is substantiated, then radar observations in the attenuated range yield information about the spectrum of buoyancy waves at small scales that is very difficult to obtain by other means. The buoyancy wave spectrum in this regime has implications on the cascade of energy in the buoyancy wave field, on the turbulent energy dissipation rate, and on turbulent mixing by the K-H breakdown of buoyancy waves.

All of the proposed mechanisms for the generation of the Fresnel refractivity irregularities, including the present one, depend upon speculative assumptions. The present model is distinguished from the others by being quantitative and therefore testable, at least under some conditions.

REFERENCES

Gage, K. S., B. B. Balsley and J. L. Green (1981), Fresnel scattering model for the specular echoes observed by VHF radar, Radio Sci., 16, 1447-1453.

Garrett, C. and W. Munk (1975), Space-time scales of internal waves: a progress report, J. Geophys. Res., 80, 291-297.

Green, J. L., J. M. Warnock, W. L. Clark, F. J. Eggert and K. J. Ruth (1981), Modifications to the Sunset radar to provide antenna beam steering, Preprint, 20th Conf. on Radar Meteorol., Am. Meteorol. Soc., 7-10.

Ottersten, H. (1969), Radar scattering from the turbulent clear atmosphere, Radio Sci., 4, 1251-1255.

Rottger, J., P. Czechowsky and G. Schmidt (1981), First low-power VHF radar observations of tropospheric, stratospheric and mesospheric winds and turbulence at the Arecibo Observatory, J. Atmos. Terr. Phys., 43, 789-800.

VanZandt, T. E. (1982), A universal spectrum of buoyancy waves in the atmosphere, Geophys. Res. Lett., 9, 575-578.

# 2.1F MESOSPHERIC SCATTER AND ITS MICROSTRUCTURE

S. A. Bowhill and K. P. Gibbs

Aeronomy Laboratory
Department of Electrical Engineering
University of Illinois
Urbana, IL 61801

The difference in character between mesospheric returns from about 70 and about 80 km has been remarked on by a number of workers. This note gives some further examples. Figure 1 (GIBBS and BOWHILL, 1983) shows simultaneous fading curves from 69 and 82.5 km altitude, and Figure 2 shows their Fourier spectra. The 69-km echo is characterized by a single return with about .1 Hz width, while the 82.5 km return extends over more than 3 Hz bandwidth; this difference is also perceptible, but to a lesser degree, on the fading curves. The conclusion seems inescapable that internal random velocities of a few m/s are present within the scattering volume for the 82.5-km echo. The most likely source for these rather large velocities is convective instability arising from deformations of the temperature profile by breaking gravity waves.

The distinction between the two types of scatter at these altitudes probably accounts for the behavior with frequency of the nighttime fading period at low and very low frequencies. BOWHILL (1957) found that the fading period of D-region reflections at night was constant at about 7 min from 16 to 43 kHz, but that at frequencies of 70 kHz and above, the fading period decreased in such a way as to indicate the presence of irregularities smaller than about 1 km in size. This suggests that frequencies of 48 kHz and below were reflected primarily from the region below 80 km where the narrow spectral irregularities of Figure 1 dominate.

Figure 3 (GIBBS and BOWHILL, 1983) shows another interesting type of behavior often seen in the spectra at the lower altitudes. The upper and lower portions of the diagram are spectra at altitudes separated by only 1.5 km compared with the 3 km vertical resolution corresponding to the 20-μsec transmitter pulse width. Two well-defined echoes are seen, each appearing at the same frequency on both plots with the different relative amplitudes. These different amplitudes are ascribed to the presence of two distinct Fresnel-type scatter regions within the scattering volume. Knowing the pulse shape, it is possible to determine the altitude at which those echoes occur, and the Doppler frequency associated with each.

Figure 4 (GIBBS and BOWHILL, 1983) shows an example of this kind of analysis; the hollow circles indicate velocities toward the radar, shaded circles indicate velocities away from it, and the diameters of the circles are proportional to the magnitudes of the velocities. This kind of plot gives the possibility of determining the location of individual scatterers with much higher precision (better than 100 m) than is normally possible with the pulse width used.

## ACKNOWLEDGMENTS

The work described was supported in part by the National Aeronautics and Space Administration under grant NSG 7506 and in part by the National Science Foundation under grant ATM 81-20371.

## REFERENCES

Bowhill, S. A. (1957), Ionospheric irregularities causing random fading of very low frequencies, J. Atmos. Terr. Phys., 11, 91.

Gibbs, K. P. and S. A. Bowhill (1983), An investigation of turbulent scatter from the mesosphere as observed by coherent-scatter radar, Aeron. Rep. 110, Aeron. Lab., Univ. Ill., Urbana-Champaign.

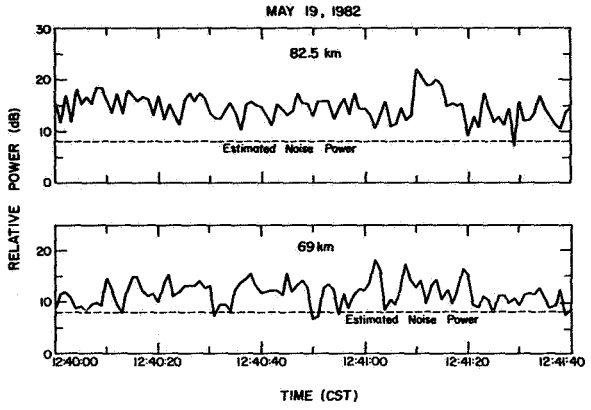


Figure 1. Power data at 1-second intervals on May 19, 1982.

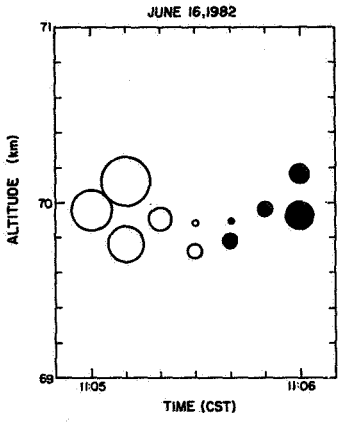


Figure 4. Scattering on June 16, 1982.

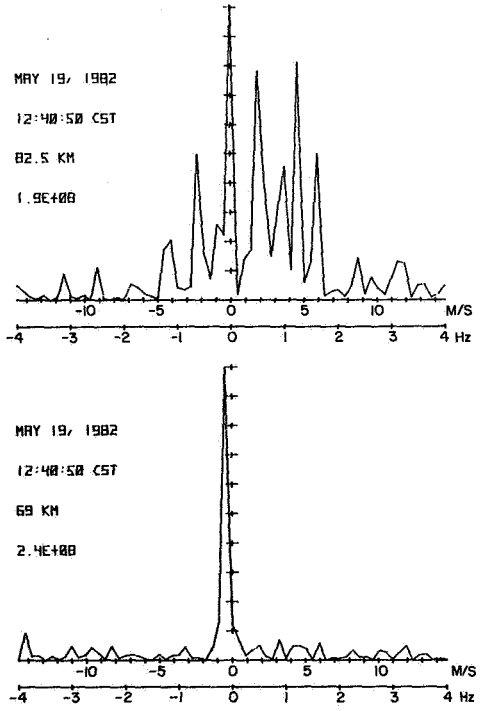


Figure 2. Spectral variation with altitude on May 19, 1982.

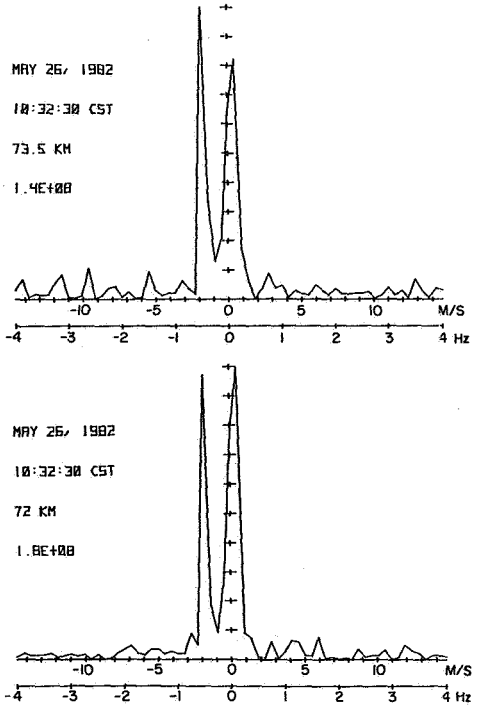


Figure 3. Comparison of spectra at adjacent altitudes.

# 2.1G FRESNEL ZONE CONSIDERATIONS FOR REFLECTION AND SCATTER FROM REFRACTIVE INDEX IRREGULARITIES

R. J. Doviak and D. S. Zrnic'

National Severe Storms Laboratory
Norman, OK 73069

## INTRODUCTION

Several different echoing mechanisms have been proposed to explain VHF/UHF scatter from clear air. GAGE and BALSLEY (1980) suggest three: (1) anisotropic scatter; (2) Fresnel reflection, and (3) Fresnel scatter, in order to account for the spatial (angle and range) and temporal dependence of the echoes. ROTTGER (1980) proposes the term "diffuse reflection" to describe the echoing mechanism when both scatter and reflection coexist. We present a unifying formulation incorporating a statistical approach that embraces all the above mechanisms and gives conditions under which reflection or scatter dominates. Furthermore, we distinguish between Fraunhofer and Fresnel scatter and present a criterion under which Fresnel scatter is important.

Scatter from anisotropic irregularities of refractive index n has, for many years, been thought to be principally responsible for microwave echoes from the clear air. Existing formulations assume that the correlation length of n irregularities generated by turbulence. are small compared to the Fresnel length. But there is experimental evidence that the contrary may be true. This paper extends the existing formulations for the case where the Fresnel zone radius is comparable to or smaller than the correlation length. LIU and YEH (1980) recognized the limitations of the existing formulations which are based upon first-order expansion of the phase term in the integral for the scattered (or reflected) electric field intensity and WAKASUGI (1981) suggested expansion to second order.

## THE FRESNEL TERM IN THE INTEGRAL FOR ECHO POWER

TATARSKI (1961, sect. 4.2) derived a formula for the field scattered from a volume $V_S$ with dimensions that implied the size of $V_S$ cannot be determined by the radar's resolution volume $V_6$ (DOVIAK and ZRNIC', 1983). (The subscript 6 is used to denote a resolution volume circumscribed by the surface giving a weight, to the scatterers, 6 dB less than the peak at the volume origin; DOVIAK et al., 1979.) In a later publication, TATARSKII (1971, sect. 2.8) extended his earlier formulation so that $V_S$ could equal $V_6$. It can be shown that for backscatter the condition assumed in this extension is

$$\rho_t << \sqrt{\lambda r_s/2\pi} = f/\sqrt{\pi} \qquad (1)$$

where $r_s$ is the range to an element of the scatter volume $\lambda$, the radar wavelength, f the first Fresnel zone radius, and $\rho_t$ is the correlation length of refractive index irregularities for lags transverse to $r_s$. Inequality (1) imposes the condition that constant phase surfaces of the incident wave are planes over the distance $\rho_t$, and the receiver is in the far field of this correlation length (i.e., $r_s > 2\rho_t^2/\lambda$).

We now develop the scatter equations which allow correlation length to be larger than that specified by (1). Assuming the Born approximation (i.e., single scatter theory), the field intensity $E_1$, backscattered by refractive index irregularities $\Delta n$ in the antenna far field is

$$E_1(\vec{r}_o,t) = k_o^2\sqrt{\frac{P_t \eta_o g}{(2\pi)^3}} \int_{V_s} \frac{f_\theta(\vec{r})\ \Delta n(\vec{r},t)}{r_s^2} \exp\{-j2k_o r_s\} dV \qquad (2)$$

where $r_s$ is the range to $\Delta n$ at $\vec{r}$ (see Figure 1), $f_\theta(\vec{r})$ is the angular pattern of the incident electric field intensity assumed to be circularly symmetric about the beam axis, $\eta_o$ is the free space wave impedance, $k_o=2\pi/\lambda$, $P_t$ is the transmitted peak power, g the antenna gain, and $\vec{r}$ the distance from the origin of $V_6$ to the scattering element. $V_s$ is a spherical shell of thickness $c\tau/2$ where $\tau$ is the transmitted pulse width and therefore $E_1(\vec{r}_o,t)$ is the intensity of echoes sampled at a range-time delay $(2r_o/c)+\tau$ after the transmitted pulse. Assume $\Delta n$ to be a zero mean random variable. In a matched filter receiver having an internal resistance R, the increment of current magnitude $|dI|$ produced by the scattering element is

$$|dI| = |dE_1|\ \lambda W(\vec{r})\sqrt{\frac{g f_\theta^2(r)}{4\pi\eta_o R}} \qquad (3)$$

where $W(\vec{r})$ is the range weighting function (ZRNIC' and DOVIAK, 1978; DOVIAK and ZRNIC', 1979). The integration now extends over all $\vec{r}$ for which $Wf_\theta\ \Delta n$ has significant value. For a receiver filter matched to a rectangular transmitted pulse, the range weighting function is

$$\begin{aligned} W(\vec{r}) &= 1 - \frac{2|\vec{r}\cdot\vec{a}_o|}{c\tau} \quad ; \ |\vec{r}\cdot\vec{a}_o| \le c\tau/2 \\ &= 0 \qquad\qquad\quad ; \text{otherwise} \end{aligned} \qquad (4)$$

where $\vec{a}_o$ is the unit vector from the origin of $V_6$ to the radar.

The received power, time averaged over a cycle of the transmitted frequency, is:

$$P_r = \frac{1}{2} II^* R \qquad (5)$$

where * denotes the conjugate.

From the integral of (3)

$$I = \frac{\lambda k_o^2 g}{(2\pi)^2}\sqrt{\frac{P_t}{2R}} \int \frac{W(\vec{r}) f_\theta^2(\vec{r})\ \Delta n(\vec{r},t) e^{-j2k_o r_s}}{r_s^2} dV \qquad (6)$$

For the condition $c\tau \ll r_o$, $r_s$ does not change significantly where $W(\vec{r})$ is appreciable so $r_s$ in the denominator of (6) can be replaced with $r_o$. Upon substituting (6) into (5) and taking the ensemble average, the expected received power becomes:

$$\langle P_r \rangle = \frac{P_t g^2}{4\lambda^2 r_o^4} \iint R(\vec{r},\vec{r}')\ W(\vec{r})\ W(\vec{r}') f_\theta^2(\vec{r}) f_\theta^2(\vec{r}')\ e^{-j2k_o(r_s-r_s')}\ dV dV' \qquad (7)$$

$$R(\vec{r},\vec{r}') = \langle \Delta n(\vec{r})\ \Delta n(\vec{r}') \rangle \qquad (8)$$

Let's assume that the irregularities have homogeneous statistical properties so that $R(\vec{r},\vec{r}') \simeq R(\vec{r}-\vec{r}')$ and that the two-way pattern function $f_\theta^2(\vec{r})$ is given by

$$f_\theta^2(\vec{r}) = \exp\{-\theta^2/4\sigma_\theta^2\} \qquad (9)$$

where $\sigma_\theta^2$ is the second central moment of the two-way power pattern and $\theta$ is the angular displacement, measured at the radar site, of $\vec{r}$ from the origin of $V_6$. In terms of the 6 dB angular width $\theta_6$ for the two way pattern $f_\theta^4$, $\theta_6=3.33\sigma_\theta$. For the assumption of narrow beams (9) can be approximated

$$f_\theta^2 \simeq \exp\{-t^2/4r_o^2\,\sigma_\theta^2\} \tag{10}$$

where $t=\sqrt{t_1^2+t_2^2}$ is the projection of $\vec{r}$ onto the plane transverse to the beam axis at $\vec{r}_o$.

The Gaussian matched filter provides the best resolution of all the receivers having the same bandwidth (ZRNIC' and DOVIAK, 1978). Because of this and because practical "matched filters" used in Doppler weather radars are Gaussian we assume that $W(\vec{r})$ is well approximated by

$$W(\vec{r}) \simeq e^{-(\vec{a}_o\cdot\vec{r})^2/4\sigma_r^2} \tag{11}$$

where $\sigma_r^2$ is the second central moment of the weighting function $W^2(\vec{r})$ and

$$\sigma_r = 0.35\ c\tau/2 = 0.30\ r_6 \tag{12}$$

for a Gaussian filter "matched" to a rectangular pulse of width $\tau$. The 6 dB range resolution is $r_6$.

Use the Taylor expansion for $r_s$

$$r_s \equiv |\vec{r}_o-\vec{r}| \simeq r_o-\vec{a}_o\cdot\vec{r}+\frac{1}{2r_o}\{r^2-(\vec{a}_o\cdot\vec{r})^2\} \tag{13}$$

for terms up to second order in $r^2$. We note that the second term of this expansion is the projection of $\vec{r}$ onto the $\vec{a}_o$ direction and the third term contains the projection on the transverse plane. Thus, in terms of the $\ell$,t coordinates centered in $V_6$,

$$r_s = r_o + \ell + t^2/2r_o \tag{14}$$

This quadratic expansion is valid (i.e., third order terms in r are negligible) provided that the scatter volume $V_s$ size is by limited by

$$d_t^2 < 2r_o\ |\sqrt{f^2/\pi+d_\ell^2}-|d_\ell|\} \tag{15}$$

where $2d_t$ and $2d_\ell$ are the dimensions of $V_s$ transverse and parallel to $r_o$. The condition (15) assumes $d_\ell \ll r_o$. As can be deduced, the farther the integration variable is displaced from the plane $\ell=0$, the smaller must be the scatter volume size perpendicular to the beam axis. However, $d_\ell$ in (15) need not be larger than the smaller of $r_6/2$ or the longitudinal projection $(d_z/\cos\psi+r_o\theta_6\tan\psi)/2$ of the scattering layer within $V_6$ (Figure 1). Substituting (14), the integral in (7) becomes

$$I_7 \equiv \iint R(\vec{r}-\vec{r}')\ W(\ell)\ W(\ell')\ \exp\{-\frac{(t^2+t'^2)}{2\sigma_t^2}-j2k_o(\ell-\ell'+\frac{t^2-t'^2}{2r_o})\}\ dVdV' \tag{16}$$

where $\sigma_t=\sigma_\theta r_o\sqrt{2}$ is proportional to the arc length of $V_6$. We now still find it convenient to define new coordinates:

$$t_1-t_1' \equiv \delta_1;\quad t_2-t_2' \equiv \delta_2;\quad \ell-\ell' \equiv \delta_3 \tag{17a}$$

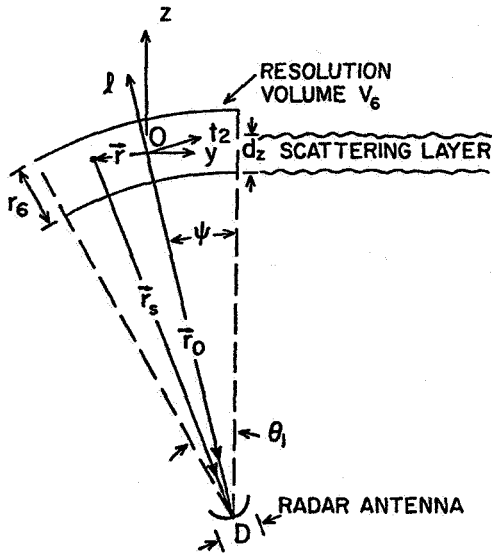


Figure 1. Geometry for backscatter. The distances $\ell$ and t are measured from the origin 0 of the resolution volume in directions parallel (longitudinal) and perpendicular (transverse) to the beam axis $\vec{r}_0$. $t_1$ is parallel to the $\chi$ axis and perpendicular to $t_2$.

$$\frac{t_1+t_1'}{2} \equiv \sigma_1; \quad \frac{t_2+t_2'}{2} \equiv \sigma_2 ; \quad \frac{\ell+\ell'}{2} \equiv \sigma_3 \tag{17b}$$

so that the $t_1$, $t_1'$ component of (16) can be written as

$$I_7(t_1) = \iint R(\vec{\delta}) \exp\left\{- \frac{\sigma_1^2+\delta_1^2/4}{\sigma_t^2} - j2k_o\sigma_1\delta_1/r_o\right\} d\sigma_1 d\delta_1 \tag{18}$$

where $\vec{\delta} = \vec{a}_1\delta_1+\vec{a}_2\delta_2+\vec{a}_3\delta_3$ is the lag vector (note $\vec{a}_3=\vec{a}_o$). The transformation from (16) to (18) is valid if, as is assumed here, the limits of integration cover the entire volume where the integrand has significant value. Thus executing the integration over $\sigma_1$

$$I_7(t_1) = \sigma_t\sqrt{\pi} \int R(\vec{\delta}) \exp\left\{-k_o\,\delta_1\,\sigma_t/r_o)^2 - \delta_1^2/4\sigma_t^2\right\} d\delta_1 \tag{19}$$

Applying similar procedures to the $t_2$ and $\ell$ coordinate integrations we obtain

$$I_7 = \sigma_r\sigma_t^2\pi^{3/2}\sqrt{2} \int R(\vec{\delta})\, e^{\underbrace{-(\delta_t^2/4\sigma_t^2 + \delta_z^2/8\sigma_r^2)}_{\text{Resolution Volume Weight}}\ \underbrace{-\pi^2\delta_t^2\sigma_t^2/f^4}_{\text{Fresnel Term}}} - j2k_o\delta_3 \; dV\delta \tag{20}$$

where $\delta_t^2 = \delta_1^2 + \delta_2^2$. The solution (20) is acceptable if the 2nd order expansion of $r_s$ in (14) is valid. Inequality (15) is the condition on $V_s$ for this expansion to be applicable. However, when the transverse dimension $\ell_t$ of $V_s$ is large such that (15) is not obeyed, we can still use (20) if $R(\vec{\delta})$ is small when

$\vec{\delta}$ has a magnitude comparable to or larger than the right side of (15). In other words the correlation length $\rho_t$ perpendicular to the beam axis must be

$$\rho_t^2 < 2r_o \{\sqrt{f^2/\pi + d_\ell^2} - |d_\ell|\} \tag{21}$$

If condition (15) is satisfied, then there is no condition on $\rho_t$. By comparing (21) with (1), it becomes evident that the second order expansion relaxes the limits placed on the scatter volume size and correlation length $\rho_t$. Now these limits are increased by the factor $(8\pi r_o/\lambda)^{1/4}$. For example, if $r_o$=10 km and $\lambda$=6 m, $\rho_t$ would have to be less than 1.4 km in order for (20) to be applicable whereas $\rho_t$ would have to be less than 100 m for a 1st order theory.

In the integral (20) the correlation is multiplied by two exponential weighting functions: (1) the resolution volume weight which depends solely upon the width $\sigma_t$ and range resolution $\sigma_r$ of $V_6$ and (2) the Fresnel terms which gives a weight in the t direction that depends upon the ratio $f/\sigma_t$. Only when the radius of the Fresnel zone is large compared to $\sqrt{\pi\sigma_t\rho_t}$ can the Fresnel term in (20) be ignored. Therefore, both beam width and correlation length enter into the comparison with f. But because $\sigma_t$ is a function of f, that is

$$\sigma_t = \frac{0.45\, r_o}{D\sqrt{\ell n 2}} = \frac{0.9f^2}{D\sqrt{\ell n 2}} \tag{22}$$

where D is the antenna diameter, we can simplify the conditions so that the Fresnel term can only be ignored if $\rho_t$ satisfies

$$\rho_t < \frac{D\sqrt{\ell n 2}}{0.9\pi} \tag{23}$$

On the other hand, because f is always smaller than $\sigma_t$ in the antenna's far field, the Fresnel term in (20) will have more weight than the beam width part of the resolution volume term. Thus situations that allow us to neglect the Fresnel term will also permit us to ignore beam width influence. If (23) is satisfied, we can use (20) (without the beam width and Fresnel terms) to obtain the scattered field, even though $V_s$ is larger than $V_6$; then we need to sum incoherent echo power from elemental volumes large compared to $\rho_t^3$ but small compared to $V_6$ (DOVIAK and ZRNIC', 1983). We call this case incoherent Fraunhofer scatter. But HODARA (1966) shows that within the lower troposphere, the correlation length has the following height dependence

$$\rho \simeq 0.4h/(1+0.01h) \quad (m) \tag{24}$$

where h is in meters. Furthermore, VHF backscatter data analyzed later in this paper suggest that $\rho_t \simeq 20$ m for irregularities in the lower stratosphere. Thus, unless the antenna diameter is of the order of 100 m or more, the Fresnel term will be important in determining the field scattered by refractive irregularities. If the scattering volume contains many subvolumes for which (20) applies, but (23) is not satisfied, we have a situation of incoherent Fresnel scatter. When $d_t < \sqrt{2r_o f}$ (from Equation 15), then we have coherent Fresnel scatter. If $d_t < f$, then signal is coherent irrespective of the transverse reshuffling of refractive index irregularities.

## THE SPECTRAL SAMPLING FUNCTION

Because it is common to describe the statistical properties of refractive index irregularities by the spectral density function the effects of the resolution volume and Fresnel terms on echo power can be examined conveniently by introducing a spectral sampling function. Equation (20) can be expressed in terms of the Fourier transform of $R(\vec{\delta})$ multiplied by the lag weighting function $H(\vec{\delta})$ where

$$H(\vec{\delta}) = \exp - \left\{ \left(\frac{1}{4\sigma_t^2}\right) + \frac{\pi^2\sigma_t^2}{f^4}\ \delta_t^2 + \frac{\delta_3^2}{8\sigma_r^2} \right\} \tag{25}$$

Thus

$$I_7 = \Phi_{nw}(0,0,2k_o) \tag{26}$$

where $\Phi_{nw}(\vec{K})$ is the three dimensional transform of $R(\vec{\delta})$ multiplied by the lag weighting function. Now $\Phi_{nw}$ is the spectrum $\Phi_n$ of refractive index irregularities convolved with the spectrum $\Phi_w$ of $H(\vec{\delta})$:

$$\Phi_{nw} = 8\sigma_r\sigma_t^2\pi^{9/2}\ \sqrt{2}\ \Phi_n * \Phi_w \tag{27}$$

where * denotes convolution and

$$\Phi_w = \frac{1}{8\pi^3} \int H(\vec{\delta})\ \exp(-j\vec{K}\cdot\vec{\delta})\ dV \tag{28}$$

is the normalized spectral sampling function. Substituting (25) into (28) and evaluating:

$$\Phi_w = \frac{\pi^{-3/2}\sigma_t^2\ \sigma_r\sqrt{2}}{(1+4\pi^2\sigma_t^4/f^4)}\ \exp\left\{-2\sigma_r^2 K_\ell^2 - \frac{\sigma_t^2 K_t^2}{(1+4\pi^2\sigma_t^4/f^4)}\right\} \tag{29}$$

where $K_t = \sqrt{K_1^2 + K_2^2}$. The second order phase term has contributed the factor $4\pi^2\sigma_t^4/f^4$ in the above equation. Thus the first order expansion is valid only if this factor is small relative to unity. However for $V_6$ in the antenna far

$$4\pi^2\sigma_t^4 f^{-4} >> 1 \tag{30}$$

For remote sensing with radar it is commonn to have $V_6$ in the antenna far field, thus the Fresnel term in $\Phi_w(\vec{K})$ cannot be ignored. As discussed earlier, this conclusion is a result of the fact that the Fresnel radius is always less than the beam width so that the Fresnel term always dominates the beam width weighting function. Thus $\Phi_w(\vec{K})$ can be well approximated by

$$\Phi_w(\vec{K}) \simeq \frac{0.44D^2\sigma_r\ell n2}{\pi^{7/2}} \exp\left\{-2\sigma_r^2 K_\ell^2 - \frac{D^2K_t^2\ell n2}{3.24\pi^2}\right\} \tag{31}$$

in which we have substituted (22) for $\sigma_t$. Equation (31) shows that the larger is the antenna diameter, the narrower is the spectral sampling function. It is surprising that the sampling function shape and size is independent of $r_o$ and, for a given antenna diameter, the spectrum $\Phi_n(\vec{K})$ of irregularities is weighted equally for all resolution volumes in space. This result differs from that derived by TATARSKII (1971) who only considered first-order phase expansion in which case $\Phi_w$ is a function of $r_o$. By combining (7), (26) and (27) the back-scattered power is given by

$$\langle P_r \rangle = \frac{2\sqrt{2}(0.45)^2\pi^{9/2}\ \sigma_r P_t g^2}{r_o^2 D^2\ \ell n2} \int \Phi_n(\vec{K})\ \Phi_w(\vec{a}_3 2k_o - \vec{K})\ dV_k \tag{32}$$

In the atmosphere it is usual for the horizontal correlation length $\rho_n$ to be larger than the vertical one $\rho_z$ so $\Phi_n(\vec{K})$ will be more sharply peaked along the $K_x, K_y$ directions and less so along the $K_z$ axis. If the irregularities have

shapes that are roughly described as oblate spheroids, then the correlation $R(\vec{\delta})$ would also have a similar form but $\Phi_n(\vec{K})$ would be prolate spheriodal in shape (Figure 2a). Equation (31) reveals that whenever range resolution $r_6=3.33\sigma_r$ is larger than 0.34D, as is usual, the sampling function (Figure 2b) along $K_\ell$ will be narrower than along $K_t$. If the beam axis is rotated by $\psi$ degrees from the vertical, $\Phi_w(\vec{K})$ will also be rotated by $\psi$ from the $K_z$ axis.

If echo power decreases significantly as $\psi$ is increased, then we have specular type reflection. The sharpness of the angular dependence is a function both of $\rho_h$ and D. Referring to Figures 2a,b and Equation (31), we see that a necessary condition to observe a specular type echoing mechanism is for $0.54\lambda/D<<1$. That is, narrow beams are required which is consistent with simple physical arguments. Assuming space is filled with $\Delta n$, specular type echoes will then be observed only if $\rho_h>>\rho_z$. However, we must be cautious in applying these criteria because we have used a specific model (i.e., Gaussian) to

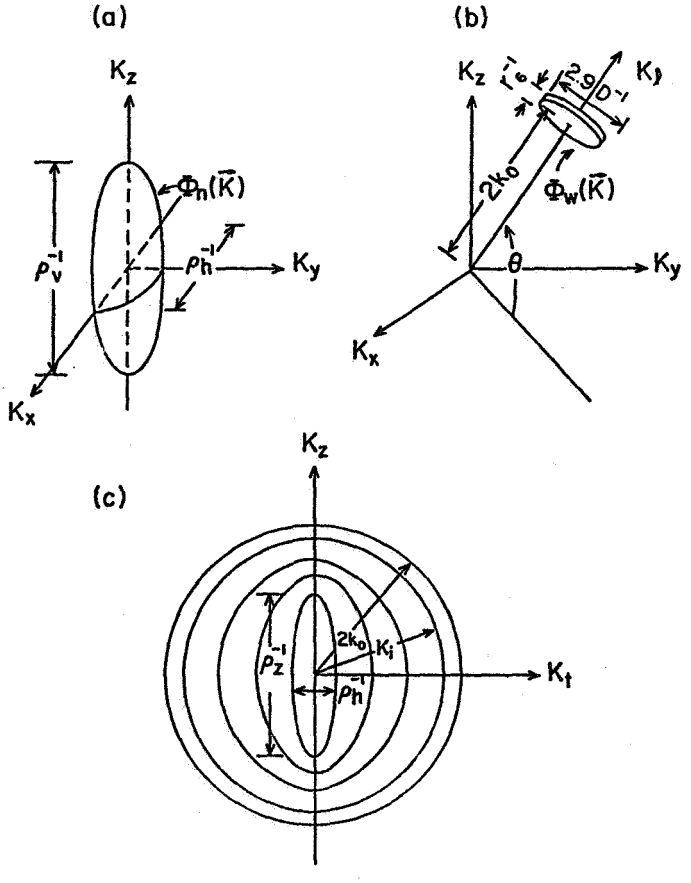


Figure 2. (a) Contour surface of constant spectra intensity $\Phi_n(\vec{K})$ for irregularities having symmetric correlation lengths along x and y that are longer than the correlation length along z. (b) Contour surface of the spectral sampling function $\Phi_w(\vec{K})$ for beam axes at elevation angle $\theta_e = \pi/2 - \psi$. (c) Contours of constant $\Phi_n(\vec{K})$ for which the small-scale irregularities produce isotropic scatter.

describe the statistical properties of n and because $\rho_h, \rho_z$ only characterize the most intense irregularities of refractive index. Thus, if the contours of constant $\Phi_n(\vec{K})$ have the dependence sketched in Figure 2c, scatter could be independent of $\psi$ (i.e., isotropic scatter) if $2k_o >> \rho_z^{-1}$ and $2k_o >> \sqrt{2} r_6^{-1}$. The $\Phi_n(\vec{K})$ depicted in Figure 2c can be represented by a sum of isotropic $\Phi_i$ and anisotropic $\Phi_a$ parts where $K_i$ is the wave number beyond which $\Phi_i \geq \Phi_a$ (independent of direction of $\vec{K}$). $\Phi_i(\vec{K})$ could have the -11/3 power law dependence on K deduced from turbulence theories.

## BACKSCATTERING FROM ANISOTROPIC IRREGULARITIES

As an example, let us consider the angular dependence of echo power when the scattering medium can be decomposed into isotropic and anisotropic components (i.e., $R(\delta)=R_i+R_a$). We further assume that $R_a$ is isotropic in the horizontal plane. To obtain an order of magnitude estimate, we take $R_a$ of the form:

$$R_a = \langle \Delta n^2 \rangle_a \exp \{ - \frac{\delta_h^2}{2\rho_h^2} - \frac{\delta_z^2}{2\rho_z^2} \}$$

where

$$\delta_h = \sqrt{\delta_x^2 + \delta_y^2} \tag{33}$$

The resolution volume coordinates are related to the natural coordinates x,y,z via:

$$\delta_x = \delta_1 ; \quad \delta_y = \delta_2 \cos\psi - \delta_3 \sin\psi ; \quad \delta_z = \delta_2 \sin\psi + \delta_3 \cos\psi \tag{34}$$

After introducing (34) into (33) and the result into (20), integration is performed giving the formula for echo power from anisotropic irregularities as being proportional to

$$I_a(\psi) = \frac{2\sqrt{2}\sigma_r \sigma_t^2 \pi^3 \langle \Delta n^2 \rangle_a}{a\sqrt{4b^2d^2 - c^4}} \exp \{ -4k_o^2 b^2 / (4b^2 d^2 - c^4) \} \tag{35}$$

where for $V_6$ in the antenna far field:

$$a^2 \simeq \frac{1}{2\rho_h^2} + \frac{\pi^2 \sigma_t^2}{f^4} \tag{36a}$$

$$b^2 \simeq \frac{\sin^2\psi}{2\rho_z} + \frac{\cos^2\psi}{2\rho_h^2} + \frac{\pi^2 \sigma_t^2}{f^4} \tag{36b}$$

$$c^2 = \left( \frac{1}{\rho_h^2} - \frac{1}{\rho_z^2} \right) \sin\psi\cos\psi \tag{36c}$$

$$d^2 = \frac{\cos^2\psi}{2\rho_z} + \frac{\sin^2\psi}{2\rho_h^2} + \frac{1}{8\sigma_r^2} \tag{36d}$$

Now for laminae of $\Delta n$ such that $\rho_z$ is smaller than the smallest of:

$$\frac{2\sqrt{2}\pi\sigma_t\sigma_r\rho_h}{f^2} , \text{ or } \frac{\rho_h f^2}{2\sqrt{2}\pi\sigma_t\sigma_r} , \text{ or } \frac{\sqrt{2}\sigma_r f^2}{\pi\rho_h\sigma_t} \tag{37}$$

we can simplify (35)

$$I_a(\psi) \simeq \frac{4<\Delta n^2>_a \rho_z \rho_h^2 \sigma_r \sigma_t^2 \pi^3}{\sqrt{TQ}} \exp\{-2k_o^2 \rho_z^2 \frac{S}{Q}\} \tag{38}$$

where

$$S(\psi) = \frac{\rho_h^2}{\rho_z^2} \sin^2\psi + \cos^2\psi + 2\pi^2\sigma_t^2\rho_h^2/f^4 \tag{39a}$$

$$T = 1 + 2\pi^2\sigma_t^2\rho_h^2/f^4 \tag{39b}$$

$$Q(\psi) = 1 + (2\pi^2\sigma_t^2\rho_h^2 \cos^2\psi/f^4) + \rho_h^2 \sin^2\psi/4\sigma_r^2 \tag{39c}$$

When height of $V_6$ is constant and laminae are infinitesimally thin, the ratio for echo powers at angle $\psi$ and zenith ($\psi$=0) is:

$$\frac{<P_a(\psi)>}{<P_a(o)>} = \sqrt{\frac{Q(o)}{Q(\psi)}} \cos^2\psi \exp\{-2k_o^2 \frac{\rho_h^2 \sin^2\psi}{Q(\psi)}\} \tag{40}$$

The term $\cos^2\psi$ accounts for the decrease in power due to the range and $\sigma_t$ increase with tilt away from the vertical because $V_6$ remains at constant height. To $<P_a(\psi)>$ we add the power $P_i(\psi)$ due to isotropic irregularities to obtain:

$$\{\frac{<P_a(\psi)>}{<P_a(o)>} + A\cos^2\psi\} \div \{1+A\} = \frac{<P(\psi)>}{<P(o)>} \tag{41}$$

where $A=P_i(0)/P_a(0)$. Equation (41) was fitted to data (Figure 3) from ROTTGER et al. (1981). Pertinent parameters for the Rottger et al. data are: $\lambda$=6.4 m; D≃260 m; heights h=16.9→18.1 km near the tropopause; beam width $\theta_1$=1.7°; and range resolution = 300 m. We find $\rho_h$=20 m for the horizontal correlation lengths, and A=0.04 fits well these data. Comparing terms in (39) it is seen that the Fresnel term (i.e., the 2nd term in $Q(\psi)$) does not contribute significantly. Although we have not distinguished any one of the mechanisms discussed in the introduction as being responsible for the echo power, we see that scattering from anisotropic irregularities can account for the observed angular dependence which is sufficiently peaked that one might believe a reflection mechanism is acting.

For sake of simplicity, it is preferable to label the echoing mechanism as scatter whenever there are several or more scattering irregularities for which only a statistical description of their properties (e.g., size, intensity, etc.) is practical. Thus, we do not need to invoke a reflective process to explain observations in this case; the scatter formulation presented here can explain all the features of the received field if indeed the medium is comprised of many irregularities of refractive index for which only statistical properties are known.

Equation (2) is the starting point for our formation for scatter from refractive irregularities. Although we refer to (2) as the scatter integral, it can be used as well in situations (i.e., $\rho_t$>>f) which might be interpreted as reflective. In order to determine echo power when irregularities have horizontal dimensions large compared to the Fresnel radius, GAGE et al. (1981) have used the general formula

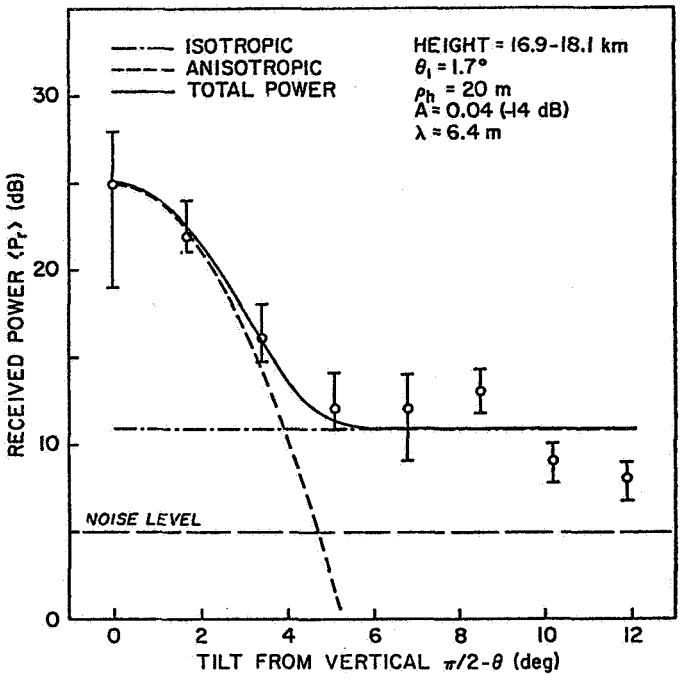


Figure 3. Angular dependence of observed mean backscatter power (open circles) from anisotropic irregularities as the radar beam axis is tilted away from the vertical (ROTTGER, 1981). Fitted to the data is a model that consists of anisotropic turbulence with a two-dimensional (horizontal isotropy) correlation function in an isotropic background.

$$|R|^2 = \frac{1}{4} \left| \int_{-\ell/2}^{\ell/2} \frac{1}{n} \frac{dn}{dz} \exp\{-j2k_o z\}\, dz \right|^2 \tag{42}$$

for the power reflection coefficient where $\ell$ is the thickness of the partially reflecting layer. In this form variations of n along the horizontal are ignored and, if the scattering layer is in the antenna far field, the echo power $P_r$ is easily found by considering an image source which gives

$$P_r = P_t A_e^2 |R|^2 / 4\lambda^2 r_o^2 \tag{43}$$

where $A_e$ is the effective area of the antenna ($A_e = g\lambda^2/4$). For exactly the same assumptions on n, the solution of (2) should produce an identical echo power. In Appendix A we prove this contention by simply using the second-order phase terms; this shows the wide applicability of the solution presented earlier.

Figure 4 illustrates the type of scatter that would be effective versus the location of the sampling wave number $2k_o$ for the case $\rho_h >> \rho_z$. The location of boundaries are functions of the parameters $\rho_h$, D, $r_o$ and the relative strengths of $\Phi_a$ and $\Phi_i$, and thus there could be a different order than presented on Figure 4. For example, if $K_i < 2r_o/\rho_h^2$, then Fraunhofer scatter could be either

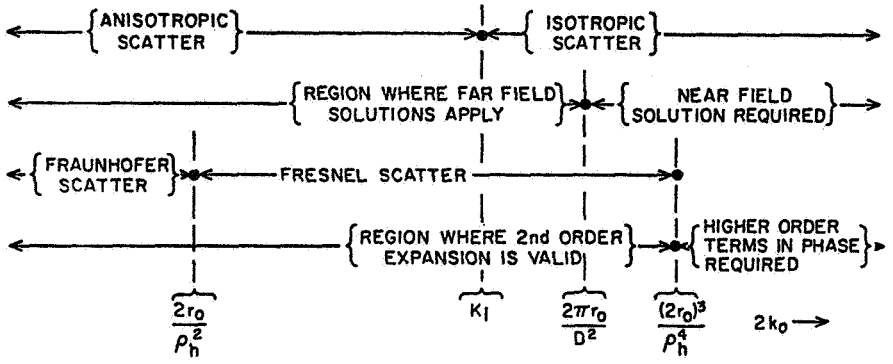


Figure 4. Types of echo mechanisms versus the location of the sampling wave number $2k_0$ for a particular ordering of boundaries. $\rho_h >> \rho_z$, and $V_6$ is uniformly filled with irregularities.

anisotropic or isotropic depending upon the value of $2k_o$. Because we had assumed infinitesimally thin laminae ($K_i \to \infty$ in that case), scatter will be anisotropic no matter how large is $2k_o$. However, it is more likely that $K_i < 2\pi r_o/\rho_h^2$ so that if $2k_o$ was larger than 2 $m^{-1}$ we could pass into a region of isotropic scatter. Data collection at various $2k_o$'s (i.e., multiple wavelength radar) could establish the correlation length $\rho_z$ and a value for $K_i$. At UHF wavelengths $2k_o$ is so large that the peak of $\Phi_w(\vec{K})$ is expected to fall most of the time in the tail of $\Phi_n(\vec{K})$ at wave numbers where turbulence is mostly isotropic and $\Phi_n$ is expected to have the same 11/3rds dependence on K as does the velocity fluctuations. However, at the longer wavelengths in the VHF band, $2k_o$ is much smaller so it can place the $\Phi_w(\vec{K})$ peak in a region where $\Phi_a$ may sometimes be larger than $\Phi_i$ or smaller than it.

ECHO POWER DEPENDENCE ON RANGE AND RANGE RESOLUTION

GAGE et al. (1981) propose a model for which echo intensity varies as the inverse square power of range but has a range resolution dependence that can vary from zero to a square law. BALSLEY and GAGE (1981) introduce the concept of a scatter volume defined, transverse to the antenna beam, by a correlation radius to derive an echo intensity that depends on the fourth power of range. It is improper to form such a condition because the scatter volume $V_S$ is defined by either the spatial distribution of intensity of $\Delta n$ fluctuations or by the resolution volume $V_6$, whichever is smaller. We shall use the solutions derived here to determine the conditions under which various dependences can occur. Recently HOCKING and ROTTGER (1983) have critically reviewed the interpretations of Balsley and Gage.

Assume vertical incidence and use (31) and (32) to obtain

$$\langle P_r \rangle = \frac{C\sigma_r}{r_o^2} \Phi_n(\vec{K})^* \Phi_w(\vec{K}) \tag{44}$$

where C is a constant independent of $\sigma_r$ and $r_o$, and $\Phi_w(\vec{K})$ can be expressed as:

$$\Phi_w(\vec{K}) = \sigma_r \Phi_w(K_t) \exp\{-2\sigma_r^2 K_z^2\} \tag{45}$$

where now $K_t^2 = K_x^2 + K_y^2$. Consider two cases: (1) $\Phi_n(\vec{K})$ broad and (2) narrow compared to $\Phi_w(\vec{K})$ along the wave number $\vec{K}_z$ coordinate (Figure 5).

(a) $\Phi_n$ Broad

Integration along $K_z$ gives a $\langle P_r \rangle$ approximated by

$$\langle P_r \rangle = \frac{C\sigma_r}{r_o^2} \iint \Phi_w(K_t)\Phi_n(K_x,K_y,2k_o)dK_x dK_y \tag{46}$$

which illustrates that the expected echo power is proportional to range resolution (assuming a uniformly filled $V_6$) and inversely proportional to the square of range $r_o$. This is the usual dependence expected when scatter is from irregularities produced by turbulence. The $r_o^{-2}$ dependence occurs irrespective of whether $\rho_h$ is large or small compared to f.

(b) $\Phi_n(\vec{K})$ Narrow

In this case (44) can be reduced to

$$\langle P_r \rangle \simeq \frac{C\sigma_r^2}{r_o^2} e^{-2\sigma_r^2(K_{sz}-2k_o)^2} \int \Phi_w(K_t)\Phi_n(\vec{K})\, dV_K \tag{47}$$

Again $\langle P_r \rangle$ depends upon the inverse square of $r_o$, a result which is independent of $\rho_h$. If $\Phi_w(\vec{K}_t)$ is also broad compared to $\Phi_n(\vec{K})$ along $K_t$ then (47) reduces to

$$\langle P_r \rangle \simeq \frac{C\sigma_r^2}{r_o^2} - \Phi_w(0)e^{-2\sigma_r^2(K_{sz}-2k_o)^2} \int \Phi_n(\vec{K})dV_K \tag{48}$$

in which $\Phi_n(\vec{K})$ is assumed to have a peak at $K_t=0$. This case occurs when refractive index irregularities have $\rho_h > f$ and strong Fourier components clustered about $2k_o$. Only if $2k_o = k_{sz}$ will $\langle P_r \rangle$ be proportional to $\sigma_r^2$; otherwise, we could have other range resolution dependencies. The integral in (48) is the variance $\langle \Delta n^2 \rangle$.

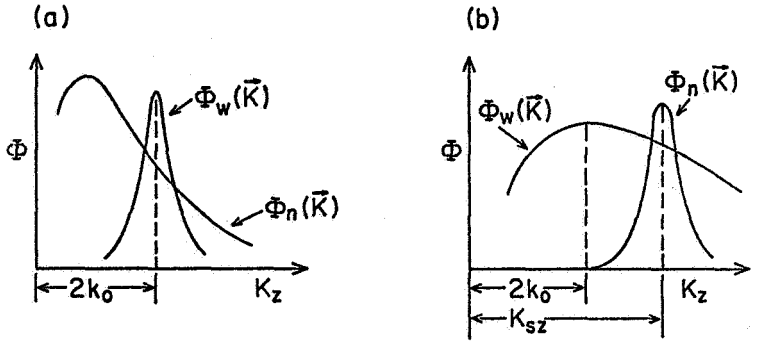


Figure 5. Cases in which $\Phi_n$ is broad (a) and narrow (b) compared to $\Phi_w$.

If the irregularities are contained in a thin layer having a vertical dimension small compared to $\sigma_r$, then echo power would be independent of $\sigma_r$, when the resolution volume is centered on the layer. For resolution volumes displaced from the layer height, echo power would have a strong dependence on $\sigma_r$ even exceeding the square law one! If the scattering irregularities are confined to horizontal dimensions small compared to beam width, then a fourth power range dependence would be obtained. However, the correlation length does not determine the scatter volume dimension as stated by BALSLEY and GAGE (1981). In the cases discussed in (a) and (b) the echo power depends on the inverse square of range because we have assumed uniformly filled $V_6$.

## CONCLUSIONS

When scattering layers are in the far field of an antenna, the Fresnel term is a more important weighting function than the antenna pattern because the width of the antenna pattern is always larger than the Fresnel radius f. Only in the case where the correlation length $\rho_t$ of refractive index irregularities $\Delta n$ perpendicular to the beam is much smaller than f will the first-order truncation of the Taylor series expansion for phase be valid. Then Fraunhofer scatter is considered to be effective. However, when retention of second-order phase terms is necessary a Fresnel term (see Equation 20) is introduced. The criterion for keeping the second-order phase term depends both upon beam width and the Fresnel radius. Thus, the condition under which incoherent Fraunhofer scatter is effective becomes solely a function of antenna diameter D (i.e., $\rho_t < 0.29D$). When the Fresnel term needs to be included in the solution we have the situation of Fresnel scatter or reflection. It is suggested that unless the antenna diameter is of the order of 100 m or more, the Fresnel term is important in determining the field scattered by refractive irregularities.

The formulas derived here establish the conditions under which a scatter or reflection mechanism can be distinguished. However it is important to have the proper statistical description of the irregularities in order to obtain the spatial and temporal dependence of echo intensity. A multiple wavelength radar, in which its beam position can be scanned, could supply invaluable data to characterize the spectrum of refractive index irregularities and help to explain the properties of the echoes. Only when irregularities have a spatial spectrum form that concentrates variance $\langle \Delta n^2 \rangle$ at wave numbers near $2k_o$ does echo power depend upon the square of range resolution. Echo power depends upon the inverse square of range $r_o$ independent of whether $\rho_t$ is less than or greater than f. However the resolution volume must be uniformly filled with $\Delta n$.

## REFERENCES

Balsley, B. B. and K. S. Gage (1981), On the vertical-incidence VHF back-scattered power profile from the stratosphere, Geophys. Res. Lett., 8, 1173-1175.

Doviak, R. J. and D. S. Zrnic' (1979), Receiver bandwidth effect on reflectivity and Doppler velocity estimates, J. Appl. Meteor., 18, 69-76.

Doviak, R. J., D. S. Zrnic' (1983), Doppler Radar and Weather Observations, Academic Press, New York, NY (in press).

Doviak, R. J., D. S. Zrnic' and D. S. Sirmans (1979), Doppler weather radar, Proc. IEEE, 67, 1522-1553.

Gage, K. S. and B. B. Balsley (1980), On the scattering and reflection mechanisms contributing to clear air radar echoes from the troposphere, stratosphere and mesosphere, Radio Sci., 15, 243-257.

Gage, K. S., B. B. Balsley and J. L. Green (1981), Fresnel scattering model for the specular echos observed by VHF radar, Radio Sci., 16, 1447-1453.

Hocking, W. K. and J. Rottger (1983), Pulse length dependence on radar signal strengths for Fresnel backscatter. Personal communication.

Hodara, H. (1966), Laser wave propagation through the atmosphere, Proc. IEEE, 54, 368-375.

Liu, C. H. and K. C. Yeh (1980), Scattering of VHF and UHF radar signals from the turbulent air, Radio Sci., 15, 277-282.

Rottger, J. (1980), Reflection and scattering VHF radar signals from atmospher refractivity structures, Radio Sci., 15, 259-276.

Rottger, J., P. Czechowsky and G. Schmidt (1981), First low-power VHF radar observations of tropospheric, stratospheric and mesospheric winds and turbulence at the Arecibo Observatory, J. Atmos. Terr. Phys., 43, 789-800.

Tatarski, V. I. (1961), Wave Propagation in a Turbulent Medium, McGraw-Hill Book Co., Inc., New York, NY. Trans. by R. A. Silverman.

Tatarskii, V. I. (1971), The effects of the turbulent atmosphere on wave propagation. Trans. by Israel Program for Sci. Transl. Jerusalem. IPST Cat. No. 5319 UDC 551.510, ISBN 0-7065-0680-4, 471 pp.

Wakasugi, K. (1981), MST radar technique for remote sensing of the middle atmosphere, Kyoto Institute of Technology, Kyoto, Japan

Zrnic', D. S. and R. J. Doviak (1978), Matched filter criteria and range weighting for weather radar. IEEE Trans. Aero. and Elec. Sys., AES-14, 925-930.

## APPENDIX A

In this appendix we shall demonstrate that (42) and (2) and identical formulations for the situation considered in this paper (i.e., a scattering layer in the far field of an antenna, and range resolution sufficiently narrow so that the $1/r^2$ term can be brought out of the integral (2)).

For pulsed transmissions the height interval that contributes to the echo sample is determined by the pulse shape if refractive index irregularities are distributed throughout the vertical. Therefore, in this case (dn/dz)/n in (42) must be multiplied by the range weighting function (e.g., (11)) and then, for pulse widths small compared to $r_o$, the limits on z in (42) can be increased to infinity without significant error. Thus the reflection coefficient takes the form:

$$R = \frac{1}{2} \int_{-\infty}^{+\infty} e^{-z^2/4\sigma_r^2} \frac{d}{dz} (\ell n n) \exp \{-j2k_o z\} \, dz \qquad (A1)$$

Using integration by parts and noting that $n = 1 + \Delta n$ where $\Delta n \ll 1$, (A1) can be reduced to

$$R = \int_{-\infty}^{+\infty} \left(\frac{z}{4\sigma_r^2} + jk_o\right) \Delta n \exp \left\{- \frac{z^2}{4\sigma_r^2} - j2k_o z\right\} dz \qquad (A2)$$

Now for range resolution many wavelengths long (i.e., $k_o\sigma_r >> 1$) the term $z/4\sigma_r^2$ can be ignored in the integral without adding appreciable error to $\rho$. Then

$$R = jk_o \int_{-\infty}^{\infty} W(z)\ \Delta n(z)\ \exp\ \{-j2k_o z\}\ dz \tag{A3}$$

We note here that W(z), as defined in this paper, also contains the weight associated with the frequency transfer function of the receiver's filter. Although this function does not rigorously belong in the integral for $\rho$, we are primarily interested in the received echo power which is dependent upon the filter function. For a linear system we could, if we ignore receiver noise, just as well consider the filter at the transmitted output thus modifying the pulse shape to give the equivalent weight W(z) considered herein. With similar consideration we can also express (2) in the form

$$E_1 = \frac{k_o^2}{r_o^2}\sqrt{\frac{P_t g \eta_o}{(2\pi)^3}} \int W(z) f_\theta^2(r)\, \Delta n\ \exp\ \{-j2k_o r_s\}\ dV \tag{A4}$$

We now consider $\Delta n$ to depend upon z as in the reflection formula and using (10) for $f_\theta^2(r)$, the second-order expansion (14) for $r_s$, and integrating over the horizontal we obtain

$$E_1 = \frac{\pi k_o^2}{r_o^2}\sqrt{\frac{P_t g \eta_o}{(2\pi)^3}}\ e^{-j2k_o r_o}\ \left(\frac{1}{2\sigma_t^2} + j\frac{k_o}{r_o}\right)^{-1} \int W\ \Delta n\ \exp\ \{-j2k_o z\} dz \tag{A5}$$

Now for $r_o$ in the antenna far field the term $jk_o/r_o$ has a magnitude larger than $1/2\sigma_t^2$. The echo power $P_r$, in terms of $E_1$, is:

$$P_r = A_e |E_1|^2 / 2\eta_o \tag{A6}$$

substitution of (A5) and (A3) into (A6) reveals

$$P_r = \frac{P_t A_e^2 |R|^2}{4\lambda^2 r_o^2}$$

which is identical to (42) derived from the reflection formula.

# 2.2A EFFECTS OF PULSE WIDTH AND CODING ON RADAR RETURNS FROM CLEAR AIR

C. R. Cornish

Schooling of Electrical Engineering
Cornell University
Ithaca, NY 14853

In MST radar studies it is desired to obtain maximum information about the atmosphere and to use efficiently the radar transmitter and processing hardware. Large pulse widths are used to increase the signal-to-noise ratio since clear air returns are generally weak and maximum height coverage is desired. Yet since good height resolution is equally important, pulse compression techniques such as phase coding are employed to optimize the average power of the transmitter. Considerations in implementing a coding scheme and subsequent effects of an impinging pulse on the atmosphere are the subject of this paper.

As noted, a large pulse width is desirable to maximize S/N which varies as the square of the pulse width. In using phase codes one pays for good height resolution in terms of decreased S/N. As height resolution increases, noise increases since the receiver bandwidth must be widened to match the decreased pulse length. The net effect is for the S/N ratio to vary as pulse width squared for uncoded pulses but for coded pulses, S/N is proportional to the pulse width. In general, one selects an optimal set of system parameters (interpulse period (IPP), pulse width, coding scheme, gate delay) to avoid range aliasing, ionospheric interference (e.g., electrojet returns at Jicamarca), code sidelobes and ground clutter.

## PULSE WIDTH EFFECTS

While a maximum duty cycle and high average power is preferred, a longer pulse causes ground clutter to be smeared over more heights. Hence strong clutter returns may overwhelm weak signals at higher altitudes.

As the scattering volume is proportional to pulse width, it is possible for one or more signal peaks to occur within a given range gate. The resolution of the structure of a particular phenomenon, e.g., wind shear, is dependent on height resolution available.

The spectral width of the signal is a measure of the distribution of velocities within the scattering volume. Velocities may be distributed due to some random process such as turbulent scattering. On the other hand, there may be some vertical structure such as velocity shear which organizes the velocity distribution. For a random distribution, one would expect no change in spectral width with pulse width, while in the case of a velocity shear the spectral width should vary with illuminated volume, i.e. pulse width.

## PULSE CODING EFFECTS

While use of phase codes yields good height resolution and maximum average transmitter power, proper selection of IPP and codes helps to eliminate range aliasing and ambiguities. Certain codes such as Barker codes are undesirable due to range sidelobes. There exists a 2-3 dB/km dropoff in signal power in the neutral atmosphere. For a 13-baud Barker code, the range sidelobes are 22 dB down from the peak but are nevertheless sufficient at a 1-km baud length to cause clutter from signals 10 km below to interfere.

Correlation times of the medium in the stratosphere and mesosphere are on the order of .5 to 1 second, which is sufficiently long that complementary codes

and coherent integration techniques can be used. The total coherent averaging time must be less than the coherence time of the atmosphere.

Ideally, perfect codes are generated, transmitted, scattered, received and decoded, but this does not happen in practice. SULZER and WOODMAN (unpublished manuscript, 1982) have considered some of the practical problems and have generated a set of quasi-complementary codes to overcome some of the deficiencies of complementary codes. Quasi-complementary codes are beneficial in eliminating ghosts from range sidelobes of complementary codes produced in the actual implementation of codes due to such effects as transmitter ringing and frequency domain asymmetry. Furthermore, quasi-complementary codes perform better than complementary codes when incomplete decoding due to truncated signals at lower altitudes occurs as a result of the loss of the first few bauds during receiver blanking. Finally quasi-complementary codes are good for suppressing interference from clutter since each individual code of the quasi-complementary code set is of higher quality (lower sidelobes) than an individual code of a complementary pair.

# 2.2B THE EFFECTS OF PULSE RATE, POWER, WIDTH AND CODING ON SIGNAL DETECTABILITY

D. A. Carter

Aeronomy Laboratory
National Oceanic and Atmospheric Administration
Boulder, CO 80303

When deciding upon radar and signal processing parameters for MST radars, the quantity that one attempts to maximize within existing constraints is the signal detectability. For Doppler spectral analysis the detectability can be defined (see BALSLEY, 1978 or GAGE and BALSLEY, 1978) as the ratio of the amplitude of the largest spectral peak of the received signal to the noise level fluctuation, $D = S_r/\Delta S_N$ (see Figure 1).

This paper will examine the effects on the detectability of varying the pulse repetition rate (PRF), peak pulse power ($P_{pk}$) and pulse width ($\tau_p$). Both coded and uncoded pulses will be considered. During this discussion the following quantities will be assumed to be constant: antenna area, echo reflectivity, Doppler shift, spectral width, spectral resolution, effective sampling rate, and total incoherent spectral averaging time. The detectability will be computed for two types of targets: 1) discrete target (i.e., a single echoing region smaller than the smallest pulse width).

First let us examine the effects of coded pulses. The received signal from a coded pulse is decoded by convolving the received voltage with the code. The phase of the received signal from the echoing region will be the mirror image of the transmitted code. Since the autocorrelation function of a code of length $L_c$ has a peak value of $L_c$, the decoding process enhances the echo signal power by a factor of $L_c^2$. For white noise which is uncorrelated between each bit of the code, the convolution will add the power incoherently and thus the noise power will be increased by a factor of $L_c$. The above is true regardless of the type of code used. For multicode processing (using complementary codes or pseudo-random codes) the signals from successive codes must be added coherently to obtain the desired autocorrelation sidelobe response. However, as long as the number of codes used is less than the normal number of coherent averages, multi-code processing will not have any additional effect on the signal detectability. Of course, the sidelobes of the code autocorrelation functions will affect range contamination of signals and influence the choice among various codes.

Now we will determine the signal detectability for coded and uncoded pulses as a function of PRF, transmitter power, pulse width, and code length. Let us define the fundamental bit length or resolution pulse width of a coded pulse to be $\tau_o$ and the total pulse length to be $\tau_p = L_c\tau_o$. The same symbols can be used for uncoded pulses by letting $L_c = 1$ and $\tau_p = \tau_o$. The returned signal power, $P_s$, is proportional to peak transmitter power for discrete targets and to peak power and pulse width for diffuse targets. Specifically, for both coded and uncoded pulses,

$$P_s \propto P_{pk} L_c^2 \quad \text{(discrete targets)}$$

$$P_s \propto P_{pk} \tau_o L_c^2 \quad \text{(diffuse targets).}$$

The noise power can be written as

$$P_N \propto B L_c/m \propto L_c/\tau_o m$$

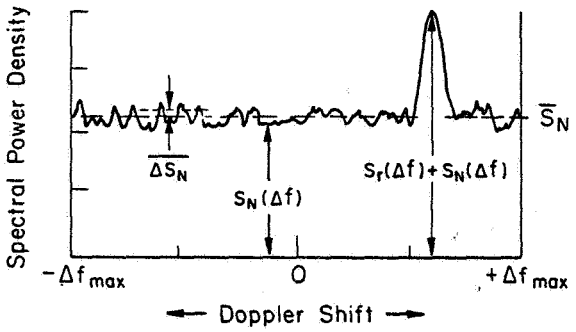


Figure 1. Typical Doppler spectrum (after BALSLEY, 1978a).

where $B \propto 1/\tau_o$ is the receiver bandwidth and m is the number of coherent averages. The signal-to-noise ratio, $SNR = P_S/P_N$, then becomes

$$SNR \propto P_{pk}\, m\tau_o\, L_c \qquad \text{(discrete)}$$

$$SNR \propto P_{pk}\, m\tau_o^2 L_c \qquad \text{(diffuse)}$$

Following the derivation of signal detectability, D, used by BALSLEY (1978) and eliminating dependencies on the fixed quantities given previously, it can be shown that

$$D \propto P_{pk}\,(PRF)\,\tau_o L_c = P_{AV} \text{ (discrete)}$$

$$D \propto P_{pk}\,(PRF)\tau_o^2 L_c = P_{AV}\,\tau_o \quad \text{(diffuse)}.$$

Table 1 summarizes these results for 4 cases with varying values of PRF, $P_{pk}$, $\tau_o$, and $L_c$ for a constant average transmitter power ($P_{AV} = P_{pk}\,(PRF)\,L_c\tau_o$) The "reference" values of each quantity are PRF = f, $P_{pk} = P$, $\tau_o = \tau$, and $L_c = 1$. Each quantity is multiplied in turn by an integer constant N, keeping the average power constant in each case. The receiver bandwidth, B, is set to $1/\tau_o$ and the number of coherent averages $n_c$ is adjusted to maintain a constant effective sampling rate, $PRF/n_c$. The resulting dependencies of the signal-to-noise ratio and detectability are shown in the last two columns.

Table 1 can be simplified by writing the first 3 independent variables in terms of dimensionless quantities PRF/f, $P_{pk}/p$, $\tau_o/\tau$ and thus showing only the dependency on N. This has been done in Table 2. For the discrete targets we can see that all 4 cases have the same signal-to-noise ratio and the same detectability. For the diffuse case, because of the dependence on the resolution pulse width, the long uncoded pulse has a detectability which is a factor of N greater than the other 3 cases.

In those diffuse cases where high resolution is obtained, we note that using coded pulses gives the same signal detectability as using short uncoded pulses with either higher PRF or higher peak power. Pulse coding becomes desirable, then, when high resolution is needed and when the peak power cannot be increased due to transmitter limitations and the PRF cannot be increased, perhaps because of range aliasing problems.

Note that, given a set of Doppler power spectra obtained with any of the high resolution systems (cases 5, 6 or 8 in Table 2) the detectability can be increased by $N^{1/2}$, at the expense of range resolution, by averaging the spectra across N range gates. This effect occurs because the spectral noise power

Table 1. Signal detectability for constant average transmitter power

| | PRF | $P_{pk}$ | Res PW $\tau_o$ | Code Size $L_c$ | Tot PW $\tau_p$ | $P_{AV}$ | B | $n_c$ | $P_s$ | $P_N$ | SNR | D |
|---|---|---|---|---|---|---|---|---|---|---|---|---|
| Discrete Targets | | | | | | | | | | | | |
| 1) High PRF | Nf | P | $\tau$ | 1 | $\tau$ | $NfP\tau$ | $1/\tau$ | Nm | $\propto P$ | $\propto 1/N\tau m$ | $\propto NPm\tau$ | $\propto NPf\tau$ |
| 2) High Peak Power | f | NP | $\tau$ | 1 | $\tau$ | $NfP\tau$ | $1/\tau$ | m | $\propto NP$ | $\propto 1/\tau m$ | $\propto NPm\tau$ | $\propto NPf\tau$ |
| 3) Long Pulse | f | P | $N\tau$ | 1 | $N\tau$ | $NfP\tau$ | $1/N\tau$ | m | $\propto P$ | $\propto 1/N\tau m$ | $\propto NPm\tau$ | $\propto NPf\tau$ |
| 4) Coded Pulse | f | P | $\tau$ | N | $N\tau$ | $NfP\tau$ | $1/\tau$ | m | $\propto N^2P$ | $\propto N/\tau m$ | $\propto NPm\tau$ | $\propto NPf\tau$ |
| Diffuse Targets | | | | | | | | | | | | |
| 1) High PRF | Nf | P | $\tau$ | 1 | $\tau$ | $NfP\tau$ | $1/\tau$ | Nm | $\propto P\tau$ | $\propto 1/N\tau m$ | $\propto NPm\tau^2$ | $\propto NPf\tau^2$ |
| 2) High Peak Power | f | NP | $\tau$ | 1 | $\tau$ | $NfP\tau$ | $1/\tau$ | m | $\propto NP\tau$ | $\propto 1/\tau m$ | $\propto NPm\tau^2$ | $\propto NPf\tau^2$ |
| 3) Long Pulse | f | P | $N\tau$ | 1 | $N\tau$ | $NfP\tau$ | $1/N\tau$ | m | $\propto NP\tau$ | $\propto 1/N\tau m$ | $\propto N^2Pm\tau^2$ | $\propto N^2Pf\tau^2$ |
| 4) Coded Pulse | f | P | $\tau$ | N | $N\tau$ | $NfP\tau$ | $1/\tau$ | m | $\propto N^2P\tau$ | $\propto N/\tau M$ | $\propto NPm\tau^2$ | $\propto NPf\tau^2$ |

PRF = Pulse repetition frequency

$P_{pk}$ = Peak transmitted power

$\tau_o$ = Resolution pulse width

$L_c$ = Number of bits in code

$\tau_p$ = Total pulse width = $L_c\ \tau_o$

$P_{AV}$ = Average transmitted = $(PRF)P_{pk}\ \tau_p$

B = Required receiver bandwidth $\propto 1/\tau_o$

$n_c$ = Number of coherent averages

$P_s$ = Returned signal power

$\propto P_{pk}\ L_c^2$ (discrete)

$\propto P_{pk}\ \tau_o\ L_c^2$ (diffuse)

$P_N$ = Noise power $\propto L_c\ B/n_c$

SNR = Signal-to-noise ratio = $P_s/P_N$

D = Signal detectability

Table 2. Relative signal detectability for constant average transmitter power

| | PRF | $P_{pk}$ | Res PW $\tau_o$ | Code Size $L_c$ | Tot PW $\tau_p$ | $P_{AV}$ | B | $n_c$ | $P_s$ | $P_N$ | SNR | D |
|---|---|---|---|---|---|---|---|---|---|---|---|---|
| Discrete Targets | | | | | | | | | | | | |
| 1) High PRF | N | 1 | 1 | 1 | 1 | N | 1 | N | 1 | 1/N | N | N |
| 2) High Peak Power | 1 | N | 1 | 1 | 1 | N | 1 | 1 | N | 1 | N | N |
| 3) Long Pulse | 1 | 1 | N | 1 | N | N | 1/N | 1 | 1 | 1/N | N | N |
| 4) Coded Pulse | 1 | 1 | 1 | N | N | N | 1 | 1 | $N^2$ | N | N | N |
| Diffuse Targets | | | | | | | | | | | | |
| 5) High PRF | N | 1 | 1 | 1 | 1 | N | 1 | N | 1 | 1/N | N | N |
| 6) High Peak Power | 1 | N | 1 | 1 | 1 | N | 1 | 1 | N | 1 | N | N |
| 7) Long Pulse | 1 | 1 | N | 1 | N | N | 1/N | 1 | N | 1/N | $N^2$ | $N^2$ |
| 8) Coded Pulse | 1 | 1 | 1 | N | N | N | 1 | 1 | $N^2$ | N | N | N |

PRF = Pulse repetition frequency

$P_{pk}$ = Peak transmitted power

$\tau_o$ = Resolution pulse width

$L_c$ = Number of bits in code

$\tau_p$ = Total pulse width = $L_c \tau_o$

$P_{AV}$ = Average transmitted = $(PRF)P_{pk} \tau_p$

B = Required receiver bandwidth $\propto 1/\tau_o$

$n_c$ = Number of coherent averages

$P_s$ = Returned signal power

$\propto P_{pk} L_c^2$ (discrete)

$\propto P_{pk} \tau_o L_c^2$ (diffuse)

$P_N$ = Noise power $\propto L_c B/n_c$

SNR = Signal-to-noise ratio = $P_s/P_N$

D = Signal detectability

fluctuations are proportional to $N^{-1/2}$. Thus by using two types of post-processing, these high resolution systems can give range resolution improved by a factor of N in regions of good SNR and, in regions of low SNR, a detectability degraded only by $N^{1/2}$, compared to the long pulse case.

REFERENCES

Balsley, B. B. (1978), Design considerations for coherent radar systems for probing the troposphere, stratosphere, and mesosphere, Preprint Vol., 18th Conf. on Radar Meteorology, March 28-31, Atlanta, GA, AMS, Boston, pp. 387-390.

Gage, K. S. and B. B. Balsley (1978), Doppler radar probing of the clear atmosphere, Bull. Am. Meteorol. Soc., 59, 1074-1093.

# 2.3A SPECTRAL CHARACTERISTICS OF THE MST RADAR RETURNS

P. K. Rastogi

Haystack Observatory
Massachusetts Institute of Technology
Westford, MA 01886

## ABSTRACT

The salient features of the spectra of atmospheric returns due to random refractivity fluctuations in the MST region are reviewed. The nonhomogeneous layered structure of turbulence is often evident as multiple peaks in the spectra. The time evolution of the spectra observed with a fine Doppler resolution provides evidence for thin regions of turbulence associated with gravity waves and shear instabilities. Embedded in these regions are horizontally extended refractivity structures that produce enhanced returns due to specular reflections. It is conceivable that some enhanced returns arise due to anisotropy of small-scale refractivity structures. Observed correlations of the strength of the returns with their Doppler spread, wind shears, and winds provide insights into the physical mechanisms that produce turbulence.

## INTRODUCTION

The use of sensitive high power radars at VHF and UHF frequencies in studies of the Mesosphere-Stratosphere-Troposphere (MST) region has been reviewed extensively in recent years (see e.g., ROTTGER, 1980; BALSLEY, 1981). These radars are sensitive to weak fluctuations in the radio refractivity of the atmosphere at a scale that usually is half the radar wavelength (BOOKER and GORDON, 1950; BOOKER, 1956). The refractivity fluctuations are induced by atmospheric turbulence and act merely as tracers for larger-scale motions associated with atmospheric winds and waves.

In most radar experiments it is usual to parametrize the spectra of the received signals by their low-order moments which are then interpreted in terms of the physical and dynamic properties of the medium (WOODMAN and GUILLEN, 1974). Details in the spectra that are not readily characterized by the low-order spectral moments, and observed interrelations between the spectral moments, provide insights into the physical mechanisms that produce the radar returns and are reviewed here.

The response of the radar to the radio refractivity fluctuations is briefly outlined in the following section, where we also discuss the consequences of layered turbulence on the spectra and the inferred parameters. In directions close to the vertical, these turbulent layers often can produce enhanced specular echoes. The spectral characteristics of these enhanced echoes are briefly outlined; observed correlations between the spectral moments, and the implications of these in terms of thin layers of turbulence generated by enhanced wind shears and subsequent thickening of layers are discussed in the respective sections. Finally, the types of observations that may resolve some conflicting evidence for the observed correlations are discussed.

## RADAR RESPONSE TO REFRACTIVITY FLUCTUATIONS

The electromagnetic aspects of scattering of radio waves from random refractivity fluctuations in radar experiments are sufficiently well understood (see e.g., TATARSKII, 1971; ISHIMARU, 1978). The refractivity fluctuations $\eta(\underline{r},t)$ constitute a random field. The received signal $z(t)$ is linearly related to the spatial Fourier component of this field at the Bragg vector

$\underset{\sim}{k}_b = (\underset{\sim}{k}_i - \underset{\sim}{k}_r)$ corresponding to the propagation vectors $\underset{\sim}{k}_i$ and $\underset{\sim}{k}_r$ or the incident and the received fields. For backscatter (usually the case for MST radars) $k_b$ corresponds to a spatial scale of half the radar wavelength. A second-order statistic of the received signal z(t), either its autocovariance function $R(\tau)$ or the power spectrum S(f), is measured in the radar experiments. These statistics can usually be related to the time or frequency behavior of these components of the field $n(\underset{\sim}{r},t)$ that have a spatial wave number $k_b$.

To proceed further, assumptions must be made about the nature of the field $n(\underset{\sim}{r},t)$. In the most widely used (and least general) information $n(\underset{\sim}{r},t)$ is assumed to be homogeneous and isotropic at least over the radar cell (BOOKER and GORDON, 1950). The signal spectrum S(f) can be characterized in this case by a single Doppler-shifted peak (ISHIMARU, 1978). Without resorting to the exact shape of the spectrum, the lowest-order moments of S(f) provide information on the turbulence-induced refractivity variance ($C_n^2$), radial velocity ($v = \underset{\sim}{k}_b \cdot \underset{\sim}{v}$), and the radial velocity spread ($\sigma_v$) (see e.g., WOODMAN and GUILLEN, 1974; ZRNIC', 1979).

The assumption of homogeneiety of the field $n(\underset{\sim}{r},t)$ over a radar cell breaks down in experiments that have a coarse altitude resolution of 1-3 km. This is principally due to a layered structure of turbulence that is characteristic of the atmosphere and ocean. Often these layers have a nominal thickness of tens to hundreds of meter. Early evidence for the occurrence of turbulent layers in the stratosphere (WOODMAN and GUILLEN, 1974) and in the mesosphere (RASTOGI and BOWHILL, 1976) was inferred from VHF radar observations at Jicamarca.

When two or more layers occur in a region of shear through a radar cell, the spectrum S(f) has characteristic multiple peaks as shown in Figure 1. In UHF radar experiments at Millstone Hill, time evolution of these spectral peaks has been observed with a fine Doppler-resolution at low elevation angles to provide evidence for breaking gravity waves, and possibly a Kelvin-Helmholtz stability in the troposphere (WAND et al., 1983). CRANE (1980) shows examples in which the multiple peaks in the spectra can be seen and tracked over contiguous radar cells.

An important consequence of the unresolved layers of turbulence is the error introduced in the estimation of the $C_n^2$ parameter from the measured signal power. Radar experiments that assume homogeneous turbulence throughout the radar cell, would tend to underestimate $C_n^2$ by a factor that depends upon the unknown volume fraction (F) of the cell that is actually filled by turbulence. VANZANDT et al. (1978) have proposed a model that can be used to infer $C_n^2$ from the back-ground wind and temperature profiles measured with radiosondes. Simultaneous radar measurements of $C_n^2$ can be used to infer the fraction F. The error in the estimates of $C_n^2$ is usually considerably smaller in fine altitude resolution experiments in which the vertical size of the radar cells is better matched to the layer thickness (SCHMIDT et al., 1979; ROTTGER et al., 1979; WOODMAN, 1980; WOODMAN et al., 1980). In these experiments, the assumption of homogeneiety over the radar cells is approximately valid, except for a possible complication due to specular returns (discussed in the next section).

The assumption of isotropy of turbulence at the Bragg scale (typically 3 meters for VHF radars and 0.3 meter for UHF radars) is reasonable if this scale is sufficiently small compared to the outer scale at which energy is fed into turbulence. For a typical layer thickness of 100 m, anisotropic Bragg-scale turbulence is more likely to occur at VHF, than at UHF frequencies. Scattering from anisotropic refractivity fluctuations (BOOKER, 1956; TATARSKI, 1971; ISHIMARU, 1978) can produce enhanced radar returns. The effect of anisotropy, however, is not expected to be significant at mesospheric heights, where the Kolmogorov scale associated with turbulence increases to 1-5 meter.

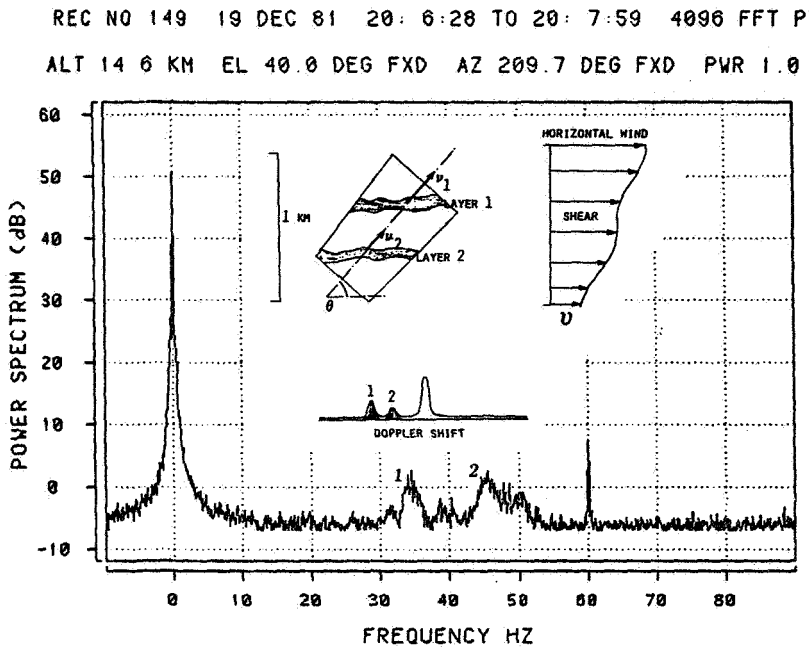


Figure 1. An example of signal spectrum with multiple peaks (identified as 1 and 2) observed with a 0.125 Hz resolution at Millstone Hill. A Doppler shift at 10 Hz corresponds to a horizontal velocity of 4.5 m/s. The ground clutter at zero frequency, and a narrow spike at the power line frequency of 60 Hz are clearly discernible. The inset shows how these peaks can arise due to layers of turbulence in a shear region.

LIU and YEH (1980) have considered scattering from thin layers of urbulence that is frozen-in with the medium, and have obtained specific results or the modified spectral moments. Their analysis is valid when the turbulent elocity component is small compared to the velocity of the medium along the adar axis. This is usually the case when the radar is pointed downwind, ufficiently away from the vertical.

PECULAR REFLECTIONS

Enhanced echoes have been observed from the S-T region (see e.g., GAGE and EEN, 1978; ROTTGER, 1978) and from the mesosphere (FUKAO et al., 1980) in VHF periments that use a radar beam pointed close to the vertical. These are tributed to weak, partial or specular reflections from sharp refractivity adients associated with turbulent layers.

The spectral characteristics of specular returns have been observed in the T region in VHF radar experiments by examining the autocovariance function of e returns (ROTTGER and LIU, 1978; RASTOGI and ROTTGER, 1982), and directly in F radar experiments (SATO, 1981). The temporal coherence of specular returns manifest in their longer correlation time or smaller spectral width. ecular returns can be discriminated, to some extent, from the scattered gnals by examining the spectra in the vicinity of the Doppler profile through ndows of different width. The Doppler resolution in the frequency spectra served with most MST radars, however, has not been adequate for fruitfully rsuing this approach.

## RELATION BETWEEN SPECTRAL MOMENTS

Empirical correlations between the low-order spectral moments, or parameters derived therefrom, have been observed in several radar experiments. Some of these correlations, e.g., those between wind (from the first-order moment), wind shear (height derivative of wind), and signal power (zeroth-order moment), can be reconciled with physical mechanisms that generate turbulence. Others, e.g., a correlation (positive or negative) between signal power and the spectral width (second-order moment) remain physically elusive, but probably depend on the growth of turbulent regions.

In the absence of convection processes, local wind shears are the principal source of turbulence. A necessary condition for the onset of turbulence is that the local Richardson number Ri should become smaller than 0.25. The signal power measured in radar experiments is an indicator of the strength of turbulence. The shear inferred from the radial wind at contiguous radar cells has a scale corresponding to the altitude resolution. An excellent similarity has been observed in the stratosphere and troposphere between the profiles of inferred shear (at a 300-m scale) and signal power in a series of fine-altitude resolution (150 m) experiments at Arecibo (SATO, 1981).

Even with altitude resolutions of 1-2 km, a correlation of the order of 0.7 between wind shear and signal power has been observed in experiments at Poker Flat (SMITH et al., 1983), and at Millstone Hill. A similar order of correlation is observed between wind and signal power, especially in regions of large (>30 m/s) horizontal wind. The fact that even the shear inferred at a 2-km scale appears to bear a good correlation with the signal power, suggests that small-scale shears probably are enhanced in regions of large background shear. The correlation of signal power with strong winds can be explained either on the basis of large Reynolds number, or alternatively because regions of strong winds (e.g., the jet streams) also have a large shear associated with them (SMITH et al., 1983).

An intriguing correlation between the signal power and fading time (inverse of spectral width) of mesospheric VHF echoes was first seen in A-scope traces by BOWLES (1958) in his pioneering incoherent-scatter experiment. A similar correlation was noticed in A-scope traces at Jicamarca (FLOCK and BALSLEY, 1967). Later experiments showed that this type of correlation is often quite pronounced in the lower mesosphere (RASTOGI and BOWHILL, 1976), though its sense is frequently reversed above 80 km (FUKAO et al., 1980; COUNTRYMAN and BOWHILL, 1979).

Since the signal power is related to the refractivity variance, and spectral width to the radial velocity variance, a positive correlation between these quantities is normally to be expected. This argument fails to explain the observed correlation, however.

RASTOGI and BOWHILL (1976) proposed that for thinner layers of turbulence, a broader range of wave numbers in the vicinity of $k_b$ are involved in scattering and the fading time would be longer. An association of stronger signals with longer fading times in the lower mesosphere then appears to imply that stronger turbulence should occur in thinner layers. In the upper mesosphere, however, stronger signals appear to be associated with shorter fading times implying that regions of stronger turbulence ought to be thicker. VHF radar observations with 150-300 m resolution actually do reveal layers 1-2 km thick at heights above 80 km. These layers are several times thinner and often unresolved in the lower mesosphere (ROTTGER et al., 1979; RUSTER et al., 1980). The increased layer thickness above 80 km is also consistent with variation of the Kolmogorov microscale with height (see e.g., BALSLEY, 1981).

Figure 2 shows a scatter plot of changes in signal power and changes in spectral width observed for a few selected tropospheric range cells in a low-elevation experiment at Millstone Hill. The two regression lines also are shown for each plot. These plots imply that an increase in the signal power is associated with a decrease in spectral width, or an increase in fading time (similar to that observed in the lower mesosphere at Jicamarca). At low elevation angles, for shear-generated turbulent layers, the spectral width is proportional to the layer thickness (WAND et al., 1983).

These observations tend to favor the notion that the observed correlations are an indication of the broadening of turbulent layers by entrainment. Thin layers are possibly generated as a consequence of instabilities in the flow. Eventually the transfer of energy from the background flow into the turbulent layers ceases, and the intensity of turbulence (hence the signal power) must decrease with time due to viscous dissipation. The outer edges of a turbulent layer, however, are usually intermittent and would entrain the ambient non-turbulent fluid into the layer, making it thicker. Regions that have just become turbulent should then show high signal powers confined to narrow spectra. Those containing decaying turbulence would exhibit lower signal power associated with wider spectra, thereby explaining the observed correlation.

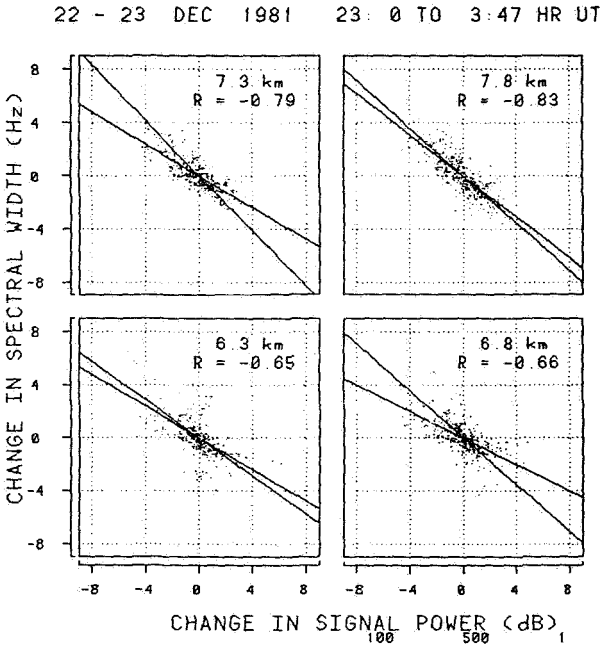


Figure 2. Scatter plots of changes in spectral width and signal power for a few heights in the troposphere observed at a 20 elevation angle with the Millstone Hill radar. The plots have about 400 points each. Trends with periods larger than 30 min have been removed. The two lines of regression and correlation coefficient also are shown. The sense of the implied correlation is similar to that observed in the lower mesosphere with VHF radars. A tentative interpretation is given in the text.

## DISCUSSION

We have briefly discussed some characteristics of the spectra observed with MST radars, that provide interesting insights into the mechanisms that may be responsible for producing the radar returns. Most of the results in this area have been obtained in experiments that use coarse altitude and Doppler resolutions by looking for "statistical" correlations between the low-order spectral moments. A better understanding of the detailed structure of regions of turbulence in the middle atmosphere - and their radar signatures - can be obtained through experiments with improved resolution in altitude (150 m or better) and radial velocity (one to few cm/s). Such experiments may also be helpful in observing isolated cases of the generation, growth and decay of turbulent layers.

## ACKNOWLEDGEMENT

This material is based on work supported by the National Science Foundation under grant number ATM-8000060.

## REFERENCES

Balsley, B. B. (1981), The MST technique - a brief review, J. Atmos. Terr. Phys., 43, 495-509.

Booker, H. G. (1956), A theory of scattering from nonisotropic irregularities with application to radar reflections from the aurora, J. Atmos. Terr. Phys., 8, 204-221.

Booker, H. G. and W. E. Gordon (1950), Theory of radio scattering in the troposphere, Proc. IEEE, 38, 401-412.

Bowles, K. L. (1958), Observations of vertical incidence scatter from the ionosphere at 41 Mc/sec., Phys. Rev. Lett., 1, 454-455.

Countryman, I. D. and S. A. Bowhill (1979), Wind and wave observations in the mesosphere using coherent-scatter radar, Aeron. Rep. No. 89, Aeron. Lab., Dep. Elec. Eng., Univ. Ill., Urbana-Champaign.

Crane, R. K. (1980), Radar measurements of winds at Kwajalein, Radio Sci., 15, 383-394.

Flock, W. L. and B. B. Balsley (1967), VHF radar returns from the D region of the equatorial ionosphere, J. Geophys. Res., 72, 5537-5541.

Fukao, S., T. Sato, R. M. Harper and S. Kato (1980), Radio wave scattering from the tropical mesosphere observed with the Jicamarca radar, Radio Sci., 15, 447-457.

Gage, K. S. and J. L. Green (1978), Evidence for specular reflection from monostatic VHF radar observations of the stratosphere, Radio Sci., 13, 991-1001.

Ishimaru, A. (1978), Wave propagation and scattering in random media, Academic, New York, 572 pp. (in two volumes).

Liu, C. H. and K. C. Yeh (1980), Scattering of VHF and UHF radar signals from the clear air, Radio Sci., 15, 277-282.

Rastogi, P. K. and S. A. Bowhill (1976), Scattering of radio waves from the mesosphere, 2. Evidence for intermittent mesospheric turbulence, J. Atmos. Terr. Phys., 36, 1217-1231.

Rastogi, P. K. and J. Rottger (1982), VHF radar reflections in the vicinity of the tropopause, J. Atmos. Terr. Phys., 44, 461-469.

Rottger, J. (1978), Evidence for partial reflection from VHF radar signals from the clear air, J. Geophys., 44, 393-394.

Rottger, J. (1980), Structure and dynamics of the stratosphere and mesosphere revealed by VHF radar investigations, Pure Appl. Geophys., 118, 494-527.

Rottger, J. and C. H. Liu (1978), Partial reflection and scattering of VHF radar signals from the clear atmosphere, Geophys. Res. Lett., 5, 357-360.

Rottger, J., P. K. Rastogi and R. F. Woodman (1979), High-resolution VHF radar observations of the mesosphere, Geophys. Res. Lett., 6, 617-620.

Ruster, R., P. Czechowsky and G. Schmidt (1980), VHF-radar measurements of dynamical processes in the stratosphere and mesosphere, Geophys. Res. Lett., 7, 999-1002.

Sato, T. (1981), Coherent radar measurements of the middle atmosphere and the design concepts of the MU radar, Ph.D. Thesis, Kyoto Univ., Kyoto, Japan.

Schmidt, G., R. Ruster and P. Czechowsky (1979), Complementary code and digital filtering for detection of weak VHF radar signals from the mesosphere, IEEE Trans. Geosci. El., GE-17, 154-161.

Smith, S. A., G. J. Romick and K. Jayaweera (1983), Poker Flat MST radar observations of shear-induced turbulence, J. Geophys. Res. (in press).

Tatarskii, V. I. (1971), The effects of the turbulent atmosphere on wave propagation, Nat. Tec. Inf. Serv., Springfield, VA, 472 pp.

VanZandt, T. E., J. L. Green, K. S. Gage and W. L. Clark (1978), Vertical profiles of refractivity turbulence structure constant: Comparison of observations with by the Sunset radar with a new theoretical model, Radio Sci., 13, 819-829.

Wand, R. H., P. K. Rastogi, B. J. Watkins and G. B. Loriot (1983), Fine Doppler resolution observations of thin turbulence structures in the tropo-stratosphere at Millstone Hill, J. Geophys. Res., 88, 3851-3857.

Woodman, R. F. (1980), High-altitude resolution stratospheric measurements with the Arecibo 430-MHz radar at Arecibo, Radio Sci., 15, 417-422.

Woodman, R. F. and A. Guillen (1974), Radar observations of winds and turbulence in the stratosphere and mesosphere, J. Atmos. Sci., 31, 493-505.

Woodman, R. F., R. P. Kugel and J. Rottger (1980), A coherent integrator-decoder preprocessor for the SOUSY-VHF radar, Radio Sci., 15, 233-242.

Zrnic', D. (1979), Estimation of spectral moments for weather echoes, IEEE Trans. Geosci. El., GE-17, 113-128.

## 2.3B SPECTRAL CHARACTERISTICS OF THE RETURN

J. Rottger

EISCAT Scientific Association
Box 705
S-981 27 Kiruna, Sweden

Doppler spectra of VHF radar returns typically indicate a Gaussian background shape with superimposed spikes as shown in Figure 1. Here an average of 10 Doppler spectra is shown which was calculated from a time series of 7 min of complex data. One accepts a proper Gaussian fit to the background distribution neglecting the strong amplitude spikes. If this background distribution is due to beam width broadening, either diffuse reflection or rather isotropic scattering is required. If beam width broadening is neglected (mean winds were only 2 m $s^{-1}$ during this observation, which supports this assumption), the width of the distribution $\sigma_S$ is given by turbulent velocity fluctuations $\sigma_w = \sigma_s/k$, where $k = \frac{4\pi}{\lambda}$. For each frequency bin the amplitudes A are Rayleigh distributed. The standard deviation around a mean amplitude $\bar{A}$ is $s_A = 0.8\ \bar{A}/\sqrt{N}$, where N is the number of averaged spectra. Any amplitudes that scatter around $\bar{A}$ by more than $2s_A = 0.5\ \bar{A}$ are not due to scattering from Gaussian-distributed irregularities (with a significance of 95%). Some amplitude spikes exceed the $2s_A$ limit, and we have to assume that these are due to Fresnel reflection. The discreteness of these spikes points to several distinct reflectors moving with radial velocity $w = \omega_o/k$, where $\omega_o$ is the frequency interval where the spikes are observed. It is assumed that the spikes result from reflection at different parts of a corrugated refractivity structure, which is consistent with the model of diffuse refelection. The scattered contribution $C_s^2$ is the integral over the power of the Gaussian background distribution, whereas the reflected contribution $C_r^2$ is the integral over the remaining spikes. From the spectrum shown in Figure 1 we estimate $C_r^2/C_s^2 \sim 0.3$, i.e. the reflected component is about 1/3 of the scattered component.

One may infer from the Doppler spectrum shown in Figure 1 that an interpretation of a "vertical" velocity has to be carefully examined. The spikes, caused by diffuse reflection from corrugated surfaces, may shift considerably the mean value of the spectrum. For a tilted surface of reflection the interpretation can become even worse if one does not measure the incidence angle to correct for off-vertical velocity components. It is assumed that the amplitude spikes due to diffuse reflection indicate a Gaussian frequency distribution such as for the amplitudes due to scattering. However, the mean spectral distribution of spikes must be calculated for a much longer time interval than is needed to determine a turbulence spectrum. This time interval to calculate the distribution of spikes may be much longer than the typical time scales of vertical velocity changes (e.g., due to gravity waves).

### MESOSPHERE

The spectral width of the returned signals is a measure of the rms velocity fluctuations in the scattering region. It has been discussed by ROTTGER et al. (1979) that thicker structures have a larger spectral width, hence larger rms velocity fluctuations. On the average the rms velocity fluctuation $\sigma_w$ found in blobs and sheets below 69 km is $\pm 0.7$ m $s^{-1}$ (corresponding correlation time $\tau = 4$ s), whereas the thicker layers exhibit the largest velocity fluctuations $\sigma_w = \pm 1.7$ m $s^{-1}$ ($\tau = 1.6$ s). This confirms the conjecture relating rms velocity fluctuations and structure thickness, which is based upon a turbulence interpretation. Since thin structures, viz. blobs and sheets, predominantly

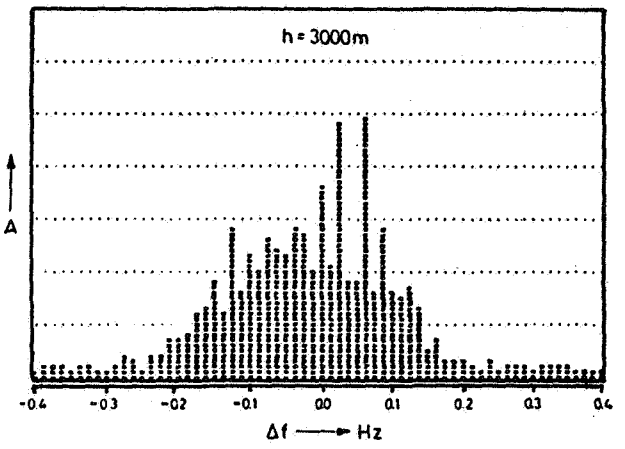


Figure 1. Doppler spectrum measured with vertically pointing antenna. Δf is the Doppler frequency, and A the amplitude in arbitrary units.

occur at lower heights and layers occur at larger heights, an increase in velocity fluctuation with height is in agreement with studies of turbulence by ZIMMERMAN and MURPHY (1977) and 2-3 MHz partial-reflection studies (VINCENT and BELROSE, 1978) that layer thickness (as opposed to the height of occurrence) gives a reasonable indication of the velocity fluctuation to be expected.

REFERENCES

Röttger, J., P. Rastogi and R. Woodman (1979), High-resolution VHF radar observations of turbulence structures in the mesosphere, Geophys. Res. Lett., 6, 617-620.

Vincent, R. A. and J. S. Belrose (1978), The angular distribution of radio waves partially reflected from the lower ionosphere, J. Atmos. Terr. Phys. 40, 35-47.

Zimmerman, S. P. and E. A. Murphy (1977), Stratospheric and mesospheric turbulence, in: Dynamical and Chemical Coupling (ed. B. Grandal and J. A. Holtet), pp. 35-47, D. Reidel Publ. Co. Dordrecht, Holland.

## 2.4A INTERPRETATION OF RADAR RETURNS FROM CLEAR AIR - DISCRIMINATION AGAINST CLUTTER

J. Rottger

EISCAT Scientific Association
S-981 27 Kiruna, Sweden

Generally, different kinds of interference may cause problems to the proper detection and analysis of the atmospheric signals, when using VHF and UHF radars. We may separate these into passive and active contributions.

Passive contributions are existent in the receiving system without the radar transmitter switched on. There are: P1) noise from the receiver/antenna system, P2) noise from cosmic sources, the sun and planets, P3) noise from the earth's surface, P4) noise from the earth's atmosphere, P5) interference from man-made sources (signals from communication and broadcast transmitter, ignition and machinery noise etc.).

Active contributions are due to scatter and reflection of the own transmitted radar signal from unwanted targets, which are called clutter. These active contributions are due to clutter from: A1) fixed and stationary targets on the earth's surface, e.g., power lines, transmitter towers, mountains, buildings and any kinds of erased structures, A2) surface waves of rivers, lakes and oceans, A3) ships, A4) motor cars, A5) aircrafts (and rockets, during special experiments), A6) satellites, A7) moon, planets (and sun), A8) atmospheric turbulence, A9) ionospheric irregularities.

The passive contributions have different effects depending on the operation frequency. P1 normally has to be regarded only at UHF, P2 is the main noise source at VHF, P3 has to be regarded only at UHF with low elevation antenna angles, P4 is negligible at UHF and VHF. P5, interference from man-made sources depends strongly on location and can be minimized by good suppression of low elevation antenna sidelobes, although strong nearby transmitters still may cause crucial interference. Also tropospheric ducting will increase the interference level from distant transmitters. A critical problem may arise in the low VHF band if transhorizon propagation via ionospheric reflection becomes possible.

In any case, care must be taken that the unavoidable interference signals do not saturate any stages of the receiver or move these into the nonlinear regime. Cross modulation effects then would prohibit proper suppression of the interference during the data analysis.

Of major importance to radar systems are active interference contributions. Different methods can be applied for elimination or at least suppressing unwanted effects. These are:

(1) Directional filtering, i.e., applying optimum suppression of antenna sidelobes,

(2) Range filtering, i.e., suppressing unwanted signals only in affected range gates,

(3) Selection by amplitude distributions,

(4) Temporal filtering, i.e., recognizing typical temporal variations of the clutter signals, viz, spectral characteristics, and applying matched filters.

Application 1, obviously needs a fairly good optimization of the antenna pattern and may need additional shielding or screening of the antenna. Since the cross sections of all the clutter targets A1-A9 may often be substantially larger than the cross sections of wanted atmospheric targets and the clutter signal still may be strong, applications 2, 3 and 4 should always be considered.

Applications 2, 3 and 4 mostly go together, since clutter targets with different characteristics will occur in different range gates. The simplest application of 2 is just for the case of stationary clutter targets (A1), yielding constant echo amplitudes in specified range gates. The easiest way then is to measure an average stationary clutter profile as a function of range and antenna position and subtract it during each following measurement. This of course has to be done according to amplitude and phase. However, all other clutter echoes A2-A9 are not stationary, and even echoes from fixed targets (A1) can fade due to tropospheric propagation effects.

Application 3, i.e., determining the amplitude distributions of signals, may help in some cases to detect an unwanted signal. The amplitude distribution of an echo from a very slowly varying target can be described by a Rice distribution, whereas atmospheric scatter has a Rayleigh distribution. Deciding which kind of distribution the echoes belong to then may allow to detect a false signal, but will not eliminate it.

One also can use a method of maximum likelihood to determine if wanted or unwanted signals are observed. One for instance does not expect clutter from ionospheric irregularities (A9) at ranges shorter than 100 km, if care is taken to avoid range ambiguities. Echoes from targets on the earth's surface (A1) and clutter from sea surface waves (A2), ships (A3), and motor cars (A4) will not occur at distances greater than the radio horizon of the antenna, if edge effects on mountain ridges, multiple scattering, ionospheric reflection or tropospheric ducting can be excluded. Echoes from moving targets are normally characterized by a U-shape variation of clutter power with range.

The most efficient way to detect and eliminate clutter echoes is by application 4, namely applying matched filters. This essentially works for slowly moving targets, since the fast moving targets, such as aircrafts, satellites, moon etc. (A5-A7) cause fast frequency changes which cannot be resolved with typical interpulse-period sampling rates of MST radars. This aliasing effect results in an increase of the noise power, since the clutter returns are non-coherent. The power due to scatter of these point sources decreases inversely with $(\text{distance})^4$, as compared to the $(\text{distance})^2$ variation of volume scatter from atmospheric turbulence. Thus, problems will not be too severe if the clutter target is at a far distance. However, it can be very critical at too close distances, since the effective cross section, or aircrafts for instance, is fairly large yielding very strong clutter signals even in the antenna sidelobes. A solution would be to set up MST radar systems far away from any aircraft flight routes.

Matched filters can be applied to eliminate clutter which exhibit "well-behaved" frequency characteristics, such as ground clutter, sea clutter and partly also the clutter from atmospheric turbulence (and ionospheric irregularities). In case of slowly varying processes, such as clutter from ships, cars, and sea clutter with frequency changing due to tides, adaptive filters can be applied.

In Figure 1 we have shown a selection of spectra-height-intensity plots to demonstrate some of these effects. The experiments to obtain these spectra were carried out at the Arecibo Observatory with a 46.8-MHz radar using the 305-m dish as antenna (ROTTGER et al., 1981). The antenna beam with 1.7° half-power width was pointed at a fixed azimuth to different zenith angles (ZE) of 1.7°,

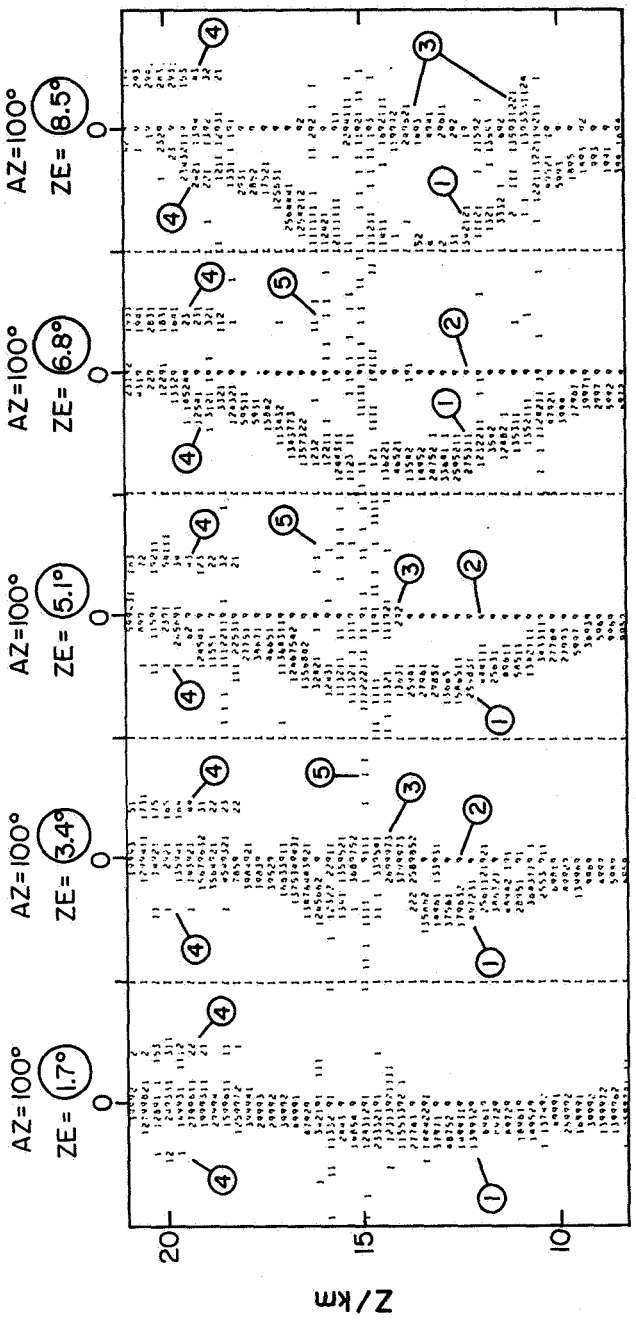


Figure 1. Spectra-height-intensity plots of VHF radar signals. ① = atmospheric echo, ② = nonfading ground clutter, ③ = atmospheric clutter due to sidelobe into zenith direction, ④ = sea clutter, ⑤ = noise.

3.4°, 5.1°, 6.8° and 8.5°. For each range gate (of 300 m increment) the amplitude of the Doppler spectra was normalized to its maximum value. The numbers 9 in the plots correspond to the maxima. The range covered by these radar experiments was from about 8 km to 21 km. Echoes from atmospheric turbulence, (1), carried with the wind, cause a Doppler shift which fairly continuously varies with range. The Doppler shift increases with zenith angle because the radial velocity component (in direction of the beam) of the horizontal wind increases with zenith angle. This effect can be used as a straightforward criterion to discriminate atmospheric echoes from clutter.

Strong ground clutter (2), having zero Doppler shift, is observed at all ranges. However, at ZE = 3.4° and some other angles this clutter widens (3). It became obvious during our experiments that this effect is due to atmospheric clutter received through sidelobes pointing towards the zenith. This kind of clutter can be strong because of the aspect sensitivity of the tropospheric and stratospheric VHF radar echoes. To reduce (or eliminate) this effect, a zenith angle of the antenna main lobe (e.g., ZE = 6.8° in these VHF radar experiments at A.O) should be chosen where sidelobes pointing close to the zenith are sufficiently suppressed.

Clutter from ocean waves (4) occur in Figure 2 at ranges larger than 18 km, which is due to sidelobes close to the horizon. This clutter occurs at positive and negative Doppler frequencies due to approaching and departing ocean waves (having different amplitudes). The phase velocity of the ocean surface waves is directly depended on their wavelength, such that the frequency offset $\pm fs$ of the scattered radar waves is fixed. It may be shifted, however, due to (tidal) currents. To eliminate the sea clutter a notch filter could be applied, which on the other hand also would affect a wanted signal. Also a low-pass filter could be used, if the atmospheric signal has lower Doppler shift than fs (e.g., at ZE = 1.7°). Too small zenith angles would yield too low accuracy and problems with separating the atmospheric scatter from ground clutter.

An optimum approach to select or separate the atmospheric signal from different types of clutter is by applying a non-linear curve fitting procedure as it was done by SATO and WOODMAN (1980). They had to apply this procedure to data taken with the 430 MHz radar at A.O., where they found that even the ground clutter faded slowly (causing a line broadening) and could not be eliminated by high-pass filtering (viz. dc-subtraction). They assumed a theoretical function shape of the power spectral components of clutter and the desired echo. They also considered some a priori knowledge of clutter/signal signatures, e.g., the ground clutter has almost a symmetrical spectrum, whereas this is not the case for almost every atmospheric signal (ZE>0°). The sea clutter also in a first approach can be expected to be in well defined frequency channels symmetrical to zero, but having different amplitudes and a small common offset due to ocean currents. The fitting procedure of Sato and Woodman allowed to detect even signals having -50 dB signal-to-clutter radio. An example of a fitting result is shown in Figure 2 (by courtesy of T. Sato), where the spectra of the atmospheric signals found by this technique are inserted. From these fitted spectra, the essential parameters signal power, Doppler shift and spectra width can be directly deduced.

In summary, we find that several methods exist and are applied to eliminate or suppress clutter effects in the data analysis. It must be regarded, however, that clutter influences should be suppressed as early as possible, i.e., by properly selecting antenna location, antenna and receiver design.

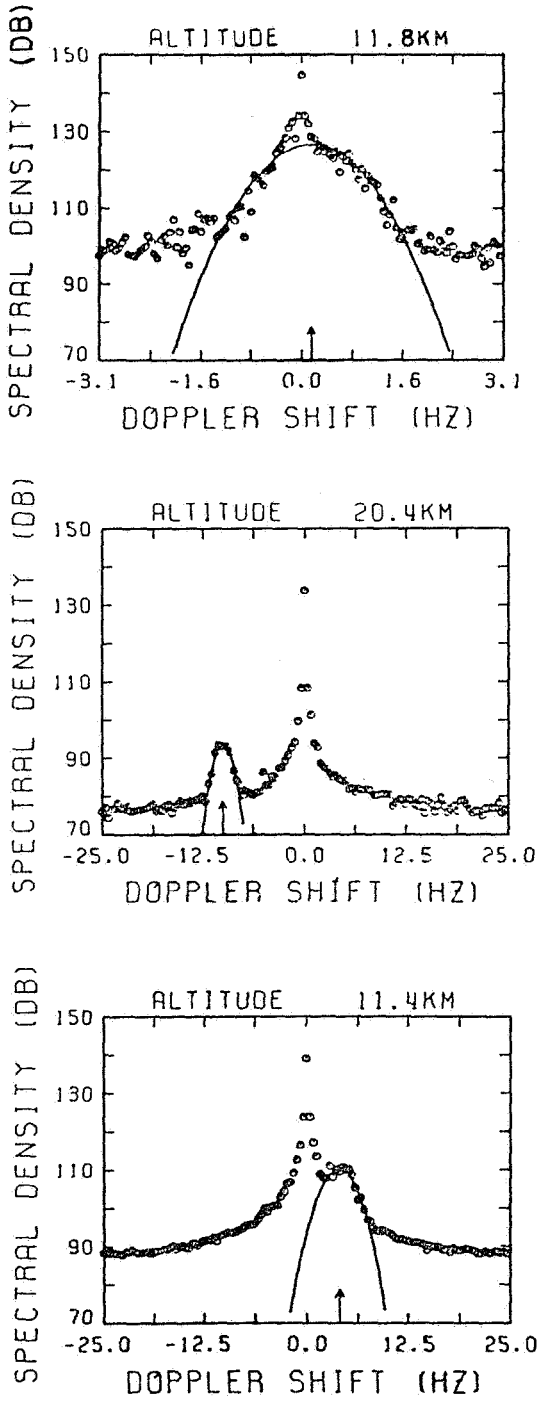


Figure 2. Optimum fitting of model signal spectra to signal + clutter data.

REFERENCES

Rottger, J., P. Czechowsky and G. Schmidt (1981), First low-power VHF radar observations of tropospheric, stratospheric and mesospheric winds and turbulence at the Arecibo Observatory, J. Atmos. Terr. Phys., 43, 789-800.

Sato, T. and R. F. Woodman (1980), Spectral parameter estimation of CAT radar echoes in the presence of fading clutter, Proc. 19th Conf. on Radar Meteorology, Miami, FL.

# 2.4B DISCRIMINATION AGAINST INTERFERING SIGNALS AT THE POKER FLAT MST RADAR

D. A. Carter

Aeronomy Laboratory
National Oceanic and Atmospheric Administration
Boulder, Colorado 80303

At the Poker Flat, Alaska, MST radar several on-line and off-line data processing techniques are used to remove interfering signals due to ground clutter, aircraft, instrumental effects, and external transmissions from the desired atmospheric echoes. The on-line, real-time techniques are necessarily simple in order to minimize processing delays, but can be of great value in improving the data operated on by the more extensive off-line, post-processing algorithms.

At Poker Flat the return from ground clutter has a very narrow spectral width. Even at the finest radial velocity spectral resolution (down to 30 cm/sec or .01 Hz) the ground return is entirely at the dc frequency point and can be filtered out by simply subtracting the mean from the time series. A more significant problem with ground returns is the large dc offset which appears on the receiver outputs. The ground return at Poker Flat actually overdrives the receiver in the first 2-3 km. The dc offset greatly increases the dynamic range needed in the ADCs to sample the atmospheric signal. In order to detect the weakest signals, the receiver output level must be large enough so that the rms noise level occupies more than one resolution bit level of the ADC and the maximum signal must be less than the full-scale range of the ADC. In order to improve the low-altitude response of the radar, the dynamic range of the receiver would have to be improved and, if the ground return signal exceeds the ADC range, higher resolution ADCs or range-variable attenuators may need to be considered.

Both the Poker Flat and Platteville MST radars have used a very simple on-line scheme for detecting short-lived contamination such as airplanes. This algorithm examines the individual Doppler spectra which are computed every 2-4 seconds (for oblique antenna beams) rather than the spectral averages which are written to magnetic tape every 1-3 minutes. The total spectral power in each individual spectrum is computed by summing all the spectral points. If this integrated power increases from one spectrum to the next by a factor greater than a pre-selected threshold, then that spectrum is not added to the spectral sum. Succeeding spectra are compared to the last acceptable spectrum. Only a certain maximum number of spectra are allowed to be rejected in succession.

This algorithm seems to work quite well. The tropospheric and stratospheric atmospheric echo power changes rather slowly on a time scale of a few seconds. By using selection criteria on individual spectra every few seconds rather than on averaged spectra every few minutes, short-term interference, such as an airplane, is easier to detect and less data are lost. This is most helpful when high time resolution data are required. The above technique is no longer being used at the Platteville radar. The primary aim of that radar at present is to obtain long-term wind profiles. A sample random consensus technique is used on mean Doppler shifts obtained every few minutes to calculate an hourly mean velocity (see Strauch, this volume, p. 528). The consensus algorithm selects the largest subset of data values which fall within a specified range of each other. This algorithm could also be applied to the unaveraged velocities and signal-to-noise ratios.

At Poker Flat it is possible to use echoes from meteor trails to obtain wind estimates at heights and times when turbulence echoes may not be present. Each meteor echo lasts for only a few seconds and because of the narrow radar beam, only a few echoes occur per hour. These short-lived echoes are therefore greatly smoothed over when spectra are averaged for several minutes. The detection rate of these echoes would be significantly improved by applying the above short-term "interference" detection algorithm to segregate the meteor echoes from the longer-averaged turbulence echoes.

Several off-line processing techniques are applied to the spectral averages recorded at Poker Flat on magnetic tape. Most of these algorithms have been developed and refined by Anthony Riddle of CIRES.

Only spectra whose signal-to-noise ratios exceed a given threshold are considered significant and used in the succeeding analysis. The time series of both signal-to-noise ratio and mean Doppler velocity at each height are examined for values which deviate beyond a certain limit from a running mean of previous values. Occurrences of external RF interference can also be detected by discarding the spectra at all ranges if the number of ranges with significant echoes increases suddenly or if echoes appear in a group of range gates near 40-km height, where no turbulence echoes are expected to be seen with the current radar configuration. Another type of spectral interference whose source appears to be equipmental occurs in the first few range gates where extraneous spikes often appear in the Doppler spectra. The true signal is extracted by examining the shape of the spectrum and the location of the spikes (see Riddle, this volume, p. 546).

In summary, we have found that by using all of these techniques in combination, good success at removing interference can be achieved.

## 2.4C PULSE STUTTERING AS A REMEDY FOR ALIASED GROUND BACKSCATTER

S. A. Bowhill

Aeronomy Laboratory, Department of Electrical Engineering
University of Illinois
Urbana, IL 61801

The Urbana MST rdar operates at a prf of 400 Hz, with a frequency of 40.92 MHz. This frequency is in fact the lowest of the operating MST radars. As a result, at times of high sunspot activity and under winter daytime conditions, when the critical frequency of the F2 layer is at its greatest, sidelobes of the antenna can provide energy which is reflected by the F2 layer. This energy can then be backscattered from the ground and reradiated into the same antenna sidelobe.

Although the antenna directivity will attenuate this signal by approximately 40 or 50 dB, it nevertheless represents a troublesome source of interference. Ranges of 1000 to 3000 km, with time delays of 7 to 20 msec, will alias the scattered energy over several transmitted pulses (at 2.5 msec intervals). Examples of this effect are shown in Figure 1, compared to a normal 2-hour period at the same season in Figure 2.

The unwanted ground scatter is shown as a sequence of velocity plots which are almost typical at the various altitudes. The reason for this is that gravity waves produce changes in the height of the F layer, thereby giving a change in range of time that falls in the same general range as that from the mesosphere. Also, the ground forms a soft target similar to mesospheric turbulence, thereby producing a fade rate which is similar to that for mesospheric echoes.

One possibility would be to reduce the transmitter prf to a value such that the ground backscatter from one pulse had completely died out before another pulse is transmitted. However, this would require a decrease of a factor of 10 in the prf, with a resulting degradation of radar performance.

A second possibility, which we have implemented successfully, is to change the interpulse period in a cyclic way, thereby destroying the coherence of the unwanted signal. To accomplish this, the interpulse period must be changed by an amount at least equal to the transmiitted pulse width, and optimum performance is obtained when the number of different interpulse periods occupies a time span greater than the coherence time of the unwanted signal. Since a 20-msec pulse width is used, it was found convenient to cycle through 50 pulses, the interpulse period changing from 2 msec to 3 msec during the 1/8-second time. This particular pattern of interpulse periods was provided by a software radar controller, using an Apple II microcomputer with the timing program written in FORTH. With application of this algorithm, the unwanted scatter signal becomes incoherent from one pulse to the next, and therefore is perceived as noise by the coherent integrator and correlator.

ACKNOWLEDGMENTS

The work described was supported in part by the National Aeronautics and Space Administration under grant NSG 7506 and in part by the National Science Foundation under grant ATM 81-20371.

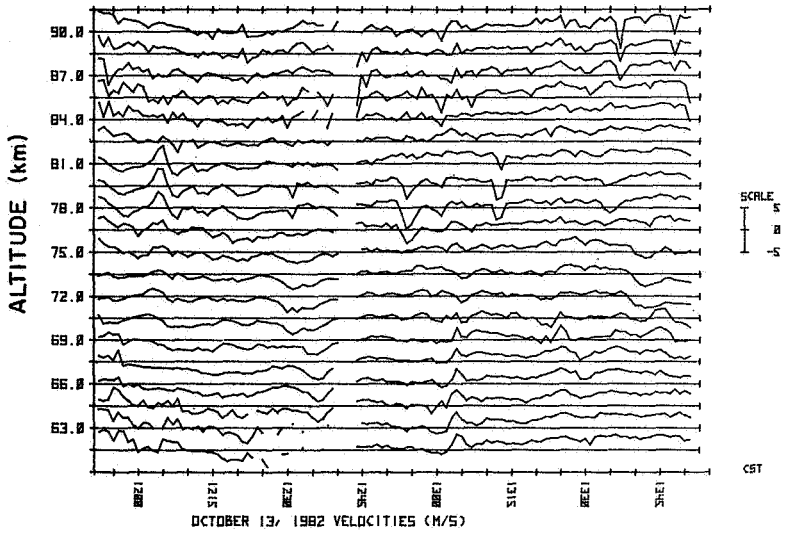


Figure 1. Typical velocity record in the presence of aliased ground backscatter.

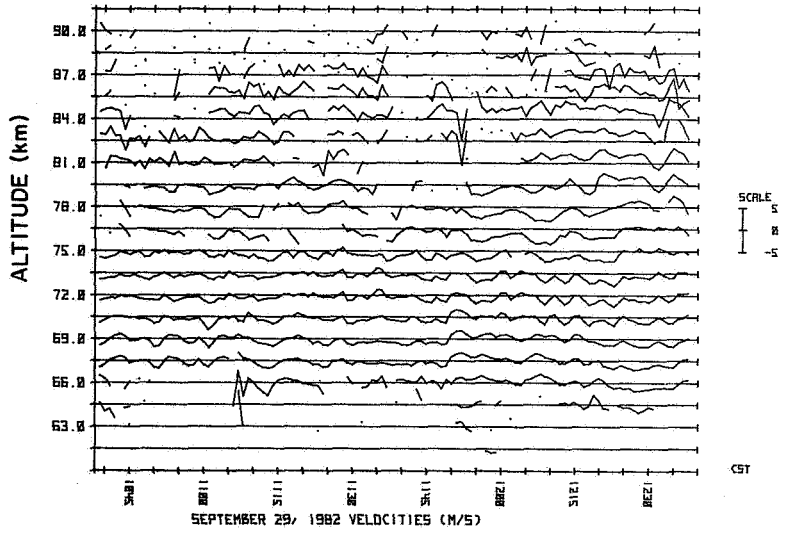


Figure 2. Typical velocity record in the absence of aliased ground backscatter.

# 2.5A THE $\Delta R$ VS $(\Delta R)^2$ QUESTION - THE PULSE-LENGTH DEPENDENCE OF SIGNAL POWER FOR FRESNEL SCATTER

W. K. Hocking

Max-Planck-Institut fur Aeronomie
D-3411 Katlenburg-Lindau, FRG

It has been proposed that the enhanced echoes from the atmosphere observed with a vertically pointing radar are due to reflections from horizontally stratified layers. The general case in which there are many closely spaced layers at random heights has been called "Fresnel scatter". The variation of received power with transmitter pulse length is examined for various models of Fresnel backscatter. It is shown that for the model most often used in previous work, the power is proportional to the pulse-length ($\Delta r$), and not to the pulse length squared. However, for more general models a pulse-length dependence more complex than either ($\Delta r$) or $(\Delta)^2$ is found.

## 1. INTRODUCTION

Radar backscatter at VHF from the troposphere and stratosphere shows at times evidence of weak partial reflections from extended horizontal irregularities. These irregularities are at least a Fresnel zone in horizontal extent, and fluctuate in the vertical by less than about $\lambda/8$ over this horizontal distance. Here, $\lambda$ is the radar wavelength. This type of reflection is in addition to scatter due to turbulence-induced irregularities (e.g., GAGE and GREEN, 1978; ROTTGER and LIU, 1978; ROTTGER, 1980a). GAGE et al. (1981a) have proposed that these scatterers occur at random heights in the atmosphere, and have then, using this simple assumption, proceeded to determine the expected dependence of backscattered power on the radar and atmospheric parameters. GAGE et al. (1981a) will be denoted by GBG here. The model was also discussed in GAGE and BALSLEY (1980), GREEN and GAGE (1980), GAGE et al. (1981b) and BALSLEY and GAGE (1981). The formula which GBG produced took the form

$$P_R = \frac{\alpha^2 P_t A^2}{4\lambda^2 r^2}[F(\lambda).\bar{M}]^2(\Delta r)^2 \qquad (1)$$

This formula is only relevant for the case in which the same array is used for both transmission and reception. $P_R$ is the received power, $\alpha$ is the array efficiency, $P_t$ is the peak transmitted power, $A_e$ is the array effective area, $\lambda$ is the radar wavelength, r is the range of the scatterers, M is the mean generalized refractive index gradient, and $F(\lambda)$ is a "calibration constant" which must be determined empirically for each radar. The term ($\Delta r$) represents the pulse width.

Most of equation (1) is intuitively reasonable, but the $(\Delta r)^2$ terms appears to be odd. In this paper, the procedures adopted in obtaining this $(\Delta r)^2$ dependence will be carefully re-examined. It will be shown that there were errors in this original formulation, and that a proper treatment leads to a ($\Delta r$) dependence.

This paper will primarily present the arguments for and against the $(\Delta r)^2$ formula, although some mention will be made of generalizations of the Fresnel model. A more complete discussion has been presented elsewhere (HOCKING and ROTTGER, 1983).

## 2. PHYSICAL PICTURE

A simplified view of the model presented in GBG is presented in Figure 1a. We will begin by discussing this simple model, and then will generalize it to gather complexity.

Imagine that a square pulse of duration $\Delta T$ is transmitted upwards into the atmosphere, and at some time $t_o/2$ the pulse is centred at a height $z_o$ ($t_o$ is the time for the pulse centre to go to height z and be reflected back to the ground). Consider a vertical region of length $c\Delta T/2$, centred on $z_o$, and assume that within this volume, there are seven reflectors, of equal reflection coefficient but at random heights. Each reflector will reflect the pulse for a time duration $\Delta T$, and at time $t_o = 2z_o/c$ (where c is the speed of the radio waves), some part of the pulse will arrive back at the ground from each of these 7 reflectors. No signal will arrive at time $t_o$ from reflectors outside of this region. (i.e., The received signal is a convolution between the pulse shape and the reflection coefficient profile.) The seven reflected signals will have approximately equal strengths, but because the reflectors have random heights, each signal will arrive back at the ground with random phase. The resultant signal may be described by the dark vector in the right-hand diagram of Figure 1a; that is, it is the sum of 7 vectors of equal strength but random phase. This is simply the classical two-dimensional random walk problem, as first described by RAYLEIGH (1894). It is well known that the modulus of the resultant vector of the two-dimensional random walk problem has a "Rayleigh distribution", and that the mean square length of the resultant vector is proportional to the number of contributing vectors. Thus if we double the pulse length to $\Delta T'$ and the mean number of reflectors per unit height remains the same at all heights, then we have approximately 14 reflectors in the new length $C\Delta T'/2$ in Figure 1a. As a result, an approximate doubling of the square of the resultant vector can be expected when the pulse length is doubled.

Of course in the above discussion we dealt with small numbers of randomly phased vectors, and strictly speaking the Rayleigh distribution is only relevant for large numbers of vectors. Nevertheless, even for the cases of these small numbers of vectors, the mean power is still proportional to the number of vectors, provided that the reflectors are allowed to fluctuate vertically in time (so that each reflected component has a uniform phase distribution between 0 and $2\pi^c$), and that the mean power is calculated over a long time interval. Naturally, however, the fluctuation in power about the true mean (relative to the true mean) will be smaller when larger numbers of reflectors contribute. More to the point, however, the above problem is only illustrative, and is unlikely to properly model the real atmosphere. Therefore, let us increase the complexity of the model. The above analysis at least gives one an intuitive feel that the power should be proportional to the pulse length.

A more general model is represented by Figure 1b. In this case, many reflectors are assumed to exist within one pulse length, but they are allowed to have varying reflection coefficients. This situation is analogous to that assumed in GBG. The situation is now far more complex than the classical random-walk problem. Nevertheless, HOCKING and ROTTGER (1983) showed that by dividing the reflectors into subsets of equal strength, it could be shown that the resultant vector will still be proportional to the number of contributing vectors, provided that the amplitude distribution of these vectors remains unchanged, and their phases are genuinely random. BECKMANN (1962) has considered the problem more rigorously and more generally, and has shown that the vector sum of a large set of vectors $\{ \underline{s}_i \}$, which have an arbritrary amplitude distribution but random phases distributed uniformly between 0 and $2\pi$, is a vector with a Rayleigh distribution of amplitudes. Furthermore, BECKMANN (1962) has shown that the mean squared length of the resultant vector is proportional to the number of contributing vectors, in line with the above discussion. These

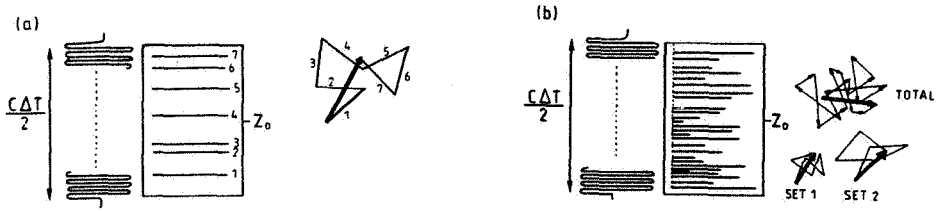


Figure 1. Pictorial description of reflection from a group of reflectors distributed randomly in height. The pulse is illustrated to the left in each figure, and the reflectors and their strengths are indicated by the horizontal lines.

results are also consistent with NORTON et al. (1955).

Therefore, it may be expected that the received power is proportional to the pulse length.

The above arguments also apply if an arbitrary form of pulse shape is used, rather than a square pulse. Provided the pulse shape is sufficiently long that many reflectors contribute to any signal, the picture is still similar to Figure 1b, but the amplitude of the pulse may change within the region $c\Delta T/2$. This simply weights the reflection coefficients, but the signals contributing to the total power at any instant are still due to signals reflected from a range of reflectors. These contributing signals are still uniformly distributed between 0 and $2\pi$ radians in phase, and the effect of the pulse is simply to modify the amplitude distribution of the component vectors. Thus the results outlined above still apply.

We may now make a general statement. If we have a sequence of vectors $\{\underline{s}_i\}$, which have an arbitrary amplitude distribution and a uniform phase distribution $(0\text{-}2\pi c)$, and this sequence is multipled by an envelope function E, then the vector sum of the resultant vectors $\{\underline{E}_i \underline{s}_i\}$ obeys the relation

$$\overline{S^2} \propto W_E, \tag{2}$$

where $W_E$ is the width of E, defined in any manner, and $\overline{S^2}$ is the mean square vector sum. This relation is true for any specific envelope shape, but cannot of course be used to compare powers between different envelopes.

It should be pointed out that if one or two of the specular reflectors are much stronger scatterers than all the others, the above statistical treatment is no longer valid. These cases require special consideration (e.g., RICE, 1944, 1945; BECKMANN, 1962), but were not considered in the model of GBG and so will not be considered here.

## 3. GBG TREATMENT

In this section, the treatment adopted by GBG will be briefly outlined. For a more detailed treatment, the original paper could be consulted, as the description given here will be largely qualitative. Nevertheless, the principle is so simple that the "pictorial" treatment given here actually describes the model adequately.

The approach adopted by GBG goes as follows. The reflection coefficient profile r(z) can be considered as the sum of many sinusoidal oscillations, of varying vertical scale, and varying amplitude. For example, the curves a, b and c in Figure 2 represent three of these. The amplitudes of these various scales can be found simply by Fourier transforming r(z).

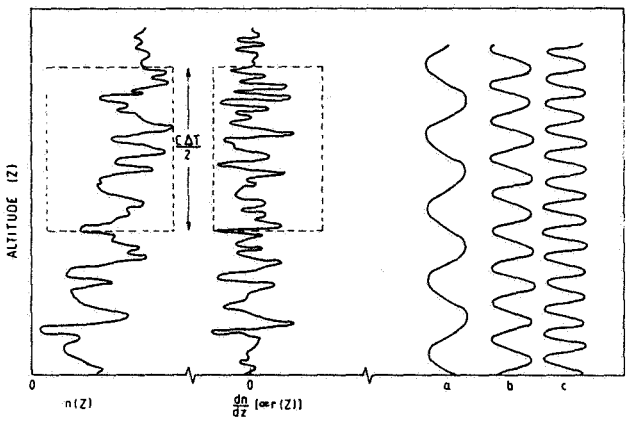


Figure 2. Typical profiles of refractive index n(z), reflection coefficient r(z), and 3 examples of Fourier components of r(z).

Then GBG state that the pulse is comprised of only one frequency, so only one of these vertical scales is important -- namely, the scale with a node-to-node distance of $\lambda/2$, $\lambda$ being the radar wavelength (i.e., this is the Bragg backscatter scale). The received signal amplitude at the ground is proportional to the number of oscillations in length $c\Delta T/2$. Doubling the pulse length effectively doubles the number of oscillations of this Bragg scale, increasing the amplitude received at the receiver by a factor of 2, and therefore the power by a factor of 4. A generalization of this discussion clearly suggests that the received power is proportional to the square of the pulse length.

## 4. THE ERROR IN THE GBG ARGUMENT

The argument in the previous section contains one error, and this is in the description of the transmitted pulse. GBG stated that a pulse consists of only one frequency, but by definition a single, pure frequency must be infinite in extent. A pulse comprises a spectrum of Fourier components, centred on the central frequency. As a result, a pulse comprises a range of wavelengths, and so in the description outlined in Figure 2, a finite spectrum of Fourier scales must produce backscatter. Since r(z) is a random function of height, the phases of these contributing Fourier components are random. Each scale therefore produces a reflected signal, and each signal arrives at the ground with different phase. These signals have random phase, so a "random-walk" type problem again results.

It can be seen that a proper analysis is more complex than the simple description given by GBG. In the following section, the pulse-length dependence of the scattered power will be re-derived from the point of view of consideration of these various scales. It will be seen that the treatment given by GBG is inadequate, and the results of section 2 will be reinforced through this alternative approach.

## 5. QUANTITATIVE TREATMENT

Suppose that the pulse field strength at time t and height z is given by

$$z^{-1} \cdot g(t-z/c) \cdot \exp\{j\omega(t-z/c)\}, \qquad (3)$$

where $\omega$ is the carrier frequency, and g describes the pulse envelope. In this simple description, it has been assumed that the pulse travels at a speed c(= the speed of light in a vacuum), and absorption has been ignored.

For simplicity, the $z^{-1}$ dependence will be ignored. Let the pulse at z=0 be written as

$$g_t(t)\, e^{j\omega t} = g_z(\xi) e^{\frac{2j\omega\xi}{c}} = \underline{g}_p(\xi). \tag{4}$$

The function $g_t$ defines the pulse envelope, we have allowed $\underline{g}_p$ to be in general complex, and $\xi = ct/2$ is a length coordinate. We will consider only the case of $g_t$ symmetric about its maximum, as this is almost always valid for real experiments. The following results are probably true generally, independent on this symmetry refinement, but these asymmetric cases will be ignored for simplicity. Let us also associate a phase with r(z), where the phase is determined by the height of the reflector above the ground, z. Then r(z) can be regarded as a complex profile, $\underline{r}(z)$. After backscatter from the reflection profile $\underline{r}(z)$, the signal received at time $\tau_o$ can be shown to be given approximately by

$$\begin{aligned} \underline{a}(z_o) &\propto \underline{r}(z_o) * \underline{g}_p(z_o) \\ &\propto \int_{-\infty}^{\infty} \underline{r}(z)\, \underline{g}_p(z_o - z)\, dz, \end{aligned} \tag{5}$$

where $z_o = c\tau_o/2$.

That is to say that the received signal is a convolution between $\underline{r}(z)$ and $\underline{g}_p(z)$ (e.g., AUSTIN et al., 1969). It is convenient to work in the spatial domain, which is the reason that $z_o$ has been used. The value $z_o$ can be approximately regarded as the height from which most of the scattered signal received at time $\tau_o$ was reflected.

Now introduce the functions $\underline{A}$, $\underline{R}$, and $\underline{G}$, defined as the Fourier transforms of the functions $\underline{a}$, $\underline{r}$ and $\underline{g}_p$. That is,

$$\begin{aligned} &\underline{a}(z) \leftrightarrow \underline{A}(\zeta) \\ &\underline{r}(z) \leftrightarrow \underline{R}(\zeta) \\ &\underline{g}(z) \leftrightarrow \underline{G}(\zeta), \end{aligned} \tag{6}$$

where $\zeta$ is the reciprocal coordinate of z. ($\zeta$ plays the same role to z as frequency does to time; the $\zeta$ coordinate will be referred to as "reciprocal space".) Then, by the convolution theorem (e.g., BRACEWELL, 1978),

$$\underline{A}(\zeta) = \underline{G}(\zeta).\, \underline{R}(\zeta). \tag{7}$$

Thus the signal strength received at the receiver can be found in the following way. First, find $\underline{r}(z)$, and then find its Fourier transform $\underline{R}(\zeta)$. Then find the Fourier transform of the pulse, $\underline{G}(\zeta)$. If $\underline{R}$ and $\underline{G}$ are multiplied, and then reverse Fourier-transformed, the signal amplitude $\underline{a}(z)$ can be found. This description is identical to the description given in section 4, except that in this case we began by assuming a convolution in the spatial domain, whereas in section 4 we went directly to the reciprocal space domain. This shows that the treatment in section 2, and the discussion in sections 3 and 4, are in fact different ways of viewing the same problem. We must now complete the analysis in the reciprocal space domain quantitatively, to show that it does in fact produce a pulse-length dependence for power. Given that GBG chose to work in the reciprocal-space domain, the following section gives the form of analysis which they should have adopted.

Since $\underline{r}(z)$ is a random function of height, then $\underline{R}(\zeta)$ is a random function of $\zeta$. Therefore the function $\underline{A}(\zeta)$ is a random function with an envelope described by $\underline{G}(\zeta)$. Schematic examples of $\underline{R}$ and $\underline{G}$ are shown in Figure 3, where $g_p(z)$ is taken as a Gaussian function, so $\underline{G}$ is a Gaussian function centred on $\zeta = 2/\lambda$.

In any physical experiment, it is normal to "mix" the central frequency down to 0 Hz, and for convenience we will do this in this theoretical consideration. This simply means that $\zeta = 2/\lambda$ is shifted to $\zeta = 0$. Figure 4a shows an example of $\underline{A}(\zeta)$ after such a shift has been performed, and this function is denoted by $\underline{A}_o(\zeta)$. Also shown (schematically only) in Figure 4 is the amplitude, $|\underline{a}|$, and phase, $\phi_a$, of $\underline{a}(\zeta)$, which might typically result after $\underline{A}_o(\zeta)$ has been reverse Fourier transformed. Notice that no large variations in $|\underline{a}|$ or $\phi_a$ can occur over distances of z of less than about one pulse length of $g_p(z)$. This is because $G(\zeta)$ defines a limited frequency band of non-zero values $A_o(\zeta)$, so no frequencies outside this band can occur in $\underline{a}(\zeta)$.

In any real situation, $\underline{r}(z)$ will change as a function of time, and therefore so will $\underline{a}(z)$. The powers $|\underline{a}(z)|^2$ at any height z may be averaged to produce a mean over some time interval T. This gives the mean power at height z. Since $\underline{r}(z)$ is random, there is no "preferred" z value, and after sufficient averaging, $|\bar{a}|^2$ will be a constant, independent of z. Therefore it is only necessary to look at one height, and for convenience we choose z = 0.

By definition,

$$\underline{a}(z) = \int_{-\infty}^{\infty} \underline{A}(\zeta) e^{j2\pi z\zeta} \, d\zeta \qquad (8)$$

so for z = 0

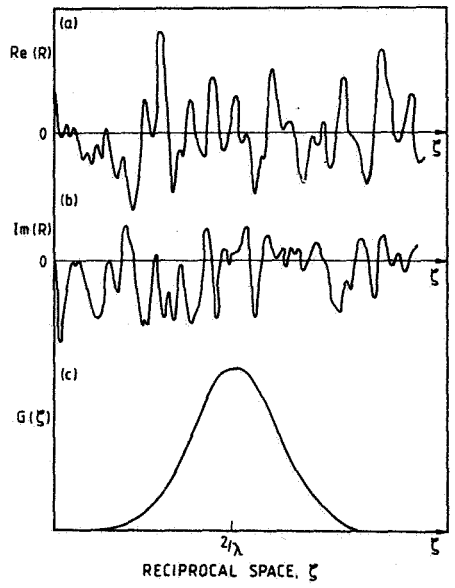


Figure 3. Schematic illustration of $R(\zeta)$, the Fourier transform of the reflection coefficient profile. (a) is the real part, (b) the imaginary component. Graph (c) shows the Fourier transform of the transmitted pulse.

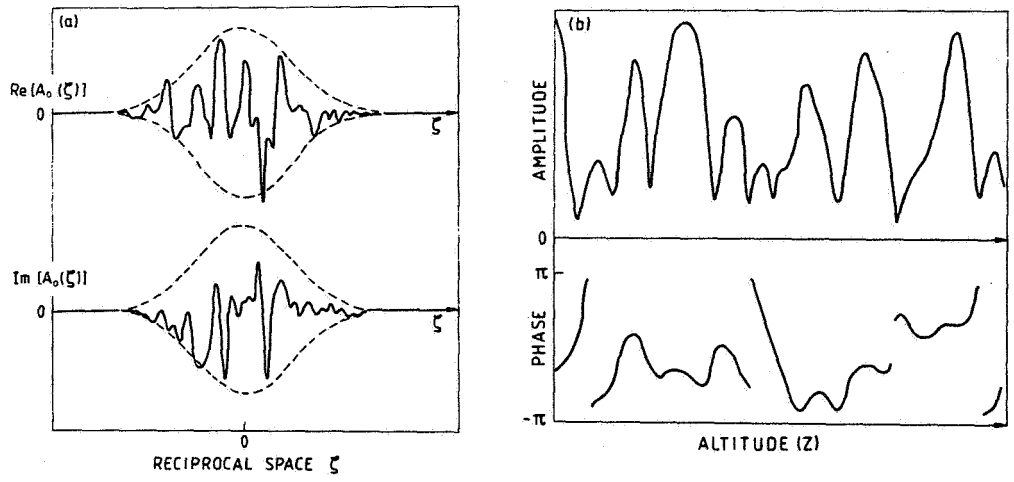


Figure 4. (a) The function $A_o(\zeta)$ (see text). (b) Typical amplitude and phase which might be recorded at any instant after reflection from the atmosphere, as a function of height, z.

$$\underline{a}(0) = \int_{-\infty}^{\infty} \underline{A}_o(\zeta)d\zeta. \tag{9}$$

In other words, $\underline{a}(0)$ can be regarded as the "complex area" under $\underline{A}_o(\zeta)$. If we take $d\zeta = \Delta\zeta$ as a sufficiently small constant,

$$|\underline{a}(0)| = |\Delta\zeta \sum_{n=1}^{N} \underline{A}_o(\zeta_i)| \quad (= |\Delta\zeta \sum_{n=1}^{N} (G(\zeta_i)R(\zeta_i)|) \tag{10}$$

This amounts to simply vectorially summing a set of vectors $\{\Delta\zeta\underline{A}_{oi}\}$. It is clear that we are confronted with a very similar problem to that in section 2 -- namely, we have a random sequence of vectors $\{\Delta\zeta R(\zeta_i)\}$, which we multiply by some envelope $G(\zeta_i)$, and then we add to produce resultant. We wish to know how the modulus of the vector sum varies as we change the envelope width. The only difference compared to section 2 is that here the vectors are functions of reciprocal space, whilst in section 2 we were dealing with vectors which were functions of z. Clearly, then, the results in section 2 apply, and we see that if we hold the peak amplitude of $G(\zeta)$ fixed, and define the "width" of $\underline{G}(\zeta)$ as $W_G$, then the vector $\underline{a}(0)$ obeys the relation (2): i.e.,

$$|\overline{\underline{a}(0)}|^2 \propto W_G. \tag{11}$$

The width W may be defined in any way (e.g., half-power width, $e^{-1}$ width, etc), provided the definition is invariant for the chosen function.

Equation (10) deals with the width of $\underline{G}(\zeta)$. It is now necessary to determine how changing the width of the Tx pulse $\underline{g}_p(\zeta)$ affects $\underline{G}(\zeta)$. Two results from Fourier transform theory are first necessarily. Firstly, the width of $g_p$ is inversely related to the width of G: i.e.,

$$W_{gp} \propto W_G^{-1} \tag{12}$$

and secondly,

$$\underline{g}_p(0) = \int_{-\infty}^{\infty} \underline{G}(\zeta) d\zeta. \tag{13}$$

(conversely, $\underline{G}(0) = \int_{-\infty}^{\infty} \underline{g}_p(z)\, dz$).

We are now in a position to examine the pulse-length dependence of the received power. As seen in equation (10), we have the following "random-walk" problem. We have a sequence of random vector $\{\Delta\zeta R(\zeta_i)\}$, and we multiply them by an envelope $\{G(\zeta_i)\}$. We know that the transmitted pulse $\underline{g}_p(z)$ may change in width but must maintain constant peak amplitude $g_p(0)$. Changing the width of $g_p(z)$ affects both the width and peak value of $G(\zeta)$. The width of $G(\zeta)$ is inversely proportional to the width of $g_p(z)$ (by (12)). This fact, together with (13), means that the peak value of $G(\zeta)$ must be proportional to the width of $g_p(z)$ when $g_p(0)$ is held fixed. Thus both the width and peak value of $G(\zeta)$ change. If we consider the rescaling of the function $G(\zeta)$ and keep its width constant for now, we see that this simply increases all the vectors $\{\Delta\zeta R(\zeta_i)\, G(\zeta_i)\}$ by a factor proportional to $W_{gp}$. This must therefore rescale the total power by $W_{gp}^2$ times. Now, we must only consider the effect of changing the width of the function $G(\zeta)$. Equation (2) can be applied here, so it is clear that changing the width of G changes the power proportionally to $W_G$.

Combining the above effects, we have

$$|\overline{\underline{a}(0)}|^2 \propto W_{gp}^{\ 2}\, W_G \tag{14}$$

for the case of unchanging pulse peak power, and using (12),

$$\overline{|a(z)|^2} \propto \underline{W}_{gp}. \tag{15}$$

(We have already shown that $\overline{|a(z)|^2} = \overline{|a(0)|^2}$ for all z).

This proves that the mean square received power is indeed proportional to the pulse width, even when viewed from the inverse space domain.

## 6. COMPUTER SIMULATION AND GENERALIZATION OF ASSUMPTION

Computer tests have been done to test equation (1), since that equation is crucial to all the arguments presented here. A Monte Carlo approach was adopted (e.g., SCHREIDER, 1967). The details of these tests will not be given here. It is suffice to say that equation (2) was completely verified by these numerical simulations.

This Monte Carlo approach also allowed a generalization of the assumptions made by GBG. In the troposphere the mean reflectivity decreases approximately exponentially with height (e.g., BALSLEY and GAGE, 1981). Therefore the situation of a pulse incident on such a reflectivity structure has been investigated. In such circumstances, varying the pulse width will vary the form of the amplitude distribution of the reflected signals, and so the pulse-length dependence for scattered power is no longer simply proportional to ($\Delta r$). The details of this simulation can be found in HOCKING and ROTTGER, (1983), but the results are summarized here with Figure 5. Suppose that the RMS reflectivity as a function of height is $\langle r^2(z)\rangle^{1/2}$, and that $\langle r^2(z)\rangle^{1/2}/z$ takes the form $\exp(-z/H)$. Suppose that a Gaussian pulse of half-power full width h is transmitted. Then the received backscattered power is a function of h/H, and follows the form indicated in Figure 5. Clearly for $h > 0.5 \times H$, the power is no longer simply proportional to the pulse width.

## 7. DISCUSSION

In any experiment to test the pulse-length dependence of backscattered power, various precautions are necessary, or else misleading results can ensue.

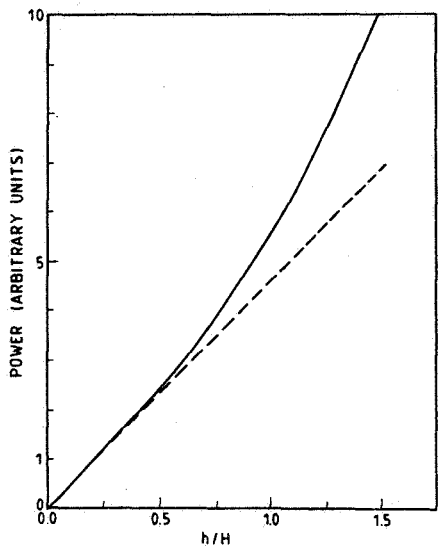


Figure 5. Plot of received power as a function of the ratio of the pulse width to the scale height of the reflection strengths, for the case of an exponential decay in reflection strength with height.

Firstly, it is important that the receiver has sufficient frequency bandwidth to accommodate the pulse. For example, imagine the situation of transmitting a Gaussian pulse, and using a receiver matched to the pulse. (This is normally done, in order to optimize the signal-to-noise ratio.) If the transmitted pulse $g_p(z)$ is now made narrower, the peak value of $G(\zeta)$ falls proportionally. But if the receiver bandwidth is not widened to accommodate the wider range of frequencies, then equation (14) becomes

$$|\underline{a}(0)|^2 \propto [W(g_p)^2] . 1, \tag{16}$$

and the received power appears to be proportional to the square of the pulse width. In fact, in any real investigations of this reflecting process, the effective pulse is not simply the transmitted pulse but rather that pulse convolved with the impulse response of the receiver. This last point is important, and care must be taken in performing receiver matching. The receiver bandwidth must not be just equal to the bandwidth of the Fourier transform of the pulse, but considerably wider. For example, suppose that the transmitted pulse is described by $g(t)$, and the Fourier transform of $g(t)$ is $G(\omega)$, $\omega$ being the angular frequency. Let the receiver response be also $G(\omega)$ -- then the effective transmitted pulse is not $g(t)$, but rather $g(t)*g(t)$ -- or a function roughly $\sqrt{2}$ times wider than the transmitted pulse. The receiver response should be flat over all non-zero values of $G(\omega)$ in order that the effective pulse is the same as the transmitted pulse.

Secondly, if the receiver is matched to the transmitted pulse on all occasions, it is interesting to look at the signal-to-noise ratio. Doubling the pulse width doubles the received power -- but if the noise is constant as a function of frequency over the bandwidth of the receiver, and the receiver band width is halved, to match the transmitter, then the received noise power also decreases by a factor of 2. For the case of VHF radars, the main noise is cosmic noise, and this can be regarded as constant over the band width of most VHF systems. Thus the signal-to-noise ratio is proportional to the square of the pulse length. It is important in any experimental test of the preceding theory to measure absolute power, and not signal-to-noise ratios.

HOCKING and ROTTGER (1983) presented a preliminary test of the above theory, using experimental data from the SOUSY radar. These results are summarized in Figures 6a-c. Figure 6a shows the experimentally observed power profile for a 150 m pulse after averaging over a period of 50 min. Figure 6b shows the profile which would have been observed had a pulse of length 1.5 km been used, with peak power equal to that of the 150 m pulse. A factor (1500/150) has been removed from this figure for ease of comparisons. This profile 6b was produced by computer manipulations; the details are discussed in HOCKING and ROTTGER (1983).

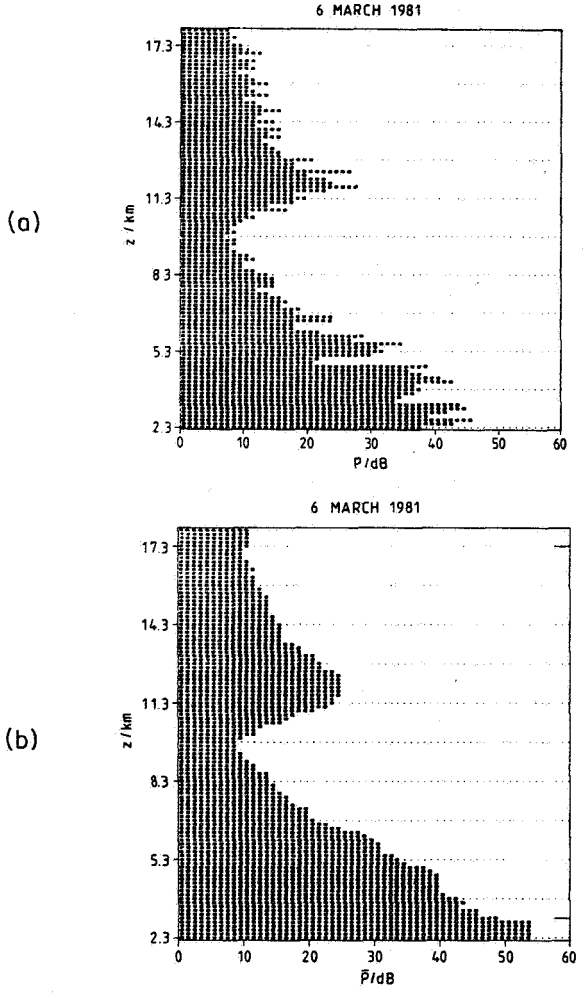


Figure 6. (a) Mean power as a function of height, recorded with the SOUSY radar on 6 March 1981. The noise has not been subtracted; the noise level was about 5-8 dB. (b) The resulting profile which would have resulted from using a pulse with a coarser resolution.

Figure 6c shows a comparison of the 2 profiles -- and it can be seen that they are in approximate agreement, now that the factor (1500/150) (i.e., the ratio of the pulse resolutions) has been removed from the low resolution profile. This is support for an approximately ($\Delta r$) power dependence. However, a great many more experimental results are necessary to properly test the theory. Also, agreement is not perfect in Figure 6c; this is discussed further in HOCKING and ROTTGER (1983).

Figure 6d shows the power as a function of height and time during this recording interval, after the mean power profile for the period has been removed. Notice the existence of certain stable, well-defined echoes. These are not consistent with the "Fresnel Scatter" model of GBG, and their existence must be borne in mind. This point is discussed further in HOCKING and ROTTGER (1983). The Fresnel scatter model may have relevance to the atmosphere, but it is not always applicable.

(c)

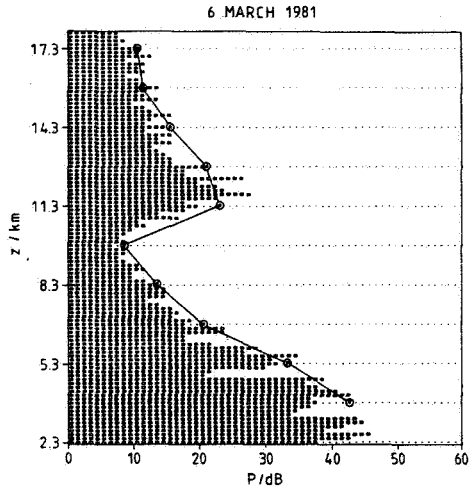


(d)

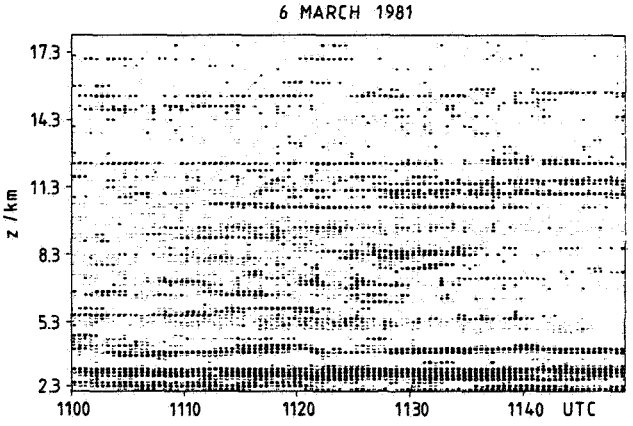


Figure 6. (c) A composite of (a) and (b). The solid line shows Figure 6(a) taken at steps of 1500 m. (d) Details of the echo strengths as a function of time during the period used to form the mean profile 6(a). Darker spots indicate greater intensity. The mean profile over the period has been subtracted, so these plots are "residual signal strengths".

## CONCLUSION

The Fresnel scatter model by GAGE et al. (1981a) has been critically examined. It has been found that equation (1) is in error, and the $(\Delta r)^2$ part should simply read $(\Delta r)$. Appropriate adjustment of $F(\lambda)$ is also necessary.

In the more general case of an exponential decay of $\langle r(z)^2 \rangle^{1/2}/z$ with height, a more complex proportionality results, and this has been illustrated with a numerical Monte Carlo approach.

## ACKNOWLEDGEMENTS

The paper was written while the author was sponsored by an Alexander von Humboldt stipend.

## REFERENCES

Austin, G. L., R. G. T. Bennett and M. R. Thorpe (1969), J. Atmos. Terr. Phys., 31, 1099-1106.

Balsley, B. B. and K. S. Gage (1981), Geophys. Res. Lett., 8, 1173-1175.

Beckmann, P. (1962), J. Res. Nat. Bur. Standards, 66D, 231-240.

Bracewell, R. N. (1978), The Fourier Transform and its Applications, McGraw-Hill Kogakusha Ltd., Tokyo, London, Paris, Sydney, 444 pp.

Gage, K. S. and B. B. Balsley (1980), Radio Sci., 15, 243-257.

Gage, K. S., B. B. Balsley and J. L. Green (1981a), Radio Sci., 16, 1447-1453.

Gage, K. S., W. L. Ecklund, J. L. Green and B. B. Balsley (1981b), Preprint vol., 20th Conf. on Radar Meteorology, Boston, Mass., pp 11-14.

Gage, K. S. and J. L. Green (1978), Radio Sci., 13, 991-1001.

Green, J. L. and K. S. Gage (1980), Radio Sci., 15, 395-405.

Hocking, W. K. and J. Rottger (1983), Radio Sci., 18, 1312-1324.

Norton, K. A., L. E. Vogler, W. V. Mansfield and P. J. Short (1955), Proc. of IRE, 43, 1354-1361.

Rayleigh, Lord. (1894), Theory of Sound, vol. I, pps 35-42, Macmillan and Co.

Rice, S. O. (1944), Bell Syst. Tech. J., 23, 282-332.

Rice, S. O. (1945), Bell Syst. Tech. J., 24, 46-156.

Rottger, J. (1980a), Radio Sci., 15, 259-276.

Rottger, J. (1980b), Pageoph., 118, 494-527.

Rottger, J. and C. H. Liu (1978), Geophys. Res. Lett., 5, 357-360.

Rottger, J. and G. Schmidt (1979), IEEE Trans. Geosc. Electr., GE17, 182-189.

Schreider, Yu. A. (1967), The Monte Carlo Method, Pergamon Press, London, New York, Sydney.

# 2.6A JICAMARCA MESOSPHERIC OBSERVATIONS

O. Royrvik

Department of Electrical Engineering
University of Illinois
Urbana, IL 61801

In explaining the scattering of VHF radar signals from the mesosphere there are two observational facts that must be accounted for. These are: 1) the aspect sensitivity of the scattered signal and that this aspect sensitivity is largest in the lower part of the mesosphere; and 2) the correlation between the scattered power and the signal correlation time. This correlation tends to be positive in the lower part of the mesosphere, but changes to negative in the upper part of the mesosphere.

This behavior is similar to that of the scattering from the troposphere/stratosphere region, and it has been suggested that the scattering mechanisms are similar in these three regions. In particular, it has been suggested that a mixture of scattering from isotropic irregularities and partial reflection from stratified layers could explain the observed characteristics of radar signal returns from the mesosphere.

Several different experiments have been performed at the Jicamarca radar in Peru. They all show strong indications of aspect sensitivity and changing correlation between scattered power and correlation time. The results from two of these experiments will be considered here.

If as suggested, the aspect dependence of scattered power and signal correlation time is due to a mixture of scattering from isotropic irregularities and reflections from stratified layers, one would expect to see a clear difference in the signal spectra in the vertical and off-vertical antennas. Perhaps a near Gaussian distribution of scattered power in the off-vertical antenna representing the turbulent scatter, and a superposition of the same Gaussian and one or more discrete peaks in the vertical antenna, representing both the scattered and the reflected component of the received signal. As can be seen from the two examples in Figure 2, the spectra in the two antennas are very similar and there is no hint of a reflecting layer in the vertical antenna. Nevertheless, there is a substantial aspect sensitivity where the scattered power in the vertical antenna is about 50% larger than that of the off-vertical antenna. There is also a slight tendency for the correlation time in the vertical antenna to be larger than that in the off-vertical antenna, as one would expect from the correlation times in Figure 1. We tentatively conclude from these data that there is no indication of stratified reflecting layers unless these layers are modulated in space and time to a degree that they cannot be distinguished from turbulence in any other way than that they cause somewhat aspect sensitive scattering.

An interferometer technique can be used to study small-scale horizontal variation in the amount and Doppler shift of the scattered signal. Data were obtained during the spaced antenna drifts experiment run on October 17, 1981 (ROYRVIK, 1983). By forming the cross spectra between sets of two antenna sections we can determine the principal direction to the scattering volume with a certain Doppler shift. Direction differences transform into horizontal distances at a certain altitude range.

In Figure 3 frequency spectra are presented for five altitudes having substantial scattered power. The phase of the frequency component has been plotted only for those frequencies with substantial power in order to reduce clut-

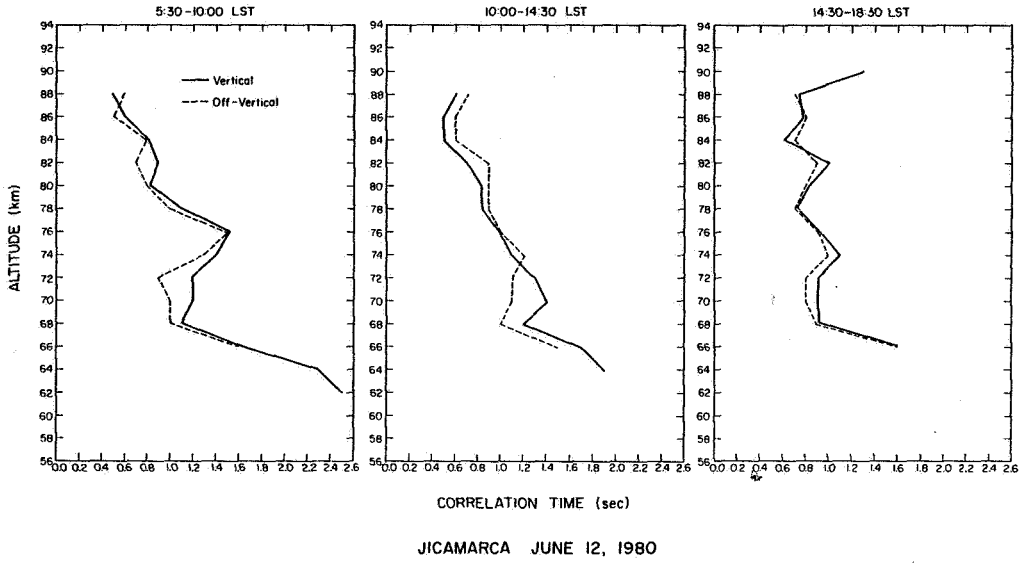


Figure 1. Signal correlation time for June 12, 1980 for vertical and west antenna sections.

ter in the figures. It can be seen from the figure that there is a tendency for the direction of the scattered signal to change systematically with changing frequency for all altitudes except 70 km. From closer study of the data it appears that the tendency at the higher altitudes is quite clear in aligning these variations in the east-west direction, whereas at 67 km the direction of alignment appears more random. Also the occurrence of these phase changes is limited to short (1-3 min) intermittent time periods. One might suspect these observations to be the result of beam width broadening due to the differential line-of-sight velocity component of the horizontal velocity. However, this differential velocity is negligible in an antenna beam of only 1° beam width. In the present case where the horizontal velocity is shown to be about 10 m/s (ROYRVIK, 1983) the broadening of the spectra will be about 0.03 Hz, or only a couple of percent Doppler broadening. Also the phase shift that would result from the observed wind field (ROYRVIK, 1983) is opposite to the phase shift actually observed. The most likely explanation appears to be one where individual peaks in the frequency spectra represent individual scattering cells with large-scale organized motions. For example, a turbulent cell caused by wind shear would have a large-scale rotating motion corresponding to the outer scale of turbulence. In the simple case where only one cell is present within the antenna beam, one would expect to observe different Doppler shifts in different directions as the one seen at 79 km in Figure 3. From the examples in Figure 3, and other examples, it is estimated that typical horizontal dimensions of these scattering cells are from 200 to 600 meters, with a few occasions where there are indications of even larger horizontal dimensions. At about 67 km the horizontal dimension seems to be somewhat smaller, but still in the range of hundreds of meters. Also the rotational velocity is smaller at lower altitudes resulting in narrower spectra. Most of the irregularities that show a directional dependence of the spectra indicate positive Doppler shift to the east and negative Doppler shift to the west. This is consistent with a rotating cell of irregularities resulting from a wind shear where higher westward wind velocities occur at higher altitudes. Seen by the radar, only the vertical velocities will show up in the spectra and one would expect the most positive Doppler shift to be to the east (Figure 4).

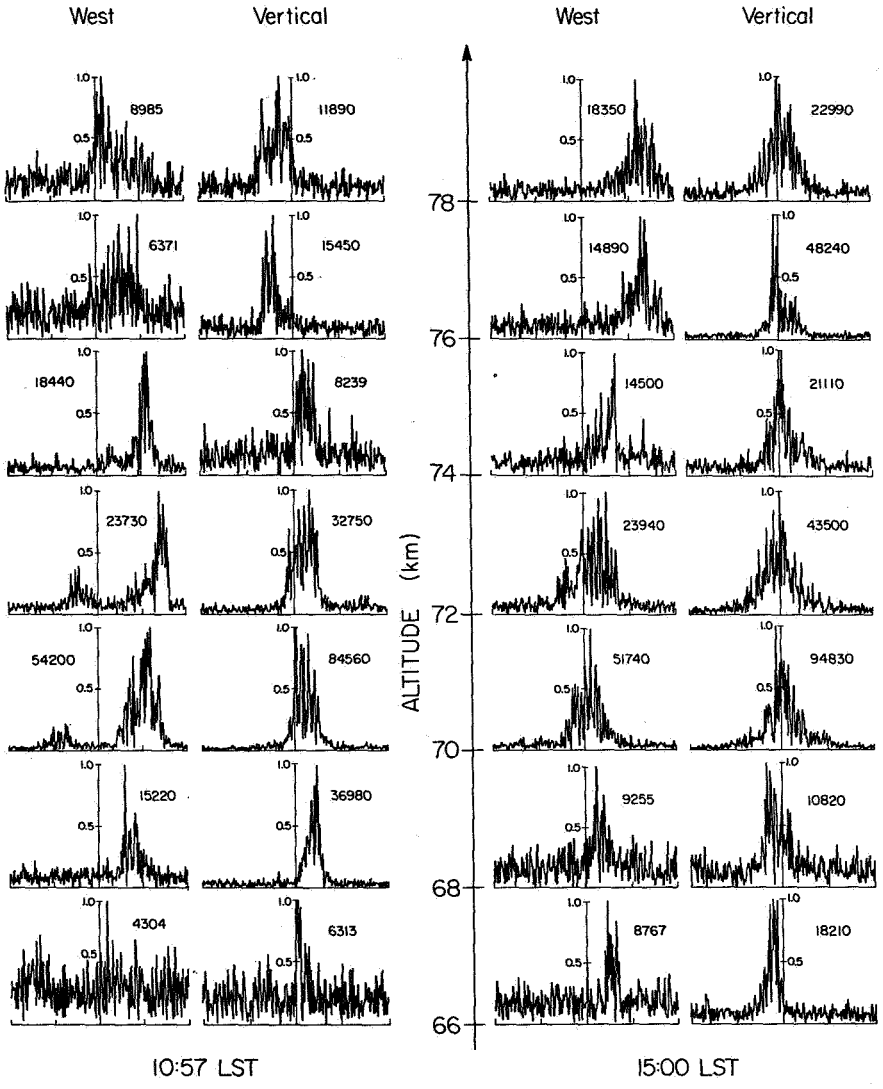


Figure 2. Frequency spectra for vertical and west antenna sections for June 12, 1980.

## DISCUSSION

A substantial amount of effort has gone into the study of the mechanism scattering HF and VHF radio waves from the mesosphere between 60 and 90 km although the question is far from settled. Stratified layers have been suggested as a source for that part of the scattered signal that is aspect sensitive. It has also generally been taken for granted that turbulence-induced irregularities in the refractive index are both isotropic and homogeneous, and thus accounts for that part of the scattered power that is not aspect sensitive. It cannot be concluded from these data that no stratified layers give rise to reflection from the mesosphere, but if stably stratified layers exist, they are not stable and stratified enough to be easily distinguished

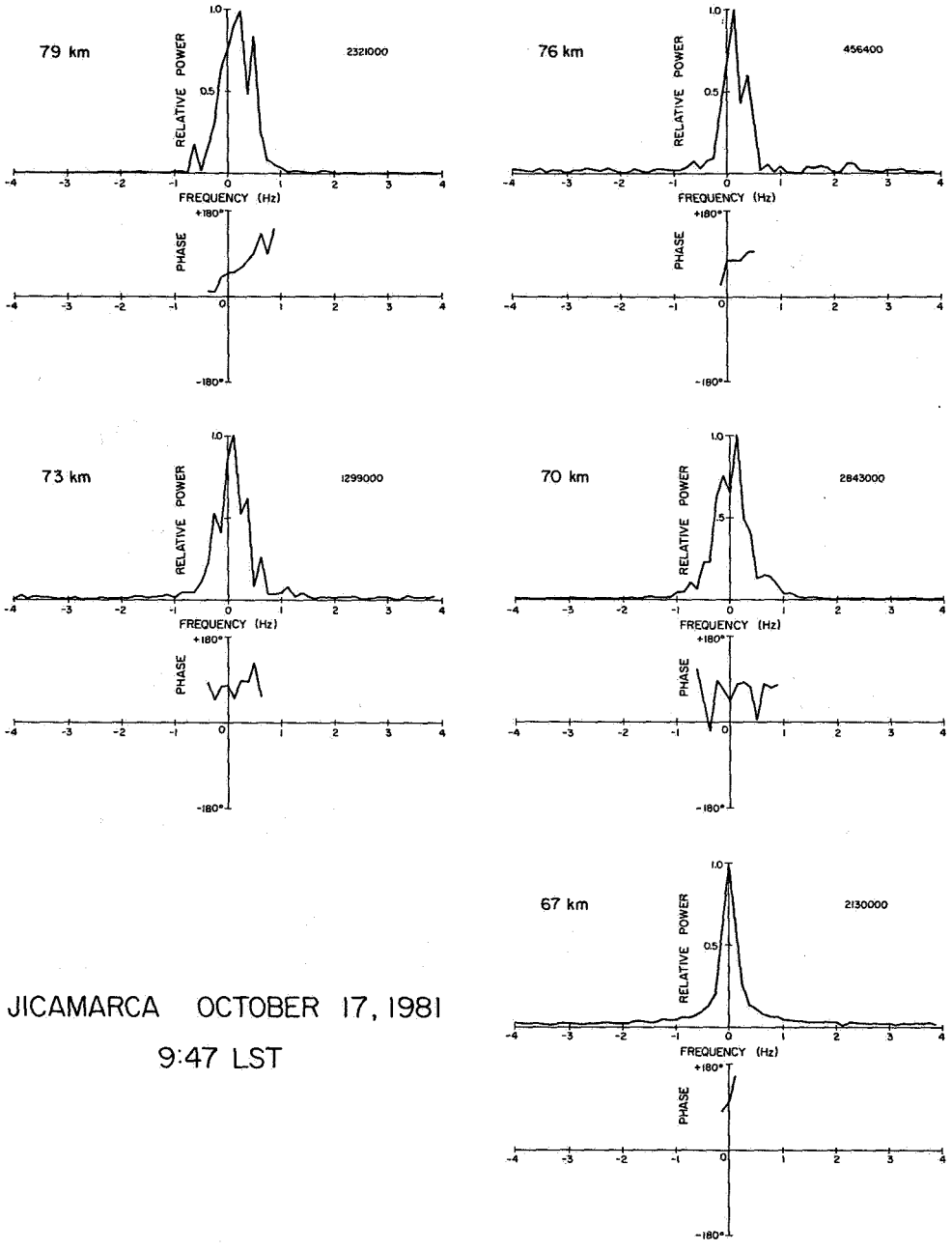


Figure 3. Cross spectra for October 17, 1981. To reduce clutter the phase has been deleted from those frequencies where the scattered power is small.

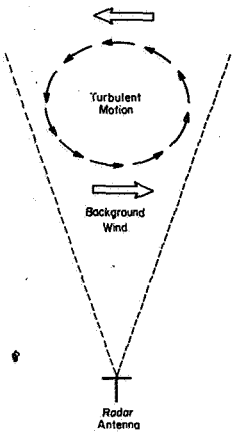


Figure 4 Diagram showing the rotating motion resulting from a wind shear.

from turbulence scatter occurring in the same range gates. It is also difficult to believe that a stratified layer could form and survive for any length of time; and it surely must take some time to form in the presence of shear induced turbulence.

Also, in the lower part of the mesosphere around 60 km, the temperature profile is such that the atmosphere is close to being convectively unstable, whereas at altitudes above 60 km it becomes more and more stable with increasing altitude throughout the mesosphere. It thus seems strange to suggest that stable stratified layers should form in the lower, but not in the upper, part of the mesosphere.

It seems more likely that the turbulence is anisotropic with larger horizontal than vertical dimensions. Such anisotropic irregularities have been reported in boundary layers observations (STEWART, 1969; MESTAYER et al., 1976 and GIBSON et al., 1977) which show anistropy in both temperature and velocity variations. To the degree that temperature is a scalar tracer in these experiments, and that the condition in surface boundary layers and jets apply to the situation of shear layers in the mesosphere, it is of interest to study these results further.

Clearly from these evidences it is not satisfactory to consider the turbulence in the mesosphere as isotropic, homogeneous and time stationary. It seems much more appropriate to discuss the scattering from the viewpoint of generation and decay of Kelvin-Helmholtz instabilities as presented by WOODS (1969); PELTIER et al. (1978); SYKES and LEWELLEN (1982) and other.

It seems reasonable to interpret the rotating cells as Kelvin-Helmholtz vortexes in the process of being "rolled-up". Given a typical observed value for the horizontal dimension of a K-H billow in the mesosphere of 300 m and assuming a Richardson number of 0.2 we find from comparison with the computer results of SYKES and LEWELLEN (1982) that the billow layer should be about 100-200 m thick.

It is also seen from the computer model study that irregularities are generated not only in the K-H billows, but also in the braids that connect the billows, and in a broader turbulent region resulting from the horizontal spreading and collapse of the billows. The large-scale irregularities are nearly horizontally stratified. It may be assumed that the mean shear that causes the large-scale anisotropy also causes anisotropy in the small-scale

irregularities responsible for the scattering of the 50-MHz radio waves. Although this does not necessarily follow from the computer study of SYKES and LEWELLEN (1982), strong experimental evidence for this anisotropy exists.

It appears that there should be no problem in explaining the aspect sensitivity of scattered radio signals as resulting from anisotropic turbulence at the scale of 3 meters. It does become a problem, however, to explain why this aspect sensitivity is substantial at 60-70 km, but decreases to almost zero at higher altitudes. Perhaps it is a result of changing turbulent conditions resulting from a change in the mean temperature gradient and/or a change in the viscosity of the atmosphere.

There remains the problem of positive correlation between scattered power and signal correlation time below 70 km and the change to a negative correlation above this altitude. The negative correlation is generally believed to be related to isotropic turbulence following the Kolmogorof model. The explanation for the positive correlation may be found in the spatial and temporal differences in the distribution of turbulent kinetic energy affecting the correlation time, and the distribution of electron-density variations representing scattered power. Comparing Figures 2 and 10 of SYKES and LEWELLEN (1982) it is seen that the strongest scatter ought to occur in the remnants of the braids, a region that has little turbulent kinetic energy. On the other hand, somewhat less scattering will occur at the periphery of the K-H billows, in a region where there is quite strong turbulent velocity fluctuations. Since the time scale of this development is on the order of 10 minutes, it is reasonable that the positive correlation between scattered power and signal correlation time should be observed when the integration period is on the order of one minute. Furthermore, it appears from the correlation between aspect sensitivity and correlation time that the largest anisotropy of the scattering irregularities ought to occur in the braids and not in the billows. Again, the question to be answered is, why does the scattering change from being dominated by the large-scale K-H instabilities at altitudes below 75 km to be almost homogeneous and isotropic above this altitude. One possible answer is that both the inner and outer scale of turbulence increases with increasing height, bringing the scattering wavelength further and further away from the horizontally stratified region at the outer scale, and close to what may be an isotropic region at the inner scale of turbulence.

On the other hand, if it is assumed that the received signal results from a mixture of scattering and partial reflection, one must conclude that the amplitude of the reflected signal varies more than that of the scattered signal, in order to explain the positive correlation between scattered power and signal correlation time. This can be proven mathematically, however, two short examples are more instructive.

First assume a constant reflecting layer with correlation time of say 1 min. Add a continuously increasing amount of scattered signal with 1 s correlation time. It is clear that as the amount of scattered signal, and thus total signal, increases the total signal correlation time will decrease. This will give a negative correlation between scattered power and signal correlation time.

Secondly, assume a constant amount of scattered power with correlation time ot 1 s. Add a continuously increasing amount of reflected signal with 1 min correlation time. As the reflected signal and the total signal increase the signal correlation time will increase from 1 s to 1 min. This gives a positive correlation between the signal power, and the signal correlation time.

This larger variation in reflecting layers than in scattering turbulence may be hard to explain.

It is concluded that there is no strong evidence for a mixture of scattered and reflected signals from the mesosphere. Anisotropic turbulent scatter appears to be a more likely explanation.

ACKNOWLEDGMENT

The work described was supported by the National Science Foundation under grant ATM 80-19563.

REFERENCES

Gibson, C. H., C. A. Freike and S. O. McConnell (1977), Structure of sheared turbulent fields, The Physics of Fluids, 20,S156.

Mestayer, P. G., C. H. Gibson, M. F. Coantic and A. S. Patel (1976), Local anisotropy in heated and cooled turbulent boundary layers, The Physics of Fluids, 19, 1279-1287.

Peltier, W. R., J. Halle and T. L. Clark (1978), The evolution of finite amplitude Kelvin-Helmholtz billows, Geophys. Astrophys. Fluid Dynamics, 10,53-87.

Royrvik, O. (1983), Spaced antenna drift at Jicamarca, mesospheric measurements, Radio Sci., 18, 461-476.

Stewart, R. W. (1969), Turbulence and waves in a stratified atmosphere, Radio Sci., 4, 1269-1278.

Sykes, R. I. and W. S. Lewellen (1982), A numerical study of breaking Kelvin-Helmholtz billows using a Reynolds-Stress turbulence closure model, J. Atmos. Sci., 39, 1506-1520.

Woods, J. D. (1969), On Richardson's number as a criterion for laminar-turbulent-laminar transition in the ocean and atmosphere, Radio Sci., 4, 1289-1298.

# 2.6B ORIGIN OF REFRACTIVE INDEX FLUCTUATIONS IN THE MESOSPHERE AS OPPOSED TO THE STRATOSPHERE AND TROPOSPHERE

J. Rottger

EISCAT Scientific Association
P.O. Box 705
S-981 27 Kiruna
Sweden

Mesospheric echoes are strongly influenced by the electron-density profile of the ionospheric D region (e.g. ECKLUND and BALSLEY, 1981). These echoes therefore are only observed during daylight hours or high-energy particle precipitation. The turbulence occurs in layers, which often confines the radar echoes to rather thin regions of several 100 m vertical extent, although layers as thick as several kilometers were also obeserved. However, it never was found with high-resolution radars that evaluable echoes were observed through the entire altitude region of the mesosphere for the given power aperture product $5 \cdot 10^7 W\ m^2$. Additionally, the echoes indicate quite some temporal variation.

To illustrate the evident temporal and spatial variation, a contour plot of signal strength is presented in Figure 1 (from ROTTGER et al., 1983). In the mesosphere four separated regions of turbulence scatter were detected after 1200 AST between 65 and 78 km altitude. At 1215 AST a noise burst was observed, followed by an abrupt increase of signal strength of turbulence scatter. The noise burst was due to enhanced solar radio emission during an $H_\alpha$ solar flare. The enhanced noise level must have been picked up through an antenna sidelobe pointing to the sun. The simultaneously increased flux of UV and X-ray radiation also resulted in an enhancement of the D-region electron density which caused sudden increase of turbulence scatter strength by some ten dB. Simultaneous incoherent-scatter observations with the 430-MHz radar showed an increase of the mean D-region electron density by a factor of 5-8 (personal communication from J. Mathews and M. Sulzer, 1981). However, even the abnormally high electron density still did not yield a continuous power profile of turbulence scatter. The reason is that the mesosphere was not totally turbulent, but the turbulence was confined to intermittent layers. In Figure 2 height profiles of average power measured before and after the solar flare are shown as well as the power difference $P_2-P_1$ in dB. It is well recognized that the power scattered due to mesospheric turbulence had increased by up to one order of magnitude. These observations show that a sudden increase or even moderate variation of signal strength of mesospheric VHF radar echoes cannot at all be attributed to an increase of turbulence strength, but rather an enhancement ot electron density or electron-density gradient.

REFERENCES

Ecklund, W., and B. Balsley (1981), Long-term observations of the arctic mesosphere with the MST radar at Poker Flat, Alaska, J. Geophys. Res. 86, 7775-7780.

Rottger, J., P. Czechowsky, R. Ruster and G. Schmidt (1983), VHF radar observations of wind velocities at the Arecibo Observatory, J. Geophys. Res., 52, 34-39.

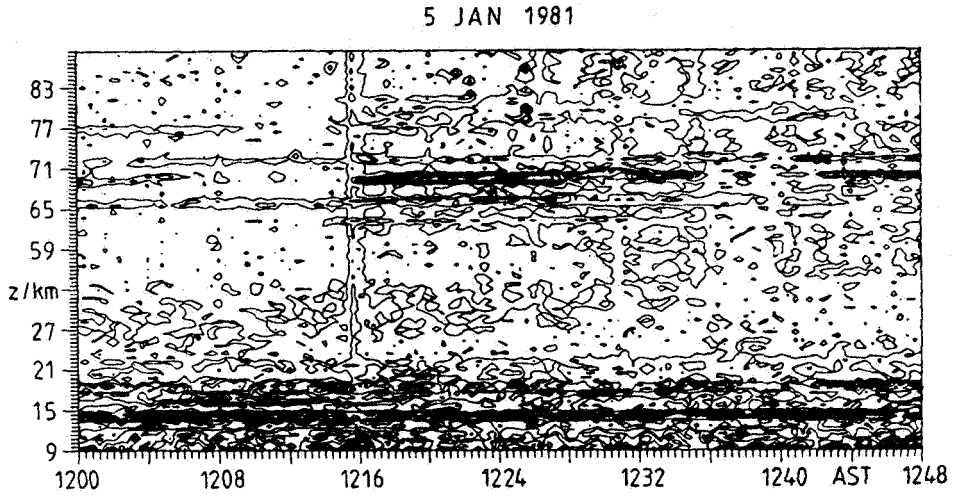


Figure 1. Contour plot of received power (signal + noise) as a function of height z and time (AST = Atlantic Standard Time). The power difference between the contour lines is 2 dB. Because atmospheric signals were not received in the height range 33-53 km, this range is suppressed in the plot. Measurements were carried out at the Arecibo Observatory with a 46.8-MHz radar with peak power of 30 kW and antenna beam pointing at a zenith angle of 2.7°.

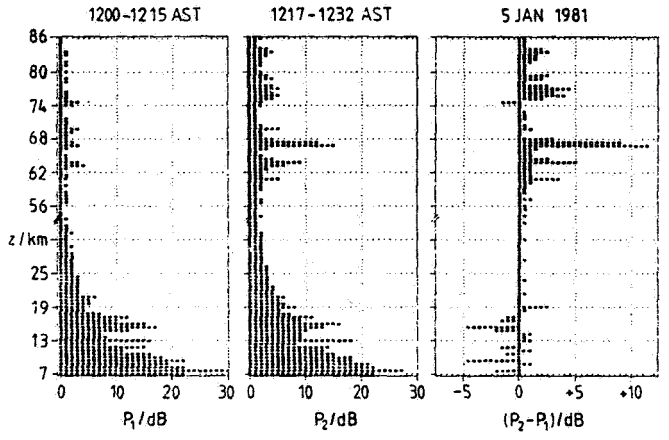


Figure 2. Profiles of average power measured before ($P_1$) and after ($P_2$) the solar flare, and power difference $P_2$-$P_1$ in dB.

# 2.6C SOLAR CONTROL OF WINTER MESOSPHERIC ECHO OCCURRENCE AT POKER FLAT, ALASKA

W. L. Ecklund and B. B. Balsley

National Oceanic and Atmospheric Administration
Boulder, CO 80303

Winter mesospheric echoes are observed between about 55 and 80 km at Poker Flat when auroral absorption is present during daylight hours (ECKLUND and BALSLEY, 1981). Relatively steady auroral absorption during sunrise and sunset periods causes a distinct onset and decay signature in mesospheric echo occurrence. Figure 1 (from ECKLUND and BALSLEY, 1981) shows the echo onset and disappearance times versus height by the inclined lines for 4 different dates. The more vertical lines give the visible sunlight height/time curves for both sunrise (SR) and sunset (SS). The data in Figure 1 have been combined and replotted in Figure 2 to give the morning onset height and the afternoon disappearance height as a function of solar zenith angle. Echoes are not observed at the lowest heights in the morning until the solar zenith angle is less than 90°. The afternoon echoes at the lowest heights also start to disappear as soon as the solar zenith angle exceeds 90°, implying that the solar component which sustains the mesospheric echo (presumably by enhancing electron density) is screened by a layer extending up to about 60 km. The morning echo at 73 km onsets near the time of visible sunrise, but in the afternoon the 73-km echo lasts well past visible sunset.

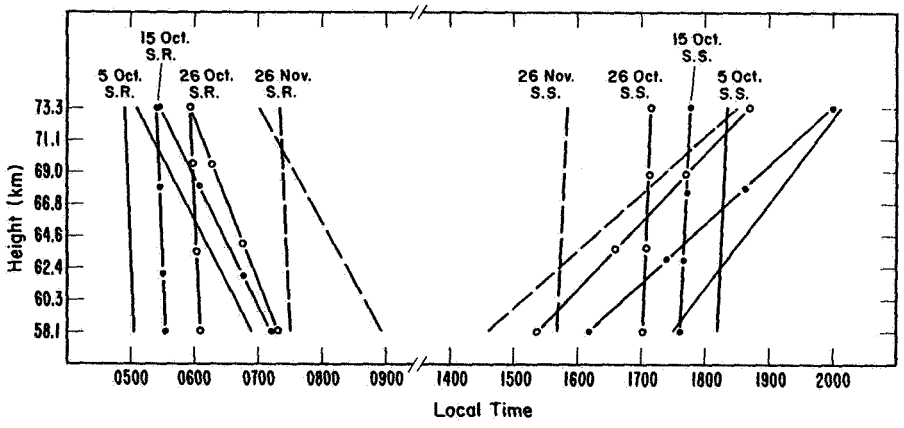


Figure 1.

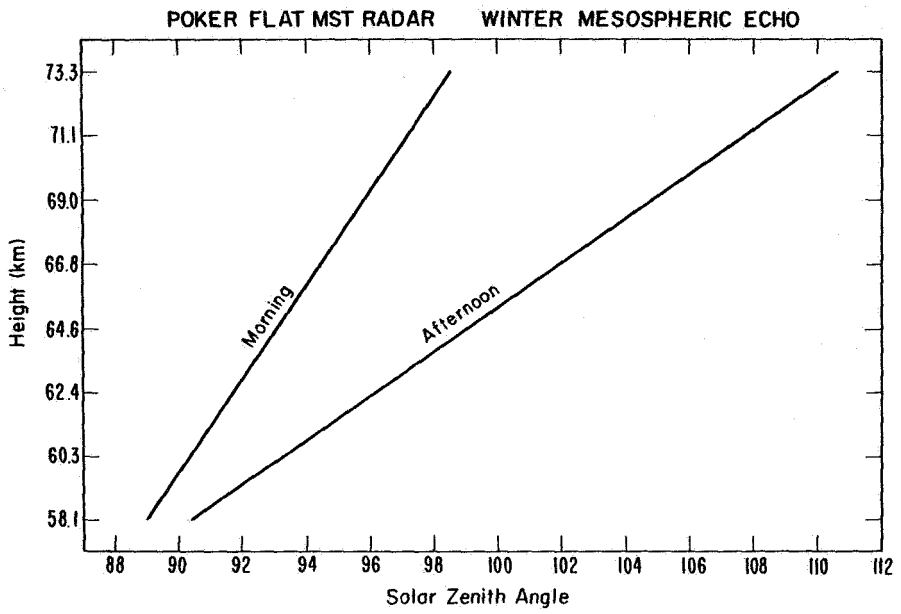


Figure 2.

REFERENCE

Ecklund, W. and B. Balsley (1981), Long-term observations of the Arctic mesosphere with the MST radar at Poker Flat, Alaska, J. Geophys. Res., 86, 7775-7780.

# 2.6D NIGHTTIME MESOSPHERIC RETURNS ASSOCIATED WITH A LARGE SOLAR FLARE EVENT

S. A. Bowhill

Aeronomy Laboratory, Department of Electrical Engineering
University of Illinois
Urbana, IL 61801

Since the source of mesospheric returns in MST radar is the formation of irregularities in electron concentration in the D region, radar measurements from the mesosphere are not available at night. However, magnetic storms associated with large flares can give D-region ionization. Special measurements were made at night during April 1982, to evaluate the nature of mesospheric returns obtained under storm conditions.

A sudden commencement was reported from Boulder at 2016 UT on April 24, 1982, followed by a magnetic storm through to 1500 UT on April 25 (i.e., 1416 CST April 24 to 0900 CST April 25). The Urbana MST radar therefore made measurements during the night of April 24-25.

Under normal circumstances, no scattered power is seen apart from sporadic meteor returns. However, on the night in question echoes were seen as indicated in Table 1. In this table, five periods of time are tabulated varying in length from 20 min to 60 min, at which scattered power was observed above the noise level. The 3-hr values of Kp corresponding to the five periods are also given, as is the mean power over noise observed.

Table 1

| Times (CST) | Altitudes (km) | Mean Power (dB) | Mean 3-hour Kp |
|---|---|---|---|
| 1930 - 2010 | 84 - 87 | 1 | 4 |
| 2245 - 2320 | 78 - 82.5 | 6 | 6 |
| 0005 - 0025 | 81 - 82.5 | 2 | 7- |
| 0030 - 0130 | 78 - 82.5 | 10 | 7- |
| 0215 - 0300 | 78 - 79.5 | 2 | 7- |

The nature of the data is illustrated by Figures 1 and 2, which show the variation of scattered power during the night at intervals of 1.5 km. Comparing these with Figure 3, a record from the previous day, reveals that the scattered powers at 78-81 km were comparable with those observed during the day, indicating that a similar ionization density was present, of several thousand $cm^{-3}$. The velocity data (Figure 4) for the night period show the presence of normal gravity-wave activity in the height range from which scattered power is returned.

There is a curious difference between the appearance of the day and night data. The peak power levels are approximately the same in both cases; but whereas the night data come from an essentially zero background, the day data arise from a substantial level of background scatter. Assuming that there is no statistical difference between incidences of turbulence by day and by night, this implies that the periods indicated in Table 1 are the only times at which any substantial particle precipitation was taking place; and that the consequent ionization was confined to the height region shown. It is possible, of course, that ionization at lower altitudes is being produced, but that the electrons form negative ions and therefore become invisible to the radar.

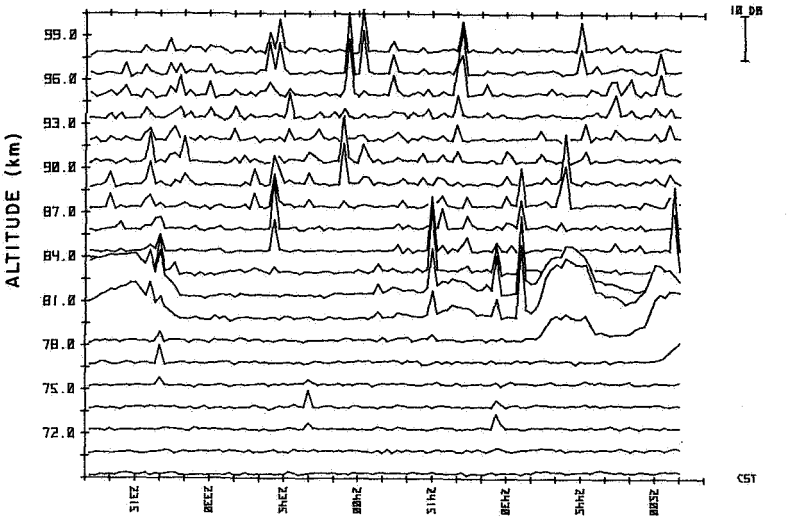


Figure 1. Logarithmic plot of scattered power on April 24-25, 1982.

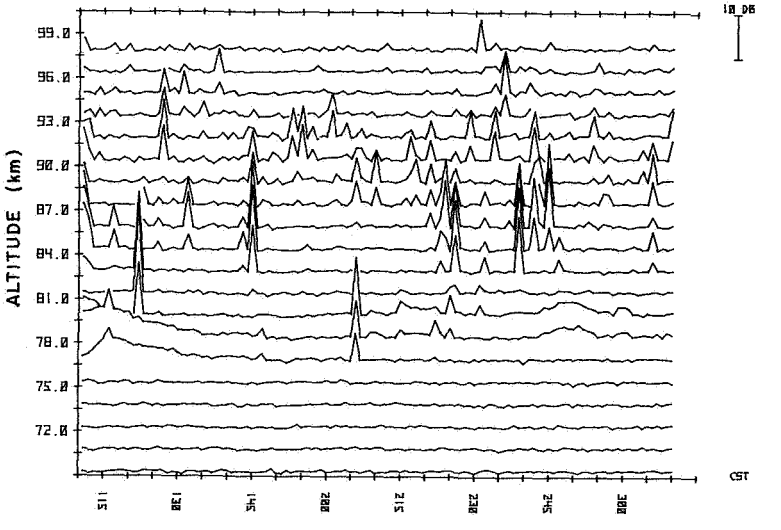


Figure 2. Logarithmic plot of scattered power on April 25, 1982.

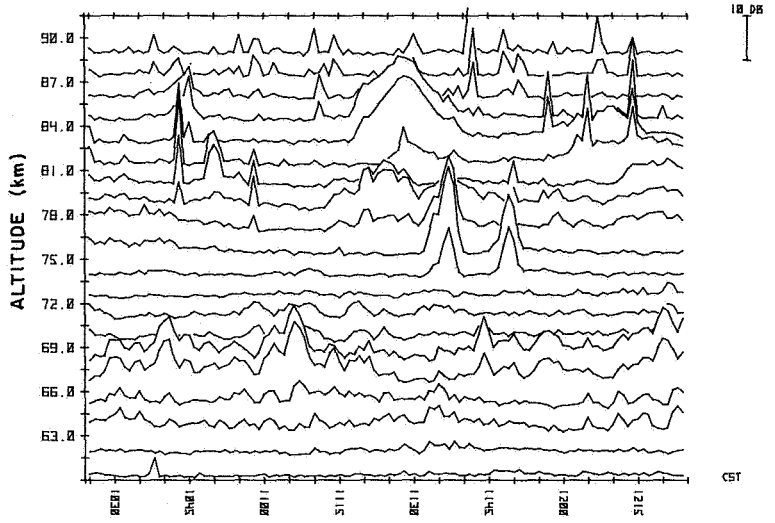


Figure 3. Logarithmic plot of scattered power on April 24, 1982.

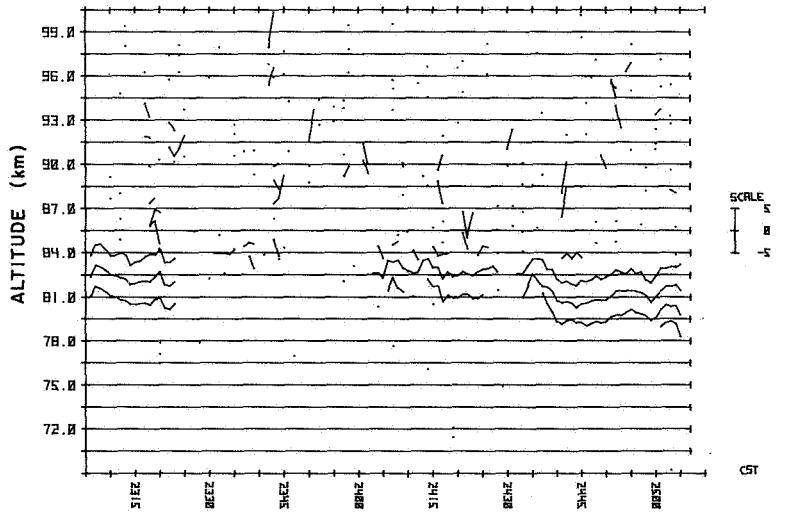


Figure 4. Line-of-sight velocities (m/s) for April 24-25, 1982.

It appears that careful use of the MST radar technique may aid in determining the altitude at which nighttime magnetic storm ionization is produced.

ACKNOWLEDGMENTS

The work described was supported in part by the National Aeronautics and Space Administration under grant NSG 7506 and in part by the National Science Foundation under grant ATM 81-20371.

# 3. TECHNIQUES FOR MEASUREMENTS OF HORIZONTAL AND VERTICAL VELOCITIES (Keynote Paper)

J. Rottger

EISCAT Scientific Association
S-981 27 Kiruna, Sweden

Techniques to measure velocities with radars make use of spectrum analysis or correlation methods, either in the time or in the space domain. The autocorrelation function of a coherently detected radar echo signal E(t) is $C(\tau) = \langle E(t)\, E^*(t+\tau)\rangle$. The power spectrum of the signal is $F(\omega) = \frac{1}{2\pi}\int C(\tau)\ \exp(-i\omega\tau)\, d\tau$. Here: t = time, $\omega$ = angular frequency, $\tau$ = temporal displacement, and * denotes complex conjugate.

The three first moments $m_0$, $m_1$, $m_2$ of the spectrum yield the essential parameters of the radio echo, namely the power P, the Doppler offset of the spectrum $\omega_d$ and the spectral width $\omega_s$. These are

$$P = m_0 = \int F(\omega)\, d\omega,$$

$$\omega_d = \frac{m_1}{m_0} \text{ with } m_1 = \int \omega F(\omega)\, d\omega,$$

$$\omega_s = \sqrt{\frac{m_2}{m_0} - \left(\frac{m_1}{m_0}\right)^2} \text{ with } m_2 = \int \omega^2 F(\omega)\, d\omega,$$

Since $F(\omega)$ and $C(\tau)$ are related through Fourier transformation, the three moments can also be deduced directly from the autocorrelation function (WOODMAN and GUILLEN, 1974), yielding

$$P = C(\tau_0), \quad (\tau_0 = 0)$$

$$\omega_d = \frac{\phi(\tau_1)}{\tau_1}$$

$$\omega_s = \left[\frac{2\ (1 - A(\tau_1)/A(\tau_0))}{\tau_1^2}\right]^{1/2}$$

where $A(\tau)$ is the amplitude and $\phi(\tau)$ is the phase of the autocorrelation function

$$C(\tau) = A(\tau)\ \exp(i\phi(\tau)).$$

The power is proportional to the intensity of the refractive index fluctuations and/or the reflection coefficient.

The Doppler shift $\omega_d = \underline{k}' \cdot \underline{V}$; the vector $\underline{k}' = \underline{k}_0 - \underline{k}_1$ defines the "mirror direction" for the direction of incidence ($\underline{k}_0$) and scattering ($\underline{k}_1$), see Figure 1. The angle $\phi$ is the scattering angle. We find

$$|\underline{k}'| = \frac{4\pi}{\lambda} \sin\phi/2 = \frac{2\pi}{\lambda'}$$

where $\lambda$ is the radar wavelength. For backscatter, $\phi = 180°$, and $\lambda' = \lambda/2$; $\lambda'$ is the Bragg wavelength, which the the important spatial scale in the

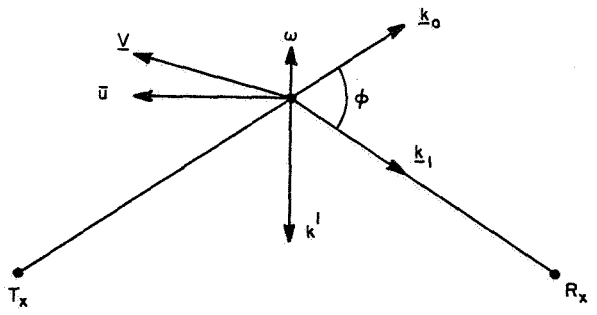


Figure 1. Scattering/reflection geometry.

scattering medium governing the radar echo intensity. For reflection, $\underline{k}'$ has to be perpendicular to the vector normal to the reflecting surface.

The bulk velocity of the scattering/reflecting target is $\underline{V} = (u,v,w)$. Measuring $\omega_d$ for different subsets of $\underline{k}'$, allows to determine $\underline{V}$. The spectral width

$$\omega_s = \frac{2 \langle \Delta v^2 \rangle \cdot \omega_0}{C}$$

is proportional to the rms velocity fluctuations $\langle \Delta v^2 \rangle^{1/2}$ of or in the radar target. $\omega_0$ is the angular frequency of the radar and C the speed of light.

Great care has to be taken to actually extract only the wanted atmospheric signal component from the correlation functions or the spectra. Contaminations occur due to noise (cosmic, receiver or interference) or clutter (ground, seasurface, ships, cars, aircraft or satellites), each having different characteristics. Also antenna sidelobes may pick up unwanted signals from other parts of the atmosphere. These problems are treated under another topic.

There are basically two methods to measure velocities. One method uses a narrow radar beam pointed into various directions to measure the 3-dimensional velocity vector $\underline{V}$. Another method uses three or more spaced antennas and the received signals are cross-correlated to determine the offset of the cross-correlation functions yielding the horizontal velocity component. The complex cross-correlation function is

$$\zeta(\underline{r}',\tau) = \langle E_k(\underline{r},t) \cdot E_1^*(\underline{r} + \underline{r}', t + \tau)$$

where k and 1 denote the different antennas and $\tau$ and $\underline{r}'$ denote the temporal and spatial displacements. Knowing the spatial displacements (i.e. the antenna separations), and measuring the temporal displacements of the cross-correlation functions allows to determine the drift speed of the field pattern on the ground, which is given by the drift speed of the scattering/reflecting radar targets. This method is the so-called "spaced antenna drift" method, whereas the former is called "Doppler method". It was shown by BRIGGS (1980) that both these methods are basically the same.

In Figure 2 both methods are compared schematically. Turbulence structures in the atmosphere scatter and reflect radar signals transmitted by a transmitter TX. Structures drifting through the antenna beam cause a drifting field pattern on the ground. The drift velocity is determined by the full correlation analysis (e.g., BRIGGS, 1977; ROTTGER, 1981). In the Doppler method the radial velocities from at least three pointing directions of the radar beam are measured. Under the assumption that the turbulence structures are advected with the background wind (Taylor hypothesis), the velocities deduced with these two methods correspond to the wind velocity.

Since these techniques have been used intensively at various places for many years, they will not be described in detail. We rather will briefly discuss some peculiarities, capabilities and limitations.

## MONOSTATIC VERSUS BISTATIC OPERATION

Bistatic operations employ separate antennas for transmission and reception, and these are separated by a distance comparable to the distance to the radar target (viz. scatter volume or reflecting structure). The height resolution is achieved by the intersection of the two beams and can be improved by applying pulse coding with short baud lengths. If the beams are matched, the echo power varies inversely as the distance of the scatter volume from the receiving antenna, instead of inversely as the square of the distance in the monostatic case. The signal-to-noise ratio does not depend on the gain of the transmitting antenna. It is proportional to the effective aperture of the receiving antenna if the horizontal width of the receiver beam at the scatter volume is larger than the width of the transmitter beam. The ideal dimensions of the two antennas are those where the two beams match. Any further improvement in gain of either antenna improves the resolution but not the signal-to-noise ratio.

Because of the change of the Bragg wavelength with incidence angle, the spatial scales to which bistatic forward scatter radars are sensitive are larger than for monostatic or bistatic backscatter radars. The forward scatter cross

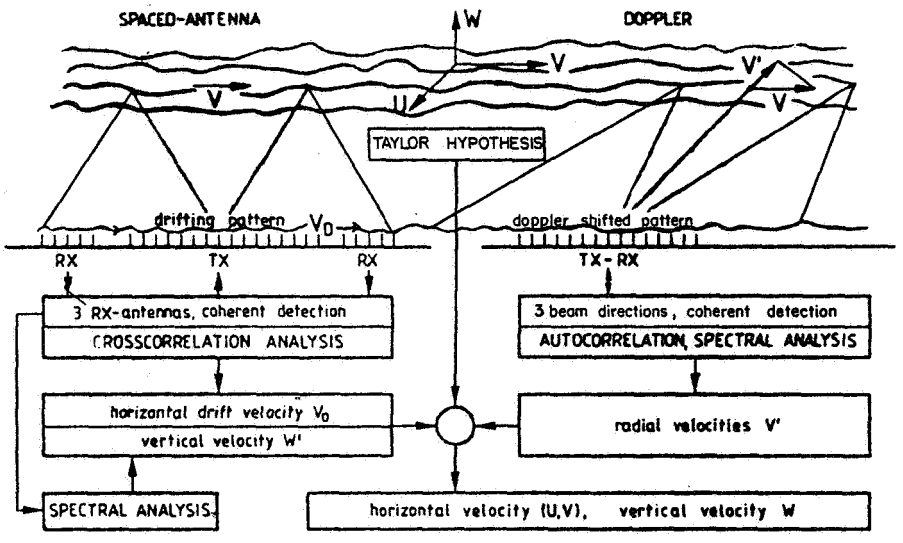


Figure 2. Scheme of spaced antenna and Doppler methods.

section mostly is larger than the backscatter cross section which significantly improves the detection capability. This on the other hand needs the scattering angle $\phi$ to be almost exactly 180°. This mostly is only the case if the target or scattering volume lies half the way along the line joining the transmitter and receiver. As a consequence, only vertical velocities can be measured.

The total velocity vector can be measured only with maintaining three receiving stations. A disadvantage of a bi- or multistatic system is further that it only observes one height at a time, although this limitation can partly be offset by antenna beam scanning or by using multi-beam receiving antennas.

## SPACED ANTENNA MEASUREMENTS

Spaced antenna measurements of wind velocities in the troposphere and stratosphere until today were carried out only with the SOUSY-VHF-Radar. These were discussed in detail in earlier papers (e.g., ROTTGER, 1981), but still questions existed on the accuracy of these measurements. Traditional calibration standards to prove the validity of radar wind measurements were always radiosonde winds. These comparisons obviously have to take into account that the winds decorrelate with distance between the sensors, but even comparisons of very close-by measurements did not yield exact equality, neither with the Doppler nor with the spaced antenna method. FUKAO et al. (1982) have shown that most of the difference between radar and radiosonde data in the lower stratosphere is caused by errors of the radiosonde winds, while the spatial and temporal variations in the wind field seem to dominate the difference in the upper troposphere. We now also take into account that the winds are modulated by propagating synoptic-scale disturbances, and calculate cross-correlation functions for radar/radiosonde and radiosonde/radiosonde data to show that very reasonable agreement exists.

A first example of winds at levels close to the tropopause height is shown in Figure 3. The radiosonde Essen is 250 km west and radiosonde Berlin 220 km east of the radar. The periodical oscillation of the meridional wind component v, seen in all three data series, is caused by planetary waves (synoptic-scale disturbances) with periods of 3-4 days, propagating from west to east.

It is evident that the radar time series is delayed with respect to the western radiosonde and advanced with respect to the eastern radiosonde station. The cross-correlation functions $\zeta_{xy}$ in Figure 4 are significantly similar in maximum amplitude for all three data sets, which proves the validity of the spaced antenna radar winds. Whereas Figure 3 shows winds in the lower stratosphere (having a fairly broad autocorrelation function, i.e., high persistency), Figure 5 shows winds of the upper troposphere which have a much lower persistency (i.e., narrower autocorrelation function). Even here the radiosonde and radar wind cross-correlations are similar, of course the correlation between the radar and the closest radiosonde (2-4) is almost 1. The similarity of wind directions is even more convincing.

One may use these results as final evidence for the equality of both methods -- the radiosonde and the spaced antenna radar. It has to be noted also that the radar winds can easily be measured in a continuous series, which is far more difficult and very impractical with radiosondes. The radar winds of Figure 5 were measured every hour during a four-minute period only, and one may accept this value as sufficient for obtaining a very reliable wind velocity estimate.

## RADAR INTERFEROMETER

The spaced antenna system that measures the quadrature components of a signal at different locations can be used as a simple form of a multielement or grating interferometer. Assume an array of N antenna modules at an equal

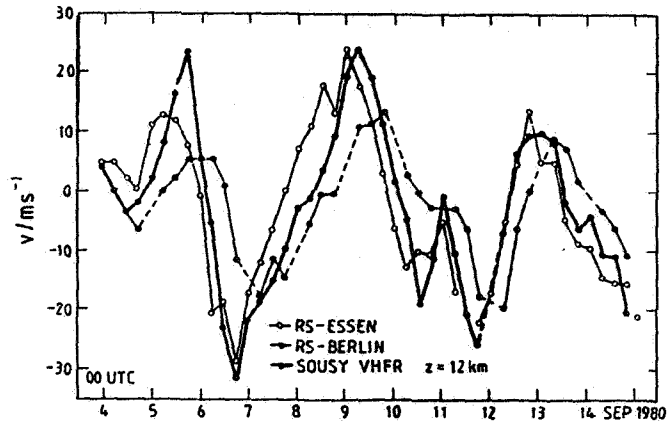


Figure 3. Meridional wind component v, measured over the period 4-15 September 1980 with radiosonde Essen, radiosonde Berlin and spaced antenna method with the SOUSY VHF radar.

spacing d to be lined up in the east-west direction. If each module with individual pattern $E_0(\phi,\theta)$ is fed with equal amplitude and phase the far field of this array is

$$E_R = \sum_{n=1}^{N} E_0(\phi,\theta) \exp(i\,(n-1)\psi)$$

with

$$\psi = 2\pi\, d/\lambda \cos\phi \sin\theta \qquad i = (-1)^{1/2}$$

where $\phi$ is the zenith angle and $\lambda$ is the wavelength. The azimuth angle $\theta$ is 90° only if the pattern in the east-west plane is considered. If the center of the array is chosen as phase reference, the array pattern in the east-west plane

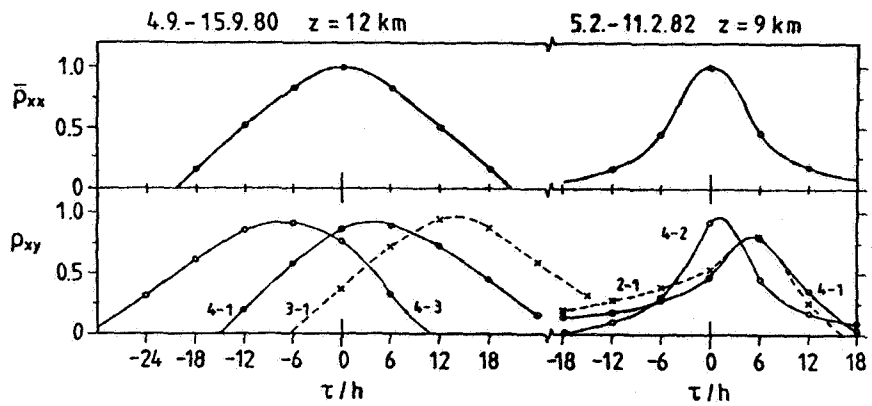


Figure 4. Auto- and cross-correlation functions for time series of wind velocity measurements with radiosondes: 1 = Essen, 2 = Hannover, 3 = Berlin, and 4 = spaced antenna radar (SOUSY near Lindau).

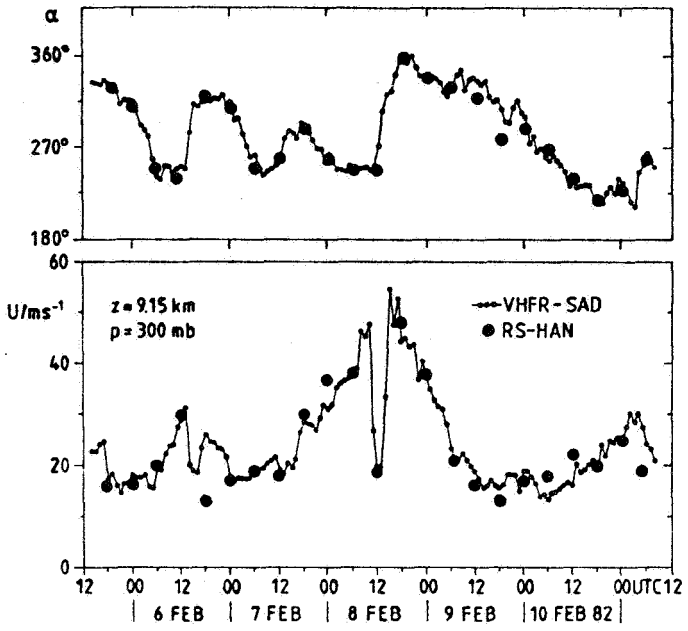


Figure 5. Wind speed U and direction α measured with the spaced antenna VHF radar method and the radiosonde of Hannover (RS-HAN).

becomes

$$E_R = E_0(\phi) \frac{\sin(N\psi/2)}{\sin(\psi/2)}$$

By reciprocity the array pattern is identical when the array is either used as a transmitting or receiving antenna.

In radar investigations an antenna with pattern $E_T(\phi)$ can be used for transmission and a grating interferometer with pattern $E_R(\phi)$ for reception. The effective pattern is

$$E(\phi) = E_R(\phi) \cdot E_T(\phi)$$

The transmitter antenna with half power beam width $\phi_T{}^h$ is assumed to point into zenith direction ($\phi = 0°$). The interferometer beam with half power beam width $\phi_R{}^h$ can be steered within the transmitter beam by changing the phase shift $\psi$ between the receiving modules. This acts like swinging the radar beam to different elevation angles and can be used to measure the aspect sensitivity, the tilt of reflecting or scattering layers and also the velocity. Since any phase shift $\psi$ can be inserted to recorded data during the evaluation process, the interferometer method appears to be more flexible than steering the antenna beam during transmission.

It has to be assured by appropriate spacing of the modules that only the main lobe of the interferometer is in the transmitter beam. This means that the spacing $\phi_R{}^g = \arcsin \lambda/d$ (with $d > \lambda$) of the grating lobe from the main lobe has to be larger than $\phi_T{}^h$. This yields

$$\sin \phi_T{}^h < \frac{\lambda}{d}$$

To obtain a reasonable angle resolution, $\phi_R{}^h$ should be equal to or smaller than $\phi_T{}^h$. Since $\phi_R{}^h = 57.3° \lambda/Nd$, the extent of the whole array in wavelengths should be

$$L = \frac{Nd}{\lambda} > \frac{57.3°}{\phi_T{}^h}$$

In Figure 6 an example is shown of an interferometer pattern which could be obtained for the spaced antenna set-up of the SOUSY-VHF-Radar (e.g., ROTTGER, 1981). This example also takes into account an angular dependence or aspect sensitivity A of diffuse reflecting structures with about 2 dB per degree decrease of received signal power. The phasing between the antenna modules was optimized to obtain a best suppression of the grating lobe. Because only three receiving modules were used, a better suppression than 5 dB was not obtained and the interferometer set-off was 1.2° only and the beam width was fairly broad. However, this system allowed to measure horizontal phase velocities and wavelengths of gravity waves in the stratosphere (described in the working paper "Determination of vertical and horizontal wavelengths of gravity waves", topic 4). It also allowed to measure horizontal wind velocities when averaging over a longer period of an hour, as is shown in Figure 7. The comparison of wind speed U and direction $\alpha$ of the three methods interferometer, drift and radiosonde appears convincing. Better sidelobe suppression and narrower beam width of course can be obtained by using more than three receiving antenna modules.

Another approach to use a spaced antenna set-up as a radar interferometer was introduced earlier to study ionospheric irregularities at Jicamarca (e.g., FARLEY et al., 1981). They used a cross-spectrum analysis, which allows determination of the phase difference between different antennas at different Doppler frequencies. This method works properly when irregularity patches or blobs are present. Since we assumed that some of the mesospheric structures, detected with the VHF radars, are blobs drifting through the antenna beam, we have applied this method, too.

The height-time intensity plot of Figure 8 shows a fairly thin and short-lived structure at about 65 km altitude after 0710 UT. Analyzing this event with the cross-spectrum interferometer technique yielded the results of Figure 9. Here $P_1$, $P_2$, $P_3$ are the power spectra measured over 30 s at the three different spaced antennas. They clearly show a change of Doppler shift from positive values at the beginning to negative values at the end of the event. In the lower diagrams the coherence $C_{13}$ and phase $\phi_{13}$ between signals measured at antennas 1 and 3 are depicted. These indicate that the phases changed during this event, which would not be expected if the scattering target would have remained overhead and moved up and down, according to the Doppler shift. The only explanation of these results is that a small scattering blob moved horizontally through the antenna beam. The combination of the interferometer and Doppler measurements yielded a zonal velocity of 43 m $s^{-1}$ and a meriodional velocity of 7.5 m $s^{-1}$ but a negligible vertical component. This analysis evidently proves the great advantage in applying the interferometer technique to avoid misinterpretation of velocity measurements.

## DOPPLER METHOD

BALSLEY and GAGE (1982) and LARSEN and ROTTGER (1982) have recently reviewed the application of radars for atmospheric wind profiling and synoptic research. Both, the spaced antenna and the Doppler method, were discussed by them and in several earlier papers referenced therein. Since the application of the Doppler method has meanwhile become a standard part of textbooks, we only discuss here two items which are specific to MST radars, namely those which operate in the VHF band. It is accepted that the scattering/reflecting structures are anisotropic, which for instance led to the suitable application

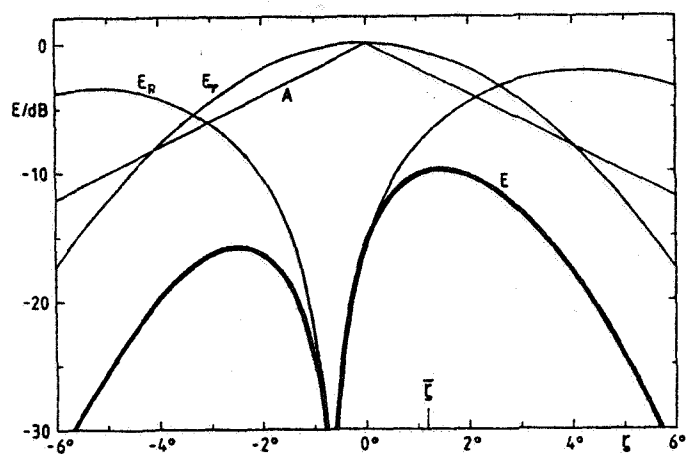


Figure 6. Interferometer pattern E, deduced from pattern of transmitter antenna $E_T$, three spaced antennas $E_R$, and angular dependence A of reflecting structures.

of the spaced antenna method. Evidently the anisotropy also leads to limitations of which the two most important shall be briefly discussed here.

## ACCURACY OF VERTICAL VELOCITY DETERMINATION

Let us assume Fresnel reflection from a refractivity structure which is slightly tilted to the horizontal. It shall be tilted by an angle $\psi$ around a horizontal rotation axis which forms an angle $\theta$ to the north direction. Let the tilted structure move with velocity $\underline{V}$, where $\underline{V}$ is given by its zonal (u), meridional (v) and vertical (w) components. A radar with vertically

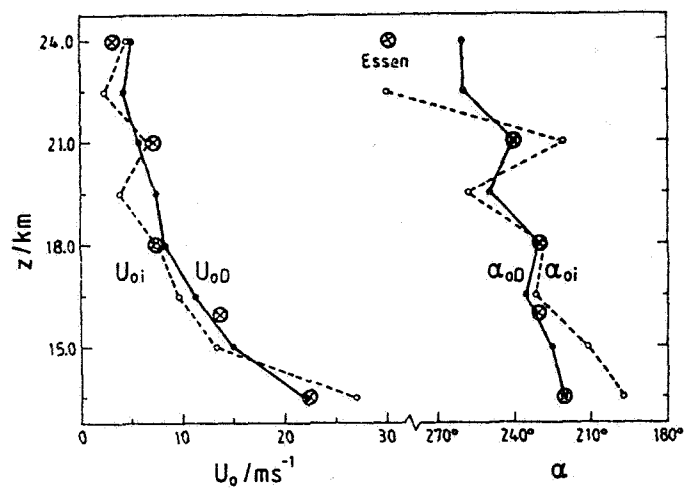


Figure 7. Average wind speed $U_0$ and direction $\alpha_0$, deduced with the interferometer (i) and the drift method (D) using spaced antenna radar on 9 September 1980, 0540-0640 UT. Circles with crosses denote corresponding radiosonde data from Essen.

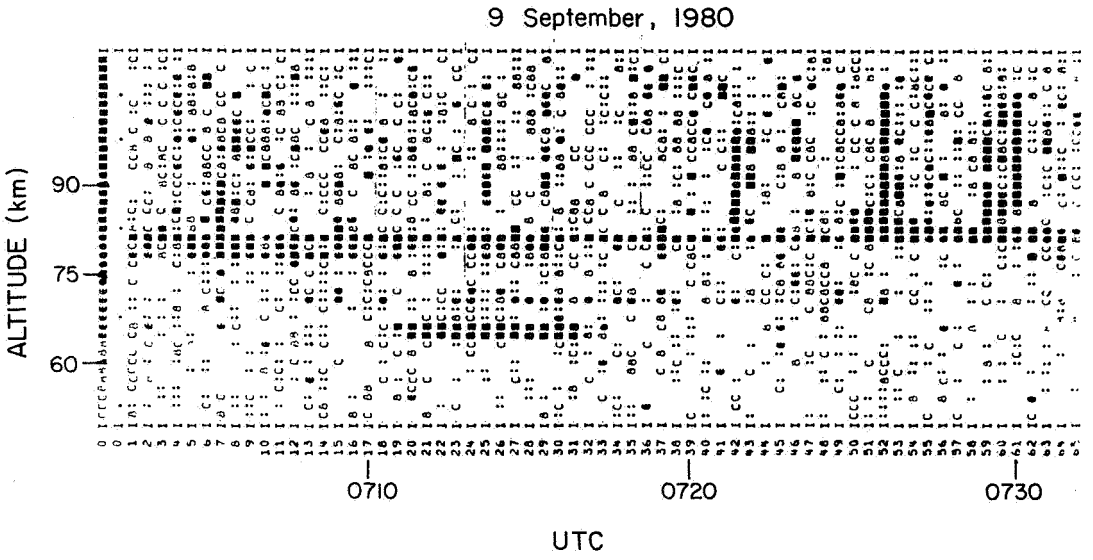


Figure 8. Height-time intensity plot of VHF radar echoes from the mesosphere.

pointing antenna, with beam width larger than the tilt angle of the structure, will measure the radial velocity

$$v_r = w \cos\psi + (u \cos\theta - v \sin\theta) \sin\psi + w^* + u^*.$$

The projections of u and v cause errors in determining w from $v_r$ which may not be negligible. These errors and possible corrections can only be determined if one can measure u, v, $\theta$ and $\psi$ independently of $v_r$. This can be achieved appropriately by spaced antenna measurements. The components u and v are deduced by the cross-correlation analysis with the spaced antenna drift method. Under realistic assumptions u and v, deduced by this method, are in a first order independent of measurements of w by means of the Doppler analysis and are not instrumentally correlated. The angles $\theta$ and $\psi$ are computed from measure-

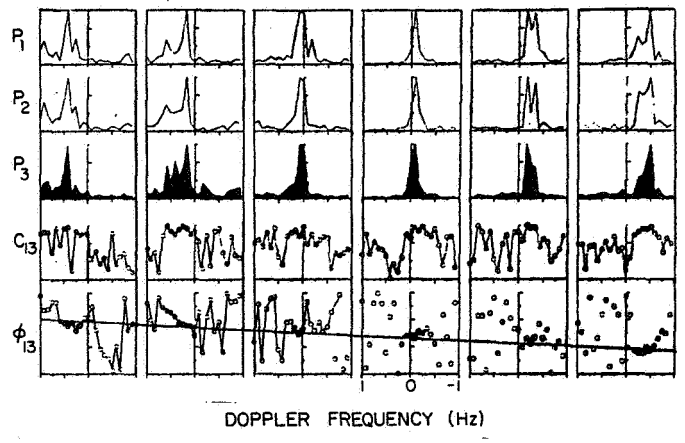


Figure 9. Power spectra $P_1$, $P_2$, $P_3$ of mesospheric echo, measured at three antennas, and coherence $C_{13}$ and phase $\phi_{13}$ measured between antennas 1 and 3.

ments of the phases of the radar echo between different spaced antennas (measurement of the incidence angles by the interferometer method).

Let, for example, two antennas being lined up in east-west direction at a distance d. For $\theta = 0°$,

$$\sin\psi = \frac{\Delta\phi}{360°} \cdot \frac{\lambda}{d}$$

Analyses of sample data from the lower stratosphere yield, for instance, for a one-hour average typical phase differences $\Delta\phi \approx 2°$ between two antennas separated by $d = 4.5\lambda$. This yields an average tilt angle $\psi = 0.07°$. Horizontal velocities of 20 m $s^{-1}$ then lead to $u^* = 2$ cm $s^{-1}$. Since typical radial velocities $v_r = 10$ cm $s^{-1}$, the average vertical velocity w is then determined with an error of 20%.

To measure the tilt for correction will therefore improve the determination of average vertical velocities and additionally yield a meteorological parameter, viz. the average inclination or tilt angles of reflecting structures which are related to baroclinic disturbances. To know the tilt angle will also be of eminent importance during pronounced gravity wave events, e.g., lee waves and propagating waves with wavelengths of several kilometers.

## OPTIMUM POINTING ANGLES

Because of the angular dependence of the anisotropic turbulence structures an apparent beam direction is manifest at off-vertical beam pointing directions (ROTTGER, 1980). This is schematically illustrated in Figure 10. Assume the angular spectrum of the diffusively reflecting irregularities to be centered at an angle $\phi_0$, which usually is the zenith direction. Let the antenna beam width be comparable to the width of the angular spectrum. The physical antenna beam pointing direction shall be off the vertical at an angle $\phi_b$. The echo power results from the convolution of the angular spectrum and the antenna beam pattern. As indicated in Figure 10, this yields an apparent beam with a pointing direction $\phi_a$, which is closer to the zenith than the physical pointing direction $\phi_b$. It was pointed out by ROTTGER (1980) that for an average angular dependence $\delta = 1.5$ dB/degrees, a beam pointing direction $\phi_b = 7°$ and a beam width of 5°, the apparent beam direction is $\phi_a = 6°$. This gives rise to an underestimate of the horizontal wind velocity by 20%. The wind direction is not affected by this effect if the irregularity structure is isometric in the horizontal plane.

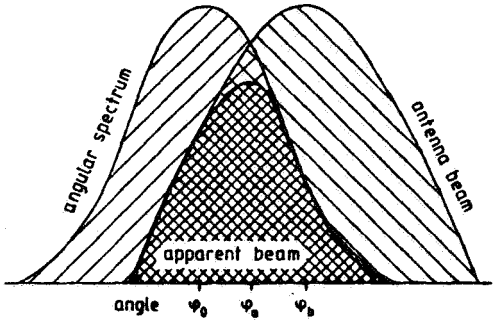


Figure 10. Formation of an apparent beam direction $\phi_a$ when the antenna beam points to direction $\phi_b$ but the angular spectrum (distribution) of the scatterer is anisotropic or the reflecting surface (seen at angle $\phi_0$) is diffuse.

ROTTGER and CZECHOWSKY (1980) have presented experimental evidence for this effect. They had evaluated horizontal velocities measured at 3.5° and 7° zenith angle with a 5° wide antenna beam. An evident difference (beam at 3.5° yielded lower velocities than at 7°) was found in the height region above the tropopause where the aspect sensitivity was most substantial. Precautions, therefore, have to be taken if one deduces horizontal velocities with the Doppler beam pointing method. The magnitude of this systematic error depends on the aspect sensitivity which has to be measured to correct the velocity estimates. One also has to bear in mind the apparent beam direction when describing the effect of beam width broadening of the Doppler spectrum (turbulence fluctuations). These errors of velocity estimates have to be considered if the off-zenith beam pointing direction is comparable to the beam width. To the author's knowledge attempts have now been made to apply such corrections to wind measurements with the Doppler method.

When choosing the optimum pointing angle, one has also to bear in mind that with increasing off-zenith angle the signal-to-noise ratio substantially decreases (e.g., Figure 11), the effective aperture of the antenna and the height resolution decrease, as well as sidelobes may be close to the zenith direction yielding again contaminations from the reflected component, but the effect of apparent beam direction (due to aspect sensitivity) gets smaller and the accuracy of the horizontal velocity estimates increases.

## QUESTIONS ON TIME RESOLUTION TO MEASURE LONG- AND SHORT-PERIOD VARIATIONS

Any kind of spectrum or correlation function measurements has to take into account ensemble averaging in order to obtain statistically significant estimates. The error of any estimate decreases with the square root of numbers of samples, and one therefore would be inclined to average over very long time periods. However, the averaging period depends obviously on the stationarity and the time scales of processes of interest. The shortest time scale, MST-VHF radars can resolve, is given by typical time scales of the variations at the Bragg wavelength $\lambda'$ of the refractive index to which these radars are sensitive. These times are typically of the order of seconds. To obtain acceptable statistics, averaging over some ten seconds must be done. Further averaging has to take into account the geophysical effects of interest, and one may decide to average over 1-2 min in order to still resolve short-period gravity waves, to average over several hours to smooth the gravity wave oscillations and obtain semi-diurnal and diurnal tidal variations. The synoptic-scale

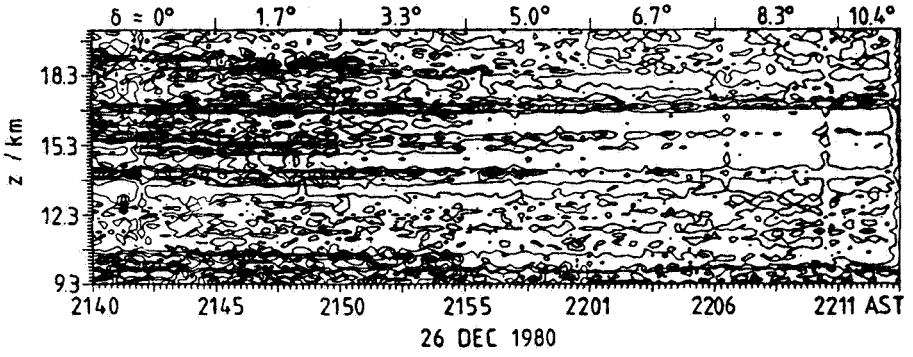


Figure 11. Contour plot of signal strength observed with 1.7° beam width and different zenith angles δ, which indicate the considerable decrease of signal with increasing δ. Observations were with the 46.8-MHz radar at the Arecibo Observatory, contour steps are 2 dB.

disturbances and planetary waves have periods of several days and averaging over 12-24 h will be suitable. However, because of the relative persistency of some of these processes, sampling during a short period at suitable time intervals often is sufficient.

As a general rule for deducing velocities from radar data, one may start with quality assessment of the autocorrelation functions and power spectra to apply an optimum fitting procedure and discard bad data. The next step would be to display short time series of velocities deduced for periods of one minute to get ideas on gravity wave oscillations and only later apply longer-term averaging.

REFERENCES

Balsley, B. B. and K. S. Gage (1982), On the use of radars for operational wind profiling, Bull. Amer. Meteorol. Soc., 63, 1009-1018.

Briggs, B. H. (1977), The analysis of moving patterns by correlation methods, Rep. ADP 148, Dept. of Physics, Univ. of Adelaide, Australia.

Briggs, B. H. (1980), Radar observations of atmospheric winds and turbulence: A comparison of techniques, J. Atmos. Terr. Phys., 42, 823-833.

Farley, D. T., H. M. Ierkic and B. G. Fejer (1981), Radar interferometry: A new technique for studying plasma turbulence in the ionosphere, J. Geophys. Res., 86, 1467-1472.

Fukao, S., T. Sato, N. Yamasaki, R. M. Harper and S. Kato (1982), Winds measured by a UHF Doppler radar and rawinsondes: Comparisons made on twenty-six days (August-September 1977) at Arecibo, Puerto Rico, J. Appl. Meteorol., 21, 1357-1363.

Larsen, M. F. and J. Rottger (1982), VHF and UHF Doppler radars are tools for synoptic research, Bull. Amer. Meteorol. Soc., 63, 996-1008.

Rottger, J. (1980), Reflection and scattering of VHF radar signals from atmospheric refractivity structures, Radio Sci., 15, 259-276.

Rottger, J. (1981), Investigations of lower and middle atmosphere dynamics with spaced antenna drifts radars, J. Atmos. Terr. Phys., 43, 277-292.

Rottger, J. and P. Czechowsky (1980), Tropospheric and stratospheric wind measurements with the spaced antenna drifts technique and the Doppler beam swinging technique using a VHF radar, Preprint Vol., 19th Conf. on Radar Meteorology, 577-584, Amer. Meteorol. Soc., Boston.

Woodman, R. F. and A. Guillen (1974), Radar observations of winds and turbulence in the stratosphere and mesosphere, J. Atmos. Sci., 31, 493-505.

REPORT AND RECOMMENDATIONS

The essential subtopics of this session were reviewed in several working papers which follow; four main subtopics (a) - (d) were discussed in detail.

(a) The meteorological requirements for the determination of vertical velocities connected with all different scales of motions was elucidated by K. S. Gage (this volume, p. 215). It was found that MST radars are most suitable tools to measure the vertical velocities. However, intensified investigations on the accuracy to be expected from MST radar measurements have to be continued. It is recommended that special emphasis shall be given to the following items:

(1) Investigations shall be carried out to determine if the turbulence structures observed with MST radars are locked into the large-scale motions, which means that they would be extended along the isentropic surfaces.

(2) Can MST radars measure the inclination of isentropic surfaces, and how accurately can this be done eventually?

(3) How accurately can the vertical velocity (defined as the velocity component in the topocentric z-direction) be measured, and how crucial are remaining contaminations from the horizontal wind?

(4) Following the Poker Flat routine observations of the vertical wind in the mesosphere, other MST radars should be used in the same mode to obtain information on global variations.

(b) The applications of the spaced antenna method to measure winds in the mesosphere by MF/HF radars and in the stratosphere and troposphere by VHF radars was reviewed by Hocking (this volume, p. 171), and he concluded that this method is as viable as any other method. Some discussion on its strengths and weaknesses followed; including the question of how bulk velocity estimates can be contaminated by gravity wave oscillations (Royrvik, this volume, p. 228). The Doppler method essentially was discussed in terms of the accuracy which can be obtained by different pointing directions of the antenna beams (Koscielny and Doviak, this volume, p. 192; and Strauch, this volume, p. 232). Considering the remaining uncertainties in measuring horizontal and vertical velocities it is recommended that investigations have to continue to solve the questions:

(1) How can the vertical velocity contamination due to the horizontal wind best be accounted for?

(2) How can the inaccuracy of horizontal wind measurements with the Doppler method be minimized, when horizontal shears in u, v and w exist?

Since troposphere and lower stratosphere radars are now seriously being proposed (and are starting to be tested) for widespread use in networks for wind measurements, definite experiments need to be conducted as soon as possible to determine:

(3) How the spaced antenna drifts methods and the Doppler method compare in terms of economics, accuracy etc. for troposphere and lower stratosphere wind profiling. An exhaustive study to compare both these methods must be done by including experts in both of these fields in a common program. It is also necessary to have other independent measurements, e.g., radiosondes, included.

(4) What range of wavelengths are suitable for profiling networks; in particular will VHF/UHF radars be more suitable to contribute to wind profiling than the new 10 cm Doppler weather radar (NEXRAD)?

(c) Another extended discussion took place on the application of MST radars to measure gravity wave parameters, since this topic was also of pronounced interest in session 4 on techniques to measure gravity waves and turbulence. The following recommendations were adopted:

(1) In order to measure horizontal and vertical wave velocities simultaneously in the same volume, the application of bistatic or tristatic MST radar systems should be considered.

(2) It is noticed that monostatic MST radars can be used to measure vertical and horizontal phase velocities of gravity waves, if these are fairly monochromatic (coherent). More use of both, the Doppler method (on-line beam steering) and the spaced antenna method (off-line beam steering), would be desirable to measure these gravity wave parameters.

(3) It is recommended that networks of MST radars have to be used for obtaining statistical information (climatology) on incoherent gravity waves.

(d) Radar interferometer techniques which recently were applied also to MST radars were reviewed by Farley (this volume, p. 237). It was noticed that these techniques have some potentials for investigating turbulence structures.

It is recommended that the application of the interferometer technique shall be encouraged. It is assumed, however that its application is not suitable for operational use rather than for basic scientific research.

# 3.1A TECHNIQUES FOR MEASUREMENT OF VERTICAL AND HORIZONTAL VELOCITIES: MONOSTATIC VS BISTATIC MEASUREMENTS

A. T. Waterman

STAR Laboratory, Stanford University
Stanford, CA 94305

First we distinguish three techniques of direct measurement from which velocities may be obtained: (1) Doppler frequency shift, (2) spaced antenna drift, and (3) spatially modulated transverse beam measurements. Although in a fundamental sense these may be considered equivalent, they differ in their experimental implementation and thus warrant the distinction. Our discussion here will concentrate on the Doppler-frequency-measurement approach. It will compare bistatic with monostatic configurations as regards received power (or sensitivity), spatial resolution, Doppler shift and avoidance of ground clutter.

## SENSITIVITY AND RESOLUTION

In the monostatic case the scattering volume is delineated by antenna beam width and pulse length. In the bistatic case the scattering volume may also be so delineated, but, since the geometry is different, so also are several other quantities: the shape and size of the scatter volume, the operative scale size in the atmospheric spectrum, and the Doppler relations. The power received bistatically may be expressed approximately as

$$P_{bi} \simeq \frac{P_T G_1}{4\pi R_1^2}\, \eta\, [b\ w\ h]\, \frac{A_2}{4\pi R_2^2} (\sin\xi)^2 \qquad (1)$$

in which

$P_T$ = transmitted power

$G_1$ = gain of the narrower-beam antenna

$R_1$, $R_2$ = distances from antennas to scale volume

$\eta$ = radar reflectivity (cross section per unit volume)

b, w, h = base, width, and height of trapezoidal shaped scatter volume, V (Figure 1)

$A_2$ = receiving aperture of the wider-beam antenna

$\xi$ = angle between electric vector of incident wave and scattering direction.

We have assumed the volume to be relatively restricted by narrow beams and a short pulse, and to be uniformly filled with the scattering medium. For the various quantities we can write, noting Figure 1 and 2,

$$b \simeq R_1 (\Delta\alpha_1) \csc (\theta/2) \qquad (2)$$

$$w \simeq R_1 (\Delta\beta_1) \qquad (3)$$

$$h \simeq \frac{C\tau}{2} \csc (\theta/2) \qquad (4)$$

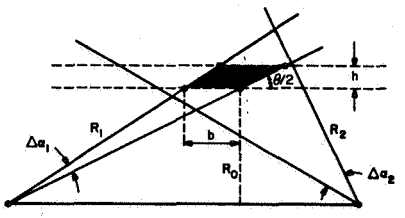


Figure 1. Scatter-volume geometry.

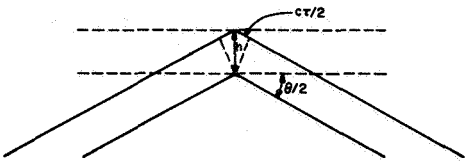


Figure 2. Delination of delay-shell width, h.

$$G_1 \simeq \frac{4\pi}{(\Delta\alpha_1)(\Delta\beta_1)} \tag{5}$$

$$\eta = 0.38\, C_n^2\, \lambda^{-1/3}\, [\csc(\theta/2)]^{11/3} \tag{6}$$

Here we have also assumed for purposes of illustration a Kolmogorov turbulence spectrum. Substituting (2) through (6) in (1), we obtain

$$P_{bi} \simeq 0.015\, P_T\, C_n^2\, \frac{A2}{R_2^2}\, \lambda^{-1/3} C\tau\, [\csc(\theta/2)]^{17/3} \tag{7}$$

where we have picked a polarization perpendicular to the plane of scattering in order to make $\xi = \pi/2$. By letting the scatter angle $\theta$ go to $\pi$, this expression reduces to the power received in the monostatic case:

$$P_{mo} \simeq 0.015\, P_T\, C_n^2\, \frac{A}{R_0^2}\, \lambda^{-1/3}\, C\tau \tag{8}$$

To compare bistatic with monostatic it is convenient to place the latter at the midpoint of the bistatic path, and let the zenith angle $\chi$ of its beam-pointing be the tilt angle of the bistatic scattering plane with respect to the great circle plane (Figure 3). If, to simplify the argument, we consider scattering from a region in the transverse midplane, then

$$R_1 = R_2 \tag{9}$$

$$\alpha_1 = \alpha_2 = \theta/2 \tag{10}$$

and so

$$\frac{R_1}{R_0} = \frac{R_2}{R_0} = \csc(\theta/2) \tag{11}$$

It will also be helpful to express antenna apertures in terms of dimensions y

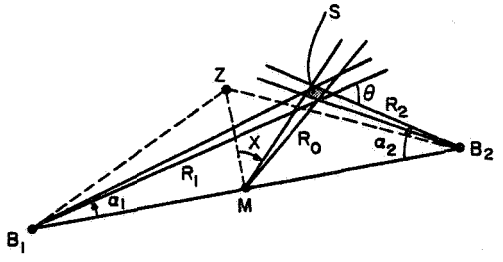


Figure 3. Geometry for bi-mono comparison. $B_1$, $B_2$ are bistatic termini. M is mono radar. Z is vertical. S is scatter volume.

(transverse to the bistatic path) and x (tilted up and in the plane of the bistatic path) so that

$$A = xy, \tag{12}$$

and

$$\Delta\alpha \simeq \lambda/x \tag{13}$$

$$\Delta\beta \simeq \lambda/y \tag{14}$$

The base, width, and height of the scattering volume, equations (2), (3), and (4), can then be written

$$b \simeq R_1 \frac{\lambda}{x} [\csc(\theta/2)] \tag{15}$$

$$w \simeq R_1 \frac{\lambda}{y} \tag{16}$$

$$h \simeq \frac{C\tau}{2} \csc(\theta/2) \tag{17}$$

With these preliminaries, we may now make comparisons of the bistatic with the monostatic case. The ratios of received powers, scattering volumes, and volume dimensions are

$$\frac{P_{bi}}{P_{mo}} \simeq \frac{P_{T,bi}}{P_{T,mo}} \frac{x_{bi}y_{bi}}{x_{mo}y_{mo}} \left(\frac{\lambda_{bi}}{\lambda_{mo}}\right)^{-1/3} \frac{\tau_{bi}}{\tau_{mo}} [\csc(\tfrac{\theta}{2})]^{11/3} \tag{18}$$

$$\frac{V_{bi}}{V_{mo}} \simeq \frac{(bwh)_{bi}}{(bwh)_{mo}} = \left(\frac{\lambda_{bi}}{\lambda_{mo}}\right)^2 \left(\frac{x_{bi}y_{bi}}{x_{mo}y_{mo}}\right)^{-1} \frac{\tau_{bi}}{\tau_{mo}} [\csc(\tfrac{\theta}{2})]^4 \tag{19}$$

$$\frac{b_{bi}}{b_{mo}} = \frac{\lambda_{bi}}{\lambda_{mo}} \left(\frac{x_{bi}}{x_{mo}}\right)^{-1} [\csc(\theta/2)]^2 \tag{20}$$

$$\frac{w_{bi}}{w_{mo}} = \frac{\lambda_{bi}}{\lambda_{mo}} \left(\frac{y_{bi}}{y_{mo}}\right)^{-1} \csc(\theta/2) \tag{21}$$

$$\frac{h_{bi}}{h_{mo}} = \frac{\tau_{bi}}{\tau_{mo}} \csc(\theta/2) \tag{22}$$

$$\frac{\ell_{bi}}{\ell_{mo}} = \frac{\lambda_{bi}}{\lambda_{mo}} \csc(\theta/2) \tag{23}$$

This last relation was obtained by noting that the geometry of Figure 2 applies also to the Bragg condition which selects scale size $\ell$, if we replace h in the figure by $\ell$, and $C\tau$ by $\lambda$.

Other things being equal (namely, powers, antennas, wavelengths, and pulse widths), the bistatic configuration has more received power to work with, since csc ($\theta$/2) is greater than unity and is raised to a moderately high power; this margin increases markedly as the bistatic baseline is lengthened. On the other

hand the size of the scattering volume $V_{bi}$ also increases drastically so that spatial resolution suffers.

For many purposes it would be desirable in the bistatic case to trade sensitivity for resolution. This can most readily be done by going to smaller wavelengths and shorter pulses -- i.e., by decreasing the ratios of $\lambda_{bi}$ to $\lambda_{mo}$ and $\tau_{bi}$ to $\tau_{mo}$. Since the monostatic antenna is probably already as large as feasible, it may be unrealistic to increase $y_{bi}$ or $x_{bi}$ over $y_{mo}$ or $x_{mo}$. Decreasing the pulse width $\tau_{bi}$ will help restore the height (or slant height) resolution $h_{bi}$ for a given scatter angle $\theta$. Similarly, decreasing the wavelength $\lambda_{bi}$ will help restore the lateral resolutions $b_{bi}$ and $w_{bi}$, for a given scatter angle and antenna size.

To illustrate with an example, if the bistatic pulse width were reduced to half the monostatic ($\tau_{bi} = \tau_{mo}/2$), then by equation (22) the scatter angle $\theta$ could drop as low as 60° before the bistatic height resolution became worse than the monostatic. Then, referring to equation (18), and still holding $\tau_{bi} = \tau_{mo}/2$, if we wish to keep the bistatic received powers no less than the monostatic for all scatter angles from 180° to 60°, we must make $\lambda_{bi} = \lambda_{mo}/8$ (assuming transmitter powers and antenna apertures are the same in the two cases). This would improve the spatial resolution, making $b_{bi}/b_{mo} = 1/2$, from equation (20), and $w_{bi}/w_{mo} = 1/4$, from equation (21). Thus if we do not insist on better resolution in the bistatic case, we can relax the size of its antennas, by a factor of at least 1/2 in elevation, and 1/4 in width. This will reduce the received power, but, since it is detectability rather than received power that is important, we are in no trouble because the antenna temperature at the higher frequency will be lower by a more-than-compensatory factor. (We are presuming that the monostatic radar operates in the VHF or UHF region and the bistatic in the UHF or SHF region).

In short, without indulging in any optimization studies, it appears safe to say that a bistatic system can retain the same spatial resolution as a monostatic, without impairment of sensitivity, if the pulse length and wavelength are shortened and the scatter angle does not get too small.

DOPPLER SHIFT

Now we turn to Doppler measurement, keeping, for purposes of comparison, the same configuration sketched in Figure 3. The monostatic radar measures the radial component of wind velocity:

$$f_{D,mo} = -\frac{2}{\lambda}(v \sin\chi + w \cos\chi) \tag{24}$$

where v and w are horizontal and vertical wind components. The bistatic radar measures the component of wind normal to the elliptical constant-delay shells. Near the midpath transverse plane, where the contribution from the along-the-path wind component u is small, the Doppler frequency is

$$f_{D,bi} = -\frac{(\sin\alpha_1 + \sin\alpha_2)}{\lambda}(v \sin\chi + w \cos\chi)$$

$$= -\frac{2 \sin(\theta/2)}{\lambda}(v \sin\chi + w \cos\chi) \tag{25}$$

When both bistatic and monostatic are looking at the same general scattering region, the ratio of the Dopplers is

$$\frac{f_{D,bi}}{f_{D,mo}} = \left(\frac{\lambda_{bi}}{\lambda_{mo}}\right)^{-1} \sin(\theta/2) \tag{26}$$

For the numbers chosen above, which keep the spatial resolutions comparable,

$$\frac{f_{D,bi}}{f_{D,mo}} = \left(\frac{1}{8}\right)^{-1} \left(\frac{1}{2}\right) = 4 \tag{27}$$

at $\theta = 60°$. For the same wind, the bistatic Doppler shift is greater owing to the shorter wavelength; less Doppler resolution is needed to achieve a given velocity resolution, and therefore a shorter measurement time is permissible. Data from two or more zenith angles (or tilt angles) permit separation of v and w components.

In order to obtain the orthogonal wind component u, the monostatic radar merely has to change its azimuthal pointing. For the bistatic system, the situation is a bit different, if the same two path terminals are to be used. When the scatter volume lies in the great-circle plane, the bistatic Doppler is given by

$$f_{D,bi} = -\frac{u}{\lambda}(\cos\alpha_1 - \cos\alpha_2) - \frac{w}{\lambda}(\sin\alpha_1 + \sin\alpha_2) \tag{28}$$

To measure u, $\alpha_1$ and $\alpha_2$ must differ appreciably -- i.e., the scatter volume must be well removed from the center of the path (Figure 4). It is not immediately apparent how best to make a comparison between bistatic and monostatic in this case, though one expects the advantage to lie with the latter.

## GROUND CLUTTER

In measuring the vertical velocity component w there is one respect in which the bistatic has an advantage. That advantage lies in the avoidance of ground clutter. Consider a bistatic configuration with the scatter volume located at midpath in the great-circle plane. Referring to Figure 3 with $\chi$ set equal to zero, the two Doppler frequencies are

$$f_{D,bi} = -\frac{2w}{\lambda}\sin(\theta/2) \tag{29}$$

$$f_{D,mo} = -\frac{2w}{\lambda} \tag{30}$$

We expect the vertical velocity w to be small and to vary about zero. Ground returns are also likely to have zero Doppler or nearly so. Confusion can arise when the ground echo has the same delay as the atmospheric. A ground feature of altitude z will extend above the transmitter's (and receiver's) horizon when (see Figure 5)

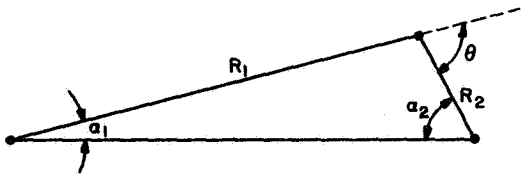


Figure 4. Off-center bistatic scattering.

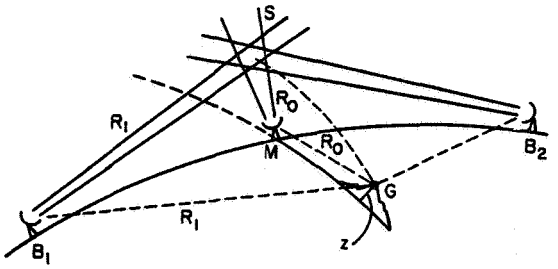


Figure 5. Interference from ground scatter into sidelobes. Ground feature at G and height z relative to radio horizons at M, $B_1$ and $B_2$.

$$z \geq \frac{R_1^2}{2r_0} \quad \text{, in the bistatic case} \tag{31}$$

and

$$z \geq \frac{R_0^2}{2r_0} \quad \text{, in the monostatic case} \tag{32}$$

Using equation (11), the ratio of these heights is

$$\frac{z_{bi}}{z_{mo}} = \left(\frac{R_1}{R_0}\right)^2 = (\csc(\theta/2))^2 \tag{33}$$

Thus, to follow the example used earlier, for $\theta = 60°$ this ratio is 4. A ground feature has to be four times as high in the bistatic, as compared with the monostatic, case before it causes the same interference problems. This advantage is of importance both for measuring vertical wind and for studying quasi-specular reflection at and near vertical incidence.

## A HYBRID SUGGESTION

This discussion should not conclude without mention of a hybrid case. Consider a transmitter located at T in Figure 6 and a scatter volume located at S. There are two bistatic receivers, located at $R_A$ and $R_B$. The planes specified by $TSR_B$ and $TSR_A$ slope toward each other and constitute two sides of a tetrahedron. There is a third receiver, at the transmitter location T, forming a monostatic radar. Doppler frequencies measured at the three receivers yield three wind components from which the vector wind can be determined. All three measurements are made on essentially the same volume of air at the same time, in contrast to most other techniques (except a triple Doppler). Futhermore the scatter volume can be moved vertically upward and downward, so that a true vertical profile of vector wind can be obtained.

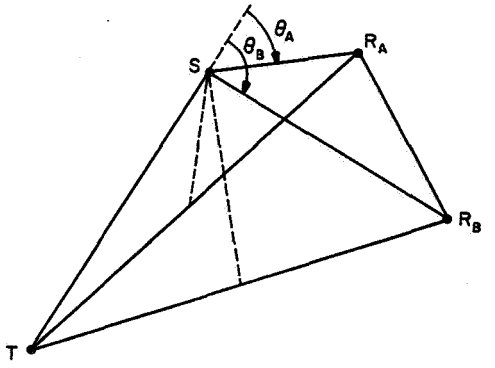


Figure 6. A combination monostatic and bistatic system.

# 3.1B A COMMENT ON SOME DRAWBACKS OF MONOSTATIC RADARS

S. A. Bowhill

Aeronomy Laboratory
Department of Electrical Engineering
University of Illinois
Urbana, IL 61801

To my knowledge, all MST radars now in operation or under construction use the monostatic mode, that is to say, the same antenna for both transmitting and receiving; or at least, transmitting and receiving antennas located adjacent to each other. This means that the only velocity information available is that corresponding to the line-of-sight direction for the radar beam. Consequently, it is never possible to determine more than one component of the atmospheric velocity at one point in space. While this is of little consequence for many practical applications, there are two important properties of gravity waves which are difficult if not impossible to determine by the monostatic method.

The first of these is the polarization of the gravity waves; that is, the complex ratio of the wave functions of vertical and horizontal motion. Some information can be gleaned on a statistical basis by comparing two different beam-pointing directions, but this cannot give information about the relative phase of the vertical and horizontal motion.

A second quantity of importance is the horizontal wavelength of gravity waves. As the pointing direction of a monostatic radar goes away from the vertical, correlation of the line-of-sight velocity with that for a vertical-pointing antenna decreases for two reasons: first, the introduction of horizontal gravity-wave velocities, to an increasing extent as the beam becomes more oblique; and the decrease in coherence of the vertical velocity itself. The second of these pertains to the horizontal wavelength of the wave; but it cannot in general be sorted out from the first effect.

Both of these problems could be overcome by use of a bistatic system. Such a system has the additional advantage of making it possible to measure at very low altitudes, and to look away from the transmitter (for example to make a horizontal section through a thunderstorm).

However, it must be recognized that bistatic operation, in the practical sense, requires not only an additional highly directive antenna, but also that both the transmitting and receiving antennas should be fully steerable.

ACKNOWLEDGMENTS

The work described was supported in part by the National Aeronautics and Space Administration under Grant NSG 7506 and in part by the National Science Foundation under Grant ATM 81-20371.

# 3.2A THE SPACED ANTENNA DRIFT METHOD

W. K. Hocking

Max-Planck-Institut fur Aeronomie
D-3411 Katlenburg-Lindau, FRG

## ABSTRACT

The spaced antenna drift method is a simple and relatively inexpensive method for determination of atmospheric wind velocities using radars. The technique has been extensively tested in the mesosphere at high and medium frequencies, and found to give reliable results. Recently, the method has also been applied to VHF observations of the troposphere and stratosphere, and results appear to be reliable. This paper discusses briefly the principle of the method, and investigates both its strengths and weaknesses. Some discussions concerning criticisms of the technique are also given, and it is concluded that while these criticisms may be of some concern at times, appropriate care can ensure that the method is at least as viable as any other method of remote wind measurement. At times, the technique has definite advantages.

## INTRODUCTION TO THE METHOD

The spaced antenna drift method was earlier applied to measurements of electron drift in the ionospheric E and F regions, and later to measurements of neutral winds in the ionospheric D region. For D-region work, the method has been denoted by "PRD" ("partial reflection D1 drifts" e.g., BRIGGS, 1977). Since its introduction to tropospheric and stratospheric measurements at VHF (e.g. ROTTGER and VINCENT, 1978), it had become known as the "SAD" ("spaced antenna drift") method (ROTTGER, 1981a). Following the Estes Park VHF conference of May, 1982, the notation "SA" was adopted ("spaced antenna"). In this paper, the latter notation will be adopted, although this is still not universally accepted.

The spaced antenna method of wind measurement began with MITRA (1949), who used a very simple approach involving measurements of time delays at three antennae. This technique was subsequently improved by a variety of workers, including BRIGGS et al. (1950), PHILLIPS and SPENCER (1955), FOOKS (1965), FEDOR (1967) and BROWN and CHAPMAN (1972). BRIGGS (1968a) presented a formal review of the method. However, possibly the best review of the method to date is one due to BRIGGS (1977b). That review is recommended to any reader who is seriously interested in understanding the spaced antenna method. Because the mathematical and conceptual details of the technique are so well covered in that article, they will not be repeated here in any great detail. Nor will a history of the method be presented; BRIGGS (1977b) presented a short history. Rather, the first objective of this paper will be to describe the basic principle of the technique, free of any mathematics. Having presented this general overview, a more extensive discussion of the shortcomings and strengths of the method will be given.

## APPARENT VELOCITY

The principle of the SA method is very simple, and is illustrated in Figure 1. Pulses of radio waves are transmitted into the atmosphere, and are partially backscattered or reflected. These scattered signals form diffraction patterns on the ground, and these diffraction patterns move at twice the speed of the scattering irregularities. The factor 2 arises because the transmitter is effectively a point source (e.g., FELGATE, 1970). The scale of these

diffraction patterns depends on the polar diagrams of the transmitting and receiving aerials, and the backscattering polar diagrams of the scatterers. The narrower the polar diagrams, the larger the scale of these diffraction patterns. The SA method measures the speed of these diffraction patterns across the ground, and this therefore gives the velocity of the scattering irregularities, after division by a factor of 2.

Figure 1 is based on an experiment conducted at Townsville in Australia to study the ionospheric D region. The experiment was designed and operated by Dr. R. A. Vincent of the Dept. of Physics, University of Adelaide, Australia. It represents perhaps the most compact and simplest form of the SA experiment. The radio waves (1.94 MHz) were transmitted from the square in the centre of Figure 1. The small black rectangle inside this square represents the transmitter and receiving building, and the four lines leading from it represent transmission lines to four half-wave dipoles, which form the outer square. Three simple crossed dipoles (A, B and C) were used for reception. The contours in the diagram represent part of the diffraction pattern amplitude (in the general case this is complex (amplitude and phase)) and the large arrow "$2\underline{W}$" represents the diffraction pattern's velocity. As it moves, the diffraction pattern will cause temporal variations at the aerials A, B and C, and these temporal variations will be similar, but will be displaced in time (see the illustrative amplitude variations as a function of time in the bottom left hand corner of Figure 1). In the simplest case, the axis of the diffraction pattern can be taken to be perpendicular to the velocity vector $2\underline{W}$, and the time displacements of the signals A, B and C can readily be used to determine the velocity $2\underline{W}$. The same formalism also applies if the contours of the diffraction pattern are, on average, circular. Determination of the "wind velocity" under either of these assumptions leads to a quantity known as the "apparent velocity". This method was first proposed by MITRA (1949).

## FULL CORRELATION ANALYSIS

Sometimes the axis of the diffraction pattern may not be perpendicular to the velocity vector, as illustrated in Figure 1. Further, the pattern may change quasi-randomly as it moves. These effects produce errors in the apparent velocity when compared to the real velocity. To remove these effects, the method of data reduction known as "full correlation analysis" (FCA) was developed. With this method, it is not only possible to more properly determine the real velocity, but it is also possible to indicate the scales of the diffraction patterns, the orientations of these patterns, and to indicate the degree of random fading. The velocity deduced by this method is termed the "true velocity". A fundamental function necessary for the application of FCA is the temporal and spatial autocorrelation function, defined by

$$p(\xi,\eta,\tau) = \frac{\langle f^*(x,y,t)f(x+\xi,y+\eta,t+\tau)\rangle}{\langle |f(x,y,t)|^2\rangle} \qquad (1)$$

where x and y are orthogonal co-ordinates on the ground (e.g., East and North), t is time, $\xi$ is the displacement in the x direction, $\eta$ the displacement in the y direction, t is the time, $\tau$ is time lag, f(x,y,t) is the (possibly complex) amplitude of the diffraction pattern (after removal of the mean) and <> denotes averaging over (in principle) all x, all y, and all t; f* is the complex conjugate of f.

In practice it is unrealistic to exactly determine $\rho(\xi,\eta,\tau)$, since it requires measurements of f(x,y,t) at all points (x,y) on the ground. Nevertheless, if some very reasonable assumptions concerning the form of $\rho$ are made (see BRIGGS, 1977b for the details of these assumptions), the $\rho(\xi,\eta,\tau)$ can be fairly accurately estimated from determinations of the temporal autocorrelations

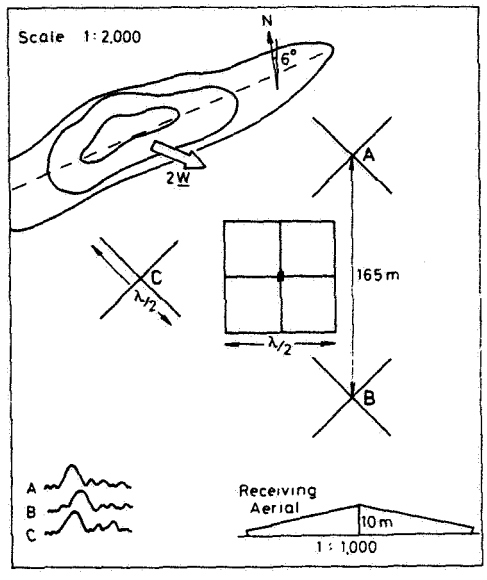


Figure 1. The principle of the spaced antenna method.

and cross correlations of 3 or more aerials. BRIGGS (1977b) described how this could be done.

Having determined an approximation to the function , it is a relatively simple matter to deduce the so-called "true velocity", as well as the variety of other parameters described earlier (BRIGGS, 1977b). These "other parameters" can provide useful information concerning the nature of the scatterers (e.g., STUBBS, 1977), but in this paper we will concentrate primarily on the "true velocity".

However, it is instructive to briefly mention the significance of one of these extra parameters. Since the backscattered signal varies as a function of time, it is of course possible to form the autocorrelation function of the signal, and thence to find the time lag for this function to fall to 0.5. This time lag will be denoted by $\tau_{0.5}$, and is sometimes called the "fading time". But FCA allows the experimentor to carry this one step further, and determine the fading time which would have been observed if the radar had been moving at the same mean speed as the scattering irregularities. Let us call this parameter $T_{0.5}$. Then BRIGGS (1980) has shown that if the scatter is due to isotropic turbulence, the Root Mean Square (RMS) vertical velocity of the turbulence scatterers, $v_{RMS}$ say, (more generally, $v_{RMS}$ is the RMS velocity of any chosen component) is related to $T_{0.5}$ by the relation

$$v_{RMS} = \lambda\sqrt{2\ln 2}/(4\pi\, T_{0.5}) \qquad (2)$$

(This formula is valid if complex data are used to estimate $T_{0.5}$.)

MANSON and MEEK (1980) and MANSON et al. (1981) have extended this formula to relate $v_{RMS}$ to the turbulent energy dissipation rate ($\varepsilon$), and the Brunt-Vaisala frequency ($\omega_B$). A relation of the form

$$\varepsilon = K\, v_{RMS}^{2}\, \omega_B \qquad (3)$$

where K is a constant (of the order of 0.3-0.5) was obtained (also see HOCKING,

1983a). Thus in principle it is possible to obtain $\varepsilon$ from Full Correlation Analysis. However, a word of warning should be sounded here. The equation (3) assumes that the RMS motions associated with horizontal and vertical directions are the same within the effective radar beam. (The effective radar beam includes consideration of the backscattering polar diagram of the scatterers.) Unfortunately, this may not be the case. The vertical motions are those associated with the Buoyancy scale of the turbulence, whilst the horizontal motions are those associated with scales of the order of the width of the effective radar beam at the height of scatter. This latter scale is often of the order of several kilometres, and the motions associated with such scales may be either two-dimensional turbulence, or gravity waves. This point was not considered either by BRIGGS (1980) or MANSON and MEEK (1980). Thus equation (3) is not really applicable for SA measurements of $v_{RMS}$, and it is necessary to distinguish between horizontal and vertical motions. This point has been emphasized by HOCKING (1983a). (Also see WRIGHT and PITTEWAY (1978)). Thus it is not really possible to estimate $\varepsilon$ by SA measurements. Equations (2) and (3) can be used to place upper limits on $\varepsilon$, but it is not possible to estimate, from simple SA measurements, just how much (3) overestimates the true value of $\varepsilon$. A more elaborate procedure, such as that described by HOCKING (1983a,b) is necessary to properly estimate $\varepsilon$, and is only possible with a large array of antenna capable of forming a narrow beam.

From now on, this paper will concentrate on estimates of wind velocities derived from the SA method. As has been seen, the principle of the method is quite simple. With modern computers, the application of the method is relatively easy, and can even be efficient with small on-site minicomputers (e.g., MEEK, 1980).

## ACCEPTANCE CRITERIA

Because the SA method requires estimation of the function $\rho(\xi,\eta,\tau)$ (equation (1)) from a few simple cross-correlation functions, it is important to take care that the fitted function $\rho$ is reasonable. Therefore proper application of the FCA method requires that certain acceptance criteria are obeyed. These acceptance criteria (also called rejection criteria) are quite stringent, and must always be applied. Failure to apply these criteria can allow many erroneous wind speed estimates to be accepted, and this can bias the results and perhaps even give the appearance that the SA method is unreliable. The rejection criteria used at Adelaide, Australia, by the University of Adelaide Physics Dept., are listed below (e.g., BALL, 1981). A data sample is rejected if

(1) The receiver was saturated for a significant time during the data record;

(2) The digitized signal levels are only of the order of a few digitial units (weak signal);

(3) The mean autocorrelation function has not fallen below 0.5 after about 20 time lags (slow fading);

(4) Any cross-correlation maxima are less than 0.2;

(5) Any cross- or auto-correlation functions are oscillatory in nature over the first 20 time lags;

(6) The polynomial fit to the cross-correlation functions breaks down, preventing determination of certain crucial time delays;

(7) The sum of the three time delays of the peaks of the cross correlations between aerial pairs AB, BC and CA is greater than 0.2 times the sum of

the moduli of these time delays (MEEK et al. 1979);

(8) The "true" and "apparent" velocities are very different;

(9) The quantity "$V_c^2$" estimated in FCA is significantly less than 0. (In the case that $V_c^2$ is only slightly less than zero, the apparent velocity can be used in place of the true velocity, since this probably indicates very little random fading);

(10) The signal-to-noise ratio is small;

(11) The contours of the diffraction pattern are non-elliptical (they become hyperbolic) in form.

Despite the apparent complexity of these tests, they are not difficult to apply with a digital computer, and they do not normally result in excessive rejection rates.

## POTENTIAL PROBLEMS WITH THE SA METHOD

As will be seen later, tests of the spaced antenna technique in the mesosphere (at MF and HF) and in the troposphere and stratosphere (VHF) have almost invariably shown it to be reliable. Nevertheless, from time to time objections to the method arise, and it is a useful exercise to consider these objections in more detail. It will be suggested that while there may be situations which can in principle produce erroneous results, they do not occur commonly in the atmosphere. Furthermore, it will be shown that objections can be raised to almost any method of remote wind measurement, and in all such remote observations a degree of care and selection is necessary.

BRIGGS (1980) has shown that, for the case that all scatterers in the radar volume move with the same horizontal velocity, and have zero vertical velocity, then the SA method must give identical results to the so-called Doppler method of wind measurement. If however, there are also vertical motions, these will affect the Doppler estimates of the horizontal velocity. Nevertheless, if a vertically pointing radar is also used, the effects of these vertical velocities can also be taken into account with the Doppler method.

The main difference of the SA method and the Doppler method lies in the direction of the radar beams. The SA method uses vertically directed beams, whilst the Doppler method uses beams tilted from the zenith to obtain horizontal wind velocities (plus a vertical beam to obtain vertical winds). Often, also, the SA method uses beams with wide half-widths, whilst Doppler estimates require very narrow beams. (Nevertheless, the SA method can also be applied with narrow beams.)

Most objections to the SA method are based on the assumption that there are two types of scatterers in the radar volume, and that these two types of scatterers move at different velocities. The most common assumption is that there are specular scatterers, aligned approximately horizontally, which scatter primarily from the vertical, and more isotropic scatterers. Specific mechanisms are then invoked which claim that the specular scatterers move at different velocities to the isotropic scatterers. It is then claimed that, since the SA method is more susceptible to scatter from the vertical, it will measure primarily a drift speed associated with these specular scatterers. It is most common to invoke gravity waves as the cause of these specular scatterers. Unfortunately it is never really stated clearly exactly how gravity waves cause these specular reflectors, and this point will be closely examined in this article.

Before proceeding to this examination, however, it is worth pointing out that gravity waves could also produce isotropic scatterers moving with the wave. For example, HODGES (1967) has shown that under certain circumstances, a gravity wave could produce turbulence during part of its cycle. If a layer of air existed which was close to statically unstable, but not quite unstable, the gravity wave temperature gradient at particular parts of the cycle may render the layer unstable. This may then cause turbulence. If the turbulence died out sufficiently quickly, then these turbulent patches would appear to move horizontally with the gravity wave, and both the SA method and the Doppler method would measure the horizontal component of the phase velocity of the gravity wave in such circumstances. Whether such a mechanism is realistic is a matter for debate; the main point is, however, that it is unfair to single out the SA method for criticism by means of specific examples without discussing similar cases for other methods of remote wind measurement.

Perhaps the most comprehensive discussions of the effects of gravity waves on the SA method can be found in HINES and RAO (1968), HINES (1972) and HINES (1976), although other authors (e.g., BROWNLIE et al., 1973) have also made contributions. However, it should be remembered that those papers primarily applied to measurements of drifts by totally reflected radio waves from the E and F ionospheric regions. In those cases, specular reflection was the main means of backscatter. Gravity waves curve the electron density isopleths, producing focusing and defocusing, and therefore fading of the radio signal at the ground. In the D region and lower atmosphere, it is not nearly so easy to make this assumption. It is necessary to carefully consider how gravity waves can influence only the specular reflectors, and also to consider the scales at which these effects occur.

To begin with, let us assume that these specular reflectors form independently of the gravity wave, by some unspecified mechanism, and are then influenced by it. Figure 2a illustrates the situation. Specular reflectors are indicated at times $t = t_1$ and $t_2$. In this case, it is assumed that the specular reflectors (thick lines and dots) are only separated by short distances, and cover most of the sky at the altitude under examination. In the limit, they may form continuous sheets. A gravity wave oscillation is assumed to tilt the reflectors at these two times. The specular reflectors are also blown by the mean wind, but this is taken to be zero in Figures 2a,b. Radio waves incident from transmitters TX1 and TX2 are "focused" and "defocused" respectively. Therefore as the gravity wave moves across the ground, it produces fading. An SA experiment may then measure the speed of this gravity wave. Is such an argument valid?

This situation may be applicable for total reflection from the ionospheric E or F regions at HF, because the isopleths of electron density are continuous, and reflection is total. However, for MF, HF and VHF scatter from the mesosphere, Figure 2a is not applicable. Rather, the specular reflectors which exist there are much more temporally and spatially intermittent (e.g., HARPER and WOODMAN, 1977; HOCKING, 1979; JONES, 1982). The same is often true for VHF tropospheric and stratospheric echoes. A situation like Figure 2b is more likely, in which only a small fraction of a gravity-wave cycle contains the reflectors. In such cases, the receiver will either receive a signal (when the reflectors are appropriately orientated), or receive no signal at all. If the oscillation has a very short period the radar signal will alternate between "high" and zero in an on-off manner. This will produce oscillatory correlation functions, and the "wind measurements" will be rejected in the FCA. Objectors to the SA method who have applied this argument have failed to recognize the importance of the "acceptance criteria" of section 4. If, on the other hand, the gravity-wave period is much longer than the typical data duration used to perform an SA measurement, then the tilting of the reflectors may be too slow to have a measurable effect. Rather "roughness" on the reflector (e.g., ROTTGER,

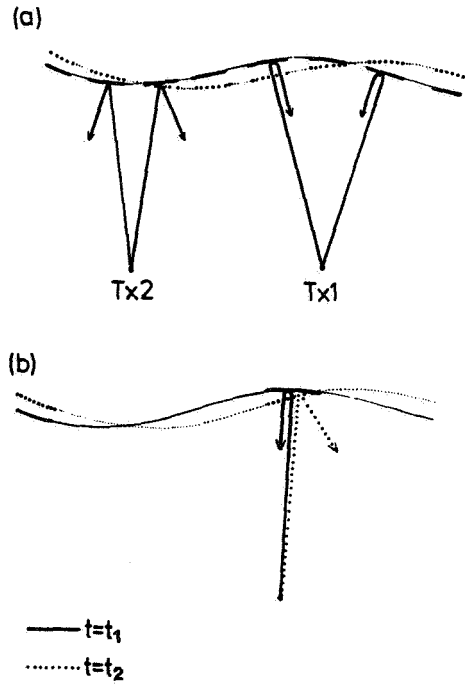


Figure 2. Illustration of gravity-wave-induced tilts to specular reflectors, and the effects of radar backscatter.

1980 refers to "diffuse reflection") will produce most of the fading, as the reflector moves with the wind, and the SA method will give the true wind velocity. When it is noted that most SA measurements use data lengths of about 1 minute or less, and that gravity waves have periods of at least 5 minutes (and at least 10 mins in the troposphere), it becomes clear that generally the scales of gravity waves are such as to reduce the possibility of this mechanism being a realistic threat to the application of the SA technique.

The point concerning the scale of the gravity waves is also pertinent to Figure 2a. If the scale of the diffraction pattern produced is similar to that of the gravity wave, then the gravity-wave-induced fading will be very slow, and faster fading (which the SA method will utilize) will occur due to motions of the more isotropic irregularities, and due to roughness on the surfaces of the reflector. Both the scatterers and the reflectors move with the wind, so that the SA method will measure this true wind speed. However, it can occur (particularly when many waves are present) that the scales of the diffraction pattern produced by gravity waves reflections can be considerably smaller than the gravity-wave scale ("interference fading": e.g., HINES and RAO, 1968; BROWNLIE et al., 1972), so that fast fading can at times occur due to gravity waves. In such cases, the SA method can produce erroneous results. Nevertheless, for VHF and HF partial reflection work, such gravity-wave-perturbed continuous reflectors seem rare; and when they do exist, it can also be difficult to obtain horizontal wind speeds by Doppler methods. One of the few catalogued tropospheric cases observed in which such stratification occurs has been presented by GAGE et al. (1981), and the wave had a period of about 18 min. It is doubtful that any effects of the phase velocity of the gravity wave

would have shown in any SA measurements of the wind in this case.

As an extra point, if high amplitude gravity waves occur, they may tilt these specular reflectors quite markedly, in which case Doppler radars may also observe the reflectors and therefore measure a finite (erroneous) wind velocity. This point has been emhasized by ROTTGER (1981a). The SA method, with its more stringent acceptance criteria, is more likely to reject the measurement. ROTTGER (1981a) also pointed out that such large amplitude waves are most likely to occur in the region of critical level interaction, in which case the phase velocity of the wave equals the mean wind anyway. But to be fair the above case may be rare and in most instances of critical level interaction, both the SA and Doppler methods will measure a wind equal to the sum of the mean wind and the wind due to the gravity wave, which is of course the desired value.

It therefore seems fair to suggest that this attempted criticism of the SA method is not, in reality, applicable, except perhaps in rare circumstances. In such circumstances, these erroneous measurements should stand out from the rest of the data, thereby enabling them to be rejected. Such rejection procedures are quite common, and would not be unique to the SA method. For example, LARSEN et al. (1982) using Doppler recorded winds, talk of rejection of questionable data.

The second way in which we could imagine gravity waves to influence the specular reflectors is that the gravity waves actually produce the reflectors, rather than simply acting on already existing reflectors. In this way the gravity wave actually carries the reflectors with it.

As mentioned earlier, this is not hard to envisage for total reflection from the E and F region. The gravity wave curves the contours of constant electron density in the region where the absolute refractive index approaches zero (i.e., the height of reflection), thereby produce focusing and defocusing. However, this scheme cannot be applied for partial reflection. For partial reflection, the refractive index gradient is the important quantity, rather than the absolute refractive index. Any change of refractive index must occur within less than about one quarter of the radar wavelength -- changes which occur more slowly are very very inefficient reflectors (e.g., ATLAS, 1964; HOCKING and VINCENT, 1982). Therefore we need only look at the case that the gravity wave wavelength is of the order of the radar wavelength. The most likely mechanism is that reflection occurs from the wavefronts of the gravity wave. For example HINES (1960) has proposed that at 60-70 km, gravity waves with vertical wavelengths of a hundred metres or so can explain observed HF and MF specular reflection from this height range. The gravity wave must have a wavelength perpendicular to its wavefronts equal to one-half of the radar wavelength. Such a process, however, would give strongest scatter from the off-vertical.

As an example, consider wavelengths of 3 m at $\simeq$ 10 km altitude. Could these exist, and produce the observed VHF specular scatter? HINES (1960, equation 49) showed that the smallest vertical wavelength which would not be dissipated by viscosity is

$$\lambda_z(\text{min}) \simeq 2\pi\sqrt{\eta T}, \qquad (4)$$

where T is the wave period (sec) and $\eta$ is the kinematic viscosity. Above 10 km, $\eta \leq 3\text{x}10^{-5}$ m$^2$ s$^{-1}$. We require $\lambda_z(\text{min}) \leq 3$ m, so T $\leq$ 100 min; at 18 km, T $\leq$ 40 min. Yet, as seen from HINES (1960, Figure 9), this means that all such wave fronts must be tilted at angles of $\geq 2°$-$3°$ from the horizontal at 10 km altitude. At 18 km altitude, the tilt must be $\geq 6°$. At 65 km, 3 m waves cannot exist, and even 75 m waves (capable of specular reflection at 150 m radio wavelength) must have tilts of greater than 10°. This effect of preferred scatter from off-zenith angles has never been observed, yet if it existed would be quite

obvious. It therefore seems unlikely that gravity waves cause specular reflections directly. Further, even if equation (4) is in error and gravity waves can cause specular reflections, the waves must be at least of very long peroid, in order to have near-horizontal wavefronts. As discussed earlier, long period oscillations do not have a substantial effect on the recorded signal when time durations of less than a minute are considered; the specular signal would just produce a constant offset. (At times, however, interference fading could be important.) Thus any fading of the signal during each data collection period would be due to other irregularities blown by the wind, and the SA method would still measure the proper wind speed.

It should also be noted that if the situation did occur in which two different types of scatterers moved at different velocities, and the two types of scatter contributed approximately equal power, and both had velocities significantly different from zero, then two peaks would often occur in the cross-correlation functions. This would also mean that the data sample would be rejected.

It therefore appears that in most cases, gravity waves do not bias SA measurements of wind velocities, and this point will be re-emphasized later by means of experimental data. However, the SA method does suffer from one weakness which must be mentioned, and this is the so-called "triangle size effect". In principle, the "true velocity" found from the SA method should be independent of the spacing of the aerials used to measure the wind, provided that the spacing is less than the typical diffraction pattern scale. However, it has been found that the "true velocity" often increases with receiver separation, tending to a limit for large separations. The same effect is observed for the "apparent velocity". The limiting values at larger separations appear to be the correct values. This effect has never been satisfactorily explained (BRIGGS, 1977b), although several proposals have been made. Nevertheless, the effect is not a major one, and appropriate choice of the aerial spacings results in reliable estimates of the wind velocity.

## ADVANTAGES OF THE SA METHOD

In the previous section, objections to the SA method were examined. It would be unfair to consider only objections to that method, however. Therefore let us consider some weaknesses of another method, namely the Doppler method. In this technique, tilted beams are used to measure radial Doppler shifts, and these are then converted to horizontal velocities. To do this, the vertical velocity must be known, and this can be obtained using a vertically pointing radar. However, it has to be assumed that the vertical velocity above the radar equals that at the scattering region for the tilted beam, and this may not always be so. Furthermore, if the radio-wave scatterers are anisotropic, with horizontal dimensions greater than their vertical dimensions, then the scatterers will also backscatter anisotropically. Radio waves will be returned more effectively from zenith angles closer to the vertical. If a radar beam is tilted at an angle $\theta_0$, the received backscattered radiation intensity will not be greatest at $\theta = \theta_0$, but a smaller angle, $\theta_1$. Thus the measured radial velocity of the scatterers will be that for scatterers at a zenith angle $\theta_1$, and this is less than the radial velocity of scatterers at $\theta_0$. When this radial velocity is converted to a horizontal velocity under the assumption that scatter was strongest from $\theta_0$, the resultant value will be an underdestimate. This has been emphasized by ROTTGER (1981a).

It is true that if the polar diagram of the scatterers is known, $\theta_1$ can be estimated, and therefore the true horizontal wind can be obtained. At present, however, such corrections are not normally applied with the Doppler method, and would be difficult to apply if the properties of the scatterers were continually changing.

Another problem can arise for the Doppler method, and this occurs when there are significant horizontal fluctuations of the wind velocity. This is illustrated in Figure 3. Doppler velocities from the region 'a' will produce a spectrum indicated by 'A' in Figure 3, and the range of velocities from region 'b' produce the spectrum 'B'. Likewise from 'c' we get the spectrum 'C'. The width of each "subspectrum" A, B and C depends on the RMS horizontal velocity of the scatterers, and the mean tilt angle for the regions a, b and c. Thus "sub-spectra" produced by scatter from larger tilt angles have a broader range of frequencies, reducing the peak power in their spectra. The result is that, when these "sub-spectra" are summed to produce the full spectrum, there is a bias towards low frequency components, and so the frequency offset of the peak of the spectrum is less than would have been obtained in the case of a constant mean wind with no horizontal fluctuations. This situation has been numerically modelled by HOCKING (1983a), who showed that if a radar with a beam half-power half-width of 4.5° is used, and if the RMS horizontal fluctuating velocity is similar to the mean wind speed in magnitude, then an underestimate in the wind velocity of ≈20% results. This is true even for isotropic backscatter.

The main point of these examples is not to downgrade the Doppler method, but rather to emphasize that all methods of remote wind measurements suffer from some form of weakness. It is important not to become too prejudiced against any method on the basis of a few speculations.

There are weaknesses and advantages of most radar methods. For example, as emphasized earlier, measurements of small scale turbulence are best done by Doppler methods (HOCKING, 1983a,b). Also, there are fewer acceptance tests necessary when the Doppler method is used. On the other hand, the SA method does not underestimate the wind velocity when scatter is anisotropic. In fact

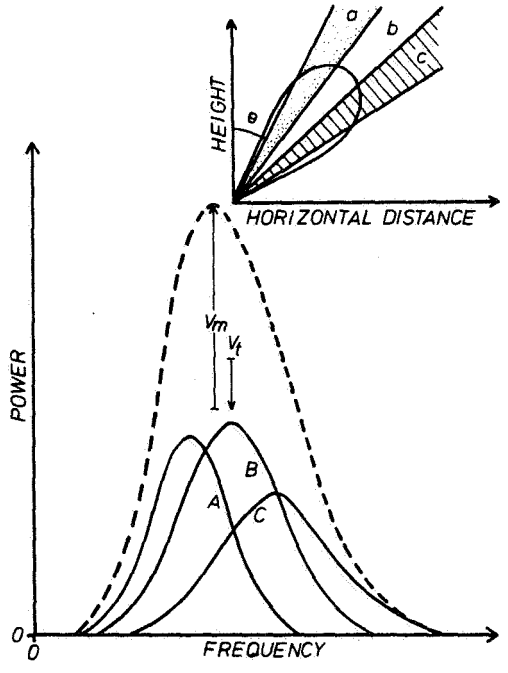


Figure 3. Distortion of radar spectra due to horizontal fluctuating motions of the scatterers.

one of the major advantages of the SA method is that it can utilize specular reflections in regions where scatter from the off-vertical is hidden by noise. For example, Figure 4 illustrates this effect. Figure 4a shows a Doppler spectrum recorded with the vertically pointing SOUSY radar beam, from a height of 25.2 km. Figures 4b and 4c show the spectra recorded with beams pointing at 7° off-zenith in the North and East directions, respectively. In Figures 4b and c the signal is hidden in the noise, and Doppler estimates of the wind velocity are not possible. However, there is plenty of signal at vertical incidence, which the SA method could utilize to obtain wind estimates. Further, as pointed out by ROTTGER (1981a) fading is slower with vertical beams, so more coherent integration can be applied with the SA method.

The SA method can also give a measure of the polar diagram of the scatterers, by virtue of its determination of the pattern scale. (In the case of gravity-wave oscillations in extended reflectors, interference fading can produce scales at the ground considerably smaller than the gravity-wave scale (see earlier). Care is necessary in such circumstances, but normally for VHF and HF partial reflections this should not be very common.) The Doppler method, in a fixed beam mode, cannot measure the polar diagram, but it can by using beam-swinging techniques.

The SA method can also apply the Doppler technique to determine vertical velocities. ROTTGER (1981a,b) has also emphasized that the SA method can be used to determine mean angles of arrival of the scattered radiation, and therefore to determine if any of the "vertical velocity" measured could be due to contamination from horizontal motions. For wide beams, this is probably most feasible over time scales of tens of minutes, since some averaging is necessary. Possibly narrow beams, such typically as those used by Doppler radars, may be better tools for estimation of short-term vertical velocity variations. Of course, the SA method can also be applied using narrow transmitter beams, and determination of angle of arrival is then an added bonus.

One of the greatest advantages of the SA method is its cheapness and simplicity. It only requires a transmitter array, and three small receiving arrays. Because of the small size, it also has advantages in regions where space for aerials is limited.

Another advantage of the SA method is that it measures wind speeds immediately above the observing array. The Doppler method measures the vertical wind overhead, but measures horizontal winds at points some distance from the overhead point. Further, the two orthogonal horizontal wind components are measured at different points in space. Thus when the three wind components are used to determine a total wind vector, it must be assumed that the wind field is homogeneous over a large area of sky.

Thus both the Doppler and SA methods have advantages and disadvantages, and the method finally adopted in any circumstances must depend largely on the requirements of the user.

## EXPERIMENTAL TESTS OF THE SA METHOD

The best way to test the SA method is, of course, by comparison with other methods. Extensive tests of the method have been carried out, and all suggest that the SA method is a reliable means of estimation of wind velocity in the mesosphere (at MF and HF) and in the troposphere and stratosphere (at VHF).

FRASER and KOCHANSKI (1970) and GREGORY and REES (1971) initially showed that SA measurements at MF and HF in the D region produced reliable winds. STUBBS and VINCENT (1973) and STUBBS (1973) then showed that the SA method agreed well with meteor measurements of winds at 80-100 km altitude. Further

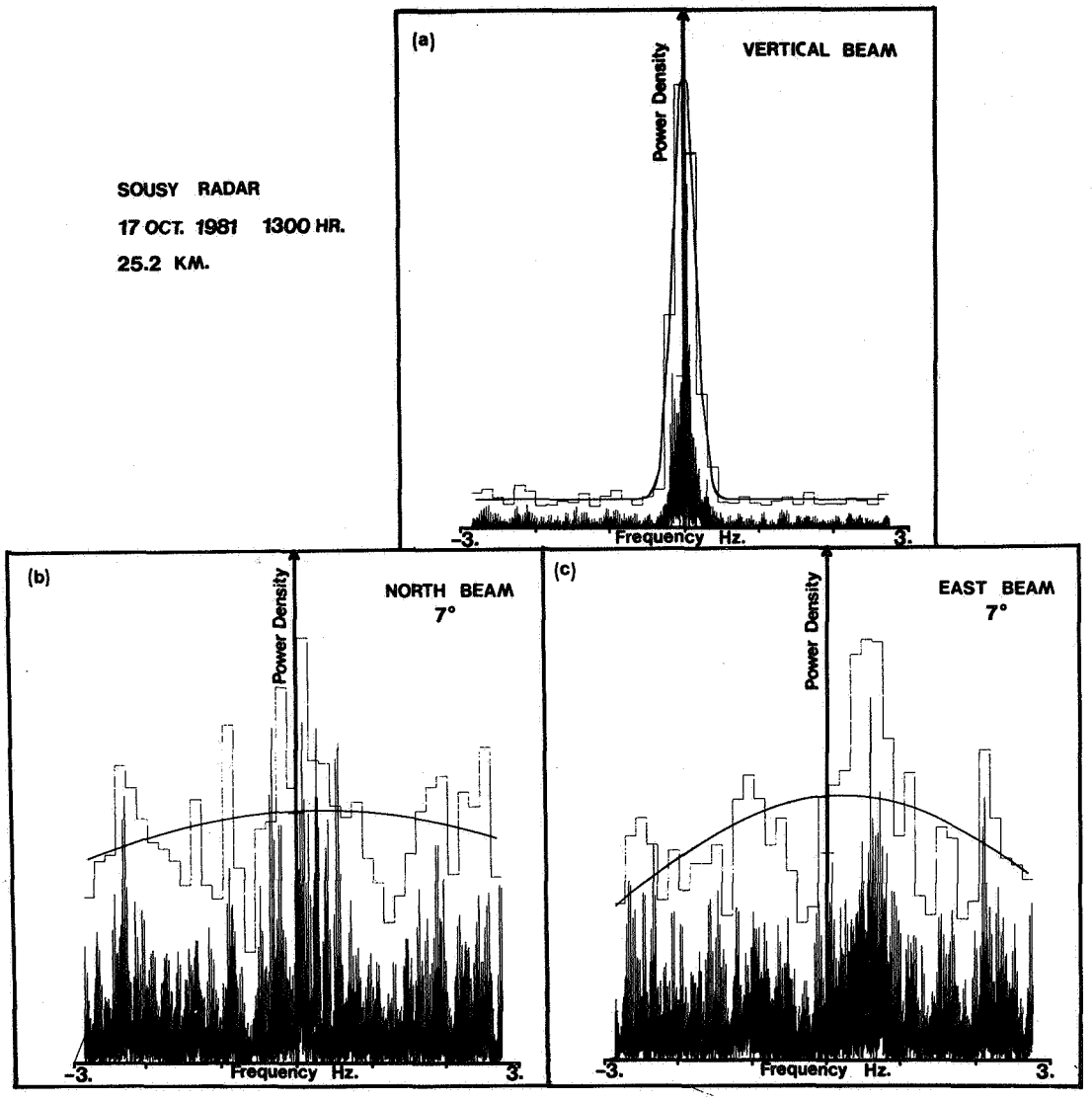


Figure 4. An example in which specular VHF backscatter is very strong (graph a) but off-vertical backscatter (b,c) is hidden in the noise. The "spikey" plots are the raw spectra -- the "histograms" are these spectra after averaging in frequency blocks. The smooth curves represent a best fit Gaussian plus offset.

comparisons with meteor measurements by WRIGHT et al. (1976) also showed good agreement. VINCENT et al. (1976) compared the SA method to measurements of D-region winds made by rocket techniques, and again good agreement was obtained. BRIGGS (1977a) presented further comparisons with meteor measurements. Measurements of means winds at Adelaide, Australia (e.g., VINCENT and BALL, 1981) and Saskatoon, Canada (e.g., MANSON et al., 1981) show that these means are consistent with accepted models of mesospheric circulation.

In the troposphere and stratosphere, several sets of SA measurements have been compared to wind measurements made by more conventional meteorological means. The first such report was by ROTTGER and VINCENT (1978). Good agreement was found between balloon measurements and VHF SA wind measurements. Likewise, results presented by VINCENT and ROTTGER (1980) showed similar good agreement. Subsequent comparisons by ROTTGER (1981a,c) and ROTTGER and CZECHOWSKY (1980) have also given no cause to doubt the SA method. More tests are probably necessary, but there are certainly no grounds yet on which to reject the method.

Recently, the Physics Dept. at the University of Adelaide, Australia, has modified the Buckland Park aerial array (which is used at 1.98 MHz to observe the ionospheric D region) to allow Doppler measurements of D-region horizontal winds. An example of a comparison between the SA method and the Doppler method is given in Figure 5. The Doppler beam had half-power, half-width of 4.5°, and was tilted at 11.6° from the vertical. The comparison was prepared by I. Reid and R. Vincent (private communication). Agreement is good; the differences can be attributed to vertical mean motion, since the horizontal winds determined by the Doppler method have been estimated under the assumption of zero vertical velocity. The effect discussed in connection with Figure 3 may also be important. HOCKING (1983b) also presented comparisons of SA and Doppler measurements, and again agreement was favourable.

The very fact that regular oscillations in winds are observed with the SA method in the D region, and that these have a cutoff at periods less than the

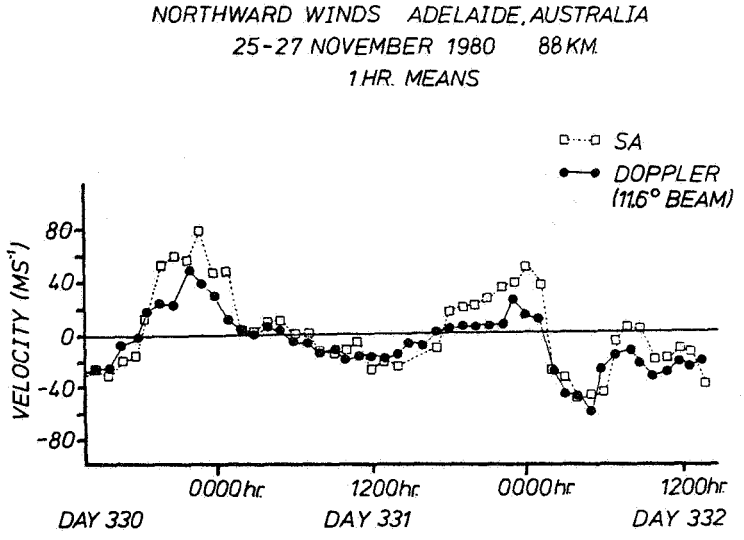


Figure 5. A comparison of wind measurements by the spaced antenna and Doppler methods, using an HF radar (REID and VINCENT, private communication).

Brunt-Vaisala frequency (e.g., VINCENT and BALL, 1977; MANSON et al., 1981) further suggests that the SA method does measure gravity-wave winds, and not the phase velocity of the gravity wave.

## DISCUSSION AND CONCLUSION

Evidence has been presented that the SA method is a reliable means of measuring neutral wind velocities in the mesosphere (at least at medium and high frequencies) and in the troposphere and stratosphere (at VHF). Some specific objections to the SA method has been considered, and it was concluded that the scales of gravity waves in the atmosphere, and the intermittency in space and time of specular reflectors, ensure that the SA method is generally quite viable when data lengths of less than 1 min are used, at least for the atmospheric regions and radio frequencies considered. (These arguments do not apply when total reflection and extremely short period waves ($\leq$ 3 min) are involved.) Further, the correct use of acceptance (rejection) tests in the SA method is emphasized. These tests must be applied in any SA measurements.

## ACKNOWLEDGEMENTS

This paper was written while the author was sponsored by an Alexander von Humboldt stipend.

## REFERENCES

Atlas, D. (1964), Advances in Geophysics, vol. 10, pp. 317, Academic Press, New York.

Ball, S. M. (1981), Upper atmosphere tide and gravity waves at mid- and low-latitudes, Ph.D. Thesis, University of Adelaide.

Briggs, B. H. (1968a), J. Atmos. Terr. Phys., 30, 1777-1788.

Briggs, B. H. (1968b), J. Atmos. Terr. Phys., 30, 1789-1794.

Briggs, B. H. (1977a), J. Atmos. Terr. Phys., 39, 1023-1033.

Briggs, B. H. (1977b), The analysis of moving patterns by correlation method, Commemorative Volume on Ionospheric and Space Physics, University of Waltair, ed. B. R. Rao. (This paper is also published as Dept. Report ADP 148, Physics Dept., University of Adelaide, Australia.)

Briggs, B. H. (1980), J. Atmos. Terr. Phys., 42, 823-833.

Briggs, B. H., G. J. Phillips and D. H. Shinn (1950), Proc. Phys. Soc., B63, 106.

Brown, G. M. and J. W. Chapman (1972), Ann. Geophys., 28, 349.

Brownlie, G. P., L. G. Dryburgh and J. D. Whitehead (1973), J. Atmos. Terr. Phys., 35, 2147-2162.

Fedor, L. S. (1967), J. Geophys. Res., 72, 5401.

Felgate, D. G. (1970), J. Atmos. Terr. Phys., 32, 241.

Fooks, G. F. (1965), J. Atmos. Terr. Phys., 27, 979.

Fraser, G. S. and A. Kochanski (1970), Annals. Geophys., 26, 675.

Gage, K. S., D. A. Carter and W. L. Ecklund (1981), Geophys. Res. Lett., 8, 599-602.

Gregory, J. B. and D. T. Rees (1971), J. Atmos. Terr. Phys., 28, 1079.

Harper, R. and R. F. Woodman (1977), J. Atmos. Terr. Phys., 39, 959.

Hines, C. O. (1960), Can. J. Phys., 38, 1441-1481.

Hines, C. O. (1971), Phil. Trans. Roy. Soc. Lond., A271, 457-471.

Hines, C. O. (1976), J. Atmos. Terr. Phys., 38, 561-563.

Hines, C. O. and R. R. Rao (1968), J. Atmos. Terr. Phys., 30, 979-993.

Hocking, W. K. (1979), J. Geophys. Res., 84, 845.

Hocking, W. K. (1983a), On the extraction of atmospheric turbulence parameters from radar backscatter Doppler spectra. I. Theory, J. Atmos. Terr. Phys., (in press).

Hocking, W. K. (1983b), Mesospheric turbulence intensities measured with a HF radar at 35°S, J. Atmos. Terr. Phys., (in press).

Hocking, W. K. and R. A. Vincent (1982), J. Atmos. Terr. Phys., 44, 843-854.

Hodges, R. R., Jr. (1967), J. Geophys. Res., 72, 3455.

Jones, K. L. (1982), J. Atmos. Terr. Phys., 44, 55-60.

Larsen, M. F., M. C. Kelly and K. S. Gage (1982), J. Atmos. Sci., 39, 1035-1041.

Manson, A. H. and C. E. Meek (1980), J. Atmos. Terr. Phys., 42, 103.

Manson, A. H., C. E. Meek and J. B. Gregory (1981), J. Atmos. Terr. Phys., 43, 35.

Meek, C. E. (1980), J. Atmos. Terr. Phys., 42, 835.

Meek, C. E., A. H. Manson and J. B. Gregory (1979), J. Atmos. Terr. Phys., 41, 251.

Mitra, S. N. (1949), Proc. IEEE, 96, 441.

Phillips, G. J. and M. Spencer (1955), Proc. Phys. Soc., B68, 481.

Rottger, J. (1980), Radio Sci., 15, 259.

Rottger, J. (1981a), J. Atmos. Terr. Phys., 43, 277-292.

Rottger, J. (1981b), Wind variability in the stratosphere deduced from spaced antenna VHF radar observations, Preprint vol., 20th Conf. on Radar Meteorology of Am. Met. Soc., Boston Mass., 30 Nov. - Dec. 3 pp 22-29.

Rottger, J. (1981c), The capabilities of VHF radar for meteorological observations, Preprint vol., of Newcasting Symposium, Third Scientific Assembly of International Association of Meteorology and Atmospheric Physics, Hamburg, FRG, 17-28 Aug. 1981.

Rottger, J. and P. Czechowsky (1980), Tropospheric and stratospheric wind measurements with the spaced antenna drifts technique and the Doppler beam swinging technique using a VHF radar, Preprint vol., 19th Conf. on Radar Meteorology of Am. Met. Soc., Miami, FL, USA. 15-18 Apr. pp 577-584.

Rottger, J. and G. Schmidt (1981), Characteristics of frontal zones determined from spaced antena VHF radar observations, Preprint vol., 20th Conf. on Radar Meteorology of Am. Met. Soc., Boston, Mass., 30 Nov - Dec 3, pp 30-37.

Rottger, J. and R. A. Vincent (1978), Geophys. Res. Lett., 5, 917-920.

Stubbs, T. J. (1973), J. Atmos. Terr. Phys., 35, 909.

Stubbs, T. J. (1977), J. Atmos. Terr. Phys., 39, 589.

Stubbs, T. J. and R. A. Vincent (1973), Australian J. Phys., 26, 645.

Vincent, R. A. and S. M. Ball (1977), J. Atmos. Terr. Phys., 39, 965-970.

Vincent, R. A. and S. M. Ball (1981), J. Geophys. Res., 86, 9159.

Vincent, R. A. and J. Rottger (1980), Radio Sci., 15, 319-335.

Vincent, R. A., T. J. Stubbs, P. H. O. Pearson, K. H. Lloyd, and C. H. Low (1977), J. Atmos. Terr. Phys., 39, 813-821.

Wright, J. W., M. Glass and A. Spizzichino (1976), J. Atmos. Terr. Phys., 38, 713.

Wright, J. W. and M. L. V. Pitteway (1978), Radio Sci., 13, 189.

# 3.2B SPACED ANTENNA DRIFT

O. Royrvik

Aeronomy Laboratory
Department of Electrical Engineering
University of Illinois
Urbana. IL 61801

## INTRODUCTION

The spaced antenna drift (SAD) technique has been used extensively for measuring horizontal wind by MF/HF radars (BRIGGS et al., 1950). Recently it has been suggested that this technique could also be successfully used by VHF radars (VINCENT and ROTTGER, 1980) and that it would be superior to a Doppler-beam-swinging (DBS) technique because it would take advantage of the aspect sensitivity of the scattered signal, and also might benefit from returns from single meteors. It appears, however, that the technique suffers from several limitations. On the basis of one SAD experiment performed at the very large Jicamarca radar it is concluded that the SAD technique can be compared in accuracy to the DBS technique only if small antenna dimensions are used.

A SAD experiment was run on the Jicamarca radar on October 17, 1981. The full antenna was used to transmit a 20 μsec pulse vertically, and the west, north, and east quarter sections were used for separate reception of the scattered signal. The 3 dB beam width of the transmitting antenna was only one degree, and the separation of the receiving antennas were 150, 150 and 211 m for the different pairs of antennas in the triangle. Horizontal velocities were calculated using the method of similar fades (BRIGGS and PHILLIPS, 1950 and FOOKS, 1965).

Minute-by-minute horizontal velocities were attempted calculated for five altitudes from 67 km to 79 km in the region of strong scattered power. Only about 50% of the minutes yielded a successfully calculated velocity. and a large fraction of these velocities were unreasonably large (>100 m/s). This compared to the vertical velocity that was successfully calculated in more than 90% of the minutes. Only by rejecting such large velocity points, and averaging the remaining velocities for one hour was it possible to get somewhat reasonable results. The reasons for this limited success are multiple, and since they all affect different size radars to a different degree we shall consider them separately and not try to give any detailed blame for the problems.

## DEPENDENCE ON ANTENNA SIZE

It is possible to use separate transmitting and receiving antennas and thus the spacing between the receiving antennas can be chosen randomly. However, since it is more convenient to use sections of the transmitting antenna for reception we will consider only this possibility. BRIGGS and VINCENT (1973) have shown that such an arrangement results in a reasonably large cross correlation between the signals in any two antenna sections regardless of the actual antenna size, if it is assumed that the scattering is isotropic.

We shall first assume semi-isotropic and homogeneous scattering and show that the accuracy of the calculated horizontal velocity depends on the antenna size. We will also assume that the signal-to-noise ratio is large.

The true drift velocity of the irregularity pattern over a one-dimensional surface is given by (FOOKS, 1965)

$$V_t = \frac{(V_c')^2}{V'}$$

Here $V' = \frac{d}{\tau'}$ and $V_c' = \frac{d}{\tau_s}$ where $\tau_s$ is the time delay at which the auto-correlation function has a value equal to that of the cross-correlation function at zero time delay. It can be shown that $\tau_s$ is a function of both the true drift velocity $V_t$ and the true fading velocity $V_c$ and can be expressed as (BRIGGS, 1980).

$$\tau_s = kT_{0.5}(1 + V_t^2/V_c^2)^{-1/2}$$

$T_{0.5}$ is the half-correlation time after the effect of the mean drift has been removed and k is a constant. Then combining these equations we get

$$V_t = \frac{d\tau'}{k^2 T_{0.5}^2}\left(1 + \frac{V_t^2}{V_c^2}\right) \tag{1}$$

At this point we make an assumption that can be shown to be valid for the Jicamarca radar and other radars with antenna dimensions of more than one hundred meters. The inequality

$$V_t^2 \ll V_c^2$$

reduces the equation (1) to

$$V_t = \frac{d\tau}{k^2 T_{0.5}^2} \tag{2}$$

As long as the correlation time is mainly a function of internal changes in the irregularity pattern and not dependent on the drift velocity the width of the peak in the cross-correlation function will be constant regardless of the amplitude of the drift velocity. The accuracy with which the location of the peak in the cross-correlation function can be determined is proportional to the width of the peak. This means it is easier to find the location of the maximum in a narrow peak, than in a broad peak. Thus it seems reasonable to introduce a fixed error $\Delta\tau'$ in the measurement of $\tau'$ since the half-width of the correlation function is virtually constant as a function of $V_t$ as long as $V_t \ll V_c$. Thus equation (2) yields

$$V_t + \Delta V_t = \frac{d\tau}{k^2 T_{0.5}^2} + \frac{d}{k^2 T_{0.5}^2}\Delta\tau' \tag{3}$$

Equation (3) expresses two related results. First, since the true velocity $V_t$ is not dependent on the antenna dimensions it is clear that an increase in d will decrease the time delay to maximum cross-correlation $\tau'$. Also since $\Delta\tau'$ is assumed to be constant we see that an increase in antenna dimensions will increase the error in the calculated horizontal velocity $\Delta V_t$.

In discussing these results it is appropriate to emphasize the findings of BRIGGS (1980) that the DBS and SAD techniques both rely on scattered signals from several off-vertical directions to measure horizontal velocities in the ionosphere. Larger off-vertical look angle will give better horizontal velocity estimates if the DBS technique is used. Thus the most natural conclusion is that also the SAD technique would give better measured horizontal velocity with increasing beam width, or smaller antenna dimensions. This is of course in accordance with the results of equation (3).

Summarizing, it is concluded that for large antenna dimensions, comparable to the Jicamarca radar, individual irregularities in the ground pattern last only a fraction of the time it takes to cover the distance separating receiving antennas, and thus it is natural that the horizontal drift velocity should be difficult to measure.

MEEK et al. (1979) have suggested using the normalized time discrepancy (NTD) as one measure of the accuracy of individual velocity measurements. A value of NTD of less than 0.2 has been advocated as a reasonable criteria for accepting the calculated horizontal velocity. It is clear however that NTD depends not only on the accuracy with which the time delay of the peak in the cross correlation can be measured, but also on the velocity of the pattern over the ground. In the extreme case of almost zero velocity and a finite pattern correlation time the equation

$$NTD = \frac{|\Sigma\tau_{ij}' + \Delta\tau_{ij}'|}{\Sigma|\tau_{ij}' + \Delta_{ij}'|}$$

reduces to

$$NTD = \frac{|\Sigma\Delta\tau_{ij}'|}{\Sigma|\Delta\tau_{ij}'|}$$

where $\Delta\tau_{ij}'$ is the error in measuring $\tau_{ij}'$. Since individual $\Delta\tau_{ij}'$ are expected to be statistically independent NTD ($V \to 0$) is expected to be randomly distributed between zero and one. If $\Delta\tau_{ij}'$ is kept constant and $\tau_{ij}$ is increased as a function of increasing velocity it can also be seen that NTD will decrease. Thus using NTD as a measure of reliability of the horizontal wind will tend to select measurements with high wind values. In Figure 1 the relationship between NTD and measured wind velocity have been plotted, and as can be seen the average wind velocity measured decreases as the NTD increases. It is concluded that NTD is not very useful as a test of the accuracy of the wind measurement, and using it can systematically change an averaged wind value. However, in practical situations use of NTD is more serious for a large radar antenna like the Jicamarca than it is for the substantially smaller SOUSY-VHF radar (ROTTGER, 1981).

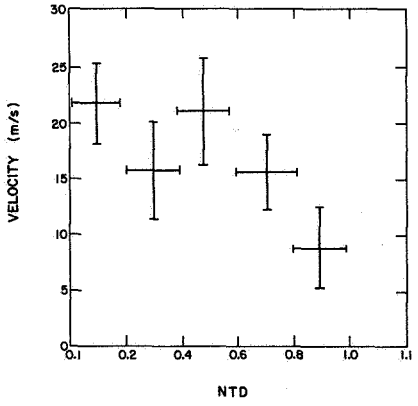


Figure 1. Normalized time discrepancy as a function of ionospheric velocity averaged for the time 9:40 to 12:30 LST and for all altitudes.

## REFLECTION FROM STRATIFIED LAYERS AND METEORS

It has been suggested that the SAD technique is superior to the DBS technique because it takes advantage of the additional power received from the vertical direction from partially reflecting stratified layers where such layers exist (VINCENT and ROTTGER, 1980). However, it can be easily shown that only that part of the signal that comes from the off-vertical direction gives any information about the horizontal velocity, and the larger off-vertical angle the better (ROYRVIK, 1983). It then becomes a matter of superposition of useless vertical signal, and useful off-vertical signal. It should be obvious that the more aspect sensitive the scattered/reflected signal is, the more of it can be attributed to the useless vertical signal. Thus increased aspect sensitivity decreases the signal-to-noise ratio where the noise is in the form of useless vertical signal. So no advantage is had from an increase in aspect sensitivity, and thus the SAD technique cannot benefit from measuring it. On the other hand, it can be argued that the DBS technique has an advantage because it can more easily distinguish between the enhanced signal in the vertical antenna, and the really useful signal in the off-vertical antenna however small this signal may be.

It has also been suggested that the SAD technique could calculate the full velocity field from one single meteor (ROTTGER, 1981). This is clearly not the case since the irregularity pattern on the ground resulting from a long train of irregularities would be a series of semi-parallel lines. Drift of the meteor trail perpendicular to the trail direction would only shift the lines in the parallel direction and thus produce no observable fading in the returned signal. It is also questionable whether the velocity parallel to the meteor trail could be measured since the SAD technique assumes an eliptical irregularity pattern, whereas the actual pattern is a series of parallel lines. In any case, great care should be taken in using meteor echoes since contamination can result from both saturation of the receiving system and reflection from the traveling meteor head. This applies to both the SAD and the DBS techniques.

It is concluded that the most useful size of a SAD antenna is such that the irregularities on the ground on the average, drifts from one receiving antenna section to another in one half-correlation time (ROYRVIK, 1983). Assuming correlation time of a VHF signal of 1 s and horizontal velocities of typically 15 m/s in the mesosphere, a transmitting/receiving antenna 60 meters on a side would be ideal. Larger antennas, although they may increase the signal-to-noise ratio, only degrades the performance of the SAD radar.

## ACKNOWLEDGMENT

The work described was supported by the National Science Foundation under Grant ATM 80-19563.

## REFERENCES

Briggs, B. H. (1980), Radar observations of atmospheric winds and turbulence, A comparison of techniques, J. Atmos. Terr. Phys., 42, 823.

Briggs, B. H., and G. J. Phillips (1950), A study of the horizontal irregularities of the ionosphere, Proc. Phys. Soc. B.LXIII, 907.

Briggs, B. H., G. J. Phillips and D. H. Shinn (1950), The analysis of observations on spaced receivers of the fading radio signals, Proc. Phys. Soc. London LXIII, 106.

Briggs, B. H. and R. A. Vincent (1973), Some theoretical considerations on remote probing of weakly scattering irregularities, Aust. J. Phys., 26, 805

Fooks, G. F. (1965), Ionospheric drift measurements using correlation analysis; methods of computation and interpretation of results, J. Atmos. Terr. Phys. 27, 979.

Meek, C. E., A. H. Hanson and J. B. Gregory (1979), Internal consistency analyses for partial and total reflection drifts data, J. Atmos. Terr. Phys., 41, 251.

Rottger, J. (1981), Investigations of lower and middle atmosphere dynamics with spaced antenna drifts radar, J. Atmos. Terr. Phys., 43, 277.

Royrvik, O. (1983) Spaced antenna drifts at Jicamarca, Mesospheric measurements, Accepted for publication, Radio Science.

Vincent, R. A. and J. Rottger (1980), Spaced antenna VHF radar observations of tropospheric velocities and irregularities, Radio Sci., 15, 319.

# 3.3A AN EVALUATION OF THE ACCURACY OF SOME RADAR WIND PROFILING TECHNIQUES

A. J. Koscielny and R. J. Doviak

National Severe Storms Laboratory
1313 Halley Circle
Norman, OK 73069

## INTRODUCTION

Major advances in Doppler radar measurement in optically clear air have made it feasible to monitor radial velocities in the troposphere and lower stratosphere. For most applications we want to monitor the three dimensional wind vector rather than the radial velocity. Measurement of the wind vector with a single radar can be made assuming a spatially linear, time invariant wind field. The components and derivatives of the wind are estimated by the parameters of a linear regression of the radial velocities on functions of their spatial locations. The accuracy of the wind measurement thus depends on the locations of the radial velocities.

PETERSON and BALSLEY (1979) point out that a tradeoff exists for a given technique between the accuracies of horizontal and vertical component measurements. Because we usually need to measure the three components of wind with different accuracy and as inexpensively as possible, we are led to evaluate the suitability of some of the common retrieval techniques for simultaneous measurement of both the vertical and horizontal wind components. The techniques we will consider are fixed beam, azimuthal scanning (VAD) and elevation scanning (VED).

## ERROR ANALYSIS THEORY

The estimation of the parameters of a linear wind field from radial velocities is discussed by KOSCIELNY et al. (1982). The measured radial velocity $v_r$ can be modelled by a linear regression equation of the form

$$v_r = P_m K_m + \varepsilon \tag{1}$$

where $P_m$ is a row vector of regressor variables which are functions of range r, azimuth $\theta$, and elevation angle $\theta_e$; $K_m$ is a column vector of m parameters. The measured $v_r$, a reflectivity weighted mean of radial velocities within the radar's resolution volume, can contain errors $\varepsilon$ due to nonuniform reflectivity, turbulence, targets such as hydrometeors that move relative to the wind, and a nonlinear wind. It can be shown that, given n measurements of $v_r$, least squares estimates of $K_m$ are computed by

$$\hat{K}_m = (P_{nm}{}^T P_{nm})^{-1} (P_{nm}{}^T V_n) \tag{2}$$

where T indicates transpose and $P_{nm}$ is an nxm matrix of the regressor variables corresponding to the n radial velocity measurements in $V_n$. Measurement errors in the radial velocities produce uncertainties in the estimate $K_m$ and the covariances of $\hat{K}_m$ about $K_m$ are given by

$$C_{mm} = (P_{nm}{}^T P_{nm})^{-1} \sigma_\varepsilon{}^2 \tag{3}$$

where $\sigma_\varepsilon{}^2$ is the variance of $\varepsilon$.

If the wind field has variations not modeled by (1), the $\hat{K}_m$ will be biased and the amount of bias $B_m$ is given by the product of a known alias matrix $A_{m\ell}$ with the vector $K_\ell$ of the $\ell$ unknown parameters of the wind field not included in $K_m$. Thus

$$B_m = A_{m\ell} K_\ell \tag{4}$$

where

$$A_{m\ell} = (P_{nm}^T P_{nm})^{-1} (P_{nm}^T P_{n\ell}). \tag{5}$$

$P_{n\ell}$ is a matrix of regressor variables for the components not included in (1).

The various techniques referred to in the introduction assume the wind to be uniform (i.e., the first and higher order derivatives are zero) over the data analysis volume. However, because w cannot be uniform for any appreciable depth of the troposphere (i.e., w must be zero at the earth's surface), the horizontal wind can never be uniform at all heights. Thus we must account for errors produced by wind shear. We propose to analyze the errors in these techniques by computing the bias and variance of the least squares estimates $\hat{K}_m$ with assumptions that $\sigma_\varepsilon^2$ is constant and the wind field is actually linear. Thus $K_3$ contains the three uniform components $u_o$, $v_o$, $w_o$ and $K_8$ contains the 8 spatial derivatives ($u_x$, $u_z$, $v_y$, $v_z$, $u_y + v_x$, $w_x$, $w_y$, $w_z$) of the linear wind. In our evaluation and comparison of techniques, we assume that a total of n measurements are available for each and these n measurements are distributed in space to estimate wind at some height h.

(a) Fixed Beam

We consider a configuration for the fixed beam technique in which three beams, one verticl and two off-vertical at elevation $\theta_e$, are sampled. The off-vertical beams usually have perpendicular horizontal projections; for convenience, we will consider them to have azimuths 0° and 90°. The total number of radial velocity measurements for a height h for all three beams is n; for generality, we let the number of vertical measurements be N.

The bias and variance properties of the estimates $\hat{K}_3^T = (u_o, v_o, w_o)$ are computed in Appendix 1 using (3) and (5), and we find that, for $n = 3N$,

$$\begin{aligned} \mathrm{VAR}(\hat{u}_o) = \mathrm{VAR}(\hat{v}_o) &= \frac{\sigma_\varepsilon^2}{n} \cdot 3 \cdot (\sec^2\theta_e + \tan^2\theta_e) \\ \mathrm{VAR}(\hat{w}_o) &= \frac{\sigma_\varepsilon^2}{n} 3 \end{aligned} \tag{6}$$

$$\mathrm{Bias} \begin{bmatrix} \hat{u}_o \\ \hat{v}_o \\ \hat{w}_o \end{bmatrix} \approx h \begin{bmatrix} u_x \cot\theta_e + w_x \\ v_y \cot\theta_e + w_y \\ 0 \end{bmatrix} \tag{7}$$

The bias equation is approximate because we have used $h \approx r\sin\theta_e$ which should be appropriate for $r \leq 30$ km. From (7) we see that the bias due to spatial derivatives is a linear function of height which is expected because the beam separation is linearly dependent on h. In addition, we see from (6) and (7)

that the variance decreases with n, but that the bias cannot be reduced by data averaging.

(b) Azimuthal Scanning

In an azimuthal scanning technique, usually called VAD (Velocity Azimuth Display), data along a circle centered on the radar are used to directly estimate the components of the uniform wind field. The results of the bias and variance equation evaluation, in Appendix 2, are that

$$\mathrm{VAR}(\hat{u}_o) = \mathrm{VAR}(\hat{v}_o) = \frac{\sigma_\varepsilon^2}{n} \cdot 2\sec^2\theta_e$$

$$\mathrm{VAR}(\hat{w}_o) = \frac{\sigma_\varepsilon^2}{n} \cdot \csc^2\theta_e \qquad (8)$$

$$\mathrm{Bias}\begin{bmatrix}\hat{u}_o\\ \hat{v}_o\\ \hat{w}_o\end{bmatrix} \approx h\begin{bmatrix}w_x\\ w_y\\ 1/2(u_x + v_y)\cdot\cot^2\theta_e\end{bmatrix} \qquad (9)$$

(c) Elevation Scanning

In the elevation scanning (Velocity Elevation Display) technique, radial velocities at a height h are collected for elevation angles $\theta_o \le \theta_e \le 180-\theta_o$. We assume $\frac{n}{2}$ data are collected for the two azimuths 0° and 90° so both horizontal components are measured. It is shown in Appendix 3 that

$$\mathrm{VAR}(\hat{u}_o) = \mathrm{VAR}(\hat{v}_o) = \frac{\sigma_\varepsilon^2}{n} \cdot \frac{4(\pi-2\theta_o)}{\{\pi-2\theta_o-\sin(\pi-2\theta_o)\}}$$

$$\mathrm{VAR}(\hat{w}_o) = \frac{\sigma_\varepsilon^2}{n} \cdot \frac{2(\pi-2\theta_o)}{\{\pi-2\theta_o+\sin(\pi-2\theta_o)\}} \qquad (10)$$

$$\mathrm{Bias}\begin{bmatrix}\hat{u}_o\\ \hat{v}_o\\ \hat{w}_o\end{bmatrix} \approx h\begin{bmatrix}w_x\\ w_y\\ (u_x + v_y)\cdot\left[\dfrac{\pi-2\theta_o-\sin(\pi-2\theta_o)}{\pi-2\theta_o+\sin(\pi-2\theta_o)}\right]\end{bmatrix} \qquad (11)$$

ERROR COMPARISON

The results of our analysis of the three techniques, summarized in Table 1 show the variances of the wind estimates all depend on $\sigma_\varepsilon^2/n$. Since the variance of an average of n independent data is $\sigma_\varepsilon^2/n$, we will divide this quantity by the variance of the estimate of the wind component. Because of its similarity to the usual statistical definition, we term this quantity the efficiency of the estimate.

The variation of the efficiences of the horizontal wind estimates with elevation angle are shown in Figure 1. The VAD technique has the highest efficiency of the techniques for all elevation angles. In addition, the VAD

Table 1. Variance and bias equations for horizontal and vertical wind estimates obtained from fixed beam, azimuth scanning or elevation scanning techniques. $VAR[\hat{v}_o] \equiv VAR[\hat{u}_o]$ and for Bias $(\hat{v}_o)$ replace x subscript with y.

| | Fixed Beam (one vertical) | Azimuth Scanning (VAD) | Elevation Scanning (VED) |
|---|---|---|---|
| VAR $(\hat{u}_o)$ | $\frac{\sigma_\varepsilon^2}{n} 3(\sec^2\theta_e + \tan^2\theta_e)$ | $\frac{\sigma_\varepsilon^2}{n} 2 \sec^2\theta_e$ | $\frac{\sigma_\varepsilon^2}{n} 2\left[\frac{\pi-2\theta_o}{(\pi-2\theta_o) - \sin(\pi-2\theta_o)}\right]$ |
| VAR $(\hat{w}_o)$ | $\frac{\sigma_\varepsilon^2}{n} 3$ | $\frac{\sigma_\varepsilon^2}{n} \csc^2\theta_e$ | $\frac{\sigma_\varepsilon^2}{n} 2\left[\frac{\pi-2\theta_o}{(\pi-2\theta_o) + \sin(\pi-2\theta_o)}\right]$ |
| Bias$(\hat{u}_o)$ | $h(u_x \cot\theta_e + w_x)$ | $hw_x$ | $hw_x$ |
| Bias$(\hat{w}_o)$ | 0 | $h(u_x + v_y) \frac{\cot^2\theta_e}{2}$ | $h(u_x + v_y)\left[\frac{\pi-2\theta_o - \sin(\pi-2\theta_o)}{\pi-2\theta_o + \sin(\pi-2\theta_o)}\right]$ |

maintains reasonable efficiency to larger elevation angles (75°) than either fixed beam or VED.

Figure 1 shows efficiencies monotonically increasing as $\theta_e$ gets smaller. But for measurements at a constant height the range increases when $\theta_e$ decreases. Because echo power reduces in proportion to the inverse square of range (assuming the echoing layer scatters isotropically and is horizontally homogeneous) the signal-to-noise ratio (SNR) falls as $\theta_e$ decreases. If measurement errors are solely due to thermal noise and SNR is less than one, ZRNIC' (1979) shows that measurement variance $\sigma_\varepsilon^2$ is proportional to $(SNR)^{-2}$. The effect of decreasing SNR as $\theta_e$ becomes small is to increase $\sigma_\varepsilon^2$ as $\csc^4 \theta_e$; the efficiency of the horizontal wind measurements thus vanishes as $\theta_e$ goes to zero. However, the variance $\sigma_\varepsilon^2$ includes meteorological effects such as turbulence that, in our experience, places a lower bound on $\sigma_\varepsilon^2$ of about 1 $m^2 s^{-2}$. Because we are mainly concerned in this paper with elevation angles larger than 40° and, consequently, ranges less than about 30 km, $\sigma_\varepsilon^2$ can be regarded as a constant.

The efficiencies of the vertical velocity estimates are shown in Figure 2. The VED has the highest efficiency, but for large elevation angles the VAD is comparable. The fixed beam has a constant efficiency of $\frac{1}{3}$ since the number of vertical estimates is fixed at $\frac{n}{3}$.

The biases of the estimates show a linear dependence on the height h. To normalize bias errors, we assume h = 1 km, so the bias for greater heights can be simply computed. The biases depend on the value of unknown spatial derivatives. Following WALDTEUFEL and CORBIN (1979) we use $u_x = v_y = 10^{-3} s^{-1}$ and $w_x = w_y = 10^{-4} s^{-1}$ as maximum values. The biases thus computed are shown in Figure 3 for the horizontal components and in Figure 4 for the vertical component. The asymmetry of the beam locations about the vertical for the fixed beam technique produces a horizontal wind bias due to $u_x$ and $v_y$ which decreases as $\cot\theta_e$. The horizontal wind biases for the VAD and VED are the same and are constant with elevation angle. For the fixed beam technique the vertical velocity is not biased by any derivatives. The vertical wind bias in the VED and VAD decreases with increasing elevation angle.

In conclusion, the vertical velocity variance and the bias errors can be decreased by using larger elevation angles. The variance for horizontal components increases with elevation angle but can be controlled to an extent by data averaging. Because bias increases with height, the higher altitudes may require a vertical measurement for vertical velocity.

(a) Example

The bias the variance equations can be used to choose an elevation angle for profiling. For example, suppose we wish to profile the winds at 5 km using 360 measurements with $\sigma_\varepsilon = 1\ m \cdot s^{-1}$. The root mean square errors (bias squared plus variance) for the horizontal and vertical components are shown in Figures 5 and 6 for each of the techniques. We have kept vertical and horizontal errors separate because vertical velocity is much smaller and requires greater accuracy. If we require horizontal and vertical velocity accuracies of $1\ m \cdot s^{-1}$ and $0.1\ m \cdot s^{-1}$ respectively, we would use an elevation angle between 83° and 85° for the VAD and 77° and 81° for the VED. Because of the bias error, the fixed beam horizontal wind error is $1.5\ m \cdot s^{-1}$ or larger.

## POSSIBLE IMPROVEMENTS

The analysis of the previous section suggests some simple improvements that can be made to increase the accuracy of the measurements.

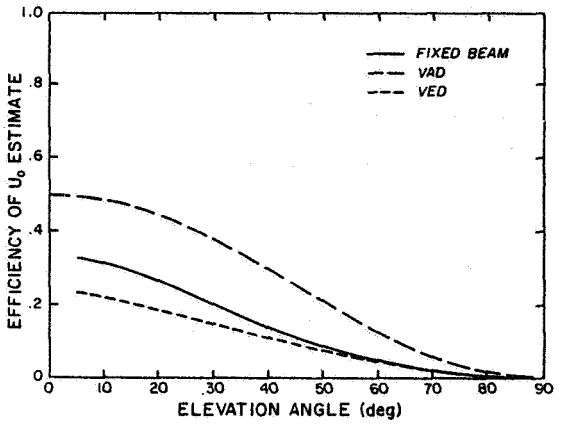


Figure 1. Variation of horizontal wind estimator efficiencies with elevation angle.

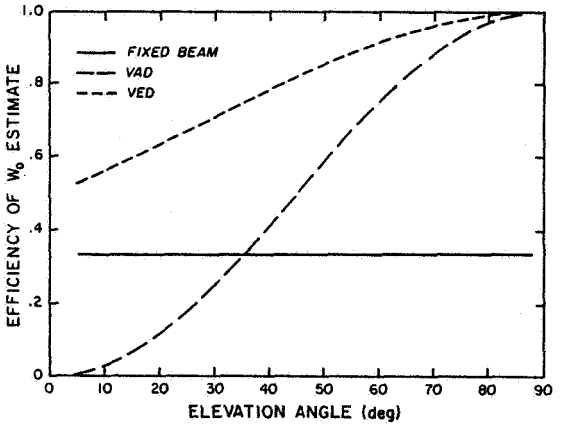


Figure 2. Variation of vertical wind estimator efficiencies with elevation angle.

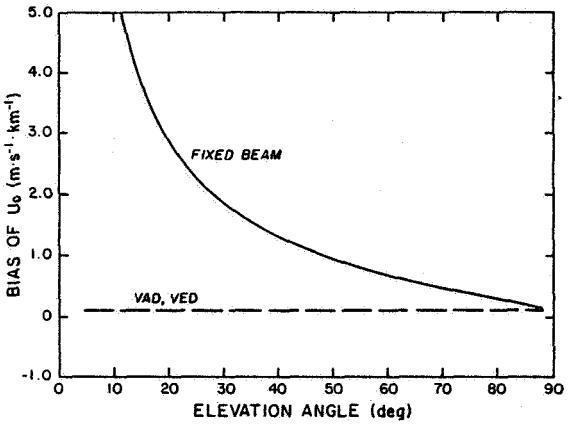


Figure 3. Bias error in horizontal wind estimator at 1 km with $u_x=v_y=10^{-3}s^{-1}$, $w_x=w_y=10^{-4}s^{-1}$. VAD and VED biases overlap.

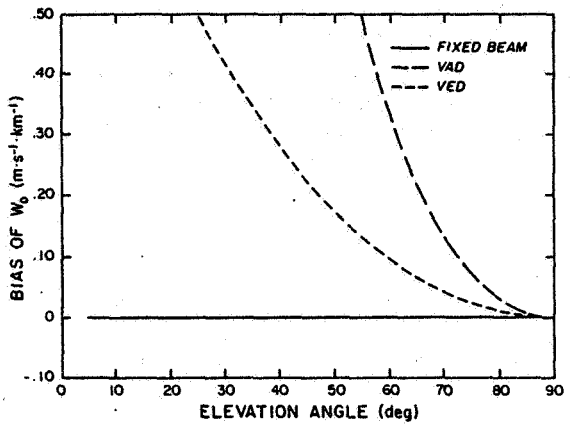


Figure 4. Bias error in vertical wind estimator at 1 km with $u_x=v_y=10^{-3}s^{-1}$, $w_x=w_y=10^{-4}s^{-1}$.

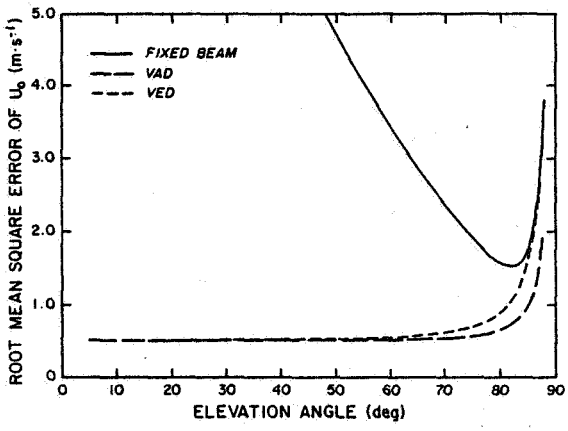


Figure 5. Root mean square error for the horizontal estimator if $\sigma=1$ $m \cdot s^{-1}$, n=360, and h=5 km.

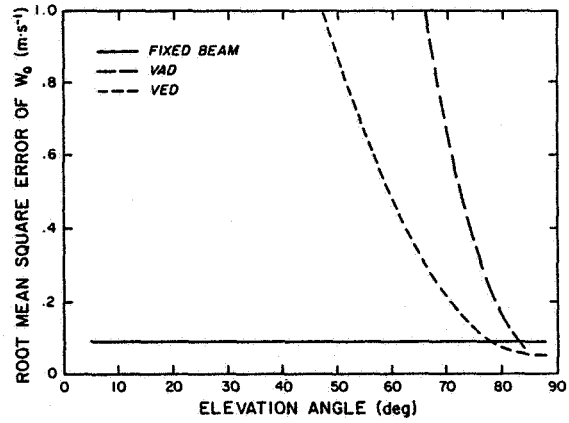


Figure 6. Root mean square error for the vertical estimator is $\sigma=1$ $m \cdot s^{-1}$, n=360, and h=5 km.

(a) Fixed Beam with Error Minimization

The wind estimate efficiencies for the fixed beam technique can be improved slightly be collecting a specified number N of vertical data. Minimizing the first diagonal element of the matrix in (A1.1), which is $VAR(\hat{u}_o) = VAR(\hat{v}_o)$ gives

$$\frac{N}{n} = \frac{\sin\theta_e}{\sqrt{2}+\sin\theta_e} \tag{12}$$

so N would vary from $\frac{n}{3}$ at $\theta_e = 45°$ to about 0.4 n for $\theta_e$ near 90°. The efficiencies are shown in Figure 7 for $u_o$ and Figure 8 for $\hat{w}_o$. It can be seen that for $\theta_e > 45°$, the efficiency of estimating $\hat{u}_o$ is unchanged but is slightly improved for $w_o$.

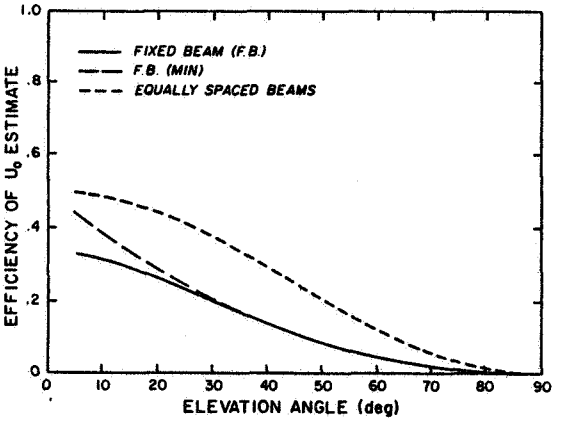


Figure 7. Horizontal wind estimator efficiency for fixed beam, fixed beam with horizontal error minimization, and fixed beam with equally spaced, off-vertical beams.

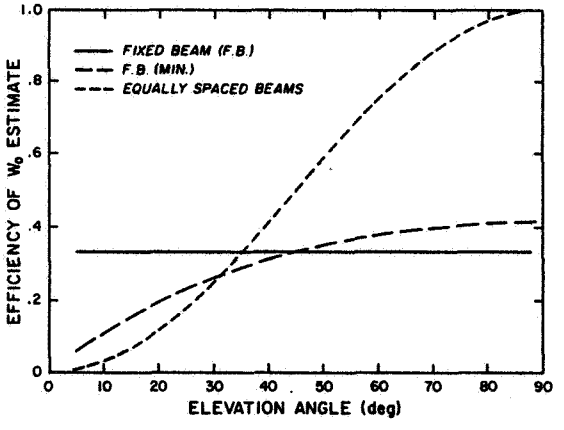


Figure 8. Vertical wind estimator efficiencies for the same techniques as described in Figure 7 caption.

The size of the variance contribution (i.e., $\sigma_\varepsilon^2 \tan^2\theta_e/N$) from the vertical velocity bias removal appears to indicate that it might be better to ignore the bias error ($w_o \tan\theta_e$). However, for observation time intervals of several minutes, a mesoscale value of $w_o$ should be used. For large elevation angles, ($\theta_e \gtrsim 75°$) the bias error could be several meters per second or larger. For tropospheric observation under all conditions, the bias should be removed if a horizontal velocity accuracy of 1 $m \cdot s^{-1}$ is required.

(b) Three Off-Vertical Beams

For some applications, ground clutter presents a problem for vertical measurements. The fixed beam technique with three off-vertical beams with elevation $\theta_e$ and azimuths 0°, 120°, 240° is analyzed in Appendix 1b. The analysis shows that the variances (and efficiencies) of the estimates are identical to those for the VAD technique (compare Figures 1, 2 with Figures 7, 8). The biases for the $u_o$ estimate is very similar to the fixed beam with one vertical but the $w_o$ estimate is biased as shown in Figure 9.

(c) Application of the Continuity Equation to VAD Data

Vertical winds as small as few centimeters per sec are important in forecasting and, as noted earlier, $w_o$ should be estimated with more accuracy than the horizontal components. Because of ground clutter it may become very difficult to estimate the radial component of air motion when the beam is pointed near the vertical since the radial velocities will have values close to zero. We now show that by assuming a linear wind field and applying the mass continuity equation, we can estimate vertical wind, averaged over the circle of measurement, with the required accuracy. When mass continuity is applied, we will call the technique indirect whereas the previously discussed techniques (e.g., VAD) are direct measurements of w.

Two VAD modes in which vertical soundings can be made are fixed $\theta_e$ variable r, and variable $\theta_e$ fixed r. With variable r however, the horizontal area for which $w_o$ is representative varies, so we prefer the second mode. Divergence is estimated by applying Gauss's theorem to the volume V (see Figure 10) enclosed by the area $S_1$ at constant range from the radar and the area $S_2$ at constant height (DOVIAK and ZRNIC', 1983). Applying mass continuity and integrating gives an areal averaged $\bar{w}$,

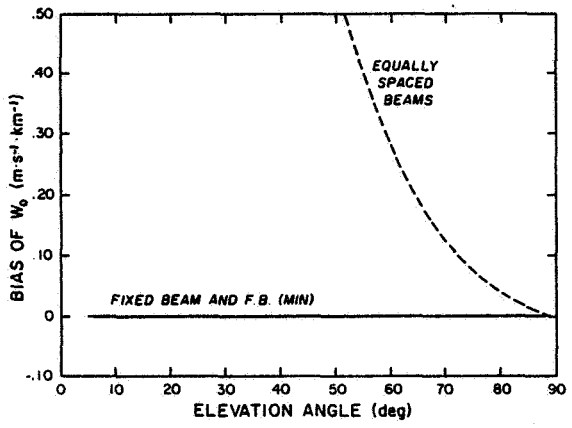


Figure 9. Vertical wind biases for the same techniques as described in Figure 7 caption.

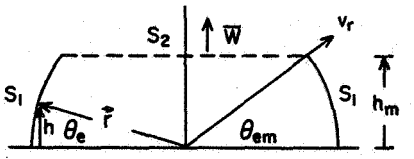


Figure 10. Geometry to estimate vertical velocity averaged over the circular area $S_2$.

$$\overline{w} = \frac{-2e^{\Gamma h}}{(1-h^2/r^2)r} \int_o^h e^{-\Gamma h} C_o(h)dh \tag{13}$$

where $\Gamma = gM/RT$ is the average lapse rate of air density versus height and

$$C_o(h) = \frac{1}{2\pi r} \int_o^{2\pi} v_r r d\phi \tag{14}$$

is the average radial velocity around the circle of measurement.

To fix the number of measurements at n, we assume M values of $v_r$ are made on each of L circles spaced at intervals $\Delta h$ from h=0 to $h=h_m$. Then

$$\hat{C}_o(h) = \frac{1}{M} \sum_{m=1}^{M} \hat{v}_{rm} \tag{15}$$

If all the radial velocities are independent with the same uncertainty, then

$$VAR[\overline{w}] = \frac{4\ e^{2\Gamma h}\ h\ VAR[v_r]}{r^2(1-h^2/r^2)^2\ N} \frac{N}{n} \left\{ \frac{1-e^{-2\Gamma h}}{2\Gamma} \right\} \tag{16}$$

For a direct measurement with a vertical beam $VAR[\hat{w}_o] = VAR[v_r]/N$. If we require that, for our maximum height $h_m$, $VAR[\overline{w}] = VAR[\hat{w}_o]$, then the range can be found by solving

$$2\Gamma h_m = \ell n \left\{ 1 + \frac{\Gamma h_m r^2}{2h_m^2} \left[ 1 - \frac{h_m^2}{r^2} \right] \frac{n}{N} \right\} \tag{17}$$

Because of the accuracy needed for vertical velocity estimates, the number N of vertical data will be much larger than the n-N data for horizontal wind component estimation. Thus in (17) we can assume $n/N \simeq 1$. Using $h_m$ = 10 km, $\Gamma = 0.113\ km^{-1}$ in (17) gives $r \simeq 40$ km, so $\theta_{em} \simeq 14°$. For heights lower than $h_m$, $VAR[\overline{w}]$ is less than for a direct measurement.

To compare the variances for direct and indirect measurements, assume that we have n/10 measurements at each level for estimating $u_o$, $v_o$, and $w_o$ at each of 10 levels spaced 1 km apart. Solving (16) assuming a specified $VAR[\overline{w}] = 10^{-3}\ m^2 s^{-2}$ at $h_m$ = 10 km with $VAR[v_r] = 1\ m^2 s^{-2}$ gives n = 1080. So there are 108 data at each level and, from (8) $VAR[u_o] \simeq 2 \times 10^{-2} m^2 s^{-2}$. With 108 data at each

level for the direct VAD measurement techniques, the VAR[$\hat{w}_o$] is larger than that obtained using the indirect method even with $\theta_e = 90°$. Because $w_o$ needs to be estimated with better accuracy than $u_o$, $v_o$, consider that most measurements are made with a vertical beam. We need at least 4 data spaced 90° apart on a circle at each level in order to remove the bias in $\hat{u}_o$, $\hat{v}_o$ due to $u_x$, $v_x$ (Equation 7). Thus from (8) we have VAR[$\hat{u}_o$]$\geq$0.5 $m^2 s^{-2}$ which should be satisfactory for horizontal wind estimates but which is an order of magnitude larger than obtained by the indirect method. Furthermore, we have at most 104 data available at each level for the vertical beam with the consequence that VAR[$\hat{w}_o$]$\simeq 10^{-2} m^2 \cdot s^{-2}$, an order of magnitude or more (at h<10 km) larger than obtained using the indirect method. A comparison of these variances is shown in Figure 11.

In reality, the variances for the indirect measurement technique may not be this much smaller, since we have neglected the dependence of signal strength (and VAR[$v_r$] with range. However, this analysis has shown that the indirect technique does not require a tradeoff between vertical and horizontal variance. It offers the advantages of low variances, an areal averaged vertical velocity, and requires no assumption about the spatial structure of the wind to measure vertical velocity.

## SUMMARY AND CONCLUSIONS

We have examined the errors in three radar techniques (three fixed beams, VAD, and VED) used to directly measure the three components of the wind. Equations were derived for the bias and variance of the uniform wind components estimates under the assumption of a spatially linear, time invariant wind field

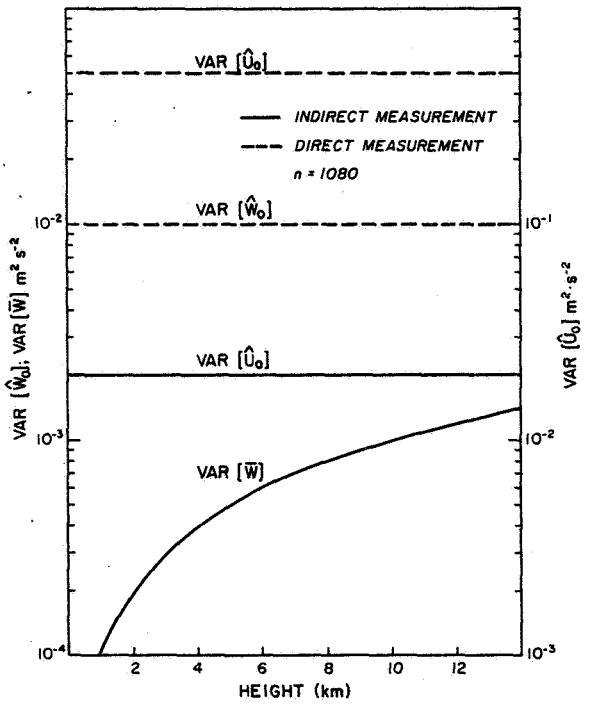


Figure 11. Comparison of wind estimate variances for direct and indirect techniques.

and a constant radial velocity measurement error. The measurement errors produce variance in the estimates and the linear wind shear biases the estimates. The variance of the estimates can be reduced by averaging more measurements but the biases cannot. Thus, for these direct measurement techniques, the selection of an elevation angle for simultaneous observation requires a compromise based on the required accuracy of the measurement.

We have also examined the errors for an indirect measurement technique based on Gauss's theorem with an equation of continuity constraint. Two advantages this indirect technique offers are that it does not require any assumptions about the spatial structure of the wind to measure vertical velocity and that its error variance can be smaller because it does not require a vertical and horizontal measurement variance compromise.

ACKNOWLEDGEMENTS

Our thanks to Joy Walton for her efficient preparation of the manuscript, to Joan Kimpel for drafting the figures, and to Robert Goldsmith for the photographic reductions.

REFERENCES

Anton, H. (1981), Elementary Linear Algebra, John Wiley, 375 pp.

Doviak, R. J. and D. S. Zrnic' (1983), Doppler Weather Radar and Weather Observations, Academic Press, New York (in press).

Koscielny, A. J., R. J. Doviak and R. Rabin (1982), Statistical considerations in the estimation of divergence from single Doppler radar and application to pre-storm boundary layer observation, J. Appl. Meteor., 21, 197-210.

Peterson, V. L. and B. B. Balsley (1979), Clear air Doppler radar measurements of the vertical component of wind velocity in the troposphere and stratosphere, Geophys. Res. Lett., 6, 933-946.

Waldteufel, P. and H. Corbin (1979), On the analysis of single Doppler data, J. Appl. Meteor., 18, 532-542.

Zrnic', D. S. (1979), Estimation of spectral moments for weather echoes, IEEE Trans. Geo. Elec., GE-17, 113-128.

## APPENDIX 1. ANALYSIS OF THE FIXED BEAM TECHNIQUES

For the fixed beam technique with one vertical, and two off-vertical beams at elevation $\theta_e$, azimuths 0° and 90°, we find, following the notations of KOSCIELNY et al. (1982), that

$$P_{nm} = \begin{bmatrix} \cos\theta_e & 0 & \sin\theta_e \\ \text{(repeats (n-N/2 times)} & & \\ 0 & \cos\theta_e & \sin\theta_e \\ \text{(repeats (n-N)/2 times)} & & \\ 0 & 0 & 1 \\ \text{(repeats N times)} & & \end{bmatrix} = P_{n3}$$

$$P_{nm}{}^T P_{nm} = \begin{bmatrix} \frac{(n-N)}{2}\cos^2\theta_e & 0 & \frac{(n-N)}{2}\cos\theta_e \cdot \sin\theta_e \\ & \frac{(n-N)}{2}\cos^2\theta_e & \frac{(n-N)}{2}\cos\theta_e \cdot \sin\theta_e \\ & & N + (n-N)\sin^2\theta_e \end{bmatrix} \equiv P_3{}^T P_3$$

Since this is a symmetric matrix, we have not entered the identical terms below the diagonal elements. We invert $P_3{}^T P_3$ by performing a sequence of row operations to reduce it to the identity matrix. Performing this same sequence on the identity matrix reduces it to $[P_3{}^T P_3]^{-1}$ (ANTON, 1981). Thus

$$(P_3{}^T P_3)^{-1} = \begin{bmatrix} \frac{2\sec^2\theta_e}{n-N} + \frac{\tan^2\theta_e}{N} & \frac{\tan^2\theta_e}{N} & -\frac{\tan\theta_e}{N} \\ & \frac{2\sec^2\theta_e}{n-N} + \frac{\tan^2\theta_e}{N} & -\frac{\tan\theta_e}{N} \\ & & \frac{1}{N} \end{bmatrix} \qquad \text{(A1.1)}$$

For an equal number of measurements on each beam, 3N=n and

$$\mathrm{VAR}(\hat{u}_o) = \mathrm{VAR}(\hat{v}_o) = \frac{3\sigma_\varepsilon^2}{n}\left(\sec^2\theta_e + \tan^2\theta_e\right) \qquad \text{(A1.2)}$$

$$\mathrm{VAR}(\hat{w}_o) = \frac{3\sigma_\varepsilon^2}{n} \qquad \text{(A1.3)}$$

The biasing of the estimates by the derivatives of the linear wind can be computed from the alias matrix of (3). Since the analysis is for constant height, all vertical derivatives cause no bias. Thus, for equal numbers of measurements,

$$P_{n\ell} = \begin{bmatrix} r\cos^2\theta_e & 0 & r\cos\theta_e \cdot \sin\theta_e & 0 \\ \vdots & \vdots & \vdots & \vdots \\ 0 & r\cos^2\theta_e & 0 & r\cos\theta_e \cdot \sin\theta_e \\ \vdots & \vdots & \vdots & \vdots \\ 0 & 0 & 0 & 0 \\ \vdots & \vdots & \vdots & \vdots \end{bmatrix}$$

$A_{34} = [P_{nm}{}^T P_{nm}]^{-1} P_{nm}{}^T P_{n\ell}$ and performing the multiplication gives

$$A_{34} = \begin{bmatrix} r\cos\theta_e & 0 & r\sin\theta_e & 0 \\ 0 & r\cos\theta_e & 0 & r\sin\theta_e \\ 0 & 0 & 0 & 0 \end{bmatrix}$$

Using the approximation $h \approx r_{\sin}\,\theta_e$

$$A_{34} = \begin{bmatrix} h\cot\theta_e & 0 & h & 0 \\ 0 & h\cot\theta_e & 0 & h \\ 0 & 0 & 0 & 0 \end{bmatrix} \qquad \text{(A1.4)}$$

and $K_\ell{}^T = [u_x, v_y, w_x, w_y]$.

For the fixed beam technique with three beams at elevation $\theta_e$ and azimuths 0°, 120°, and 240°, we find that

$$P_{nm} = \begin{bmatrix} \sin 0° \cdot \cos\theta_e & \cos 0° \cdot \cos\theta_e & \sin\theta_e \\ \vdots & \vdots & \vdots \\ \sin 120° \cdot \cos\theta_e & \cos 120° \cdot \cos\theta_e & \sin\theta_e \\ \vdots & \vdots & \vdots \\ \sin 240° \cdot \cos\theta_e & \cos 240° \cdot \cos\theta_e & \sin\theta_e \\ \vdots & \vdots & \vdots \end{bmatrix}$$

so

$$(P_{nm}{}^T P_{nm}) = \begin{bmatrix} \frac{n\cos^2\theta_e}{2} & 0 & 0 \\ 0 & \frac{n\cos^2\theta_e}{2} & 0 \\ 0 & 0 & n\sin^2\theta_e \end{bmatrix}$$

and

$$(P_{nm}{}^T P_{nm})^{-1} = \begin{bmatrix} \frac{2\sec^2\theta_e}{n} & 0 & 0 \\ 0 & \frac{2\sec^2\theta_e}{n} & 0 \\ 0 & 0 & \frac{\csc^2\theta_e}{n} \end{bmatrix} \qquad \text{(A1.5)}$$

The alias matrix can be computed as before. For this case the predictor function for deformation is nonzero so

$$P_{n\ell} = \begin{bmatrix} 0 & 0 & r\cos^2\theta_e & 0 & r\sin\theta_e\cdot\cos\theta_e \\ \vdots & \vdots & \vdots & \vdots & \vdots \\ -abr\cos^2\theta_e & a^2r\cos^2\theta_e & b^2r\cos^2\theta_e & ar\cos\theta_e\cdot\sin\theta_e & -br\sin\theta_e\cdot\cos\theta_e \\ \vdots & \vdots & \vdots & \vdots & \vdots \\ abr\cos^2\theta_e & a^2r\cos^2\theta_e & b^2r\cos^2\theta_e & -ar\cos\theta_e\cdot\sin\theta_e & -br\sin\theta_e\cdot\cos\theta_e \\ \vdots & \vdots & \vdots & \vdots & \vdots \end{bmatrix}$$

where $a = \sqrt{3/2}$ and $b = 1/2$. Computing A as before,

$$A_{35} \approx \begin{bmatrix} \frac{h\cot\theta_e}{2} & 0 & 0 & h & 0 \\ 0 & \frac{-h\cot\theta_e}{2} & 0 & 0 & \frac{h}{3} \\ 0 & \frac{h\cot^2\theta_e}{2} & \frac{h\cot^2\theta_e}{6} & 0 & \frac{h\cot\theta}{3} \end{bmatrix} \qquad \text{(A1.6)}$$

and $K_\ell^T = [u_y + v_x,\ u_x,\ v_y,\ w_x,\ w_y]$.

---

## APPENDIX 2. ANALYSIS OF THE VAD TECHNIQUES.

For the VAD technique, n radial velocity data are collected on a circle at height h. So

$$P_{nm} = \begin{bmatrix} \cos\theta_e\cdot\sin\phi_1 & \cos\theta_e\cdot\cos\phi_1 & \sin\theta_e \\ \cos\theta_e\cdot\sin\phi_2 & \cos\theta_e\cdot\cos\phi_2 & \sin\theta_e \\ \vdots & \vdots & \vdots \\ \cos\theta_e\cdot\sin\phi_n & \cos\theta_e\cdot\cos\phi_n & \sin\theta_e \end{bmatrix}$$

and

$$P_{nm}{}^T P_{nm} = \begin{bmatrix} \Sigma\cos^2\theta_e\cdot\sin^2\phi_i & \Sigma\cos^2\theta_e\cdot\sin\phi_i\cos\phi_i & \Sigma\cos\theta_e\cdot\sin\theta_e\cdot\sin\phi_i \\ & \Sigma\cos^2\theta_e\cdot\cos^2\phi_i & \Sigma\cos\theta_e\cdot\sin\theta_e\cdot\cos\phi_i \\ & & \Sigma\sin^2\theta_e \end{bmatrix}$$

where all summations are for i=1, 2,..., n. To simplify $P_{nm}{}^T P_{nm}$, we approximate the summations by integrals. For example,

$$\Sigma\cos^2\theta_e\sin\phi_i \approx \cos^2\theta_e\frac{n}{2\pi}\int_{-\pi}^{\pi}\sin^2\phi d\phi = \frac{n}{2}\cos^2\theta_e.$$

A similar evaluation of the remaining summations gives

$$P_{nm}^{T} P_{nm} = \begin{bmatrix} \frac{n \cos^2\theta_e}{2} & 0 & 0 \\ & \frac{n}{2}\cos^2\theta_e & 0 \\ & & n \sin^2\theta_e \end{bmatrix}$$

Thus

$$(P_{nm}^{T} P_{nm})^{-1} = \begin{bmatrix} \frac{2 \sec^2\theta_e}{n} & 0 & 0 \\ & \frac{2 \sec^2\theta_e}{n} & 0 \\ & & \frac{\csc^2\theta_e}{n} \end{bmatrix}$$

and

$$VAR(\hat{u}_o) = VAR(\hat{v}_o) = \frac{\sigma_\varepsilon^2}{h} \; 2 \sec^2\theta_e \tag{A2.1}$$

$$VAR(\hat{w}_o) = \frac{\sigma_\varepsilon^2}{n} \csc^2\theta_e \tag{A2.2}$$

To find the bias caused by neglecting the parameters of a linear wind field, we compute the alias matrix where $K_5^T = [u_y + v_x, u_x, v_y, w_x, w_y]$. For analysis at constant height,

$$n\ell = r \cos\theta_e \begin{bmatrix} \cos\theta_e \cdot \cos\phi_1 \cdot \sin\phi_1 & \cos\theta_e \cdot \sin\phi_1 & \cos\theta_e \cdot \cos\phi_1 & \sin\theta_e \cdot \sin\phi_1 & \sin\theta_e \cdot \cos\phi_1 \\ \cos\theta_e \cdot \cos\phi_2 \cdot \sin\phi_2 & \cos\theta_e \cdot \sin\phi_2 & \cos\theta_e \cdot \cos\phi_2 & \sin\theta_e \cdot \sin\phi_2 & \sin\theta_e \cdot \cos\phi_2 \\ \vdots & \vdots & \vdots & \vdots & \vdots \\ \cos\theta_e \cdot \cos\phi_n \cdot \sin\phi_n & \cos\theta_e \cdot \sin\phi_n & \cos\theta_e \cdot \cos\phi_n & \sin\theta_e \cdot \sin\phi_n & \sin\theta_e \cdot \cos\phi_n \end{bmatrix}$$

Performing the matrix multiplications in (5), approximating summations by integrals, and using $h \tilde{} r\sin\theta_e$ gives

$$A_{35} = \begin{bmatrix} 0 & 0 & 0 & h & 0 \\ 0 & 0 & 0 & 0 & h \\ 0 & \frac{h \cot^2\theta_e}{2} & \frac{h \cot^2\theta_e}{2} & 0 & 0 \end{bmatrix} \tag{A2.3}$$

## APPENDIX 3. ANALYSIS OF VED TECHNIQUE.

In the VED technique, the azimuth is fixed and the elevation angle is scanned. The range r is selected so the data are for a constant height h. To measure both horizontal components, another azimuth, preferably at 90° to the first, must be scanned. We assume $\frac{n}{2}$ data are collected for each scan. For convenience, we introduce the horizontal distance s which is directed along the azimuth $\phi$. We make estimates of a horizontal component $u_o$ (directed along s) and the vertical component $w_o$. The predictor function matrix is

$$P_{nm} = \begin{bmatrix} \cos\theta_1 & \sin\theta_1 \\ \cos\theta_2 & \sin\theta_2 \\ \vdots & \vdots \\ \cos\theta_n & \sin\theta_n \end{bmatrix}$$

so

$$P_{nm}^T P_{nm} = \begin{bmatrix} \Sigma \cos^2\theta_i & \Sigma \cos\theta_i \cdot \sin\theta_i \\ & \Sigma \sin^2\theta_i \end{bmatrix}$$

where the summations are for i=1, 2,..., $\frac{n}{2}$ and $\theta_i$ is the elevation angle. Approximating the summations by integrals,

$$\Sigma \cos^2\theta_i \approx \frac{n}{2(\pi-2\theta_o)} \int_{\theta_o}^{\pi-\theta_o} \cos^2\theta d\theta = \frac{n}{4}\left[\frac{(\pi-2\theta_o) - \sin 2\theta_o}{\pi-2\theta_o}\right]$$

$$\Sigma \sin\theta_i \cos\theta_i \approx 0$$

$$\Sigma \sin^2\theta \approx \frac{n}{4}\left[\frac{(\pi-2\theta_o) + \sin 2\theta_o}{\pi-2\theta_o}\right]$$

so

$$(P_{nm}^T P_{nm})^{-1} = \begin{bmatrix} \frac{4}{n}\left[\frac{(\pi-2\theta_o)}{(\pi-2\theta_o) - \sin 2\theta_o}\right] & 0 \\ 0 & \frac{4}{n}\left[\frac{(\pi-2\theta_o)}{(\pi-2\theta_o) + \sin 2\theta_o}\right] \end{bmatrix}$$

and

$$\begin{aligned} VAR(\hat{u}_o) = VAR(\hat{v}_o) &= \frac{\sigma_\varepsilon^2}{n}\, 4\left[\frac{\pi-2\theta_o}{(\pi-2\theta_o) - \sin\theta 2\theta_o}\right] \\ VAR(\hat{w}_o) &= \frac{\sigma_\varepsilon^2}{n}\, 2\left[\frac{\pi-2\theta_o}{(\pi-2\theta_o) + \sin 2\theta_o}\right] \end{aligned} \qquad \text{(A3.1)}$$

The variance of $w_o$ is halved since we assume the results from the two scans will be averaged.

The bias by the linear terms is again computed by the alias matrix. The prediction functions corresponding to the excluded parameters are

$$P_{n\ell} = \begin{bmatrix} r\cos^2\theta_1 & r\sin\theta_1\cdot\cos\theta_1 \\ r\cos^2\theta_2 & r\sin\theta_2\cdot\cos\theta_2 \\ \vdots & \vdots \\ r\cos^2\theta_n & r\sin\theta_n\cdot\cos\theta_n \end{bmatrix}$$

Performing the matrix multiplications, approximating summation by integrals and using $h \sim r\sin\theta$ gives

$$A_{22} = \begin{bmatrix} 0 & h \\ h\left[\dfrac{(\pi-2\theta_o) - \sin 2\theta_o}{(\pi-2\theta_o) + \sin 2\theta_o}\right] & 0 \end{bmatrix}$$

For the combined analysis of two scans at 0° and 90°,

$$A_{34} = \begin{bmatrix} 0 & 0 & h & 0 \\ 0 & 0 & 0 & h \\ h\left[\dfrac{(\pi-2\theta_o) - \sin 2\theta_o}{(\pi-2\theta_o) + \sin 2\theta_o}\right] & \left[h\dfrac{(\pi-2\theta_o) - \sin 2\theta_o}{(\pi-2\theta_o) + \sin 2\theta_o}\right] & 0 & 0 \end{bmatrix}$$

and the vector of excluded parameters is

$$K_4^T = (u_x,\ v_y,\ w_x,\ w_y).$$

# 3.3B ESTIMATING UNBIASED HORIZONTAL VELOCITY COMPONENTS FROM ST/MST RADAR MEASUREMENTS: A CASE STUDY

W. L. Clark, J. L. Green and J. M. Warnock

Aeronomy Laboratory
National Oceanic and Atmospheric Administration
Boulder, CO 80303

In this paper we present a self-editing quick-look procedure in use at the Sunset radar (GREEN et al., 1979) for determining relatively unbiased hourly estimates of the u and v components of the wind with an example application to data taken when a jet stream was overhead. The technique presented here should be applicable to all height ranges, though only ST results are presented here.

## ESTIMATING THE HORIZONTAL WIND COMPONENTS

The vertical wind component, w, may be measured directly by pointing the radar beam straight up. The east and west components of the wind, u and v, however, must be estimated by projecting to the horizontal plane the radial velocity, vr, actually observed by pointing the radar suitably off zenith (see Figure 1):

$$u = [vr * \csc(T) - w * \mathrm{ctn}(T)] * \sin(A)$$

$$v = [vr * \csc(T) - w * \mathrm{ctn}(T)] * \cos(A)$$

where T is the zenith angle and A is azimuth angle measured from north. The above equations apply when the sign of vr is taken positive for a reflecting volume moving away from the radar. At most ST/MST radars the azimuth angle A is restricted to a multiple of 90 degrees, so that the cos(A) and sin(A) factors merely provide the proper sign.

## PRACTICAL IMPORTANCE OF THE W TERM

A rough estimate of u or v may be obtained by neglecting the vertical motion term. Figure 2 exhibits the error thus produced in these estimates for various values of w. Note that for a value of w greater than .27 m/s, an error in u or v greater than 1 m/s is produced for the typical zenith angle of 15 degrees.

Time series of vertical velocities observed at the Sunset radar located in the foothills about 12 km east of the continental divide and at the Platteville radar in the plains 60 km further east are shown in Figure 3 (ECKLUND et al., 1982). Supposing that we want u and v components accurate to 1 m/s we see that for the mountain location the .27 m/s threshold of w is nearly always exceeded during this period in March. At the Platteville radar, on the other hand, perhaps only a third of this nearly three week period contains velocities which excede the threshold. However, the periods that do need correction tend to appear in the later part of the day, and could cause a systematic diurnal bias. In any event, this third of the data must be corrected for vertical velocity effects if the 1 m/s criterion is to be satisfied.

## THE QUICK LOOK

It is not too hard to see from this same figure that the large ws are often accompanied by large changes in w with time. This presents a problem if these changes occur frequently enough that the w measured at one time is not appropriate to correct radial velocities measured at another, since the vertical

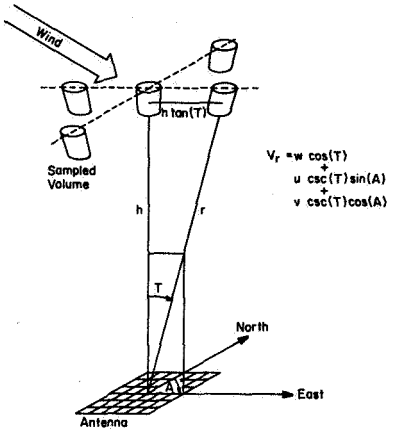


Figure 1.

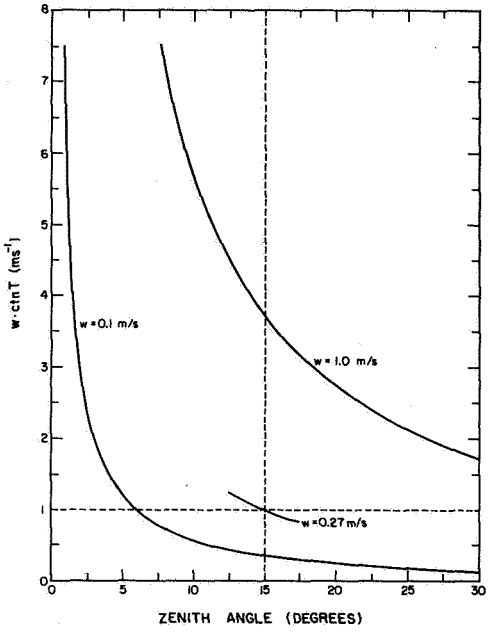


Figure 2. Size of w correction for for various values of w.

and horizontal components are usually measured sequentially. The solution, when it is not necessary to have closely spaced data, is to apply a filter to the observed components. To obtain hourly values a simple filter choice would be to take the hourly mean. This would require data editing, however, as a few non-atmospheric echoes nearly always occur in a long data set. We have chosen instead, for a quick-look procedure, to use the hourly median, which has similar characteristics for good data but is more resistent to occasional bad values. Thus the medians of all the radial components (including w) are found over each hour, then the u and v are calculated from the projection equations above using these median values.

## A CASE STUDY

A good example of the effectiveness of this technique is demonstrated by the data taken on March 28, 1983 while a small jet stream was moving over the Sunset radar. The radar was set to look sequentially in 5 directions as shown in Figure 1: vertical, 15 degrees north, 15 degrees east, 15 degrees south and finally 15 degrees west. This sequence was repeated continuously for four hours. The vertical direction, of course, provides direct measurement of w over the radar, two of the orientations provide information on the u and two on the v component. Figure 4a shows an example of the three components estimated with neglect of the effect of w on u and v, and Figure 4b the three components estimated by including the effect of w.

The greatly improved agreement demonstrates the correction is significant and appropriate. The remaining substantial differences between the two u profiles and the two v profiles, however, are also of interest. They indicate real spatial variations due to orographic effects, including a lee wave induced in the atmospheric flow by the nearby continental divide. In this situation the seemingly redundant measurements of the horizontal components of the wind are,

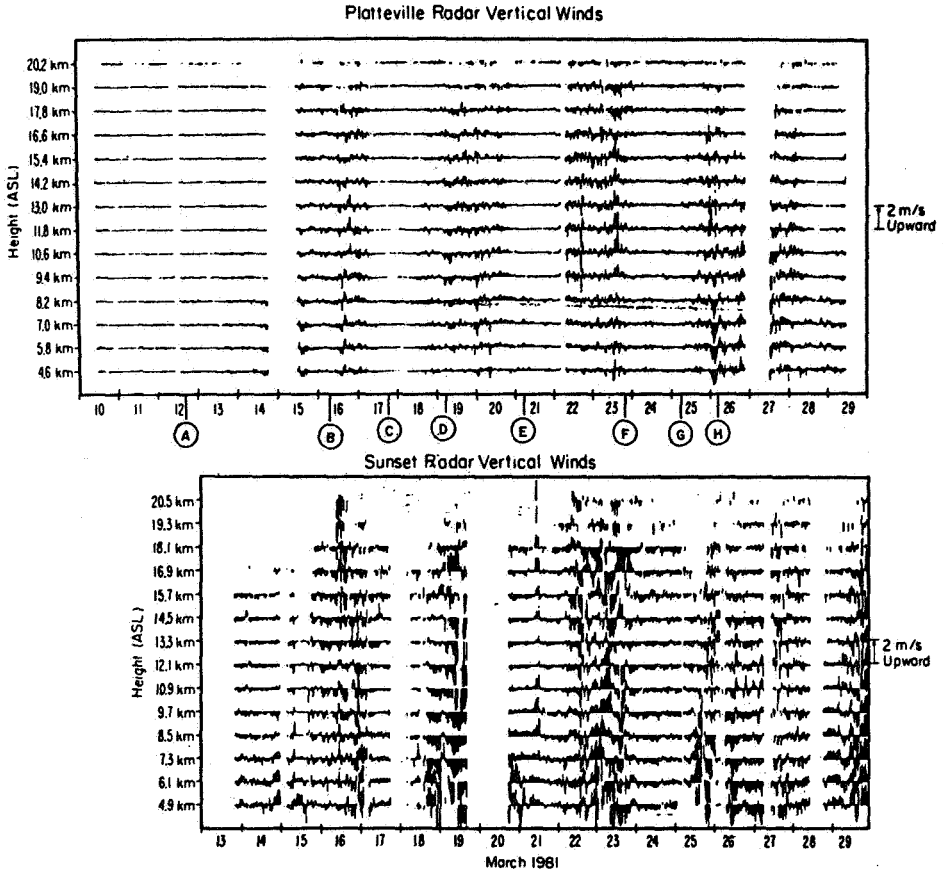


Figure 3. Fifteen-minute-averaged vertical velocities over Platteville and Sunset, Colorado, for the complete experimental period (after ECKLUND et al., 1982).

in fact, not redundant. They provide information crucial to the modelling of an atmospheric flow containing horizontal shear.

REFERENCES

Ecklund, W. L., K. S. Gage. B. B. Balsley, R. G. Strauch and J. L. Green (1982), Vertical wind variability observed by VHF radar in the lee of the Colorado Rockies, Mon. Wea. Rev., 110, 1451-1457.

Green, J. L., K. S. Gage and T. E. VanZandt (1979), Atmospheric measurements by VHF pulsed Doppler radar, IEEE Trans. Geo. Sci. Elec., GE-17, 262-280.

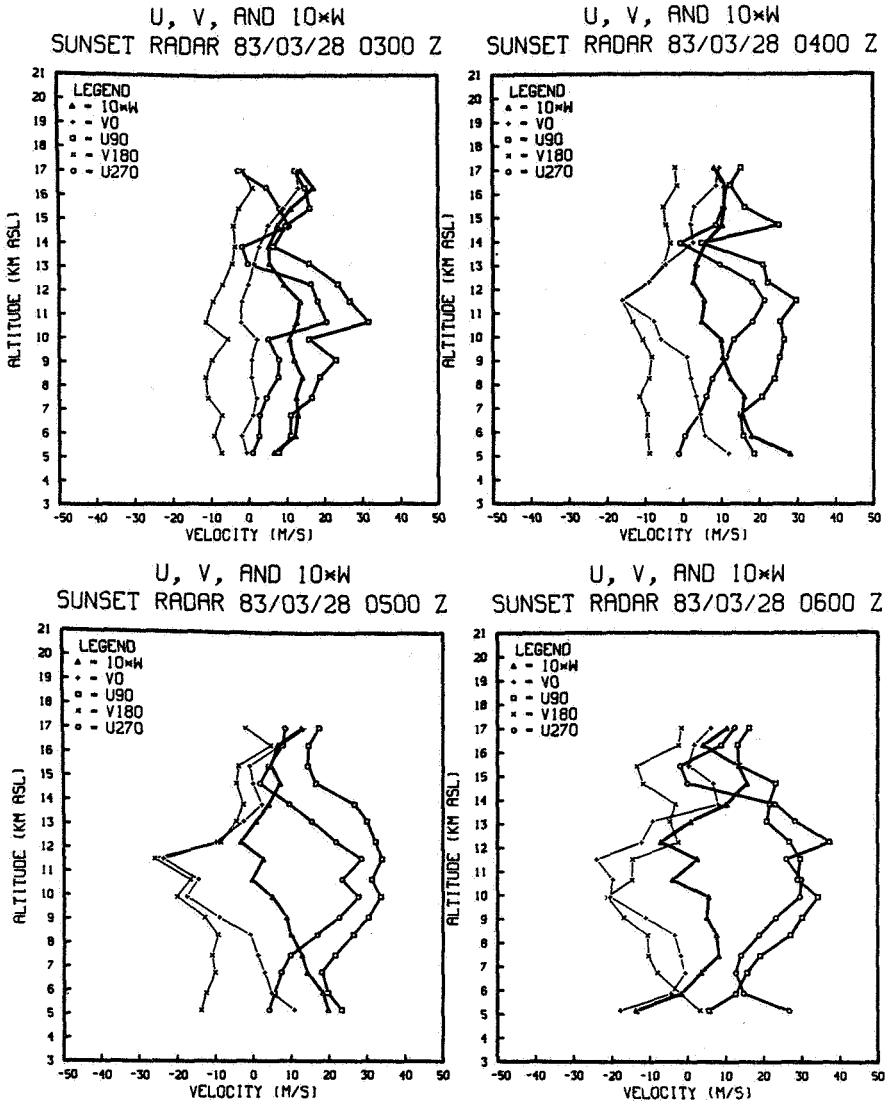
U, V, AND 10×W
SUNSET RADAR 83/03/28 0300 Z
U, V, AND 10×W
SUNSET RADAR 83/03/28 0400 Z
U, V, AND 10×W
SUNSET RADAR 83/03/28 0500 Z
U, V, AND 10×W
SUNSET RADAR 83/03/28 0600 Z
LEGEND
10×W
V0
U90
V180
U270
ALTITUDE (KM ASL)
VELOCITY (M/S)

Figure 4a.

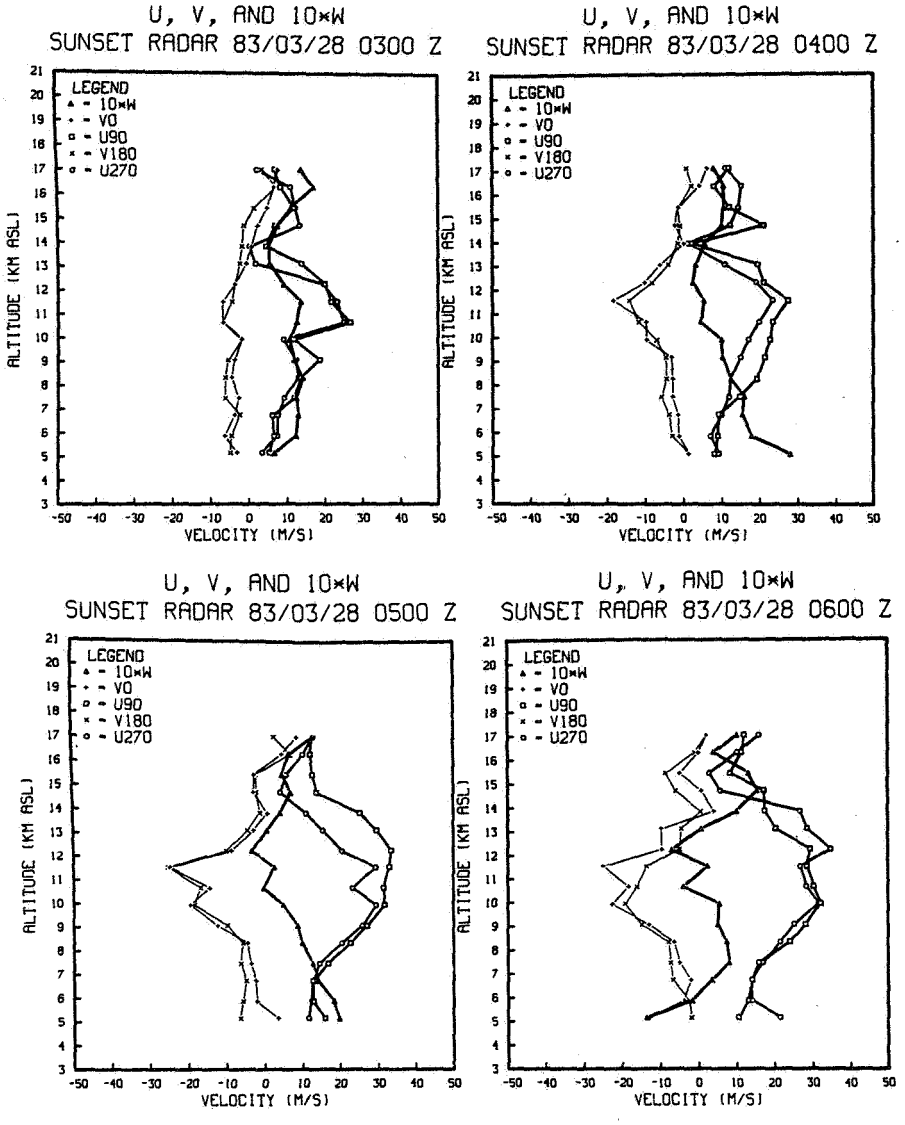
U, V, AND 10×W
SUNSET RADAR 83/03/28 0300 Z
U, V, AND 10×W
SUNSET RADAR 83/03/28 0400 Z
U, V, AND 10×W
SUNSET RADAR 83/03/28 0500 Z
U, V, AND 10×W
SUNSET RADAR 83/03/28 0600 Z
LEGEND
▲ - 10×W
+ - V0
□ - U90
× - V180
○ - U270
ALTITUDE (KM ASL)
VELOCITY (M/S)

Figure 4b.

# 3.4A ON THE MEASUREMENT OF VERTICAL VELOCITY BY MST RADAR

K. S. Gage

Aeronomy Laboratory
National Oceanic and Atmospheric Administration
Boulder, CO 80303

## ABSTRACT

An overview is presented of the measurement of atmospheric vertical motion utilizing the MST radar technique. Vertical motion in the atmosphere is briefly discussed as a function of scale. Vertical velocity measurement by MST radars is then considered from within the context of the expected magnitudes to be observed. Examples are drawn from published vertical velocity observations.

## INTRODUCTION

MST radar measurements of atmospheric vertical motion have been available for about 5 years. The first measurements were associated with case studies and invariably of short duration. More recent observations are nearly continuous over long periods and provide a basis for evaluating the climatology of the vertical wind.

In view of the large amount of vertical wind data available for analysis, surprisingly little has been published. Nevertheless, the vertical wind data constitutes a valuable resource. I believe that part of the reason that more has not been done with the vertical winds lies in the lack of suitable techniques for verification. Also, since the (specular) scattering mechanism thought to be responsible for much of the vertical echoes seems to differ from the turbulent scattering mechanism which is thought to cause the off vertical echoes, one may reasonably question whether the observed vertical velocities are an accurate measurement of vertical air motion. Furthermore, routine direct vertical wind measurements have never been available from any source. It is therefore very difficult to form any independent judgment of the reasonableness of the observations.

In this paper I shall consider the meaning and possible significance of the vertical wind measurement within the context of current knowledge of the magnitudes of atmospheric vertical motion at different scales.

## THE MAGNITUDE OF ATMOSPHERIC VERTICAL MOTION AS A FUNCTION OF SCALE

The magnitude of atmospheric vertical motion varies greatly with scale. The magnitude of the large-scale vertical motion is very small and has been determined by inference rather than by direct observation. Small-scale vertical motion on the other hand has been measured directly by several methods.

Estimates of mean vertical velocities associated with the general circulation of the atmosphere are given by the analysis of NEWELL et al. (1972). The largest vertical velocities averaged over a season are on the order of a few millimeters per second. These values occur in the equatorial zone and are associated with the ascending branch of the Hadley cell. They decrease considerably in magnitude in the lower stratosphere. Of course, larger vertical velocities would be anticipated higher in the middle atmosphere.

On the synoptic scale, vertical velocities show considerable variability. The dynamics of large-scale vertical motion is discussed by FLEAGLE (1958). Diverse methods for calculating large-scale vertical velocities are discussed in many papers (PANOFSKY, 1946; FLEAGLE, 1958; O'BRIEN, 1970; KUNG, 1972; STUART,

1974; SMITH and LIN, 1978; and PEDDER, 1981).

Qualitatively, it is easy to think of large-scale vertical motion as a consequence of nearly horizontal motion on isentropic surfaces. Isentropic surfaces are surfaces of constant potential temperature. Since parcels of air in adiabatic motion conserve potential temperature, it is reasonable to anticipate motion along isentropic surfaces. The consequences for vertical motion are clear when one considers the fact that (in the Northern Hemisphere) isentropic surfaces generally slope upwards from south to north. Northward motion is generally ascending and often associated with clouds and precipitation due to adiabatic cooling (PANOFSKY, 1946). In contrast, southward motion is typically descending and free of clouds. DANIELSEN (1961) pointed out the significance of isentropic analysis for trajectory calculations. He gave an example of a twelve-hour isentropic trajectory over the U.S. from northwest to southeast which implied a -7.4 cm $s^{-1}$ average vertical velocity. KUNG (1972) presented an analysis of the synoptic scale vertical motion field in the troposphere over North America. Typical vertical velocities were on the order of 1 cm $s^{-1}$ with extreme values about an order of magnitude larger. Large-scale vertical motions have been analyzed in the stratosphere (MILLER, 1970) and found to be in the same range at 2 mb (43 km).

Several studies have shown larger synoptic scale vertical velocities in the vicinity of jet streams and severe weather. WILSON (1976) analyzed 3-hr soundings made during NASA's Atmospheric Variability Experiment (AVE) and found extreme values of vertical motion of about 25 cm $s^{-1}$ associated with severe convective storms. In an earlier study of vertical velocities associated with jet streams, ENDLICH (1953) concluded that values of 10 cm $s^{-1}$ are common and that extreme values of the order of 25 cm $s^{-1}$ are possible.

Clearly, the magnitude and variability of atmospheric vertical motions can be expected to increase with decreasing spatial and temporal scale. This is especially true on the mesoscale where disturbances of the smallest scale can possess large vertical velocities. While the mesoscale is not routinely observed, special studies have been made to determine the magnitude of mesoscale vertical motions (HARDMAN et al., 1972; TUCKER, 1973). FANKHAUSER (1974) has analyzed data collected from a special mesoscale sounding network used in Oklahoma by the National Severe Storms Laboratory (NSSL). His analysis revealed a systematic pattern of tropospheric vertical motion associated with a squall line. Maximum vertical velocities were on the order of 1 $ms^{-1}$. Vertical velocities have also been reported from a mesoscale analysis of BOMEX data by SMITH et al. (1975). They were found to be as large as .5 $ms^{-1}$ in an active mesoscale disturbance.

On the cloud scale vertical velocities have been measured directly by aircraft, radar and balloons. Aircraft measurement of vertical velocity is discussed by LENSCHOW (1976) and LAWSON (1980). LeMONE and ZIPSER (1980) report vertical velocities measured by aircraft during GATE on the order of 5 $ms^{-1}$. They present statistical distributions of vertical velocities which show great variability. Vertical motions have also been deduced from ascent rate variations of rising Jimspheres tracked by radar (DeMANDEL and KRIVO, 1971). By subtracting out buoyancy and drag variations, estimates were made of vertical air motion. Vertical velocities on the order of .5 $ms^{-1}$ were reported during ascent through clear skies. Vertical velocities on the order of 1 $ms^{-1}$ have been obtained by precise tracking of constant level balloons (GAGE and JASPERSON, 1976). In convective storms vertical motions as high as 10 $ms^{-1}$ have been observed by Doppler radar (BATTAN, 1973).

## A BRIEF SURVEY OF VERTICAL VELOCITY MEASUREMENT BY MST RADAR

It should be clear from the material presented in the previous section that the entire spectrum of atmospheric vertical velocities is not well observed. It

should also be clear that the magnitude of vertical motion decreases with increasing scale so that large-scale atmospheric motions are quasi-horizontal. It is only on the smallest scale that vertical velocities have been directly measurable and these have never been routinely available in the past.

Since MST radars measure the radial component of motion, the principle of measurement of vertical velocity is the same as for horizontal velocity. The most straightforward way to measure vertical velocity is to direct the antenna beam vertically. Since horizontal velocities are typically so much larger than vertical velocities, care must be taken that the antenna is directed truly vertically; otherwise, the measured velocity will be contaminated by a small component of the horizontal wind.

Another method for obtaining vertical velocity is from VAD analysis (PETERSON and BALSLEY, 1979; RABIN and ZRNIC', 1980). To employ this method the radar antenna must be capable of making a complete azimuth scan for fixed zenith angle. The horizontal velocity is determined by fitting a sinusoid to the radial velocity over the azimuth scan. The amplitude yields horizontal wind speed, the phase gives horizontal wind direction and any offset of the sinusoid about zero determines the vertical velocity. A third method is to perform an elevation scan. By this method radial velocity is plotted as a function of zenith angle and the vertical velocity is then determined by the intercept of the radial velocity at zero zenith angle. Vertical velocities from all three methods have been determined using the Chatanika radar (PETERSON and BALSLEY, 1979). The profiles of vertical velocity are reproduced in Figure 1 and show a reasonable consistency, especially at the lower heights where the vertical velocity is largest.

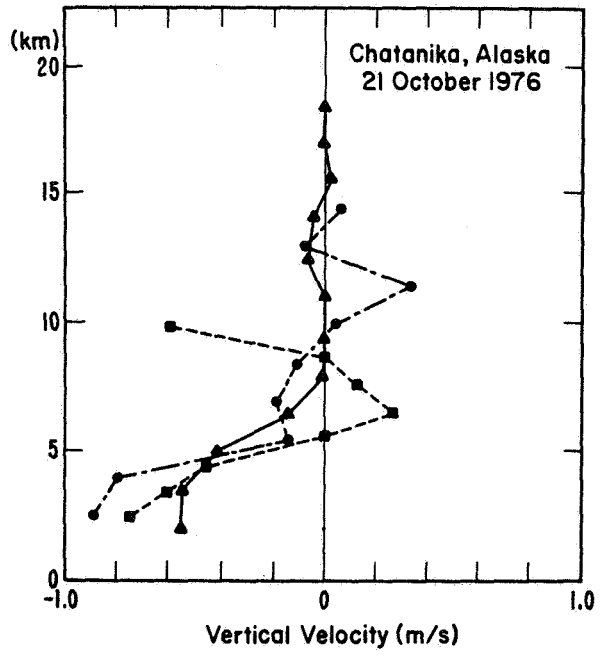


Figure 1. Comparison of the vertical component of wind velocity obtained by three different methods. (After PETERSON and BALSLEY, 1970.) [ ■...■ AZSCAN data, ● ... ● ELSCAN data, ▲ ... ▲ Zenith data]

Most MST radars do not have the capability of scanning and consequently the antenna must be directed at the zenith to measure vertical velocities. Several case studies have been made of vertical velocities observed in this manner. GREEN et al. (1978) observed the vertical wind associated with the passage of a strong southerly jet stream over the Sunset radar. They reported upward vertical motion as high as .5 $ms^{-1}$ in the vicinity of the tropopause. GAGE et al. (1978) and ROTTGER (1980a) report vertical motion associated with convective storms. They found complicated patterns of updrafts and downdrafts with vertical velocities of several $ms^{-1}$.

The vertical velocities associated with a jet stream and upper level frontal zone were reported by LARSEN and ROTTGER (1982, 1983). The reflectivity and vertical velocities are reproduced in Figure 2. Upward vertical motion of about .5 $ms^{-1}$ was found on the warm side of the front in the vicinity of the jet stream core. Downward motion of equal magnitude was found on the cold side of the front through most of the troposphere. Note the structure in the vertical velocity field. With some smoothing these velocities would reduce to the magnitude of synoptic scale vertical velocities.

Continuous measurements of vertical velocities are now available using MST radar. The longest uninterrupted data records are from the Poker Flat MST radar. A 34-day record of hourly-averaged vertical winds at Poker Flat is reproduced in Figure 3 (ECKLUND et al., 1981). This figure shows that the magnitude of the vertical wind varies greatly from day to day with occasional active periods disrupting a relatively quiet background. A sample of vertical velocities for a quiet period is given in Figure 4 and a sample of vertical velocities for an active period is shown in Figure 5. The accompanying 500 mb maps show that the active period is associated with the strong winds found in baroclinic zones. The correlation of vertical wind variability with wind speed has been verified in a recent climatological study by NASTROM and GAGE (1983).

The large magnitude and extreme variability of the vertical wind observed by MST radar has been attributed to internal gravity waves (or buoyancy waves). An example of a wave-like disturbance observed by the Poker Flat MST radar is reproduced in Figure 6 (GAGE et al., 1981). No apparent variation of phase with altitude was observed during this wave event suggesting that a trapped mode was observed.

Other MST vertical wind observations can be found in ROTTGER (1980c, 1981), FUKAO et al. (1978) and ECKLUND et al. (1982, 1983). In all cases the magnitude of observed vertical velocities are in reasonable agreement with the magnitudes of vertical velocities observed under similar circumstances using other techniques. However, no direct verification by independent means has yet been reported.

Vertical velocities have also been measured at mesospheric altitudes. Quasi-vertical motions showing gravity wave activity have been reported by WOODMAN and GUILLEN (1974) and by MILLER et al. (1978). More recently, BALSLEY and RIDDLE (1983) have analyzed the mean vertical motion observed at Poker Flat over several years. The mean wind is downward during the summer which suggests that upward motion in the summer mesosphere is confined poleward of 65°N.

## THE ACCURACY OF VERTICAL WIND MEASUREMENT BY MST RADARS

As mentioned above, direct vertical wind measurement is a new commodity in meteorology. As a consequence, it is difficult to form an independent judgment concerning the validity of the MST radar vertical velocities. In marked contrast horizontal velocities determined from the Doppler shift due to turbulent scattering have been compared to balloon and aircraft derived velocities. While a few outstanding problems can compromise the validity of the

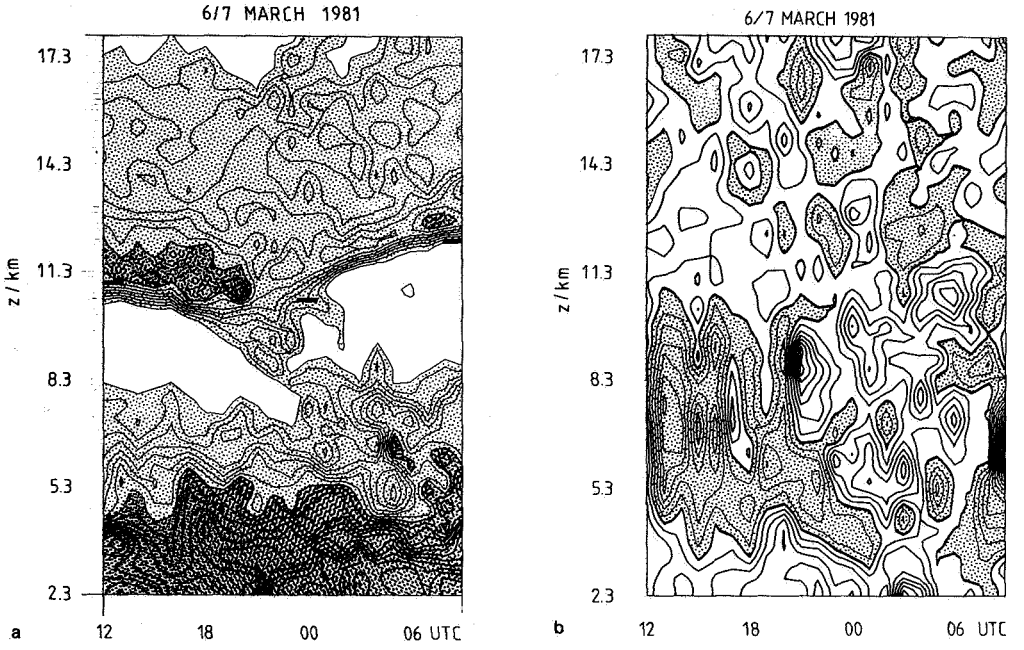


Figure 2. Observations of the SOUSY radar. a. Reflectivity contour plot. Difference between contour lines is 2 dB. Intensity of shading corresponds to intensity of echoes. b. Contour plot of vertical echoes. Shading indicates downward velocity. The interval between contours is 7.5 cm $s^{-1}$. (After LARSEN and ROTTGER, 1982.)

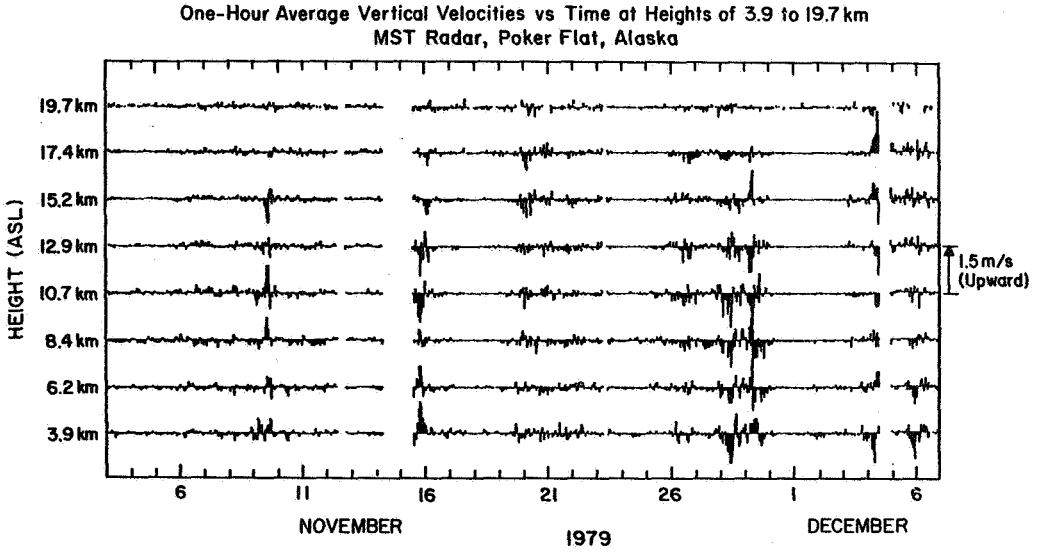


Figure 3. 34-day record of hourly averaged vertical wind velocites at heights of 3.9 - 19.7 km as observed by the Poker Flat MST radar. (After ECKLUND et al., 1981.)

horizontal winds, they are generally in excellent agreement with winds obtained by other accepted techniques.

Two features make the validity of vertical winds difficult to evaluate. First, the magnitude of vertical winds is much smaller than the magnitude of horizontal winds. Second, at least at lower VHF, MST radars obtain their echoes at vertical incidence from a quasi-specular scatter mechanism. Thus, the fact that horizontal winds are accurately measured cannot be used without qualification to justify the validity of the vertical wind measurement.

Local vertical winds observed by MST radars vary greatly but are usually less than 1 $ms^{-1}$. Because mean vertical motions are very small, it is appropriate and advantageous when measuring vertical velocity to reduce the limits of maximum unambiguous velocity to a few $ms^{-1}$. Doing this greatly

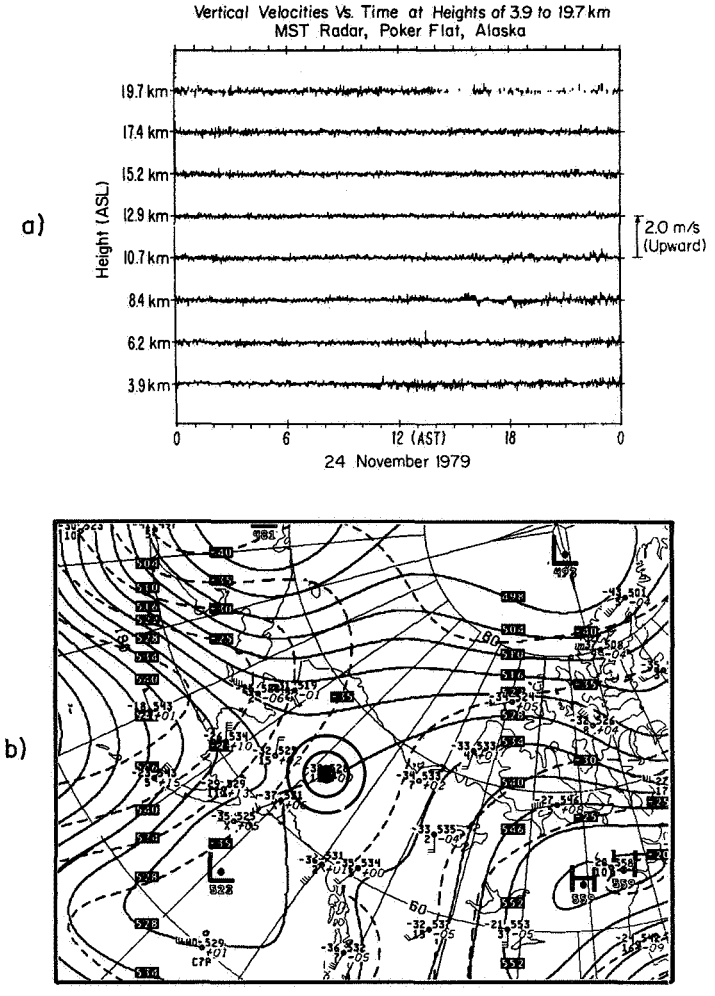


Figure 4. a. Vertical velocities observed by the Poker Flat MST radar on a quiet day (24 November 1979). b. The 500 mb analysis map for the quiet day. (After ECKLUND et al., 1981.)

improves the resolution of the vertical velocity measurement. For example, if 4 $ms^{-1}$ is used as a maximum unambiguous velocity and 256 points are used in an FFT, then vertical velocities as small as 3 cm $s^{-1}$ should be resolvable in individual spectra. Averaging, of course, further reduces the magnitude of vertical motion that can be resolved.

GAGE et al. (1981) considered the measurement of vertical velocity in relation to scattering mechanisms in an analysis of a wave event observed by the Poker Flat MST radar. The wave event as a time series of vertical velocity is shown in Figure 6. A comparison of the time series of velocities with the time series of received power and spectral width at 10.7 km is contained in Figure 7. The spectra reproduced in Figure 8 show that the observed spectral shape changed dramatically with the phase of the wave disturbance. Only when the vertical velocity was close to zero did the spectra truly appear specular. When the

a)

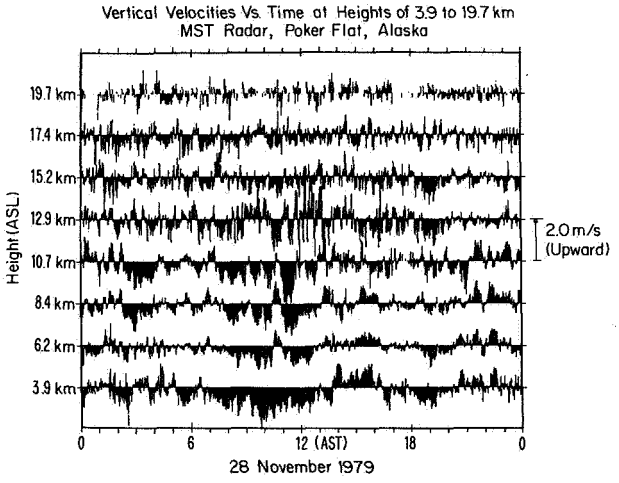


b)

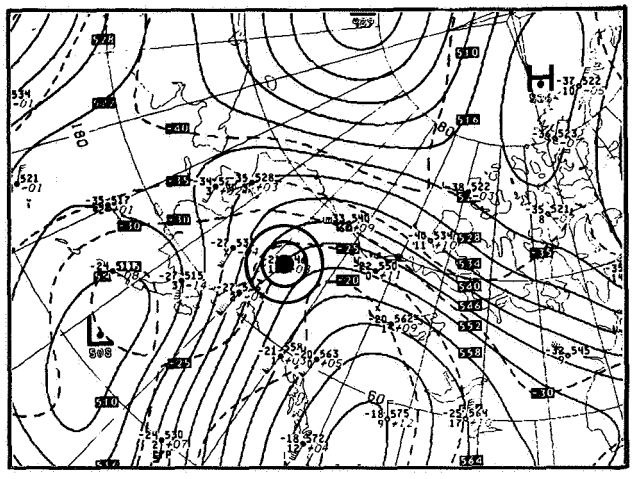

Figure 5. a. Vertical velocities observed by the Poker Flat MST radar on an active day (28 November 1979). b. The 500 mb analysis map for the active day. (After ECKLUND et al., 1981.)

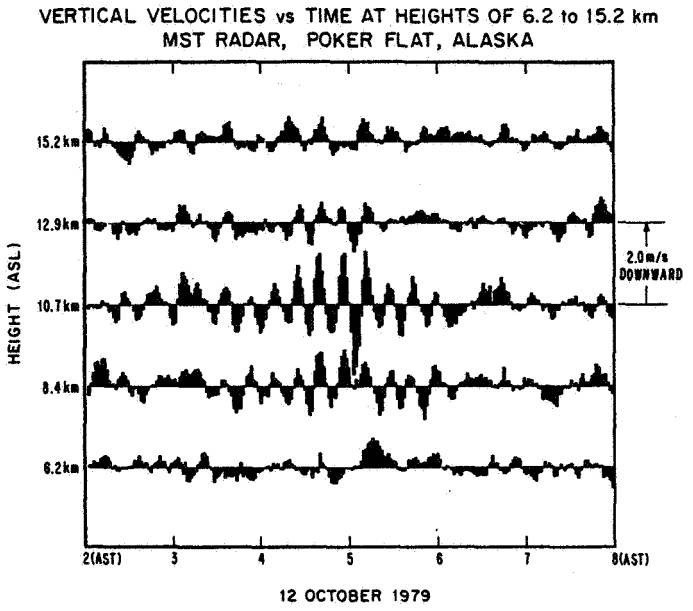


Figure 6. Vertical velocities observed from 6.2 km to 15.2 km for 6 hours on 12 October 1979. (After GAGE et al., 1981.)

vertical velocity departed significantly from zero, the spectral shape broadened and the magnitude dropped sharply. Thus, there is some evidence to suggest that the larger vertical velocities are a result of turbulent scattering and should therefore be valid.

There has been some concern that MST measured vertical velocities may not be valid under certain circumstances. ROTTGER (1980b) raised the concern that tilting of reflecting layers contributing to diffuse reflection could adversely bias the mean vertical velocities deduced from MST observations. Another related concern (ROTTGER, 1981) arises when a VHF radar determines the vertical velocity from a slightly tilted layer. The sloping layer can effectively tilt the incident beam slightly off-vertical and, as a consequence, a small component of the horizontal velocity would contaminate the vertical velocity measurement. In evaluating this concern it should be borne in mind that atmospheric motions are not strictly two-dimensional. Thus, a large-scale vertical velocity component can be anticipated even for an antenna beam directed strictly vertically. Whether tilting effects are a practical concern for the measurement of vertical velocities observed by MST radars needs to be evaluated more fully. It should be clear, however, that UHF radars should not experience these problems. The practical importance of these effects could be determined by careful comparisons of vertical velocity measurements obtained simultaneously at UHF and at lower VHF. Indeed, preliminary comparisons of vertical velocities measured by the Chatanika radar and the Poker Flat radar show close agreement (WATKINS and JAYAWEERA, 1983). Comparitive vertical velocity measurements with Doppler lidar should also be pursued.

## CONCLUDING REMARKS

In this overview I have attempted to evaluate MST radar measurements of vertical velocities in the context of the magnitudes of vertical motion pertaining to varying scales of atmospheric motion. While no definitive conclusions can be made on the validity of MST vertical velocity measurement,

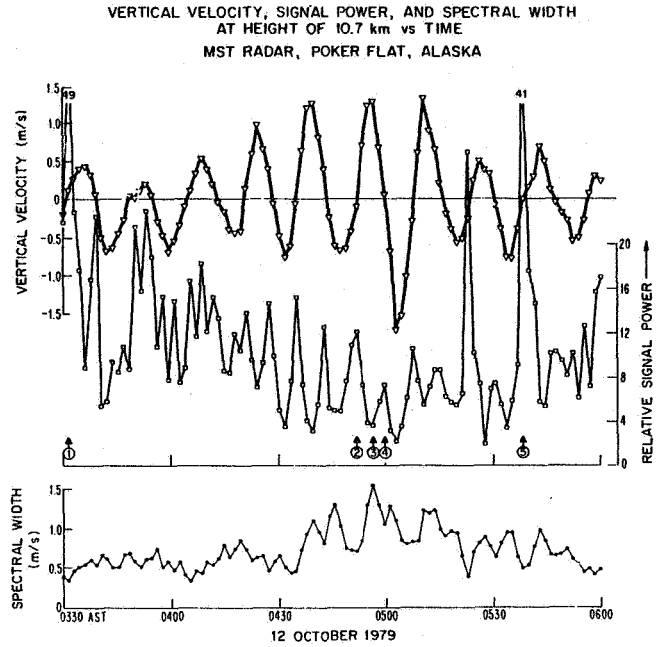


Figure 7. Time series of vertical velocity signal power, and spectral width observed during the wave event of 12 October 1979. The circled numbers refer to the spectra shown in Figure 8. Positive velocity values are downward (after GAGE et al., 1981.)

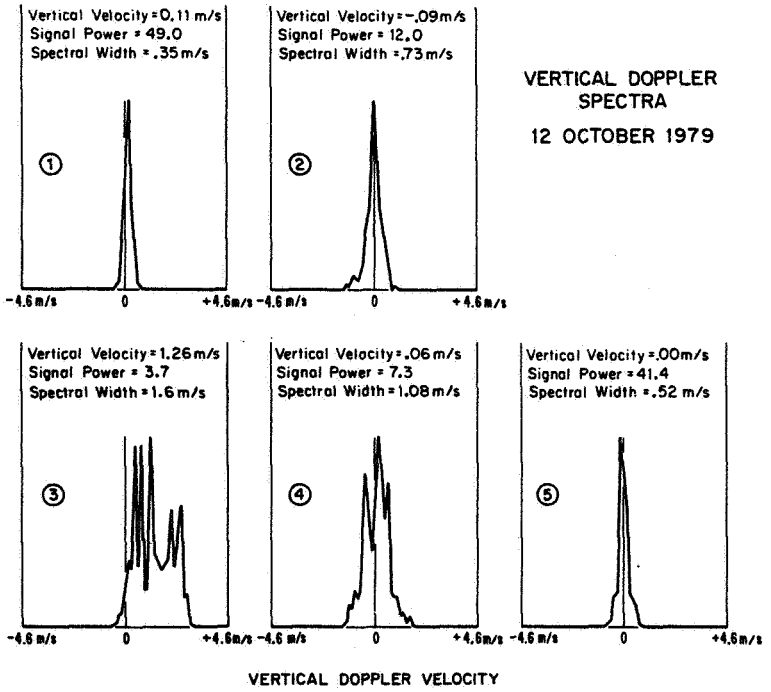


Figure 8. Doppler spectra observed at various stages of the wave event of 12 October 1979 (after GAGE et al., 1981).

observations to date are consistent with the magnitudes of vertical motion obtained by other methods. While some uncertainty remains due to the specular nature of lower VHF echoes at vertical incidence, there are indications that layer tilting effects will not limit the usefulness of MST vertical velocity measurements in practice. Remaining unresolved is the issue of whether synoptic scale vertical motions are measurable.

REFERENCES

Balsley, B. B. and A. C. Riddle (1983), Monthly mean values of the horizontal and vertical wind field in the mesosphere over Poker Flat, Alaska, submitted to J. Atmos. Sci.

Battan, L. J. (1973), Radar Observation of the Atmosphere, University of Chicago Press, Chicago, 324 pp.

Danielsen, E. F. (1961), Trajectories: isobaric, isentropic and actual, J. Meteorol., 18, 479-486.

DeMandel, R. E. and S. J. Krivo (1971), Radar/balloon measurement of vertical air motions between the surface and 15 km, J. Appl. Meteorol., 10, 313-319.

Ecklund, W. L., K. S. Gage and A. C. Riddle (1981), Gravity wave activity in vertical winds observed by the Poker Flat MST radar, Geophys. Res. Lett., 8 285-288.

Ecklund, W. L., K. S. Gage, B. B. Balsley, R. G. Strauch and J. L. Green (1982), Vertical wind variability observed by VHF radar in the lee of the Colorado Rockies, Mon. Wea. Rev., 110, 1451-1457.

Ecklund, W. L., K. S. Gage, B. B. Balsley, R. G. Strauch and A. C. Riddle (1983), Vertical wind observations using VHF clear-air radars, Preprint Vol., Symp. on Meteorological Observations and Instrumentation, April 11-15, Toronto, Ontario, Canada.

Endlich, R. M. (1953), A study of vertical velocities in the vicinity of jet streams, J. Meteorol., 10, 407-415.

Fankhauser, J. C. (1974), The derivation of consistent fields of wind and geopotential height from mesoscale rawinsonde data, J. Appl. Meteorol., 13, 637-646.

Fleagle, R. G. (1958), On the mechansim of large-scale vertical motion, J. Appl. Meteorol., 15, 249-258.

Fukao, S., S. Kato, S. Yokoi, R. M. Harper, R. F. Woodman and W. E. Gordon (1978), One full-day radar measurement of lower stratosphere winds over Jicamarca, J. Atmos. Terr. Phys., 40, 1331-1338.

Gage, K. S. and W. H. Jasperson (1976), Diffusion coefficients estimated from turbulence data measured by the METRAC positioning system in Minneapolis Field Test, Preprint vol., Third Symposium on Atmospheric Turbulence, Diffusion and Air Quality, Raleigh, NC), AMS, Boston.

Gage, K. S., J. L. Green and T. E. VanZandt (1978), Application of the VHF pulsed Doppler radar to cloud physics research, Preprint Vol., Conference on Cloud Physics and Atmospheric Electricy, Issaquah, WA, AMS, Boston.

Gage, K. S., D. A. Carter and W. L. Ecklund (1981), The effect of gravity waves on specular echoes observed by the Poker Flat MST radar, Geophys. Res. Lett. 8, 599-602.

Green, J. L., K. S. Gage and T. E. VanZandt (1978), Three-dimensional wind observations of a jet stream using a VHF Doppler radar, Preprint Vol., 18th Conf. on Radar Meteorology, Atlanta, GA, March 28-31, pp 184-189.

Hardman, M. E., D. G. James and D. Goldsmith (1972), The measurement of mesoscale vertical motions in the atmosphere, Quart. J. Roy. Met. Soc., 98, 38-47.

Kung, E. C. (1972), A scheme for kinematic estimate of large-scale vertical motion with an upper-air network, Quart. J. Roy. Met. Soc., 98, 402-411.

Larsen, M. F. and J. Rottger (1982), VHF and UHF Doppler radars as tools for synoptic research, Bull. Amer. Meteorol. Soc., 63, 996-1007.

Larsen, M. F. and J. Rottger (1983), Comparison of tropopause height and frontal boundary locations based on radar and radiosonde data, Geophys. Res. Lett., 10, 325-328.

Lawson, R. P. (1980), On the airborne measurement of vertical air velocity, J. Appl. Meteorol., 19, 1416-1419.

LeMone, M. A. and E. J. Zipser (1980), Cumulonimbus vertical velocity events in GATE. Part 1: Diameter, intensity and mass flux, J. Atmos. Sci., 37, 2444-2457.

Lenschow, D. H. (1976), Estimating updraft velocity from an airplane response, Mon. Wea. Rev., 104, 618-627.

Miller, A. J. (1970), A note on vertical motion analyses for the upper stratosphere, Mon. Wea. Rev., 98, 616-620.

Miller, K. L., S. A. Bowhill, K. P. Gibbs and I. D. Countryman (1978), First measurements of mesospheric vertical velocities by VHF radar at temperate latitude, Geophys. Res. Lett., 5, 939-942.

Nastrom, G. D. and K. S. Gage (1983), A brief climatology of vertical wind variability as seen by the Poker Flat, Alaska MST radar, submitted to J. Climate and Appl. Meteorol.

Newell, R. E., J. W. Kidson, D. G. Vincent, and G. J. Boer (1972), The General Circulation of the Tropical Atmosphere, MIT Press, Cambridge, MA

O'Brien, J. J. (1970), Alternative solutions to the classical vertical velocity problem, J. Appl. Meteorol., 9, 197-203.

Panofsky, H. A. (1946), Methods for computing vertical motion in the atmosphere, J. Meteorol., 3, 45-49.

Pedder, M. A. (1981), On the errors of kinematic vertical motion estimation using divergence bias adjustment procedures, Mon. Wea. Rev., 109, 1814-1816

Peterson, V. L. and B. B. Balsley (1979), Clear air Doppler radar measurements of the vertical component of wind velocity in the troposphere and stratosphere, Geophys. Res. Lett., 6, 933-936.

Rabin, R. and D. Zrnic (1980), Subsynoptic-scale vertical wind revealed by dual Doppler-radar and VAD analysis, J. Atmos. Sci., 37, 644-654.

Rottger, J. (1980a), Development of refractivity structures during anticyclonic weather conditions, Preprint Vol., Ninteenth Conf. on Radar Meteorology, Miami, FL, AMS, Boston.

Rottger, J. (1980b), Reflection and scattering of VHF radar signals from atmospheric refractivity structures, Radio Sci., 15, 259-276.

Rottger, J. (1980c), Structure and dynamics of the stratosphere and mesosphere revealed by VHF radar investigations, Pure and Appl. Geophys., 118, 494-527

Rottger, J. (1981), Wind variability in the stratosphere deduced from spaced antenna VHF radar measurements, Preprint Vol., 20th Conf. on Radar Meteorology, 30 Nov-3 Dec 1981, Boston.

Smith, C. L., E. J. Zipser, S. M. Daggupaty and L. Sapp (1975), An experiment in tropical mesoscale analysis: Part 2, Mon. Wea. Rev., 103, 893-903.

Smith, P. J. and C. P. Lin (1978), A comparison of synoptic-scale vertical motions computed by the kinematic method and two forms of the Omega equation, Mon. Wea. Rev., 106, 1687-1694.

Stuart, D. W. (1974), A comparison of quasi-geostrophic vertical motion using various analyses, Mon. Wea. Rev., 102, 363-374.

Tucker, G. B. (1973), Vertical velocities and vertical eddy fluxes derived from serial soundings at one station, Quart. J. Roy. Met. Soc., 99, 520-539.

Watkins, B. J. and K. Jayaweera (1983), Comparisons of vertical winds measured with the Poker Flat MST radar and the Chatanika ST radar, (manuscript in preparation).

Wilson, G. S. (1976), Large-scale vertical motion calculations in the AVE IV experiment, Geophys. Res. Lett., 3, 735-738.

Woodman, R. F. and A. Guillen (1974), Radar observations of winds and turbulence in the stratosphere and mesosphere, J. Atmos. Sci., 31, 493-505.

# 3.4B ACCURACY OF VERTICAL VELOCITY DETERMINATION

A. C. Riddle

CIRES/NOAA Aeronomy Laboratory
Boulder, CO 80303

Typical wind spectra taken at Poker Flat, Alaska, using the vertically oriented antenna show velocities of 10's of cm to meters per second and spectral widths winds of 0.5 to 1 m/s. The potential errors in such measurements can be broken down into three categories: (1) those due to instrumental parameters and data processing, (2) those due to specular returns from non-horizontal surfaces, and (3) those due to other physical effects.

At Poker Flat the typical vertical velocity spectrum has data points every 10 to 20 cm $s^{-1}$. This spacing is small enough to prevent velocity determination errors. The central point in the spectrum (0 velocity) is replaced by the average of the two adjacent points in order to avoid dc offset problems. For small velocities and narrow spectral widths, this could cause systematic errors of $\sim$ 1 cm/s. However, since the errors are symmetric with respect to zero velocity they will not cause noticeable errors in velocities averaged over significant times ($\geq$ 1/2 hr). Hence we expect no significant errors due to instrumental parameters or data processing.

On the other hand, for finite width antenna beams, specular returns from nonhorizontal surfaces can occur. We have no real estimate of the errors caused by this effect. However, we do expect it to be a random effect with zero mean and hence again we expect no errors in long-term averages of vertical velocity. These expectations are borne out in the mesosphere where vertical velocities derived from turbulent echoes and vertical velocities at higher altitudes from meteor echoes show the same general trend. Since the meteor echoes cannot be so affected we assert that, on the average, specular returns in the mesosphere from tilted surfaces cause no systematic error.

There are a number of potential effects in the third category. First we consider the possibility that the beam is not vertical. For a typical horizontal velocity of $\sim$ 50 meters per second to cause an error of less than 10 cm/s it is essential that the beam is no more than 0.1° off vertical. At Poker Flat the typical monthly mean vertical velocity in the troposphere is less than 1 cm/s and hence the beam is considerably less than 0.1° off vertical.

In the mesosphere several physical effects could cause an error in the vertical velocity measurements that should increase with height. We have considered beam bending by the magnetic field, beam bending by nonvertical ionospheric gradients, phase shifts (interpreted as velocities) introduced by changing electron density and electric fields in the ionosphere (REID, 1983). Even under extreme conditions only the latter mechanism could introduce measurable effects. The similarity of Poker Flat mesospheric vertical monthly averages over 25 km range (70 to 95 km) indicate that none of these potential error sources are significant.

## REFERENCE

Reid, G. C. (1983), The influence of electric fields on radar measurements of winds in the upper mesosphere, Radio Science, 18, 1028-1034.

# 3.5A IMPLICATION ON DATA INTERPRETATION BY SHORT- AND LONG-PERIOD OSCILLATIONS

O. Royrvik

Aeronomy Laboratory
Department of Electrical Engineering
University of Illinois
Urbana, IL 61801

## OBSERVATION OF HORIZONTAL VELOCITY VARIATIONS

Measurements of horizontal velocities in the upper atmosphere have been attempted using a multitude of techniques with associated assumptions about the wind field. One example is the Doppler beam swinging radar where line-of-sight wind measurements are made with the antenna positioned in three different directions and then the three-dimensional wind field is calculated under the assumption that the wind field is constant over time and space spanning these measurements. This assumption is reasonable when tidal oscillations and the mean wind are considered. Tides have wavelengths of thousands of kilometers and periods that are integral fractions of a solar day (24-12-8 hours). For the mean wind the scale of the temporal and spatial variations are even larger. Thus it is concluded that there are no problems in measuring the mean wind and tides using the Doppler beam swinging (DBS) technique, or any other technique based on the assumption of stationary wind fields.

The problem arises when short-period horizontal oscillations are measured. COUNTRYMAN and BOWHILL (1979) using the Jicamarca radar in a DBS experiment have shown that the horizontal wavelength of short-period gravity waves are of the order of 20 km. This agrees well with observations of gravity waves in the OH layer observed by MOREELS and HERSE (1977) showing horizontal wavelengths as short as 20 km. It is thus clear that a DBS radar with angular separation in beam directions of about 5° or more will span a substantial fraction of the horizontal wavelength in the mesosphere and thus the assumption of similar wind fields is violated. So it appears that short-period horizontal velocity oscillations can not be easily measured by the use of the DBS technique. This appears to be generally accepted in the MST radar community.

Similar considerations are valid for the spaced antenna drifts technique (SAD). However, there have been claims in the literature that this technique should be able to measure short-period horizontal oscillations, so it is reasonable to discuss this technique in more detail. The SAD technique is based upon the recognition of an interference pattern drifting across a set of spaced receiving antennas (ROYRVIK 1983a).

Under ideal conditions, it is clear that the velocity of the interference pattern over the ground can be measured with reasonable accuracy. However, it remains to be shown that this velocity is related to the bulk horizontal motion of the ionosphere at the altitude probed. It is reasonable to expect to find short-period gravity waves in the mesosphere that have approximately the same amplitude in the horizontal and vertical wind component, and horizontal wavelength as short as 20 km. The effect of such short-period waves upon the SAD experiment's ability to measure wind has not previously been taken into account.

Consider the simplified situation given in Figure 1 where only two scattering irregularities are present in the antenna beam at equal but opposite angular distances away from the zenith. The same amount of power is scattered from each irregularity. The electric fields on the ground resulting from scattering from each of the two irregularities may be written

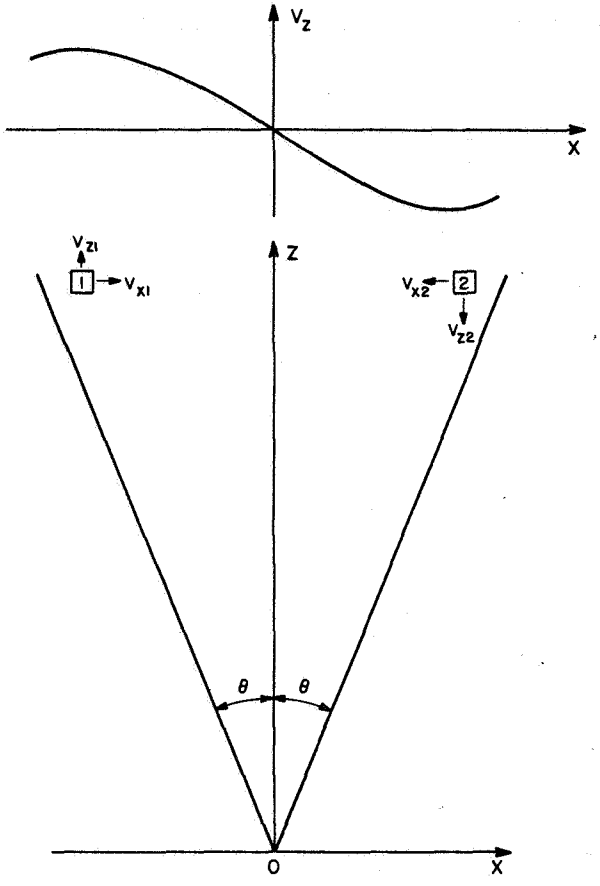


Figure 1. Radar situation with two scattering irregularities moving under the influence of a short-wavelength gravity wave.

$$E_1 = E_0 \exp i[(\omega_0 + \omega_1)t - \frac{2\pi \ x \sin\theta}{\lambda} + \frac{2\pi \ z \cos\theta}{\lambda}]$$

$$E_2 = E_0 \exp i[(\omega_0 + \omega_2)t + \frac{2\pi \ x \sin\theta}{\lambda} + \frac{2\pi \ z \cos\theta}{\lambda}]$$

In these equations $E_0$ is the amplitude of the scattered wave, $\omega_0$ the angular frequency of the transmitted radar wave, $\omega_1$ and $\omega_2$ the Doppler shifts in frequency, and $\lambda = \frac{2\pi c}{\omega_0}$ is the free space wavelength. Generally, $\omega_1$ and $\omega_2$ are independent, and we can express them as a function of a mean frequency shift $\omega_m$ and a differential frequency shift $\omega_d$ so that

$$\omega_1 = \omega_m - \omega_d \text{ and } \omega_2 = \omega_m + \omega_d$$

Since the antenna beam width is generally small we may add the electric fields without accounting for polarization effects. The total electric field on the ground then becomes

$$E = E_1 + E_2 = E_0 \exp i\,[(\omega_0 + \omega_m)t + \frac{2\pi \ z \cos\theta}{\lambda}]$$

$$2\cos(\frac{2\pi \ x \sin\theta}{\lambda} - \omega_d t)$$

The exponential part of this function represents a wave propagating vertically in the negative z direction with a frequency ($\omega_0 + \omega_m$). The amplitude of this wave is modulated in the horizontal plane in the form of a propagating wave given by

$$A(x,t) = 2E_0\cos(\frac{2\pi\ x\ \sin\theta}{\lambda} - \omega_d t)$$

where the frequency of the wave is given by $\omega_d = (\omega_2 - \omega_1)/2$. The two Doppler shift frequencies $\omega_1$ and $\omega_2$ resulting from the action of an internal gravity wave can be expressed as a function of the two line-of-sight velocities

$$\omega_1 = \frac{2\omega_0}{c}(V_{1z}\cos\theta + V_{1x}\sin\theta)$$

and

$$\omega_2 = \frac{2\omega_0}{c}(V_{2z}\cos\theta - V_{2x}\sin\theta)$$

For radars with half beam width $\theta$ less than 15° it is a good approximation to set $\cos\theta = 1$ thus simplifying the expressions for $\omega_1$ and $\omega_2$. Using the asymptotic relationships for internal gravity waves we can express $\omega_1$ and $\omega_2$ as a function of amplitude, frequency and wavelength of the gravity wave giving

$$\omega_1 = \frac{2\omega_0}{c}(V_z\sin\Omega\ t + V_x\cos\Omega\ t\ \sin\theta)$$

and

$$\omega_2 = \frac{2\omega_0}{c}[V_z\sin(\Omega\ t - \theta_d) - V_z\cos(\Omega\ t - \theta_d)\sin\theta]$$

Here it has been assumed that the vertical and horizontal velocity components are 90° out of phase. This may not be very realistic under all circumstances, but leads to simplifications of the result and will not affect the basic conclusions. $\Omega$ is the frequency of the internal gravity wave, and $V_z$ and $V_x$ are the vertical and horizontal components of the wind field, respectively. $\theta_d$ is the phase difference between the oscillations in the two scattering volumes which can be approximated by

$$\theta_d = \frac{4\pi z\ \sin\theta}{L}$$

where L is the horizontal wavelength of the gravity wave. Combining these equations give the expression

$$\omega_d = \frac{\omega_0}{c}\{V_z[\sin(\Omega\ t - \theta_d) - \sin\Omega\ t]$$

$$-V_x\sin[\cos(\Omega\ t - \theta_d) + \cos\Omega\ t]\}$$

and

$$\omega_m = \frac{\omega_0}{c}\{V_z[\sin(\Omega\ t - \theta_d) + \sin\Omega\ t] + V_x\sin\theta[\cos\Omega\ t - \cos(\Omega\ t - \theta_d)]\}$$

It is clear from the expression for $\omega_d$ that the horizontal velocity of the ground pattern will be a quite complicated function of several physical parameters unless $\theta_d \approx 0$. However, consider a not unreasonable situation of an antenna half beam width of 5°, two scattering irregularities at 85 km as shown in Figure 1, a horizontal wavelength of 30 km and a wave period of 10 minutes. Then $\theta_d \approx \pi$ and $\omega_d$ reduces to

$$\omega_d = \frac{\omega_0}{c} V_z(-2\sin\Omega t)$$

Thus it is seen that for this, and other similar choices where $\theta_d \approx \pi$ the horizontal motion of the pattern over the ground is caused by the horizontal variations in the vertical velocity only. However, even for other values where $0 \ll \theta_d < \pi$, $\omega_d$ will be dominated by vertical velocity differences because of the additional factor $\sin\theta$ in the contribution from the horizontal velocity.

The preceding calculations show that small spatial variations in the vertical velocity within the antenna beam can drastically affect the horizontal velocity measured. It was shown that if the antenna beamwidth is of the order of 10° such vertical velocity variations could be caused by short-period gravity waves. For an antenna beamwidth of the order of 1° large-scale turbulent motion is more likely to cause erroneous horizontal wind measurements. As is shown in another paper (ROYRVIK, 1983b) there are indications of large-scale (200-400 m) Kelvin-Helmholtz billows with a circular motion in the mesosphere. These occur intermittently and may cause large disturbances in the calculated horizontal velocities when a narrow beam antenna is used.

Thus it appears that both the SAD and the DBS techniques require integration over several periods of the short-period oscillations to obtain a horizontal velocity measurement. Estimates show that integration over approximately one hour gives reasonably accurate horizontal velocity estimates.

Two other less known techniques may be better suited to measure short-period horizontal velocity oscillations. These are the interferometer (IFR) technique and the cross-beam drift (CBD) technique. Both these techniques are based upon the horizontal drift of spatially limited scattering volumes. In the IFR mode the horizontal motion of the irregularities could be traced as a change in relative phase between the signals received in a set of spatially separated receivers. In the CBD mode the horizontal drift would manifest itself as a lagged maximum in the cross correlation of signal amplitudes received in a set of antennas in looking different directions.

The use of these techniques will depend on a proper spatial and temporal distribution of the scattering irregularities in the upper atmosphere, and as far as is known it has not been shown that these distributions exist.

## ACKNOWLEDGMENT

The work described was supported by the National Science Foundation under Grant ATM 80-19563.

## REFERENCES

Countryman, I. D. and S. A. Bowhill (1979), Wind and wave observations in the mesosphere using coherent-scatter radar, Aeron. Rep. No. 89, Aeron. Lab., Dep. Elec. Eng., Univ. Ill., Urbana-Champaign.

Moreels, G. and M. Herse (1977), Photographic evidence of waves around the 85 km level, Planet. Space Sci., 25, 265.

Royrvik, O. (1983a), Spaced antenna drifts at Jicamarca, Mesospheric measurements, Radio Sci., 461-476.

Royrvik. O. (1983b), VHF radio signals scattered from the equatorial mesosphere, Radio Sci., 1325-1335.

# 3.6A TECHNIQUES FOR MEASUREMENT OF HORIZONTAL AND VERTICAL VELOCITIES: OPTIMUM POINTING ANGLE

R. G. Strauch

NOAA/ERL/Wave Propagation Laboratory
Boulder, CO 80303

The factors that influence the choice of pointing angle for measurement of vertical profiles of the horizontal wind with monostatic Doppler radar are summarized in this paper.

We assume that fixed pointing directions are used; this avoids the costs and complexities of large mechanically or electronically steered antennas. Three antenna beam-pointing directions are needed to measure the vector wind; for simplicity the pointing directions are chosen to observe orthogonal horizontal wind components u and v, and the vertical component w. Horizontal winds are measured with an antenna elevation pointing angle $\theta_e$ that allows observation at all altitudes of interest.

The radial Doppler velocities $V_i$ measured by the radar are related to the wind as follows:

$$V_1 = u \cos\theta_e + w \sin\theta_e$$

$$V_2 = v \cos\theta_e + \sin\theta_e$$

$$V_3 = w$$

where the antenna azimuth angles for $V_1$ and $V_2$ are assumed to be 0° and 90° respectively. At each altitude h the three measurements are made at volumes separated in space, so an assumption of horizontal uniformity is needed to combine the measurements to form a wind profile assumed to apply in the vertical direction above the radar location. Two types of errors can result from this assumption: first, u and v measured at the observation volume will be in error by $h \frac{\Delta w}{\Delta x}$ and $h \frac{\Delta w}{\Delta y}$, respectively; and second, the measured u and v will differ from the u and v directly above the radar by $\frac{\Delta u}{\Delta x} h \cot\theta_e$ and $\frac{\Delta v}{\Delta y} h \cot\theta_e$, respectively.

It is commonly assumed that w can be ignored for sufficiently long averaging times so that horizontal winds can be measured with just two pointing directions. In some clear-air cases the averaging time needed may be hours (much longer than is commonly used), and during precipitation the measured Doppler velocity spectra may be from a combination of scattering from refractive turbulence and hydrometeors. Hydrometeors generally trace the mean wind but also have fall speeds that may be as large as 9 m/s (even larger for hail, ATLAS ET AL., 1973). The hydrometeor scattering signal can be stronger than the signal from refractive turbulence, even for VHF radars. If the horizontal winds are measured without correction for vertical motion, then the (two) pointing angles used are generally the same as for radars that use three pointing directions.

Factors that dictate high elevation angles are the following:

1. If the physical axis of the antenna is directed toward the zenith (the usual case for large phased arrays or large fixed reflectors) the elevation pointing angle should be as high as possible to keep the effective aperture nearly the same as for zenith pointing. The loss in sensitivity varies as $\csc\theta_e$ and is given in Table 1.

2. The elevation pointing angle should be as high as possible to minimize the range to a given height. The range is $h/\sin\theta_e$ and the loss in sensitivity varies as $(\text{range})^2$. This loss is double that of the effective aperture loss as shown in Table 1.

3. The height resolution of the radar depends on the range resolution and the cross-beam dimensions of the antenna illumination. The antenna elevation angle should be high enough so that the height resolution is not degraded by cross-beam resolution at the highest altitude of interest. We want radar range resolution $\Delta R$ to determine height resolution because range resolution is controllable by system bandwidth whereas cross-beam resolution is fixed by antenna dimensions. Thus, the cross-beam dimension, $h_m\ \beta_2 \cot\theta_e$, should be less than $\Delta R \sin\theta_e$ where $h_m$ is the maximum height of interest and $\beta_2$ is the two-way antenna beam width. Cross-beam height resolution at a height of 20 km is given in Table 1 for two-way beam widths of 2°, 3°, 4°, and 5°.

4. The elevation angle should be as high as possible to minimize the effects of horizontal gradients of the wind as discussed earlier.

Opposing these factors that mandate elevation angles near zenith are those that dictate lower elevation angles:

1. The elevation angle should be as low as possible to produce accurate wind measurements because uncertainty in the measurement of radial velocity causes an uncertainty in horizontal wind that increases with elevation angles. If vertical velocities are neglected,

$$\text{STD DEV}\ (\hat{v}_h) = [\text{STD DEV}\ (\hat{v}_i)]\ \sec\theta_e$$

where the superflex denotes an estimated quantity. Our ability to obtain unbiased estimates of $v_i$ with low standard deviation depends on radar wavelength, signal-to-noise ratio, observation time, and the width of the Doppler spectrum (ZRNIC', 1979). We want to obtain estimates at low signal-to-noise ratios where STD DEV $(\hat{v}_i)$ may be 1 m/s or more for individual observations. If we derive average horizontal winds from N independent observations with an uncertainty of 1 m/s, then sec $\theta_e$ must be at most $\sqrt{N}$ if the individual radial measurements have an uncertainty of 1 m/s. Table 2 gives the uncertainty in horizontal wind for an uncertainty in measured radial velocity of 1 m/s. For a VHF radar that obtains hourly wind averages from 15 observations, the elevation angle should not be greater than 75°.

Table 1. Loss factor and resolution for various elevation angles

| $\theta_e$ (deg) | Aperture loss (dB) | $(\text{Range})^2$ loss (dB) | Cross-beam height (m) | | | |
|---|---|---|---|---|---|---|
| | | | 2° | 3° | 4° | 5° |
| 90 | 0 | 0 | 0 | 0 | 0 | 0 |
| 85 | 0.016 | 0.032 | 60 | 90 | 120 | 150 |
| 75 | 0.15 | 0.30 | 187 | 280 | 375 | 467 |
| 60 | 0.62 | 1.24 | 400 | 600 | 800 | 1000 |
| 45 | 1.5 | 3.0 | 700 | 1050 | 1400 | 1750 |

Table 2. Uncertainty and bias of wind measurements for various elevation angles.

| $\theta_e$(deg) | STD DEV ($\hat{v}_h$)(m/s) | Bias errors (%) 2° | 3° | 4° | 5° |
|---|---|---|---|---|---|
| 90 | ∞ | --- | --- | --- | --- |
| 85 | 11.5 | 11 | 17.6 | 24.9 | 33 |
| 75 | 3.9 | 3 | 5 | 7 | 9 |
| 60 | 2 | 1.5 | 2 | 3 | 4 |
| 45 | 1.4 | 0.9 | 1.3 | 1.8 | 2.6 |

2. Bias errors in the wind measurements caused by errors in antenna pointing direction increase with increasing elevation angle. Table 2 gives the bias error for antenna beam widths of 2°, 3°, 4°, and 5° when the antenna pointing is in error by 1/4 of the beam width, a value that should be achieved in practice with a non-steerable antenna.

3. At long wavelengths (6-10 m) enhanced radar reflections are observed on a zenith-pointing beam. These reflections are caused by horizontally stratified atmospheric layers; their intensity decreases as the antenna elevation angle decreases from zenith. However, if the antenna is pointed too close to zenith, the effective pointing angle will be biased toward zenith, and this pointing error will bias wind measurements toward low values. At 15° off-zenith this effect should be negligible (ROTTGER, 1980).

## CONCLUSION

The selection of the elevation angle for measurement of vertical profiles of horizontal winds and Doppler radar must satisfy conflicting demands. Elevation angles near zenith result in intolerable uncertainties in wind measurement; elevation angles too far off-zenith result in a loss of sensitivity that must be compensated by increased transmitted power or antenna size. An elevation angle of 75° yields an acceptable compromise for typical clear-air radars.

## REFERENCES

Atlas, D. A., R. C. Srivastava and R. S. Sekhon (1973), Doppler radar characteristics of precipitation at vertical incidence, Rev. Geophys. Space Phys., 11, 1-35.

Rottger, J. (1980), Reflection and scattering of VHF radar signals for atmospheric refractivity structure, Radio Sci., 15, 259-276.

Zrnic', D. S. (1979), Estimation of spectral moments for weather echoes, IEEE Trans. Geosci. Elec., GE-17, 113-128.

# 3.6B EFFECTS OF GEOPHYSICAL NOISE ON THE ACCURACY OF WIND DETERMINATION

S. A. Bowhill

Aeronomy Laboratory
Department of Electrical Engineering
University of Illinois
Urbana, IL 61801

Let us assume that hourly mean zonal wind values at a range of altitudes are to be determined by an MST radar capable of pointing either vertically or at an angle s to the east. The simplist approach is to measure the line-of-sight velocity in the east pointing direction, take the hourly mean, and multiply by cosec s. The line-of-sight velocity contains a component w cos s of the vertical velocity w in the scattering volume, and the hourly mean of this quantity is not zero. Gravity-wave activity is an rms values per w of about 2 m/s, resulting in an rms error in each observation of 2 cot s.

The effects of vertical velocity may be partially eliminated by simultaneously measuring the vertical velocity with the vertically pointing radar direction. However, this introduces a difficulty in that the two antenna beams are examining different portions of the atmosphere, where the vertical velocity may not be the same. In general, for a gravity-wave field, the horizontal correlation function of the vertical velocity at a given altitude will decrease to 1/e of its value in some horizontal distance d. The effect of this on the rms error in each individual measurement of horizontal velocity is shown in Figure 1. Interestingly, for d = 40 km, corresponding to a horizontal wavelength of about 150 km, the resulting error is almost independent of s, indicating that little is to gained by the use of a very large zenith angle. Probably, the value of s of about 10° would be appropriate.

The effects of horizontal wave velocity on measurements of horizontal wind are, of course, independent of s, and must simply be compounded with the error arising from vertical velocities.

A further important point is that the resulting error in the mean velocity is obtained by dividing the rms error from Figure 1 by $N^{1/2}$, where N is the number of <u>equivalent</u> independent points in 1 hour of data. For a gravity wave of period 8 min, for example $N \sim 6$, even though line-of-sight velocity measurements may be made every minute. This geophysical noise problem is clearly the limiting factor in determining horizontal winds by MST radar.

ACKNOWLEDGMENTS

The work described was supported in part by the National Aeronautics and Space Administration under Grant NSG 7506 and in part by the National Science Foundation under Grant ATM 81-20371.

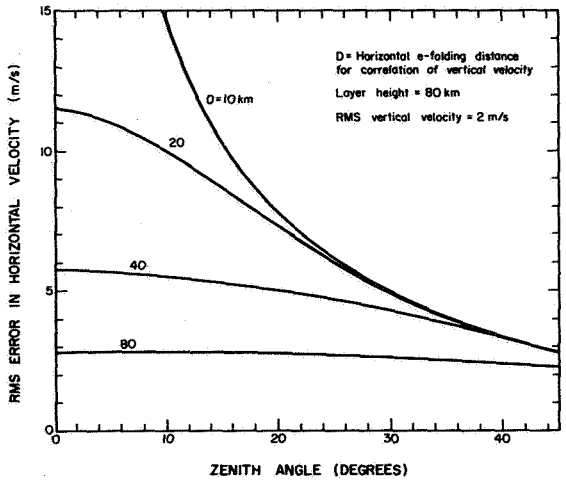


Figure 1.* rms error in estimates of horizontal velocity obtained from 1-hr average of line-of-sight velocities measured by an antenna beam pointing at a given zenith angle to the vertical, and corrected by the mean line-of-sight velocity measured by a vertically pointing antenna.

# 3.7A RADAR INTERFEROMETER MEASUREMENTS

D. T. Farley

School of Electrical Engineering
Cornell University
Ithaca, NY 14853

## INTRODUCTION

WOODMAN (1971) appears to have been the first to use the interferometer technique in scatter probing of the ionosphere. His observations allowed him to determine the position at which the radar beam was normal to the magnetic field (and hence the dip angle) above the Jicamarca Observatory with very high accuracy. More recently the technique has been extended, with the inclusion of Doppler information, and applied to studies of equatorial E-region electrojet plasma turbulence (FARLEY et al., 1981; KUDEKI et al., 1982), equatorial F-region irregularities (KUDEKI et al., 1981), and auroral electrojet irregularities (PROVIDAKES et al., 1983). There have been a few references to interferometer observations in the MST radar literature also, but the observations have been of various types, usually different from those in the ionosphere. One purpose of this paper is to try to clear up any possible confusion. As yet there do not appear to have been any successful 'true' (in the sense that we describe below) MST radar interferometer observations, but only a few brief attempts have been made.

## THE BASIC IDEA

In its simplest form, a radar interferometer consists of two separated receiving antennas, each with its own receiver, and a single transmitting antenna, which could be either a third antenna or one of the two receiving antennas. Suppose all the antennas are pointed vertically (extending the results to oblique observations is trivial) and that there is a single small (~ point) target located at some small angle $\theta$ from the zenith in the plane defined by the vertical and the line joining the phase centers of the two receiving antennas. If the range to the target is much greater than the separation, L, between the receiving antennas (as is always the case in practice), then there will be a small time delay, given by $L\sin\theta/c$, between signal reception at the two antennas. This delay translates into a phase difference of

$$\Delta\phi = kL\sin\theta \simeq kL\theta \qquad (1)$$

where $k=2\pi/\lambda$ is the radar wave number. In the absence of noise, this phase difference can be measured easily by forming the complex cross product of the two signal voltages; i.e.,

$$F = \frac{\langle V_1(t)V_2^*(t)\rangle}{\left[\langle|V_1|^2\rangle\right]^{\frac{1}{2}}\left[\langle|V_2|^2\rangle\right]^{\frac{1}{2}}} = e^{i\Delta\phi} \qquad (2)$$

where $\langle\cdot\rangle$ represents an ensemble or time average. This phase measurement determines the angular position of the target; changes in time of this angle determine an angular velocity, to which range information can be added to give a linear velocity component in the direction of the interferometer baseline. In order to avoid ambiguities of multiples of $2\pi$ in the phase measurement, it is desirable to have the beamwidth of one or more of the antennas narrower than the interferometer lobe spacing. As a rough rule of thumb, this is accomplished if the two receiving antennas, for example, are 'touching' (their linear dimension in the baseline direction is equal to L).

## COMPLICATING FACTORS

There are a number of effects encountered in practice which also must be kept in mind. For example:

1. Receiver noise. Since the noise in the two receivers is uncorrelated, it will not contribute to the cross produce in (2). It will change the normalization constant, but this is not important.

2. Cosmic noise and/or other correlated interference. These are common to both interferometer channels and so will cause problems. They must be measured separately (with the transmitter off, say) and subtracted out. If the signal is weak and the correlated interference changes with time and/or is somewhat changed by the presence or absence of the transmitter, the subtraction is somewhat changed by the presence or absence of the transmitter, the subtraction may be difficult to do accurately.

3. Multiple targets. If there are several targets in the beam at once, the cross product in (2) will be a vector sum of phasors whose magnitude and direction represent the strength and angular position of the separate targets, and the magnitude of F will be less than unity even if the signal/noise ratio is high. If all the targets move with the same velocity and maintain the same relative strengths, the velocity can still be determined from the rate of change of the mean phase angle, but if the situation is more complicated it may become impossible to interpret the phase changes.

4. Broad target. Much the same arguments apply to a target with an appreciable angular width. The magnitude of F gives a measure of the width; i.e., if we can describe the target as having an angular variance $\sigma^2$, the magnitude of F is roughly $\exp(-k^2L^2\sigma^2/2)$.

## RADIAL MOTION AND CROSS-SPECTRAL ANALYSIS

So far we have neglected target motion in the direction of the radar beam. Such motion will produce Doppler shifts in the received signals. The Doppler shifts thus give additional information about the scattering medium and also often can be used to separate the contributions to the signal from multiple targets, if the individual targets have different radial velocities as well as different angular positions. The analysis of the signals in this case is similar to that given above, but we introduce the additional step of first Fourier transforming the two signals. Next, we replace the simple voltage cross product with the cross spectrum of the two individual spectra; i.e., we compute

$$S_{12}(\omega) = \frac{\langle V_1(\omega)V_2^*(\omega)\rangle}{\langle|V_1(\omega)|^2\rangle^{\frac{1}{2}}\langle|V_2(\omega)|^2\rangle^{\frac{1}{2}}} \qquad (3)$$

where $V_1(\omega)$ and $V_2(\omega)$ are the (voltage) Fourier transforms of $V_1(t)$ and $V_2(t)$. By analogy with (2) and from the discussion above of broad targets, it is fairly easy to see that, in terms of the target parameters, the cross spectrum is

$$S_{12}(\omega) = e^{ikL\bar{\theta}\omega}\exp(-\tfrac{1}{2}k^2L^2\sigma_\omega^2)$$

where $\bar{\theta}_\omega$ and $\sigma_\omega$ are the mean angular position and spread of the target giving a Doppler shift of $\omega$. This result neglects noise contributions, etc. For a more complete discussion see FARLEY et al. (1981).

This measurement and analysis procedure has proved to be a very powerful

tool for investigating plasma turbulence in the ionosphere, as mentioned in the introduction, but full cross spectral analysis does not appear to be useful for MST applications. To see why, let us assume a typical vertical velocity to be ~.5 m/s (e.g., WOODMAN and GUILLEN, 1974), which would give a Doppler shift of 0.1-0.2 Hz at a radar frequency of 50 MHz. To achieve a reasonable frequency resolution of ~.01 Hz, say, would require an observation time of at least 1 min for each Fourier transform, and several computations of the cross spectrum must be averaged to obtain a meaningful result. In the required integration time of several minutes, a scattering center traveling with a horizontal velocity of say 10 m/s will move several kilometers, probably enough to move the scatterer out of the radar beam and certainly enough to give a phase change of many radians. Operating at higher radar frequencies will improve the situation, but probably not by enough.

In practice, then, one must revert to the analysis of (2), which is also much simpler computationally, and ignore the vertical velocity information in the interferometer calculations. It is still of course possible to obtain mean estimates of the vertical velocity by calculating the power spectrum of either of the received signals, or even the magnitude of the cross spectrum, which is essentially the same thing. It is only the phase information in the cross spectrum which is of no use in MST applications.

## MST INTERFEROMETER OBSERVATIONS

Some attempts to observe horizontal velocities at Jicamarca in the way just described have been mentioned by RUSTER and WOODMAN (1976) and RUSTER et al. (1978). The attempts were unsuccessful, however. The successive phase angles were more or less randomly distributed, indicating that scattering centers were distributed throughout the radar beam and that the scattering could not be modeled as coming from one or two discrete moving centers. The horizontal velocities shown in RUSTER et al. (1978) were obtained from a version of Spaced Antenna Drift (SAD) analysis. The two time series of the vertical velocities obtained from Fourier analysis of the signals received on the two separated antennas were cross correlated and the horizontal velocity was determined from the delay at which the cross correlation maximized. The attempts at the 'true' interferometer analysis were not very exhaustive, however, and there is some reason to hope that they might be successful at times in the mesosphere at least (WOODMAN, private communication, 1983). Some more recent observations at Jicamarca have led to similar conclusions (CORNISH, private communcation, 1983). (Added note: One successful mesospheric observation was described at this workshop by M. Ierkic and J. Rottger.)

Some work using the SOUSY radar with spaced antennas and phase coherent receivers has been described by ROTTGER and VINCENT (1978) and VINCENT and ROTTGER (1980). The voltages were cross correlated, and the lag at which the magnitude of the cross correlation was greatest was used to determine the velocity (the SAD technique). In contrast, the technique discussed here utilizes the phase of the cross correlation at zero lag to determine position. The SOUSY work did involve using phase information to determine the character of the scattering medium. The 'radiation pattern', so to speak, of the medium was measured by steering the lobe pattern of the interferometer array numerically in the data processing. In one example it was found that the echoes from an altitude of 2.44 km corresponded to isotropic scatterers but those from 3.79 km closely approximated a specular partial reflection. This sort of analysis is related to, but not quite the same as, measuring the magnitude of F in (2) to determine in some sense the angular width of the distribution of scatterers. This width would be very small for a quasi-specular reflection, but would roughly equal the antenna beam width for isotropic and uniformly distributed scatterers.

REFERENCES

Farley, D. T., H. M. Ierkic and B. G. Fejer (1981), Radar interferometry: A new technique for studying plasma turbulence in the ionosphere, J. Geophys. Res., 86, 1467-1472.

Kudeki, E., D. T. Farley, and B. G. Fejer (1982), Long wavelength irregularities in the equatorial electrojet, Geophys. Res. Lett., 9, 684-687.

Kudeki, E., B. G. Fejer, D. T. Farley and H. M. Ierkic (1981), Interferometer studies of equatorial F region irregularities and drifts, Geophys. Res. Lett., 8, 377-380.

Providakes, J. F., W. E. Swartz, D. T. Farley and B. G. Fejer (1983), First VHF auroral radar interferometer observations, Geophys. Res. Lett., 10, 401-404

Rottger, J. and R. A. Vincent (1978), VHF radar studies of tropospheric velocities and irregularities using spaced antenna techniques, Geophys. Res. Lett., 5, 917-920.

Ruster, R., J. Rottger and R. F. Woodman (1978), Radar measurements of waves in the lower stratosphere, Geophys. Res. Lett., 5, 555-558.

Ruster, R. and R. F. Woodman (1976), Radar measurements in the tropo-, strato-, and mesosphere, Preprints, 17th Radar Meteor. Conf., 354-358.

Vincent, R. A. and J. Rottger (1980), Spaced antenna VHF radar observations of tropospheric velocities and irregularities, Radio Sci., 15, 319-335.

Woodman, R. F. (1971), Inclination of the geomagnetic field measured by an incoherent scatter technique, J. Geophys. Res., 76, 178-184.

Woodman, R. F. and A. Guillen (1974), Radar observations of winds and turbulence in the stratosphere and mesosphere, J. Atmos. Sci., 31, 493-505.

# 4. TECHNIQUES FOR STUDYING GRAVITY WAVES AND TURBULENCE (Keynote Paper)

M. A. Geller

NASA Code 964
Goddard Space Flight Center
Greenbelt, Maryland 20771

In the 1960s, there was great interest in studying gravity waves and turbulence in the middle atmosphere. The main emphasis at that time was to look at small-scale observed structures in the wind and temperature fields and to understand the relation between observed chemical composition and "eddy diffusion." The idea that internal gravity waves can be important in generating turbulence in an otherwise stably stratified medium was also being pursued during this period as was the idea of internal gravity waves providing a medium of physical communication between distant regions of the atmosphere. During the 1970s and 1980s it has become more fully appreciated how important it is to understand the interaction of gravity waves and turbulence with the large scale flow sufficiently to be able to parameterize these effects in global models of the middle atmosphere.

To understand this more fully, let us consider what the zonally symmetric structure of the middle atmosphere would be if differential heating was present but the effects of wave motions and mechanical dissipation were absent. An acceptable mathematical solution would be that of radiative equilibrium with a balanced thermal wind. The form of this solution state for solstice conditions is shown in Figure 1 (taken from GELLER, 1983). Obviously, this solution gives a winter stratosphere that is much too cold and a summer mesosphere that is much warmer than the winter mesosphere which is contrary to observations. Also, both the winter westerlies and the summer easterlies are much too strong and do not form closed jet structures as are observed. There is no vertical or meridional wind in this solution state since the local heating rates and accelerations are everywhere zero. It should be pointed out that this solution state is not an acceptable physical solution state since it is unstable due to the very large lateral wind shears.

If we now impose mechanical dissipation in the form of a Rayleigh friction acting on the mean zonal wind state (still remaining in a zonally symmetric framework), we get results shown in Figure 2 (also taken from GELLER, 1983) which are much closer to the observed state of the middle atmosphere. Physically, this altered solution results by the drag on the zonal flow diminishing the mean zonal flow and requiring a zonal accelerative effect to counter the drag's decelerative effect. This sets up a summer to winter meridional flow upon which the Coriolis torque produces the required accelerations. By continuity, a rising motion is set up in the summer hemisphere and a sinking motion in the winter hemisphere which, in turn, elevates the winter middle atmosphere temperatures and reduces the summer middle atmosphere temperatures to be more in line with observations.

It is believed that much of this mechanical dissipation has its source in gravity waves breaking into turbulence. A cartoon of this process is illustrated in Figure 3 (GELLER, 1983). Gravity waves tend to grow exponentially with altitude as is shown and give rise to a vertical flux of horizontal momentum that is constant with altitude until the breaking level where the wave becomes statically or shear unstable. Above this breaking level, the wave amplitude ceases to increase with height giving rise to a diminished magnitude of the momentum flux. This tends to accelerate (or decelerate) the mean zonal flow so as to bring the flow in this region toward the wave's phase velocity

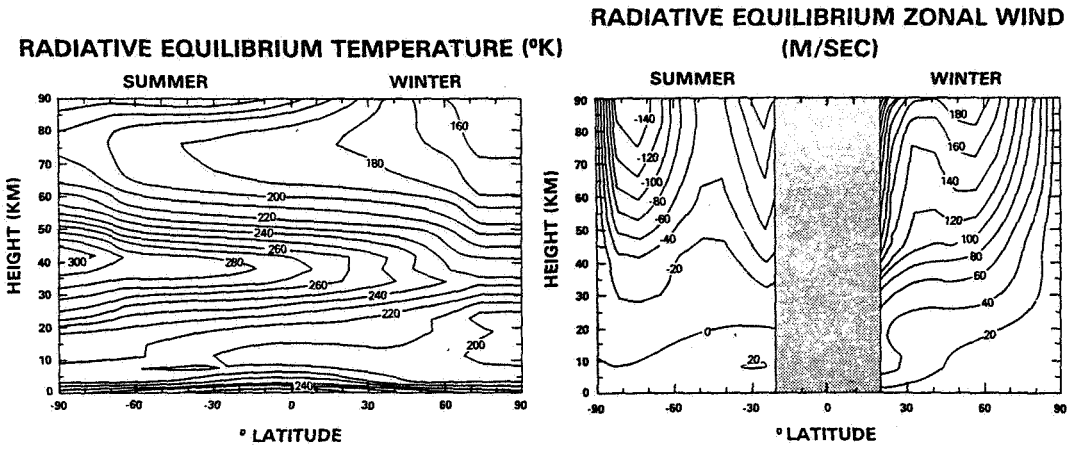


Figure 1. (Left) Calaculated radiative equilibrium temperatures. Units are K. (Right) Geostropic mean zonal winds calculated from the radiative equilibrium temperatures shown above. No values are shown near the equator because of the inapplicability of the geostropic formula there. Units are m/s, and westerly winds are positive while easterly winds are negative. (from GELLER, 1983.)

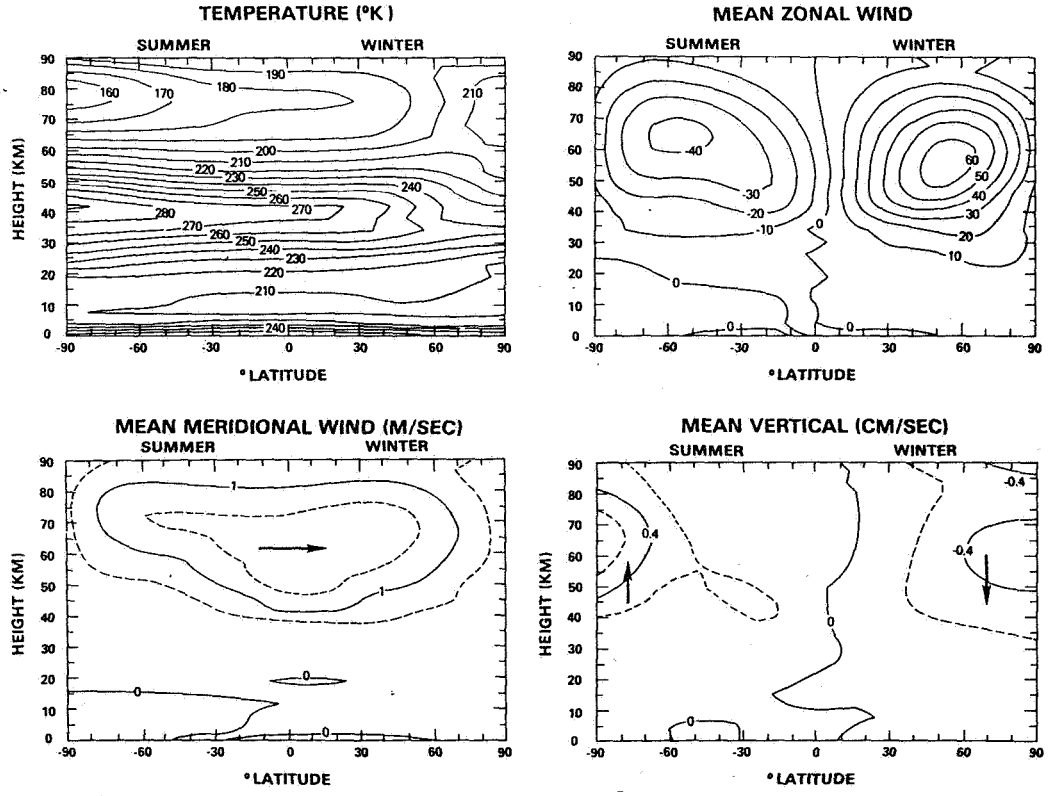


Figure 2. Model calculated zonally averaged temperature field in K (left-top); mean zonal wind in $ms^{-1}$ (right-top); mean meridional wind in $ms^{-1}$ (left-bottom); and mean vertical motion in cm $s^{-1}$ (right-bottom).

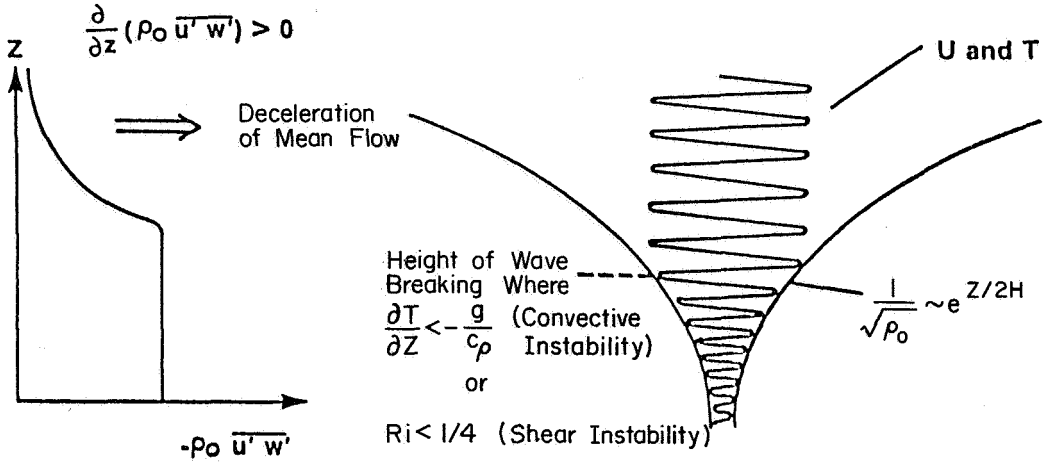


Figure 3.

which should be equal to the mean zonal flow velocity in its source region. Given that these gravity waves have their source in the troposphere where the zonal winds are relatively weak, the fast moving middle atmosphere flow will experience a drag. Gravity waves are thought to be essential to produce these effects since the other candidate, stationary planetary waves, are virtually absent in the summer hemisphere, but, as we have seen, mechanical dissipation is required in both hemispheres.

The mathematical basis for this mechanism was introduced by LINDZEN (1981). His formulae for the wave-induced drag and diffusion are shown in equations (1) and (2), respectively.

$$-\frac{1}{\rho_0}\frac{d}{dz}\rho_0\overline{uw} \approx \frac{-k}{2H}\frac{(\bar{u}-c)^3}{N(1+\ell^2/k^2)^{3/2}}\Bigg|_{z=z_{break}} \quad \text{eval at} \tag{1}$$

$$D_{eddy} \approx \frac{k|\bar{u}-c|^4}{N^3(1+\ell^2/k^2)^{3/2}}\left[\frac{1}{2H} - \frac{3}{2}\left(\frac{1}{\bar{u}-c}\frac{d\bar{u}}{dz}\right)\right] \quad \text{eval above } z_{break} \tag{2}$$

In equations (1) and (2), k is the east-west wave number; $\ell$ is the north-south wave number, $\bar{u}$ is the eastward mean flow; c is the gravity wave phase velocity; $N^2$ is the Brunt-Vaisala frequency squared; H is the scale height; z is the altitude; $\rho_0$ is the background density; $\overline{uw}$ is the covariance of the eastward and upward gravity wave velocity; and $z_{break}$ is the altitude at which the wave plus environmental lapse rate exceeds the dry adiabatic lapse rate of 9.8°C/km. MST

radars appear to have the capability of observing $-\frac{1}{\rho_0}\frac{d}{dz}(\overline{uw})$ by the methods of VINCENT and REID (1983), for example, as well as $D_{eddy}$ by measuring $C_n^2$, for example. They also can measure $\bar{u}$ and $\frac{d\bar{u}}{dz}$. One thing we will wish to discuss is how the remaining terms on the right-hand side of equations (1) and (2) can be either measured or inferred. This line of research will allow us to relate the theory of gravity wave breaking more closely to observations. Of course, LINDZEN'S (1981) formulation was only the beginning of theoretical formulations on this subject. Other factors to be considered are now becoming evident. These include the heat transports in breaking gravity waves (SCHOEBERL et al., 1983); the geographical nonuniformity of gravity wave propagation to breaking altitudes (SCHOEBERL and STROBEL, 1983); and nonlinear interactions among the gravity waves (WEINSTOCK, 1982).

MST radars represent a most powerful technique for obtaining the needed parameters for gravity-wave-induced drag and diffusion effects as well as measuring wave accelerations and diffusion directly. During this workshop, we will be discussing several of the factors relating to these measurements. We will be discussing the following topics as well as others that will arise:

(1) Required horizontal, vertical and temporal resolution.
(2) Wavelength dependence of the turbulence spectrum.
(3) Existence of a persistent background of turbulence.
(4) Determination of vertical and horizontal wavelengths of gravity waves.
(5) Parameterization of Fresnel returns.
(6) Minimization of bias and errors due to sampling and short-term fluctuations.
(7) Relationship of strength of turbulence to the received power.

## REFERENCES

Geller, M. A., (1983), Middle atmosphere dynamics, (to appear in Space Science Reviews).

Lindzen, R. S. (1981), Turbulence and stress owing to gravity wave and tidal breakdown, J. Geophys. Res., 86, 9707-9714.

Schoeberl, M. R., and D. F. Strobel (1983), Nonzonal gravity wave breaking in in winter mesosphere, (to appear in collection of papers from U.S.-Japan Seminar on Middle Atmospheric Dynamics).

Schoeberl, M. R., D. F. Strobel, and J. Apruzese (1983), A numerical model of gravity wave breaking and stress in the mesosphere, J. Geophys. Res., 88, 5249-5259.

Vincent, R. A., and J. M. Reid (1983), Radar measurements of gravity wave momentum fluxes, J. Atmos. Sci., 40, 1321-1333.

Weinstock, J. (1982), Nonlinear theory of gravity waves: Momentum deposition, generalized Rayleigh friction, and diffusion, J. Atmos. Sci., 39, 1698-1710.

## ISSUES AND RECOMMENDATIONS

### INTRODUCTION

It is now generally accepted that gravity waves and their associated breaking into turbulence are very important in producing the overall picture of middle atmosphere global dynamics and associated transport. It is also accepted

that the ST and MST radar techniques play an important role in assessing these effects. During the cause of this meeting, we have focussed on some important issues that arise in applying the ST and MST techniques to the study of gravity waves and turbulence.

(b) Issues

1. Eddy Diffusivities in the Lower Stratosphere: ST radars find effective eddy diffusivities of $\sim 0.1\ m^2 s^{-1}$ in the tropical lower stratosphere. This is about one order of magnitude larger than previous analyses of aircraft observations have indicated. This discrepancy is presently unresolved and deserves further attention.

2. Turbulent Layering: There commonly exist long-lived thin turbulent layers of large horizontal extent ($\sim$100 km) in both the stratosphere and mesosphere. This requires theoretical explanation.

3. Validity of Homogenous and Isotropic Turbulence Theory: Given the fact that the VHF radars commonly probe eddy sites that are comparable to the thickness of thin turbulent layers, it is questionable if the formulations of homogenous and isotropic turbulence can be used to interpret these observations. Further work is required on this situation.

4. Monochromatic Gravity Waves: Much of the analysis of gravity waves takes place on the rather rare occasions when significant energy is found in almost monochromatic wave activity. Given that these events occur infrequently, it is questionable whether their analysis yield results that are representative of average atmospheric behavior.

(c) Recommendations

1. Programs to Verify Radar Measurements of Turbulent Parameters: We recommend increased activity toward using in situ aircraft, balloon, and rocket techniques to achieve simultaneous measurements of atmospheric turbulent parameters with ST and MST radars.

2. Colocation of Ground-Based Instrumentation with MST Radars: Given that MST radars are powerful major ground-based facilities but that they produce incomplete observations of atmospheric parameters by themselves (e.g., wind only and the 40-60 km gap), we recommend that other ground-based instrumentation (e.g., lidar, meteor radar, and partial reflection drifts) be colocated with major MST radar facilities.

3. Needed Spatial and Temporal Resolution: Given that gravity wave periods down to several minutes exist and that time averaging the radar signals before recording data is an irreversible process, we recommend that signal averaging <u>before recording</u> be done for as short times as is practical. In most cases, this should be a fraction of a minute.

ST and MST radars should be capable of range resolutions on the order of 150 m. The coarser the vertical resolution of MST and ST radars, the more difficult results are to interpret due to multiple returns.

4. $\overline{V^2}$ is Preferred Over $C_n^2$: Velocity variance measurements are preferred over $C_n^2$ measurements to characterize the energetics of atmospheric turbulence. Narrow beam width ($\sim 1°$) systems are required to obtain measurements of $\overline{V^2}$ that can be easily interpreted.

5. Simultaneous Spectra: It is desired to obtain simultaneous spectra of horizontal and vertical velocities versus frequency and horizontal and vertical

wavelengths to resolve theoretical models.

6. HF Radars: We urge that the use of sensitive HF radars be explored for MST observations.

7. Radar Networks for Gravity Waves: We urge that networks of ST and MST radars be set up for a variety of spacings and representative of a variety of geophysical conditions to measure gravity-wave parameters.

8. Gravity-Wave Sources: We recommend that observational programs be planned to increase our understanding of gravity-wave sources.

9. Gravity-Wave Momentum Fluxes: Given the importance of understanding gravity wave drags on the large-scale flow, we recommend that MST radar facilities determine $\overline{v'w'}$ as a function of season and geographical location either by the methods of VINCENT and REID (1983) or by other methods.

10. Rotary Spectra: It is recommended that vector spectral analysis be applied to time series of the two components of horizontal wind at all available altitudes in order to determine the fraction of low-frequency gravity-wave energy associated with up-going and downgoing phase velocities.

# 4.1A TECHNIQUES FOR STUDYING GRAVITY WAVES AND TURBULENCE: HORIZONTAL, VERTICAL AND TEMPORAL RESOLUTION NEEDED

S. K. Avery* and D. A. Carter**

*CIRES, University of Colorado, Boulder, CO 80309
**Aeronomy Laboratory, NOAA, Boulder, Co 80303

One of the most important atmospheric measurements that is needed is a measure of the gravity-wave spectrum. Theoretical modeling of the breakdown of gravity waves and the resulting generation of turbulence has shown that this mechanism is crucial in understanding the general circulation of the middle atmosphere (LINDZEN, 1981; HOLTON, 1982; MATSUNO, 1982). In these models a knowledge of the gravity-wave periods and horizontal phase velocities is necessary. To date a thorough observational study to help delineate the gravity-wave parameters has not been done although a measure of the gravity-wave upward energy flux has been made by VINCENT and REID (1983). A detailed analysis of the sources of gravity waves is also lacking.

According to the dispersion relationship for gravity waves (HINES, 1960), the periods of these waves, including the tidal oscillations, range from minutes to hours. Corresponding horizontal wavelengths range from $10^2$m to $10^7$m and vertical wavelengths range from $10^2$ to $10^5$m. Thus there is a wide band of frequencies and wavelengths that are associated with gravity-wave motions. Since the background atmosphere acts as a filter for upward propagating gravity waves, the spectrum observed at mesospheric heights should be different than that at tropospheric heights.

The large temporal and spatial scales of tidal oscillations require continuous data collection (at least over 48 hours) and a global network of stations.* Coordinated observational periods have been made amongst meteor radar, partial reflection drifts, and MST radar groups. A workshop discussing the results of one such global campaign will be held in Hamburg at the IUGG meeting, August 1983.

Shorter period oscillations will require temporal resolution on the order of minutes or less. This time resolution is already available on many MST or ST radars (BALSLEY and GAGE, 1980). An indication of the spatial resolution required for observations can be obtained from vertical velocity data taken simultaneously by 3 ST radars a few km apart during the ALPEX experiment in southern France in 1982. Figure 1 displays vertical velocity power spectra, coherence, and cross-phase (phase of the cross-spectrum) for two sites which were separated by 4.6 km. The curves at short periods are averaged over 18 consecutive 4-hour periods and over 5 adjacent 750-meter range gates in the troposphere and 3 range gates in the stratosphere. The curves between 3 and 24 hour periods were obtained from 3 24-hour data sets averaged over the same range gates. For the short-period sections of the coherence curves, the 99% confidence level for zero coherence is at a value of 0.22 for the troposphere and 0.29 for the stratosphere.

Note that the power drops off dramatically in the troposphere below the Brunt-Vaisala period ($T_B$). A lesser drop-off in power is seen in the stratosphere. The coherence between the two sites for periods less that $T_B$ is small and increases rapidly with increasing period. For periods greater than 3 hours the coherence is greater than 0.7 and the cross phase between the sites is zero. The coherence is still relatively high for periods between 3 H and 1 H and a gradual increase in the cross phase is seen in the stratosphere. The cross

*The time resolution only needs to be on the order of one hour or less unless one is studying the interaction with shorter period gravity waves.

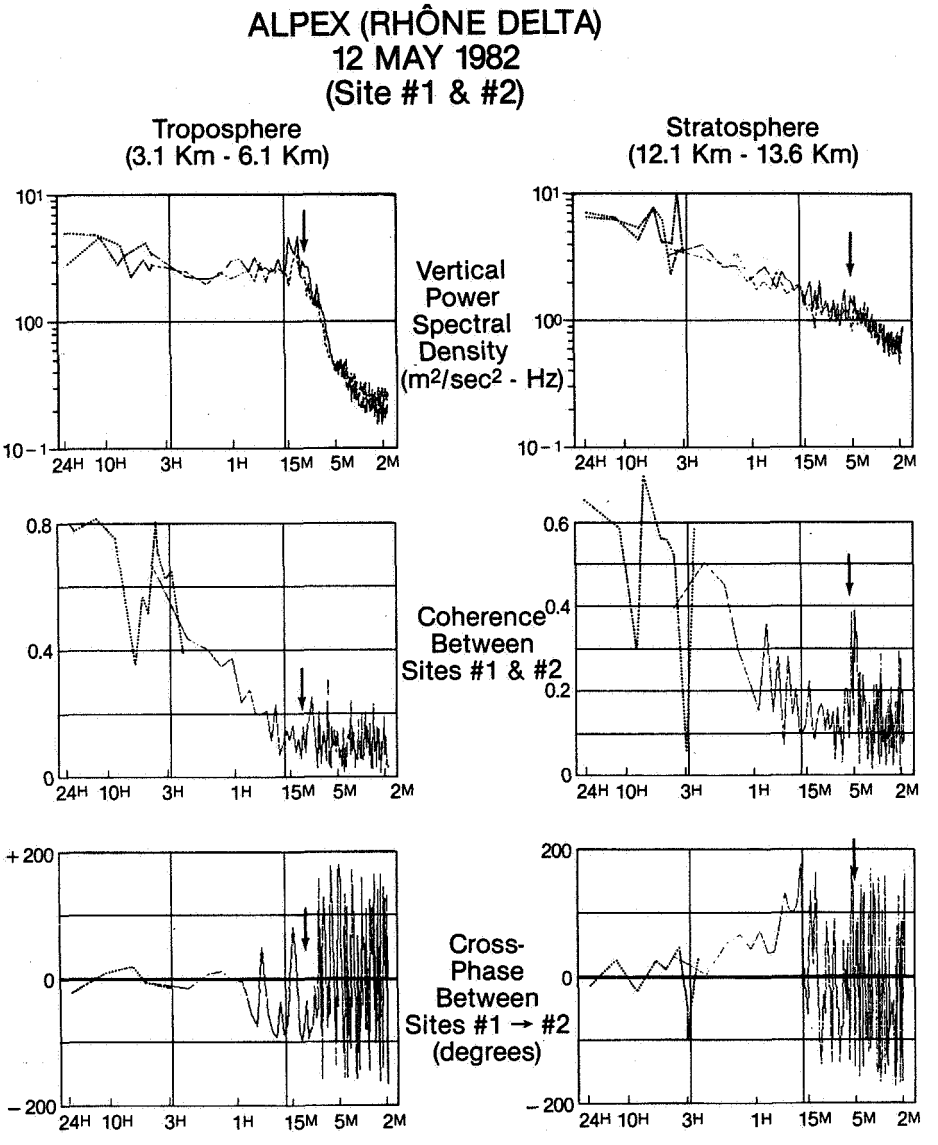


Figure 1.

phase is approximately 50° for waves with periods of 2 H which corresponds to a horizontal wavelength component of 35 km and a phase speed of 4.5 m/s.

From this type of analysis we can obtain a measure of the horizontal spacing required to measure horizontal wavelengths. Below $T_B$ the horizontal resolution needed is less than 5 km. For wave periods between 3 H and 1 H the 5 km spacing appears to be adequate. Periods greater than 3 H in the stratosphere will require a horizontal resolution greater than 5 km. It is difficult to obtain an upper limit on the required horizontal spacing since it will depend on the periods of wave motion that one wishes to determine.

The vertical resolution needed is also dependent on the periods of interest. Two km resolution over several heights has been adequate to resolve vertical wavelengths greater than 10 km (CARTER and BALSLEY, 1982). However, oscillations near the Brunt-Vaisala frequency appear to be coherent over 1-2 height ranges. This has been seen in the Alpex data which has a vertical resolution ot 750 m and the Urbana data which has a vertical resolution of 3 km. These oscillations do not appear to be propagating waves.

In addition GIBBS and BOWHILL (1983) has shown that within the Urbana 3-km spacing, several smaller scale features of the scatterers exist. He was able to obtain finer vertical resolution by using a parbolic fit of the amplitude of the Doppler frequency. Thus it is possible to use signal processing techniques to enhance the vertical resolution.

In summary, the MST radar has the temporal resolution required to determine gravity-wave oscillations. Of course the amount of temporal averaging that is required to obtain a significant measurement of the wind will vary depending on the signal-to-noise ratio. However, 4-minute averaged data have been routinely available at Poker Flat, which is probably sufficient for gravity wave motions. With the radar operating at full power, one minute data are available. The required vertical and horizontal resolution will depend on which particular part of the gravity-wave spectrum one wishes to analyze. It appears that 5-km horizontal spacing is adequate to resolve the horizontal structure of 3 H - 1 H oscillations.

REFERENCES

Balsley, B. B. and K. S. Gage (1980), The MST radar technique: Potential for middle atmospheric studies, P. Appl. Geophys., 118, 452-493.

Carter, D. A. and B. B. Balsley (1982), The summer wind field between 80 and 93 km observed by the MST radar at Poker Flat, Alaska (65°N), J. Atmos. Sci., 39, 2905-2915.

Gibbs, K. P. and S. A. Bowhill (1983), An investigation of turbulent scatter from the mesosphere as observed by coherent-scatter radar, Aeronomy Rep. No. 110, Aeronomy Lab., Dept. Elec. Eng., Univ. of Ill., Urbana-Champaign.

Hines, C. O. (1960), Internal atmospheric gravity waves at ionospheric heights, Can. J. Phys., 38, 1441-1481.

Holton, J. R. (1982), The role of gravity wave induced drag and diffusion in the momentum budget of the mesosphere, J. Atmos. Sci., 39, 791-799.

Lindzen, R. S. (1981), Turbulence and stress owing to gravity wave and tidal breakdown, J. Geophys. Res., 86, 9707-9714.

Matsuno, T. (1982), A quasi one-dimensional model of the middle atmospheric circulation interacting with internal gravity waves, J. Met. Soc. Japan, 60, 215-226.

Vincent, R. A. and I. M. Reid (1983), H.F. Doppler measurements of mesospheric gravity wave momentum fluxes, Submitted to J. Atmos. Sci.

# 4.2A THE MST RADAR TECHNIQUE: A TOOL FOR INVESTIGATIONS OF TURBULENCE SPECTRA

M. F. Larsen

School of Electrical Engineering
Cornell University
Ithaca, New York 14853

## INTRODUCTION

The MST radar technique has vastly improved our ability to measure turbulence spectra and turbulence intensity at all altitudes between the ground and the thermosphere, particularly at temporal scales characteristic of mesoscale motions. The only limitations have been the height resolution of the order of a hundred meters and the time resolution of the order of a minute. However, the instrument is still far superior to any other instrument used for this purpose in measuring frequency power spectra.

## POWER SPECTRAL MEASUREMENTS

As an example, the Poker Flat radar has provided a data set that can be used to study turbulence at periods from a few minutes to several years at altitudes in the troposphere, stratosphere, and mesosphere. The only limitation of the technique is that since the radars are not scanning radars, velocity profiles are measured as a function of time and provide only frequency spectra. The frequency spectra then have to be related in some way to the wave number spectra since most of the theoretical results relate to wave number spectra and do not make any direct predictions about frequency spectra. Also, none of the spectra of the thermodynamic variables can be measured with the radar, but, on the other hand, vertical velocity spectra can be investigated, and that is difficult to do with any other instrument.

So far, only a few studies of turbulence spectra have been carried out using the radar data. LARSEN et al. (1982) calculated the frequency power spectra for 40 days of data from the Poker Flat, Alaska, MST radar. The height range covered was from 3.79- to 14.99-km altitude. The results showed that on the average, the spectral slope over that height range was $-1.60 \pm 0.24$, very close to -5/3. BALSLEY and CARTER (1982) used a much longer time series from the same radar for both tropospheric and mesospheric winds. The much longer time series allowed a large number of spectra for shorter time frames to be composited in order to get a better estimate of the spectral slope. The details of how the spectra were produced are given in their paper. The resulting frequency power spectra at both 8- and 86-km altitude deviate very little from the $f^{-5/3}$ power law.

There have been a number of observations using other types of instruments that also found a -5/3 spectral power law at scales typical of the mesoscale. GAGE (1979) summarizes much of the observational evidence available at the time of his paper. LARSEN et al. (1982) cite further studies with similar results.

## CHARACTERISTICS OF STRATOSPHERIC TURBULENCE

A different approach to the study of turbulence has been that of Dr. R. F. Woodman, formerly of the Arecibo Observatory in Puerto Rico. Together with Drs. T. Sato and P. Rastogi, he has been interested primarily in the frequency of occurrence of turbulent layers in the stratosphere. It has been known at least since the HICAT studies (LILLY et al., 1974) that turbulence in the stratosphere occurs in thin layers. HICAT involved turbulence measurements made with U2 aircraft. The 430-MHz radar at the Arecibo Observatory is capable of making

observations with a height resolution of 300 m. The resolution is sufficiently good and the distribution of layers is such that generally only a single layer will be found within the sampling volume. The thickness of the layers is usually much less than the thickness of the sampling volume. The echo strengths can be used to study the frequency of occurrence of the layers and how they move as a function of time. Also, information on the distribution of layer thicknesses can be obtained (RASTOGI and WOODMAN, 1983).

WOODMAN et al. (1981) and RASTOGI and WOODMAN (1983) have used the data to investigate the effectiveness of stratospheric turbulent layers in mixing and transport processes. Calculations of the magnitude of the diffusion coefficient based on this approach have yielded values that are larger, perhaps by as much as an order of magnitude, than the values estimated originally by LILLY et al. (1974) based on HICAT data. The values derived from the new approach are in fact closer to the values needed to explain stratospheric residence times if large-scale circulation effects are neglected. However, the measured residence times have been attributed to large-scale transport processes in the past rather than diffusion. If diffusion really is more effective than had originally been thought, then how do we explain the role of the large-scale transport processes since they are also thought to be important? There is much room for more investigations of these problems, and the radar measurements will likely be a valuable tool.

## TWO-DIMENSIONAL TURBULENCE VS. A UNIVERSAL SPECTRUM

Although it is generally agreed that the spectral slope of mesoscale horizontal velocity fluctuations lies near -5/3, the interpretation of the significance of this fact is far from resolved. GAGE (1979) summarized the data from various sources indicating the existence of a -5/3 slope. He then argued, based on scaling arguments, that mesoscale motions are more likely to be associated with a two-dimensional inertial subrange rather than a three-dimensional inertial subrange. The most important implication of two-dimensionally rather than three-dimensionally is that there is a reverse cascade of energy from small scales to large scales, the so-called red cascade as opposed to the blue cascade.

LILLY (1983) became interested in the problem and dealt more directly with the problem of where the energy sources for the cascade are located. He was also able to show that two-dimensional turbulence can exist in the presence of gravity waves and other three-dimensional structures. LILLY (1983) postulated that the source of energy is associated with convection, shear instabilities, mountain waves, and other small-scale dynamic structures. Although most of the energy from such a process will decay towards smaller scales, a small fraction of the energy may be able to reach larger scales to become part of a red cascade process. He estimated that even as little as 5-10% of the energy generated in this way would be enough to have a significant effect on mesoscale variance spectra. The general physical process proposed by LILLY (1983) is described in this way, but he also points out that there may be competing processes involved.

An alternative interpretation of the observed spectra was proposed by VANZANDT (1982). In his view, the -5/3 slope is only significant in that it represents the existence of a universal spectrum in analogy to the universal spectrum that has been found to exist in the oceans. The GARRETT-MUNK (1975) spectrum is an empirically derived description of the frequency spectra measured in the oceans, and the empirical spectrum has been found to fit the measurements made at a wide variety of locations and under a wide variety of conditions. Thus, it is really appropriate to characterize the spectrum as being universal.

Since the model is empirical, the physical basis for the model is not immediately evident. However, there is general agreement that in the oceans the

spectrum is the result of a steady interaction of gravity waves. There is still discussion about the energy flow budget associated with such a spectrum. However, McCOMAS and MULLER (1980) have modeled the interactions of a spectrum of gravity waves, and the study showed that the energy flow was from large to small scales, the same as the energy flow direction in three-dimensional turbulence. See LeBLOND and MYSAK (1978) for a discussion of the dynamics of the GM spectrum.

## NEED FOR FUTURE OBSERVATIONS

There are a number of important reasons for resolving the question of which model best represents mesoscale turbulent processes, aside from improving our general understanding of the dynamics of the atmosphere. A reverse energy cascade would create a serious limitation on our ability to make mesoscale forecasts. The implication is that to resolve scales of say a few hundred kilometers, we need to have good information about scales of motion that are much smaller than that.

At this point, I would like to be able to make a very specific list of the observations that are needed to distinguish between the two models. However, this is not possible. I can only describe some general considerations that might be used by anyone who is interested in pursuing the topic in the future.

A -5/3 spectral slope is a strong requirement for the existence of a two-dimensional inertial subrange, and the observations to date do seem to indicate that such a slope is representative of conditions on the average. However, the GM model does not make a prediction of what the slope should be. Therefore, a -5/3 slope is not contradictory to the model, though the slope is closer to -2 in the oceans. Once the spectral slope associated with the horizontal velocity fluctuations is known, the slopes for other quantities such as the vertical velocity, temperature etc., are given by the theory. But, if the atmospheric vertical velocity spectra are found to be consistent with the predictions of the GM model, that in itself does not argue against the existence of two-dimensional turbulence at that scale. Since two-dimensional turbulence theory does not consider vertical variations explicitly, any variability in that direction is incidental to the theory. It is clear that at this point it is not trivial to devise a test of the competing models. It may be that advancements in our understanding of the theory will have to take place first.

Suggestions made to date involve testing the basic premise of the interacting gravity-wave hypothesis. Gravity waves in the ocean are in some sense trapped by the imposed boundaries of the ocean floor and the water surface. Thus, it is possible for the waves to interact over long periods of time to establish a steady-state spectrum. Gravity waves generated in the atmosphere can propagate away vertically to be dissipated in the high atmosphere. It is crucial then to determine what the interaction time is and whether waves are propagating out of the troposphere before the interactions can take place. Another suggestion has been to test the universality of the spectrum in the atmosphere. Of course, if the spectral slope is found to vary to some extent, that would only prove that the interacting gravity-wave spectrum may be overwhelmed by other processes on occasion.

Although LILLY (1983) has proposed a model of two-dimensional mesoscale turbulence with energy flow from small to large scales, he qualifies this viewpoint by noting that if the motions really act as two-dimensional turbulent motions, they will eventually decorrelate in the vertical to the extent that instabilities will arise. The effect of such instabilities would be to reverse the flow of energy, and if such effects are too large, the proposed physical picture could be invalid. If the energy flow reversals associated with instabilities are not too large in magnitude then it may be possible that both

processes can coexist.

## MESOSCALE GAP

Throughout the last half of the sixties and first half of the seventies, there was another ongoing debate in the literature about the nature of mesoscale turbulence. Specifically, the argument centered on whether or not a gap in the energy spectrum at spatial scales charactertistic of the mesoscale actually exists. It was argued by proponents of the idea that since there are no real sources of energy for mesoscale motions, there should be a gap in the energy spectrum corresponding to those scales. The implication was that there is a clear separation between synoptic scale motions and microscale motions. The most surprising aspect of the argument was that both points of view were apparently supported by observational data. The most recent papers discussing the evidence for the existence of a mesoscale gap in the spectrum of turbulence were published between 1972 and 1975 (FRYE et al., 1972; HESS and CLARKE, 1973; SMEDMAN-HOGSTROM and HOGSTROM, 1975). The arguments and an excellent summary of the literature are presented in the introduction to the book by ATKINSON (1981) on mesoscale meteorology.

Proponents of the no-gap theory claimed that energy should decrease smoothly from large scales to small, as predicted by Kolmogoroff, according to the -5/3 power law, and they showed clear observational evidence of this type of behavior (e.g., VINNICHENKO and DUTTON, 1969; VINNICHENKO, 1970). There is now general agreement that there is no lack of energy at the mesoscale, and indeed, much of the present day research emphasis is on mesoscale motions (see LARSEN (1983) in this volume for further discussion and references).

Part of the "gap" controversy was fueled by a lack of adequate data. The mesoscale has always been the most difficult to observe, especially above the boundary layer. However, improvements in radar technology, instrumented aircraft, and satellites has made it possible to make an increasing number of measurements of turbulence spectra at these scales. The evidence is clearly in favor of the continuous energy distribution rather than the gap theory.

## NONUNIVERSAL SPECTRA

The controversy was resolved when it was realized that the spectra that had been interpreted as being supportive of the gap model, in fact, showed an increase in energy above the normal level at small scales. The data used by VAN DER HOVEN (1957) was collected in hurricane conditions and had an energy peak at periods of a few minutes. It was the associated "valley" on the low frequency side of the anomalous peak that had been incorrectly interpreted as evidence of the mesoscale gap.

The arguments for and against the mesoscale gap are less interesting now, but not so the data that was used to support these arguments. There are clearly strong sources of energy at small scales, and the sources are evident in more than a few isolated cases. In fact, the -5/3 slope that has been found in the frequency spectra at different heights and different locations only appears if the mean behavior or the atmosphere is considered. Spectra usually have to be added, averaged, or composited in some way before consistent behavior appears. The oceans appear to be much less variable than the atmosphere in this respect. Anomalous peaks and deviant spectra should be considered along with the effort to improve our understanding of the mean or average turbulence spectra. It is possible that spectra measured at times when strong energy sources are present may hold the key to resolving the question of whether mesoscale turbulence is characterized by a universal gravity-wave spectrum or two-dimensional turbulence.

ACKNOWLEDGEMENTS

The author was supported by the National Aeronautics and Space Administration under grant NAGW 362 and by the National Science Foundation under grant ATM 81-08381.

REFERENCES

Atkinson, B. W. (1981), Meso-scale Atmospheric Circulations, Academic Press, New York.

Balsley, B. B., and D. A. Carter (1982), The spectrum of atmospheric velocity fluctuations at 8 km and 86 km, Geophys. Res. Lett., 9, 465-468.

Frye, D. E., S. Pond, and W. P. Elliott (1972), Note on the kinetic energy spectrum of coastal winds, Mon. Wea. Rev., 100, 671-673.

Gage, K. S. (1979), Evidence for a $k^{-5/3}$ law inertial range in mesoscale two-dimensional turbulence, J. Atmos. Sci., 36, 1950-1954.

Garrett, C., and W. Munk (1975), Space-time scales of internal waves: A progress report, J. Geophys. Res., 80, 291-297.

Hess, G. D., and R. H. Clarke (1973), Time-spectra and cross-spectra of kinetic energy in the planetary boundary layer, Quart. J. Roy. Meteorol. Soc., 99, 130-153.

Larsen, M. F. (1983), The MST radar technique: Requirements for operational weather forecasting, Preprints, Workshop on MST Radar, in this volume.

Larsen, M. F., M. C. Kelley, and K. S. Gage (1982), Turbulence spectra in the upper troposphere and lower stratosphere at periods between 2 hours and 40 days, J. Atmos. Sci., 39, 1035-1041.

LeBlond, P. H., and L. A. Mysak (1978), Waves in the Ocean, Elsevier Oceanogrphy Series, Elsevier, New York.

Lilly, D. K. (1983), Stratified turbulence and the mesoscale variability of the atmosphere, J. Atmos. Sci., in press.

Lilly D. K., D. E. Waco, and S. I. Adelfang (1974), Stratospheric mixing estimated from high-altitude turbulence measurements, J. Appl. Meteorol., 13, 488-493.

McComas, C. H., and P. Muller (1981), The dynamic balance of internal waves, J. Phys. Oceanography, 11, 970-986.

Rastogi, P. K., and R. F. Woodman (1983), Vertical transport in the tropo-stratosphere by intermittent turbulence: A simulation study, Extended Abstracts, Sixth Symp. on Turbulence and Diffusion, March 22-25, 1983, Boston, Mass., AMS, Boston, Mass.

Smedman-Hogstrom, A.-S., and U. Hogstrom (1975), Spectral gap in surface-layer measurements, J. Atmos. Sci., 32, 340-350.

van der Hoven, I. (1957), Power spectrum of horizontal wind speed in the frequency range from 0.0007 to 900 cycle per hour, J. Meteorol., 14, 160-164.

VanZandt, T. E. (1982), A universal spectrum of buoyancy waves in the atmosphere, Geophys. Res. Lett., 9, 575-578.

Vinnichenko, N. K. (1970), The kinetic energy spectrum in the free atmosphere - 1 second to 5 years, Tellus, 12, 158-166.

Vinnichenko, N. K., and J. A. Dutton (1969), Empirical studies of atmospheric structure and spectra in the free atmosphere, Radio Sci., 4, 1115-1126.

Woodman, R. F., P. K. Rastogi, and T. Sato (1981), Evaluation of effective eddy diffusive coefficients using radar observations of turbulence in the stratosphere, Handbook for MAP, 2, S. K. Avery (ed.), University of Illinois, Urbana, Illinois.

# 4.3A EXISTENCE OF A PERSISTENT BACKGROUND OF TURBULENCE

T. E. VanZandt

Aeronomy Laboratory
National Oceanic and Atmospheric Administration
Boulder, Colorado 80303

Before the advent of VHF Doppler radars, it was generally believed, on the basis of direct measurements by balloons and aircraft and indirect measurements by incoherent radars, that turbulent layers in the free atmosphere have median thicknesses of at least 100 m. Since it was also believed that in the lower stratosphere only about 3% of the atmosphere is turbulent on the average (LILLY et al., 1974), then the mean separation between turbulent layers had to be at least 3 kilometers. If this were true, then a radar with 1-km range gates would detect an echo only about one third of the time and the fading of the echo strength would be very deep.

Instead, VHF Doppler radars with 1-km resolution usually detect echoes in every range gate up to the upper altitude of detectability. In the troposphere, echoes are detected in every range gate even with a resolution as small as 150 m. These results required that turbulence be much more uniformly distributed than had been thought. But since constraints on the total turbulent energy dissipation rate make it impossible for the entire volume of the lower atmosphere to be turbulent, the turbulence must be distributed among many, thin, relatively closely spaced layers. This distribution constitutes a persistent background of turbulence.

The principal mechanism for the generation of turbulence in the free atmosphere is thought to be shear instability in regions where the Richardson number Ri is less than 1/4. The existence of many thin turbulent layers then requires many thin regions of large shear. Such regions were suggested by vertical shear profiles from smoke trails (Figure 1) and high-vertical resolution balloon ascents during the 1960s. More recently, BARAT (1983) has used very high resolution balloon data to show that the turbulent layers do indeed occur in regions of large shear.

In order to interpret the early VHF Doppler radar measurements, VANZANDT et al. (1978) assumed that the total shear in the denominator of Ri is the sum of the steady background shear and a fluctuating mesoscale shear, which they described by a probability distribution. They then calculated the probability of occurrence of regions where $Ri \leq 1/4$. Such regions occur more frequently where the background shear is large or where the background stability ($N_B^2$, the numerator of Ri) is small. They assumed, lacking evidence to the contrary, that the probability distribution in the troposphere is the same everywhere, independent of altitude or location, and similarly in the stratosphere.

In their model the mean thickness of turbulent layers was taken to be 10 m. This value might be in error due to deficiencies in the model or errors in the absolute calibration of the radar. Nevertheless, 10 m was so much smaller than the then generally accepted median thickness, that it did strongly suggest that the previous estimated thicknesses were too large.

Later more direct measurements confirmed that the median turbulent layer thickness is considerably less than 100 m. WOODMAN (1980b), using a 2380-MHz radar at Arecibo, found that the thickness of the echoing (turbulent) layers was usually not much larger than the altitude resolution used, that is, with 150 m resolution, they were often 150 m thick, with 60 m resolution, they were 60-200 m thick, and with 30 m resolution, they were 30-60 m thick.

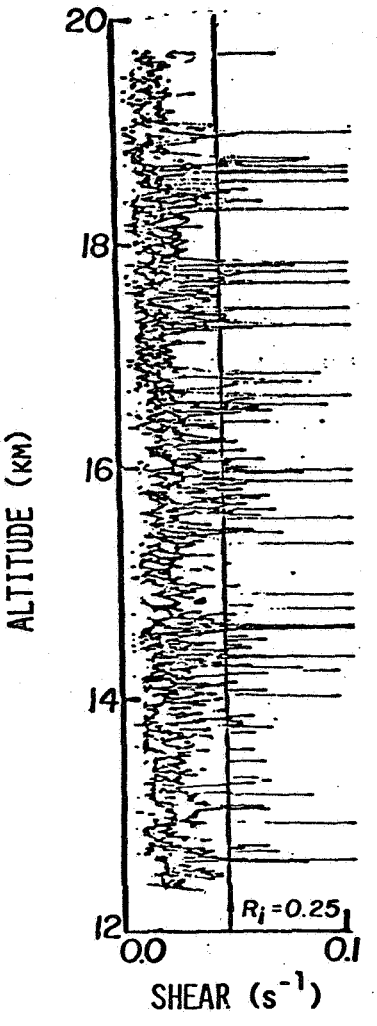


Figure 1. Superposition of eight vertical shear profiles from smoke trails with 25 m resolution. (Adapted from ROSENBERG and DEWAN, 1974.)

Indeed, when the earlier reports of direct measurements of turbulent layer thickness are examined, it is found that in almost every case the median or mean thickness reported is close to the resolution of the experiment. This suggests that the probability of occurrence of a turbulent layer of thickness in the range (L,dL) is a strongly decreasing function of L, at least for L larger than about 30 m.

In a very high resolution balloon experiment in the mid-stratosphere (27.5 to 29.5 km), BARAT (1982) found seven turbulent layers ranging in thickness from 3 to 240 m, with a median of 27 m and a mean of 56 m.

Although the VANZANDT et al. (1978) model provided a plausible scenario for the persistent background of turbulence it did not attempt any explanation for a persistent fluctuating distribution of mesoscale shears. Indeed, there was no generally accepted explanation for such shears.

Later VANZANDT (1982) showed that the mesoscale fluctuations of wind and temperature, hence of shear and stability, in the troposphere and lower stratosphere can be explained as the result of a spectrum of buoyancy (internal gravity) waves. The shape of this spectrum tends to be universal and, indeed, can be described by a slight modification of the GARRETT and MUNK (1972, 1975) model spectrum for oceanic internal gravity waves. There also appears to be a considerable degree of universality of the amplitude of this spectrum as a function of altitude, geographical location, etc., consistent with the assumption in the VANZANDT et al. (1978) model that the probability distribution of the shear fluctuations is invariant.

The universal shape of the oceanic internal waves spectrum is thought to be maintained by weakly nonlinear resonant wave interactions that cause a cascade of wave energy in frequency-wave-number space. The same process should operate in the atmosphere with some modifications. The scenario for energy flow is illustrated in Figure 2. Energy is put into the buoyancy wave field at vertical wave numbers smaller than $\beta_*$ (vertical wavelength $\geq 1/\beta_*$). The sources of buoyancy wave energy are not well understood. They include wave generation by shear instability, on the upper and lower sides of jet streams, for example, generation of waves by convective storms, extraction of energy from lee waves by wave interaction, etc. The order of magnitude of the rate of energy input is not known even for the sources that have been identified.

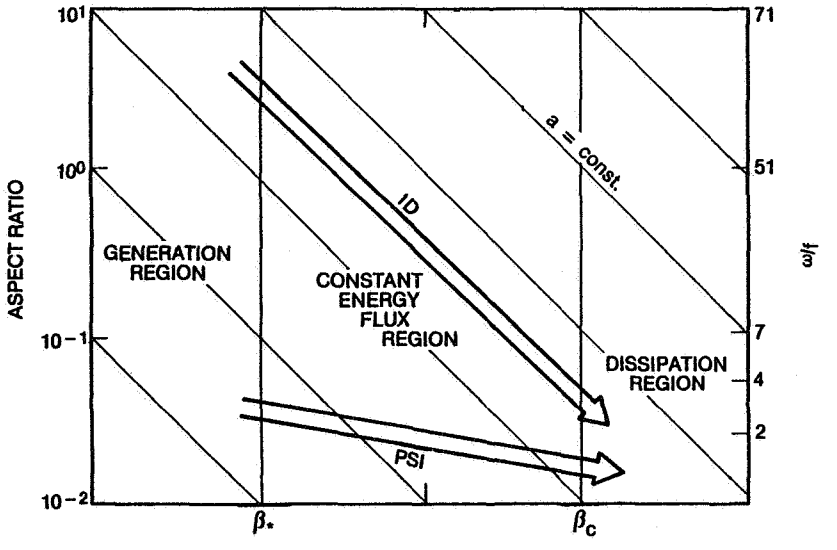


Figure 2. Schematic scenario for energy flow in the buoyancy wave field. *a* is the horizontal wave number. (Adapted from McCOMAS and MULLER, 1981.)

The energy is cascaded through the constant energy flux region by the wave interactions. McCOMAS and BRETHERTON (1977) showed that the dominant resonant wave interactions can be classified as "elastic scattering," which simply reverses the vertical phase velocity, and "induced diffusion" (ID) and "parametric subharmonic instability" (PSI), both of which move energy in frequency-wave-number space toward the inertial frequency, f = sin (latitude)/12 hr, and large vertical wave numbers (small wavelenghs). Since the variance of the shear versus log $\beta$ increases about as $\beta^{1/2}$, as the energy moves to smaller and smaller vertical wavelengths the occurrence of shear instability (Ri $\leq$ 1/4) becomes more and more common. The critical wave number $\beta_c$ is where the flux of energy by cascade from larger wave numbers can no longer keep up with the turbulent dissipation of wave energy. In the ocean $\beta_c \sim 1/10$ m (GARGETT et al., 1981); its value in the atmosphere is unknown, but the observed spectrum of horizontal wind versus $\beta$ does not show any breakdown to at least 20 m, the shortest scale observed (R. E. GOOD, private communication).

This scenario also automatically results in long-lived, pancake shaped patches (blini) of turbulence, consistent with observations (ROTTGER and SCHMIDT, 1979; WOODMAN et al., 1981; SATO and WOODMAN, 1982; BARAT, 1983). Since the frequency spectrum is red, the dominant contribution to the shear at any particular scale is likely to be made by low-frequency waves, which have nearly horizontal surfaces of constant phase and small vertical phase velocities. Thus, most turbulent patches will be long-lived pancakes that move slowly upward or downward, as in Figure 3.

According to this scenario, because the stability is greater in the stratosphere than in the troposphere, the rate of occurrence of turbulence should be

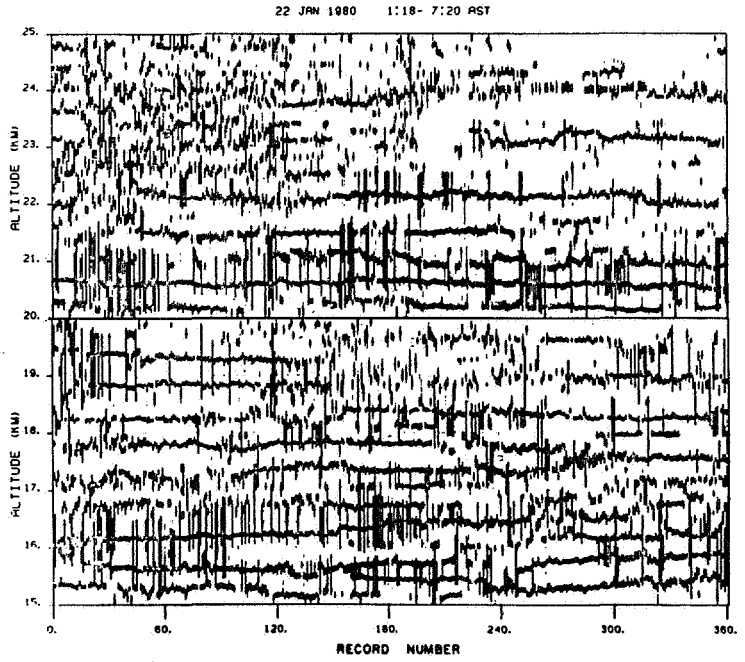


Figure 3. Locus of echo power maxima observed by the Arecibo 430-MHz radar with 150 m resolution. A turbulent layer is assumed to exist at every power maximum. (From WOODMAN et al., 1981).

less in the stratosphere. Also, the critical wavelength of $1/\beta_c$ will increase with increasing altitude due to the attenuation of buoyancy waves by the increaasing kinematic viscosity. This will result in fewer and fewer thin turbulent layers with increasing height. These predictions are qualitatively consistent with observations. With 150 m resolution, WOODMAN (1980) found that in the troposphere turbulence occurred in every range gate, but in the stratosphere above 16 km there were gaps. The thickness of these gaps increased with altitude, to about 1 km at about 24 km. The maximum height at which a turbulent echo was detected was 31 km. (At the greatest heights, the detectability of turbulence might have been strongly diminished by the approach of the inner scale of turbulence to the half-wavelength of the radar.) BARAT (1982) also found that turbulent layers are sparse in the middle stratosphere.

The foregoing constitutes a plausible scenario for the existence of a persistent background of turbulence. Other scenarios may be possible, but they have not been developed as far as this one has. The present scenario is generally accepted as the explanation for most, if not all, of the turbulence in the deep ocean (MUNK, 1981; GARGETT et al., 1981; DESAUBIES and SMITH, 1982). Nevertheless, many aspects of the scenario need to be quantified, not only in the ocean but even more so in the atmosphere. The MST radar technique can make crucial contributions to this study. It is the only existing technique that can be used to describe the morphology of occurrence of turbulence as a function of altitude, wind speed, shear, weather conditions, geographical location, etc. It is also the only technique that can describe the buoyancy wave spectrum versus frequency (BALSLEY and CARTER, 1982) and vertical wave number under a wide range of conditions. Such observations are essential to assess the degree of universality of the shape and amplitude of the buoyancy wave spectrum and the relation between the buoyancy wave spectrum and turbulence.

## REFERENCES


Balsley, B. B., and D. A. Carter (1982), The spectrum of atmospheric velocity fluctuations at 8 km and 86 km, Geophys. Res. Lett., 9, 465-468.

Barat, J. (1982), Initial results from the use of ionic anemmeters under stratospheric balloons: Application to the high-resolution analysis of stratospheric motions, J. Appl. Meteorol., 21, 1489-1496.

Barat, J. (1983), The fine structure of the stratospheric flow revealed by differential sounding, J. Geophys. Res., 88, 5219-5228.

Desaubies, Y., and W. K. Smith (1982), Statistics of Richardson number and of instability in oceanic internal waves, J. Phys. Ocean., 12, 1245-1259.

Gargett, A. E., P. J. Hendricks, T. B. Sanford, T. R. Osborn, and A. J. Williams III (1981), A composite spectrum of vertical shear in the upper ocean, J. Phys. Oceanography, 11, 1258-1271.

Garrett, C., and W. Munk (1972), Space-time scales of internal waves, Geophys. Fluid Dynamics, 2, 225-265.

Garrett, C., and W. Munk (1975), Space-time scales of internal waves: a progress report, J. Geophys. Res., 80, 291-297.

Lilly, D. K., D. E. Waco, and S. I. Adelfang (1974), Stratospheric mixing estimated from high-altitude turbulence measurements, J. Appl. Meteorol., 13, 488-493.

McComas, C. H., and F. P. Bretherton (1977), Resonant interaction of oceanic

internal waves, J. Geophys. Res., 82, 1397-1412.

McComas, C. H., and P. Muller (1981), The dynamic balance of internal waves, J. Phys. Oceanography, 11, 970-986.

Munk, W. (1981), Internal waves and small-scale processes, in Evolution of Physical Oceanography, ed. B. A. Warren and C. Wunsch, pp 264-291.

Rosenberg, N. W., and E. M. Dewan (1974), Stratospheric turbulence and vertical effective diffusion coefficients, Proc. Third Conf. on the Climatic Impact Assessment Program, ed. A. J. Broderick and T. M. Hard, Rep. No. DOT-TSC-OST-74-15, pp 91-101; or AFCRL-TR-75-0519 (29 Sept. 1975), Hanscom AFB, MA.

Rottger, J., and G. Schmidt (1979), High-resolution VHF radar sounding of the troposphere and stratosphere, IEEE Trans. Geosci. Electr., GE-17, 182-189.

Sato, T., and R. F. Woodman (1982), Fine altitude resolution observations of stratospheric turbulent layers by the Arecibo 430 MHz radar, J. Atmos. Sci., 39, 2546-2552.

VanZandt, T. E. (1982), A universal spectrum of buoyancy waves in the atmosphere, Geophys. Res. Lett., 9, 575-578.

VanZandt, T. E., J. L. Green, K. S. Gage and W. L. Clark (1978), Vertical profiles of refractivity turbulence structure constant: Comparison of observations by the Sunset Radar with a new theoretical model, Radio Sci., 13, 819-829.

Woodman, R. F. (1980a), High-altitude resolution stratospheric measurements with the Arecibo 430-MHz radar, Radio Sci., 15, 417-422.

Woodman, R. F. (1980b), High-altitude resolution stratospheric measurements with the Arecibo 2380-MHz radar, Radio Sci., 15 423-430.

Woodman, R. F., P. K. Rastogi, and T. Sato (1981), Evaluation of effective eddy diffusive coefficients using radar observations of turbulence in the stratosphere, in Handbook for MAP, 2, Extended abstracts from Intern. Symp. on Middle Dynamics and Transport, July 28-August 1, 1980, Urbana, Ill., ed. S. K. Avery.

# 4.4A DETERMINATION OF VERTICAL AND HORIZONTAL WAVELENGTHS OF GRAVITY WAVES

J. Rottger

EISCAT Scientific Association
P.O. Box 705
S-98127 Kiruna, Sweden

The determination of horizontal and vertical wavelengths of gravity waves obviously relies on measurements of wave parameters in horizontal and vertical directions, if one does not want to use the dispersion relation for model calculations. A very suitable parameter, measured fairly easily with MST radars, is the fluid velocity.

Average velocities and superimposed turbulent fluctuations are much larger in the horizontal than in the vertical direction. Vertical and horizontal fluid velocities due to wave-like events are mostly about equal in magnitude. Vertical fluid velocities due to waves therefore can be more reliably detected than horizontal velocities. This is confirmed by MST radar observations.

Other parameters, measured by MST radars, also give information about wave parameters. The radar reflectivity for instance can be modulated, viz. by the turbulence intensity or the undulation of reflecting surfaces. This indirectly could be used to determine spatial and temporal scales. However, from experience, the vertical fluid velocity appears to be most suitable.

To investigate wave events, we at least have to detect a full period of a wave, but longer wave trains of course would be much more suitable. For most reliable estimates the wave event should be fairly monochromatic and stationary. It may be possible to filter different waves from a continuous spectrum if these are separated widely enough in frequency and have amplitudes significantly different from the amplitudes of background turbulence. Only these conditions will allow to deduce acceptable estimates of vertical and horizontal wavelengths.

The vertical velocity w due to gravity wave is proportional to

$$\exp[i(k_x x+k_y y+k_z z-wt)],$$

where $k_x = \frac{2\pi}{\lambda_x}$, $k_y = \frac{2\pi}{\lambda_y}$, $k_z = \frac{2\pi}{\lambda_z}$

and x, y, z denote a proper coordinate system (e.g., east, north, vertical), t is the time, and $w = \frac{2\pi}{T}$, where T is the period of the wave. We have to take into account that the radar measurements of w are in a fixed frame of reference and actually $w_o = w - \underline{k}\cdot\underline{U}o$ is Doppler shifted, if a background wind $\underline{U}o$ is observed. Thus, also the deduced wavelengths $\lambda_x, \lambda_y$ and $\lambda_z$ are given in this fixed reference frame and have to be converted if one would know $\underline{k} = (k_x, k_y, k_z)$ and $\underline{U}o$.

Keeping x, y and z constant (i.e., measuring in a fixed portion) allows determination of $\omega$. If a significant amplitude of w is detected at frequency $\omega$, measuring the phase of its oscillation as function of x, y and z allows determination of $\lambda_x$, $\lambda_y$ and $\lambda_z$. This schematically is depicted in Figure 1. Assume a wave in the x-z plane and pointing the antenna beams to two directions; this yields radial velocities $w_I$ and $w_{II}$ being caused by vertical fluid velocities of the wave and a background wind Uo. Assuming that the background wind is the

same at both beam positions, and neglecting horizontal fluid velocities (this is permitted as long as the beam directions are close to the zenith), the vertical fluid velocities can directly be deduced from the measurements. Swinging the beam can most appropriately be done with the interferometer technique, described in another workshop paper. Of course it also can be done by the traditional method pointing transmitter beams at different directions and receiving with the same beam direction. Briefly speaking, complex data are taken at 3 antennas (only 2 are shown in Figure 1 for clearness) and phase shifts $\Delta\gamma$ are introduced during the data analysis to swing the receiver antenna beam. Complex addition of the 3 data sets yields the velocities according to the different antenna beam directions.

An example of such an experiment is shown in Figure 2, where the interferometer beam was pointed at 1.2° zenith angle to an azimuth 207° (closed circles and 27° (open circles). This corresponds to an average horizontal probing distance of 800 m at 20 km altitude. It is very evident that the oscillations of the vertical velocity w are displaced in phase at the two positions. This indicates that a horizontally propagating wave was observed. Making use of three beam positions, one can calculate the horizontal wave vector $k_h = (k_x, k_y)$ and find the horizontal wavelength $\lambda_h$. This was done by applying a cross spectrum analysis, which of course also yields the mean amplitude of the vertical velocity $\overline{w}$ and the mean period $\overline{T}$ of the wave. Results are shown in Figure 3. In this diagram additionally the horizontal width b of the volume probed with the applied beam widths is indicated. Since b is much smaller than the horizontal wavelength $\lambda_h$, there are no objections that this method of beam swinging is applicable. It also proves that obviously phase velocities of gravity waves cannot be measured with fixed vertical beams as often was used as an argument against the spaced antenna drifts method.

Knowing $k_h$ from these measurements, one can find the horizontal phase velocity $V_p$ and the propagation direction $\alpha_v$ of the wave. These are shown in Figure 4, where additionally the average background wind speed Uo and its direction $\alpha_u$, measured with the same interferometer set-up are inserted. It shall be mentioned that Uo and $\alpha_u$ are in agreement with radiosonde data. When investigating further wave parameters one can make use of the measured wind speed and direction as well as the measured frequency and propagation vector of the gravity wave to correct for the Doppler shift.

From the phase shift of the vertical velocity oscillations with height, the vertical wavelength can be deduced. Since we observed coherent wave events only over a few kilometers height range and the phase differences are not too pronounced, the measurement of the vertical wavelength is not so consistent. Firstly, the vertical wavelength may change with altitude, secondly the mean frequency of the wave changes with altitude and we always observed much less than one cycle of the wave in the vertical direction. Anyhow, by filtering the different spectral amplitudes, one could deduce an average phase shift with height as is shown in Figure 5 for a shorter observation period than in Figures 3 and 4. From the average phase shift of the dominating component at 4.6 min, one can find a mean vertical wavelength of about 15 km. This value has to be taken with care because of the indication of non-coherency of these wave events.

In summary we find from the analyses of these wave events between 15 km and 25 km altitude that

1) horizontal wavelengths are about 10-20 km, and increasing with height,
2) vertical wavelengths are fairly similar to horizontal wavelengths,
3) wave periods increase with altitude from about 250 s to 300 s,
4) mean vertical velocity amplitude increases with height from about 8 cm $s^{-1}$ to 10 cm $s^{-1}$,
5) direction of wave propagation is almost constant with altitude,

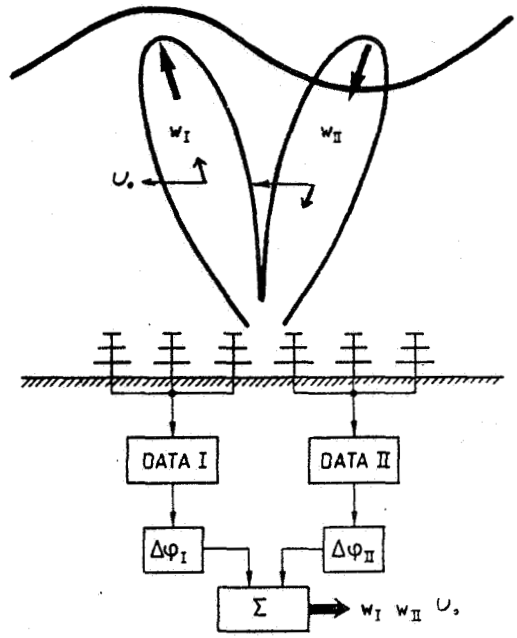


Figure 1. Principle of an MST radar interferometer. Complex data are taken independently with at least 2 antenna sets, introducing a phase shift allows swinging the antenna beam to observe the horizontal velocity Uo and vertical velocities w at different positions of a gravity wave.

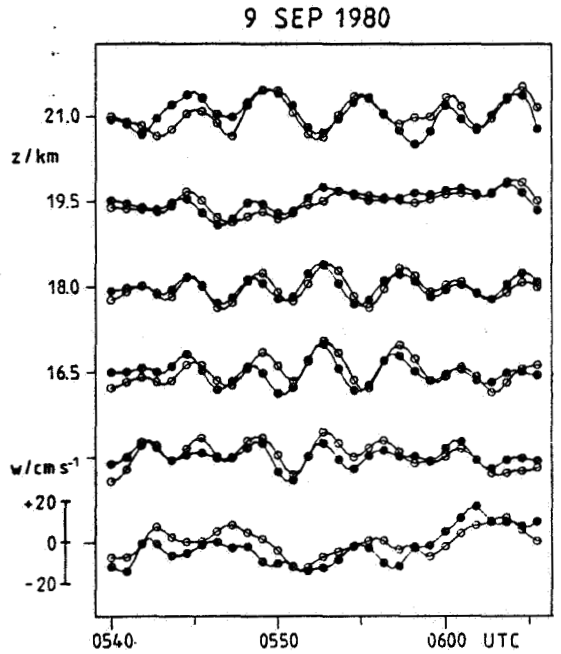


Figure 2. Vertical velocities w, measured at zenith angles of $\pm$ 1.2°.

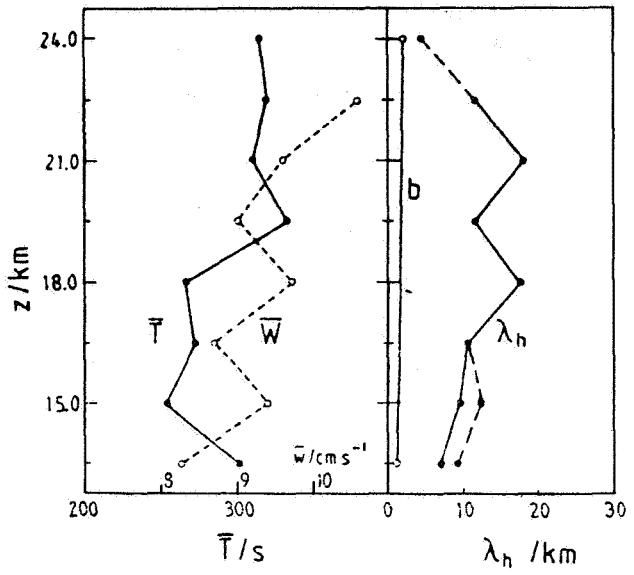


Figure 3. Average period $\overline{T}$, average vertical velocity amplitude $\overline{w}$, and horizontal wavelength $\lambda_h$. Averaging was done over the period range 3.5-7.5 min, with the amplitude as weighting function. Observation period is 0446-0616 UTC, on 9 September 1980.

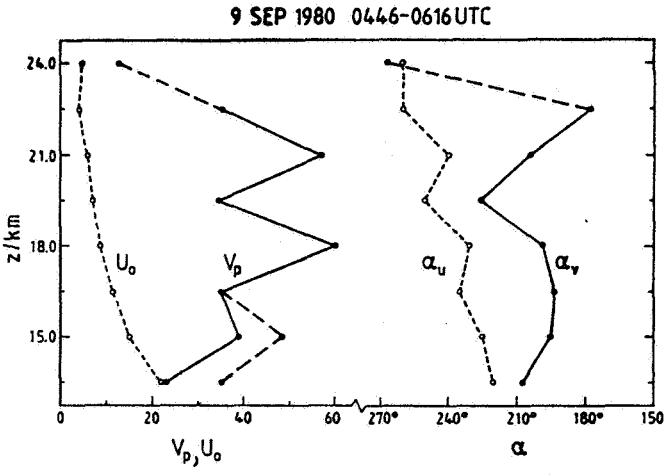


Figure 4. Height profiles of wave's phase velocity $v_p$ and propagation direction $\alpha_v$ as well as background wind speed Uo and direction $\alpha_u$.

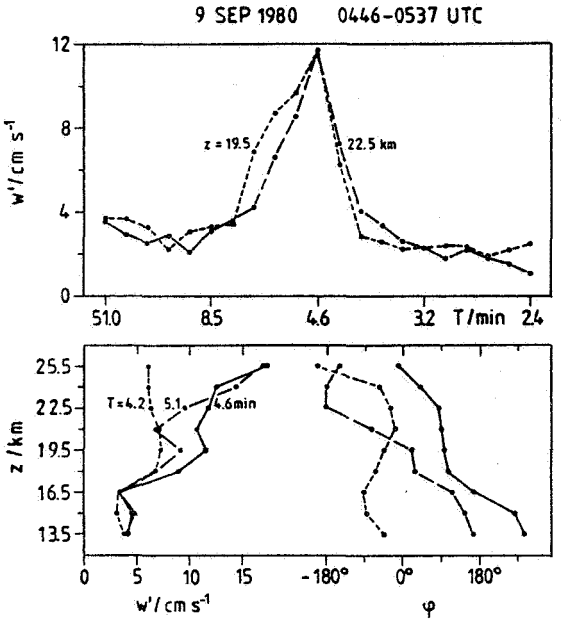


Figure 5. Spectra of vertical fluid velocity $w^1$, measured at 19.5 km and 22.5 km altitude (upper diagram). Height profile of vertical velocity amplitude and phase of oscillations at T = 4.2, 4.6 and 5.1 min.

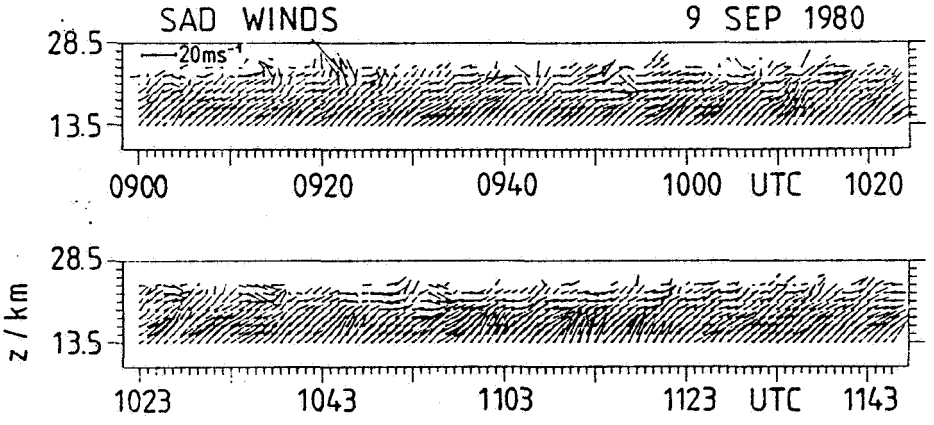


Figure 6. Vector field of lower stratospheric winds measured with the spaced antenna drifts method.

6) phase speed of waves ($\approx$40 $ms^{-1}$) is almost constant with altitude,
7) phase speed and direction are similar to wind speed and direction close to the lowest heights observed ($\approx$ 13.5 km),
8) wave phases propagate downward,
9) from 7) and 8) it is deduced that these waves are probably generated at wind shear regions close to 13.5 km.

Horizontal fluid velocities occasionally also could be used to detect gravity waves, as is for instance shown in Figure 6. The wind arrows in the lower altitudes obviously indicate some oscillation in direction at periods of 4-8 minutes (e.g., around 1000 UTC and 1115 UTC) which can be explained by atmospheric gravity waves. These measurements would have been fairly difficult with the Doppler method which always measures a superposition of vertical and horizontal velocities. These cannot easily be separated for wave events since the beam would point to different phase locations of the wave.

Waves with shorter vertical wavelength, such as mountain lee waves may have a substantial variation of the horizontal velocity which then could be used to determine the wavelength. In Figure 7 an example of wind speed and direction measured during a lee wave event is presented (from ROTTGER et al., 1981). One clearly summarizes an oscillating pattern with altitude which also was observed in the vertical velocity. Lee waves are standing waves and stationary as long as the background wind does not change. As the background wind increases with height, also the vertical wavelength does. To find a relation of the wavelength and the background wind, a polar plot as shown in Figure 8, may be useful to measure the vertical wavelength (e.g., by determining the height difference between the crossovers of the velocity phasor), one also can easily obtain the sense of rotation of the wave vector with height from this polar plot. Analyses of vertical wavelengths of tides are done in a similar way.

In summary we recognize that a single MST radar can contribute substantially to investigations of many parameters of atmospheric gravity waves by applying the interferometer technique or the traditional beam steering technique. Investigations of long period gravity waves may need multistatic systems, but just one radar can be used to determine some essential parameters of standing waves, such as lee waves.

## REFERENCE

Rottger, J., T. Y. Kang, and M. Y. Zi (1981), Mountain lee waves in radar wind profiles, MPAe-Report, W-00-81-36.

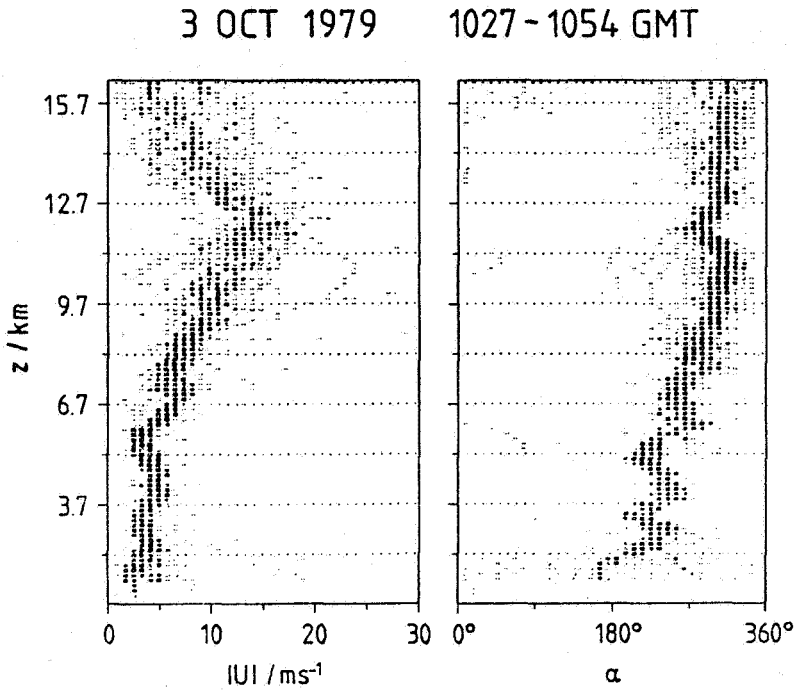


Figure 7. Height profiles of speed /U/ and direction α of the horizontal wind measured during a lee wave event over the Harz mountains.

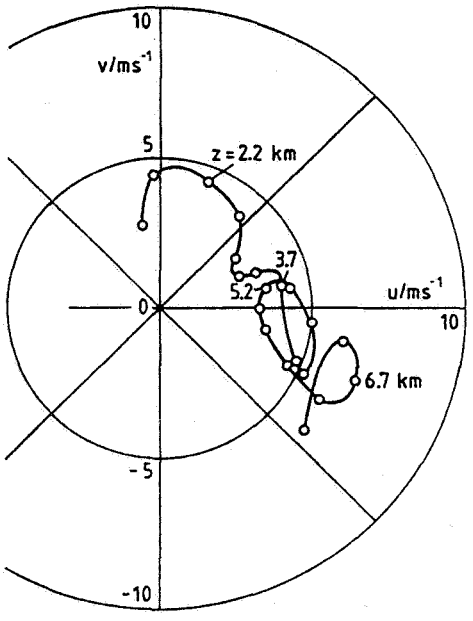


Figure 8. Polar plot of horizontal wind velocity measured during a lee wave event. The open circles denote height increments of 300 m.

# 4.4B TECHNIQUES FOR STUDYING GRAVITY WAVES AND TURBULENCE: VERTICAL WIND SPEED POWER SPECTRA FROM THE TROPOSPHERE AND STRATOSPHERE OBTAINED UNDER LIGHT WIND CONDITIONS

W. L. Ecklund, B. B. Balsley, M. Crochet*, D. A. Carter,
A. C. Riddle and R. Garello

Aeronomy Laboratory, National Oceanic and Atmospheric Administration,
Boulder, CO 80303

*L.S.E.E.T., "La Gippone" Boulevard des Amaris, Toulon 83100, France

In April and May 1982 a joint France/U.S. experiment was conducted near the mouth of the Rhone river in southern France as part of the ALPEX program. This experiment used 3 vertically directed 50 MHz radars separated by 4 to 6 km. The main purpose of this experiment was to study the spatial characteristics of gravity waves. The good height resolution (750 meters) and time resolution (1 minute) and the continuous operation over many weeks have also allowed us to obtain high resolution vertical wind speed power spectra under a variety of synoptic conditions. The complete set is being prepared for journal publication. It is our purpose here to present vertical spectra obtained during very quiet (low wind) conditions in the troposphere and lower stratosphere from a single site. The spectra shown in Figure 1 were obtained by averaging spectra from 4 heights in the troposphere for 12, 13 and 14 May (solid line) and from 4 heights in the lower stratosphere for 17 and 18 April (dashed line). The arrow near the peak of each spectrum indicates the average Brunt-Vaisala period calculated from the nearby Nimes sounding balloon data. In our experience, spectra like those shown in Figure 1 are typically not observed; this may be due to the apparent requirement that background winds be unusually low. For example, during the 2-month observing period in France, spectra such as those shown in Figure 1 were only observed on 5 or 6 days.

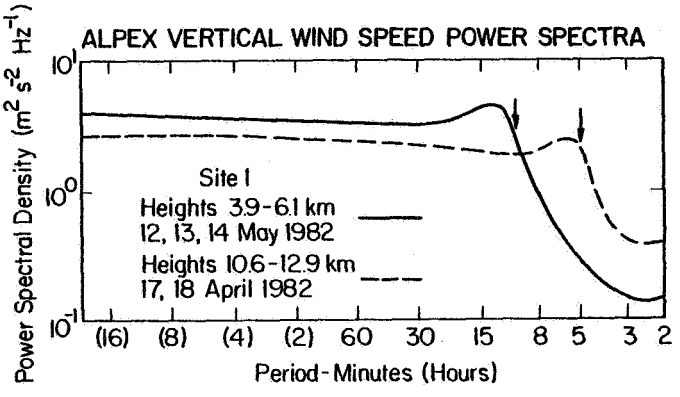


Figure 1.

# 4.4C MEASUREMENT OF THE HORIZONTAL VELOCITY OF WIND PERTURBATIONS IN THE MIDDLE ATMOSPHERE BY SPACED MF RADAR SYSTEMS

C. E. Meek, A. H. Manson and M. J. Smith

Institute of Space and Atmospheric Studies
University of Saskatchewan
Saskatoon, Canada

## ABSTRACT

Two remote receiving sites have been set up at a distance of $\sim$ 40 km from the main MF radar system. This allows measurement of upper atmosphere winds from 60-120 km (3 km resolution) at the corners of an approximately equilateral triangle of side $\sim$ 20 km. Some preliminary data are compared through cross correlation and cross spectral analysis in an attempt to determine the horizontal velocity of wind perturbations and/or the horizontal wavelength and phase velocity of gravity waves.

## INTRODUCTION

The three sites are illustrated in Figure 1. Figure 2 describes the equipment at each of the remote receiving sites. The remote data are similar to those of the main site (e.g., GREGORY et al., 1982) except for a higher noise level due to smaller receiving antennas (single dipoles) and the proximity of overhead power lines. Examples of data from the three sites are shown in Figure 3 (the scale vectors indicate 50 m/s). The important limitations of the system are the transmitter antenna beam width (nominally $\sim$ 150 km at a height of 100 km, but the effective area depends on the scattering process), the time resolution of the wind measurement (5 min, at present) and the site spacing. The latter two parameters mean that periods < 10 min and wavelengths $\lesssim$ 50 km are folded back to higher values, although the wide Tx beamwidth will probably reduce the effect of wavelength folding.

Two possibilities which must be considered are that (1) the perturbations are all travelling in the same direction with the same speed, in which case cross correlations between wind vectors at the three sites are sufficient to determine velocity, and (2) the perturbations are caused by independent gravity waves with different speeds and directions; here cross spectral analysis is required to separate out the different waves.

In case (1), the maximum measurable speed is determined by the minimum measurable time delay. For reasonable accuracy, given well-behaved cross correlations, the lowest delay should be greater than half a lag from zero lag (2.5 min). This puts an upper limit of $\sim$ 120 m/s on speed. In case (2), the absolute phase differences between sites must all be less than 90° so that the direction of travel may be deduced (although this is still not a unique solution). This puts a lower limit on the wavelength of $\sim$ 100 km. In addition, there must be some way of confirming the presence of the "same wave" at all sites, otherwise the phase differences will be spurious.

## FIRST RESULTS

Figures 4 and 5 show cross correlation and spectral analyses for the one day available, over the height range $\sim$ 100-112 km. The data have been detrended for the correlation analysis. The autocorrelation phase shows a dominant period of $\sim$ 1 hr. The cross correlation does not show single clear peaks, however it appears that the P-D and D-W peaks are at positive lag (+5 to +10 min) and the W-P peak is at negative lag ($\sim$-5 min).

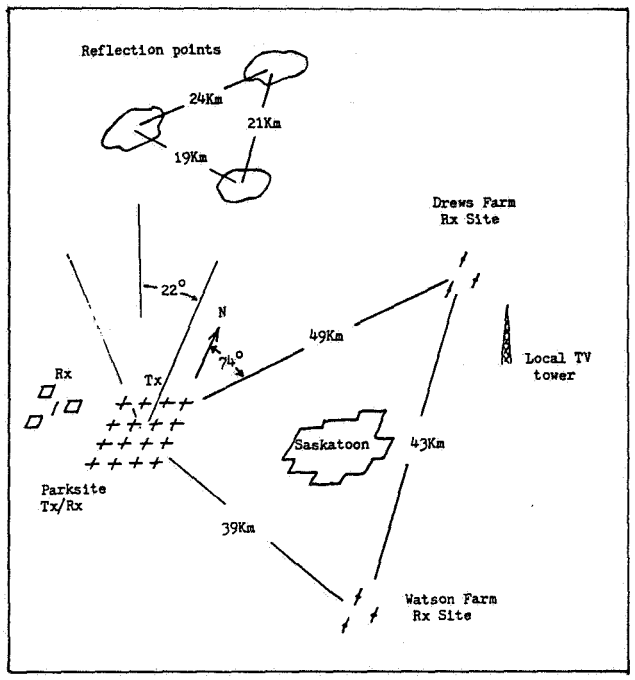


Figure 1. Geometry of spaced radio sites.

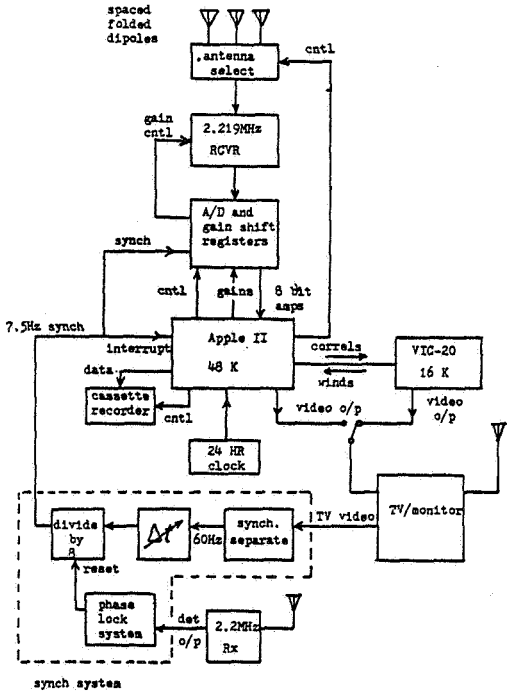


Figure 2. Block diagram of remote receiving/analysis/ recording system.

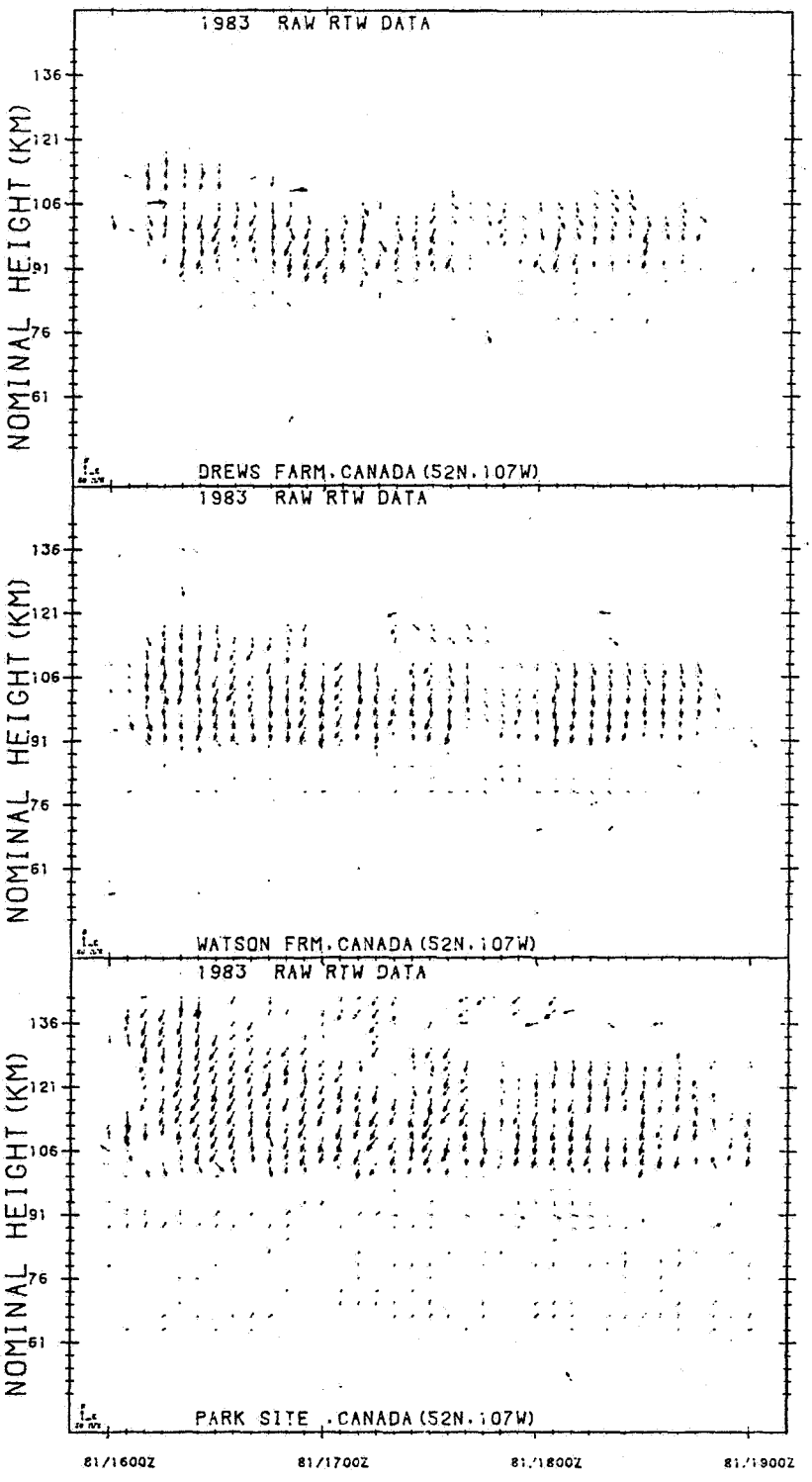


Figure 3. Sample wind vectors from the three sites. Note that Drews' and Watson's height labels are ∿12 km low.

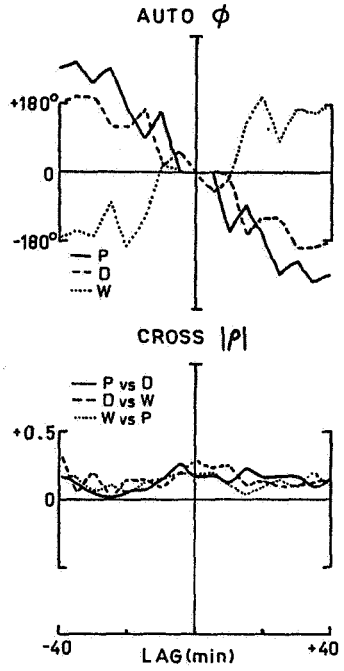


Figure 4. Cross correlation analysis between spaced wind vectors over a 4-hr period (1982 Mar 21, 1600-1955 GMT).

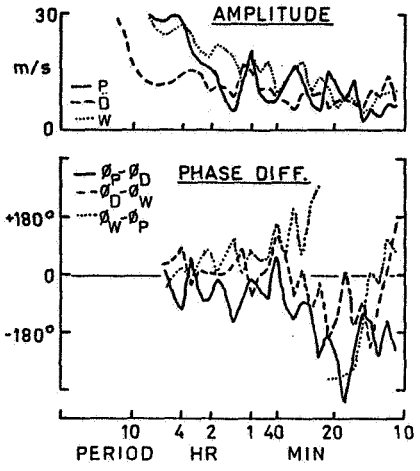


Figure 5. Cross spectral analysis between spaced wind vectors. Note that the frequency ("period") scale is linear in $f^3$ (not f, as is usual) and extends from 0 to the Nyquist frequency (10 min period).

The spectral analysis (Figure 5) is more illuminating. The spectra have been calculated by separate harmonic analysis (least squares) at each frequency, and the frequency scale distorted to give more resolution at the longer periods. The peak at ∿ 1 hr period is clear, and the slopes of the phase differences (which define time delay) are also fairly clear. They indicate delays of ∿ 10 min (P→D), 1 min (D→W), and 10 min (P→W) . This gives a rough velocity estimate of 30 m/s, 100° east of north. Apparently, on the average all frequency components have the same delay between sites. The phase differences show large fluctuations, however, which means that wavelength and velocity calculations for a single period would be almost random. One way around this is to select significant periods on the basis of coherence from an average cross spectrum over height or frequency. This will be done in the future when longer data sequences are available.

## CONCLUSIONS

Preliminary spaced wind observations have been analysed to determine the velocity of wind perturbations. There is some indication that all frequency components have a common speed and direction. Since there is only one day of simultaneous data available at the time of writing, general conclusions are impossible.

## REFERENCE

Gregory, J. B., C. E. Meek and A. H. Manson (1982), J. Atmos. Terr. Phys., 44, 649.

# 4.4D EVIDENCE FOR PARALLEL ELONGATED STRUCTURES IN THE MESOSPHERE

G. W. Adams*, J. W. Brosnahan** and D. C. Walden***

*Center for Atmospheric and Space Sciences, Utah State University, Logan, UT 84322
**Tycho Technology, Inc., P. O. Box 1716, Boulder, CO 80306
***Space Environment Laboratory, NOAA/ERL, Boulder, CO 80302

## ABSTRACT

The physical cause of "partial reflection" from the mesosphere has been sought for some time. We present data from an image-forming radar at Brighton, Colorado, that suggest that some of the radar scattering is caused by parallel elongated structures lying almost directly overhead. Possible physical sources for such structures include gravity waves and roll vortices.

## INTRODUCTION

Radar soundings of the mesosphere have indicated anisotropic scattering since the initial work of GARDNER and PAWSEY (1953) and GREGORY (1961). Signals scattered from this region are often characterized by well-defined amplitude fading, or pulsation, patterns, with quasi-periods of one to some tens of seconds, and by scattering that is stable in altitude for minutes to days. A number of models have been proposed to explain the "partial reflection" results: (GARDNER and PAWSEY, 1953; HINES, 1960; GREGORY, 1961; BELROSE and BURKE, 1964; PIGGOTT and THRANE, 1966; FLOOD; 1968; AUSTIN et al., 1969; AUSTIN and MANSON, 1969; GREGORY and MANSON, 1969; MANSON et al., 1969; VON BIEL, 1971; BEER, 1972; COHEN and FERRARO, 1973; MANSON et al., 1973; MATHEWS et al., 1973; NEWMAN and FERRARO, 1973; TANENBAUM et al., 1973; HARPER and WOODMAN, 1977; SCHLEGEL et al., 1978; HOCKING, 1979; JONES and GRUBB, 1980; SCHLEGEL et al., 1980; and JONES et al., 1982).

We report here on mesospheric measurements made with an imaging radar at Brighton, Colorado, that indicate occasional large differences in returns on two orthogonal linear polarizations. Echo location indicates that these returns come from within 2.5 degrees of zenith. We present first a description of the experiment and of the resulting data. Our interpretation of the data in terms of parallel elongated structures is then given, followed by speculation about the possible physical cause of the inferred structures.

## EXPERIMENTAL CONFIGURATION

The data reported here were obtained with the NOAA/NSF HF Radar (GRUBB, 1979) and the Middle-Atmosphere Image-Forming Radar (MAIFR) which are located near Brighton, Colorado. The HF radar is a flexible dual-Doppler radar, used in the work described here to drive the large 2.66-MHz MAIFR antenna array, and to sample the ten antennas that comprise the array sequentially in pairs. Each of the ten antennas consists of a coaxial-collinear (BALSLEY and ECKLUND, 1972) string of eight half-wave dipoles as shown in Figure 1, fed at the center. The pattern of a single antenna is fan-shaped, being 16 degrees wide in the direction parallel to the antenna, and 100 degrees wide in the transverse direction (Figure 2). Five of the antennas are parallel to each other and to the north-south axis; the other five are parallel and east-west. Dipole-to-dipole spacing along an antenna is $0.33\lambda$; antennas are spaced $0.707\lambda$ apart. Pulses of length 4.5 km (30 $\mu$sec) were transmitted at 50 pulses/sec, with 50 kW peak-pulse-power at the antenna terminals. For transmission, we used either the center antenna of each linear array, giving a crossed-fan-shaped beam, or all ten antennas, giving an approximately circular beam about 16 degrees wide. In both configurations, the two polarizations were fed together and in phase. For reception, a

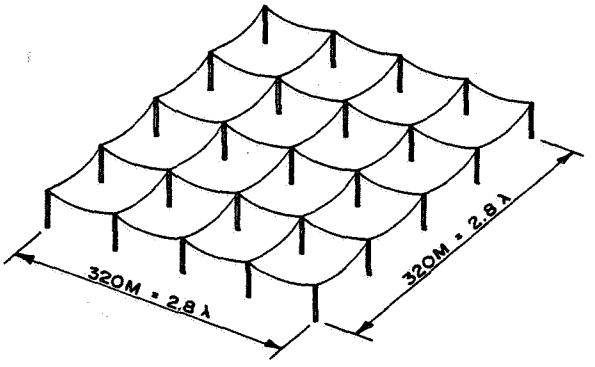


Figure 1. Middle-atmosphere image-forming radar antenna. Location: Boot Lake (Brighton) Colorado, Area: 25.6 acres = $10^5$ $m^2$, height: 0.15 λ, frequency: 2.66 MHz, λ: 112 m.

four-pulse average was used on each antenna, so that one complete data set was obtained every 0.4 seconds.

DATA

Figure 3 shows log amplitude vs. altitude plot for one of the east-west antennas (top), one of the north-south antennas (center), and a composite of the two plots (bottom). The feature of interest here is the well-defined layer around 70 km, which is much more noticeable on the east-west antenna than on the north-south. (This figure was taken with a camera directly from the HF radar's on-line graphics display, and relabeled. This display shows the six most recent soundings for a single antenna, which corresponds to a time spread of 2.4 seconds in this experiment.)

Figure 4 is a time history of the linear voltage amplitude at 70 km for the same pair or antennas as in Figure 3. Notice that the north-south antenna shows a smaller but quite distinct signal which is often correlated, but sometimes anticorrelated, with the voltage on the east-west antenna. Notice also the characteristic fading pattern and deep nulls.

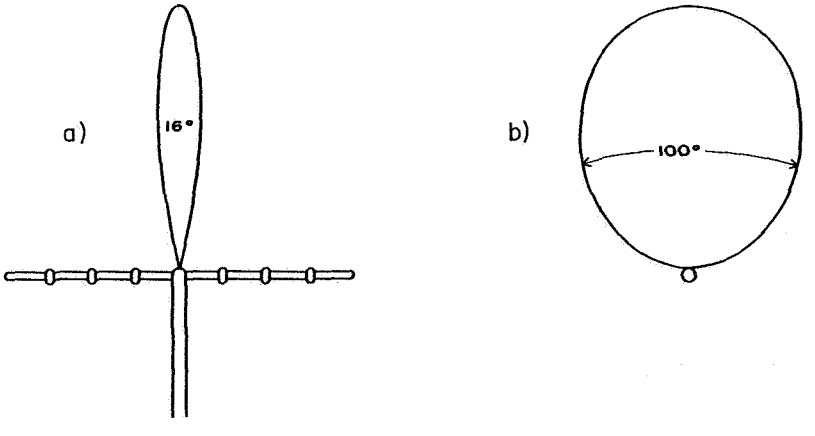


Figure 2. Single antenna (a) longitudinal view, (b) transverse view.

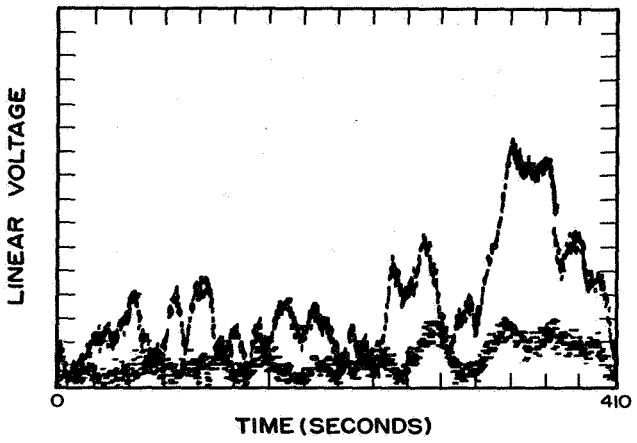


Figure 4.

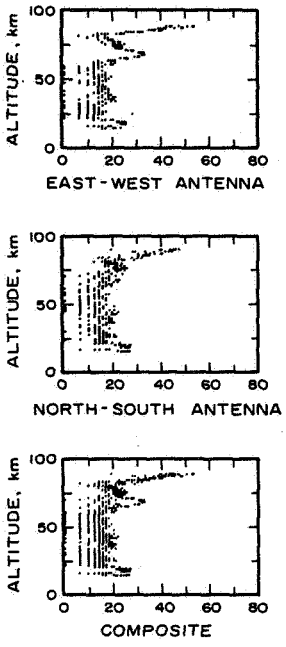


Figure 3.

Figure 5 shows the corresponding phase histories of four of the east-west antennas. Unfortunately, the northernmost antenna was not operative at this time, so we show data from the #1 (southernmost) through #4 (next-to-northernmost) antennas. While there are some differences in detail among the four plots, the largest significant differences across the array are less than 30 degrees. The antenna spacing is 0.707λ, so a maximum 30-degree phase difference between #1 and #4 corresponds to a location within 2.5 degrees of zenith in the north-south meridian. The north-south antennas have phase histories (not shown) that also indicate a location within 2.5 degrees of zenith in the east-west meridian. The main transmit beam is 16 degrees wide, so the indicated centroid

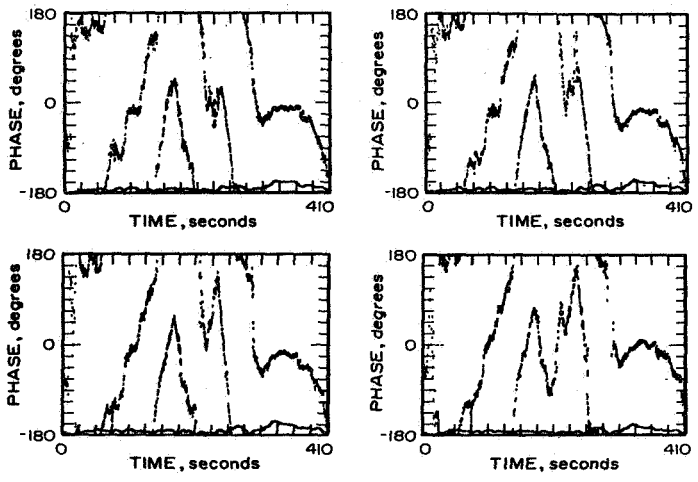


Figure 5.

of the scatterer is well within the main beam. Notice that there is less than 90 degrees net phase difference across the almost 7-minute phase history of the first three antennas. However, there is a 180-degree phase discontinuity, indicative of interference among multiple targets, at t = 200 seconds. The fourth antenna recovers from this discontinuity oppositely from the other three, indicating that the "perfect" discontinuity lay between the third and fourth antennas.

These measurements were made using a narrow transmit beam (all ten antennas). Measurements at other times using a much wider beam gave results not noticeably different from these.

## DISCUSSION

The first suspicion, of course, is that the observed differences between the two polarizations were caused by sidelobe activity. The echo-location results in Figure 5, however, show that the radar returns come from very nearly overhead.

Since the individual antenna beams are fan-shaped, it would be possible for a large elongated structure (20 x 170 km, say) to fill one antenna beam while only intersecting the orthogonal beam. Indeed, we have recently found a high correlation between the occurrence of infrared structures of similar dimensions and increased radar scattering, particularly around 85 km (PETERSON and ADAMS, 1983; ADAMS et al., 1983). However, such large structures seem unlikely to explain the results presented here for two reasons. First, the first Fresnel zone is 4 km in diameter at 70 km, so a continuous scatterer much larger than this would not return much more power. Second, our measurements made at other times with alternating wide and narrow transmit beams also indicate that there is no substantial off-vertical scattering. (There is no requirement that the observed radar scattering correspond in scale to the observed infrared structures, of course. The radar scattering may be specular, caused by the overhead gradient maxima of some very large structure.)

The voltages shown in Figure 4 indicate power ratios of as high as 20 to 1. If we suppose that the scattering results from the presence of a simple elongated structure, and that the structure lies within the first Fresnel zone, then maximum dimensions of 4 km x 200 meters are indicated. Notice, however, that if the transverse dimension is less than the radar's half-wavelength of 56 meters, then the transverse cross section will be much smaller than dimensional scaling would indicate. A single elongated structure, however, would not explain the fading pattern and deep nulls seen in Figure 4. Multiple structures might. Such deep fading is frequently accompanied by 180-degree phase discontinuities such as the one at t = 200 seconds discussed above. Deep fading and phase discontinuities are symptomatic of multitarget interference patterns. KELLEHER (1966) reported frequent quasi-periodicities in the spatial structure of the ground diffraction pattern of radar pulses. MARKER (1981) has directly observed groups of parallel rolls in the troposphere. Optical observations (PETERSON and ADAMS, 1983, and references therein) typically show several parallel bands. Such a model seems to have potential for explaining our observations.

## SUMMARY AND CONCLUSIONS

We have shown data indicating that returns on two orthogonal polarizations can differ by a factor of 20, while simultaneous echo-location measurements locate the scatterer to within 2.5 degrees of zenith. Deep fading and 180-degree pnase discontinuities are seen. These data can be explained by parallel elongated structures.

Either gravity waves or roll vortices are possible sources for parallel elongated structures. The polarization-dependent returns, when they are present, tend to be stationary in altitude for many minutes, so we would suggest that either horizontal waves or long columnar rolls, probably generated by passing gravity waves or local wind shears, are the most likely cause. Since such waves or rolls would manifest themselves in the manner presented here only when they were in alignment with one of the polarizations (we see both east-west and north-south domination at different times), our casual observation that such phenomena are present about 10% of the time would indicate that such scatterers are actually present most of the time.

ACKNOWLEDGEMENTS

We appreciate the considerable effort made by John W. Neuschaefer. This material is based upon work supported by the National Science Foundation under Grant No. ATM-8117275.

REFERENCES

Adams, G. W., A. W. Peterson, J. W. Brosnahan, J. W. Neuschaefer and D. C. Walden (1983), Mesospheric structures observed simultaneously with 2.6-MHz radar and infrared photography, submitted to J. Atmos. Terr. Phys.

Austin, G. L., R. G. T. Bennett and M. R. Thorpe (1969), The phase of waves partially reflected from the lower ionosphere (70-120 km), J. Atmos. Terr. Phys., 31, 1099-1106.

Austin, G. L. and A. H. Manson (1969), On the nature of the irregularities that produce partial reflections of radio waves from the lower ionosphere (70-100 km), Radio Sci., 14, 35-40.

Balsley, B. B. and W. L. Ecklund (1972), A portable coaxial collinear antenna, IEEE Trans. Ant. Prop. AP-20, 513-516.

Beer, T. (1972), D-region parameters from the extraordinary component of partial reflections, Ann. Geophys. 28, 341-347.

Belrose, J. S. and M. J. Burke (1964), Study of the lower ionosphere using partial reflection, J. Geophys. Res. 69, 2799-2818.

Cohen, D. J. and A. J. Ferraro (1973), Modeling the D-region partial reflection experiment, Radio Sci., 8, 459-465.

Flood, W. A. (1968), Revised theory for partial reflection D-region measurements, J. Geophys. Res., 73, 5585-5598.

Gardner, F. F. and J. L. Pawsey (1953), Study of the ionospheric D-region using partial reflections, J. Atmos. Terr. Phys., 3, 321-344.

Gregory, J. B. (1961), Radio wave reflections from the mesosphere, J. Geophys. Res., 66, 429-445.

Grubb, R. N. (1979), The NOAA SEL HF radar system (ionospheric sounder), NOAA Tech. Memo. No. ERL SEL-55.

Harper, R. M. and R. F. Woodman (1977), Preliminary multiheight radar observations of waves and winds in the mesosphere over Jicamarca, J. Atmos. Terr. Phys., 39, 959-963.

Hines, C. O. (1960), Internal atmospheric gravity waves at ionospheric heights,

Can. J. Phys., 38, 1441-1481.

Hocking, W. K. (1979), Angular and temporal characteristics of partial reflections from the D-region of the ionosphere, J. Geophys. Res., 84, 845-851.

Jones, R. M., G. W. Adams and D. C. Walden (1982), Preliminary ionospheric partial reflection measurements at Brighton, Colorado, on 9 January 1981, NOAA Tech. Mem #ERL SEL-60.

Jones, R. M. and R. N. Grubb (1980), D-region partial reflection Doppler measurements with the NOAA/MPI digital HF radar, Max-Planck Institut fur Aeronomie, Report No. MPAE-W-02-80-20.

Kelleher, R. F. (1966), Some statistical properties of the ground diffraction patterns of vertically reflected radio waves, J. Atmos. Terr. Phys., 28, 213-223.

Manson, A. H., J. B. Gregory and D. G. Stephenson (1973), Winds and wave motions (70-100 km) as measured by a partial reflection radiowave system, J. Atmos. Terr. Phys., 35, 2055-2067.

Manson, A. H., M. W. J. Merry and R. A. Vincent (1969), Relationship between the partial reflection of radio waves from the lower ionosphere and irregularities as measured by rocket probes, Radio Sci., 4, 955-958.

Marker, W. S. (1981), Dual Doppler observations of diffusion and rolls, Preprint 20th Conf. Radar Meteorol., AMS, 536-545.

Mathews, J. D., J. H. Shapiro and B. S. Tanenbaum (1973), Evidence for distributed scattering in D region partial-reflection processes, J. Geophys. Res., 78, 8266-8275.

Newman, D. B., Jr. and A. J. Ferraro (1973), Sensitivity study of the partial reflection experiment, J. Geophys. Res., 78, 774-777.

Peterson, A. W. and G. W. Adams (1983), OH airglow phenomena during the July 5-6, 1982 total lunar eclipse, to appear in Applied Optics.

Piggott, W. R. and E. V. Thrane (1966), The effect of irregularities in collision frequency on the amplitude of weak partial reflections, J. Atmos. Terr. Phys., 28, 311-314.

Schlegel, K., A. Brekke and A. Haug (1978), Some characteristics of the quiet polar D-region and mesosphere obtained with the partial reflection method, J. Atmos. Terr. Phys., 40, 205-213.

Schlegel, K., E. V. Thrane and A. Brekke (1980), Partial reflection results in the auroral D-region explained in terms of acoustic waves, J. Atmos. Terr. Phys., 42, 809-814.

Tanenbaum, B. S., J. H. Shapiro and J. E. Reed (1973), Phase-difference distributions in a D-region partial-reflection experiment, Radio Sci., 8, 437-448.

von Biel, H. A. (1971), Amplitude distributions of D-region partial reflections, J. Geophys. Res., 76, 8365-8367.

# 4.5A PARAMETRIZATION OF FRESNEL RETURNS IN MIDDLE-ATMOSPHERE RADAR EXPERIMENTS

P. K. Rastogi
Haystack Observatory
Massachusetts Institute of Technology
Westford, MA 01866

## ABSTRACT

Weak reflections from sharp discontinuities in radio refractivity have been invoked over many years to explain the results of radio propagation experiments. In this contribution, the characteristics of refractivity structures required to produce Fresnel returns are first examined. The experimental evidence for Fresnel returns in middle-atmosphere radar experiments is then reviewed. The consequences of these returns on estimating the turbulence and wind parameters are briefly outlined.

## INTRODUCTION

The role of turbulence-induced irregularities in producing scattering and reflection of radio waves was first considered over two decades ago in connection with tropospheric and ionospheric forward-scatter experiments. The shape of the irregularities that could cause the supposed reflections was described in terms such as blinis (pancakes) or feuillets (sheets or leaves) to emphasize their planar nature. Regions of sharp transitions in radio refractivity, that are required to produce the reflections, were indeed observed with microwave refractometers carried aloft by balloons to heights of several kilometers. Much of the related work is described in texts such as BECKMANN and SPIZZICHINO (1963) and DU CASTEL (1966). A similar mechanism was invoked to explain the weak "partial-reflections" of 2-3 MHz radio waves from the D-region (GARDNER and PAWSEY, 1953).

The relevance of such reflections to the middle atmosphere radar experiments (ROTTGER, 1980; BALSLEY 1981), in addition to backscatter from the turbulence-induced refractivity fluctuations at half the radar wavelength (BOOKER, 1956), has been emphasized by several groups in recent years (GAGE and GREEN, 1978; ROTTGER, 1978; FUKAO et al., 1979). The terms that have been used for these reflections -- partial, specular, diffuse, aspect-sensitive and Fresnel -- tend to ascribe an underlying physical mechanism to explain the returns. Thin regions of refractivity gradients that extend horizontally over a a Fresnel zone are crucial to all these mechanisms. The term "Fresnel reflection" is therefore more appropriate.

Here, we first examine those characteristics of refractivity structures that are effective in producing reflections as opposed to scattering. Evidence for the occurrence of reflections in middle-atmosphere radar experiments is reviewed next, and finally, the consequences of such reflections on inferring the parameters of turbulence and the wind field from radar observations are discussed briefly.

## REFLECTIONS FROM REFRACTIVITY STRUCTURES

The scattering of radio waves from a random field of refractivity fluctuations, assumed homogeneous and isotropic for simplicity, has been discussed in detail by TATARSKII (1971) and ISHIMARU (1978). The scale of refractivity

that is half the radar wavelength for monostatic radars. The refractivity fluctuations are produced locally by turbulent mixing of refractivity gradients. There now is ample evidence that, in a convectively stable atmosphere, turbulence occurs in thin layers. The assumption of homogeneity of turbulence throughout the radar cell often is invalid due to the presence of such layers. Depending on the Bragg scale and the length scales associated with turbulence, the assumption of isotropy of Bragg-scale turbulence may also be violated within thin layers. Radio waves would be scattered by refractivity fluctuations within the layers, but are liable to be reflected by sharp refractivity gradients at the layer interfaces.

In order that reflections may be a viable mechanism for producing the radar returns, the refractivity structures must satisfy several conditions. First, the surfaces of constant refractivity must be oriented approximately normal to the Bragg vector, and the average direction of the refractivity gradients at these surfaces must be parallel to the Bragg vector. Second, these surfaces must be sufficiently smooth. Finally, they must be horizontally extended to cover a substantial part of a Fresnel zone.

Due to the horizontal stratification of the atmosphere, the iso-refractivity structures also are predominantly horizontal and will produce reflections for vertical Bragg-vector orientations. For monostatic radars, the radar must be pointed close to the vertical. For bistatic radars, the transmitter and receiver antenna must be oriented symmetrically about the vertical. The criterion for smoothness of iso-refractivity surfaces is stated by the Rayleigh condition, that a roughness-scale for these surfaces (parametrized e.g., by the standard deviation of the surface height above a reference level) be smaller than one-fourth of the Bragg scale (BECKMANN and SPIZZICHINO, 1963; ISHIMARU, 1978). For middle-atmosphere applications, this roughness-scale should be smaller than 0.75m for VHF and 0.1 m for UHF radars. For horizontally extended iso-refractivity surfaces, the contributions from those parts of the surface that are in a Fresnel zone arrive in phase at the receiver and therefore add coherently. This is illustrated schematically in Figure 1. In the far field, the diameter of the first Fresnel zone exceeds the antenna dimension, and is smaller than the size of the region illuminated by the radar beam.

When the individual layers of turbulence are not adequately resolved by the radar, a radar cell may contain several reflecting structures distributed along the range. The contributions of these structures can mutually interfere to produce large amplitude and phase fluctuations. If the other conditions are satisfied, then the requirement on the horizontal size of the structures is not too stringent. Within a Fresnel zone, the signal power attributable to the reflected component increases approximately as the square of the surface area contributing to the reflections. It is not necessary that the structures be uniform. For structures of larger size, contributions over different Fresnel zones would mutually interfere.

It is also instructive to consider the reflecting structures as antenna. These structures should then produce a diffraction pattern at the ground level. The size of this diffraction pattern depends inversely on the horizontal size of the reflecting structures. Movement of "drift" of this diffraction pattern provides information on horizontal motion of the structures using the spaced antenna drifts method (ROTTGER, 1981).

## RADAR EVIDENCE FOR FRESNEL RETURNS

Three different methods have been used to discriminate reflections from scattering in radar observations of the middle atmosphere -- (1) from observations of signal power along the vertical and off-vertical directions, (2) from temporal coherence of the reflected components, and (3) from observations of the

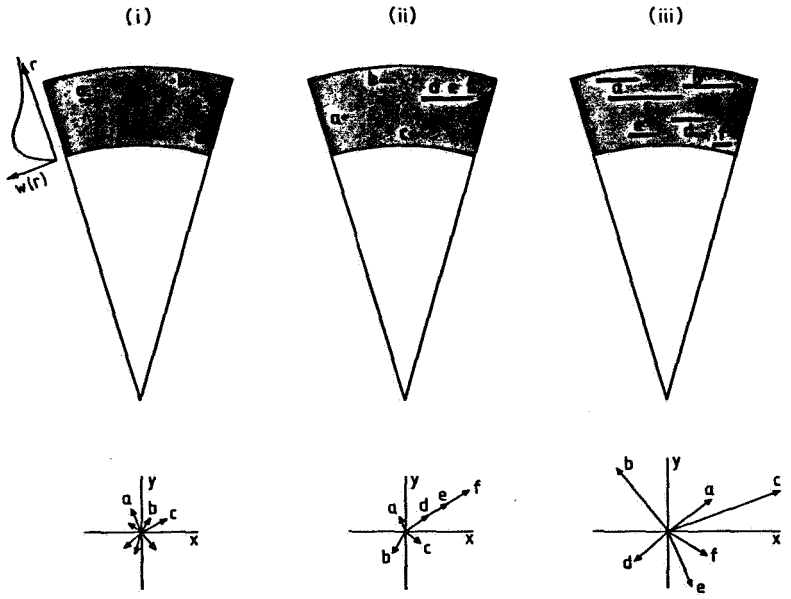


Figure 1. A schematic illustration of scattering and reflection from refractivity structures in a radar cell (shaded region). w(r) is a weighting function along the range. In case (i), signals scattered from randomly distributed irregularities (a,b,c..) add incoherently at the receiver as shown by the vector diagram at the bottom. In case (ii), signals scattered from the different parts (d,e,f..) of a horizontally extended surface arrive in phase at the receiver to produce a reflected component. In case (iii), irregularities at several horizontally extended surfaces (a,b,c..) produce reflections that mutually interfere at the receiver (from RASTOGI and HOLT, 1981).

diffraction pattern at the ground with spaced antennas. These methods are schematically shown in Figure 2. Almost all the observations of reflections have been made with VHF radars. There is yet scant empirical evidence for UHF radar reflections from the troposphere and stratosphere. This is probably because the roughness scale (0.1 m) required for UHF reflections becomes comparable to the Kolmogorov microscale.

Radar measurements along the vertical and an off-vertical direction show an enhancement in signal power along the vertical direction. Such observations have been reported by GAGE and GREEN (1978) at Sunset for the stratosphere, and by FUKAO et al. (1979) at Jicamarca for the stratosphere and the mesosphere. GAGE and GREEN interpreted their results as due to reflection from an extended layer of 1-m thickness. GAGE and BALSLEY (1980) considered anisotropic scattering from model irregularities to show that the observed enhancements along the vertical direction can be reconciled with weakly anisotropic disc and rod-shaped irregularities. GAGE et al. (1981) suggest that the observations at Sunset can also be reconciled with scattering from Bragg-scale fluctuations within a thin, extended layer - a process for which they suggest the term "Fresnel Scattering". Enhanced mesospheric reflections along the vertical have been observed only below 75-km altitude (FUKAO et al., 1979; ROTTGER et al., 1979; FUKAO et al., 1980). This is probably due to the increase in the

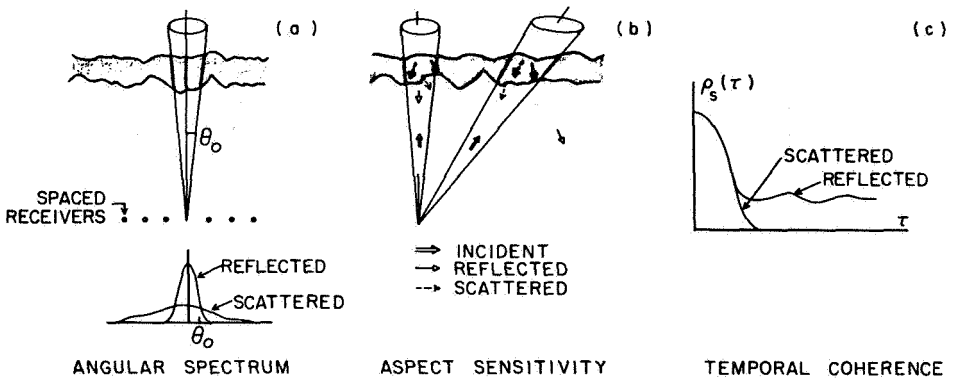


Figure 2. A schematic illustration of three methods of discriminating reflections from scattering. In the spaced-receiver method (a), the diffraction pattern produced by the irregularities is measured at ground level. Reflected components produced by a horizontally extended irregularity produce a diffraction pattern with a narrow angular spectrum. In the angular variation or aspect sensitivity method (b), signals received from the vertical and an off-vertical direction are compared. In the temporal-coherence method (c), reflections are detected on the basis of their longer correlation time. $\rho_S(\tau)$ is the autocovariance function of the received signal (from RASTOGI and ROTTGER, 1982).

Kolmogorov microscale associated with turbulence, that makes the Rayleigh condition rather difficult to satisfy in the upper mesosphere.

ROTTGER and LIU (1978) have used the longer coherence time of the reflected signals (up to several tens of seconds) to discriminate tropospheric reflections from scattering. ROTTGER (1980) and RASTOGI and ROTTGER (1982) have used the temporal coherence of the reflected returns to detect stable structures in the lower stratosphere.

The diffraction characteristics of the reflected and scattered components in the troposphere have been studied with spaced antennas by VINCENT and ROTTGER (1980) and the applicability of this method to measure winds up to mesospheric heights has been established by ROTTGER (1981). The spaced-antenna technique has also been used to detect in some cases a slight tilt in the refractivity structures (VINCENT and ROTTGER, 1980).

The statistical distribution of the received signals is affected significantly by the presence of reflected components. For scattering alone, the real and imaginary parts of the received signal envelope are expected to have a Gaussian distribution and its amplitude, a Rayleigh distribution (ISHIMARU, 1978). In presence of a constant reflected component, the amplitude has a Rice distribution. For several dominant reflectors, the distribution reverts to Rayleigh. RASTOGI and HOLT (1981) discuss the use of these distributions to detect strong reflections in the presence of scattering. The statistical distribution of MST radar signals does not seem to have received much attention.

## DISCUSSION

The characteristics of radar reflections from the middle atmosphere have been studied in several VHF experiments. It is generally recognized that thin, horizontally extended refractivity structures play a significant role in

producing these reflections. Several mechanisms have been proposed to explain the observed characteristics of reflections, on the basis of assumed or inferred properties of small-scale refractivity fluctuations.

At directions close to the vertical, reflections can produce undesirable effects. In the presence of reflections, care is needed to estimate the turbulence parameters (e.g., $C_n^2$) from the received signal power. Measurements of vertical wind are also likely to be biased by the winds at reflection heights, especially when the altitude resolution is coarse.

Most of the reported radar studies of reflections tacitly assume that the iso-refractivity surfaces are planar. Weak undulations of these surfaces are expected, however, in the presence of atmospheric waves and shears. These undulations can produce a focussing and defocussing effect on the signals received at ground level. Such effects become important with small antennas, and also influence the validity of estimating instantaneous horizontal velocity from simultaneous Doppler observations along beams pointed in different directions.

ACKNOWLEDGEMENT

This material is based on work supported by the National Science Foundation under grant number ATM-8000060.

REFERENCES

Balsley, B. B. (1981), The MST Technique - A brief review, J. Atmos. Terr. Phys., 43, 495-509.

Beckmann, P. and A. Spizzichino (1963), The Scattering of Electromagnetic Waves From Rough Surfaces, Pergamon, New York, 503 pp.

Booker, H. G. (1956), A theory of scattering by nonisotropic irregularities with applications to radar reflections from the aurora, J. Atmos. Terr. Phys., 8, 204-221.

du Castel, F. (1966), Tropospheric Radio Wave Propagation Beyond the Horizon, Pergamon, New York.

Fukao, S., T. Sato, R. F. Woodman and W. E. Gordon (1979), Mesospheric winds and waves over Jicamarca on May 23-24, 1974, J. Geophys. Res., 84, 4379-4386.

Fukao, S., T. Sato, R. M. Harper and S. Kato (1980), Radio wave scattering from the tropical mesosphere observed with the Jicamarca radar, Radio Sci., 15, 447-457.

Gage, K. S. and J. L. Green (1978), Evidence for specular reflection from monostatic VHF radar observations of the stratosphere, Radio Sci., 13, 991-1001.

Gage, K. S. and B. B. Balsley (1980), On the scattering and reflection mechanisms contributing to clear air radar echoes from the troposphere, stratosphere and mesosphere, Radio Sci., 15, 243-257.

Gage, K. S., B. B. Balsley and J. L. Green (1981), Fresnel scattering model for the specular echoes observed by VHF radar, Radio Sci., 16, 1447-1453.

Gardner, F. F. and J. L. Pawsey (1953), Study of ionospheric D-region using partial reflections, J. Atmos. Terr. Phys., 3, 321-344.

Ishimaru A. (1978), Wave Propagation and Scattering in Random Media, Academic, New York, 572 pp. (in two volumes).

Rastogi, P. K. and O. Holt (1981), On detecting reflections in presence of scattering from amplitude statistics with application to D-region partial reflections, Radio Sci., 16, 1431-1443.

Rastogi, P. K. and J. Rottger (1982), VHF radar observations of coherent reflections in the vicinity of the tropopause, J. Atmos. Terr. Phys., 44, 461-469.

Rottger, J. (1978), Evidence for partial reflection of VHF radar signals from the troposphere, J. Geophys. Res., 44, 393-394.

Rottger, J. (1980), Structure and dynamics of the stratosphere and mesosphere revealed by VHF radar investigations, Pure Appl. Geophys., 118, 494-527.

Rottger, J. (1981), Investigation of lower and middle atmosphere dynamics with spaced antenna drifts radar, J. Atmos. Terr. Phys., 43, 277-292.

Rottger, J. and C. H. Liu (1978), Partial reflection and scattering of VHF radar signals from the clear atmosphere, Geophys. Res. Lett., 5, 357-360.

Rottger, J., P. K. Rastogi and R. F. Woodman (1979), High-resolution VHF radar observations of turbulence structures in the mesosphere, Geophys. Res. Lett., 6, 617-620.

Tatarskii V. I. (1971), The effects of the turbulent atmosphere on wave propagation, Nat. Tech. Inf. Serv., Springfield, Va., 472 pp. (translated from the Russian).

Vincent, R. A. and J. Rottger (1980), Spaced antenna VHF radar observations of tropospheric velocities and irregularities, Radio Sci., 15, 319-335.

# 4.5B PARAMETERIZATION OF FRESNEL RETURNS

J. Rottger

EISCAT Scientific Association
P.O. Box 705
S-98127 Kiruna, Sweden

It appears appropriate to use the intensity correlation function $\rho(\tau)$ to investigate variations of a reflected signal component, $C_r^2$, and a scattered signal component, $C_s^2$, because it is determined by the relative motions, i.e., fluctuations of irregularities or structural changes.

An example of a correlation function $\rho(\tau)$ is shown in Figure 1. It can be separated into three parts. (1) A very fast drop between zero and the neighboring lag which is due to uncorrelated noise. (2) A smooth decrease at small lags up to a few seconds which is due to scattering. This decrease can be approximated by a parabola (equation (1)). (3) A rather slow fadeout which is due to Fresnel reflection and very gradually approaches zero correlation for longer lags.

The noise contribution (part (1)) has to be eliminated by normalizing the correlation function by means of the zero-lag value $\rho'$ which follows from a parabolic approximation. As signal intensity variations are directly connected to turbulent variations in a scattering medium or the changes of a reflecting discontinuity, we can evaluate parts (2) and (3) of the normalized correlation functions in terms of characteristic structure parameters (e.g., FROST and BITTE, 1977):

(1) The microscale correlation time is defined as

$$\tau_e = \left[ -\frac{1}{2} \frac{\partial^2 \rho}{\partial \tau^2} \right]^{-1/2} \qquad (1)$$

The value of $\tau_e$ is given by the interception of the $\rho = 0$ axis by the parabolic curve fitted through $\rho(\tau)$ at $0 \lesssim \tau << T$ (see Figure 1). The microscale correlation time is a measure of the most rapid changes that occur in the fluctuations on the radar Bragg scale. The time $\tau_e$ is also called "coherence time" or "time to independence" (e.g., ATLAS, 1964), since this is the time after which the turbulent fluctuations at half the radar wavelength $\lambda$ become statistically independent.

(2) The average persistency of a structure is given by the integral-scale correlation time

$$T_e = \int_0^T \rho(\tau)\, d\tau \qquad (2)$$

where T is the length of the correlation function. The persistency $T_e$ is a measure of the longest-lived coherence in structural behavior.

It can be shown that $\tau_e \sim \lambda/(4\pi\sigma_w)$, where $\sigma_w$ is the rms deviation of the velocity distribution. In a similar way, the integral-scale correlation time or persistency $T_e$ can be expressed by a characteristic length L and a velocity u, with which a reflecting structure is advected through the radar beam. We find $T \sim L/u$. This assumption is based on the Taylor hypothesis that the time scale for evolution of a structure of dimension L is so long that there is no

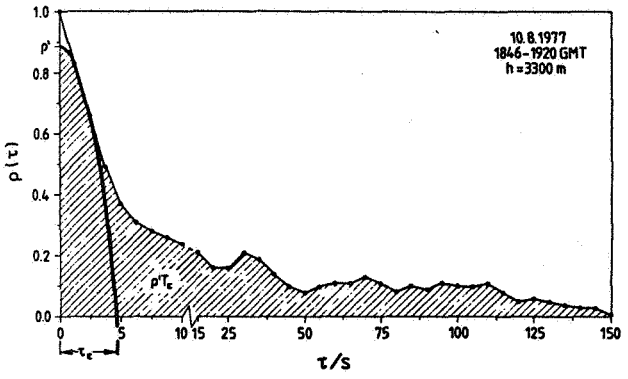


Figure 1. Intensity correlation function $\rho(\tau)$. The scaling of the $\tau$ axis is different for the lags $0 \text{ s} < \tau < 10 \text{ s}$ and $15 \text{ s} < \tau < 150 \text{ s}$; $\rho'$ is the offset correlation at zero lag due to noise contributions; $\tau$, is the microscale correlation time, and the area $\rho'T$, determines the integral-scale correlation time $T_e$.

significant change during its advection through the radar beam. The persistency $T_e$ is large for a slowly changing discontinuity and for minor contributions due to scattering, $C_s^2 \ll C_r^2$. If $C_s^2 \gg C_r^2$, the integral-scale correlation time will approach the microscale correlation time ($T_e \to \frac{2}{3} \tau_e$). In most realistic conditions, scattering and reflection are observed, i.e., $C_s^2 \sim C_r^2$. The correlation function then indicates a Gaussian shape approximated by a parabola near zero lag. Zero correlation is gradually approached for long time lags because or contributions from reflection (e.g., Figure 1). The integrals $I(\tau_e) = \int_0^{\tau_e} \rho \, d\tau$ and $I(T_e) = \int_0^{T} \rho \, d\tau - I(\tau_e)$ yield a rough estimate of the scattered and reflected contributions. We expect $I(T_e) \sim I(\tau_e)$ if $C_r^2 \sim C_s^2$.

For $\tau < \tau_e$, $\rho(\tau)$ is essentially determined by turbulence scatter, whereas it is determined by reflection for $\tau > \tau_e$. An estimate of the scattered contribution can also be obtained by high pass filtering ($f > \tau_e^{-1}$) and an estimate of the reflected contribution by low pass filtering ($f < \tau_e^{-1}$) of the intensity time series.

RASTOGI and ROTTGER (1982) used a high-pass and low-pass filter procedure to separate the scattered from the reflected component. They defined a specularity index R which is the ratio of the rms outputs from the low-pass and the high-pass filters. This procedure of course needs an a priori definition of the cutoff frequencies of these filters. If $R > 1$, the reflected component is dominant; if $R < 1$, the scattered component is dominant.

Another most preferred way would be to evaluate the spectra as suggested by Rottger (this volume, p. 112). As mentioned there, the scattered contribution is the integral over the Gaussian background distribution, whereas the reflected contribution is the integral over the remaining spikes which are assumed to be caused by diffuse reflection.

REFERENCES

Atlas, D. (1964), Advances in radar meteorology, in: Advances of Geophysics, (ed. H. E. Landsberg and J. van Mieghem), Academic, New York, 317-478.

Frost, W. and J. Bitte (1977), Statistical concepts of turbulence, in: Handbook for Turbulence, 1, (ed. W. Frost and T. H. Mouldon), Plenum, New York, 53-83.

Rastogi, P. K. and J. Rottger (1982), VHF radar observations of coherent reflections in the vicinity of the tropopause, J. Atmos. Terr. Phys., 44, 461-469.

# 4.6A THE RELATIONSHIP BETWEEN STRENGTH OF TURBULENCE AND BACKSCATTERED RADAR POWER AT HF AND VHF

W. K. Hocking

Max-Planck-Institut fur Aeronomie
D-3411 Katlenburg-Lindau
Federal Republic of Germany

## ABSTRACT

The formulae relating turbulence and other atmospheric parameters to backscattered power for radar observations are reviewed. The paper considers primarily the case of scatter from turbulent irregularities which have scales corresponding to the range of isotropic, inertial range turbulence, although some brief discussion of the applicability of this assumption is given. A new formula is introduced for the mesosphere which relates ionospheric electron densities to backscattered power.

## INTRODUCTION

Discussions and the relationship between the intensity of turbulence and backscattered radar signal strengths have, in recent literature, been largely based upon the Kolmogoroff theory of inertial range isotropic turbulence (e.g., BATCHELOR, 1953; TATARSKI, 1961, 1971). This is not to say, however, that this is the only possible approach. For example, BOOKER and GORDON (1950) and STARAS (1952) adopted an alternative procedure for examination of turbulence (e.g., see review by GAGE and BALSLEY,1980). This second approach has not been as extensively applied as that due to Kolmogoroff, but, as pointed out by GAGE and BALSLEY (1980), it does allow extensions to conditions of anisotropic turbulence. Whether in fact the assumptions of inertial range, isotropic turbulence are valid for the atmosphere is to some extent an unresolved topic. For example the inertial range theory requires high Reynolds numbers (BATCHELOR, 1953, p 116), and Reynolds numbers in the atmosphere tend to be only moderate. Furthermore, observations of turbulence in the stratosphere often show very thin ($\approx$50-200 m thick) well-defined layers of turbulence (e.g., CRANE, 1980). This is not predicted by the Kolmogoroff theory. Nevertheless, it is normally assumed that Kolmogoroff theory still applies within the layer, at scales smaller than the layer thickness. BOLGIANO (1968) has proposed a turbulence model in which thin well-mixed layers of turbulence form, and in this model radio-wave backscatter is not produced by the turbulence within the layer but by discontinuities in refractive index at its top and bottom. The scatter from such discontinuities should be very different in character to turbulent scatter. It should show an aspect sensitivity, with most scatter coming from the vertical, and should have slow fading times. Such "specular reflections" are well known to occur in the stratosphere at VHF (e.g., GAGE and GREEN, 1978; ROTTGER and LIU, 1978), but whether the mechanism proposed by Bolgiano explains these reflections has not been resolved. Other refinements to Kolmogoroff theory have been presented by some authors (e.g., HILL and CLIFFORD, 1978; WEINSTOCK, 1978a).

Despite these potential problems, however, the Kolmogoroff theory of inertial range turbulence appears to model the atmosphere reasonably well in the range of scales for which it is applicable. Therefore this model will be the main one discussed in this short essay.

A short introduction of the formulae of the inertial range theory will first be given, and then it will briefly be shown how these formulae extend to radio-wave scattering. Some discussion on the accuracy of these formulae will then follow.

It will be assumed initially that the radar looks at the atmosphere at an off-zenith angle, so that the role of specular reflectors can be ignored. The complexities introduced by specular scatter will not be discussed in detail; more complete discussions can be found in, for example, HARPER and GORDON (1980), and ROTTGER (1980a,b).

## INERTIAL RANGE TURBULENCE

Atmospheric turbulence causes random fluctuations of various atmospheric parameters, such as density, velocity, refractive index, etc. The statistics of the turbulence is usually described using one of these parameters. However, the parameter chosen to describe the fluctuations must be a passive tracer. This means that its statistical properties must not depend on the position in the turbulence patch. For example, density is not a good passive tracer, as displacement of a parcel of air vertically alters its density. This matter was discussed more deeply by TATARSKI (1961), and will also be considered again shortly. Potential temperature is a good tracer. So are the velocity fluctuations.

For the present, let this passive tracer by a scalar, denoted by $\theta$.

There are at least two ways to describe the statistical properties of the turbulence. One way is by means of the structure function, viz

$$D_\theta(\underline{r}) = \langle|\theta(\underline{x}) - \theta(\underline{x}+\underline{r})|^2\rangle. \tag{1}$$

Here, $\underline{x}$ represent a position vector, and $\underline{r}$ a spatial displacement. $\langle\rangle$ represents an average over space and time. It can be shown that for inertial range turbulence,

$$D_\theta(\underline{r}) = C_\theta{}^2 r^{2/3} \tag{2}$$

e.g. TATARSKI (1961), where $C_\theta{}^2$ depends on the intensity of turbulence. The turbulence fluctuations can also be expressed as the Fourier sum of wave numbers $\underline{k} = 2\pi/\Lambda$, $\Lambda$ being the Fourier scale. Then TATARSKI (1961) showed that the spectrum of fluctuations is

$$\phi_\theta(\underline{k}) = 0.033\ C_\theta{}^2\ |\underline{k}|^{-11/3} \tag{3}$$

A normalization has been chosen such that $\iiint_{-\infty}^{\infty} \phi_\theta(\underline{k})d\underline{k} = \langle\theta^2\rangle$.

It can be shown (TATARSKI, 1961) that $C_\theta{}^2$ is related to the outer scale of turbulence, $L_o$ (i.e., the approximate transition scale between the inertial and buoyancy ranges of turbulence) by the relation

$$C_\theta{}^2 = a^2\alpha' L_o{}^{4/3} \left(\frac{d\bar{\theta}}{dz}\right)^2 \tag{4}$$

Here, a is a constant, $\approx 2.8$ (e.g., VANZANDT et al., 1978), $\alpha'$ is a constant which is approximately 1., and $(d\bar{\theta}/dz)$ is the gradient of the mean quantity $\theta$.

The formulae (3) and (4) form the basis of theories which relate backscattered radar power to turbulence. However, before discussing how this is done, some other spectral forms should be briefly discussed. It is important to note that the spectral form shown in (3) is not the only form which appears in the literature. It is the full three-dimensional spectrum. But at times the spectrum of wave numbers with magnitude $k = |\underline{k}|$ is given viz

$$E_\theta(k) = 4\pi k^2 \phi_\theta(\underline{k}) = 0.132\pi\ C_\theta\ k^{-5/3}. \tag{5}$$

No distinction between the directions of the $\underline{k}$ vectors is made in this formula. Another very important spectrum is the spectrum of fluctuations which would be seen by a probe moving in a straight line through the turbulence. This is not the same as (3), since that only looks at 1 scale direction. But for a probe, all scales produce an effect along the path of the probe, but their "effective scales" change because they are not all orientated along the probe path. Then this produces a spectrum

$$S_\theta(k) = \int_{-\infty}^{\infty}\int_{-\infty}^{\infty} \phi_\theta(\underline{k})\,dk_y\,dk_z \qquad (6)$$

whence $S_\theta(k) \approx 0.25\ C_\theta^2 k^{-5/3}$ (7)

OTTERSTEN (1969) has emphasized the difference between (3) and (7), and pointed out that (3) is applicable for radar experiments, whilst (7) is applicable for in situ measurements. The two expressions should not be confused.

## POTENTIAL REFRACTIVE INDEX GRADIENT

In considering backscatter of radio waves from the atmosphere, it is of course necessary to look at the fluctuations in refractive index caused by the turbulence. The refractive index n of air at centimetre and metre wavelengths is (TATARSKI, 1961).

$$n = 1 + 10^{-6} \times (79/T) \times (p + 4800\ e/T) \qquad (8)$$

where T is temperature (absolute), p is pressure (millibars) and e is the water vapour pressure. However, it is more convenient to express n as a function of the potential temperature H and the specific humidity, q [$= e/(1.62p)$]. Then

$$n = n(p, H, q) \qquad (9)$$

But n here is not a good passive tracer. This can be seen by the following consideration. Suppose an eddy moves from height $z_1$ to a height $z_2$. Suppose that at $z_1$ the eddy was in equilibrium with its environment, and that at this height there was pressure $p_1$, potential temperature $H_1$ and specific humidity $q_1$. Suppose that at height $z_2$, the atmospheric pressure is $p_2$, and the environmental H, q are $H_2$ and $q_2$. However, at $z_2$ the parcel itself has $H = H_1$ and $q = q_1$, since it is assumed to have moved adiabatically. Of course the pressure in the parcel is now $p_2$. Hence the difference in refractive index between the parcel and its environment at $z_2$ is

$$\Delta n = \underbrace{n(z_2, p_2, H_1, q_1)}_{\text{parcel}} - \underbrace{n(z_2, p_2, H_2, q_2)}_{\text{environment}}$$

$$\Delta n = \left(\frac{\partial n}{\partial H}\frac{\partial H}{\partial z} + \frac{\partial n}{\partial q}\frac{\partial q}{\partial z}\right)\Delta z \qquad (10)$$

where $\Delta z = z_2 - z_1$.

This is not simply the difference in refractive index at heights $z_1$ and $z_2$, which would be

$$\Delta n = \left[\frac{\partial n}{\partial p}\frac{\partial p}{\partial z} + \left(\frac{\partial n}{\partial H}\frac{\partial H}{\partial z} + \frac{\partial n}{\partial q}\frac{\partial q}{\partial z}\right)\right]\Delta z \qquad (11)$$

The formula discussed in the previous section can be applied for refractive index

with $\theta = n$, but in equation (4), the term $(d\bar{\theta}/dz)$ should not simply be $(dn/dz)$ as given by (11), but rather, from (10),

$$\frac{d\bar{n}}{dz} = \left(\frac{\partial n}{\partial H}\frac{\partial H}{\partial z} + \frac{\partial n}{\partial q}\frac{\partial q}{\partial z}\right) \tag{12}$$

This quantity is often denoted by M, and is called the generalized potential refractive index gradient.

For metre and centimetre scatter from the un-ionized atmosphere, (TATARSKI, 1961),

$$M = \frac{-79\times10^{-6}p}{T^2} \cdot \left(1 + \frac{15{,}500\ q}{T}\right)\left(\frac{dT}{dz} + \Gamma_a - \frac{7800}{\left(1+\frac{15{,}500}{T}\right)} \cdot \frac{dq}{dz}\right) \tag{13}$$

The term $\Gamma_a$ is the adiabatic lapse rate.

In the stratosphere and mesosphere, $q = 0$. However, once heights of greater than 50-60 km are reached, scatter from turbulence is enhanced by the existence of free electrons (ionization), and in this case M needs modification.

For these circumstances

$$n = n(N, \nu_m) \tag{14}$$

Where N is the electron density, and $\nu_m$ is the collision frequency of electrons with neutral particles. (Pressure and temperature fluctuations also produce weak changes in n, as for the troposphere and stratosphere, but these effects are very weak compared to the effects of N and $\nu_m$, and so can be ignored).

HOCKING (1980, 1981) has shown that the appropriate generalized refractive index gradient for the ionospheric D region is given approximately by

$$M_e = \frac{\partial n}{\partial N} \cdot \left[\frac{N}{T}\left(\frac{dT}{dz} + \Gamma_a\right) - \frac{dN}{dz} + \frac{N}{\rho}\frac{d\rho}{dz}\right) + \frac{\partial n}{\partial \nu_m}\frac{\partial \nu_m}{\partial z}, \tag{15}$$

where $\rho$ is the neutral air density.
For the region 0-120 km, this equals

$$M_e = \frac{\partial n}{\partial N}\left[\frac{N}{T}\left(\frac{dT}{dz} + \Gamma_a\right) - \frac{dN}{dz} - (1.4\times10^{-4})N\right] + \frac{\partial n}{\partial \nu_m}\frac{\partial \nu_m}{\partial z} \tag{16}$$

At VHF in the D region n is related quite simply to N by the relation

$$n^2 = 1 - \pi^{-1} r_e N \lambda^2$$

where $r_e$ is the classical electron radius, and $\lambda$ is the radar wavelength, so $\partial n/\partial \nu_m = 0$, and

$$\frac{\partial n}{\partial N} = \frac{1}{2}\pi^{-1} r_e \lambda^2.$$

At HF and MF, the relation between n and N is more complex (e.g., BUDDEN, 1965). Thus $M_e$ depends on the potential temperature gradient, the electron density gradient, and the neutral atmospheric density gradient.

In deriving (15), it was assumed that when a parcel of ionosphere is displaced, the ratio of electron density to neutral density remains constant, and that no change in the photochemical reaction rates occurs during such a displacement. HILL and BOWHILL (1979) have suggested that this might not be exactly true, but nevertheless equations (15) and (16) should provide a reasonable estimate of $M_e$.

## SCALES OF THE INERTIAL RANGE

Before proceeding to show how these turbulence formulae relate to radar backscatter, it is important to illustrate over what scales they can be applied.

At very small scales, the kinetic energy density contained by the eddies is diminished due to viscous effects, and much of the turbulent energy is dissipated as heat. This small scale range is often called the "viscous range". At very large scales, buoyancy effects become important, and turbulent eddies taken on a "pan-cake"-like appearance, with horizontal scales much larger than their vertical dimensions.

An important scale for determining the boundary of the inertial-range to viscous range transition is the Kolmogoroff microscale, defined by

$$\eta = (\nu^3/\varepsilon)^{1/4}. \qquad (17)$$

Here, $\nu$ is the kinematic viscosity, and $\varepsilon$ is the turbulent energy dissipation rate. This is a scale well within the viscous range. The scale

$$\ell_o = 7.4\eta \qquad (18)$$

is known as the "inner scale" (e.g., HILL and CLIFFORD, 1978) and defines the approximate transition scales between the inertial and viscous ranges. (The constant 7.4 is only relevant for air.)

The scale for determining the transition region between the inertial and buoyancy ranges is (WEINSTOCK, 1978b)

$$L_B = (2\pi/0.62)\ \varepsilon^{1/2}\ \omega_B^{-3/2}, \qquad (19)$$

where $\omega_B$ is the Brunt-Vaisala period of the atmosphere at the height of the turbulence. This $L_B$ should not be confused with $L_o$ in (4): they are different parameters, as will be seen later.

The inertial range of turbulence strictly only applies for scales somewhat less than $L_B$ and larger than $\ell_o$.

Approximate values of $L_B$ and $\ell_o$ are shown in Figure 1. For a radar wavelength $\lambda$, backscatter occurs for scales of $\lambda/2$. Thus if a 50 MHz radar is used ($\lambda$ = 6 m), then scatter should be possible from isotropic inertial range turbulence up to altitudes of about 65-70 km. Figures similar to Figure 1 have appeared elsewhere in the literature (e.g., GAGE and BALSLEY, 1980), and show similar values for $\eta$ and $\ell_o$.

## RADIO-WAVE BACKSCATTER

Having illustrated some appropriate formulae for relating refractive index fluctuations to turbulence parameters, it is now necessary to determine how these formulae relate to radio-wave backscatter.

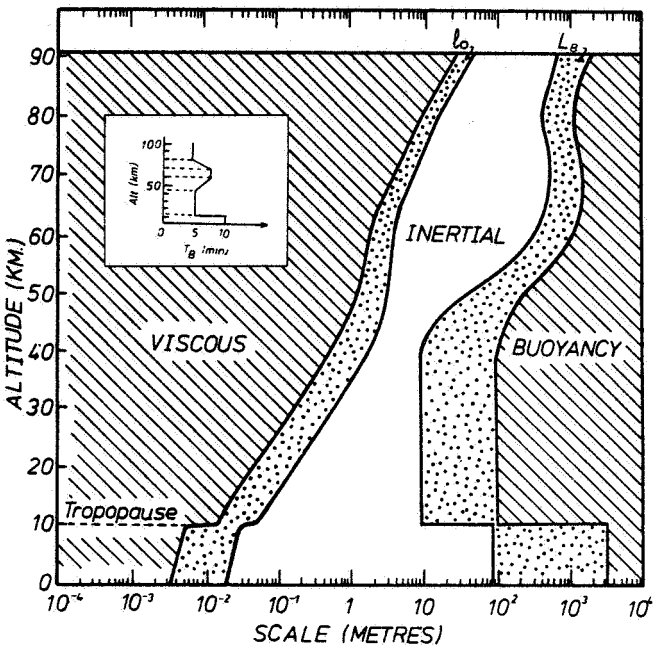


Figure 1. Typical inner and outer scales ($\ell_o$ and $L_B$ respectively) for inertial-range turbulence in the atmosphere. The formulae used are given in the text. The profile of the Brunt-Vaisala period is also shown. It was assumed that the mean value of $\varepsilon$ was $10^{-1}$ W kg$^{-1}$ at 90 km, decreasing exponentially to $10^{-2}$ W kg$^{-1}$ at 80 km. Between 80 and 60 km, this mean was taken at $10^{-2}$ W kg$^{-1}$. In the region 60-90 km, the bounds of the dotted areas correspond to turbulent energy dissipation rates of 1/3 rd and 3 times these mean values. Below 40 km, and downto the tropopause, the upper and lower limits of $\varepsilon$ were taken as $10^{-3}$ and $10^{-5}$ W kg$^{-1}$. $L_B$ and $\ell_o$ were assumed to vary smoothly between 40 and 60 km. (The region between 30 and 80 km is perhaps the most uncertain part of the graph.) Below the tropopause, $\varepsilon$ was assumed to be limited between $10^{-4}$ and $10^{-1}$ W kg$^{-1}$. Larger $\varepsilon$ values correspond to smaller $\ell_o$ and larger $L_B$ values (i.e. the inertial range widen at both ends, when $\varepsilon$ increases).

BOOKER (1956) has shown that the power backscattered from refractive index fluctuations with mean square value $N(\underline{k})d\underline{k}$ at scales $\Lambda = 2\pi/k$, per unit solid angle, per unit incident power density, and per unit volume (i.e., the cross section of backscatter) is

$$\sigma = [4\pi^2/\Lambda^2]N(\underline{k}). \tag{20}$$

(this expression is true at VHF, but at lower frequencies may not be) $P(\underline{k})$ is similar to $\phi_n(k)$ in equation (3) ($\theta$=n), but BOOKER (1955) used the normalization

$$(2\pi)^{-3} \iiint_{-\infty}^{\infty} N(\underline{k})dk_1\, dk_2\, dk_3 = |\overline{\Delta n}|^2$$

Hence $N(\underline{k}) = (2\pi)^3 \phi_n(\underline{k})$. (21)

For radar backscatter at wavelength $\lambda$, $k = 4\pi\lambda^{-1}$, and so using (21) and (29), and using (3) for $\phi_n(\underline{k})$,

$$\sigma = .00654\pi^{4/3} C_n^2 \lambda^{-1/3} \tag{22}$$

Sometimes an alternative definition of backscatter cross section is used. This is the total power which would be scattered if power were scattered isotropically with an intensity equal to that of the backscattered radiation, per per unit incident power density, per unit volume of scatterer. It is often denoted by $\eta$, and although this can at times be confused with the Kolmogoroff microscale, this convention will be maintained here. Then

$$\eta = 4\pi\ \sigma, \tag{23}$$

and hence

$$\eta = 0.38 C_n^{\ 2}\ \lambda^{-1/3}, \tag{24}$$

as also derived by OTTERSTEN (1969). It should be noted that, at least for the ionosphere, the wavelength dependence for $\eta$ is more complex than $\lambda^{-1/3}$, since $C_n^{\ 2}$ is itself a function of wavelength. This can be seen by considering a given patch of turbulence in the ionosphere. For this patch, there is a constant electron density structure constant, which we may denote by $C_N^{\ 2}$. Then $C_N^{\ 2} = (\partial n/\partial N)^2\ C_N^{\ 2}$ (e.g., HOCKING and VINCENT, 1982), and $(\partial n/\partial N)$ is strongly wavelength dependent, as has already been seen.

Now it is necessary to show how $\sigma$ (or $\eta$) relates to the power received in a backscatter experiment. Consider scatter from a height h. Then the peak power per unit area incident at h is

$$P_h = (P_T G_T e_T)/(4\pi h^2), \tag{25}$$

where $P_T$ is the transmitter peak power, $G_T$ is the transmitter array directivity and $e_T$ is the transmitter efficiency. To obtain the power backscattered per unit steradian, we simply multiply this by $\sigma V$, where V (the "radar volume") is the volume defined by the locus of the half-power points of the radar, and the pulse length. The receiving array subtends a solid angle $A_R/h^2$ to this scattering region at height h, so the peak power received by the receiver is (ignoring absorption)

$$P_R = \frac{P_T\ G_T\ V\sigma\ e_T\ e_R\ A_R}{4\pi\ h^4} \tag{26}$$

where $e_R$ is the receiver efficiency and $A_R$ is the effective area of the receiving array.

Thus by (22) and (26),

$$C_n^{\ 2} = \frac{16\pi^2\ P_R\ h^4\ \lambda^{1/3}}{0.38V\ P_T\ G_T\ e_T\ e_R\ A_R} \tag{27}$$

In the case of a circularly symmetric array, $V \approx \pi(h\theta_{1/2})^2$. L, where L is the pulse-length and $\theta_{1/2}$ is the half-power-half-width of the polar diagram. If the same array is used for transmission and reception, $e_T = e_R$, and $A_R = G_T\lambda^2/4\pi$, so

$$C_n^{\ 2} = \frac{1662.25\ P_R\ h^2\ \lambda^{-5/3}}{P_T\ G_T^{\ 2}\ e_T^{\ 2}\ \theta_{1/2}^{\ 2}\ L} \tag{28}$$

For a radar, it can be shown that $G_T\ \theta_h^{\ 2} \approx \pi^2/4$, where $\theta_h$ is the half-power-half-width. For the case in which the same radar is used for transmission and

reception, the effective half-power width reduces by $\sqrt{2}$, so $\theta_{1/2}=\theta_h/\sqrt{2}$, and $G_T\,\theta_{1/2}^2 = \pi^2/8$. Then

$$C_n^2 = \frac{128\,\lambda^{1/3}\,h^2\,P_R}{0.38\pi\,e^2\,A\,L\,P} \tag{29}$$

Either (30) or (31) can be used to estimate $C_n^2$ from absolute measurements of received power. This has been done, for example, by NASTROM et al. (1982) and GOOD et al. (1982).

## APPLICATION OF THE FORMULAE IN THE REAL ATMOSPHERE

Clearly (28) or (29) can be used to estimate $C_n^2$ with a radar, but unfortunately this does not give the structure constant $C_n^2$ for the turbulence itself. It would, if the turbulence filled the radar volume, but in reality turbulence appears to occur in thin horizontal layers, with depths of 10s to 100s of meters (e.g., VANZANDT et al., 1978; CRANE, 1980; WEINSTOCK, 1981, and references therein). Thus the scattering within the radar volume is usually from a few thin turbulent layers, and the effective volume V should not be $\pi h^2\theta_{1/2}^2 L$ as proposed earlier, but $(\pi h^2\theta_{1/2}L)\cdot F$, where F represents the fraction of volume within the radar volume which is filled with turbulence. VANZANDT et al. (1978) obtained a formula enabling F to be determined from a knowledge of the mean wind shear (taken with a resolution of about a kilometer or so), the standard deviation of the fine-scale shear, and a "critical wind shear" $S_c$. Then, if $\overline{C_n^2}$(turb) is the refractive index structure constant for the turbulence, and $\overline{C_n^2}$(radar) is the value measured by the radar,

$$\overline{C_n^2}(\text{turb}) = \overline{C_n^2}(\text{radar})/F. \tag{30}$$

VANZANDT et al.(1978) used meteorological data to estimate M (equation 13) and then applied (4) and (30) to estimate $\overline{C_n^2}$(radar). They found that with a value of $L_o$ equal to 10 m, good agreement occurred between the model and radar observations, particularly in the stratosphere. Agreement was not so good in the lower troposphere, because the model did not account for humidity fluctuations.

VANZANDT et al. (1981) improved the theory of VANZANDT et al. (1978) by considering these humidity fluctuations, by considering small-scale fluctuation in potential temperature, by letting the layer thicknesses be non-constant, and also by using a more realistic distribution for the wind shears.

VANZANDT et al. (1978) compared $\overline{C_n^2}$(radar) estimates from their model to experimental radar values, assuming $L_o$= 10 m. GAGE et al. (1980) applied this principle in reverse, using radar estimates of $C_n^2$ to effectively estimate $L_o$ (through equation 14). They then drew on an equation relating $L_o$ and the turbulent energy dissipation rate $\varepsilon$, to estimate $\varepsilon$. This relation was (TATARSKI, 1961)

$$\varepsilon = b\,S^{3/2}\,L_o^2 \tag{31}$$

where b was taken as a constant equal to unity, and $S = (d\bar{u}/dz)^2$ is the shear in the mean wind. By replacing S with $\omega^2 B/R_i$, where $R_i$ is the Richardson number and $\omega_B$ is the Brunt-Vaisala frequency, and assuming that turbulence exists if $R_i = R_i(\text{crit})$, (a critical value), they obtained, using $L_o$ from (4),

$$\varepsilon_{turb} = [C_n^2(\text{turb})\cdot(a^2\alpha' R_i(\text{crit})\,\omega_B^2\,M^2)^{-1}]^{3/2}. \tag{32}$$

They took $R_{i(crit)} = 1/4$. Then $\varepsilon_{turb}$ is the mean turbulent energy dissipation

rate. GAGE et al. (1980) also calculated a quantity which they denoted by $\overline{\varepsilon}$, which was the mean turbulent energy dissipation rate averaged over the radar volume. They took

$$\overline{\varepsilon} = F^{-1}\varepsilon_{turb} \tag{33}$$

From radar measurements GAGE et al. (1980) estimated $\overline{C_n^2}$(radar). Then they made some reasonable assumptions concerning F, and so were able to estimate $\varepsilon_{turb}$ and $\overline{\varepsilon}$ from their radar data. M was calculated from meteorological measurements of T and p, and it was assumed that the humidity terms in M were unimportant. It should also be noted that F is dependent on $\omega_B$, although this may not be obvious in the simplified discussion given above. This dependence of F on $\omega_B$ can cause some problems in estimating F, but GAGE et al. (1980) were careful to reduce this error as much as was reasonable.

The technique outlined above is, at least in principle, the primary means by which $\varepsilon$ is obtained for the atmosphere using VHF radars. Variations on the details of these formulae have been presented (e.g., CRANE, 1980; WEINSTOCK, 1981), but the principle remains similar - namely, to determine the fraction of the radar volume actually filled by turbulence, and then to correct $C_n^2$ values measured by the radar to give $\varepsilon_{turb}$ and $\overline{\varepsilon}$.

In their model calculations, VANZANDT et al. (1978) chose $L_o \approx 10$ m. It should be noted that $L_o$ is not equivalent to $L_B$ in (19). If $S = \omega_B^2/R$ is substituted in (31), as was proposed, then

$$L_o = 0{,}35\ \varepsilon^{1/2}\ \omega_B^{-3/2} \tag{34}$$

and comparison with (19) shows that

$$L_o = .035\ L_B \tag{35}$$

The difference arises because of the different definition used to define these "outer scales". $L_B$ is probably a better measure of the transition scale between the inertial and buoyancy subranges, but $L_o$ is quite appropriate wherever the formulae of TATARSKI (1961) are applied. This of course means that (31) and (4) are only applicable for $L_o$ as defined by TATARSKI (1961). The choice of $L_o = 10$ m used by VANZANDT et al. (1978) corresponds to a choice of $L_B$ of about 290 m. WEINSTOCK (1981) developed his theory relating $\varepsilon$ and $C_n^2$(radar) using $L_B$ as an estimate of the sum of the thicknesses of the turbulent layers in the radar volume, and achieved numerical results similar (to within a factor of 2) to those of GAGE et al. (1980).

It is also possible to apply (32) for the mesosphere, using $M_e$ (equation 16) in place of M. However, there are some problems in estimating F for this case. For example, CZECHOWSKY et al. (1979), using a 150 m resolution radar, have shown that at mesospheric altitudes of ≈80 km, the scattering layers can be quite thick (up to ≈1 km) and so F may approach unity. Further, at VHF the appropriate scattering scales may be within the viscous range, so (3) and hence (29) may not be applicable. At HF and MF radar wavelengths (e.g., $\lambda$ = 150 m), however, scatter should be from the inertial range and these formulae should be appropriate.

## DISCUSSION

Interestingly, RASTOGI and BOWHILL (1976) presented some formulae relating turbulence parameters to backscattered power, and concluded that for the mesosphere the backscattered power was independent of $\varepsilon$. They based their conclusions on dimensional arguments. However, these arguments were nowhere near

as rigorous as those presented in this paper, and it is felt that (32) more appropriately represents the relation between $\varepsilon$ and $C_n^2$. The appropriate generalized refractive index gradient can be obtained from (13) (troposphere and stratosphere) or (16) (mesosphere), provided that scatter can be assumed to be from within the inertial range of turbulence. It will be noted that (32) is indeed dimensionally correct, since $C_n^2$ has units of $m^{-2/3}$.

Direct, independent measurements of $\varepsilon$ and $C_n^2$(radar) have not been extensively made, so it is difficult to comment on the validity of these theories. Certainly, however, the estimates of $\varepsilon$ presented by GAGE et al. (1980) are of the correct order of magnitude.

Recently, HOCKING (1983a,b) has presented an alternative method for measurement of turbulent energy dissipation rates with radars. This utilizes not the signal strength backscattered, but the spectral widths of the received signal. The principle of the method has been known for many years (e.g., ATLAS, 1964; FRISCH and CLIFFORD, 1974; FRISCH and STRAUCH, 1976) but the major advance presented by HOCKING (1983a,b) was the accurate removal of both (i) spectral broadening due to the motion of the mean wind across the finite beamwidth and (ii) spectral "broadening" (or "narrowing" in some cases) due to vertical wind shears in the horizontal wind. These two factors have previously been considered separately (e.g., ATLAS, 1964), but never coherently. HOCKING (1983a) also illustrated that there was a necessity to distinguish between vertical and horizontal fluctuating motions, and showed how this could be done. This technique was illustrated using an HF radar to measure energy dissipation rates in the mesosphere.

The technique can readily be applied at VHF, and the author is currently doing this with the "SOUSY" radar (ROTTGER et al., 1978) in West Germany. The estimates of $\varepsilon$ appear to be of the correct order of magnitude, and will be reported separately in a later paper. Application of this method can allow independent comparisons of $\varepsilon$ and $C_n^2$(radar), and therefore can check the equation (32). This new method of obtaining involves less assumptions than (32), and may prove to be a more reliable method in the future. Previously, some authors made comparisons of signal fading time and received power (e.g., FUKAO et al., 1980a,b; RASTOGI and BOWHILL, 1976b), but it is difficult to decide how much the fading time (or equivalently the spectral width) is contaminated be beam- and wind-shear broadening. Therefore these measurements cannot really be regarded as comparison of $\varepsilon$ and $C_n^2$.

For approximate estimates of the effects of beam-broadening, the following formula may be useful. If $\theta_{1/2}$ is the half-power-half-width of the effective radar beam, and V is the mean velocity of the scatterers tangential to the beam (usually this amounts to the horizontal velocity), then the half-power spectral half-width due to beam broadening is

$$f_{1/2} = (1.0)2/\lambda\ \theta_{1/2} V \qquad (36)$$

This is very nearly exact, provided beam widths of less than 3° - 4° are used. A similar formula was presented by ATLAS (1964), and was originally derived by HITSCHFELD and DENNIS (1956). [Atlas gives an equation $\sigma_v = 0.3\ \theta V$. However, this equation is for the case in which the same radar is used for transmission and reception, and $\theta$ is the half-power-full-width for the transmitter (or receiving) polar diagram only. Thus $\theta$ in this equation is equal to $2\sqrt{2}$ times $\theta_{1/2}$ in (36), since $\theta_{1/2}$ there is the half-width for the effective polar diagram (transmitter and receiver polar diagram included).] For proper removal of beam-broadening and shear-broadening, however, the complete treatment presented by HOCKING (1983a) is recommended.

As discussed in the introduction, there may be problems with the assump-

tion of inertial range turbulence, and it is useful to list some of these. Specular reflection has already been mentioned, and the cause of this has not been fully explained. It is sometimes assumed to be a process separate from turbulence, but this may not be. For example, the model proposed by BOLGIANO (1968), which was discussed earlier, may be important. In this case, tilting the radar beam from the vertical may cause the layer to disappear, since one of the assumptions of Bolgiano's model was that turbulence mixes the layer so well that no parameters such as density vary with height within the layer. Thus the generalized refractive index gradient within the layer is close to zero, and very little radio-wave scatter from the turbulence itself can occur. If such layers do exist, and are not seen by tilted VHF radars, this could lead to biases in estimates of $\overline{\varepsilon}$ for the atmosphere. For vertically beamed radars, the relation between the specular scatter and the degree of turbulence may not be simple. Investigations of this matter await more experiments. The possibility that turbulence could be anisotropic even at scales of meters has also been briefly mentioned. Multifrequency experiments may help resolve some of these issues.

## CONCLUSIONS

If it is assumed that radio-wave scatter is from inertial range turbulence, then the back-scattered power and the energy dissipation rate can be simply related through equations (28) (or 29), (30), (32), (16), (19) and (33). The derivation of these equations assumed inertial range isotropic turbulence, and the scales within which this is probably true are indicated in Figure 1. Considerable experimental work remains to be done to determine when these relations are valid, and when they break down.

## ACKNOWLEDGEMENTS

This paper was written while the author was sponsored by an Alexander von Humboldt stipend.

## REFERENCES

Atlas, D. (1964), Advances in Geophysics, Vol 10, 317, Academic New York

Batchelor, G. K. (1953), The theory of homogeneous turbulence, Cambridge University Press, England.

Bolgiano, R. Jr. (1968), Winds and Turbulence in the Stratosphere, Mesosphere and Ionosphere, 371-400, North-Holland.

Booker, H. G., and W. E. Gordon (1950), Proc. IEEE, 38, 410-412.

Booker, H. G. (1956), J. Atmos. Terr. Phys., 8, 204-221.

Budden, K. G. (1965), Radio Science, 69D, 191-211.

Crane, R. K. (1980), Radio Science, 15, 177-194.

Czechowsky, P., R. Ruster and G. Schmidt (1979), Geophys. Res. Lett., 6, 459-462.

Frisch, A. S., and S. F. Clifford (1974), J. Atmos. Sci., 31, 1622-1628.

Frisch, A. S., and R. G. Strauch (1976), J. Appl. Met., 15, 1012-1017.

Fukao, S., K. Wakasugi and S. Kato (1980a), Radio Sci., 15, 431-438.

Fukao, S., T. Sato, R. M. Harper and S. Kato (1980b) Radio Sci., 15, 447-457.

Gage, K. S., and J. L. Green (1978), Radio Sci., 13, 991-1001.

Gage, K. S., and B. B. Balsley (1980), Radio Sci., 15, 243-257.

Gage, K. S., J. L. Green and T. E. VanZandt (1980), Radio Sci., 15, 407-416.

Good, R. E., B. J. Watkins, A. F. Quesada, J. H. Brown and G. B. Loriot (1982), Applied Optics, 21, 3373-3376.

Harper, R. M., and W. E. Gordon (1980), Radio Sci., 15, 195-212.

Hill, R. J., and S. F. Clifford (1978), J. Opt. Soc. Am., 68, 892-899.

Hill, R. J., and S. A. Bowhill (1979), J. Atmos. Terr. Phys., 41, 607-623.

Hitschfeld, W., and A. S. Dennis (1956), Measurement and calculation of fluctuations in radar echoes from snow, Scientific Report MW-23, McGill University, Montreal, Canada.

Hocking, W. K. (1980), An introduction to atmospheric turbulence (with particular emphasis on radio studies of turbulence), Physics Dept. University of Adelaide, Australia, report ADP164.

Hocking, W. K. (1981), Investigations of the movement and structure of D-region ionospheric irregularities, Ph.D. Thesis, University of Adelaide, Adelaide, Australia.

Hocking, W. K., and R. A. Vincent (1982), J. Atmos. Terr. Phys., 44, 843-854.

Hocking, W. K. (1983a), On the extraction of atmospheric turbulence parameters from radar backscatter Doppler spectra - I. Theory, J. Atmos. Terr. Phys., in press.

Hocking W. K. (1983b), Mesospheric turbulence intensities measured with a HF radar at 35 S, J. Atmos. Terr. Phys., in press.

Nastrom, G. D., K. S. Gage and B. B. Balsley (1982), Optical Eng., 21, 347-351.

Ottersten, H. (1969), Radio Sci., 12, 1251-1255.

Rastogi, P. K., and S. A. Bowhill (1976a), J. Atmos. Terr. Phys., 38, 399-411.

Rastogi, P. K., and S. A. Bowhill (1976b), J. Atmos. Terr. Phys., 38, 449-462.

Rottger, J., J. Klostermeyer, P. Czechowsky, R. Ruster and G. Schmidt (1978), Naturwissenschaften, 65, 285-296.

Rottger, J., and C. H. Liu (1978), Geophys. Res. Lett., 5, 357-360.

Rottger, J. (1980a), Radio Sci., 15, 259-276.

Rottger, J. (1980b), Pageoph., 118, 494-527.

Staras, H. (1952), J. Appl. Phys., 23, 1152-1156.

Tatarski, V. I. (1961), Wave propagation in a turbulent medium, McGraw Hill N. Y. Lond.

Tatarski, V. I. (1971), The effects of the turbulent atmosphere on wave propagation, Keter Press, Jerusalem.

VanZandt, T. E., J. L. Green, K. S. Gage and W. L. Clark (1978), Radio Sci., 13, 819-829.

VanZandt, T. E., K. S. Gage and J. M. Warnock (1981), Preprint vol., 20th Conf. on Radar Meteorology, Bost. Mass., Nov. 30 - Dec. 3.

Weinstock, J. (1978a), J. Atmos. Sci., 35, 634-649.

Weinstock, J. (1978b), J. Atmos. Sci., 35, 1022-1027.

Weinstock, J. (1981), Radio Sci., 16, 1401-1406.

# 4.6B RELATIONSHIP OF STRENGTH OF TURBULENCE TO RECEIVED POWER

J. Rottger

EISCAT Scientific Association
P.O. Box 705
S-98127 Kiruna, Sweden

Because of contributions due to reflection, the determination of the turbulence refractive index structure constant $C_n^2$ may be affected (e.g., ROTTGER, 1980). For pure scattering from turbulence in the inertial subrange the radar echo power can be used to calculate $C_n^2$, as applied in several investigations (e.g., GREEN et al., 1978; VANZANDT et al., 1978). The radar power is determined by the convolution

$$P \propto \int E^m(\psi_T - \psi, \theta_T - \theta)\, A(\psi_A - \psi, \theta_A - \theta) \cdot \sin\theta \, d\theta \, d\psi \qquad (1)$$

where $\psi$ is the elevation angle and $\theta$ the azimuth angle. The term $E^m$ is the pattern of the radar antenna pointing into the direction given by $\psi_T$ and $\theta_T$. The angular distribution $A(\psi_A - \psi, \theta_A - \theta)$ expresses the aspect sensitivity of the radar target, where the angles $\psi_A$ and $\theta_A$ determine a tilt of the target. Height variations of these parameters are not considered here for simplification. If the radar target is a scattering medium, $m = 1$. The distribution A determines the anisotropy of the scattering irregularities. If the radar target is an ideal reflector, $m = 2$, and A is given by the Dirac delta function. It is found from experiments that $1 < m < 2$, providing evidence that the radar echo power is given by a composition of scattering and reflection or by diffuse reflection.

It was assumed by VINCENT and ROTTGER (1980) that in a two-dimensional approach ($\theta$ = const), the aspect sensitivity can be expressed by a Gaussian angular distribution with its maximum near the zenith.

If one swings the antenna beam to sufficiently large off-zenith angles (>12.5°, e.g., Figure 9 in ROTTGER, 1980) so that a quasi-isotropic response from the tail ends of the Gaussian angular distribution can be anticipated, the evaluation of the integral (1) depends only on the known antenna pattern of the radar. This procedure, swinging the radar beam to attenuate the reflected component, may be called "angular or directional filtering". Under this condition of volume scattering, $m = 1$, and $A$ = const for isotropic scatterers. It has to be assumed, on the other hand, that the outer part of the angular distribution really is due to pure turbulence scattering and not due to diffuse reflection. The tilted antenna also may pick up reflected components from near the zenith through the sidelobes. This can be tested by the evaluation of the correlation function (e.g., RASTOGI and ROTTGER, 1982). This method applies a "time domain filtering" of the intensity time series but needs a very careful selection of the high pass filters. Provided that these two methods of angular and time domain filtering can be properly applied to separate the contribution from reflection and scattering and that VHF radars can determine if a volume is filled with homogeneous turbulence, it is accepted that reliable estimates of the refractive index structure constant and eddy dissipation rate due to turbulence can be deduced.

## REFERENCES

Green, J. L., K. S. Gage and T. E. VanZandt (1978), VHF Doppler radar studies of CAT in the troposphere and lower stratosphere, in: Proc. Conference on Atmospheric Environment of Aerospace Systems and Applied Meteorology, Amer. Meteorol. Soc., Boston.

Rastogi, P. K. and J. Rottger (1982), VHF radar observations of coherent reflections in the vicinity of the tropopause, J. Atmos. Terr. Phys., 44, 461-469.

Rottger, J. (1980), Reflection and scattering of VHF radar signals from atmospheric refractivity structures, Radio Sci., 15, 259-276.

VanZandt, T. E., J. L. Green, K. S. Gage and W. L. Clark (1978), Vertical profiles of refractivity turbulence structure constant: Comparison of observations by the Sunset radar with a new theoretical model, Radio Sci., 13, 819-829.

Vincent, R. A. and J. Rottger (1980), Spaced antenna VHF radar observations of tropospheric velocities and irregularities, Radio Sci., 15, 319-335.

## 4.6C ON THE EXTRACTION OF ATMOSPHERIC TURBULENCE PARAMETERS FROM RADAR BACKSCATTER DOPPLER SPECTRA - I. THEORY

W. K. Hocking

Max-Planck-Institut fur Aeronomie
D-3411 Katlenburg-Lindau
Federal Republic of Germany

The following abstract is taken from this paper which was published in the Journal of Atmospheric and Terrestrial Physics, Vol. 45, No. 2/3, 89-102, 1983.

ABSTRACT

A theory is developed for the extraction of r.m.s. velocities of scatterer motions from spectra measured with a Doppler backscatter radar. The effects of finite beam-widths, finite pulse lengths, beam broadening, shear broadening and other such spectral 'contaminants' are considered. It is shown that these 'contaminants' can play a major role in determining the measured spectral widths (and, equivalently, the signal fading time), and so must be properly considered if the spectral widths are to be used to extract the r.m.s. motions of the scatterers. It is also shown that these r.m.s. motions can be used to estimate turbulence intensities, in those cases where turbulence is the dominant cause of the scatterer motions.

## 4.6D MESOSPHERIC TURBULENCE INTENSITIES MEASURED WITH A HF RADAR AT 35°S - II

W. K. Hocking

Max-Planck-Institut fur Aeronomie
D-3411 Katlenburg-Lindau
Federal Republic of Germany

The following abstract is taken from this paper which was published in the Journal of Atmospheric and Terrestrial Physics, Vol. 45, No. 2/3, 103-114, 1983.

ABSTRACT

A theory has been developed for extraction of turbulence energy dissipation rates from spectra measured with a radar. It was shown that factors apart from turbulence contribute to the observed spectral widths, and that these factors must be considered if accurate estimates of energy dissipation rates are to be obtained. In particular, beam-width broadening and shear broadening were important. In this paper, the first results obtained with this theory are presented. The rules were obtained using the large HF array at Adelaide, Australia, primarily during the southern hemisphere winter of 1981. Results are consistent with rocket measurements of turbulence, with typical values varying between 0.01 and 0.2 W $kg^{-1}$ at 80-90 km altitude.

# 5.1A CAPABILITIES AND LIMITATIONS OF EISCAT AS AN MST RADAR

J. Rottger*, M. Baron**, K. Folkestad***

*EISCAT Scientific Association, Box 705, S-98127 Kiruna, Sweden
**SRI International, 333 Ravenswood Avenue, Menlo Park, CA 94025
***The Norwegian Defence Research Establishment, Box 25-N-2007, Kjeller, Norway

EISCAT is the European Incoherent Scatter radar facility established and operated by research institutions of Finland, France, W. Germany, Norway, Sweden, and the United Kingdom. Its facilities, which also can be used for coherent scatter research of the middle atmosphere, are located in Northern Scandinavia.

The observatory consists of two independent systems which will allow observations of the upper, middle and lower atmosphere: a tri-static UHF radar capable of vector drift measurements, and a monostatic VHF system. The geographic locations of the installations are shown in Figure 1. Ramfjordmoen, near Tromso, Norway, is the transmitter location for both systems. The additional receiver sites for the tristatic system are Kiruna, Sweden, and Sodankyla, Finland.

## TRANSMITTERS

The transmitter characteristics are shown in Table 1. Each is capable of CW or phase-coded pulses, in single- and multi-pulse sequences. The transmitted frequency can be changed from pulse to pulse or within a pulse, providing great flexibility in designing pulse codes.

Both transmitters employ klystrons as final power amplifiers: one tube in the UHF system and two tubes in the VHF system. The UHF system started its operation in summer 1981, but still has not yet reached its final reliability because of remaining transmitter problems. The VHF transmitter is still under construction. Since both systems are basically developed for ionospheric incoherent-scatter investigations, they are not yet too suitable for middle atmosphere investigations. Some modifications, such as fast T/R switching and short pulses, are feasible and shall be applied in future.

Because of the dual tube VHF configuration, the polarization of the transmitted signal may be easily changed by altering the phase relationship between the low-power RF signals driving the two klystrons.

## ANTENNAS

The UHF antennas (Table 2) are identical fully steerable parabolic dishes having Cassegrain feeds. The feed horn design is somewhat different at the transmitter site. A polarizer preceding the feed horn enables the transmitted/received polarization to be made circular, linear or elliptical to optimize the experimental arrangement (for a multi-static system, the optimum polarization is a function of site location and pointing angles). The polarizer settings are controlled by motor-driven phase changers.

With the narrow beam widths of the tristatic system, accurate pointing is essential in order to have the beams intersect in space. Small misalignments of each antenna's true pointing direction relative to the encoder readings are measured by systematic tracking of known radio stars. A model, fitted to the measurements, is used to correct the antenna pointing directions, also taking

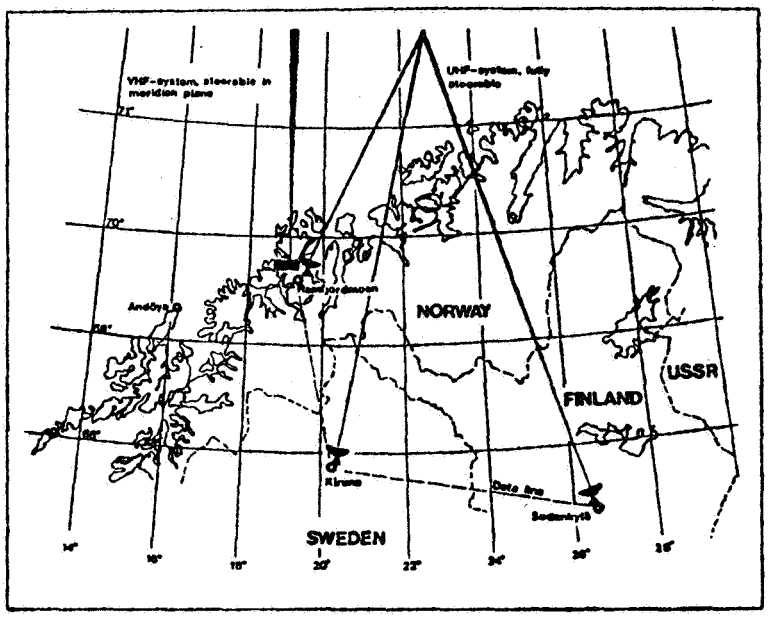


Figure 1. The EISCAT system in Northern Scandinavia.

Table 1 Characteristics of the EISCAT transmitters

| | UHF | VHF |
|---|---|---|
| Frequencies | 933.5 ± 3.5 MHz | 224.0 ± 1.75 MHz |
| Frequency steps | 0.5 MHz | 0.25 MHz |
| Peak power | 2 MW | 5 MW |
| Average power | 250 kW | 625 kW |
| Pulse lengths | 2 μs - 10 ms | 10 μs - 1 ms |
| Pulse repetition frequencies | 0 - 1000 Hz | 0 - 1000 Hz |
| Maximum duty cycle | 12.5% | 12.5% |

Table 2 UHF antenna specifications

| | |
|---|---|
| Diameter of main reflector | 32 m |
| Diameter of subreflector | 4.6 m |
| Overall efficiencey | 0.65 |
| Half-power beam width | 0.6° |
| Gain | 48 dB |
| Speed of mechanical movement | 80°/min |

into account tropospheric refraction, which is essential at low elevation angles.

The VHF antenna is a parabolic cylinder consisting of four identical 30 m x 40 m elements. The antenna may be operated in two modes. In mode I, the four elements are mechanically aligned and move together as one antenna. In this mode the antenna may radiate right or left circular polarization with the possibility of changing polarization from pulse to pulse or within a pulse. Linear polarization with the field $\pm 45°$ to the antenna axis may also be used. In mode II, the split-beam option, the four individual reflector elements act in pairs, producing two independent beams. Only left circular polarization is possible in this mode. By mechanical motion of the cylinder elements the beam can be steered 30° south and 60° north of the zenith in the meridional plane.

The VHF antenna is fed by a linear array of 128 crossed dipoles. The beam may be steered 21° from broadside by manually changing phasing cables to the dipoles. The VHF antenna is operational at the Tromso site and its characteristics are summarized in Table 3.

## RECEIVERS

To minimize the system noise, the UHF front-end receivers are installed in instrument cabins immediately behind the feed horns of the antennas. At Kiruna and Sodankyla, helium-cooled parametric amplifiers are used, yielding an overall system noise temperature of about 40 K. At the transmitter site, the first stage of the receiver is an uncooled GaAs-FET amplifier, resulting in an overall system noise temperature of about 140 K.

The received signals are converted to an intermediate frequency of 120 MHz before being channelled to the main buildings for further down-conversion to 30 MHz second IF, filtering and processing.

The back-end receivers at each station consist of 8 channels for simultaneous reception of up to 8 transmitted frequencies. On each channel the signal is detected in quadrature. A complement of Bessel and Butterworth filters with several band widths is available.

The detected and filtered signals are fed to 8-bit A/D converters capable of independently sampling the 8 receiver channels at rates up to 500 kHz. If a phase-coded pulse is used, the samples are transferred to a decoder matched to a 13-bit Barker code. Otherwise, the decoder is bypassed and the samples passed directly to the correlator.

Table 3 VHF antenna characteristics

| | |
|---|---|
| Orientation of plane of mechanical movement | 0.5° west of north |
| Effective area in mode I, broadside: | |
| - Circular, calculated | 3250 $m^2$ |
| - Horizontal, measured | 3330 $\pm$ 240 $m^2$ |
| - Vertical, measured | 2890 $\pm$ 210 $m^2$ |
| Beam widths, calculated for broadside: | |
| - Mode I | 0.6° east/west<br>1.7° north/south |
| - Mode II | 1.2° east/west<br>1.7° north/south |
| Range of steering in transit plane | 30° south to 60° north of zenith |
| Speed of mechanical movement | 5°/min |

For the VHF system where the sky noise is 100-200 K, transistor amplifiers are sufficient for the receiver front-end. Otherwise, the receiving system is identical to the UHF one, except of different intermediate frequencies.

## CORRELATORS

As described earlier, most of the information from the radar echoes is obtained from the spectrum. The same information, of course, is also contained in the complex autocorrelation function of the received signal. The EISCAT signal processing system is configured around a fast digital correlator. The correlator is a special purpose micro-programmable computer capable of handling the large number of multiplications and additions involved in calculating the complex correlation function. It operates at a clock-rate of 5 MHz and has a pipeline structure enabling parallel processing with a through-put rate of 50 Mega operations/sec. Its input buffer has 4 k memory for real and imaginary part. After calculation of the correlation function (ACFs), these can be integrated over software specified integration periods. The result memory covers 2 k words with 32 bit per real and imaginary part of the ACFs. Input buffer and result memory are extendable.

## RADAR CONTROLLERS

All high-precision timing signals used to pulse control transmitter, receiver, ADC etc., are generated by a radar controller, one unit assigned to the VHF system and one at each site for the UHF radar. The central component is a 4 k word matrix of 2 x 16 words. Half of the matrix constitutes the "Instruction timetable", ITT, the other half the "Instruction table", IT. Each of the bits 0-13 is routed to a signal line having a particular control function in the transmit-receive operations. For instance, while the radar controller is in the transmit mode, defined by bit 14 being set, bit number 11 controls the RF modulation; the klystron beam is switched on upon setting of bit 12. The elements in the "dwell time array", ITT, determine how long (in μs) the corresponding instructions in the complementary array, IT, are to last.

The radar controller is programmed in a high-level language called TARLAN (Transmission And Receiver LANguage). Instructions are transferred by the TARLAN compiler into a bit pattern corresponding to the IT and ITT tables which determine the state of the signal lines. The tables are then loaded, on command, from the sites' general purpose computer into the radar controller.

## FREQUENCY AND TIMING STANDARDS

Because the EISCAT UHF radar is a pulsed tristatic system, timing at the three sites must be synchronized to within a few microseconds. For this purpose, each EISCAT station is equipped with a Cesium standard giving the frequencies 1, 5 and 10 MHz with an accuracy specified as $10^{-11}$. A fourth standard is available as a "travelling clock" for occasional comparison and adjustments. Long-term variations in the standards are corrected by noting the trend in long-term comparisons of the Cesium signals with Loran C signals received at 100 kHz from a transmitter in Vesteralen, Norway.

A real-time clock takes its input from the Cesium standard and feeds the radar controller with suitably shaped second-pulses. A provision is made in the clock for delaying the second-pulse in microsecond steps to compensate for long-term drifts in the standards and for the difference in propagation time

for the scatter volume to the different sites. The delay is computed and set by the routines governing the antenna pointing.

## COMPUTERS AND INTER-SITE COMMUNICATION

At the transmitter station there is a Norsk Data NORD-10S computer with two 75 Megabyte discs. In addition, each station has a NORD-10 computer, having 128 k word memory, two 10 Megabyte discs and a standard complement of peripheral equipment, e.g., 1600 bpi tape drives. The standardized interfacing system CAMAC is used for interchanging data and control signals between the computer and the devices and processes which it serves. Permanent telephone lines operating at 9600 baud link the three site computers together, allowing for mutual transfer of programme routines and data. For scientific data analysis, EISCAT shares a larger computer, NORD 500, with the Kiruna Geophysical Institute.

## ON-LINE DISPLAYS

Display software has been developed to use the on-site graphical terminals for real-time quick-look assessment of the quality of the received data. These displays have proved to be almost indispensable in supervising the operational states of the equipment during experiments. Options exist for plotting the complex autocorrelation functions, power spectra, and received signal as a function of range. All may be displayed with or without noise subtraction and for one of many range gates. The display also contains housekeeping information (e.g., time, antenna position) and system parameters (e.g., transmitted power and system temperature). Monitoring of operations at all three sites can be (sequentially) done from any one site through inter-computer transfer of the data.

## REAL-TIME OPERATING SYSTEM

The EISCAT system, while performing experiments, is almost entirely computer controlled by EROS, which is the acronym for EISCAT's Real-time Operating System. To the user EROS appears as an assembly of high-level commands, about 75 altogether, for pointing antennas, setting the receivers, loading and controlling the correlators and the radar controllers, handling tapes and data transfer, activating and terminating real-time programmes and experiments. Using EROS in the remote mode at one station, one may control system parameters at one or both of the other two sites. This feature provides the possibility for supervising the operations at all three stations from one site.

A detailed technical description of the EISCAT facility can be found in an article by FOLKESTAD et al. (1983).

## MIDDLE ATMOSPHERE OBSERVATIONS WITH THE EISCAT UHF RADAR

First stratosphere and mesosphere echoes were detected with the EISCAT UHF radar in summer 1982 after a special correlator program for coherent signals (pulse-to-pulse correlation) was prepared (Kofman, 1982). These experiments yielded basic experiences on the capabilities of the UHF radar for middle atmosphere research.

## STRATOSPHERE

In contrast to incoherent scatter from the ionosphere, the stratosphere echoes are due to coherent scatter from clear air turbulence. Because of the not yet optimized transmit-receive switching, some limitations exist in the

monostatic mode when observing at short ranges. To records echoes from the stratosphere, the antenna has to be pointed at fairly low elevation angles below about 20°. Then problems arise because of ground clutter and shielding due to the mountains surrounding Tromso. The shielding also sets limits for bistatic observations. The elevation of the mountain ridges can be read from the horizon profile of Figure 2.

An example of stratospheric records is shown in Figure 3 which depicts a typical real-time display of autocorrelation functions (ACFs) and spectra for subsequent range gates. During this test operation on 3 August 1982, 2055 UT, the antenna pointed at 17.4° elevation and 325° azimuth. The transmitter was operated with 750 kW pulse peak power and 4% duty cycle. The pulse repetition rate was 1 ms and the pulse length 40 μs. The first range gate was at 400 μs, corresponding to 54 km (considering 40 μs post-detection filter delay). This corresponds to the lowest sampled height at 16.4 km and a height resolution of 1.8 km. It evidently can be seen that receiver transition (saturation) effects occur out to range gate 2, corresponding to 440 μs. This value obviously has to be improved in future experiments.

The records of Figure 3 clearly show evaluable echoes out to heights of about 22 km. The signal-to-noise ratio at this height is around 0 dB. Not too much signal power can be expected here because of the viscous subrange limitations discussed earlier. However, first test measurements in the bistatic mode prove that signals can be detected from maximum heights up to 30 km, because the Bragg wavelength is greater in this mode. This will allow measurements of vertical velocity and turbulence intensity up to the middle stratosphere.

The off-set of the power or Doppler spectra in Figure 3 proves that the signals are due to scatter from clear air turbulence carried by the background wind. This very clearly can be seen when operating the radar in the velocity-azimuth-display (VAD) mode, as shown in Figure 4. The change in sign of Doppler frequency when rotating the azimuth by 180° (upper diagrams) is obvious. Rotating the azimuth in steps of 20° and plotting the mean values of the spectra in the lower diagram of Figure 4 proves the expected sinusoidal variation. The mean wind speed of 4 m $s^{-1}$ and direction from east, deduced from these radar data, is consistent with radiosonde wind data of Sodankyla.

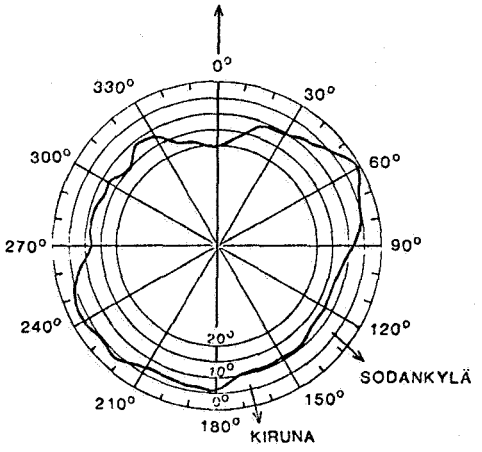


Figure 2. Horizon profile for the UHF transmitter at Tromso. The elevation scale extends from 0° to 20°.

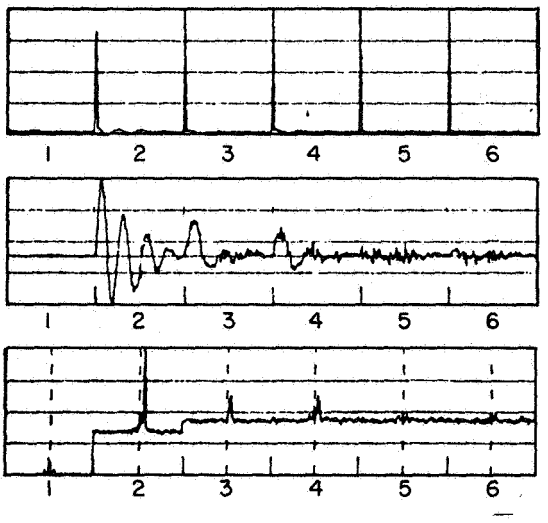


Figure 3. Autocorrelation functions (upper diagram: real part, center diagram: imaginary part) and power spectra (lower diagram) of stratosphere signals. Numbers denote range gates, corresponding to altitudes 16.4 (1), 18.2 (2), 20.0 (3), 21.8 (4), 23.6 (5) and 25.4 km. Receiver saturation is evident in range gates 1 and 2, signals disappear in gates 5 and 6. The ACFs were postintegrated over 30 s.

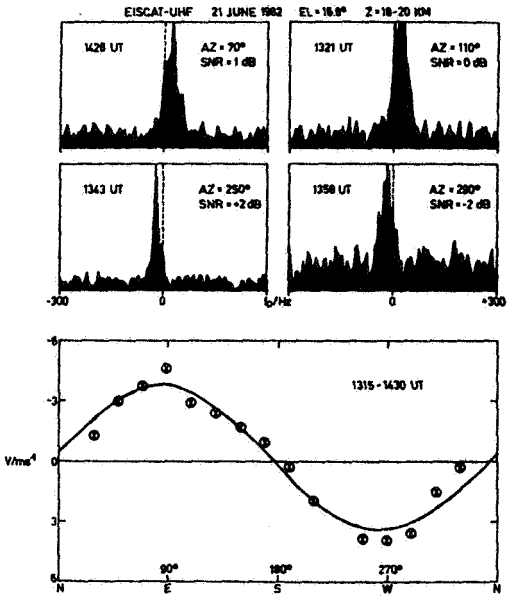


Figure 4. Spectra of stratosphere echoes (upper part), averaged over 30 s, and velocity-azimuth display in lower part.

MESOSPHERE

Signals from mesospheric altitudes were also observed in the monostatic and bistatic mode. In an extended series of operations to support the rocket campaign CAMP (Cold Arctic Meso-Pause) at Esrange in July/August 1982, a fairly clear view on the occurrence frequency of these mesospheric echoes was obtained. Their appearance was mostly limited to a short duration up to some ten minutes, intense echoes often were connected with high absorption events recorded with riometers. It is fairly evident, therefore, that the mesospheric echoes are due to incoherent scatter from D-region ionization which was enhanced by high-energy particle precipitation. The comparison of the riometer reading and the average signal power (Figure 5), received from a scattering volume at 88 km altitude half the way between Tromso and Sodankyula, clearly indicates the correlation between these two measurements. Although an absolute calibration of the electron density in the probed volume is not yet done, it is found that the ionization had increased shortly by almost three orders of magnitude during the peak of the precipitation event.

The pulse-to-pulse correlation scheme allowed for the first time to measure the ion component spectra of these events (Figure 6). The signal-to-noise ratio was fairly low (-10 dB), but significant spectra were detected between 2135-2140 UT. In Figure 7 spectra-time intensity plots are shown which were obtained from monostatic observations at an elevation angle of 40°. The spectra exhibit a displacement when turning the antenna from south to west and v.v. This is caused by a wind, and the wind profile deduced from these data is consistent with mean circulation models. Since the spectra which are averaged over 10 s are each normalized to the peak power, these plots also indicate the signal-to-noise ratio. This obviously increased when the antenna turned to north, which is explained by a north-south gradient of the electron density in the D region. The spectral width is dependent on the temperature, collision frequency, and negative ion to electron ratio. Under model assumptions on two of these parameters, the remaining parameter can be deducted. By these means

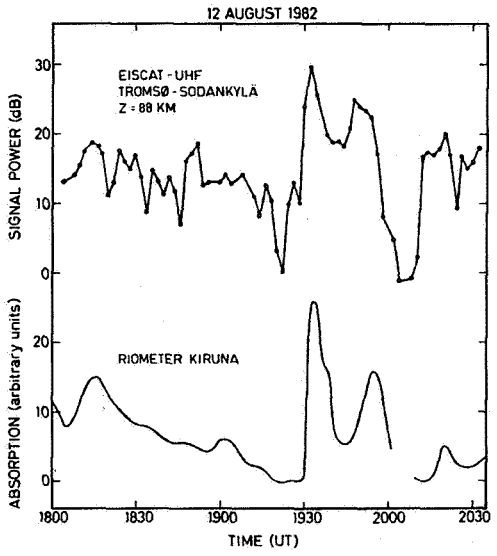


Figure 5. Incoherent-scatter signal power compared with riometer data.

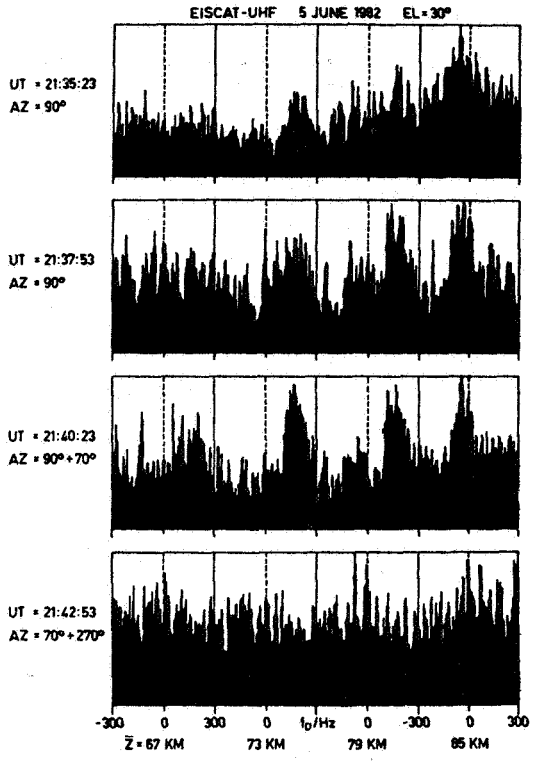


Figure 6. Spectra (2.5 min averages) of incoherent-scatter returns from the D region, obtained in the monostatic mode with 1.2 MW pulse peak power.

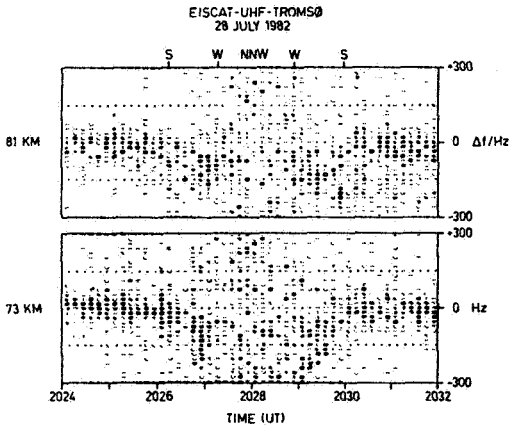


Figure 7. Spectra-time intensity plots of incoherent-scatter echoes. Between 2026 and 2030 UT the azimuth of the antenna was rotated, leading to a displacement and a disappearance of the spectra.

it may be possible to find indications on negative ions. In continuing these analyses, a unique chance exists to compare these EISCAT measurements with simultaneous in situ probes by rockets flown during the CAMP campaign.

## CONTRIBUTIONS TO FUTURE RESEARCH OF THE M.A.

The analysis of about 60 hours of middle atmosphere observations in 1982 leads to the conclusion that EISCAT's capabilities to measure mesospheric parameters will improve during moderately or strongly disturbed conditions. It then will be possible to measure profiles (with height resolution down to about 1 km) of wind velocity, electron density, and temperature/collision frequency. It also should be possible in some instances to determine ion masses. The accuracy of these partly interdependent estimates will strongly improve by having available information on temperature or collision frequency and ion mass from other experiments. Of course, observations of these parameters in the lower thermosphere (90-130 km) are possible with EISCAT even under fairly undisturbed conditions. The steerability of the UHF system will allow to measure the geographical distribution of some scalar parameters within some 100 km distance around Tromso.

By recording in the monostatic VAD mode (velocity-azimuth display), stratospheric wind velocities up to the maximum height of 24 km can be recorded. In the bistatic mode, echoes from stratospheric heights up to about 30 km can be received and estimates of the vertical velocity and turbulence refractive index constant can be deduced.

More details on experiments to investigate the middle atmosphere with EISCAT and the interpretation of coherent and incoherent scatter echoes are discussed in a paper by ROTTGER (1983).

The EISCAT Scientific Association is funded and operated by Suomen Akatemia/Finland, Centre Nationale de la Recherche Scientifique/France, Max-Planck-Gesellschaft/W. Germany, Norges Naturvitenskapelige Forskningsrad/ Norway, Naturvetenskapliga Forskningsradet/Sweden and Science and Engineering Research Council/United Kingdom.

(References in this paper are included in the Publications listed below).

## PUBLICATIONS RELATED TO EISCAT MST CAPABILITIES

Folkestad, K., T. Hagfors and S. Westerlund (1983), EISCAT - an updated description of technical characteristics and operational capabilities, Radio Sci., 18, 867-879.

Kofman, W. (1982), A mesospheric experiment: measurement scheme and program implementation, EISCAT Techn. Note 82/35, EISCAT-HQ, Kiruna, Sweden.

Kofman, W., F. Bertin, A. Crenieu, J. Rottger and P. J. S. Williams (1983), The EISCAT Mesospheric Measurements during the CAMP Campaign, IAMAP/IAGA Symposium during IUGG Assembly, Hamburg, August 1983.

Rottger, J. (1983), The use of the EISCAT radar facility for middle atmosphere research, Proc. 6th ESA Symposium on European Sounding-Rocket and Balloon Research (to be published).

Rottger, J. (1983), Some capabilities of the EISCAT UHF radar for investigation of the stratosphere, Preprint Volume 21th Conference on Radar Meteorology, (in press).

# 5.2A CAPABILITIES AND LIMITATIONS OF THE JICAMARCA RADAR AS AN MST RADAR

R. F. Woodman*, and D. T. Farley**

*Institute Geofisico del Peru, Apartado 3747, Lima, Peru
**Phillips Hall, Cornell University, Ithaca, NY 14853

## LOCATION

The Jicamarca radar (Long. 76.52W, Lat. 11.56S) is located at 20 km from Lima at approximately 500 meters over sea level. It is surrounded by mountains which provide a good shield from man-made interference. The radio horizon goes from a few hundred meters, across the dry valley where it is located, to 15 km, along the valley in the direction of the continental divide. This limits the clutter to 15 km, except for one high peak at 21 km. It is the most equatorial of all existing MST radars. Its proximity to the Andes, makes its location unique for the study of lee waves and orographic-induced turbulence.

## ANTENNA

The Jicamarca antenna is the largest radar antenna in the world. It is a flat and almost horizontal array of cross-dipoles, covering an area of 300 m by 300 m (9 Ha). It has a center frequency of 50 MHz with a bandwidth of 1 MHz (determined by power combiners and splitters at the feed point of the antenna).

The antenna consists of 64 identical and fixed squared modules of 144 cross-dipoles each. They are grouped into 4 squared sections with 2 independent feeds for each quarter, one for each linear polarization. Steering of the full antenna, or of each of the quarters, can be accomplished by manually inserting phasing cables into each of the modules. Each linear polarization can be steered independently, at both the quarter and full antenna level. Maximum practical steering is $\pm 3°$ from the on-axis position. On-axis position is 1.4° to the SW from zenith. Exact vertical pointing can be achieved with a special set of cables. Positions $\pm 3°$ from zenith have been used to determine vertical and E-W and N-W projections of MST horizontal velocities (WOODMAN and GUILLEN, 1974). Full aperture radar beam width is of the order of 0.5 degrees. This is an important parameter for MST spectral width interpretation, since it reduces the effect of beam width spectral broadening to a fraction of turbulent broadening.

Maximum power handling capacity is at least 6 MW.

Performance of the antenna is very close to that of a full squared aperture with an ohmic efficiency of 0.8-0.9.

Vertical as well as horizontal projections of MST velocities are obtained by simultaneously pointing with different sections of the antenna into 3 or 4 different directions. Usually positions at $\pm 3°$ and north or south from the on-axis vertical position are used for this purpose.

The possibility of splitting the antenna into different sections permits observations in an interferometer mode to determine size, position and velocity of structure smaller than the beam width (RUSTER and WOODMAN, 1976).

## TRANSMITTERS

The transmitting system consists of a battery of 4 independent transmitters with a nominal power of 1.5 MW each. Maximum real obtainable power, when the tubes are new is of the order of 4 MW total. Maximum duty cycle is

5%, which translates into 200 kW of average power.

The output power of the transmitters can be combined, or split, in a variety of modes to feed either the full antenna or fractions of each, forming in this way independent transmitter-antenna units. The relative phase of the transmitters can be changed at exitation level permitting the synthetization of different polarization via Hybrid combiners.

The bandwidth of the transmitters is limited by a fairly large cathode to grid capacitance, which, when turned, produces a high Q circuit with a bandwidth of the order of 50 kHz. This relative narrow bandwidth limits the altitude resolution to ≃2 km.

The combination of antenna size, power and frequency makes Jicamarca the most sensitive MST radar in the world. Even at this level, its sensitivity to obtain echoes at 45-km altitude is marginal.

The operating frequency at 50 MHz is an asset. Given sufficient power aperture product the maximum altitude obtainable by an MST radar is determined by the altitude at which the turbulence inner scale is comparable to the radars wavelength. The longer the wavelength the higher the altitude.

The Jicamarca radar is the only MST radar in existence which can obtain echoes all the way from tropospheric to mesospheric altitudes, including a region of very weak echoes around 45-km altitude.

A part of the large power transmitters, there are four smaller transmitters, similar to the ones used at the Poker Flat array. Each unit is capable of transmitting 10 kW of peak power at 1% maximum duty cycle. Their bandwidth is much wider than the larger transmitters, permitting 1 μsec pulses which correspond to 150 meter resolution.

Recently, one ot the 1 MW transmitters has been modified to take a different final amplifier tube. The new tubes, apart from costing a fraction of the cost of the present ones, has one order of magnitude wider baudwidth. Preliminary tests with the new design indicate that 1.5 MW peak power and 1 μsec rise could be obtained. At present the only limitation of the radar for optimum MST observations is its reduced altitude resolution. With the new modifications a 150-meter resolution will be achieved with the largest power aperture of all MST radars.

## RECEIVERS

There are 4 independent receivers, sharing a common L.O. Signals are converted to a 30 MHz IF, where most amplification is performed and then converted down to two quadrature signals (complex coherent detection) at zero frequency. Bandwidth is determined at this level with Bessel filters. They are manually adjusted to match 1, 3, 5, 10, 30, 50, 100, 300 or 500 μsec pulses. Receiver noise figure is of the order of 3 dB. But signal sensitivity at these frequencies is determined by sky noise.

## DATA ACQUISITION, PROCESSING AND CONTROL

Data acquisition, processing and control is based on a general-purpose computer and two in-house-designed units, one for control of the radar and sampling and the other for data acquisition.

The computer is Harris/6 model, with 156 kiloword (24 bit) of memory running under a Vulcan System. It has two disk units with 80 Megabytes of

storing capacity each. Bulk recording is made on a 25 in/sec tape recorder for 800 and 1600 bbi/sec (three other 24/sec, 800 bbi. Transports from a previous unit are being modified and integrated.) There are two CRT, 1 graphics, 1 alphanumeric terminals and 2 Heathkits Z-81 microcomputers connected to the computer. Usually two, one CRT and one graphics, are assigned to the radar for operations. There is a Versatec electrostatic and an Annadex dot-matrix printer, both with graphic possibilities, connected to the system.

The data acquistion system is under development. A minimum working configuration is already in operation. Plans include a preprocessor, capable of coherent integrating and other incoherent scatter processing operations, which is now under construction.

The working configuration consists of an 8 bit ADC with a maximum converting speed of 20 Mega-samples per second. Eight channels can be sampled and processed simultaneously. The 8 input signals are connected to 8 sample-and-hold units whose output is multiplexed into the ADC. The ADCs are now connected to a computer channel assigned exclusively to this function, eventually through a buffer memory and preprocessor. Maximum input rate into the computer is closed to 1.2 megabytes per second. When the buffer memory of the preprocessor becomes operational, the maximum sampling rate will be .8 $\mu sec^{-1}$ for two receiver channels in parallel corresponding to a maximum resolution of 125 meters.

The radar controller is designed around the original idea of the first radar controller built at Jicamarca, now a popular scheme in many incoherent scatter and MST radars. A sequence of two parallel words, one defining the state of 8 control lines and the other the duration of the state, are read consecutively from a memory unit preprogrammed by the main computer.

Experiments can be pre-scheduled using a Harris Job Control language sequence which is defined by the user. At any time, the defining parameters can be changed interactively by editing the contents of a software panel which is displayed continuously on a CRT and contains all variable parameters. These parameters can also be preset by editing a set of the panels to be used in an experiment beforehand, in accordance with the requirements. Usual observing programs are provided by the Observatory. The user can also write his own programs. There are existing real-time data acquisition and control subroutines, which relieve the user from the need of familiarizing himself with the computer and data-acquisition system. (See Figure 1 for schematic diagram of the Jicamarca radar.)

(The reference in this paper is included in the Publications listed below.)

PUBLICATIONS RELATED TO THE JICAMARCA MST RADAR

Ochs, G. R., (1965), The large 50 Mc/s dipole array at Jicamarca radar observatory, NBS Rep. 8772, 61pp., U.S. Dept. of Commer. Nat. Bur. of Stand. Boulder, Colorado.

Woodman, R. F., and A. Guillen (1974), Radar observations of winds and turbulence in the stratosphere and mesosphere, J. Atmos. Sci., 31, 493-505.

Rastogi, P. K., and R. F. Woodman (1974), Mesospheric studies using the Jicamarca incoherent-scatter radar, J. Atmos. Terr. Phys., 36, 1217-1231.

Ruster, R., and R. F. Woodman, Radar measurements in the tropo-strato- and mesosphere, Proceedings AMS 19th Conf. on Radar Meteorology, Oct., 1976 Seattle, Wash.

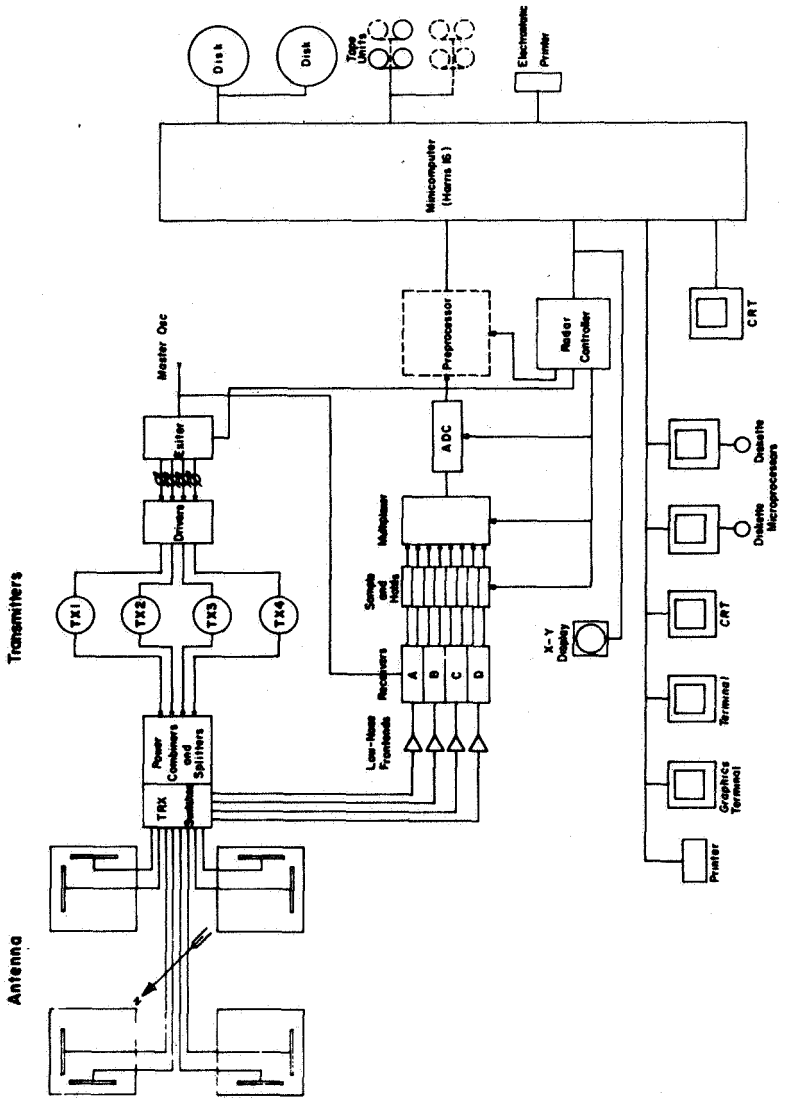


Figure 1. Schematic diagram of the Jicamarca radar.

Rastogi, P. K., and S. A. Bowhill (1976a), Gravity waves in the equatorial mesosphere, J. Atmos. Terr. Phys., 38, 51-60.

Rastogi, P. K., and S. A. Bowhill (1976b), Scattering of radio waves from the mesosphere-1. Theory and observations, J. Atmos. Terr. Phys., 38, 399-411.

Rastogi, P. K., and S. A. Bowhill (1976c), Scattering of radio waves from the mesosphere-2. Evidence for intermittent mesospheric turbulence, J. Atmos. Terr. Phys., 38, 449-462.

Fleisch, D. A. (1976), Stratospheric scattering of radio waves and the Jicamarca radio telescope, M.S. thesis, Rice Univ., Houston, Texas.

Harper, R. M., and R. F. Woodman (1977), Preliminary multiheight radar observations of waves and winds in the mesosphere over Jicamarca, J. Atmos. Terr. Phys., 39, 959-963.

Fukao, S., S. Kato, S. Yokoi, R. M. Harper, R. F. Woodman and W. E. Gordon (1978), One full-day radar measurement of lower stratospheric winds over Jicamarca, J. Atmos. Terr. Phys., 40, 1331-1337.

Fukao, S., T. Sato, S. Kato, R. M. Harper, R. F. Woodman and W. E. Gordon (1979), Mesospheric winds and waves over Jicamarca on May 23-24, 1974, J. Geophys. Res., 84, 4379-4386.

Countryman, I. D., and S. A. Bowhill (1979), Wind and wave observations in the mesosphere using coherent-scatter radar, Aeronomy Rep. No. 89, Aeronomy Lab., Dept. Elec. Eng., Univ. of Ill., Urbana-Champaign.

Fukao, S., K. Wakasugi, and S. Kato (1980), Radar measurement of short period atmospheric waves and related scattering properties at the altitude of 13-25 km over Jicamarca, Radio Sci., 15, 431-438.

Fukao, S., T. Sato, R. M. Harper, and S. Kato (1980), Radio wave scattering from the tropical mesosphere observed with the Jicamarca radar, Radio Sci., 447-457.

Fukao, S., T. Sato, I. Hirota, and S. Kato (1980), A preliminary radar observation of long-period waves in the tropical mesosphere over Jicamarca, J. Geophys. Res., 85, 1955-1957.

Countryman, I. D., and P. M. Dolas (1982), Observations on tides in the equatorial atmosphere, J. Geophys. Res., 87, 1336-1342.

# 5.3A CHARACTERISTICS OF SUNSET RADAR

J. L. Green

NOAA, Aeronomy Laboratory
325 Broadway
Boulder, CO 80303

The Sunset radar is a VHF, pulsed Doppler radar located in a narrow canyon near the Sunset townsite 15 km west of Boulder, CO. This facility is operated by the Aeronomy Laboratory, ERL, NOAA, exclusively for meteorological research and the development of the MST and ST radar technique.

## ANTENNA

The antenna system consists of two colocated arrays, each containing 16 lines of coaxial-colinear dipoles. One of these arrays can be steered in the N-S vertical plane and the other in the E-W plane. The phase progression necessary for steering the antenna beam is provided by the insertion of remotely controlled phase shifters in the transmission line to each line of dipoles. The phase shifters have binary format (i.e., phase increments of $\lambda/2$, $\lambda/4$,..... $\lambda/256$ can be summed). The practical range of beam steering for meteorological experiments is $\pm 45$ due to the loss of antenna gain with increasing zenith angle. The beam steering increment near the zenith is 0.4° to take advantage of the sharp nulls in the antenna pattern. The phase shifters also perform the switching between the two arrays. Each phase shifter is controlled by the on-line computer.

## DATA PROCESSING

On-line data processing is performed by a Nova 800 computer. This computer provides radar control, antenna steering control, spectral analysis by a FFT algorithm, spectral averaging, on-line spectral plotting, and output to a tape recorder and a hard copy unit. Control of the radar is by a "menu" subroutine that allows immediate changes in range gate altitudes, range gate length, number of spectra averaged, and antenna beam position. Sequences of antenna positions may also be specified.

Coherent averaging is provided by analogue filters on each of the 16 range gates. The effects of ground clutter are reduced by a 0 - 0.1 Hz notch in the response of these filters. Coherent averaging is especially effective because of the high pulse repetition frequency of the radar (typically 6 kHz).

Since March, 1981, calibration signals from a stable noise generator have been placed on each data tape for each mode of operation used. These calibrations, along with the recorded transmitted power, are used to determine absolute radar reflectivity.

Magnetic data tapes are further processed by a scaling program on the central computing facility of the Boulder Laboratories of NOAA. The output of this program contains radial velocity, velocity width, received power, $C_n^2$, and the magnitude of the reflection coefficient for each range gate.

## HISTORY AND SIGNIFICANT ACCOMPLISHMENTS

The Sunset radar was the first radar designed and constructed specifically

Summary of Sunset radar characteristics

| | |
|---|---|
| Frequency | 40.475 MHz |
| Wagelength | 7.41 m |
| Transmitter power | |
| Peak | 100 kW |
| Average (maximum) | 16 kW |
| (typical) | 2.5 kW |
| Antenna | |
| Phased array of coaxial-colinear dipoles with computer-controlled phase shifters for each line of dipoles | |
| Area | 3600 $m^2$ |
| Aperture efficiency | 0.58 |
| Resistive loss | 0.30 |
| Steerability | |
| (E-W or N-S vertical plane only) | $\pm$ 60° |
| Beam width H plane (steerable) | 4.8° |
| E plane | 4.4° |
| Steering increment | 0.2° |
| Practical steering rate | 1 record/minute/position to any arbitrary antenna beam position |

as a VHF ST radar. Construction was begun in 1973 and the first clear-air echoes and wind velocity measurements were obtained in 1974 (GREEN et al., 1975). The Sunset radar has been used to demonstrate the feasibility of using an ST radar to measure wind velocity (WARNOCK et al., 1978), all three vectors of wind velocity (GREEN et al., 1978a), turbulence (VANZANDT et al., 1978), wind variability (GAGE and CLARK, 1978), variation of clear air turbulence near and above thunderstorms (GREEN et al., 1978b), simultaneous measurement of hydrometeor and air velocity (GREEN et al., 1978b), turbulence intensity using velocity width (1978c) specular reflection from stable layers (GAGE and GREEN, 1978), gravity (buoyancy) waves (VANZANDT et al., 1979), the height of the tropopause (GAGE and GREEN, 1979b), turbulence parameters (GAGE et al., 1980); devise a practical and economical method of steering ST radar antennas (GREEN et al., 1981); and estimate the gradient of temperature in the stratosphere (GAGE and GREEN, 1982).

(References in this paper are included in the Publications listed below.)

PUBLICATIONS RELATED TO THE SUNSET RADAR

Green, J. L., J. M. Warnock, R. H. Winkler and T. E. VanZandt (1975), Studies of winds in the upper troposphere with a sensitive VHF radar, Geophys. Res. Lett., 2, 19.

Green, J. L., J. M. Warnock, R. H. Winkler and T. E. VanZandt (1975), A sensitive VHF radar for the study of winds, waes, and turbulence in the troposphere, stratosphere, and mesosphere, 16th Radar Meteorol. Conf., Houston, Am. Meteorol. Soc.

VanZandt, T. E., J. L. Green, J. M. Warnock and R. W. Winkler (1975), Studies of winds in the upper troposphere with a sensitive VHF radar, 16th Radar Meteorol. Con., Houston, AMS, April 22-24.

VanZandt, T. E., J. L. Green, J. M. Warnock, K. S. Gage and W. L. Clark (1977), Reflectivity studies with the Sunset VHF pulsed Doppler radar, Proc. Symp. on Radio Prop. and Non-ionized Media, 28 April - 6 May, Centre National d'Etudes des Telecommunications, Paris, France, 519-524.

B. B. Balsley and J. L. Green (1978), Coherent radar systems for probing the troposphere, stratosphere, and mesosphere, Proc. 4th Symp. on Meteorol. Observations and Instrumentation, April 10-14, 1978, Denver, CO, 227-230.

Gage, K. S. (1978), Comparison of sensitive Doppler radar observations of winds and turbulence with in situ observations, Proc. 4th Symp. on Meteorol., Observations and Instrumentation, April 10-14, Denver, CO, 231-238.

Gage, K. S. and J. L. Green (1978), Evidence for specular reflection from monostatic VHF radar observations of the stratosphere, Radio Sci., 13, 991-1001.

Gage, K. S., J. L. Green and T. E. VanZandt (1978), Application of the VHF pulsed Doppler radar to cloud physics research, Proc. Conf. on Cloud Physics and Atmospheric Electricity, July 31 - August 4, 1978, Issaquah, Wash. 394-401.

Gage, K. S. and B. B. Balsley (1978), Doppler radar probing of the clear atmosphere, Bull. Amer. Meteorol. Soc., 59, 1074-1093.

Gage, K. S. and W. L. Clark (1978), Mesoscale variability of jet stream winds observed by the Sunset VHF Doppler radar, J. Applied Meteorol., 17, 1412-1416.

Gage, K. S., T. E. VanZandt and J. L. Green (1978), Vertical profiles of $C_n^2$ in the free atmosphere: Comparison of model calculations with radar observations Proc. 18th Conf. on Radar Meteorol., March 28-31, 1978, Atlanta, GA, 184-189.

Green, J. L., K. S. Gage and T. E. VanZandt (1978c), VHF Doppler studies of CAT in the troposphere and lower stratosphere, Preprint Vol, Conf. on Atmos. Environment of Aerospace Systems and Appl. Meteorol., Nov. 14-16, New York, NY, 159-164.

Green, J. L., K. S. Gage and T. E. VanZandt (1978a), Three dimensional wind observations of a jet stream using a VHF Doppler radar, Proc. 18th Conf. on Radar Meteorol., March 28-31, Atlanta, GA, 184-189.

Green, J. L., R. H. Winkler, J. M. Warnock, W. L. Clark, K. S. Gage and T. E. VanZandt (1978b), Observations of enhanced clear air reflectivity associated with convective clouds, Proc. 18th Conf. on Radar Meteorol., March 28-31, Atlanta, GA, 88-93.

VanZandt, T. E., J. L. Green, K. S. Gage and W. L. Clark, (1978), Vertical profiles of refractivity turbulence structure constant: comparison of observations by the Sunset radar with a new theoretical model, Radio Sci., 13, 818-829.

Warnock, J. M., T. E. VanZandt, J. L. Green and R. H. Winkler (1978), Comparisons between wind profiles measured by Doppler radar and by rawindsonde balloons, Geophys. Res. Lett., 5, 109-112.

Gage, K. S., J. L. Green, W. L. Clark and T. E. VanZandt (1979), Doppler radar measurement of turbulence in the clear atmosphere, Proc. Conf. Fourth Symp. on Turbulence, Diffusion and Air Pollution, January 15-18, Reno, Nevada, 522-529.

Gage, K. S. and J. L. Green (1979b), Tropopause detection by partial specular reflection using VHF radar, Science, 203, 1238-1240.

Green, J. L., K. S. Gage and T. E. VanZandt (1979), Atmospheric measurements by VHF pulsed Doppler radar, IEEE Trans. on Geosci. Elec., GE-17, 262-280.

VanZandt, T. E., K. S. Gage and J. M. Warnock (1979), A statistical model for the probability of turbulence and the calculation of vertical profiles of turbulence parameters, Proc. Conf. Fourth Symp. on Turbulence, Diffusion, and Air Pollution, January 15-18, Reno, Nevada, 52-55.

VanZandt, T. E., J. L. Green, W. L. Clark and J. R. Grant (1979), Buoyancy waves in the troposphere: Doppler radar observations and a theoretical model, Geophys. Res. Lett., 6, 429-432.

Gage, K. S., J. L. Green and T. E. VanZandt (1980), Use of Doppler radar for the measurement of atmospheric turbulence parameters from the intensity of clear-air echoes, Radio Sci., 15, 407-416.

Green, J. L. and K. S. Gage (1980), Observations of stable layers in the troposphere and stratosphere using VHF radar, Radio Sci., 15, 395-405.

VanZandt, T. E., K. S. Gage, and J. M. Warnock (1980), Progress in modelling turbulence parameters from profiles of background winds, temperature, and humidity, Proc. AMS 19th Conf. on Radar Meteorol., April 15-18, 613-615.

Gage, K. S. and J. L. Green (1980), Prospects for a quantative measurement of atmospheric stability using VHF radar, Proc. AMS 19th Conf. on Radar Meteorol., April 15-18, Miami Beach, FL, 605-612.

Green, J. L., J. M. Warnock, W. L. Clark and F. J. Eggert (1980), Modifications to the Sunset radar to provide beam steering, Proc. AMS 19th Conf. on Radar Meteorol., April 15-18, Miami Beach, FL, 575-576.

Green, J. L., K. S. Gage, W. L. Clark, T. E. VanZandt and P. H. Hildebrand (1980), Joint instrumented aircraft and VHF Doppler radar measurements of wind near Boulder, CO, Proc. AMS 19th Conf. on Radar Meteorol., April 15-18, Miami Beach, FL, 624-628.

VanZandt, T. E., K. S. Gage and J. L. Green (1979), The use of Doppler radar measurement of atmospheric turbulence parameters in the clear atmosphere, Collection of Extended Abstracts Presented at ICMUA Sessions and IUGG Symp. 18, XVII IUGG Gen. Assemb., Canberra, Australia, 285-292.

Gage, K. S. and J. L. Green (1979a), Observations of stable layers in the middle atmosphere using VHF radar, Collection of Extended Abstracts Presented at ICMUA Sessions and IUGG Symp. 18, XVII IUGG Gen. Assemb., Canberra, Australia, 325-332.

Gage, K. S., B. B. Balsley and J. L. Green (1981), Fresnel scattering model for the specular echoes observed by VHF radar, Radio Sci., 16, 1447-1453.

Gage, K. S. and J. L. Green (1982), A technique for determining the temperature profile from VHF radar observations, J. Appl. Meteorol., 21, 1155-1158.

Balsley, B. B., J. L. Green, W. L. Ecklund, W. L. Clark, R. G. Strauch and A. C. Riddle (1981), Joint observations of gravity wave activity in vertical winds in the troposphere and lower stratosphere over a 63 km baseline obtained with clear-air VHF radars at Platteville and Sunset, Colorado, Preprint Vol, 20th Conf. on Radar Meteorol., Boston, Nov 30 - Dec 3, AMS, 110-115.

Green, J. L., J. M. Warnock, W. L. Clark, F. J. Eggert and K. J. Ruth (1981), Modifications to the Sunset radar to provide antenna beam steering, Preprint Vol., 20th Conf. on Radar Meteorol., Boston, Nov 30 - Dec 3, AMS, 7-10.

VanZandt, T. E., K. S. Gage and J. M. Warnock (1981), An improved model for the calculation of profiles of $C_n^2$ and in the free atmosphere from background profiles of wind, temperature and humidity, Preprint Vol., 20th Conf. on Radar Meteorol., Boston, MA, Nov 30 - Dec 3, AMS, 129-135.

Ecklund, W. L., K. S. Gage, B. B. Balsley, R. G. Strauch and J. L. Green (1982), Vertical wind variability observed by VHF radar in the lee of the Colorado Rockies, Mon. Wea. Rev., 110, 1451-1457.

# 5.4A CAPABILITIES AND LIMITATIONS OF EXISTING MST RADARS: COLORADO WIND PROFILERS

R. G. Strauch

NOAA/ERL/Wave Propagation Laboratory
Boulder, Colorado 80303

The Wave Propagation Laboratory (WPL) is developing a ground-based remote-sensing system called PROFILER (HOGG et al., 1983) to measure tropospheric parameters currently measured in operational meteorology by radiosondes. The prototype PROFILER uses two radars for wind sounding: a 6-m radar located at Platteville, Colorado, and a 33-cm radar located at Denver's Stapleton International Airport. The Platteville radar was originally developed by NOAA's Aeronomy Laboratory (AL) and is being operated jointly by WPL and AL. In addition, a network of three 6-m wind-profiling radars is being installed in Colorado, and a fourth site is planned. Figure 1 shows the location of the five radars. Their characteristics and limitations are described in this paper.

1. The 6-m radar at Platteville -- This radar is described by ECKLUND et al. (1979). It has been operating continuously and unattended since about mid-1981, except for brief periods of downtime caused by computer problems. Since January 1982 data have been tape-recorded routinely.

The radar alternates between two modes of operation: one mode is for measuring vertical profiles of the horizontal wind, and the other is optimized for zenith-pointing observations. Each mode is used every 5 min. The data-processing scheme is described in another paper (STRAUCH, 1983). Data are transmitted by telephone to the central PROFILER computer in Denver as well as recorded on magnetic tape at Platteville. There are three antennas, transmitters, and receivers so data are obtained simultaneously in the three viewing directions. Table 1 summarizes the radar characteristics and operating parameters.

The major limitations are caused by the data system. A minicomputer performs all the time-domain integration in software, and this restricts the maximum pulse repetition frequency, the minimum spacing of range gates, and the number of range gates allowed. As a result the radar is operated with coarse range resolution and relatively poor minimum height coverage ($\sim$2 km above ground). The data system also limits sensitivity by restricting the duty cycle. There are 13 range cells for monitoring winds in the troposphere and 10 range cells for monitoring mesospheric echoes. Present plans are to replace the data system with a more versatile system that includes a preprocessor (used with the four radars described below) and to replace the two off-zenith antennas. A minicomputer will still be used for data processing (including spectral analysis), so the number of range cells would be restricted to about 40 to keep the data-processing time small compared with the acquisition time. Range resolution would then be limited by the bandwidth authorized (400 kHz).

2. The 33-cm radar at Denver -- This radar is used only for tropospheric wind measurements. It has a 10-m offset paraboloidal reflector antenna with offset feeds to generate the same three beam-pointing positions as the radar at Platteville (EARNSHAW et al., 1982). For this radar the viewing directions are not observed simulatenously; a single transmitter and receiver are switched to the desired direction. The transmitter is solid state and is capable of up to 25% duty cycle. The T/R function is accomplished by a circulator with a diode limiter providing additional protection for the low-noise r-f preamplifier. The radar operates in three resolution modes: a 1-$\mu$s pulse width for high

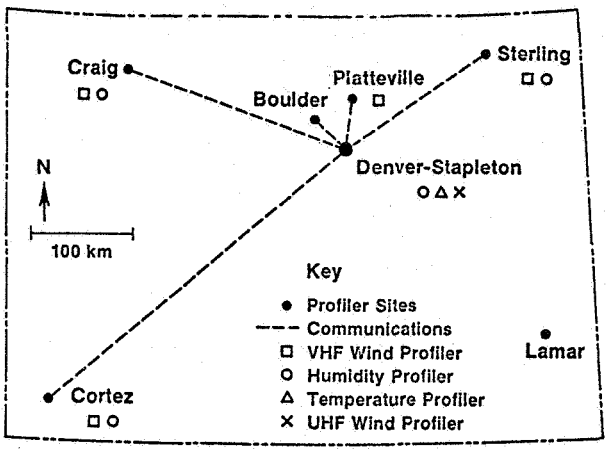


Figure 1. Colorado Profiler Network. A UHF (915 MHz) radar is located at Denver's Stapleton International Airport; VHF (50 MHz) radars are at Craig, Sterling, Cortez, and Platteville. Lamar is a possible future site for a VHF radar.

Table 1. Platteville radar characteristics and operating parameters

| | | |
|---|---|---|
| **Radar** | | |
| Frequency | 49.92 mHz | |
| Authorized bandwidth | 0.4 mHz | |
| Peak power | 27 kW (maximum ≈60 kW) | |
| Average power | 180 W (maximum ≈1 kW) | |
| Pulse width | 16 μs | |
| Pulse repetition period | 2400 μs | |
| Antenna aperture | 100 m x 100 m | |
| Antenna pointing | zenith, 15° off-zenith to north and east (3 antennas) | |
| Antenna type | fixed phased array of colinear-coaxial dipoles | |
| Two-way beamwidth | 2.5° | |
| **Data Processing** | **Vertical Mode** | **Horizontal-Wind Mode** |
| Time domain averaging | 256 pulses | 32 pulses |
| Spectral averaging | 2 | 16 |
| Maximum radial velocity | ±2.44 m/s | ±19.55 m/s |
| Spectral resolution (64 points) | 0.076 m/s | 0.61 m/s |
| **Tropospheric sampling** | | |
| 1st height | 1.85 km | 2.5 km |
| Height spacing | 1.5 km | 1.45 km |
| Number of heights | 13 | 13 |
| **Mesospheric sampling** | | |
| 1st height | 67.5 | 66 km |
| Height spacing | 3.6 km | 3.48 km |
| Number of heights | 10 | 10 |

resolution in the lowest 2 km, a 4-μs pulse width to measure winds to about 7-km altitude, and a 16-μs pulse to measure winds to the highest altitude possible. Time-domain integration is performed in a laboratory-built preprocessor that also operates the radar under computer control. The main PROFILER computer performs the data processing; it has an array processor so that spectral-processing overhead time is small compared with data acquisition time. (The rate at which power spectra must be calculated is much higher for a 33-cm radar than for a 6-m radar.) Radar characteristics and the anticipated operating parameters are shown in Table 2. Radar hardware is complete, and tests have been made to ensure that the system will operate properly. Software for automated operation is not complete. Limitations of this radar will not be known until it has been in continuous operation for some time. Operation should start early in 1983. It is expected that a major limitation will be that the maximum height coverage will not extend to the tropopause routinely. Future plans are to add pulse coding so that longer pulses can be used to take advantage of the high duty cycle available.

3. The 6-m radar network — These three radars are similar to the Platteville, radar, but they will not have zenith-pointing antennas. The antenna apertures are 1/4 that of the Platteville antennas. These radars are designed for tropospheric wind measurements. They observe the north and east wind components simultaneously, perform all required data analysis at the radar site, and send hourly wind profiles to Denver by telephone. They use the same preprocessor and radar-computer interface as the 33-cm radar. Two resolution

Table 2. Stapleton radar characteristics and operating parameters

| | | | |
|---|---|---|---|
| **Radar** | | | |
| Frequency | 915 mHz | | |
| Maximum bandwidth | 2 mHz | | |
| Peak power | 5.6 kW | | |
| Duty cycle | ≤25% | | |
| Antenna aperture | ≈10 m x 10 m | | |
| Antenna pointing | zenith, 15° off-zenith to north and east | | |
| Antenna type | offset paraboloidal reflector with offset horn feeds | | |
| Two-way beam width | 1.7° | | |
| System noise temperature | 240 K | | |
| **Data Processing** | **1** | **2** | **3** |
| Pulse width | 1 μs | 3 μs | 9 μs |
| Pulse repetition period | 50 μs | 64 μs | 110 μs |
| Average power | 110 W | 260 W | 450 W |
| Time domain averaging | 136 pulses | 80 pulses | 46 pulses |
| Spectral averaging | 8 spectra | 32 spectra | 32 spectra |
| Maximum radial velocity | ——— | 12.02 m/s | ——— |
| Spectral resolution (64 points) | ——— | 0.375 m/s | ——— |
| **Height sampling** | | | |
| 1st height | 1.06 km | 1.64 km | 2.7 km |
| Height spacing | 100 m | 290 m | 870 m |
| Number of heights | 24 | 24 | 18 |

Table 3. Sterling radar characteristics and operating parameters

| | | | | |
|---|---|---|---|---|
| **Radar** | | | | |
| Frequency | 49.8 mHz | | | |
| Authorized bandwidth | 0.4 mHz | | | |
| Peak power | 30 kW (maximum ≈60 kW) | | | |
| Average power | 400 W (maximum ≈1 kW) | | | |
| Pulse width | 4, 16 μs (3, 9) | | | |
| Pulse repetition period | 300, 1200 μs (225, 675) | | | |
| Antenna aperture | 50 m x 50 m | | | |
| Antenna pointing | 15° off-zenith to north and east (2 antennas) | | | |
| Antenna type | fixed phased array of colinear-coaxial dipoles | | | |
| Two-way beam width | 5° | | | |
| **Data Processing** | 4-μs pulse | (3) | 16-μs pulse | (9) |
| Time domain averaging | 320 pulses | (426) | 64 pulses | (113) |
| Spectral averages | 8 | | 16 | |
| Maximum radial velocity | ±15.7 m/s | | ±19.6 m/s | |
| Spectral resolution (64 points) | 0.49 m/s | | 0.31 m/s | |
| **Height sampling** | | | | |
| 1st height | 1.4 km | (0.6) | 3.0 km | (3.0) |
| Height spacing | 290 m | (290) | 1.160 km | (.870) |
| Number of heights | 20 | (22) | 14 | (18) |

( ) -- new values as of 5/1/83.

modes are used: a 4-μs pulse width for low and midlevels and a 16-μs pulse width to extend the height coverage as high as possible. Table 3 lists the characteristics and anticipated operating parameters. These radars are to be installed by January 1983 and in operation in early 1983.

(References in this paper are included in the Publications listed below.)

PUBLICATIONS RELATING TO THE COLORADO WIND PROFILING NETWORK

Ecklund, W. L., D. A. Carter and B. B. Balsley (1979), Continuous measurement of the upper atmospheric winds and turbulence using a VHF radar: Preliminary results, J. Atmos. Terr. Phys., 41, 983-994.

Hogg, D. C., C. G. Little, M. T. Decker, F. O. Guiraud, R. G. Strauch and E. R. Westwater (1980), Design of a ground-based remote sensing system using radio wavelengths to profile lower atmospheric winds, temperatures, and humidity; Remote Sensing of Atmosphere and Oceans, Academic Press, 313-364.

Strauch, R. G., M. T. Decker, D. C. Hogg, C. G. Little and R. Bunting (1981), The ERL Profiler and aviation meteorology; Proc. of First Int. Conf. of Aviation Weather System, Montreal, P.Q., Canada, May 4-6, 153-156.

Strauch, R. G. (1981), Radar measurement of tropospheric wind profiles, Preprints 20th Conf. on Radar Meteorol., Nov 30 - Dec 3, Boston, MA, 430-434.

Strauch, R. G., M. T. Decker and D. C. Hogg (1982), An automatic profiler of the troposphere, AIAA-82-0014, Proceedings of AIAA 20th Aerospace Science Meeting, January 11-14, 1982, Orlando, FL.

Decker, M. T., R. G. Strauch and E. R. Westwater (1982), Ground-based remote sensing of atmospheric temperatures, water vapor and winds, Proc. 1982 International Geoscience and Remote Sensing Symp., (IGARSS 1982) Munich FRG.

Earnshaw, K. B., D. C. Hogg and R. G. Strauch (1982), A triple-beam antenna for wind-profiling radar, NOAA Tech Memo, ERL WPL-108.

Shapiro, M. A., D. C. Hogg and C. G. Little (1983), The wave propagation laboratory Profiler system and its applications, Proc. of 5th Symp. on Meteorol. Observations and Instrumentation, Toronto, Ontario, Canada, April 11-15, 174-182.

Strauch, R. G., D. A. Merritt, K. P. Moran, K. B. Earnshaw and D. vande Kamp (1983), Tropospheric wind profiling with Doppler radar, Proc. of 21st Conf. on Radar Meteorol., Edmonton, Alta., Canada, (in press).

Strauch, R. G., M. T. Decker and D. C. Hogg (1983), Automated profiling of the troposphere, J. of Aircraft, 20, 359-362.

Hogg, D. C., M. T. Decker, F. O. Guiraud, K. B. Earnshaw, D. A. Merritt, K. P. Moran, W. B. Sweezy, R. G. Strauch, E. R. Westwater and C. G. Little (1983), An automatic profiler of the temperature, wind, and humidity in the atmosphere, J. Appl. Meteorol., (in press).

Strauch, R. G. (1983), Data analysis techniques: Spectral processing, SCOSTEP/URSI/MAP Workshop on Technical aspects of MST Radar, Urbana, IL, May 22-27, 1983, paper 8.5A, this volume.

# 5.5A CAPABILITIES AND LIMITATIONS OF EXISTING MST RADARS: POKER FLAT

B. B. Balsley, W. L. Ecklund and D. A. Carter

Aeronomy Laboratory
National Oceanic and Atmospheric Administration
Boulder, CO 80303

The Poker Flat MST Radar was designed as a prototype system to continuously monitor the atmosphere up to ∿100 km. Initial funding was received from the National Science Foundation in September, 1978. The system began operations -- at a relatively low sensitivity -- some five months later. Since that time the system has been in almost continuous operation, and the sensitivity has increased steadily toward its ultimate design characteristics. Both the current and the final parameters are shown in Table 1. A more complete description of the system appears in BALSLEY et al. (1980). The current (fixed-position) antenna beams are shown in Figure 1, and a picture of the site is shown in Figure 2.

In addition to the parameters listed in Table 1, the Poker Flat radar embodies both a number of specific design features and an operating philosophy that are reasonably unique. These are discussed briefly below.

The modular system design incorporated in the Poker Flat radar uses 64 transmitting modules distributed throughout the 200m x 200m antenna array. Each transmitter is connected to four coaxial-collinear (COCO) dipole chains in one of two possible orthogonal polarizations. Each of these subsets (1 transmitter - 4 COCOs) is independently controlled from low-power RF pulse drivers located in the main building. Reception is accomplished by a similar process: the same four antennas feed a low-noise 50-MHz amplifier located at the output of the TR (Transmit-Receive) switch in the same transmitter. Each set of eight receiver outputs (i.e., one polarization-quarter) is combined in the field, so that eight separate inputs (i.e., eight separate polarization-quarters) are fed into the main building.

This modular design has a number of advantages relative to that for single transmitter/antenna systems. One of the most important advantages lies in the fact that the scientific observational program can begin with the completion of the first module; it is not necessary to await completion of the full system. A second advantage is that the probablity of catastrophic failure is considerably reduced. The loss of a single transmitter, power supply, or antenna module merely reduces the system sensitivity, and the observational program can continue. For example, the loss of one transmitter in the final system reduces the system sensitivity by only a fraction of 1 dB. A third advantage of modularity is the relatively simple maintenance procedures necessary to keep the system operational. Any single transmitter, for example, can be replaced in less than an hour, and repaired subsequently (a transmitter module weighs less than 20 kgm and can be changed by one person). These and other advantages to a modular design are listed in Table 2.

The operational philosophy adopted at Poker Flat is one of continuous, uninterrupted operation. This precludes all but the most crucial "campaign-type" experiments. It also precludes -- at least for the time being -- a number of desirable long-term studies using either higher temporal or spatial resolution. This latter limitation arises primarily from the amount of taped records (see Figure 3 for an example of the taped spectra) that would accumulate at the higher data rates if data were to be taken at all possible heights: currently Poker Flat uses a single standard digital tape every two days; improved resolution studies using, say, 300 m resolution instead of the standard

Table 1. Poker Flat MST radar* parameters

| | | CURRENT (FEBRUARY 1983) | FINAL |
|---|---|---|---|
| Transmitter | Frequency | 49.920 MHz | 49.920 MHz |
| | Peak pulse power (oblique) | 1.2 MWatts/polarization | 3.2 MWatts/polarization |
| | (vertical) | 0.35 MWatts | 3.2 MWatts |
| | Average power (oblique) | 22 kW/polarization | 64 kW/polarization |
| | (vertical) | 6 kW | 64 kW |
| | Pulsewidth | 2-16 μsec | 2-16 μsec (coded) |
| | Pulse rate | 1.2 kHz | 1.25 kHz |
| Receiver | Noise figure | ≃ 3 dB | ≃ 3 dB |
| | Bandwidth | Matched to pulse width | Matched to pulse width |
| | Filtering | Bessel | Bessel |
| Antenna | Area (oblique) | $3 \times 10^4$ m$^2$ | $4 \times 10^4$ m$^2$ |
| | (vertical) | $1 \times 10^4$ m$^2$ | $4 \times 10^4$ m$^2$ |
| | Beamwidth (two-way) | ≃ 1° | ≃ 1° |
| | Direction | Oblique/vertical | Oblique/vertical |
| Processing | Coherent averaging (oblique) | 58 pulses | 58 pulses |
| | (vertical) | 412 pulses | 412 pulses |
| | Spectral resolution | 64 points | 64 points |

*Location 65° 07' 58" N, 147° 21' 30" W

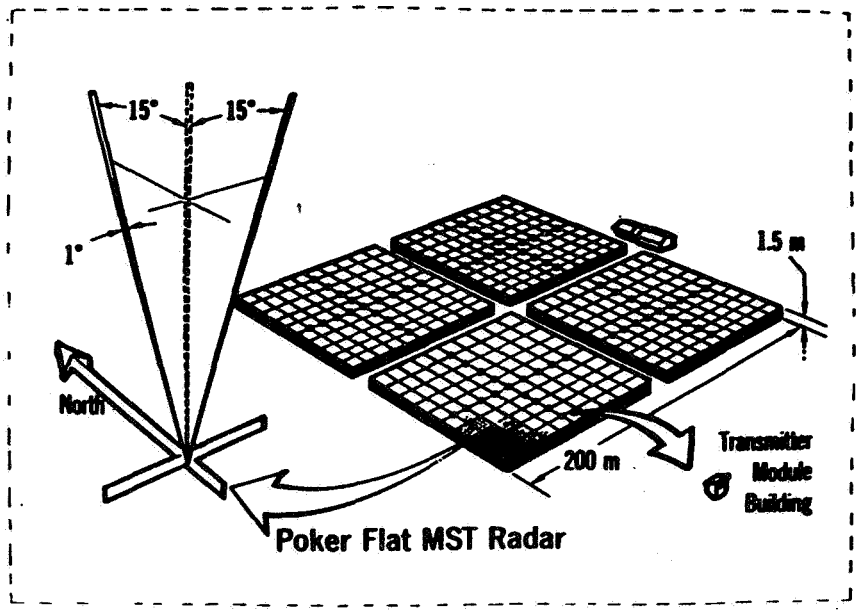


Figure 1. Showing the current three fixed-beam arrangement of the Poker Flat MST radar.

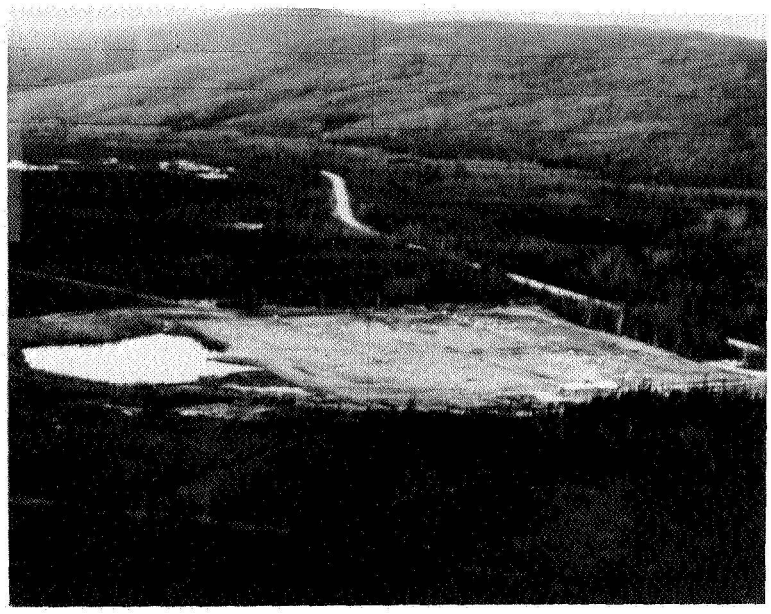

Figure 2. Aircraft view of the Poker Flat radar (foreground) and the University of Alaska Geophysical Institute's Poker Flat rocket range (upper left area). View looking approximately WNW.

Table 2. Poker Flat MST radar

Advantages

Modular Design

- Allows operation using only a portion of the system
- No catastrophic failures (distributed elements)
- Easy maintenance
- Beam switching using very low power phase switching
- Air-cooled (not water cooled) transmitting tubes
- Heat exchangers not required
- Small spare parts reserve (∿ 10%) relative to single unit system
- Lower feedline costs (not major)
- No moving parts (i.e., dishes, mechanical switches)

Continuous, uninterrupted operation (> 4 years)

- Virtually unattended (except for maintenance)
- Reliability (> 90%): no start-up problems
- Cost effective
- Operates well in climate extremes (+ 30°C to - 56°C)
- Power supply "bleeder" resistors heat main building

Miscellaneous

- Remote site: less man-made interference (RF, aircraft, etc.)
- Proximity to University of Alaska rocket range (Met rockets and balloons and experiments)

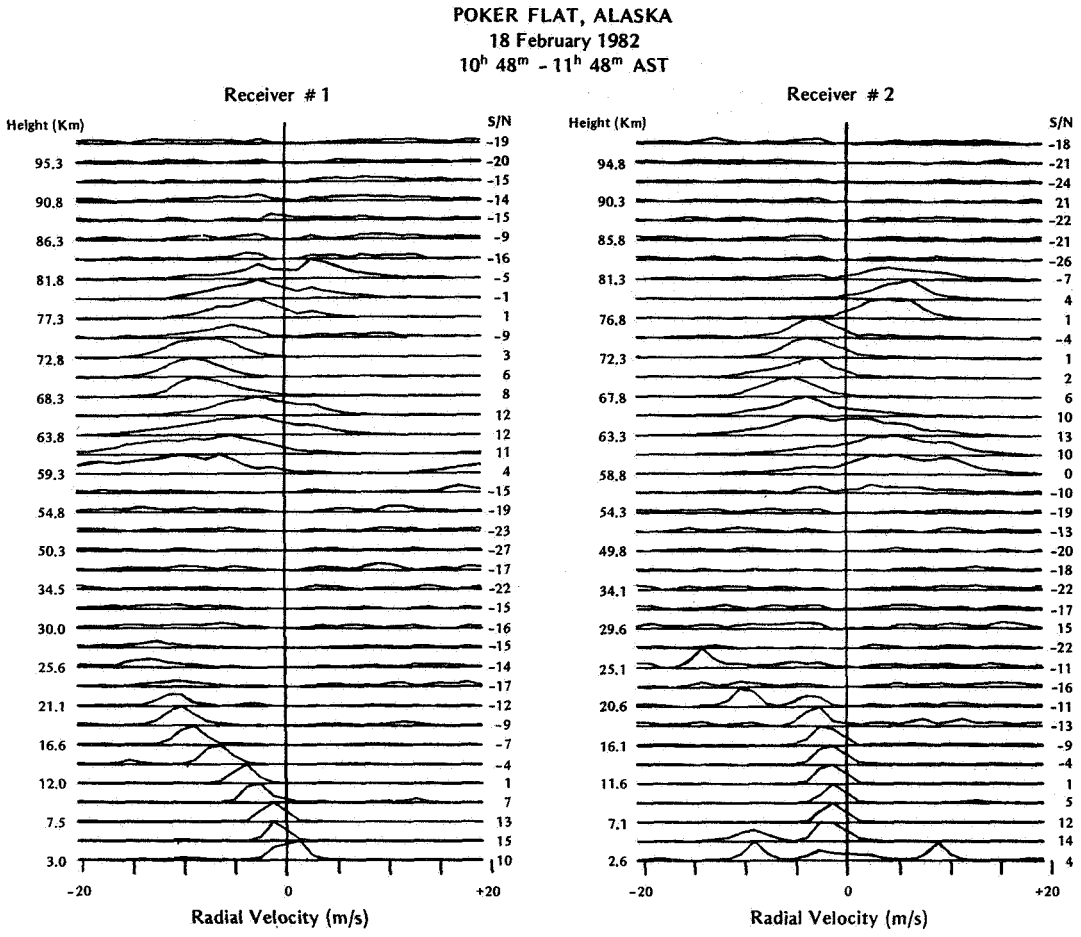


Figure 3. Example of the spectral information obtained from Poker Flat taped data. Shown are one-hour averaged values of normalized Doppler power spectra for "EAST" receiver (#1) and "NORTH" receiver (#2). S/N values are printed on right of each spectrum.

2.2 km resolution would require three tape changes per day. While this is not an unreasonable rate for a few days, it becomes prohibitive for long-term studies. In the final operational mode at Poker Flat, however, such data will be obtained using a separate recording system with minimal interruption.

Continuous operation has a number of advantages. For example, continuous operation combined with every-two-day tape changes enables an essentially unattended operation (except for maintenance tasks and special experiments). It also results in a cost effective operation and an enhanced reliability (owing in part to the lack of normally expected "turn on" problems). As an example, during 1982, the system was operational ~92% of the time, with much of the off-time arising from tape changing discontinuities. Figure 4 shows an example of the percentage of echoes received at Poker Flat versus height and time. Also, although the ambient temperature during this period ranged between about +30°C and -56°C, the system operation was not affected. This can be attributed in part to the continuity of data taking. These advantages, along with other less-important ones, are listed in Table 2.

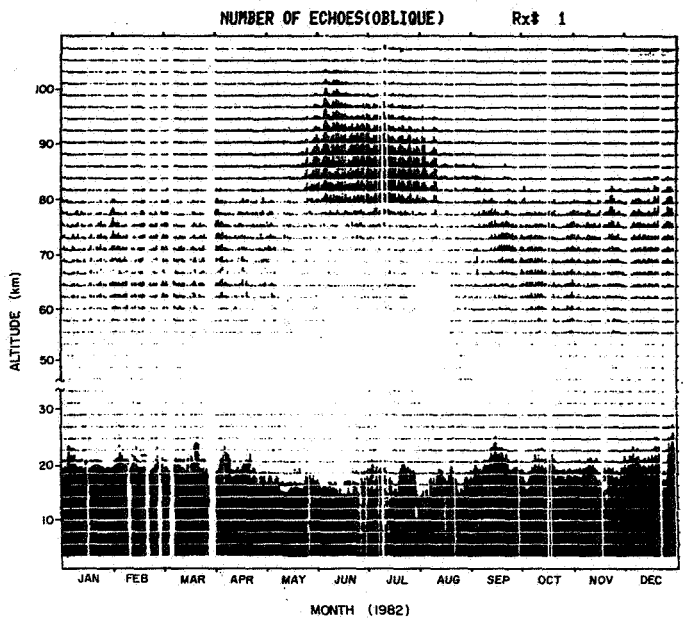


Figure 4. Example of the continuity of the Poker Flat observations (R. Garello, private communication). For each height, the percentage of possible echoes for each hourly averaged period is scaled in terms of the full height range at that time and height (e.g., the full-height lines for all seasons below $\sim$ 12.5 km indicate 100% echo rate; half-height lines at 23.3 km in mid September indicate 50% echo/no-echo rate). Note the seasonal change in the mesospheric echo heights and occurrence rates. The relatively darkened lines that maximize at $\simeq$ 92 km arise from meteor echoes.

Table 3. Poker Flat MST radar

| |
|---|
| Disadvantages |
| Not-Yet-Finished Problems |
| Not yet steerable (3 fixed beams) |
| Three-quarters of antenna only on oblique beam |
| One-quarter of antenna only on vertical beam |
| Continuous observations with < 2.2 km resolution requires separate tape unit |
| Preprocessor unit (for maximum sensistivity) under construction |
| Current reliable peak Tx power $\leq$ 60 kW |
| No ancillary measurements on-line yet |
| Full sensitivity on vertical to "see through" still in the future |
| General Problems |
| Reasonably expensive operation (power bill $\sim$ $\$10^5$/year) |
| Remote site (cold in winter, muddy in spring, mosquitoes in summer) |
| Continuous operation mode precludes some special studies |
| Not portable |
| Mountain echoes added to atmospheric echoes below $\simeq$ 7 km |
| Moose in the (fenced-in) antenna array |

The disadvantages of the Poker Flat system are shown in Table 3. Many of the current disadvantages stem from the fact that the system is not yet completed. For example, maximum sensitivity in the vertical will not be realized until the full system is steered between vertical and oblique positions (this will allow us to examine the region of weak echoes near 45 km with full system sensitivity). Also, higher resolution studies not currently possible will be enabled with the advent of an additional recording system and a digital "preprocessing" system currently under construction. We also lack a series of ancillary measurements (surface wind, temperature, all-sky camera, riometer, airglow, etc.) at the site, which will be eventually included on the standard data format. Finally, the system in some 5-1/2 dB below the final sensitivity. This is due in part to transmitter tube HV arc-over problems, to the (current) lack of a fast preprocessor, and to the fact that only three-quarters of the full antenna is currently used for oblique operation. Additional disadvantages along with those mentioned above, are included in Table 3.

(The reference in this paper is included in the Publications listed below.)

PUBLICATIONS RELATING TO THE POKER FLAT RADAR

Balsley, B. B., W. L. Ecklund, D. A. Carter and P. E. Johnston (1979), The Poker Flat MST radar: First results, Geophys. Res. Lett., 6, 921-924.

Balsley, B. B. and K. S. Gage (1980), The MST radar technique: Potential for middle atmospheric studies, Pure Appl. Geophys., 188, 452-493.

Balsley, B. B., W. L. Ecklund, D. A. Carter and P. E. Johnston (1980), The MST radar at Poker Flat, Alaska, Radio Sci., 15, 213-223.

Ecklund, W. L., B. B. Balsley and D. A. Carter (1980), The Poker Flat MST radar: Preliminary results between 3-20 km, Preprints, AMS 19th Conf. on Radar Meteorol., April 15-18, Miami Beach, FL, 557-562.

Balsley, B. B., W. L. Ecklund and D. A. Carter (1980), The Poker Flat MST radar: An outline of the primary echoing mechanisms and a description of the facility Preprints, AMS 19th Cong. on Radar Meteorol., April 15-18, Miami Beach, FL, 557-562.

Carter, D. A., B. B. Balsley and W. L. Ecklund (1980), The Poker Flat MST radar: Signal analysis and data processing technique with examples, Preprints 19th Conf. on Radar Meteorol., April 15-18, Miami Beach, FL, 563-567.

Gage, K. S. and B. B. Balsley (1981), Recent advance in Doppler radar probing of the clear atmosphere, Atmos. Tech., 13, 3-21.

Nastrom, G. D., K. S. Gage and B. B. Balsley (1981), The variability of $C_n^2$ at Poker Flat, Alaska from MST Doppler radar observations, SPIE, 227, 10-15.

Ecklund, W. L. and B. B. Balsley (1981), Long term observations of the Arctic mesosphere with the MST radar at Poker Flat, Alaska, J. Geophys. Res., 86, 7775-7780.

Balsley, B. B. and K. S. Gage (1981), On the vertical-incidence VHF backscattered power profile from the stratosphere, Geophys. Res. Lett., 8, 1173-1175.

Balsley, B. B., W. L. Ecklund, D. A. Carter, P. E. Johnston and A. C. Riddle (1981), The Poker Flat MST radar system: current status and capabilities, Preprint, Vol., 20th Conf. on Radar Meteorol., Boston, MA, Nov 30 - Dec 3, AMS, 1-6.

Gage, K. S., D. A. Carter and W. L. Ecklund (1981), The effect of gravity waves on specular echoes observed by the Poker Flat MST radar, Geophys. Res. Lett., 8, 599-602.

Nastrom, G. D., B. B. Balsley and K. S. Gage (1981), Changes with season of $C_n^2$ at Poker Flat, AK, from MST Doppler radar observations, Preprint, Vol., 20th Conf. on Radar Meteorol., Boston, MA, Nov 30 - Dec 3, AMS.

Nastrom, G. D., B. B. Balsley and D. A. Carter (1982), Mean meridional winds in the mid- and high-latitude summer mesosphere, Geophys. Res. Lett., 9, 139-142.

Gage, K. S., W. L. Ecklund and B. B. Balsley (1982), Comparison of Poker Flat MST radar observations with the Fresnel scattering model, submitted to Radio Science.

Balsley, B. B. and D. A. Carter (1982), The spectrum of atmospheric velocity fluctuations at 8 km and 86 km, Geophys. Res. Lett., 9, 465-468.

D. A. Carter and B. B. Balsley (1982), The summer wind between 80 km-93 km observed by the MST radar at Poker Flat, Alaska (65°N), J. Atmos. Sci., 39, 2905-2915.

Nastrom, G. D., K. S. Gage and B. B. Balsley (1982), Variability of $C_n^2$ at Poker Flat, Alaska, from mesosphere, stratosphere, troposphere (MST) Doppler radar observations, Optical Engineering, 21, #2, 347.

Fritts, D. C., B. B. Balsley and W. L. Ecklund (1982), Evidence of tidal breakdown at the summer mesopause, submitted to Radio Science.

Balsley, B. B., D. A. Carter and W. L. Ecklund (1982), On the potential of radar observations for studying coupling processes between the ionosphere and middle atmosphere, Proc. Second International Symp. on Solar-Terrestrial Influences on Weather and Climate, submitted 11/3/82.

Larsen, M. F., Kelley, M. C. and K. S. Gage (1982), Turbulence spectra in the upper troposphere and lower stratosphere at periods between 2 hours and 40 days, J. Atmos. Sci., 39, 1035-1041.

Gage, K. S. and W. L. Ecklund (1982), Objective tropoapuse height determination using a low resolution VHF radar, Radio Science.

Avery, S. K., A. C. Riddle and B. B. Balsley (1983), The Poker Flat, Alaska MST radar as a meteor radar, Radio Sci., 18, 1021-1027.

Balsley, B. B., W. L. Ecklund and D. C. Fritts (1983), Mesospheric radar echoes at Poker Flat, Alaska: Evidence for seasonally-dependent generation mechanisms, Radio Sci., 18, 1053-1058.

Balsley, Ben B. (1983), Poker Flat MST radar measurement of winds and wind variability in the mesosphere, stratosphere and troposphere, Radio Sci., 18, 1011-1020.

Balsley, B. B., W. L. Ecklund and K. S. Gage (1983), On the use of clear-air ST radars to observe winds, waves and turbulence in the troposphere and lower stratosphere, Preprint Vol., Fifth AMS Symp. on Meteorol. Observations and Instrumentation, April 11-15, Toronto, Ontario, Canada.

Ecklund, W. L. and K. S. Gage, Vertical wind observations using UHF clear-air radars, Preprint Vol, Fifth AMS Symp. on Meteorol., Observations and Instrumentation, April 11-15, 1983, Ontario, Canada.

Luhmann, J. G., R. M. Johnson, M. J. Baron, B. B. Balsley and A. C. Riddle (1983), Observations of the high latitude ionosphere with the Poker Flat MST radar: Analyses using simultaneous Chatanika radar measurements, submitted to Geophys. Res. Lett.

Balsley, B. B., W. L. Ecklund and D. C. Fritts (1983), VHF echoes from the artic mesosphere and lower thermosphere, Part I: Observations, 1983 Proc. of U.S.-Japan Seminar.

Fritts, D. C., B. B. Balsley and W. L. Ecklund (1983), VHF echoes from the artic mesosphere and lower thermosphere, Part II: Interpretations, Proc. of U.S.-Japan Seminar.

Balsley, B. B. and A. C. Riddle (1983), Monthly mean values of the mesospheric wind field over Poker Flat, Alaska, and a proposed polar circulation cell, submitted to J. Atmos. Sci.

Balsley, B. B., W. L. Ecklund and D. C. Fritts (1983), VHF echoes from the high-latitude mesosphere and lower thermosphere: Observations and interpretations, J. Atmos. Sci., 40, 2451-2466.

# 5.6A COMPLEMENTARY CODE AND DIGITAL FILTERING FOR DETECTION OF WEAK VHF RADAR SIGNALS FROM THE MESOSPHERE

G. Schmidt, R. Ruster and P. Czechowsky

Max-Planck-Institut fur Aeronomie
D-3411 Katlenburg-Lindau 3, Germany

The following is an excerpt from this paper which was published in IEEE Transactions on Geoscience Electronics, Vol. GE-17, No. 4, 1979, 154-161.

## THE SOUSY RADAR FACILITY

The SOUSY-VHF-Radar operates at a frequency of 53.5 MHz in a valley in the Harz mountains, Germany, 90km from Hanover. Figure 1 presents a block diagram of the radar facility with the main system parameters. The radar controller, which is programmed by a 16-bit computer, is the central unit. It holds 1024 program steps in core and controls, via 8 channels, the whole radar system: in particular the master oscillator, the transmitter, the transmit-receive-switch, the receiver, the analog to digital converter, and the hardware adder.

The transmitter operates as a linear amplifier with a bandwidth of 2.5 MHz. The peak pulse power is 600 kW and the duty cycle 4 percent. The pulse length can be varied from 0.8 to 100 μs. The maximum height resolution is somewhat larger than 120 m because the receiver bandwidth is 1 MHz. Pulse length, pulse coding, and pulse repetition frequency are easily adjustable to the requirements of the different observational programs by software instructions.

The transmitter, the receiver, and the antenna are connected to a high-speed transmit-receive switch with a recovery time of less than 5 μs, corresponding to a minimum radar range of about 750 m. The transmitting antenna consists or a system of 196 four-element Yagis with a total gain of 31 dB and a half-power beamwidth of 5°. To reduce interference with commercial TV stations and to reduce the influence of ground clutter from the surrounding mountains, the suppression of the first side lobes of the antenna pattern is about 20 dB and the antenna response far off-axis (which corresponds to low elevation angles) is approximately 40 dB. At present the antenna beam is directed to the zenith. By means of a system of 4-bit phase shifters, which are computer controlled, the extended version of this array will be steerable continuously in any direction within a cone of 30° vertex angle centered on the vertical. The high-sensitivity receiver has a dynamic range of 70 dB and a video bandwidth of 1 MHz. The complex signals at the receiver output are digitized by an analog-to-digital converter. The maximum sample frequency is 2 megawords/s, with a word length of 10 bits, corresponding to a dynamic range of 57 dB. These digitized complex signals can be coherently added by a hardware adder with a maximum core for 1024 complex values. The adder also is used for coding techniques. Phase coding schemes are applied, in particular for investigations at mesospheric heights, in order to carry out measurements with the maximum duty cycle and the maximum height resolution. The computer takes the data from the adder to store it in magnetic tape or disc.

The central unit of the radar facility is the radar controller, which synchronously controls the whole system. The radar controller is programmed by the computer using simple Fortran IV statements. After the program has been loaded and the computer has started the radar controller, it runs automatically, stopping at the program end. In case of errors or failures occurring during the radar operation, the radar controller is shut off caused either by a

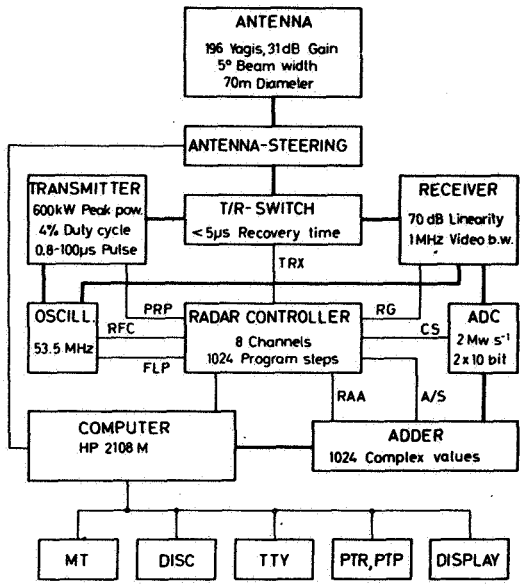


Figure 1. Block diagram of the SOUSY-VHF-Radar facility. (MT-magnetic tape, DSC-moving head disc, TTY- eletype, PTR, PTP-paper tape read/punch, DISPLAY-storage oscilloscope.

safety circuit from the transmitter and the transmit-receive-switch or by a power failure circuit or by a parity check system in the radar controller. The response time of a shutdown in only 50 ns.

Figure 2 shows the block diagram of the radar controller. Its program, generated by the computer, is stored in two different memories and two latches. The core size of each memory is 1024 storage locations of 8-bit length. An additional bit is used for parity check. The first memory (program memory) contains the various commands and the second (rate memory) the respective time intervals for which the commands have to be carried out. These execution times are counted in clock periods, which can be chosen to be 0.5, 1, 2, or 4 µs each. Since a storage location in the rate memory consists of 8 bits, the maximum length to be stored is 255 clock periods. If, however, a program step longer than 255 clock periods is required, this command is divided into several

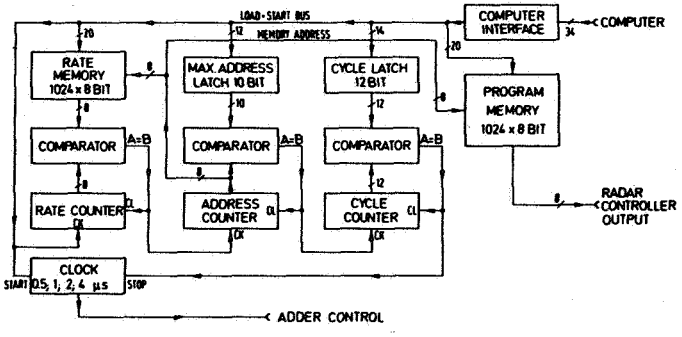


Figure 2. Block diagram of the radar controller.

sequential program steps. The two latches contains the number of repetitions of the radar cycle (cycle latch) and the maximum address for the program in the rate and program memory (maximum address latch). Three cascaded counters with comparators for reset are used as address counter, rate counter, and cycle counter.

PUBLICATIONS RELATING TO THE SOUSY RADAR

"Forschungsschwerpunkt 'Untere Atmosphare' - Vorlaufige Studie der Arbeitsgruppe SOUSY" Interner Bericht, Max-Planck-Institut fur Aeronomie, Lindau/Harz, Juni 1974.

Czechowsky, P. (1976), Optimierung des Antennensystems fur die Lindauer VHF-Radaranlage, Kleinheubacher Ber. 19, 123-126.

Czechowsky, P., J. Klostermeyer, J. Rottger, R. Ruster and G. Schmidt (1976), Ein kontinuierlich steuerbares VHF-radarantnnensystem zur Beobachtung von Scattersignalen aus der mittleren Atmosphare, Kleinheubacher Berichte, 19, 117-122.

Czechowsky, P., J. Klostermeyer, J. Rottger, R. Ruster, G. Schmidt and R. F. Woodman (1976), The SOUSY-VHF radar for tropo-, strato- and mesospheric sounding, Preprint Volume, 17th Conf. on Radar Meteorol., 349-353, AMS, Boston, MA.

Ruster, R. and R. F. Woodman (1976), Radar measurements in the tropo-, strato-, and mesosphere, Preprints, 17th Conf. Radar Meteorol., Seattle, Wash., Amer. Met. Soc., 353-358.

Rottger, J. and P. Czechowsky (1977), Clear-air turbulence and tropospheric refractivity variations observed with a new VHF-radar, Naturwissenschaften, 64, 580.

Klostermeyer, J. and C. H. Liu (1978), Indication of gravity wave-mean flow interaction in upper atmospheric radar observations, Geophys. Res. Lett. 5, 507-510.

Czechowsky, P., R. Ruster and G. Schmidt (1979), Variations of mesospheric structures in different seasons, Geophys. Res. Lett., 6, 459-462.

Rottger, J. and P. Czechowsky (1978), VHF-radar echoes from the troposphere and stratosphere, Kleinheubacher Berichte, 21, 279-290.

Rottger, J. (1978), Evidence for partial reflection of VHF radar signals from the troposphere, J. Geophys., 44, 393-394.

Rottger, J. and P. K. Rastogi (1978), High resolution VHF radar observations of turbulence structures in the mesosphere, Report MPAE-W-00-78-30, Max-Planck-Institut fur Aeronomie, Katlenburg-Lindau.

Rottger, J. and C. H. Liu (1978), Partial reflection and scattering of VHF signals from the clear atmosphere, Geophys. Res. Lett., 5, 357-360.

Rottger, J., J. Klostermeyer, P. Czechowsky, R. Ruster and G. Schmidt (1978), Remote sensing of the atmosphere by VHF radar experiments, Naturwissenschaften, 65, 285-296.

Rottger, J. and R. A. Vincent (1978), VHF radar studies of tropospheric velocities and irregularities using spaced antenna techniques, Geophys. Res.

Lett., 5, 917-920.

Ruster, R., J. Rottger and R. F. Woodman (1978), Radar measurements of waves in the lower stratosphere. Geophys. Res. Lett. 5, 555-558.

Ruster, R. and R. F. Woodman (1978), Digital filtering, calibration and correlation analysis of radar-echoes from the tropo- and stratosphere. Kleinheubacher Berichte 21, 239-246.

Klostermeyer, J., R. Ruster, P. Czechowsky, J. Rottger, and G. Schmidt (1979), VHF-radar erkundet atmosphare, Umschau 79, 514-515.

Schmidt, G., R. Ruster and P. Czechowsky (1979), Complementary code and digital filtering for detection of weak VHF radar signals from the mesosphere, IEEE Trans. Geosci. Electron., GE-17, 154-161.

Rottger, J. (1979), VHF radar observations of a frontal passage, J. Applied Meteorol., 18, 85-91.

Rottger, J., P. K. Rastogi and R. F. Woodman (1979), High-resolution VHF radar observations of turbulence structures in the mesosphere, Geophys. Res. Lett., 6, 617-620.

Rottger, J. and G. Schmidt (1979), High-resolution VHF radar sounding of the troposphere and stratosphere, IEEE Trans. Geosci. Electr., GE-17, 182-189.

Czechowsky, P. and K. Meyer (1980), Das antennensystem des SOUSY-VHF-radars internal report, MPAE-T-00-80-19, Max-Planck-Institut fur Aeronomie, 3411 Katlenburg-Lindau, FRG.

Czechowsky, P., R. Ruster and G. Schmidt (1980), VHF-radar observations of structures and their dynamics in the stratosphere and mesosphere, Preprints, 19th Conf. Radar Meteorol., Miami, Amer. Met. Soc., 588-592.

Klostermeyer, J. and R. Ruster (1980), Radar observation and model computation of a jet stream-generated Kelvin-Helmholtz instability, J. Geophys. Res. 85, 2841-2846.

Rottger, J. (1980), Structure and dynamics of the stratosphere and mesosphere revealed by VHF radar investigations, J. Pure Appl. Geophys., 118, 494-527.

Rottger, J. (1980), Reflection and scattering of VHF radar signals from atmospheric refractivity structures, Radio Sci., 15, 259-276.

Ruster, R. and P. Czechowsky (1980), VHF radar measurements during a jet stream passage, Radio Sci. 15, 363-369.

Ruster, R., P. Czechowsky and G. Schmidt (1980), VHF-radar measurements of dynamical processes in the stratosphere and mesosphere, Geophys. Res. Lett. 7, 999-1002.

Vincent, R. A. and J. Rottger (1980), Spaced antenna VHF radar observations of tropospheric velocities and irregularities, Radio Sci., 15, 319-335.

Woodman, R. F., R. P. Kugel and J. Rottger (1980), A coherent integrator-decoder preprocessor for the SOUSY-VHF-Radar, Radio Sci., 15, 233-242.

Rottger, J. (1980), Development of refractivity structures during anticyclonic

weather conditions, Preprint Volume, 19th Conf. on Radar Meteorol., April 15-18, Miami, FL, 593-598, AMS, Boston, MA.

Rottger, J. and P. Czechowsky (1980), Tropospheric and stratospheric wind measurements with the spaced antenna drifts technique and the Doppler beam swinging technique using a VHF radar, Preprint Volume, 19th Conf. on Radar Meteorol., April 15-18, Miami, FL, 577-584, AMS, Boston, MA.

Rastogi, P. K. and J. Rottger (1980), Radar detection of tropopause by coherent reflections at very high frequencies, Preprint Volume, 19th Conf. on Radar Meteorol., April 15-18, Miami, FL, 616-623, AMS, Boston, MA.

Rottger, J. (1980), Utilization of the lower VHF band for radar experiments at the Arecibo Observatory, Technical Rep. MPAE-T-00-80-01, Max-Planck-Institut fur Aeronomie, Katlenburg-Lindau.

Klostermeyer, J. (1981), MST radars: advanced tools for gravity wave studies, Nature 292, 107-108.

Klostermeyer, J. and R. Ruster (1981), Further study of a jet stream-generated Kelvin-Helmholtz instability, J. Geophys. Res. 86, 6631-6637.

Rottger, J. (1981), Investigations of lower and middle atmosphere dynamics with spaced antenna drifts radars, J. Atmos. Terr. Phys., 43, 277-292.

Rottger, J., T. Y. Kang and M. Y. Zi (1981), Mountain lee waves detected in radar wind profiles, Report MPAE-W-00-81-36, Max-Planck-Institut fur Aeronomie, Katlenburg-Lindau.

Rottger, J., P. Czechowsky and G. Schmidt (1981), First low-power VHF radar observations of tropospheric, stratospheric and mesospheric winds and turbulence at the Arecibo Observatory, J. Atmos. Terr. Phys., 43, 789-800.

Rottger, J. (1981), The dynamics of stratospheric and mesospheric fine structure investigated with an MST VHF radar, Handbook for MAP, 2, Extended abstracts from Int. Symp. on Middle Atmosphere Dynamics and Transport, 341-350, ed. S. K. Avery, SCOSTEP Secretariat, Univ. Ill. Urbana/Champaign.

Rottger, J. (1981), The capabilities of VHF radars for meteorological observations, ESA SP-165 (Nowcasting: Mesoscale Observations and Short-Range Prediction, Proc. of an International Symp., 25-28 August, Hamburg, Germany (Part of the IAMAP Third Scientific Assembly), 143-148 (Publ. by European Space Agency, Paris, June 1981).

Rottger, J. (1981), Wind variability in the stratosphere deduced from spaced antenna VHF radar measurements, Preprint Volume, 20th Conf. on Radar Meteorol., Nov 30- Dec 3, Boston, MA, 22-29, AMS, Boston, MA.

Rottger, J. and G. Schmidt (1981), Characteristics of frontal zones determined from spaced antenna VHF radar observations, Preprint Volume, 20th Conf. on Radar Meteorol., Nov 30 - Dec 3, Boston, MA, 30-37, AMS, Boston, MA.

Czechowsky, P. (1982), Phasengesteuerte Flachenantenne im VHF-Bereich, NTG-Fachberichte 78, 16-20, VDE-Verlag GmbH, Berlin, Offenbach.

Czechowsky, P., R. Ruster and G. Schmidt (1982), VHF-Radarmessungen wahrend ALPEX, Annalen der Meteorologie 19, 124-126.

Klostermeyer, J. (1982), Fernerkundung mit MST-Radars, Ann Meteorol. 18, 91-93.

Rastogi, P. K. and J. Rottger (1982), VHF radar observations of coherent reflections in the vicinity of the tropopause, J. Atmos. Terr. Phys., 44 461-469.

Rottger, J. (1982), Mesosphere-stratosphere-troposphere radar, EISCAT Meetings 82/7, Vol. I (Proc. of the EISCAT Annual Review Meeting 1982, Riksgransen, Sweden, 8-12 March, editor: Kristen Folkstad), 155-169.

Larsen, M. F. and J. Rottger (1982), VHF and UHF Doppler radars as tools for synoptic research, Bull. Amer. Met. Soc., 63, No. 9, 996-1008.

Larsen, M. F. and J. Rottger (1982), Analysis of VHF radars and radiosonde data during a frontal passage, Manuscript, Cornell University, EISCAT.

Ruster, R., P. Czechowsky, G. Schmidt and K. Labitzke (1982), VHF-radar observations in the stratosphere and mesosphere during a stratospheric warming, J. Atmos. Terr. Phys. 45, 161-168.

Weber, G. R. and R. Ruster (1982), Occurrence of a dry front over the Alpine Region and Central Europe, ALPEX Preliminary Scientific Results, Geneva, December 1982, GARP-ALPEX Series Nr. 7, 108-117.

Weber, G. R., R. Ruster, and J. Klostermeyer (1982), VHF-Radarbeobachtungen von Frontenpassagen im Voralpengebiet, Annalen der Meteorologie 19, 99-101.

Czechowsky, P., G. Schmidt and R. Ruster (1983), The mobile SOUSY-Doppler radar - Technical design and first results, Internal Report, MPAE-W-00-83-09, Max-Planck-Institut fur Aeronomie, 3411 Katlenburg-Lindau, FRG, 1983.

Rottger, J., P. Czechowsky, R. Ruster and G. Schmidt (1983), VHF radar observations ot wind velocities at the Arecibo Observatory, J. Geophys. Res., 52, 34-39.

Larsen, M. F. and J. Rottger (1983), Comparison of tropopause height and frontal boundary locations based on radar and radiosonde data, Geophys. Res. Lett., 10, No. 4, 325-328.

Hocking, W. K. and J. Rottger (1983), Pulse-length dependence of radar signal strengths for Fresnel backscatter, Radio Sci., 18, 1312-1324.

Hocking, W. K., G. Schmidt and P. Czechowsky (1983), Absolute calibration of the SOUSY VHF stationary radar, Internal Report, MPAE-W-00-83-14, Max-Planck-Institut fur Aeronomie, 3411 Katlenburg-Lindau, FRG.

Rottger, J. (1983), The correlation of winds measured with a spaced antenna VHF radar and radiosondes, Proc. 21st Radar Meteorol. Conf., in press.

Ruster, R. and J. Klostermeyer (1983), VHF Radar observations of a Kelvin-Helmholtz instability in a subtropical jetstream, accepted for publication in: Geophys. Astrophys. Fluid Dynamics.

# 5.6B VHF RADAR MEASUREMENTS DURING MAP/WINE

P. Czechowsky, J. Klostermeyer, R. Ruster, G. Schmidt and J. Rottger*

Max-Planck-Institut fur Aeronomie, 3411 Katlenburg-Lindau,
Federal Republic of Germany

*Presently on leave at EISCAT, Kiruna, Sweden

In the past ten years, a new type of sensitive Doppler radars has been developed which operate in the very high frequency (VHF) band, usually near 50 MHz (wavelength $\lambda \sim 6$ m). These radars can measure profiles of background winds, tides, atmospheric gravity waves and turbulence at tropospheric, stratospheric and mesospheric heights. Their ability to observe simultaneously large- and small-scale processes makes them unique instruments for studying not only each process separately but also their nonlinear interactions.

The radar echoes are produced by scattering from refractive index structures with scales equal to $\lambda/2$ and partial reflections from refractive index gradients. Refractive index variations in turn are due to changes in temperature, pressure, humidity and free electron concentration. Free electrons play a major role only at mesospheric heights. In the troposphere and stratosphere, the radar echo power decreases strongly with height due to the exponential decrease of the air density whereas in the mesosphere, the free electrons may produce one or more local power maxima. Depending on geographic latitude, daytime and mode of radar operation, there is always a more or less extended height range around the stratopause yielding no radar echoes.

The distance at which a radar signal is scattered or reflected is obtained from the signal travel time and the speed of light. Doppler radars are phase coherent so that transmitted and received signals can be compared to get both amplitude and phase of the echoes. The usual procedure is to find the echo power as a function of the Doppler shift from the transmitter frequency. This Doppler spectrum contains all necessary information about the intensity of the refractive index variations at scales equal to $\lambda/2$, the mean velocity of the scattering volume in the direction of the antenna beam (radial velocity) and the distribution of random velocities within the scattering volume. The 3-dimensional velocity vector can be obtained by operating the radar in three independent antenna beam directions. The optimum temporal and spatial resolutions are about 1 min and 150 m, respectively.

The mobile VHF radar to be used during the MAP/WINE campaign on Andoya is a modified version of the SOUSY VHF radar being in operation for six years in the Harz Mountains (ROTTGER et al., 1978). The main system parameters are shown in figure 1a, paper 6.4B, this volume. The radar controller, which is programmed by a 16-bit computer, is the central unit. It holds 1024 program steps in core and controls the whole system: the master oscillator (OSCILL), the transmitter, the transmit-receive-switch (T/R-switch), the receiver, the analog-digital converter (ADC), and the hardware adder.

The transmitter operates as a class-C push-pull amplifier with a bandwidth of 3 MHz. The maximum pulse peak power is 200 kW with a duty cycle of 4%. The pulse length can be varied from 1 to 100 μs corresponding to a height resolution of 150 m to 15 km. To increase the signal-to-noise ratio, a pulse coding technique is applied (for details see SCHMIDT et al., 1979). The pulse length, coding and repetition frequency are easily adjustable to the requirements of the different observational programs by software instructions. The transmitter, the receiver and the antenna are connected to a high-speed transmit-receive-switch with a recovery time of less than 10 μs, corresponding to a minimum radar range

of 1.5 km.

The antenna array consists of 576 four-element Yagis with a total gain of 35.5 dB and a half power beam width of 3°. By means of a system of 110 four-port coaxial relays, the antenna diagram is steerable in three independent directions. To reduce interference and clutter, the suppression of sidelobes of the antenna pattern is about 25 dB at angles close to the zenith and about 40 dB for low deviation angles.

REFERENCES

Rottger, J. (1978), Naturwissensch., 65, 285.

Schmidt et al. (1979), IEEE Trans. Geosci. Electr., GE-17, 154.

# 5.7A THE URBANA MST RADAR, CAPABILITIES AND LIMITATIONS

O. Royrvik and L. D. Goss

Aeronomy Laboratory, Department of Electrical Engineering
University of Illinois, Urbana, Illinois 61801

## ABSTRACT

The 41-MHz coherent-scatter radar located northeast of the University of Illinois at Urbana, Illinois has been used during the last five years for studies of the troposphere, stratosphere and mesosphere regions. The antenna consists of 1008 halfwave dipoles with a physical aperture of 11000 $m^2$. Transmitted peak power is about 750 kW. Clear-air returns may be received from 6 km to 90 km altitude. Autocorrelation functions of the scattered signal are calculated on-line. From the autocorrelation functions the scattered power, line-of-sight velocity and signal correlation time are calculated. Some aspects of the troposphere/stratosphere and the mesosphere observations are described. Capabilities and limitations of the Urbana MST radar are pointed out, and recent and planned improvements to the radar are described.

## THE URBANA MST RADAR

The Urbana monostatic VHF radar has been in operation since 1978 (MILLER et al., 1978). It is located at the Aeronomy Laboratory Field Station approximately 10 km northeast of the University of Illinois at Urbana (40° 10'N, 88°10'W). Transmitted frequency is 40.92 MHz and peak transmitted power is, at the present, approximately 750 kW. The antenna consists of 1008 half-wavelength dipole elements divided into three parallel sections. This arrangement allows for limited steerability of the antenna by inserting different lengths of cable in the feedline to each of the three sections. The ground where the antenna is located slopes 1.5° to the to the southeast (36° south of east) so that the on-axis antenna position is off-vertical by the same amount. In addition, off-vertical antenna beam positions pointing approximately 2.5° off-vertical to the east and south, can be obtained by changing the relative phasing of the three antenna sections. The change of the antenna beam direction is done manually and is therefore not very practical for day-to-day operation. Both transmitter and receiver are connected to the antenna via a transmit/receive switch which consists of a set of gas-filled tubes. Due to recovery time of the switch only signals from above 9 km altitude can be received.

The receiver system consists of a low noise, broad band preamplifier, a filter and a single conversion receiver with a bandwidth of 230 kHz centered around 40.92 MHz (Figure 1). A toggle-switch attenuator is located between the mixer and the IF section to provide control of the 5.5 MHz IF frequency. The signal is quadrature phase detected, and the two components fed through a multiplexer and a 10-bit analog-to-digital converter with a conversion time of 10 $\mu$s. Data processing has until recently been done on a Digital Equipment Corporation PDP-15 minicomputer with 32 k of core memory. Data collection is under the control of a radar director that allows the pulse repetition frequency, number of samples, and altitude of first sample to be preset. Pulse repetition frequency is normally 400 Hz and due to computer limitations only 20 altitudes can be sampled. Samples of the returned signal can be taken anywhere from the upper part of the troposphere through the mesosphere, however, only a 30 km altitude range can be sampled at any one time. Fifty consecutive samples from each altitude range are coherently integrated so as to give an integrated sample each 1/8 s. Autocorrelation functions are calculated on line with 12 lags 1/8 s each. The correlation functions are

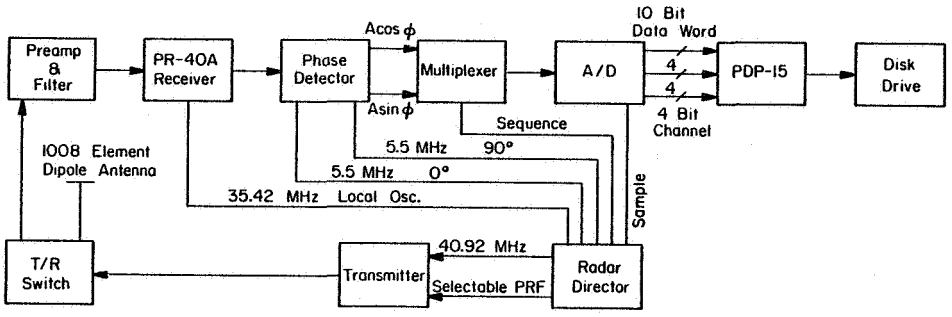


Figure 1. Block diagram of the Urbana MST radar in its most used configuration.

then incoherently integrated for one minute. The one-minute averaged autocorrelation functions are stored on magnetic tape for later processing. Scattered power, line-of-sight velocity and signal half-correlation time are calculated from the autocorrelation function. Hourly averages of power and velocity are also calculated. The radar parameters are summarized in Table 1.

## MESOSPHERIC EXPERIMENT

The mesosphere between about 60 and 90 km has been probed on a regular basis approximately once a week since the spring of 1978. Twenty μs Gaussian-shaped transmitted pulses have been used for the mesosphere in order to obtain maximum transmitted power. The resulting 3-km transmitted pulse has been sampled every 1.5 km, thus allowing some improvement in height resolution deconvoluting the returned signal. This technique, however, is not used on a regular basis. Data are normally taken in two-hour blocks during daylight hours and it is rare to find a day of no mesospheric scattered signal large enough to be detected above the noise level. Usually the scattering occurs in one or more layers that are stable in altitude. On a few occasions mesospheric data have been obtained under nighttime conditions, and the signal in those instances are believed to be due to meteor precipitation or high-energy particle precipitation from solar flares.

An example of a data set from the mesosphere is seen in Figures 2-4. The data were obtained on May 12, 1982 between 13:15 and 15:15 CST. The scattered power in Figure 2 shows a moderately disturbed day with a strong scattering layer in the region between 80- and 86-km altitude, and some scattered signal in most of the range gates below 80 km. Figure 3 shows the line-of-sight velocity for the same time period. The short period (5-15 min) velocity oscillations have relatively large amplitudes (2-5 m/s) and are likely to be the vertical velocity component of internal gravity waves. Since the antenna beam is off-vertical by 1.5° the line-of-sight velocity includes a small but important component of the horizontal velocity that has been reduced by a factor sin 1.5° $\approx$ 1/38. By averaging the line-of-sight velocity for one hour, and assuming that the one-hour-average of the vertical velocity component is zero, we can multiply the resulting averaged velocity by a factor of 38 and obtain the horizontal velocity in the southeast direction.

One may consider further the assumption of zero averaged vertical velocity. Any oscillation with periods shorter than one hour will not systematically contribute to the averaged hourly velocity; however they will

Table 1. Parameters of the Urbana MST radar

| | Mesosphere | Stratosphere/Troposphere |
|---|---|---|
| Radar frequency | 40.92 MHz | 40.92 MHz |
| Peak power | 750 kW | 750 kW |
| Pulse repetition frequency | 400 Hz | 400 Hz |
| Pulse width | 20 s | 10 μs 20 μs |
| Receiver system bandwidth | 100 kHz | 100 kHz |
| Range resolution | 3 km | 1.5 km |
| Antenna | 1008 dipole | |
| Antenna efficiency | -7.6 dB | |
| Physical aperture | 11000 $m^2$ | |
| Effective aperture | 450 $m^2$ | |
| Power gain | 27 dB | |
| Data | 12-lag ACF 1/8 sec lag | 12-lag ACF 1/8 sec lag |
| Time resolution | 1 min | 1 min |
| Maximum radial velocity | ± 14 m/s | ± 14 m/s |
| Number of range gates | 20 | 20 |
| Lowest altitude | 58 km | 6 km |

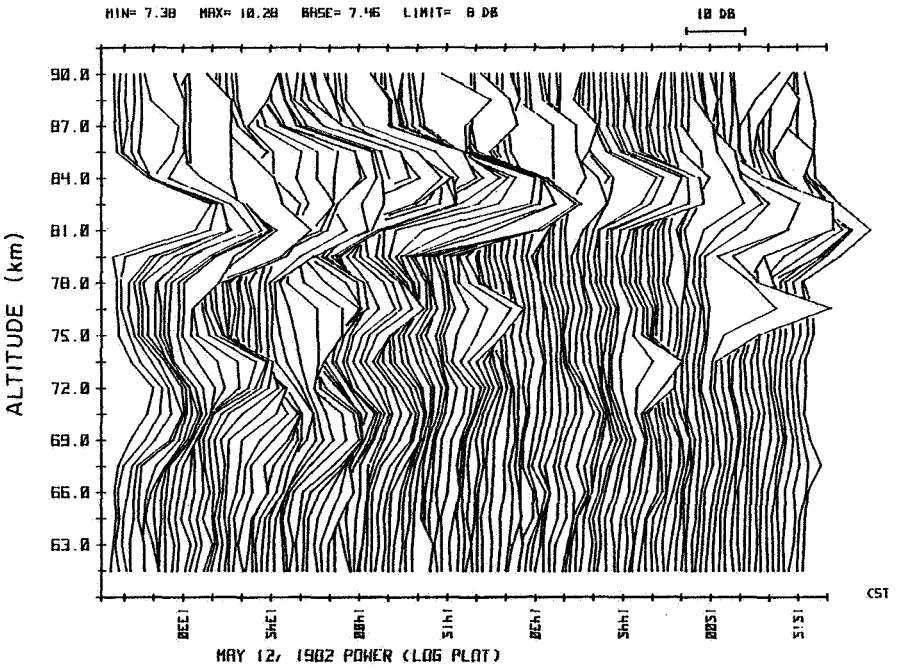


Figure 2. Scattered power map for May 12, 1982, 13:15 to 15:15 CST.

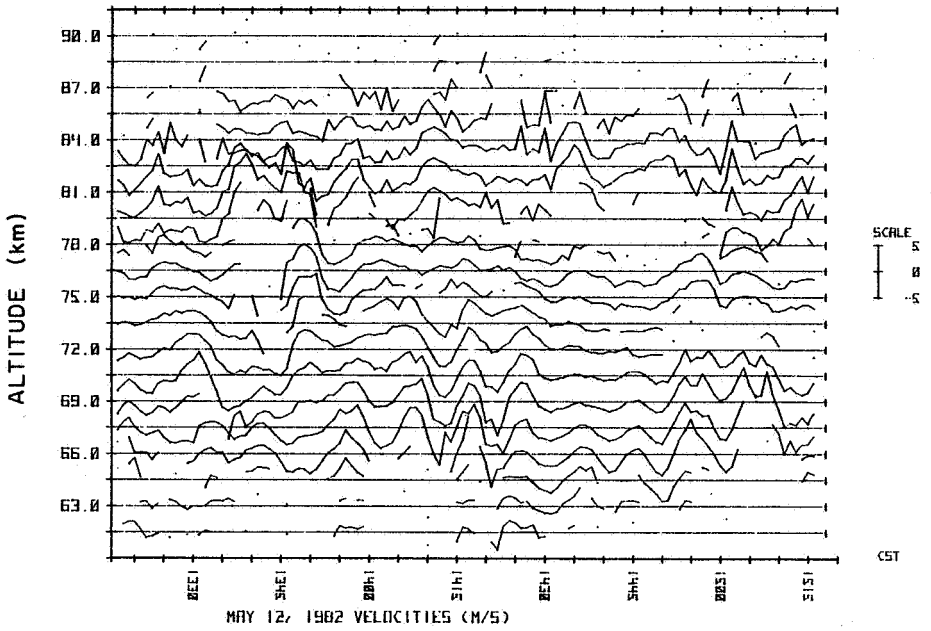


Figure 3. Line-of-sight velocities for May 12, 1982, 13:15 to 15:15 CST. The scale is 5 m/sec.

contribute to the uncertainty of the velocities. This contribution is considered to be geophysical noise. For velocity oscillations with periods larger than one hour we can apply the asymptotic relation that relates the velocities and periods; $\frac{\tau}{\tau g} \approx \frac{V_x}{V_z}$ (HINES, 1960). Here $\tau_g$ is the Brunt-Vaisala period, $\tau$ the period of oscillation, and $V_x$ and $V_z$ the horizontal and vertical velocities, respectively. Solving for the relationship we find that any oscillation with periods less than three hours will contribute to the average mainly through the vertical velocity component while those with periods longer than three hours will contribute mainly with the horizontal component. Thus observed tidal oscillations with periods from 6-24 (48) hours can safely be assumed to yield horizontal velocity components in these observations. This makes it necessary to assume that oscillations with periods of one to six hours have velocity amplitudes considerably smaller than the tidal oscillations. That this appears to be the case is apparent from most of the mesospheric data.

Figure 4 shows two examples of hourly averages from the two-hour data set in Figure 3. The top two plates show the averaged line-of-sight velocity as a function of height for each of the two one-hour sections. The two curves show the limits of the standard deviation, thus the actual velocity profile has a high probability of lying mainly between these curves. As can be seen by comparison, the details of the velocity profile change from one hour to the next; however, the overall picture of a wave with a vertical wavelength of 14-16 km is obvious in this example. In a large fraction of the data this kind of wave profile persists throughout the day while slowly descending making it obvious that tidal components dominate the wind velocity, and that oscillations or 1-6 hours are not usually large enough to mask the presence of tidal components. It is thus concluded that it is possible to study some

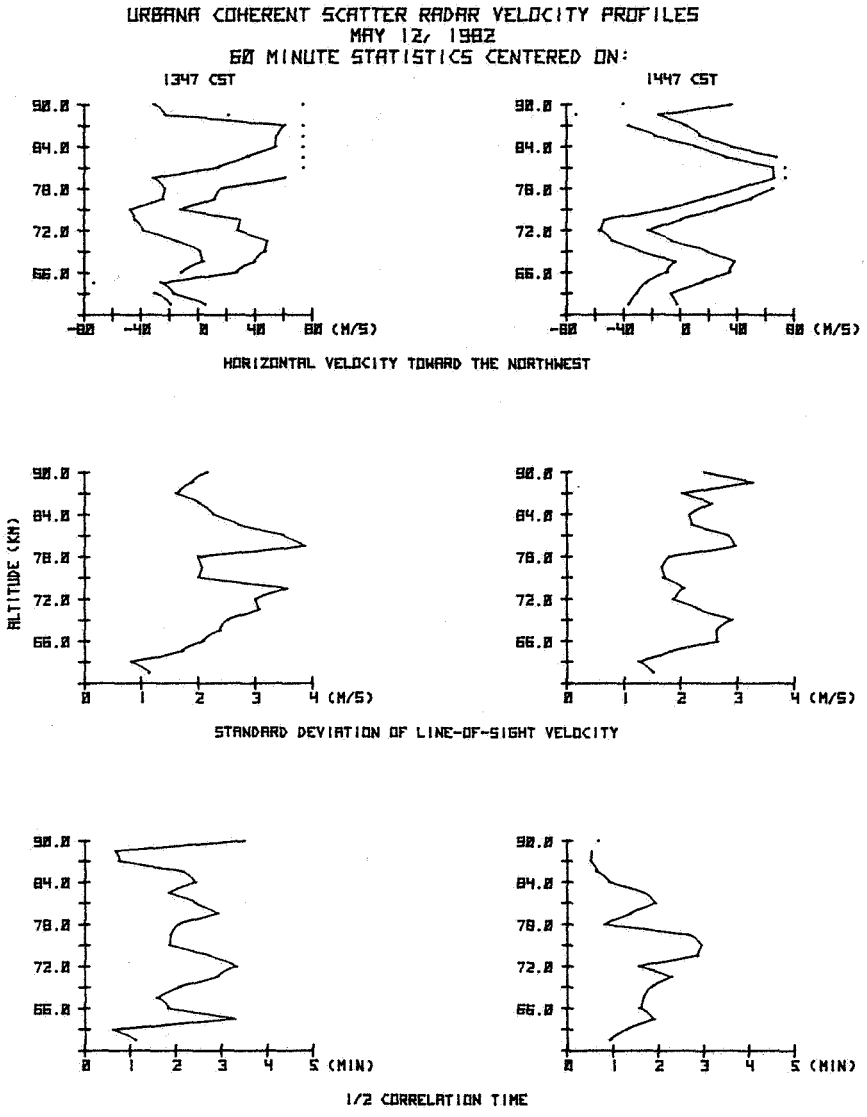


Figure 4. Diagram showing two one-hour averaged; (a) horizontal velocity towards the northwest; (b) standard deviation of the line-of-sight velocity; and (c) half-correlation time of the line-of-sight velocity oscillations. The data cover the two-hour period from 13:15 to 15:15 CST on May 12, 1982.

features of the long-period horizontal wind field using the Urbana radar although some care must be taken.

However, one complicating factor in interpreting these data is the aspect sensitivity of the scattered signal in the lower part of the mesosphere (FUKAO et al., 1980). The result of this aspect sensitivity is that the horizontal velocity is almost certainly being underestimated in the lower part of the mesosphere; however it is not a simple task to estimate by how much. A factor of two, however, seems like a reasonable upper limit.

The second set of plates in Figure 4 show the standard deviation of the line-of-sight velocity. This gives a good estimate of the amplitude of the velocity oscillations at any altitude averaged over one-hour periods. Thus a profile of gravity-wave activity is found. It can be seen that there is a slight tendency for an increase in amplitude with increasing altitude in both the hourly profiles. There are also two distinct peaks in the profiles at about 70 and 82 km. The reason for these peaks is not clear, however, they appear to be real since they are present in both profiles.

The last two plates in Figure 4 show the half-correlation time of the line-of-sight velocity time series. This gives a convenient estimate of the dominant frequency of the velocity oscillations. If a sinusoidal wave is assumed, a half-correlation time of 2 min is equivalent to a period of 12 min. Although there are substantial variations in the correlation time, it indicates that the dominant period is between 10 and 15 minutes for most altitudes especially during the first one-hour period.

## TROPOSPHERE-STRATOSPHERE OBSERVATIONS

Some troposphere-stratosphere observations have been made using the Urbana MST radar. There have been two main problems with this study, however. First of all, the transmit/receive switch presently used limits the lowest observable altitude to about 10 km. Secondly, the altitude resolution is 1.5 km, corresponding to a transmitted pulse width at its lowest possible limit of 10 μs. Useful scattered power is received from 9 to approximately 24 km on most occasions. An attempt was made to lower the observable altitude by receiving separately on a single 13-element Yagi antenna pointing vertically. This allowed data to be obtained down to 6 km as the lower altitude. However, the upper limit on useful data was 18 km in this case and the data were not nearly as continuous as that obtained by the large antenna. Thus a smaller amount of useful data was obtained when using the Yagi as a receiving antenna.

It has been possible to compare calculated horizontal velocities in the southeast direction to data obtained by a rawinsonde released from Peoria, Illinois 168 km to the northwest of Urbana. Figure 5 shows two wind profiles from the Peoria rawinsonde on July 15, 1982 at 6:00 CST and 18:00 CST. As can be seen, the southeast wind profile has changed substantially during the 12 hours between the two profiles. In particular, a large shear region has developed between 13 and 14 km. Figure 6 shows four velocity profiles obtained by the Urbana radar between 9:41 CST and 12:45 CST for the same day of July 15, 1982. In this set of profiles it is apparent that the large shear region is developing over the two-hour time interval between 10:41 CST and 12:45 CST. It is also apparent that the radar profiles at 9:41 CST and 12:45 CST compare reasonably well to the rawinsonde profiles of 6:00 CST and 18:00 CST, respectively. The differences can easily be attributed to differences in time and distance separating the two sets of observations. It is suggested that the significant wind shift that occurred in the 12-14 km region was associated with a warm front that moved through during the morning hours on July 15, 1982.

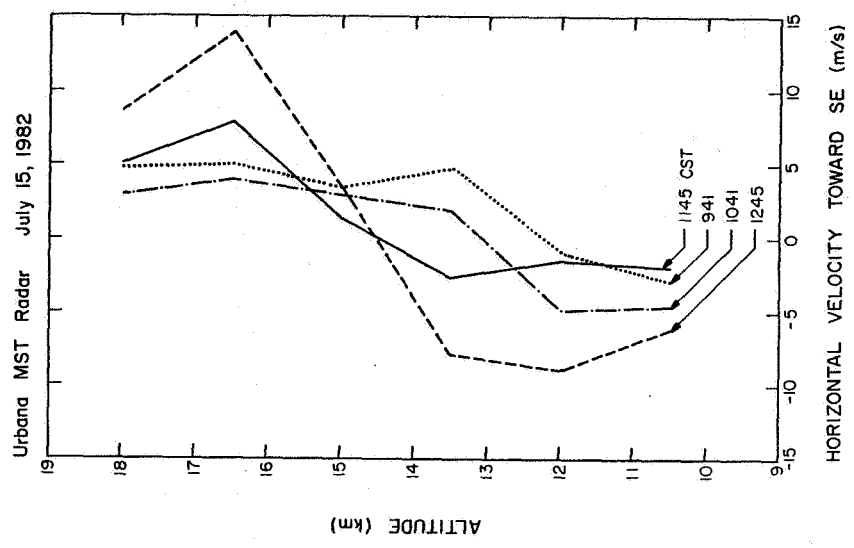


Figure 6. Profiles of horizontal velocity component towards the southeast from Urbana MST radar on July 15, 1982. Times are 9:41, 10:41, 11:45 and 12:45 CST.

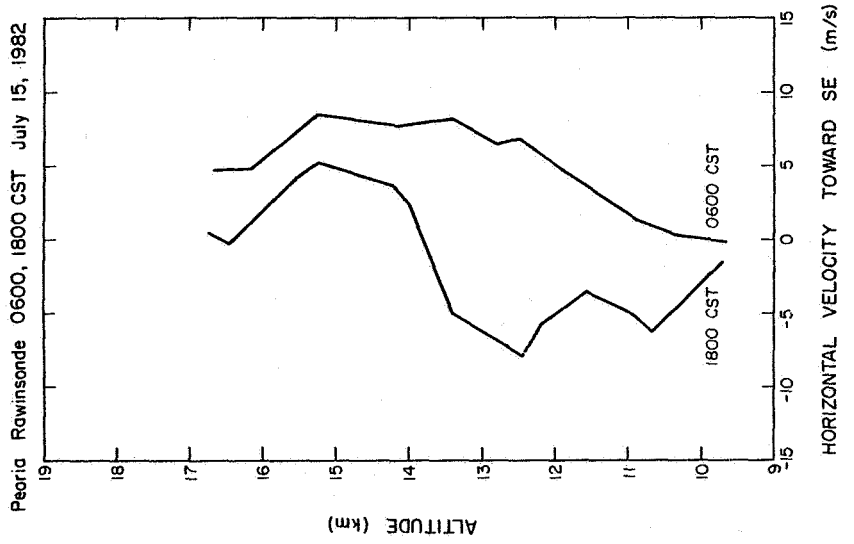


Figure 5. Profiles of horizontal velocity component towards the southeast from two Peoria rawinsonde releases on July 15, 1982. Times are 6:00 CST and 18:00 CST.

Interesting data have also been taken in the vicinity of thunderstorms. One example of this is shown in Figure 7. On the evening of June 29, 1982 a severe thunderstorm passed from west-to-east over the Urbana radar. Data taking was started as the main part of the storm had just passed. The updraft region of the storm can easily be seen between 18:40 and 19:00 CST between 12 and 15 km. These observations are compared to the National Weather Service radar summary at 1735 CST, approximately 1 hour before data collection began. The summary shows cloud top heights of 55,000 feet or 16.7 km in an area just west of Urbana. Thus, the observation of an updraft at 15 km is entirely possible for this storm. Gravity-wave activity, possibly related to the storm, was very strong reaching amplitudes of several m/s. This is several times the amplitude of 0.2 m/s that is normal for the troposphere/stratosphere region over Urbana. A large increase in gravity wave activity has been encountered during all observations involving strong convective activity.

Many groups using VHF radars have reported enhanced radio returns at vertical incidence in the troposphere/stratosphere region. These returns are thought to be caused by specular reflection from horizontally stratified layers in the lower stratosphere as opposed to scattering from isotropic turbulence (GAGE and GREEN, 1978).

Figure 8 shows hourly averaged power levels from the radar data compared to changes in potential temperature ($d\theta/dz$) as a function of altitude for July 22, 1982. The potential temperature is calculated from data available from nearby National Weather Service balloon soundings at five altitudes common to the range probed by the radar. The potential temperature is a good measure of the stability and stratification of the atmosphere at any given altitude in the stratosphere. There is a rough agreement between stability as represented by the potential temperature changes and the power profile. In particular, a layer of enhanced stability (positive $d\theta/dz$) exist around 12 km and a corresponding layer of enhanced scattering is evident in the power profile. Similar agreements are seen in other profiles of potential temperature changes and scattered power.

## POSSIBILITIES AND LIMITATIONS

It is clear that the Urbana MST radar has the capability to measure the line-of-sight velocities in parts of the troposphere/stratosphere and mesosphere regions. The slight off-vertical pointing direction of the antenna also allows a measurement of tidal and other long-period components of the horizontal wind in the southeast direction. Velocity measurements can be obtained from those altitude regions where the scattered signal exceeds the detection threshold set by the noise level. In order to increase the scattered signal level it is desirable to increase pulse length of the transmitted signal. However, this has the unfortunate side effect of decreasing the range resolution. One way of increasing transmitted power and still retaining high range resolution is to phase code the transmitted signal (WOODMAN, 1980). However, the Urbana transmitter has a narrow bandwidth so that the baud length has to be at least 6 μs, thus giving a 900 meter range resolution. This is not much better than the 1.5-km range resolution presently used in the troposphere/stratosphere region. Another way of increasing range resolution has been suggested by Bowhill (private communication) and will be implemented for the Urbana radar in the near future. In this scheme the radar will transmit a series of pulses at different but closely spaced frequencies. The signal phase values obtained from each of the different frequencies can then be combined to obtain a high altitude resolution (150 meters) while maintaining maximum transmitted power.

One problem that appears to be unique to the Urbana MST radar is oblique

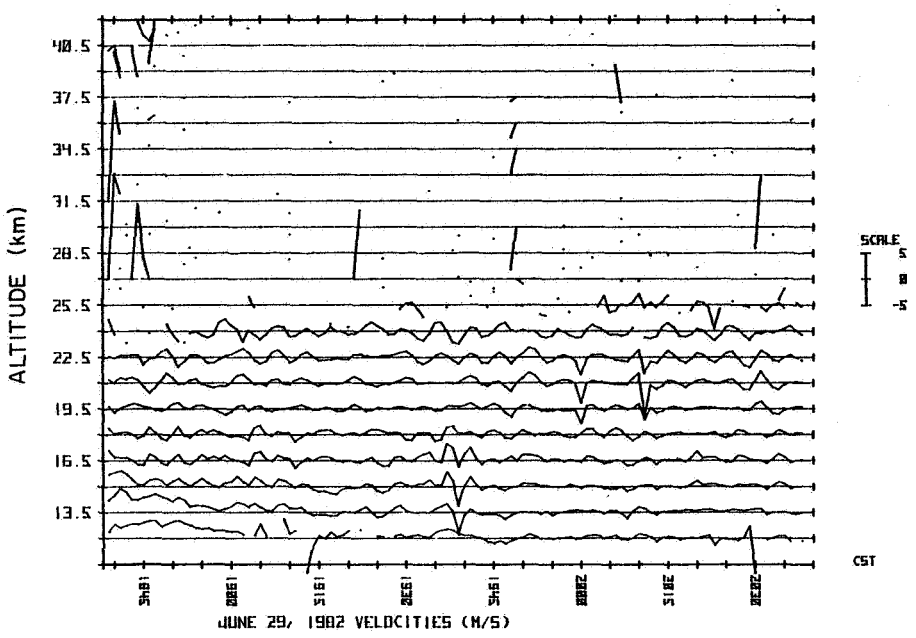


Figure 7. Line-of-sight velocity in the troposphere/stratosphere region between 18:40 and 20:40 CST on June 29, 1982.

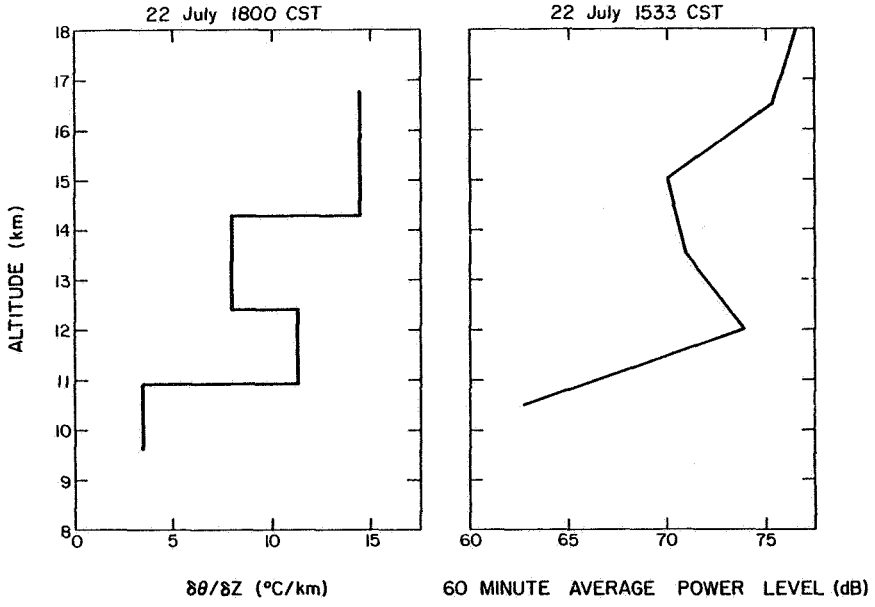


Figure 8. Profiles of potential temperature variations ($d\theta/dz$) from Peoria rawinsonde July 22, 18:00 CST; and scattered power profiles from the Urbana MST radar at 15:33 CST, same date.

reflection and backscatter. At times, especially during the November to March period, we have observed quite strong scattered power at all altitudes from ground level and up. The calculated velocities are identical in all range gates and slowly changing with a period of the order of one hour. Line-of-sight velocities can reach as much as 3-4 m/sec. It is believed that this signal is over-the-horizon ground reflection where the signal is obliquely reflected off the F layer, and transmitted/received in low elevation sidelobes of the antenna. Thus the received signal is range aliased. By using a variable interpulse period (IPP) and coherently integrating, it has been possible to reduce the strength of the aliased signal relative to the real signal from the troposphere/stratosphere and mesosphere region. In order to generate a variable IPP, an Apple II microcomputer has been implemented as a radar director. This allows software control of all radar parameters except for transmitted power and transmitted pulse length. Sets of 50 pulses are transmitted all with different IPP, thus the aliased signal will be incoherent from pulse to pulse, and will contribute only to the noise level.

The PDP-15 minicomputer used for data taking has deteriorated significantly during the last few years, and as a backup and possible replacement, an Apple II-based data-taking system is being implemented. The number of range gates sampled by the Apple system has been limited to 20, and correlation functions are being calculated on-line although with somewhat less accuracy than that of the PDP-15 data. The Apple data-collection system uses separate analog-to-digital converters and can be run independently from the old computer. We therefore now have the capability to take both tropospheric/stratospheric and mesospheric data simultaneously.

The Urbana radar also has the advantage of being located on a site where there are other instruments for probing similar regions of the atmosphere. These are: an HF partial-reflection drifts radar operating at 2.6 MHz, a meteor radar (40.92 MHz), a sodium LIDAR, and an ionosonde. The ionosonde is at the present not operational, but could be made so if desired. Of the other experiments the partial-reflection drift radar is probably the most interesting support for the MST radar. It is totally independent of, and can be run in parallel with, the MST radar. A preliminary comparison between velocities in the two radars show reasonable agreement (RUGGERIO and BOWHILL, 1982). In addition, there are some indications that the scattered power profiles at both 40.92 and 2.66 MHz are very similar between 60 and 90 km altitude, a point awaiting further study. The meteor radar and the MST radar cannot be run simultaneously since they use the same transmitter and receiving system. However, alternating between the two will allow comparison of long-period waves in the altitude region where the two experiments overlap between 80 and 90 km. The LIDAR is mainly a nighttime experiment and not very well suited for daytime operation so comparison with the MST radar cannot be made simultaneously.

Presently, modifications to the transmitter are underway to allow an increase of transmitted power, hopefully by a factor of 2. However, the most desirable improvement to the Urbana MST radar is an upgrading of the present antenna system.

REFERENCES

Fukao, S., T. Sato, R. M. Harper and S. Kato (1980), Radio wave scattering from the tropical mesosphere observed with the Jicamarca radar, Radio Sci., 15, 447-457.

Gage, K. S. and J. L. Green (1978), Evidence for specular reflection from monostatic VHF radar observations of the stratosphere, Radio Sci., 13, 991-1001.

Hines, C. O. (1960), Internal atmospheric gravity waves at ionospheric heights, Can. J. Phys., 38, 1441-1481.

Miller, K. L., S. A. Bowhill, K. P. Gibbs and I. D. Countryman (1978), First measurements of mesospheric vertical velocity by VHF radar at temperate latitude, Geophys. Res. Lett., 5, 939-942.

Ruggerio, R. and S. A. Bowhill (1982), New advances in the partial-reflection drifts experiment using microprocessors, Aeronomy Rep. No. 106, Aeronomy Lab., Dept. Elec. Eng., Univ. Ill., Urbana-Champaign.

Woodman, R. F. (1980), High-altitude resolution stratospheric measurements with the Arecibo 430-MHz radar, Radio Sci., 15, 417-422.

PUBLICATIONS RELATING TO URBANA MST RADAR

Allman, M. E. and S. A. Bowhill, Feed system design for the Urbana incoherent-scatter radar antenna, Aeron. Rep. No. 71, Aeron. Lab., Dep. Elec. Eng., Univ. Ill., Urbana-Champaign, 1976.

Miller, K. L., S. A. Bowhill, K. P. Gibbs and I. D. Countryman (1978), First measurements of mesospheric vertical velocities by VHF radar at temperate latitudes, Geophys. Res. Lett., 5, 939-942.

Countryman, I. D. and S. A. Bowhill, Wind and wave ovservations in the mesosphere using coherent-scatter radar, Aeron. Rep. No. 89, Aeron. Lab., Dep. Elec. Eng., Univ. Ill., Urbana-Champaign, 1979.

Gibbs, K. P. and S. A. Bowhill, The Urbana coherent-scatter radar: Synthesis and first results, Aeron. Rep. No. 90, Aeron. Lab., Dep. Elec. Eng., Univ. Ill, Urbana-Champaign, 1979.

Royrvik, O., K. P. Gibbs and S. A. Bowhill (1982), VHF power scattered from the mesosphere at midlatitudes, J. Geophys. Res., 87, 2501-2508.

Zendt, F. L. and S. A. Bowhill, A preprocessor for the Urbana coherent-scatter radar, Aeron. Rep. No. 102, Aeron. Lab., Dep. Elec. Eng., Univ. Ill., Urbana-Champaign, 1982.

Loane, J. T., S. A. Bowhill and P. E. Mayes, Feed system design and experimental results in the UHF model study for the proposed Urbana phased array, Aeron. Rep. No. 107, Aeron. Lab., Dep. Elec. Engin., Univ. Ill., Urbana-Champaign, 1982.

Tanner, D. R., P. E. Mayes and S. A. Bowhill, Phased array design including consideration of mutual coupling with application to the Urbana coherent-scatter radar, Aeron. Rep. No. 108, Aeron. Lab., Dep. Elec. Eng., Univ. Ill., Urbana-Champaign, 1982.

Herrington, L. J., Jr. and S. A. Bowhill, Phase modulating the Urbana radar, Aeron. Rep. No. 109, Aeron. Lab., Dep Elec. Eng., Univ. Ill., Urbana-Champaign, 1983.

Gibbs, K. P. and S. A. Bowhill, An investigation of turbulent scatter from the mesosphere as observed by coherent-scatter radar, Aeron. Rep. No. 110, Aeron. Lab., Dep. Elec. Eng., Univ Ill., Urbana-Champaign, 1983.

Goss, L. D., and S. A. Bowhill, Observations of the upper troposphere and lower stratosphere using the Urbana coherent-scatter radar, Aeron. Rep. No. 111, Aeron. Lab., Dep. Elec. Eng., Univ. Ill., Urbana-Champaign, 1983.

# 5.8A STRATOSPHERE AND TROPOSPHERE (S-T) STUDIES AT MILLSTONE HILL RECENT RESULTS, CAPABILITIES AND LIMITATIONS

P. K. Rastogi

Haystack Observatory
Massachusetts Institute of Technology
Westford, MA 01886

## ABSTRACT

The 440-MHz incoherent-scatter radar at Millstone Hill has been used in recent years for studies of the troposphere and lower stratosphere with a fully steerable 150' antenna. The configuration of the radar system is briefly outlined. Clear-air returns are received over an altitude range 4-25 km. The power spectra of these returns can be measured with a range resolution of up to 300 m and a Doppler resolution of up to 4 cm/sec. Due to the lack of a natural shield around the radar, the ground clutter at Millstone is more severe than at other installations. With the use of a fine Doppler resolution, however, the atmospheric returns are readily discriminated from the clutter. Recent observations of turbulence structures, spatial inhomogeneity of turbulence, and enhanced turbulence associated with convective phenomena are described. Capabilities and limitations of the Millstone S-T radar are pointed out.

## THE MILLSTONE HILL RADAR

For close to two decades, the 440-MHz UHF radar at Millstone Hill has been used for ionospheric studies with the incoherent-scatter technique (EVANS 1969). These studies initially were carried out with a 220' fixed antenna pointed 2° off zenith towards the south. A fully steerable 150' diameter antenna was added to the radar in 1977. The radar system was upgraded during 1981 with a CAMAC system for radar control and a Harris H-100A minicomputer in conjunction with a Floating Point Systems FPS-120B array processor (AP) for real-time data acquisition and processing. In the past, the UHF radar shared parts of its transmitter system with an L-band satellite-tracking radar. Recent upgrading efforts also have involved considerable modification to the transmitter system (EVANS and REID 1982) that make the operation of the UHF radar independent of the satellite tracking radar. The UHF radar system is used in several different experimental modes for studies of the ionosphere (HOLT et al., 1983), and in recent years also of the stratosphere and troposphere (S-T) region. A brief technical description of the radar is included in the Appendix. A list of publications related to the S-T work at Millstone Hill is appended to the references.

## THE S-T EXPERIMENTS AT MILLSTONE HILL

For studies of the stratosphere and troposphere, the 440-MHz radar is used as a pulsed Doppler radar, with either of the two antennas, at a peak power of 1.4 MW and a pulse repetition interval of 2 msec. Two experimental modes designated "I" and "M" have been utilized thus far. The I-mode is used at low elevation angles with an effective altitude resolution of 1 km. The M-mode obtains a finer altitude resolution (300 m), especially at high elevation angles, with the use of phase codes.

In the I-mode, pulses of 10 μs width are transmitted. The atmospheric returns are detected coherently with a receiver system of 100 kHz bandwidth (matched to the transmitted pulse width), sampled in range, digitized to a

12-bit accuracy and temporarily stored in the array processor. When a preset number of pulses has been transmitted, the array processor computes the periodogram of the samples for each range from the stored values. The periodograms are averaged over a time duration of 0.5 to 1 min to obtain a reasonable estimate of the power spectrum of the atmospheric returns. These power spectrum estimates, together with the radar-system parameters in effect, are added periodically to records on a disc file.

Owing to the radar location on a hilltop, the power-spectrum estimates contain a strong contribution due to ground clutter at the radar frequency. This contribution is smeared in frequency since samples taken over a finite duration only are used for computing the periodogram. As a consequence of this smearing, the clutter contribution falls off inversely as the square of the Doppler shift. The atmospheric returns are several orders of magnitude weaker than the ground clutter and are detected solely on the basis of their Doppler shift. For this reason, the I mode is used to cover the region (4-25 km) over which useful atmospheric returns can be obtained, at low elevation angles (10°-30°). This provides a viable experiment when the coarse altitude resolution (1 km) imposed by the pulse length and the beamwidth is acceptable.

The M-mode uses a longer sequence of atmospheric returns to compute the periodogram -- thus reducing the smearing of the ground clutter, and employs phase codes to achieve a better range resolution (300 m). To make full use of the fine range resolution available in this mode, use of high elevation angles (> 75°) is desirable.

In the M-mode, the transmitted pulses are of 32 μs width, and are successively phase modulated with a 16-baud complementary code pair. The receiver system has a 500-kHz bandwidth matched to the 2 μs baud length. The signals received following each pulse are decoded (i.e., correlated) with the code that is used to modulate the pulse. The complementary codes have the desirable property that, when the decoded returns due to the two codes in the pair are added, the contributions in the range sidelobes cancel. Complementary codes have been used in earlier experiments with the SOUSY (SCHMIDT et al., 1979) and the Arecibo radars (WOODMAN, 1980). At Millstone Hill, the decoding scheme has been implemented in software using the array processor.

The slow fading rates and smaller Doppler shifts of the atmospheric returns obtained at high elevation angles can be exploited to reduce the data-input rate to the processor with the use of coherent integration (WOODMAN, 1980). Thus the atmospheric returns for a code can be summed coherently over several successively transmitted pulses prior to the decoding operation. Further, the dc or zero-frequency contribution can be reduced by transmitting the alternate code pairs with a 180° phase shift and then correcting the received signal for this phase shift. Following the coherent integration and decoding operations, the power spectrum estimates are obtained as in the I-mode.

At present the altitude coverage in the M-mode is limited to 5 km by the size of the AP memory (32 kilo words). Efforts are underway to double the AP memory to 64 kilo words. This will provide a 10-km altitude coverage with a 300-m altitude resolution. The entire S-T region below 30 km then can be covered in two 10-km segments with a time resolution of 1-2 min for a fixed antenna pointing direction.

Table 1 summarizes the parameters of the S-T experiments used at Millstone Hill. Figure 1 shows a typical example of power spectra obtained at Millstone Hill with the I-mode. Examples of M-mode spectra are discussed in the following section.

Table 1. Parameters of the Millstone Hill radar for ST studies

| | | I-mode | M-mode |
|---|---|---|---|
| Radar frequency | $f_o$ | 440 MHz | 440 MHz |
| Peak power | $P_T$ | 1.4 Mw | 1.4 Mw |
| Pulse repetition interval | T | 2 ms | 2 ms |
| Pulse width | $\tau$ | 10 μs | 32 μs |
| Phase code | | none | 16 baud complementary |
| Baud rate | | none | 2 μs |
| Receiver bandwidth | | 100 KHz | 500 KHz |
| Range resolution | $\Delta r$ | 1.5 km | 300 m |
| Typical elevation angle | $\theta$ | 15°-30° | > 75° |
| Altitude resolution | $\Delta z$ | ~ 1 km | ~ 300 m |
| *Doppler window | $\pm f_{max}$ | ± 250 Hz | ± 62.5 Hz |
| Points in spectra | N | 256 | 512 |
| *Doppler resolution | $\Delta f$ | 2 Hz | 0.24 Hz |
| *Maximum radial velocity | $\pm v_{max}$ | ± 85.2 $ms^{-1}$ | 21.3 $ms^{-1}$ |
| *Radial velocity resolution | $\Delta v$ | 0.66 $ms^{-1}$ | 0.08 $ms^{-1}$ |
| †Number of range bins | $N_h$ | 38 | 17 |
| Lowest altitude | $Z_{min}$ | ~ 4 km | ~ 9 km |
| †Altitude coverage | | ~ 20 km | ~ 5 km |
| §Antenna | | 150' | 150' or 220' |
| System temperature | | 150 K | 150 K |

Notes: * These parameters can be scaled down by coherent integration. The I-mode usually is run without coherent integration. In M-mode, the coherent-integration interval is a multiple of 4 T.

† The number of range bins is constrained by the Array-processor memory (currently 32 K words) for given number of points (N) in the spectra. The choice of N indicated is dictated by the extent of ground-clutter smearing that can be tolerated. Efforts are underway to double the AP memory to 64 K, to increase the altitude coverage for the M-mode.

§ The 150-foot antenna is fully steerable. It can be moved in azimuth at 1° per second. It provides a beamwidth of 1°. The 220-foot antenna is pointed permanently at an elevation angle 88° due south and provides a beamwidth of 0.7°.

## RECENT RESULTS

The data acquisition programs for the upgraded Millstone Hill radar were developed and tested by R. H. Wand in June, 1981. These programs were used in a month-long campaign, jointly with the Air Force Geophysics Laboratory, to measure the refractive-index structure parameter ($C_n^2$) simultaneously by the radar, radiosondes and an optical scintillometer (GOOD et al., 1982).

In a series of observations during July - November 1981, the Doppler structure of atmospheric returns from regions of strong wind shear was observed at low elevation angles with a frequency resolution of 0.125 Hz, or a radial velocity resolution of 4 cm/sec. These experiments revealed a variety of thin turbulent structures, often dominated by breaking gravity-wave events and attributable, in one case, to Kelvin-Helmholtz instability. A comparison with radiosonde data indicates that the onset of one clear-air turbulence feature seen in the vicinity of the tropopause covered a horizontal extent of several hundred km (WAND et al., 1983).

During the remaining parts of 1981-82, over 400 hr of observations were made in several different configurations, primarily with the I mode. These configurations include observations along a fixed pointing direction for detecting short-period gravity-wave fluctuations, and observations along two

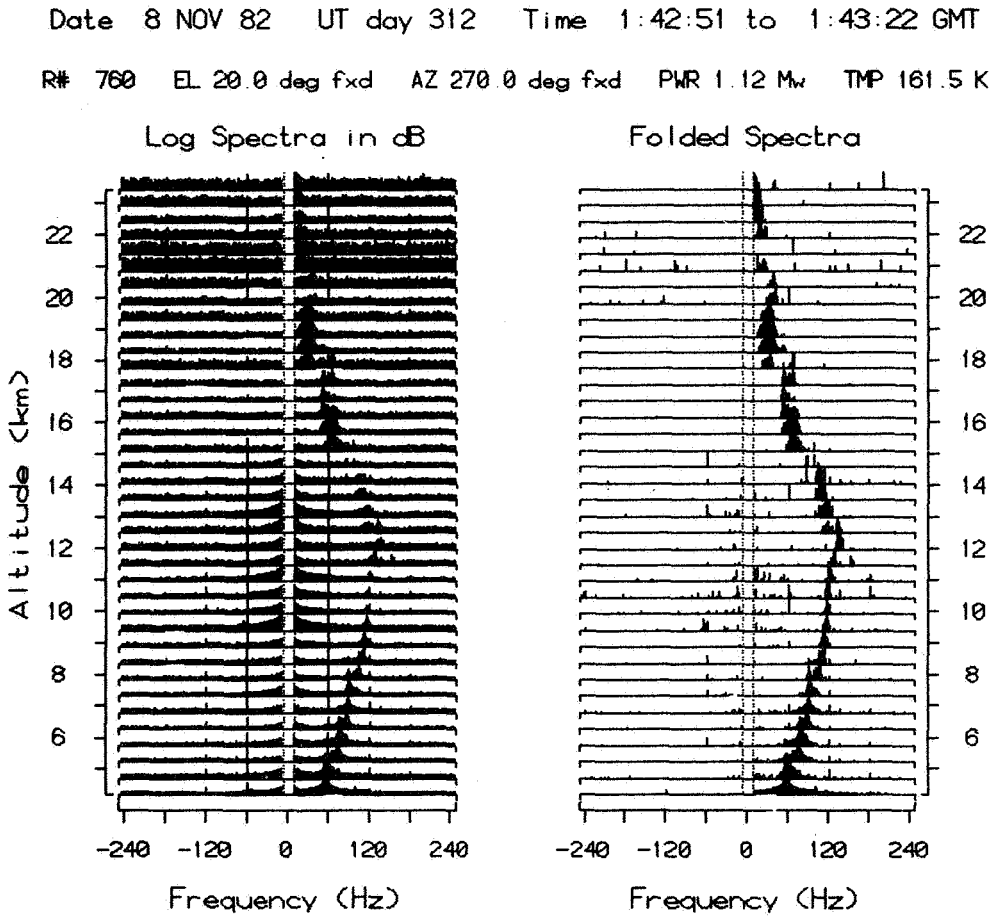


Figure 1. An example of power spectra obtained with the I mode. A narrow band of frequencies near the center has been suppressed. Spectra on the left show unusually strong clutter at 9-14 km. Spectra on the right are obtained by removing the part symmetric about the zero Doppler shift. A Doppler shift of + 60 Hz corresponds roughly to an eastward wind of 22 m/s in this case.

or more fixed azimuths to obtain the parameters of the horizontal wind field and turbulence. Limited observations (about 100 hr) also were made with the M mode on both the antennas. Most of these observations still are being analyzed. Preliminary results are described below.

Figure 2 shows the profiles of horizontal wind and signal power from measurements along two orthogonal azimuth directions at an elevation angle of 20°. The large difference of signal power along the two azimuth directions is indicative of patches of clear-air turbulence in the vicinity of the tropopause. Often, this difference persists for several hours. Enhanced turbulence appears to occur in regions of strong shear in the horizontal wind. Further analysis of these observations shows that the correlations between wind or wind shear and signal power are typically 0.5 to 0.7. At selected heights, these correlations can be even better for short intervals (3 hr or less).

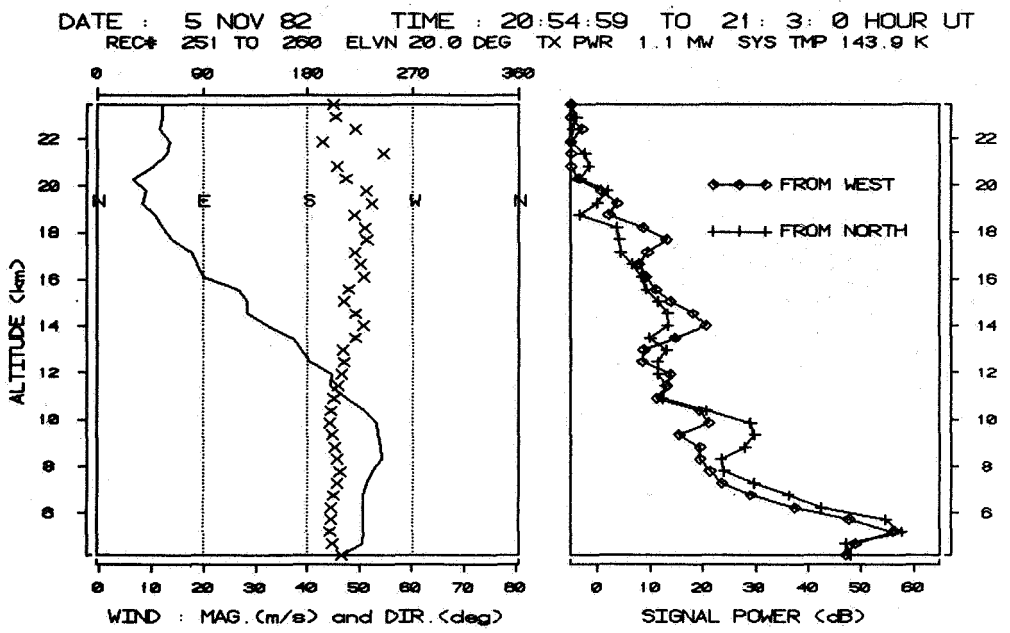


Figure 2. Profiles of horizontal wind and its direction (left) inferred from measurements along east and north at an elevation of 20°. Intensities of signals received along the two directions are shown on the right.

During one run on 8-9 September 1981, a moderate thunderstorm associated with the westerly passage of a cold front traversed Westford. The effect of this thunderstorm on the intensity of the signals received along twelve equispaced azimuths is shown in the series of plots in Figure 3. The asymmetric enhancement of the tropospheric signals corresponds roughly to the passage of the storm from the west to southeast. Enhanced echoes above the tropopause appear first to the north, then to the southeast as the storm moves away. These observations suggest that the turbulence in the lower stratosphere can be enhanced in the vicinity of a thunderstorm, probably as a consequence of the decay of short-period gravity waves that are generated by convection forced below the tropopause (LARSEN et al., 1982).

Figure 4 shows a plot of contours of constant signal power for a two-day interval on 17-19 July 1982. Throughout this interval the antenna was pointed towards east at a 20° elevation. A variable but persistent layer of turbulence at 14 km, in proximity of the tropopause level, is clearly visible. During the middle of this interval, two plume-like structures of turbulence can be seen that penetrate across the tropopause to heights of 19-20 km. Scattered precipipation was reported over southern New Hampshire on this day. It is possible that the observed plume-like structures are related to tropospheric convection associated with these precipipation events.

The modifications to the data-taking program for a 300-m altitude resolution, and the development of the software for decoding was completed by G. B. Loriot in November 1982. Observations with the 220' antenna during a day-long run in December 1982 indicate that stratospheric echoes can be received from altitudes as high as 25-26 km (as opposed to 28-29 km for Arecibo). Figure 5

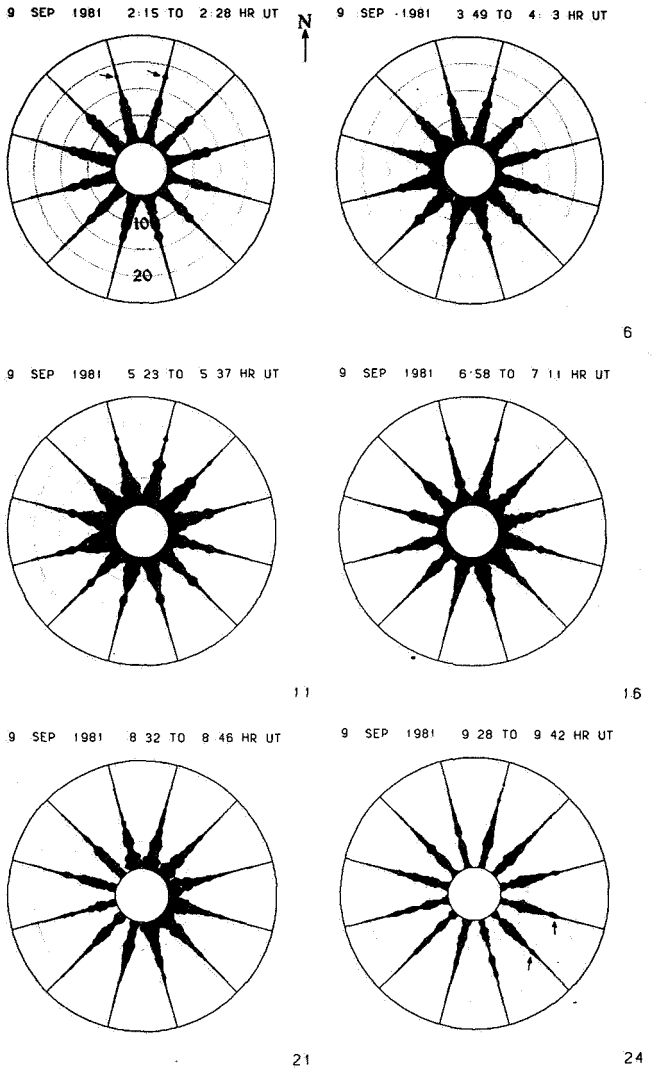


Figure 3. A sequence of plots (a through f) showing the log intensity of the received signals in a 12 position azimuth scan during the passage of a thunderstorm over Millstone Hill. Dotted circles are at a 5-km altitude interval and are spaced 17.5 km horizontally. The storm moves from the west towards the southeast. Stratospheric echoes enhanced by about 10 dB are marked with arrows and appear first to the north, then to the southeast.

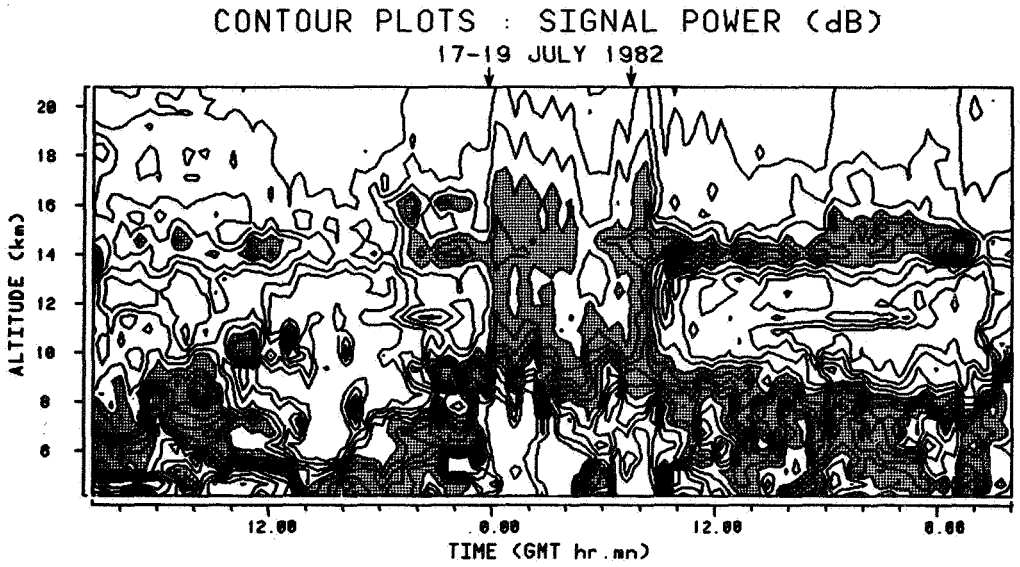


Figure 4. A plot showing the evolution of turbulence during a two-day period in the vicinity of the Millstone Hill radar. Contours are plotted at 2-dB intervals for detrended signal power. Shaded regions show signals that are 10-20 dB above the base power. A persistent layer is seen at 14 km. Arrows show the onset of two plume-like events that, probably, are related to convective activity to the north of the radar.

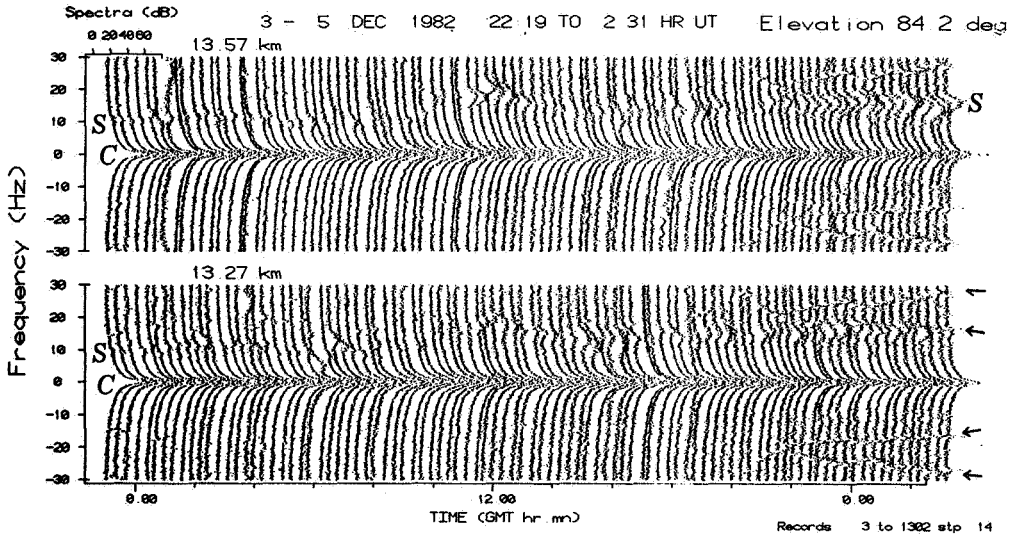


Figure 5. Time evolution of signal spectra for a 30-hr period at two heights and constant elevation in an elevation scan with 300-m altitude resolution (M mode). Each spectrum has 512 points. The ground clutter (C) and the Doppler-shifted signal peaks (S) are identified. Arrows show persistent external interference that complicates the task of inferring the spectral moments.

shows a sequence of spectra observed with the 150 antenna in the vicinity of the tropopause for a 30-hr interval. A program for obtaining wind and turbulence parameters from these spectra is under development.

## CAPABILITIES AND LIMITATIONS

The availability of two antennas at the Millstone Hill radar -- one pointed close to the vertical and the other fully steerable -- gives it a unique capability for studies of the dynamic phenomena in the troposphere and lower stratosphere. Its location is quite favorable for studying phenomena related to the polar-front jet stream.

Perhaps the most serious limitation of the radar is the lack of a natural shield around it. For this reason the radar suffers strong ground clutter at close ranges. Contamination of the atmospheric returns by the ground clutter is minimized, however, with the use of 12-bit analog-to-digital converters and by using a sufficiently large number of points (typically 512) in the spectra. This latter step provides better accuracy in estimating the spectral width of the atmospheric returns, and offers the possibility of obtaining improved estimates of the energy-dissipation rate due to turbulence (see e.g. SATO 1981). Due to the constraint of the finite processor memory, the number of range cells for which the spectra can be measured simultaneously at 512 points is reduced, however. Efforts currently underway to increase the array processor memory from 32 k words to 64 k words, and possibly to 256 k words, will circumvent this problem.

Further modifications to the transmitter to provide a 1 msec pulse repetition interval have recently been successful [W. A. REID, personal communication], albeit with a lower (1 MW) peak power. These modifications, if implemented for routine operation, will improve the detectability of signals above 25-km altitude.

## ACKNOWLEDGMENT

It is a pleasure to acknowledge the contributions of Dr. G. B. Loriot and Dr. R. H. Wand to the program described here. The development and maintenance support of Mr. W. A. Reid, Mr. P. M. Chizinski, Mrs. A. M. Gorczyca and Mr. R. R. Norander is gratefully acknowledged. The advice and guidance of Dr. J. V. Evans was invaluable throughout this work.

This material is based on work supported by the National Science Foundation under grant number ATM-8000060.

## REFERENCES

Evans, J. V. (1969), Theory and practice of ionosphere study by Thompson scatter radar, Proc. IEEE, 57, 496-530.

Evans, J. V. and W. A. Reid (1982), Upgrading the Millstone Hill radar for dual radar capability, Report, MIT Lincoln Lab., 54 pp., November 1982.

Good, R. E., B. J. Watkins, A. F. Quesada, J. H. Brown and G. B. Loriot (1982), Radar and optical measurements of $C_n^2$, Appl. Optics, 21, 3373-3376.

Holt, J. M., J. V. Evans, W. L. Oliver and R. H. Wand (1983), The upgraded Millstone-Hill radar, Radio Sci., in press.

Larsen, M. F., W. E. Swartz and R. F. Woodman (1982), Gravity-wave generation by thunderstorms observed with a vertically-pointing 430 MHz radar, Geophys. Res. Lett., 9, 571-574.

Sato, T. (1981), Coherent radar measurements of the middle atmosphere and design concepts of MU radar, Ph.D. thesis, Kyoto University, Kyoto, Japan, 219 pp.

Schmidt, G., R. Ruster and P. Czechowsky (1979), Complementary codes and digital filtering for detection of weak VHF radar signals from the mesosphere, IEEE Trans, Geosci. El., GE-17, 154-161.

Wand, R. H., P. K. Rastogi, B. J. Watkins and G. B. Loriot (1983), Fine Doppler resolution observations of thin turbulence structures in the tropo-stratosphere at Millstone Hill, J. Geophys. Res., 88, 3851-3857.

Woodman, R. F. (1980), High-altitude resolution stratospheric measurements with the Arecibo 430 MHz radar, Radio Sci., 15, 417-422.

PUBLICATIONS RELATED TO S-T WORK AT MILLSTONE HILL

The early observations of clear-air turbulence using the L-band radar at Millstone Hill have been reported by :

Crane, R. K. (1970), Measurements of clear-air turbulence in the lower stratosphere using the Millstone-Hill L-band radar, preprints, 14th Radar Meteor. Conf., pp. 101-106, AMS, Boston, MA.

Crane, R. K. (1980), A review of radar observations of turbulence in the lower stratosphere, Radio Sci., 15, 177-193.

The first observations with the UHF radar at Millstone Hill have been reported by :

Watkins, B. J. and R. H. Wand (1981), Observations of clear air turbulence and winds with the Millstone Hill radar, J. Geophys. Res., 86, 9605-9614.

Recent modifications and upgrading of the Millstone Hill UHF radar are described in :

Holt, J. M., J. V. Evans, W. L. Oliver and R. H. Wand (1983), The upgraded Millstone-Hill radar, Radio Sci., in press.

A comparison or refractivity-structure parameter measured at optical and UHF frequencies is made by :

Good, R. E., B. J. Watkins, A. F. Quesada, J. H. Brown and G. B. Loriot (1982), Radar and optical measurements of $C_n^2$, Appl. Optics, 21, 3373-3376.

Observations of thin structures of turbulence generated by wind shear have been reported by :

Wand, R. H., P. K. Rastogi, B. J. Watkins and G. B. Loriot (1983), Fine Doppler resolution observations of thin turbulence structures in the tropo-stratosphere at Millstone Hill, J. Geophys. Res., 88, 3851-3857.

# APPENDIX

## THE RADAR AT MILLSTONE HILL FOR S-T STUDIES

A block diagram of the 440-MHz UHF radar at Millstone Hill, as presently configured for S-T studies is shown in Figure A.1. Two antennas may be used in conjunction with the UHF transmitter: a fixed 220-foot antenna pointed due south at an elevation angle of 88 degrees, and a 150-foot fully steerable antenna. The transmitter normally is operated at a 1.4 to 1.6 MW peak power with either coded or uncoded pulses at a 2 ms pulse repetition interval. Three experimental modes, designated I, K and M, are used to S-T work. The I and K modes use uncoded pulses of 10 and 5 μs (2 μs in some cases), respectively. In the M mode, 32 μs pulses, phase coded with a 16-baud complementary code at a 2 μs baud rate, are used, Only the I and M modes are used routinely. Each of the two antennas is equipped with a low noise parametric amplifier, though the rest of the receiver is common. The overall system noise temperature typically is 150 K. The received signals are successively down converted to a 30-MHz intermediate frequency (IF) for the M mode, and to a 2 MHz IF for the I and K modes. Following the IF stage, bandlimiting is applied to match the receiver to the pulse length (for I and K modes), or the baud rate (for the M mode).

The receiver IF is detected coherently with a pair of quadrature phase detectors to obtain the inphase and quadrature (or the sine and cosine) components of the complex received signal. These components are sampled through a "comb" at range intervals corresponding to the pulse length (for I and K modes) or the baud rate (for the M mode), and digitized by 12-bit A-D converters. The Formatter is a locally built unit that sign-extends the 12-bit samples to 16 bits, and packs them pairwise into 32-bit words.

The GPIOP (General Purpose Input Output Processor) is a programmable controller that runs in parallel with the Array Processor (AP). It has two independently programmable processors: a Control Processor (CPROC) and a Formatting Processor (FPROC). The Formatting Processor unpacks the 32-bit words supplied by the Formatter, converts them to a 38-bit floating point format required by the Array Processor, and then transfers these 38-bit words to the Array Processor by a direct memory access channel. The Control Processor initiates transfer of blocks of radar data from the formatter in response to interrupts from the radar timer.

In the Array Processor are performed all the computation-intensive tasks, viz., coherent integration, decoding, Fourier transforms (FT) and the power spectrum estimation. The Array Processor runs as a peripheral to the H-100 computer, connected to it as a UBC (Universal Block Controller) channel. The processed results from the Array Processor, usually in the form of the time-averaged periodograms, are transferred to the H-100 computer. These results are stored on a disk file and saved later on magnetic tape. Current or past spectra on this disk file can be examined on a fast vector display (256 kHz rate).

The H-100 computer controls and monitors the various radar functions through a CAMAC (Computer Automated Measurement and Control) system that utilizes the same UBC as the Array Processor for an input-output path. The radar information input to the H-100 includes the antenna azimuth and elevation, peak transmitter power, a refractometer reading, day number, time and other radar status parameters. Settings of 24 operator-selectable sense switches also are input to the H-100, and provide a ready means of controlling the various program functions.

Program output commands via the CAMAC channel are used to supply the

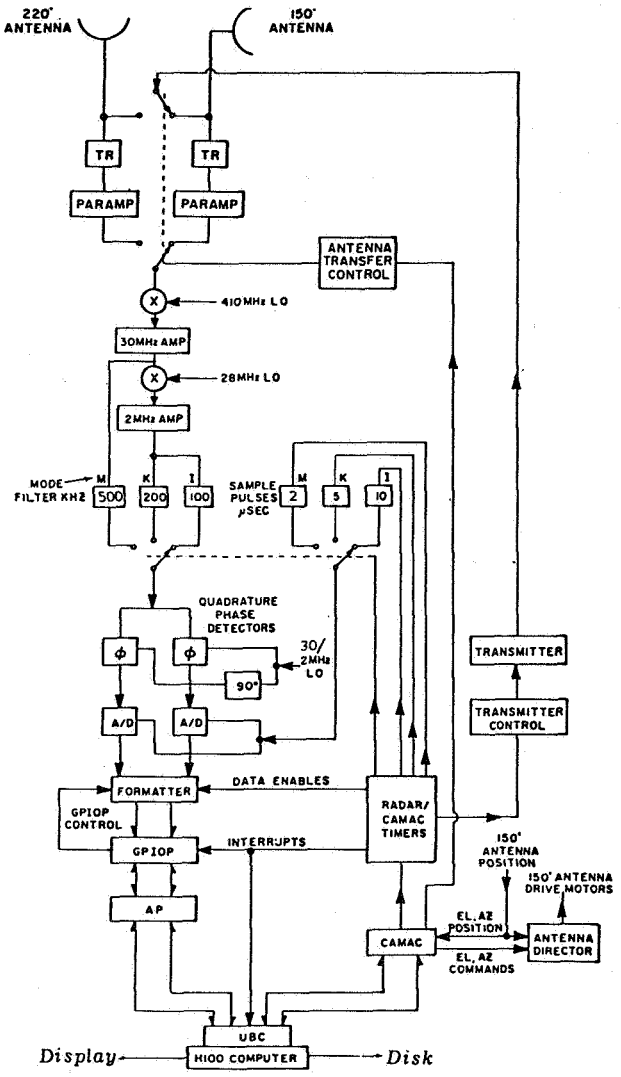


Figure A.1. A block diagram of the 440-MHz radar system at Millstone Hill.

azimuth and elevation commands to the 150-foot antenna director, to select one of the several radar timer modes, to select either the 150-foot or the 220-foot antenna, and to control various other radar functions. The CAMAC elevation and azimuth commands are sent directly to the Antenna Director which uses the difference between the command and true position to steer the antenna through elevation and azimuth servos.

A number of adjustable parameters for each mode, set usually through an input parameter file for the H-100, allow considerable control over the experiments. The most important of these are the range spacing, the number of ranges, the number of pulses to be coherently integrated, the number of Fourier-transform points and the number of periodograms to be added incoherently to obtain the power-spectrum estimates. The current 32-kilo word limitation on the Array Processor memory restricts the selection of the number of ranges and the number of Fourier-transform points. Typically, the I mode is used with 256 point Fourier transforms for 39 ranges, and the M mode with 512 point Fourier transforms for 18 ranges. One range usually is reserved for monitoring the system noise sampled at a distant range. Efforts presently underway to double the memory size of the Array Processor to 64 kilo words will allow 36 ranges for the M mode with a $\sim$10-km altitude coverage for the 2 $\mu$s baud rate. A wider altitude coverage over 8-25 km, say, in 5 or 10 km steps is possible with cycle times of 1-2 minutes.

# 5.9A THE ARECIBO OBSERVATORY AS AN MST RADAR

R. F. Woodman

Instituto Geofisico Del Peru
Apartado 3747
Lima, Peru

The radars and other systems at the Arecibo Observatory were designed and built, originally, for incoherent-scatter and radio-astronomy research. More recently, important additions have been made for planetary radar and artificial RF heating of the ionosphere. Although designed and built for a different application, these systems have shown to be very powerful tools for tropospheric, stratospheric and mesospheric research. The Observatory at present has two main radars: one at 430 and the other at 2380 MHz. In addition, 50-MHz MST radar work has been done using portable transmitters brought to the Observatory for this purpose. This capability will become permanent with the recent acquisition of a transmitter at this frequency. Furthermore, control and data processing systems have been developed to use the powerful HF transmitter and antennas of the HF-heating facility as an HF-bistatic radar.

The present paper will make a brief description of the four radars available at the Observatory. We have included in the bibliography a list of references where more detailed descriptions of these systems can be found. The list also includes papers of scientific nature which further illustrate the capabilities of the Arecibo Observatory as an MST radar. We will not cover the capabilities of the observatory for mesospheric research using incoherent scatter techniques. These capabilities have been recently reviewed by MATHEWS [1981, 1984].

## THE 430-MHz RADAR

The 430-MHz Arecibo radar in its ST mode configuration has been described by WOODMAN (1980a). Some recent improvements are described by WOODMAN et al. (1979) and SULZER and WOODMAN (1983). A block diagram of this configuration is shown in Figure 1. The most outstanding characteristics of the system are its large power-aperture product, a very powerful processing system and a very flexible radar control.

The transmitter has 2 MW of maximum power at a 6% maximum duty cycle. Its phase-coding bandwidth permits a minimum code length of 1 μsec which corresponds to a maximum altitude resolution of 150 meters.

The antenna is the largest reflection antenna in the world. The reflector is spherical with a diameter of 300 meters. Steering is performed by moving the position of the feed point. The feed illuminates the reflector almost evenly. It can point in any direction within 20° of zenith. Control is commanded by the central control and processing computer. Beam width at MST altitudes is cylindrical, since these altitudes are in the nearfield of the antenna. The effective beam width is sufficiently narrow to produce negligible effects on the altitude resolution or beam width broadening of the spectral width.

Receiving performance is determined by the noise level of the front end. System temperature is of the order of 100° K. Receiver bandwidth is selectable at both, the IF (30 MHz) and dc level. Gaussian-shaped filters of different bandwidths can be patched at IF frequency, and square-shaped pulse filters at the coherently detected level.

The control and processing system works around a central Harris/6 mini-

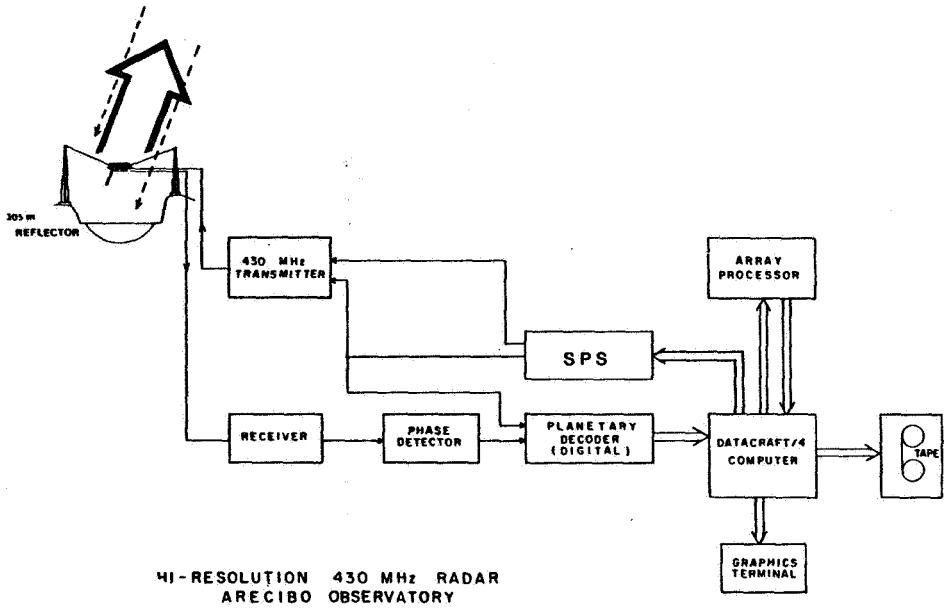


Figure 1.

computer. But, the flexibility and processing capabilities of the system are mainly determined by a special purpose controller, a powerful decoder and an array processor.

Control pulses for the radar to the ADC and the decoder, including the code sequences, are generated by a Synchronous Programmable Sequencer (SPS) (WOODMAN et al., 1979). This sequence can generate 16 independent, TTL level, arbitrary sequences with arbitrary length and transition resolution of 0.1 μsec. It is capable, for instance, of clutter which makes the evaluation of vertical velocities difficult.

## THE 2380-MHz BISTATIC RADAR

The S-band 2380 radar was built for planetary radar research, but it has been adapted for stratospheric research in a bistatic mode. The system techniques and capabilities is described in detail by WOODMAN (1980b). Here we will limit ourselves to a short description underlining its more important features and limitations.

A block diagram of the system is depicted in Figure 2. The transmitter is the most powerful radar presently in use for MST applications. It transmits continuously 500 kW of average power. The transmitter does not have a transmit-receive switch, hence the need for a bistatic approach. It uses the 300-meter-diameter spherical reflector as a transmission antenna and a 30-meter parabolic at Higuiales, 11 km north of the Observatory, for reception. The receiver has a low-noise parametric receiver, with a 25° K system temperature. The received signal is sent back to the Observatory via a wide band telemetry link for processing.

At any one time scattered signals are received mainly from turbulent fluctuations within the common volume defined by the intersection of both antennas. One of the outstanding features of this system is its high altitude resolution. Resolutions as small as 30 meters have been obtained. Higher resolution than the size of the common volume is obtained by means of phase-

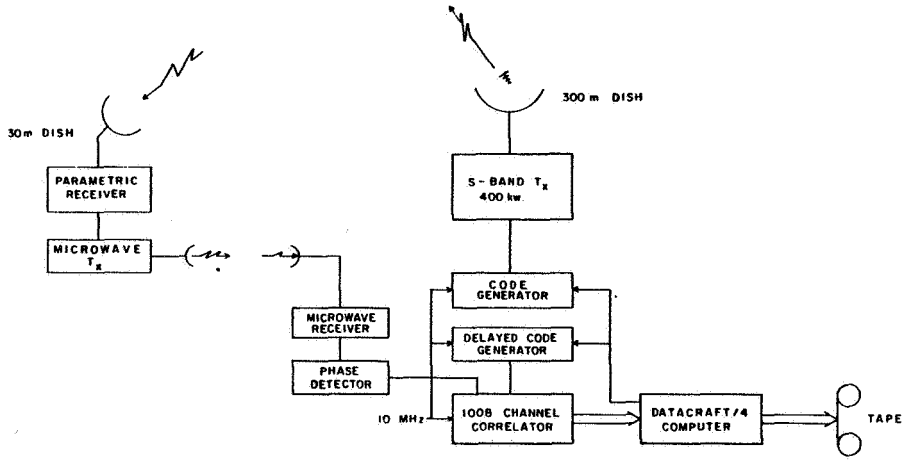


HI-RESOLUTION S-BAND STRATOSPHERIC SYSTEM
ARECIBO OBSERVATORY

Figure 2.

shift coding. Continuous periodic pseudorandom codes are used with adjustable baud and period length.

Typical values for the above-mentioned resolution are 0.2 μsec baud length with a period of 1023 bauds. Decoding is performed with the Arecibo's 1008 lag correlator, by cross-correlating the real and imaginary components of the coherently detected signal with the transmitter code. The altitude range of observations is from 14 to 19 km. The lower altitude is determined by the geometry of the antennas at maximum zenith angles (20°), and the highest by the sensitivity of the system. Sensitivity at this altitude is apparently determined by the sharp cut-off of the fluctuations k-spectrum at the inner scale, which becomes comparable to the wavelength of the radar at this altitude. The small probing wavelength should also permit the study of the turbulence spectrum shape at ks close to the inner scale.

The original observations gave only power information, because of the slowness of the correlator to dump the decoded profiles to the computer. This has been circumvented recently with a scheme in which two consecutive decoded profiles are dumped at any one time, permitting the evaluation of velocity and spectral width information. A new correlator is being built which will allow the evaluation of full spectral information and greater sensitivity. The sensitivity is improved by reducing the amount of processing idle time.

There is a project to provide the transmitter with a fast transmit receive switch which would allow the use of the radar as a monostatic radar. This will permit the study of lower tropospheric altitudes.

## THE MPI-ARECIBO 50-MHz RADAR

During 1980-81 the Max-Planck Institute brought their mobile radar to the Arecibo Observatory (ROTTGER et al., 1983). The system used a self-contained transreceiver, control and processing system and the large 300-meter Arecibo reflector with a specially designed feed for this frequency. This equipment is no longer available to the Observatory. Recently the Observatory has placed an order for a 50-100 kW MHz transmitter, which with existing receivers

control and processing system, (Figure 1) including software will allow MST research at these frequencies. The possibility of observing at 3 different frequencies from the same location will be an important capability of the Arecibo Observatory.

## THE ARECIBO HF BISTATIC RADAR

A large antenna and a powerful HF transmitter has been recently constructed north of the Arecibo Observatory for the purpose of artificially heating the ionosphere. The antenna consists of an array of 8 x 16 log-periodic vertically pointing antennas covering an area of 340 x 680 meters. The transmitter has a continuous rating of 800 kW. Both systems have a nominal frequency range of 3 to 12 MHz.

A bistatic radar has been recently implemented (GONZALES and WOODMAN, 1983) for partial-reflection and backscatter studies. The HF-heating facility is used for transmission and the large Arecibo disk for reception. The system uses pulse coding on transmission with a maximum resolution of 8-16 μsec. Coherent addition is performed on reception and full spectrum information is obtained in parallel from "ground wave altitudes" to F-region ionospheric heights (256 altitude). A new coding scheme has been used; it is based on a continuous set of complementary codes which vary from pair to pair. The sequence has the property of cancelling echoes which have been range folded into the altitudes of interest, i.e., only the echoes which belong to the previous pulse contribute to the profile. This is important, since it allows for the cancellation of strong-multiple reflections from the F- and E-region ranges.

A schematic diagram of the system is shown in Figure 3.

The Arecibo HF bistatic radar, because of its power, antenna gain and sophisticated processing is today perhaps the most sensitive HF radar in the world.

(References in this paper are included in the publications listed below.)

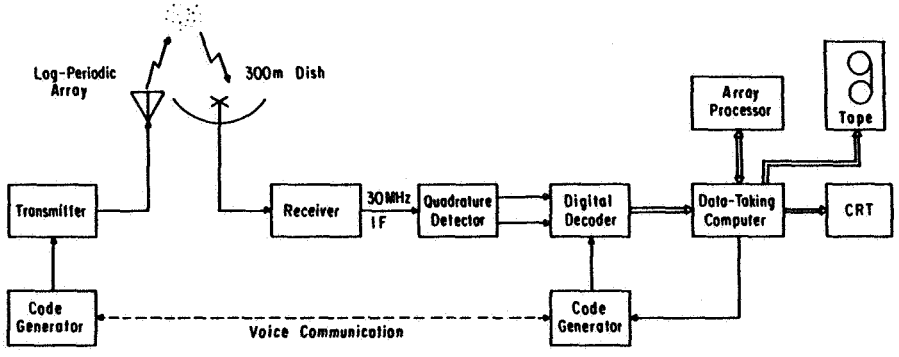


Arecibo Observatory
HF Bistatic Radar

Figure 3.

PUBLICATIONS RELATING TO THE ARECIBO OBSERVATORY

Walker, J. C. G. (1963), Radar measurements of the upper atmosphere, Science, 206, 180.

Aso, T., S. Kato and R. M. Harper (1977), Arecibo middle atmosphere experiment Geophys. Res. Lett., 4, 10-12.

Harper, R. M. (1978), Preliminary measurements of the ion component of the incoherent scatter spectrum in the 70-90 km region over Arecibo, Geophys. Res. Lett., 5, 784-786.

Farley, D. T., B. B. Balsley, W. E. Swartz and C. La Hoz (1979), Winds aloft in the tropics measured by the Arecibo radar, J. Appl. Meteorol., 18, 227-230.

Shames, P. M. (1979), AEOULUS: Ionosphere data taking system. NAIC, Computer Dept. Rep. No. 11, Arecibo Obs. POB No. 995, Arecibo, P.R.

Woodman, R. F., Haseltine, and Tabaja (1979), The Arecibo synchronous programmable sequencer, Arecibo Observatory, Internal Report.

Woodman, R. F. (1980a), High-altitude resolution stratospheric measurement with the Arecibo 430 MHz radar, Radio Sci., 15, 417-422.

Woodman, R. F. (1980b), High-altitude resolution stratospheric measurement with the Arecibo 2380 MHz radar, Radio Sci., 15, 423-460.

Fukao, S., T. Sato, N. Yamasaki, R. M. Harper and S. Kato (1980), Radar measurement of tidal winds at stratospheric heights over Arecibo, J. Atmos. Sci., 37, 2540-2544.

Fukao, S., T. Sato, Y. Maekawa, S. Kato and R. F. Woodman (1981a), Tidal vector wind measurement at stratospheric heights over Arecibo, in preparation.

Fukao, S., T. Sato, N. Yamasaki, R. M. Harper and S. Kato (1981b), Vertical sounding of the lower stratosphere by the Arecibo radar, in preparation.

Mathews, J. D. (1981), D-region research at Arecibo, J. Atmos. Terr. Phys., 43, 549-556.

Woodman, R. F. (1981), Turbulence in the middle atmosphere: A review, Handbook for MAP, 2, S. K. Avery Ed., SCOSTEP Sec., Univ. Ill., Urbana, Ill.

Woodman, R. F., P. K. Rastogi and T. Sato (1981), Evaluation of effective eddy diffusive coefficients using radar observations of turbulence in the stratosphere. Handbook for MAP, 2 S. K. Avery Ed., SCOSTEP Sec., Univ. Ill, Urbana, Ill.

Sato, T., and R. F. Woodman (1982a), Fine altitude resolution radar observations of upper-tropospheric and lower stratospheric winds and waves, J. Atmos. Sci., 39, 2539-2545.

Sato, T., and R. F. Woodman (1982b), Fine altitude resolution observations of stratospheric turbulent layers by the Arecibo 430 MHz radar, J. Atmos. Sci., 39, 2546-2552.

Sato, T., and R. F. Woodman (1982c), Spectral parameter estimation of CAT

radar echoes in the presence of fading clutter, Radio Sci., 17, 817-826.

Larsen, M. F., W. E. Swartz and R. F. Woodman, (1982), Gravity-wave generation by thunderstorms observed with a vertically-pointing 430 MHz radar, Geophys. Res. Lett., 9, 571-574.

Gonzalez, C. A. and R. F. Woodman (1983), Phase coding techniques with application to HF partial reflection experiments, to be submitted to Radio Science.

Mathews, J. D. (1984), Incoherent scatter radar studies of the mesosphere, to be published in MAP Handbook No. 13.

Rottger, J., P. Czechowsky, R. Ruster and G. Schmidt (1983), VHF radar observations ot wind velocities at the Arecibo Observatory, J. Geophys. Res., 52, 34-39.

Rottger, J., P. Czechowsky and G. Schmidt (1983), First low-power VHF radar observations of tropospheric, stratospheric and mesospheric winds and turbulence at the Arecibo Observatory, Submitted to J. Atmos. Terr. Phys.

Ruster, R. and J. Klostermeyer, (1983), VHF radar observations of a Kelvin-Helmholtz instability in a subtropic jet stream, Geophys. Astrophys.

Sulzer, M. P. and R. Woodman (1983), Quasi-complementary codes: A new technique for MST radar sounding, Submitted to Radio Science.

# 5.10A CAPABILITIES AND LIMITATIONS OF THE SONDRESTROM RADAR FOR ST OBSERVATIONS

B. J. Watkins

Geophysical Institute
University of Alaska
Fairbanks, Alaska 99701

## INTRODUCTION

The Sondrestrom radar is located on the western side of Greenland (67°N, 51°W) near the U.S. air base and Danish community at Sondre Stromfjord. The radar was previously located at Chatanika, Alaska where its primary role was incoherent-scatter studies of the auroral ionosphere. Stratosphere/troposphere studies have occupied a very small portion of the radar observing schedule. Ionospheric research is still the radar's primary function and was the reason for its re-location from Alaska to a very high magnetic latitude. The radar was moved from Alaska during the second half of 1982 and was first operational in Greenland in January 1983 and commenced regular operations in April 1983. It is managed and operated by SRI International although there are users from other institutions.

The high operating frequency (1290 MHz) implies that the radar may only be used for turbulence-scatter studies in the troposphere and lower stratosphere. While the inner scale sizes of turbulence imply that the radar should be able to obtain data up to at least 20 km, in practice about 15 km seems to be the usual limit, due to lack of system sensitivity. However, this upper height limit varies from day to day and data have been obtained up to 23 km when a long (50 μsec) pulse has been used (BALSLEY et al., 1977). At high latitudes the tropopause is typically about 8-11 km altitude, therefore the radar is particularly suited to studies at tropopause heights.

Figure 1 shows the antenna and buildings. The surrounding terrain provides relatively little protection from ground clutter echoes compared to the previous Alaskan site. The stronger ground clutter may compromise experiments when the turbulence signals have a small Doppler shift; this occurs, for example, when the antenna is directed vertically.

## HARDWARE

### Transmitter

The radar transmitter operates at 1290 MHz and uses a single Litton L3938 Klystrom as its final power amplifier. It was originally designed for incoherent-scatter ionospheric research. With the longer pulses and lower pulse repetition frequency (PRF) used for ionospheric studies (up to 320 μsec pulses and PRF < 75 Hz) the peak pulse power is typically 4 MW. However, this is reduced to 3 MW with the short (5μsec) pulses and higher PRF (250 Hz) used for ST studies. As will be discussed later, the maximum 250 Hz PRF value is too low; it compromises the signal detectability and may result in spectral aliasing. Other priorities have precluded any modifications to the transmitter.

No hardware is presently available to support phase-coded pulses, and only uncoded 5 or 10 μsec pulses have so far been used. There is also a limitation with the receiver analog-to-digital (A/D) converters that precludes the use of transmitter pulses less than 2 μsec long. The maximum A/D sample rate is 500 kHz.

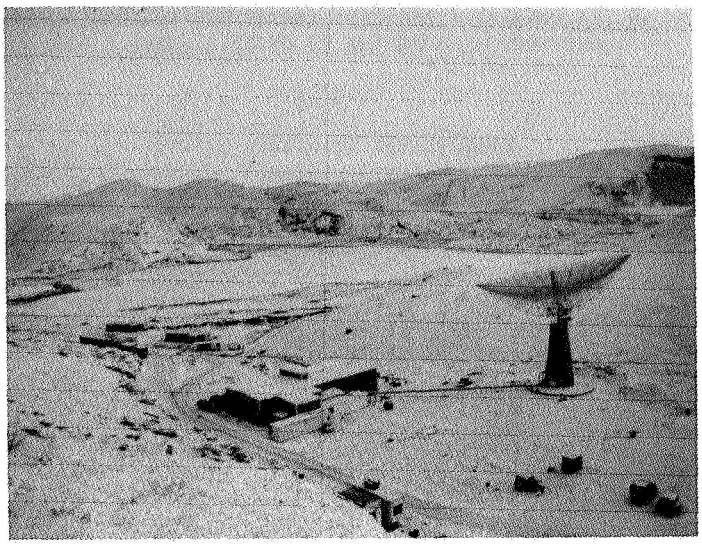

Figure 1. The Sondrestrom radar.

Receiver

The first receiver stage is a GaAs FET amplifier located in the antenna mount just behind the antenna surface. Following this, the first mixer produces a 30 MHz IF (10 MHz bandwidth) that is amplified and directed to the receiver room. A directional coupler which is located just before the parametric amplifier is used to inject a calibrated noise source into the received signal. The noise source is pulsed on briefly near the end of each interpulse period; it permits an accurate calibration of the received signals and hence turbulence intensities.

The 30-MHz IF is subsequently filtered, coherently demodulated and then digitally sampled.

Antenna

The antenna is a fully steerable dish of 32 meters diameter. After relocating the radar to Sondrestrom the antenna was increased in diameter from

Table 1. Sondrestrom radar parameters

| | |
|---|---|
| Frequency | 1290 MHz |
| Peak pulse power* | 3 MW |
| Pulse repetition frequency* | 250 Hz |
| Pulse length* | 5-10 μsec |
| Maximum duty cycle | 3 % |
| Polarization | Circular |
| Antenna diameter | 32 m |
| Antenna gain | 49.6 dB |
| Antenna efficiency | 52 % |
| System temperature | 100° K |

*Typical values for ST observations

its original 26 meters and the efficiency has been increased from 43 to 52%. The effective aperture is now 418 $m^2$ which is almost a factor of 2 increase which should aid future ST observations.

The antenna can be slewed rapidly at 5°/second and elevation scans are permitted over a range of 120 degrees and possibly more in the future.

## SOFTWARE

### Real-Time Program

The real-time data-acquisition program was written by C. Dawson at SRII for the on-site Harris computer. It is capable of determining power spectra with up to 512 point FFTs; we have usually used either 256 or 512 points. No dc clutter subtraction is performed before the FFT calculations, therefore a central clutter spike is evident in our spectra, especially the lower heights.

The program is limited to a maximum of 24 range gates. Due to memory limitations some disk accesses have been necessary thereby slowing the effective processing rate.

While the program has so far performed well for simple wind measurements, the program efficiency is very low. There is too much time used in processing for the worst case of 512 point spectra and four coherent integrations (the maximum allowed by the program) only about 20% of the radar pulses are used and the signal returns from the remainder are discarded while processing takes place. This limitation lies with the computer which has too little available memory and is too slow. An array processor with a large amount of memory would significantly enhance the programming speed and increase the effective signal/noise ratio because more spectra could be averaged in a given time.

The real-time program is also responsible for controlling the antenna motion and providing graphics output of spectra on an HP-2648A CRT terminal. Data may be gathered either with the antenna moving, or stationary in a sequence of fixed directions. We prefer to take data with the antenna stationary because it avoids spectral spreading of signals and clutter. The antenna can be moved quickly to the next position while the computer is doing the processing and writing data to tape.

### Off-line Analysis Programs

The off-line analysis programs have been written by this author to run on the Geophysical Institute's VAX 11/780 computer. Programs are available to analyze and plot power spectra. As well as the usual wind and power measurements, we can analyze complex multi-peaked spectra. The Doppler velocity, power and width of several individual peaks in a spectrum can be determined.

Other programs have been written to plot these spectral parameters as a function of height or time.

## MEASUREMENT CAPABILITIES AND LIMITATIONS

The ST measurements have so far focussed on wind measurements using azimuth and elevation scans (BALSLEY and PETERSON, 1981; CHANG, 1980). Recent observations in Alaska just prior to the relocation to Greenland involved data comparisons with the nearby Poker Flat MST radar.

The steerable dish antenna can be moved rapidly (5 degrees per second) so that an azimuth or elevation scan can be quickly completed (e.g. Figure 2). This is important for wave studies. The ability to direct the antenna to low elevation angles (minimum of 30 degrees) can be useful for reducing clutter because the range to a given height can be increased so that clutter is minimal. Low antenna elevations permit experiments similar to that performed by CRANE (1980) who studied the horizontal extent of turbulent structures.

Another feature of the radar we are beginning to exploit is its ability to easily derive Doppler spectra with high frequency resolution. We have used 512 point FFTs with 4 coherent integrations to obtain a frequency resolution of 1.4 cm/sec. An example of one of these spectra is shown in Figure 3. With high frequency resolution data we have been able to accurately determine the small vertical wind motions (WATKINS and JAYAWEERA, 1983) with the antenna directed vertically.

The radar is also capable of incoherent-scatter studies of the ionosphere (80 - 600 km). It should be feasible to operate the radar in both incoherent-scatter and turbulence-scatter modes simultaneously. This would probably require alternately switching rapidly between modes. It may be useful for investigating possible coupling between the two height regions but has not so far been attempted.

There are several limitations of the radar when used for ST studies. A major intrinsic limitation is its inability to receive usable signals much higher than about 15 km. However, if long pulses ($\geq$ 50 μsec) are used (BALSLEY et al., 1977) the upper height limit can be extended to about 25 km.

The present use of 5 μsec pulses gives a range resolution of 750 meters. This is inadequate for resolving individual turbulent layers. It would be desirable to obtain at least 150 - 200 meter resolution by phase-coding. It is not practical to use an uncoded pulse shorter than the present 5 μsec because the radar is already sensitivity limited.

The relatively low transmitter PRF can pose a problem of spectral aliasing for some experiments and it needs to be increased. The Nyquist frequency for the spectra is given by (PRF/2) Hz which corresponds to (1/4 $\lambda$ PRF) = 14.4 m/s Doppler velocity. The horizontal wind speed is often greater than this value. Thus experiments with low antenna elevations often produce aliasing of the turbulence-scattered signals, and this makes it difficult to determine the real wind velocity. Increasing the PRF would also aid system sensitivity because of higher average power.

An associated minor problem is that it is usually not feasible to perform coherent integration because the narrow spectral bandwidth is further reduced by $N_c$, the number of coherent integrations. However, for experiments with the antenna near vertical we have successfully used up to four coherent integrations.

The major limitation at present is the data-acquisition computer which is too slow and cannot process spectra fast enough in real time. For simple wind measurements where time resolution is unimportant, this is not a problem. However, if vector wind data are to be acquired quickly enough to resolve gravity waves, improvements need to be made.

While the full potential of the radar has yet to be exploited, the system can provide very good wind data up to about 24 km. If phase-coding and an upgraded data-acquisition system can be implemented it will be possible to take advantage of the antenna steerability to study wave and turbulence structures with good spatial and temporal resolution.

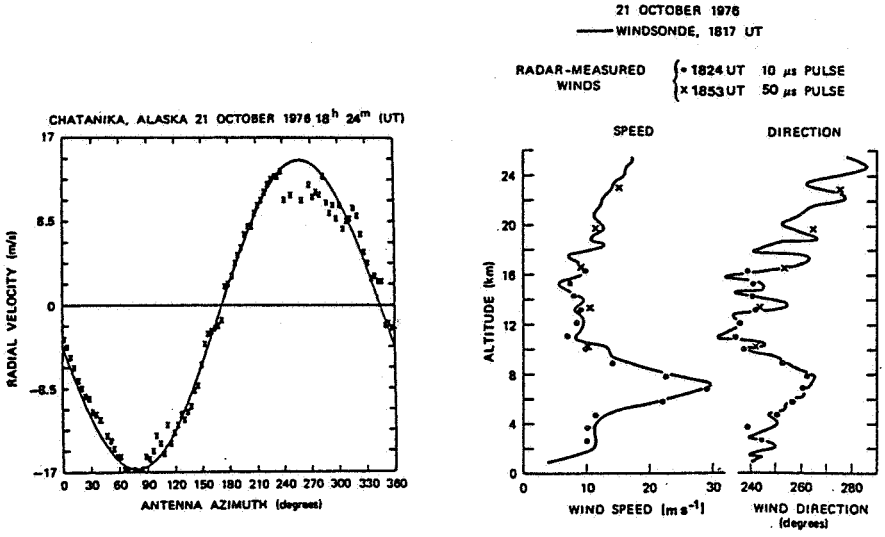


Figure 2. Left: An example of data from an azimuth scan at constant elevation (45 deg). The crosses are data points and the continuous curve is a best-fit sine function. The amplitude of the sine curve gives the horizontal wind speed, the phase gives the horizontal direction, and the vertical offset gives the vertical wind component. Right: Wind profiles (dots and crosses) obtained from a radar azimuth scan. For comparative purposes, radiosonde-measured winds are shown as the continuous curve (from BALSLEY et al., 1977).

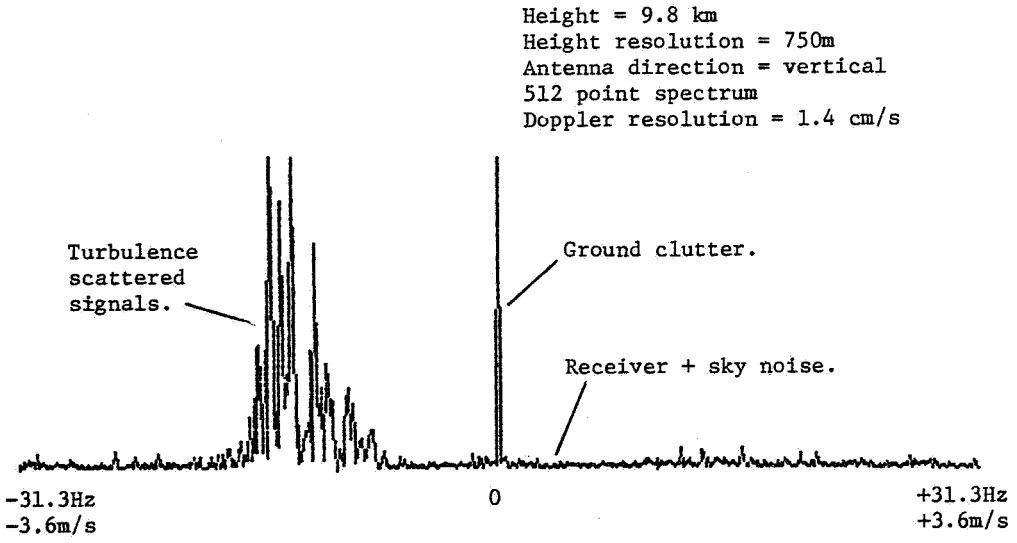


Figure 3. Example of a high resolution spectrum. The width of the turbulence signals is about 0.9 m/s. The mean (vertical component) is about 1.5 m/s downward.

In summary, the major advantages and limitations are listed below:

ADVANTAGES

1. Fast steerable dish antenna
2. Good Doppler resolution easily attained
3. Possibility of "simultaneous" incoherent-scatter operation.

LIMITATIONS

1. ST operation only - low maximum height for stratospheric returns (15-20 km) due to short wavelength.
2. Long runs (> 24 hours) generally not possible. This limits radar's usefulness for synoptic type studies.
3. Slow data processing capability. This limits the usefulness of the steerable antenna.
4. Average transmitter power is too low thereby reducing sensitivity. Implementation of phase-coding would increase sensitivity and also permit better range resolution.
5. Maximum transmitter pulse repetition frequency (250 Hz) is too low.

It should be noted that the limitations 3, 4, 5 could all be corrected with an appropriate investment in money and manpower.

REFERENCES

Balsley, B. B., N. Cianos, D. T. Farley, and M. J. Baron (1977), Winds derived from radar measurements in the Arctic troposphere and stratosphere, J. Appl. Meteorol., 16, 1235-1239.

Balsley, B. B. and J. L. Peterson (1981), Doppler-radar measurements of clear air turbulence at 1290 MHz, J. Appl. Meteorol., 20, 266-274.

Chang, N. J. F. (1980), Precision of tropsopheric/stratospheric winds measured by the Chatanika radar, Radio Sci., 15,371-383.

Crane, R. K. (1980), Radar measurements of wind at Kwajalein, Radio Sci., 15 383-394.

Watkins, B. J. and K. Jayaweera (1983), Comparisons of vertical winds measured with the Poker Flat MST radar and the Chatanika ST radar, in preparation.

PUBLICATIONS RELATING TO THE CHATANIKA/SONDRESTROM RADAR

Balsley, B. B. and D. T. Farley (1976), Auroral zone winds detected near the tropopause with the Chatanika UHF Doppler radar, Geophys. Res. Lett., 3 525-528.

Balsley, B. B., N. Cianos, D. T. Farley, and M. J. Baron (1977), Winds derived from radar measurements in the Arctic troposphere and stratosphere, J. Appl. Meteorol., 16, 1235-1239.

Chang, N. J. (1979), The potential of the Chatanika radar to investigating possible solar/atmosphere coupling, in solar-terrestrial influences on weather and climate, M. B. McCormac and T. A. Seliga, eds., 329-334, D. Reidel, Dordrecht, Holland.

Chang, N. J. F. (1980), Precision of tropospheric/stratospheric winds measured by the Chatanika radar, Radio Sci., 15, 371-382.

Peterson, V. L. and B. B. Balsley (1979), Clear air Doppler radar measurements of the vertical component of wind velocity in the troposphere and stratosphere, Geophys. Res. Lett., 6, 933-936.

# 5.11A OUTLINE OF THE MU RADAR

S. Kato

Radio Atmospheric Science Center
Kyoto University
Gokanosho, UJI,
Kyoto, 611, Japan

The MU radar is expected to be partly in operation in summer or fall 1983. The number of antennas in this partial operation is 57 or three groups, each of which consists of 19 Yagis. It is our idea that even such limited operation can work as an ST radar. In 1984 the rest of the antenna groups will be added, completing the total 25 groups, i.e. 475 (19 x 25) antennas. This complete system makes it possible for us to observe both the middle and upper atmosphere, probably up to 300 km.

Technical specifications are given in Table 1 and the system is shown in block diagram (Figure 1). Among other things, the MU radar has the following two outstanding features:

1. The antenna array consists of 25 groups each of which consists of 19 crossed-Yagis with three elements; each antenna has semiconductor transmitter and receiver, called a module, and each group of 19 antennas works as an independent small radar steering its radar beam under the control of a microcomputer. Thus, the total system consists of 25 small radars of this kind, enabling us to do various sophisticated operations with the system.

2. The system is controlled by two other computers, one for radar controlling (HP9835A) and the other for data taking and on-line analysis (VAX11/750). The computer-controlled system is simple in operation for users and reliable in observation. Very quick beam steering (as quick as in a msec) is also possible because of electronic phase-changing of each module output under control of the microcomputer which is further controlled by the radar controller.

Table 1. Basic parameters of the MU radar

| | |
|---|---|
| Location: | Shigaraki, Shiga, Japan (34.85°N,136.10°E) |
| Frequency: | 46.5 MHz |
| Antenna configuration: | circular array of 475 crossed Yagi antennas |
| Aperture: | 8330 $m^2$ (103 m in diameter |
| Beam width | 3.6° |
| On-axis gain: | 34.0 dB |
| Polarizations: | linear or circular |
| Beam directions: | 0-30° zenith angle |
| Transmitter: | |
| Power amplifier: | 475 solid-state amplifiers |
| Peak power: | 1 MW min |
| Average power: | 50 kW min |
| Bandwidth: | 1 MHz |
| TR switch: | PIN diodes with a directional coupler |
| Receiver: | |
| Bandwidth: | 1 MHz |
| Dynamic range: | 70 dB min |
| IF: | 3 MHz |
| A/D converter: | 12 bit x 4 channel |

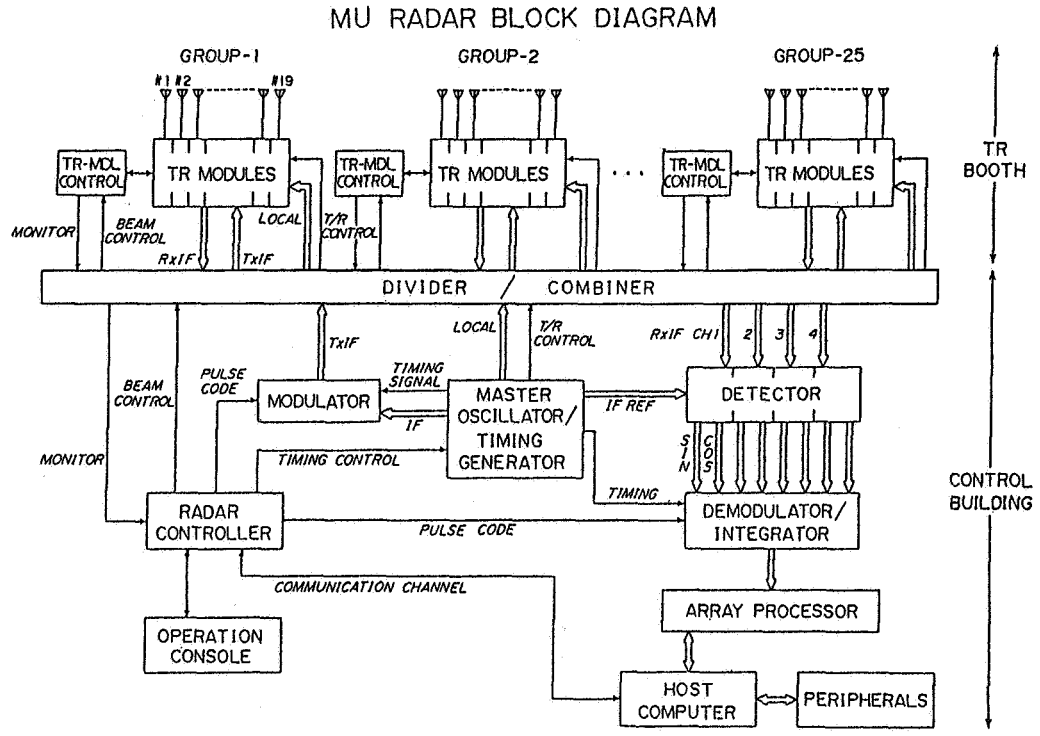
MU RADAR BLOCK DIAGRAM
GROUP-1
GROUP-2
GROUP-25
#1 #2
#19
TR-MDL CONTROL
TR MODULES
TR BOOTH
MONITOR
BEAM CONTROL
LOCAL
T/R CONTROL
RxIF
TxIF
DIVIDER / COMBINER
RxIF CH1 2 3 4
PULSE CODE
TIMING SIGNAL
MODULATOR
MASTER OSCILLATOR/ TIMING GENERATOR
IF REF
DETECTOR
IF
SIN
COS
TIMING CONTROL
TIMING
RADAR CONTROLLER
PULSE CODE
DEMODULATOR/ INTEGRATOR
CONTROL BUILDING
COMMUNICATION CHANNEL
ARRAY PROCESSOR
OPERATION CONSOLE
HOST COMPUTER
PERIPHERALS

Figure 1.

# 5.12A CHUNG-LI, TAIWAN DUAL MODE (DOPPLER AND SPACED ANTENNA) VHF RADAR: PRELIMINARY SPECIFICATIONS

J. Brosnahan*, J. Chao**, and J. Rottger***

*Tycho Technology, Inc., P. O. Box 1716, Boulder, CO 80306
**Dept. of Atmospheric Physics, National Central University, Chung-Li, Taiwan 320, Republic of China
***EISCAT Scientific Association, Box 705, S-981, 27 Kiruna, Sweden

In February 1982 a workshop on VHF coherent radar was held in Chung-Li, Taiwan. The workshop was sponsored by the National Science Council of the Republic of China and the National Central University. A VHF radar design with unique capabilities is the result of this conference.

A major unresolved question in the field of atmospheric research using VHF radar techniques is the relative merit of the two most widely used systems. These systems are the Doppler method as described by GAGE and BALSLEY (1978) at the Poker Flat, Alaska MST radar, and the spaced antenna method as described by ROTTGER (1981) at the SOUSY-VHF radar in Germany.

It has been suggested that one radar of each type be operated side by side for a direct comparison of the two techniques. This duplication of effort is not cost effective. The major components of both systems are identical, and one radar could be operated in both modes by proper design of a suitable antenna system and by proper data analysis. The Chung-Li radar will be able to switch between modes on a time scale of seconds and is the first VHF radar to be able to directly compare the Doppler data with spaced antenna data. The system will have performance comparable with the present SOUSY spaced antenna system and will provide mesospheric data in addition to stratospheric and tropospheric data. Table 1 lists the major specifications of the Chung-Li radar.

Figure 1 is the block diagram of the system. The radar is a monostatic system using commercially available components to minimize development time and cost. The minicomputer will initially be utilized only to write integrated data to tape and provide a minimum of real-time displays. All data analysis will be done off line on the National Central University's CDC Cyber computer. In designing a VHF radar facility the antenna system provides the greatest opportunity to maximize the system performance cost ration. Because of the requirement to operate the Chung-Li radar in both the Doppler and spaced antenna modes, Yagi antenna elements were chosen to provide symmetry in both horizontal axes. Three separate subarrays are required for the spaced antenna system of analysis. Subarrays of 64 elements each provide a symmetrical array of 8 x 8 elements and a number of feed points that can be easily matched with equal power distribution utilizing a simple power divider scheme. The Yagi elements are oriented at 45 degrees to the directions of lobe steering (Figure 2) to provide identical patterns when the beam is steered in azimuth in 90 degree steps.

By choosing a delay line system requiring only 0, 90, 180, and 270 degree delays, a very simple beam-steering system can be implemented, as shown in Figure 3. Once the delay line system is determined, the angle of the beam from the zenith is dependent on array element spacing. This spacing is chosen to simultaneously provide a main beam at a zenith angle of between 10 and 20 degrees, provide an array null at the zenith, and provide adequate sidelobe suppression, especially at the horizon. The beam angle is equal to the arc sine of 90 degrees (the basic delay line increment) divided by the element

Table 1. Specifications

| |
|---|
| SITE: National Central University, Chung-Li, Taiwan, R.O.C. |
| LATITUDE: 25 degrees north longitude: 121 degrees east |
| TYPE: Dual mode (Doppler-Spaced Antenna) |
| FREQUENCY: 52 Megahertz |
| ANTENNA: Three arrays of 64 Yagis each |
| AREA: Three 2900 square meter arrays |
| TRANSMITTER: 180 kW |
| MAXIMUM RESOLUTION: 150 Meters |
| ESTIMATED COMPLETION DATE: Late 1983 |

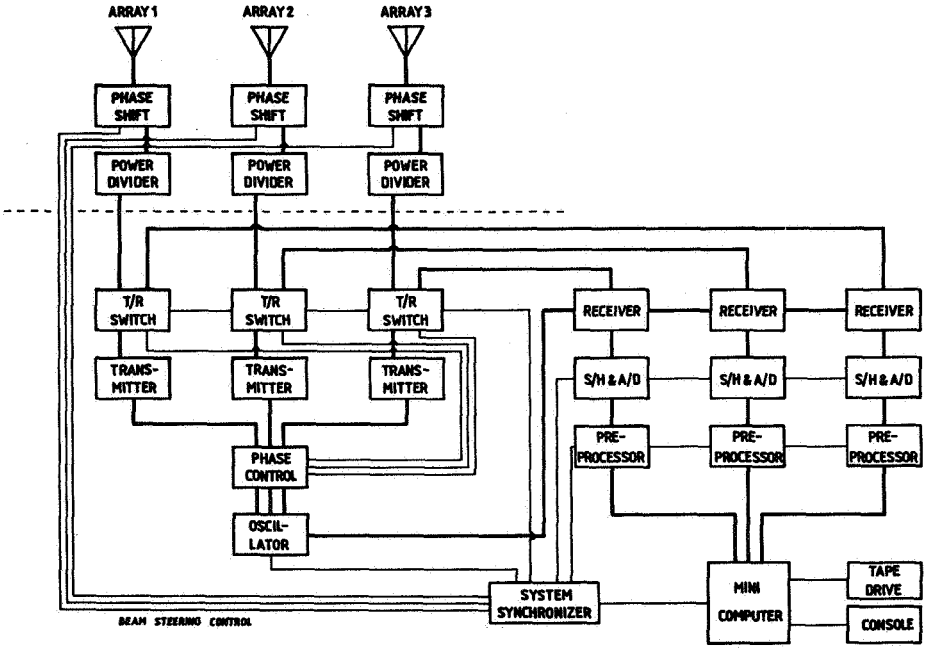


Figure 1. Chung-Li radar block diagram.

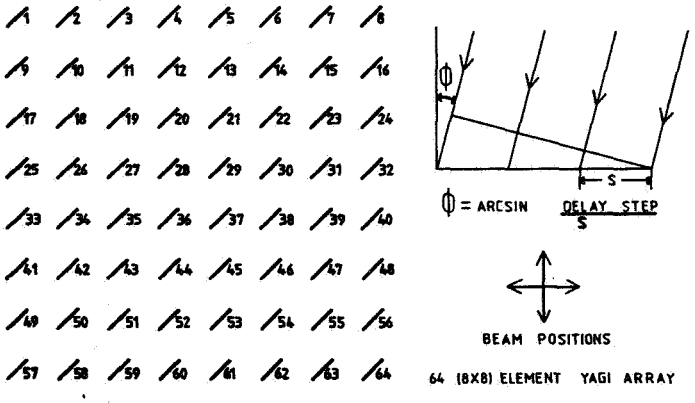


Figure 2. Yagi array orientation.

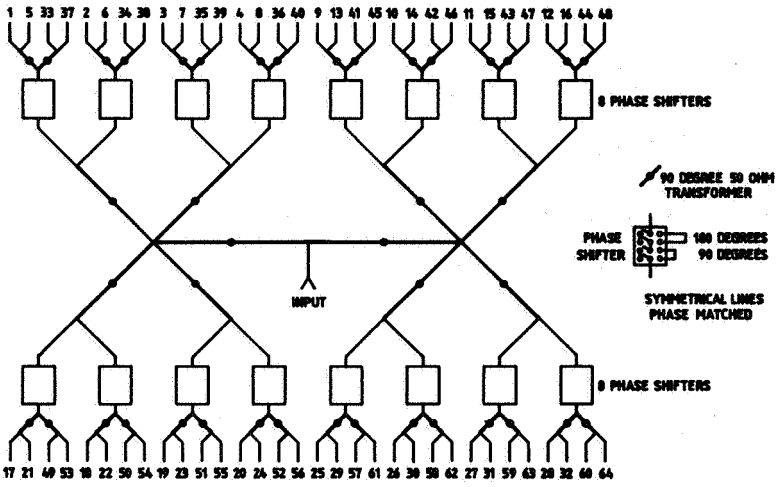


Figure 3. Power divider and beam steering phase delay.

spacing in degrees. A spacing of between 0.75 and 1.5 wavelengths provides a main lobe of between 19.5 degrees and 9.6 degrees, respectively. Element spacing in the 1 to 1.25 wavelength look the most promising, and computer modeling is presently being done to optimize the system. Table 2 shows the element phasing for the seven available beams.

Once the optimum spacing is selected the individual Yagi design is determined to best fill the aperture while having a pattern consistent with the overall array pattern. Four- or five-element Yagis are appropriate. The 45 degree orientation of the Yagi arrays tends to help reduce the mutual coupling between elements of the array. The beam-steering system also allows alternate Yagis to be fed out of phase to provide two orthogonal twin lobe patterns

Table 2. Beam steering element phasing

| | Delay Line Phase Lag in Degrees | | | | | | |
|---|---|---|---|---|---|---|---|
| ELEMENT | VERT | NORTH | EAST | SOUTH | WEST | NORTH SOUTH DUAL | EAST WEST DUAL |
| 1, 5,33,37 | 0 | 270 | 0 | 0 | 270 | 0 | 0 |
| 2, 6,34,38 | 0 | 270 | 90 | 0 | 180 | 0 | 180 |
| 3, 7,35,39 | 0 | 270 | 180 | 0 | 90 | 0 | 0 |
| 4, 8,36,40 | 0 | 270 | 270 | 0 | 0 | 0 | 180 |
| 9,13,41,45 | 0 | 180 | 0 | 90 | 270 | 180 | 0 |
| 10,14,42,46 | 0 | 180 | 90 | 90 | 180 | 180 | 180 |
| 11,15,43,47 | 0 | 180 | 180 | 90 | 90 | 180 | 0 |
| 12,16,44,48 | 0 | 180 | 270 | 90 | 0 | 180 | 180 |
| 17,21,49,53 | 0 | 90 | 0 | 180 | 270 | 0 | 0 |
| 18,22,50,54 | 0 | 90 | 90 | 180 | 180 | 0 | 180 |
| 19,23,51,55 | 0 | 90 | 180 | 180 | 90 | 0 | 0 |
| 20,24,52,56 | 0 | 90 | 270 | 180 | 0 | 0 | 180 |
| 25,29,57,61 | 0 | 0 | 0 | 270 | 270 | 180 | 0 |
| 26,30,58,62 | 0 | 0 | 90 | 270 | 180 | 180 | 180 |
| 27,31,59,63 | 0 | 0 | 180 | 270 | 90 | 180 | 0 |
| 28,32,60,64 | 0 | 0 | 270 | 270 | 0 | 180 | 180 |

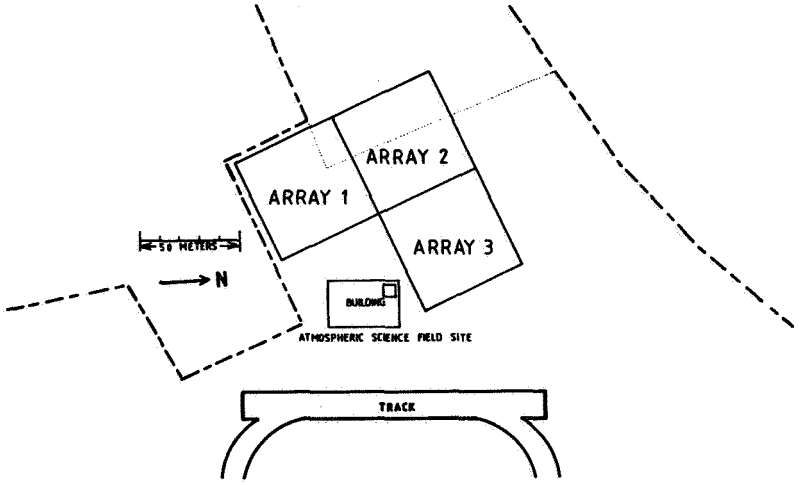


Figure 4. Chung-Li radar site.

providing a null at the zenith. These twin lobe patterns provide Doppler data with both positive and negative components, the difference between the two sidebands providing data on momentum transport [VINCENT, 1982].

The spaced antenna mode prefers 120 degree array symmetry and the Doppler mode prefers 90 degree symmetry. Final array configuration will be determined by computer modeling. Figure 4 shows one possible array orientation for the Chung-Li site which dictates a three-element array. Of course a total of four arrays could be utilized to provide more gain and symmetry in all axes if the site is available. The three arrays can be operated independently or together in all combinations of the seven beam patterns (vertical, off zenith in four azimuths, and two dual-beam patterns with a null at the zenith). This provides maximum flexibility for a relatively simple antenna system.

System installation will be completed in late 1983, and will provide a new and unique capability to make measurements in the mesosphere, stratosphere, and troposphere. Of special interest is the capability to provide excellent data during the many typhoons that come near or hit Taiwan.

REFERENCES

Balsley, B. B. and K. S. Gage (1980), The MST radar technique: Potential for middle atmospheric studies, Pure and Appl. Geophys., 118, 452-493.

Gage, K. S. and B. B. Balsley (1978), Doppler radar probing of the clear atmosphere, Bull. Amer. Meteorol. Soc., 59, 1074-1093.

Rottger, J. (1981), Investigations of lower and middle atmospheric dynamics with spaced antenna drifts radars, J. Atmos. Terr. Phys., 43, 277-292.

Vincent, R. A. (1982), The use of multibeam Doppler radars to study gravity wave momentum fluxes, presented at the Workshop on Equatorial Middle Atmosphere Measurements and Middle Atmosphere Radars, Estes Park, CO., 10-12 May 1982.

# 5.13A DESIGN CONSIDERATIONS OF A PROPOSED UK VHF RADAR

A. J. Hall

Rutherford Appleton Laboratory
Chilton, Didcot
OXON OX11 OQX
United Kingdom

The proposal that a VHF radar should be established in the UK as a national facility for the study of the dynamics of the middle atmosphere was first submitted to the SERC in 1980 by Sir Granville Beynon and others from ICW, Aberystwyth. As part of the subsequent evaluation of the proposal, a discussion meeting attended by about 50 scientists was held at the Royal Society on 30 September 1981 and it was agreed at this meeting that a more definitive version of the Aberystwyth proposal should be prepared by Professor L. Thomas (who succeeded Sir Granville Beynon at UCW on 1 October 1981) and submitted to the Solar System Committee at its meeting on 2 December 1981. At that meeting the Committee, after considering the report prepared by Professor Thomas, approved the carrying-out of a design study at RAL and appointed Professor Thomas as the Project Scientist.

The timeliness of the proposal that the UK should construct an MST radar can be gauged from the fact that at the present time different atmospheric radar systems already exist or are being planned, upgraded or constructed in nine different countries. During the last few years the international scientific community has identified middle atmospheric studies as an important branch of geophysics -- hence, for example the Middle Atmosphere Programme being carried out under the auspices of SCOSTEP. Work in this field is likely to be particularly fruitful, especially if it is based on data obtained using the MST radar technique which is now widely recognized as one of the most powerful ways of studying the atmosphere right from the Earth's surface into the mesosphere.

The provision of an MST radar in the form of a national facility open to any member of the interested community (which is already of a significant size, but which is expected to expand once the radar becomes operational) would constitute an important step in the progress of atmospheric science in this country; if the radar is not forthcoming, however, the UK will be left outside one of the mainstreams of international geophysics.

One of the most difficult aspects of providing a radar as a central facility for any or all of the UK science groups has been to arrive at a possible configuration which meet most of their aims at a cost which the Solar System Committee of the SERC can afford, and to retain the possiblity of later improvement in such a way that little original expenditure will be wasted.

The list of user interests is listed in Appendix I from which it may be seen that 30 priority projects are to be supported by 15 user groups in universities and government stations, covering the broad field of study summarized in Appendix II.

Many users have neither the computer access nor the staff time available to deal with preprocessed data and have urged strongly that the radar should have its own dedicated computer facility on site and a small permanent complement of Research Council staff capable of routine operation, maintenance and engineering of the radar as well as reduction of data required within programs arranged by a user committee. Some on-site accommodation for visiting users is needed to cover non-routine program development and campaign needs.

An impression of the proposed site is given in Figure 1. Several users have asked us to reconsider making the radar containerised and transportable, but it seems better to retain this concept as a second stage separate project as the SOUSY team has done.

When UK VHF television ceases in 1984, it will still be active in neighboring states. The plan to find a Welsh mountain valley fairly near to Aberystwyth University is not favored by Met. Office users who wish to make measurements clear of the effects of mountains. On the other hand it could prove difficult to persuade our licensing authorities to allow us a 2 MHz band at 50 MHz elsewhere.

The full design study, a copy of which is available for discussion by interested workshop attendees, was presented in February 1983 to the Solar Systems Committee. The committee decided to appoint a small panel under the chairmanship of Prof. T. B. Jones (Leicester) to consider it. The panel, which invited Dr. R. Ruster to act as consultant, reported in favor of the proposal and whilst recommending some reconsideration of detail, endorsed a pre-implementation phase costing about 10% of the projected total in which the major cost features could be tested experimentally.

## MAJOR FEATURES OF PROPOSED UK RADAR

From Appendix III, it may be seen that the aims of the radar are very similar in range and facility to the SOUSY Radar. Indeed some workers see benefit in collaboration using both radars, and look forward to developing their plans for using the UK radar, during the period of construction, by consultation with MPI colleagues.

1) It has been decided to limit the radar initially to DBS operation, reserving the possibility of SAD operation later either by subdividing the array or by using smaller movable subarrays.

2) To minimize the initial outlay on relays be limiting operation to vertical plus two discrete angles along two orthogonal directions.

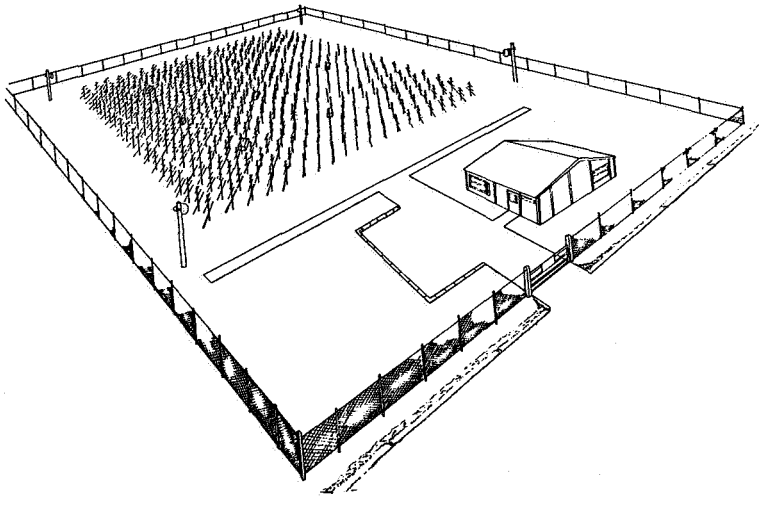

Figure 1. An artist's impression of the proposed MST radar site showing the array of 400 Yagis.

3) To modularize the assembly by energizing groups of the antenna array using about 10 medium power amplifiers producing a total of about 250 kW peak with a 5% duty ratio.

4) To opt for a 20 x 20 array off 10 x 10 co-phased subarrays of Yagi 3-element antennas.

5) To include complementary code pulse facilities.

6) To leave consideration of remote operations to a later date.

Figures 2-7 show some of the details of the proposed antenna arrangements.

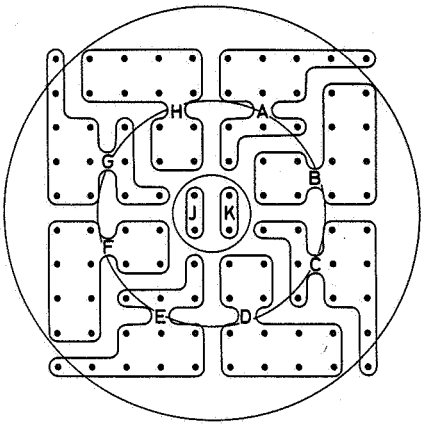


Figure 2. Plan of the 10 x 10 array of quads showing the radial power zoning necessary for sidelobe suppression. The letters A-K denote the positions of the feed points from the 10 RF amplifiers each having a mean output of 1.2 kW.

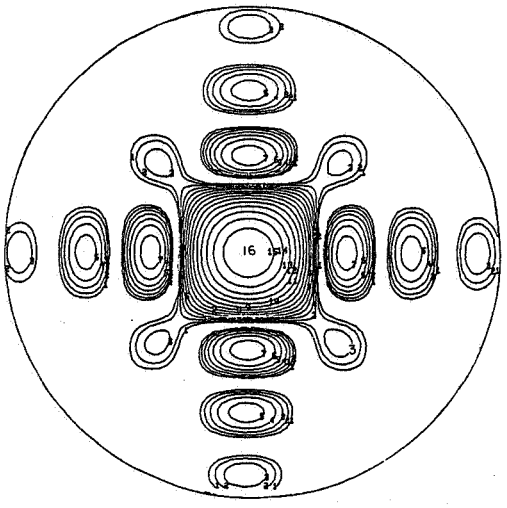


Figure 3. Zenithal projection of the spherical distribution of radiated power produced by the 400-Yagi array proposed. Contours are plotted at 2 dB intervals and the map extends to a zenith angle of 18°.

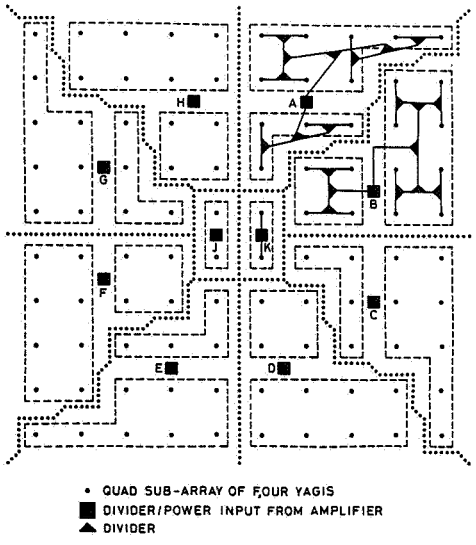


Figure 4. Plan of the 10 x 10 array of quads illustrating the power fan-out from the ten power input points A-K. The ten areas bounded by dotted lines are the sections of the array each powered by a transmitter; apart from the two small inner areas the array has an octantal structure.

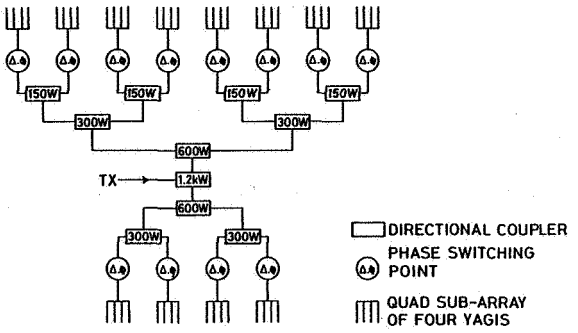


Figure 5. Power distribution network for the two outer rings of the array in one of the octants.

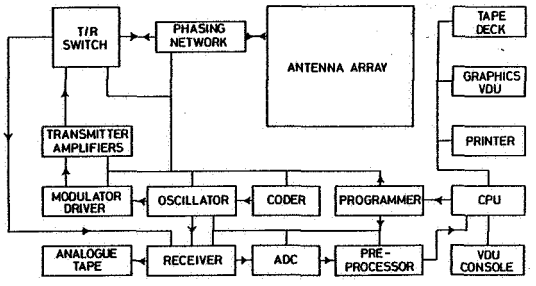


Figure 6. Block diagram of the proposed radar system.

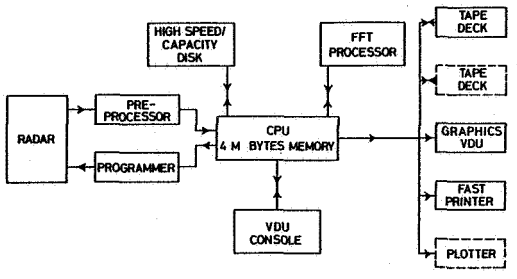


Figure 7. Configuration of the real-time data processing system.

## APPENDIX I

Priority Programmes

| | | |
|---|---|---|
| Mesosclae eddy transport in the low stratosphere | Atmospheric Physics, Oxford | SERC |
| Mesoscale Frontal Structure | Reading University | NERC |
| Coordinated measurements of wind shears (VHF) and atmospheric densities (lidar) to identify dynamically and statically unsuitable regions, gravity waves (VHF) and turbulence ($C_n^2$ from VHF) | University College of Wales, Aberystwyth | SERC |
| Coordinated measurements of motion field, including vertical component, and tropopause height (VHF), properties of cirrus clouds (lidar) and temperature and water (radiosonde) | | NERC |
| An investigation of the role of jet stream and frontal layer instabilities in the formation and launching of freely propagating gravity waves | | SERC/ NERC |
| A study of the coherence of waves as they propagate through the middle atmosphere | | SERC |
| Nonlinear interactions of gravity waves | | NERC/ SERC |
| The evolution of the wave spectrum | | NERC/ |
| Planetary waves in the troposphere, stratosphere, and mesosphere from day-to-day variability in average wind profiles | | SERC |
| Acoustic wave and pulsation studies | University of Leciester | SERC |
| Upward propagation of internal gravity waves (using MST HF Doppler) | | SERC |
| VHF communication link performance | | SERC |
| Investigation of air flow around jet streams with particular emphasis on investigation of the occurrence of intrusions of tropospheric air into the stratosphere | Meteorological Office | MOD |

| | | |
|---|---|---|
| Comparison of radar-measured winds, tropopause height and static stability with those obtained by coincident sequential radio-sonde ascents | Meteorological Office | MOD |
| Gravity-wave mode structure | RAL | SERC |
| Critical level motions | | SERC |
| Horizontal extent of atmospheric structures (with MPI). | | |
| LONG-TERM PROGRAMMES | | |
| Upper mesospheric cellular structures and transport dynamics | QUB | UGC/ SERC |
| Statistical study of turbulent layers (thickness, occurrence frequency and duration) in stratosphere for studies of vertical transport by turbulence | University College of Wales, Aberystwyth | SERC/ NERC |
| A determination of the seasonal behavior of gravity-wave propagation in the middle atmosphere; the effect of the summer mesopause on wave reflection and dissipation | | SERC |
| Trans-tropopause interchange | University of Edinburgh | UGC/ NERC |
| Lunar tidal analysis | Exeter University | SERC/ UGC |
| Studies of short period pulsations | University of Leicester | SERC |
| Synoptic studies of gravity waves and neutral wind interaction | | SERC |
| Obtaining long period (1 year) data on the frequency of stratosphere-troposphere exchange events | Meteorological Office | MOD |
| Collection of statistics of stength of return as function of height, time of day/year, synoptic situation, etc., with a view to characterizing the performance required of an operational wind profiler | | MOD |

| | | |
|---|---|---|
| Climatology of turbulence in the mesosphere | RAL | SERC |
| Correlative studies of tropopause height and temperature | | SERC |
| Off-vertical wave propagation (with MPI) | | SERC |
| Dependence of upward wave coupling on temperature field (with Oxford, PMRs) | | SERC |

## APPENDIX II

1. Middle Atmosphere Motions - Problem Areas

   (i) Mean circulation - particularly above 50 km;

   (ii) Planetary waves - particularly above 50 km;

   (iii) Tides:

   Morphology - temporal and spatial variability

   Effects on mean winds and temperatures

   Generation of gravity waves and turbulence;

   (iv) Gravity waves:

   Morphology - seasonal and geographical variability

   Sources - orography, penetrative convection, wind shears (jet stream)

   Propagation - temperature and winds (critical layers)

   Breaking and dissipation - turbulence

   (v) Turbulence:

   Generation by breaking and dissipation of tides and gravity waves (intermittent, spatially and temporally)

   Importance of convective and shear turbulence (average large scale flow?)

   Origin of laminar and turbulent structures

   Relationships between turbulence parameters (diffusion, eddy dissipation rate) to radar scatter.

2. Proposed Usage of MST System

1. Gravity-wave generation, propagation and dissipation.
2. Role of dynamics in formation of cirrus clouds.
3. Association of structures in height variation of stratospheric constituents with features of small-scale motion field.
4. Interchange of material between stratosphere and troposphere.
5. Vertical propagation of acoustic waves.
6. Propagation and scattering mechanisms for VHF waves.
7. Structure and velocities of fronts.
8. Generation of gravity waves at fronts leading to enhanced convection and rainbands.
9. Generation and characteristics of tides.
10. Vertical propagation of planetary waves.
11. Vertical structure of winds for synoptic studies of troposphere and stratosphere.
12. Statistics and characteristics of turbulent and stable layers as input to numerical models.
13. Small-scale turbulence and waves in stratosphere and mesosphere.
14. Nonlinear processes involving gravity waves.
15. Vertical momentum transport by gravity waves and influence on mesospheric circulation.

3. Exploitation of MST System

Development of operational wind sounder by Meteorological Office

Observations of troposphere and stratosphere in Antarctica by British Anarctic Survey.

## APPENDIX III

Performance Specification of the Proposed System

Engineering parameters

The values of the radar engineering parameters are given below:

| | | |
|---|---|---|
| **Transmitter** | | |
| Frequency: | 50 MHz | The exact frequency cannot be specified before further discussions with the Home Office |
| Peak pulse power: | 240 kW | This figure represents the total power from the ten amplifiers |
| Duty cycle: | 5% | |
| Mean power: | 12 kW | |
| Pulse length: | 1 to 64 μs in 1 μs steps | Pulse codes of up to 32 bits could be used |
| Pulse repetition frequency: | 1 to 6 kHz | continuously |
| Bandwidth: | 2 MHz | Determined by the shaping of the minimum pulse length desired |
| **Antenna** | | |
| Area: | 5184 $m^2$ | The array will comprise 400 3-element Yagis arranged in a 10 x 10 matrix of 2 x 2 quads |
| Gain: | Total array: >33 dB<br>Each quad: >19 dB<br>Each Yagi: 6 dB | |
| Half-power beam width: | 3.6° | |
| Beam directions: | 0° and approximately 5° and 10° off zenith in both the x and y directions | |
| First null: | 5.2° off zenith | |
| First maximum: | 7.2° off zenith | |
| Second null: | 9.5° off zenith | |
| Side-lobe suppression: | Better than 17 dB (at first maximum) and better than 20 dB beyond 12° | |
| Mean power aperture | $6.2 \times 10^7$ $Wm^2$ | |
| **Receiver** | | |
| Dynamic range: | 70 dB | |

| | | |
|---|---|---|
| Noise figure: | 3 dB | |
| IF bandwidth: | 4 MHz | |
| Protection: | Up to 20 V peak RF input | |
| Outputs: | In-phase and quadrature | |
| Filters: | Four Bessel filters with values between 1 and 500 μs selected by user | |

T/R switch

| | | |
|---|---|---|
| Switch time: | <5 μs | This together with cable delays, will limit the minimum height range to 1 km |

A/D converters

| | | |
|---|---|---|
| Conversion time: | 1 μs | |
| Resolution: | 10 bits linear | |

Pre-processor

| | | |
|---|---|---|
| No. of coherent integrations: | 1024 | |
| Memory capacity: | 2 x 1024 20-bit words | |

Performance parameters

The values of the performance parameters of the radar are indicated below; they are based on the values of the engineering parameters.

| | | |
|---|---|---|
| Height-resolution | 150, 300 and 600 m | These correspond to effective pulse lengths of 1, 2, and 4 μs |
| Maximum height achievable | Between 75 and 85 km by day | |
| Operating height ranges: | 1-25, 1-30, 1-37.5 1-50, 1-75 and 1-150 km | These figures correspond to pulse repetition frequencies of 6, 5, 4, 3, 2, and 1 kHz |
| Doppler frequency bandwidth: | 3, 6, or 12 Hz | These figures depend on the data sampling rate i.e., the PRF divided by the number of coherent integrations |
| Dwell times: | 5, 10 or 20 s | |

| | | |
|---|---|---|
| Doppler frequency resolution: | 0.05, 0.1 or 0.2 Hz | These figures are the reciprocals of the dwell times |
| Velocity resolution: | 2, 1, or 0.5 $ms^{-1}$ | The velocity resolution is directly proportional to the Doppler frequency resolution and therefore depends on the dwell time. The figures quoted are estimates for time-resolutions of 15, 30 and 60 s, respectively. |
| Time resolution: | 15, 30 or 60 s | |

# 5.14A THE PROUST RADAR

M. Glass

RPE/PAB
3, Avenue de la Republique
Issy-les-Moulineaux, France

Operating frequency: 935 MHz
Location: St Santin incoherent facility
A pre-experiment and 3 phases

PRE-EXPERIMENT

-Bistatic
-Transmitting facility

| | |
|---|---|
| Incoherent scatter transmitter | 150 kW |
| and antenna | 2000 $m^2$ |
| Pulse width | 4 µs |
| PRF | 7.5 kHz |

-Receiving facility

| | |
|---|---|
| Parabolic antenna | 95 $m^2$ |
| Receiver noise | 300 K |

-Analogic recording (March 1983)
-Coherent integrator (64 pulses)
and digital recording (October 1983)

PHASE I

-Bistatic
-2 working modes with the same pulse width 4 µs

| | | |
|---|---|---|
| Profile: | height resolution | 600 m |
| | altitude gates | 32 |
| Magnifier: | | |
| | pseudo complementary coding with 20 subcodes | |
| | height resolution | 30 m |
| | 4 independent groups of 8 contiguous altitude gates | |

-On-line coherent integration and FFT

-Klystron switch

PHASE II

-Monostatic with the large antenna

PHASE III

-Monostatic with a steerable disk

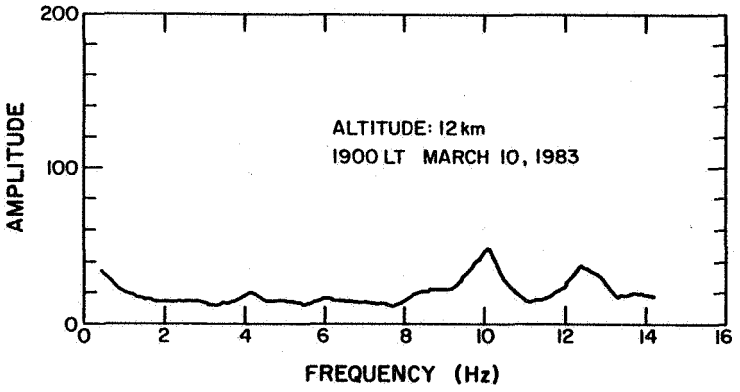


Figure 1. 69 sec sum of 32 spectra, each of 256 samples. Each sample consists of 64 coherently integrated pulses.

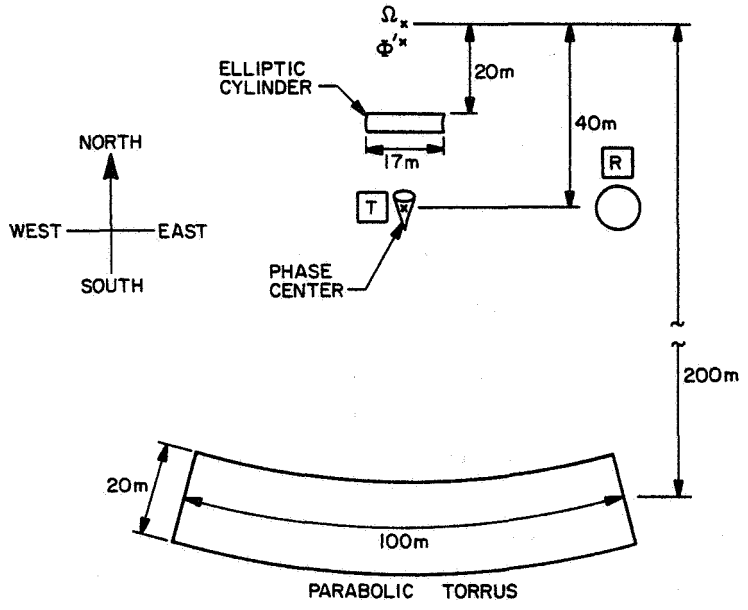


Figure 2. Top view of the antenna system.

# 5.15A FRENCH PROGRAM OF A VHF TRANSPORTABLE ST RADAR

M. Crochet

Laboratoire de Soudages Electromagnetiques
de 1'Environment Terrestre (L-S-E-E-T)
C-N-R-S, Universite de Toulon
France

## INTRODUCTION

This low cost project is mainly oriented towards specific experiments (ALPEX - FRONTS 84 ...) and comparisons with other techniques (UHF Doppler radars, high resolution radio soundings, radio stars scintillations, lidars ...). Developments are planned to decrease the minimum altitude of observations and define an "optimum" frequency for transportable S-T radars.

## DESCRIPTION OF THE RADAR AND PRELIMINARY INVESTIGATIONS

The actual radar is of the "Platteville" type

| | |
|---|---|
| Frequency: | 47.80 MHz |
| Power: | 50 kW peak |
| Pulse width: | 2 to 16 μs |
| Antennas: | 3 arrays of 50 x 50 $m^2$ |

## PRELIMINARY INVESTIGATIONS

-ALPEX-Provence (April - July 1982) with NOAA in the Rhone Delta in France
-winds measurements and comparisons with radio soundings (July 1982 - May 1983)
-scattering processes studies (July 1982 - May 1983)

## PLANS FOR THE FUTURE

1) Participation in a mesoscale experiment:

"Fronts 1984" - Spring 1984 - Southwest of France; Cooperative study of the fronts, rainbands, clouds and atmospheric waves generated by deep convection involving "precipitations" Radar (Doppler 5 cm, Doppler 8 mm, multipolarisation, meteorological radars), in situ measurements (planes and balloons), satellites and ground measurements.

2) Studies of waves generated by the Mistral wind:

-lee waves, gravity waves and turbulence studies from different sites (plain and mountain)
-sea wave generation in the Mediterranean Sea involving HF Doppler radar, VHF ST radar and in situ measurements of the wind variations.

3) Multifrequency investigations of the clear air:

-20-30 MHz HF radar
-50 MHz VHF radar
# 220 MHz VHF radar

For investigation of the scattering processes and definition of an optimum frequency for a transportable radar and wind profiles of the troposphere.

## 5.16A PUBLICATIONS RELATING TO THE SASKATOON PARTIAL-REFLECTION RADAR

Gregory, J. B., C. E. Meek, A. H. Manson and D. G. Stephenson (1979), Development in the radiowave drifts technique for measurement of high altitude winds. J. Appl. Met., 18, 682-691.

Meek, C. E., A. H. Manson and J. B. Gregory (1979), Internal consistency analyses for partial and total reflection drifts data. J. Atmos. Terr. Phys., 41, 251-258.

Manson, A. H. and C. E. Meek (1980), Gravity waves of short period (5-90 min), in the lower thermosphere at 52°N (Saskatoon, Canada). J. Atmos. Terr. Phys., 42, 103-113.

Gregory, J. B., C. E. Meek and A. H. Manson (1981), Mean zonal and meridional wind profiles for the mesosphere and lower thermosphere at 52°N, L=4.4, during solar maximum. Atmosphere-Ocean, 19, 24-34.

Gregory, J. B., C. E. Meek and A. H. Manson (1981), Solar Cycle Modulation of middle atmosphere circulations at Saskatoon, 52°N, 107°W. Report #5, Dynamics Group, Institute of Space and Atmospheric Studies.

Manson, A. H., J. B. Gregory and C. E. Meek (1981), Atmospheric waves ( 10 min - 30 days) in the mesosphere and thermosphere at Saskatoon (52°N, 107°W) October 1978 - September 1979. Planet. Space Sci., 29, 615-625.

Manson, A. H., C. E. Meek and J. B. Gregory (1981), Gravity waves of short period (5-90 min), in the lower thermosphere at 52°N (Saskatoon, Canada); 1978/1979. J. Atmos. Terr. Phys., 43, 35-44.

Manson, A. H., C. E. Meek and J. B. Gregory (1981), Winds and waves (10 min - 30 days) in the mesosphere and lower thermosphere at Saskatoon (52°N, 107°W, L=4.3) during the year, October 1979 - July 1980. J. Geophys. Res., 86, 9615-9625.

Manson, A. H., C. E. Meek and J. B. Gregory (1981), Long-period oscillations in mesospheric and lower thermospheric winds (60-110 km) at Saskatoon (52°N, 107°W, L=4.3). J. Geomag. and Geoelectr., 33, 613-621.

Meek, C. E. and A. H. Manson (1981), Use of the full polarization measurement in the partial reflection experiment. J. Atmos. Terr. Phys., 43, 45-58.

Meek, C. E., A. H. Manson and J. B. Gregory (1981), Monthly mean winds (zonal and meridional) and tides (24-, 12-h) from 60-110 km, at Saskatoon (52°N, 107°W) during the year July 1980 - May 1981. Report #3, Dynamics Group, Institute of Space and Atmospheric Studies.

Chakrabarty, P., C. E. Meek, D. K. Chakrabarty and A. H. Manson (1982), Results inferred from electron density measurements at Saskatoon, Canada (L = 4.4) by a partial reflection technique -- I. Variations of nitric oxide in the D-region during quiet periods. J. Atmos. Terr. Phys., 44, 957-962.

Gregory, J. B., C. E. Meek and A. H. Manson (1982), An assessment of winds data (60-110 km) obtained in real-time from a medium frequency radar using the radio wave drifts technique. J. Atmos. Terr. Phys., 44, 649-655.

Manson, A. H., C. E. Meek, J. B. Gregory and D. K. Chakrabarty (1982), Fluctuations in tidal (24-, 12-h) characteristics and oscillations (8-h - 5-d) in the mesosphere and lower thermosphere (70-110 km): Saskatoon (52°N, 107°), 1979-1981. Planet. and Space Sci., 30, 1283-1294.

Manson, A. H., C. E. Meek, J. B. Gregory and M. J. Smith (1982), Monthly mean winds (zonal, meridional) and tides (24-, 12-h) from 60-110 km, at Saskatoon (52°N, 107°W) during the year, June 1981 - May 1982. Report #4, Atmospheric Dynamics Group, Institute of Space and Atmospheric Studies. (p. 1-7).

Meek, C. E., A. H. Manson, J. B. Gregory and M. J. Smith (1982), Observations of mean winds and tidal oscillations at Saskatoon (52°N, 107°W) for November 9 - December 3 (1981): the co-ordinated global campaign of the ICMUA working group on tides in the mesosphere and lower thermosphere. Report #5, Atmospheric Dynamics Group, Institute of Space and Atmospheric Studies. (p. 1-8).

Meek, C. E. and A. H. Manson (1983), Measurements of the structure and drift velocities of airglow ( 557.7 nm) irregularities: Saskatoon (52°N, 107°W), Canada, J. Atmos. Terr. Phys., 45, 203-212.

Chakrabarty, D. K., C. E. Meek and A. H. Manson (1983), Asymmetry in the diurnal variation of temperature and electron loss coefficient in the mesosphere. J. Atmos. Terr. Phys., 45, 309-314.

Chakrabarty, P., C. E. Meek, D. K. Chakrabarty and A. H. Manson (1983), Results Results inferred from electron density measurements at Saskatoon, Canada (L = 4.4) by a partial reflection technique -- Part II: Ion production rates and nitric oxide in the D-region during post storm periods. J. Atmos. Terr. Phys., 45, 303-308.

Manson, A. H., C. E. Meek and J. B. Gregory (1983) The semidiurnal tide at the equinoxes: M.F. radar observations for 1978-1982 at Saskatoon (52°N, 107°W). J. Atmos. Sci., 40, 969-976.

Smith, M. J., J. B. Gregory, A. H. Manson, C. E. Meek, R. Schminder, D. Kurschner and K. Labitzke (1983), Responses of the upper middle atmosphere (60-110 km) to the stratwarms of the four pre-MAP winters (1978/9 - 1981/2). Advances in Space Research, 2, 173-176.

# 6. DESIGN CONSIDERATIONS FOR HIGH-POWER VHF RADAR TRANSCEIVERS (Keynote Paper)

J. W. Brosnahan

Tycho Technology, Inc.
Boulder, CO 80306

The importance of the MST radar technique has been clearly established by the more than ten facilities presently operating in the clear-air radar mode. Some of the facilities such as Poker Flat and SOUSY were designed specifically as MST radars. Other facilities such as Arecibo and Millstone were designed for other applications, but are capable of being operated in the MST radar mode. Now that the MST technique has been demonstrated, many new groups are setting out to establish facilities. Some of the new groups are clearly research oriented, while others are applications oriented.

The facilities already established and operating in the MST mode have developed all of the equipment required for an MST radar. Because development of the electronic building blocks has already been accomplished, new research facilities can concentrate their efforts on engineering enhancements rather than "reinventing the wheel". Research facilities are now able to begin scientific work much sooner since much of the required electronics is commercially available. Applications oriented facilities are now feasible without lengthly design and development efforts.

Topic 6 -- "Design considerations for high-power VHF radar transceivers" provides an opportunity for the pioneers in the MST radar field to exchange status reports and results of the previous and current hardware developments. Topic 6 also provides an opportunity for those currently beginning to establish facilities to learn what has been done in the way of hardware development and integrate this information into their plans. In addition, Topic 6 provides a forum for discussion on the future directions of VHF radar transceiver development.

The subtopics to be discussed in Topic 6 include, (1) distributed versus single transmitters, (2) coded pulses and decoder design, (3) large transmitter design considerations, and (4) T/R switch design. A number of papers on each subtopic has been submitted and they will provide a reference point for the current status of engineering development. In addition the papers will provide a departure point for the discussion on future directions in transceiver development.

The topics to be included in the discussion on future directions will include the following, (1) enhanced receiver performance, (2) transmitter systems for unattended operation, (3) limitations of the current T/R switch designs, (4) data processing (is eight bits enough), and (5) new frequencies (200 MHz and/or 400 MHz).

Enhanced receiver performance will include discussions on the optimum noise figure versus dynamic range tradeoffs, the usefullness of fast attenuators (< 5 microsecond switching time) to increase dynamic range, and the requirements for bandwidth filtering.

Transmitter systems for unattended operation will include discussions on the control and monitoring systems, the optimum power level to maximize performance versus cost, and reliability versus cost tradeoffs.

Limitations of the current T/R switch designs discussion topic will include

isolation limitations, and recovery time limitations.

Data processing will include discussions on 8-bit versus 10- or 12-bit A/D converters, preprocessor (preintegrator) requirements, and recent developments in the computer industry that can provide enhanced performance at a greatly reduced cost.

New frequencies discussions will include the advantages of higher frequencies, the cost tradeoffs of 50 MHz versus 200 MHz versus 400 MHz, the increase in resolution with higher frequencies, the lowering of the minimum height limitations, and the availability of various frequency allocations.

Hopefully during this session of the Workshop on Technical Aspects of MST Radar the current state of the art of high-power VHF radar transceivers will be defined, and the engineering development goals for the next year or two will be established.

## SUMMARY AND RECOMMENDATIONS

The session on Topic 6 -- "Design Considerations for High Power VHF Radar Transceivers" was a detailed discussion on hardware design. The question of distributed transmitters versus a single large transmitter was studied. The two categories were expanded to three categories to include small, medium, and large transmitters. The small transmitters are characterized by power outputs of less than 10 kW peak power, such as the MU radar modules. The medium-sized transmitters have outputs in the range of 10 kW to 200 kW, such as the transmitters at the Poker Flat facility. The large transmitters provide outputs in excess of 200 kW, such as the transmitters at Jicamarca.

An MST radar based on small transmitters, such as the MU radar, appears to cost more per watt than a radar utilizing medium or large transmitters. Using small transmitters allows the system to be steered in many directions quite easily. The cost of small transmitters can only be justified if the potential steering ability of a system of this type is fully implemented.

The cost per watt of transmitter systems consisting of an array of medium-sized transmitters versus a single large transmitter appears to be about equal. The multiple transmitter approach utilizes smaller, more readily available components and has the advantage that a single transmitter failure does not make the entire system inoperative. A single large transmitter requires essentially 100 percent spares to allow continuous operation. In addition, the parts for a large transmitter are more difficult to obtain, with lead times on components such as high power capacitors running six months or more.

There was lively discussion on the optimum size of transmitters, with no clear conclusions reached. The engineering decisions should be based on the particular scientific and operational requirements, availability of equipment (some of the proponents of large transmitters had obtained their equipment surplus), and the type of technical support available for operation and maintenance.

T/R switch discussion centered on the importance of recovery time in order to obtain data from lower altitudes. Switching time is limited by the time constants of the components required for operation at 50 MHz. Present state of the art is about 1-km height for the first data; though this can probably be lowered somewhat with a few tricks, such as adding shorted quarter-wave transmission line stubs on the antenna feedlines, and lowering the Q of the RF chokes that isolate the PIN diodes from their driver circuitry.

There are many valid approaches to receiver design. The important require-

ments are dynamic range, rejection of interference, and sensitivity. With currently available components, it is relatively easy to approach an optimum design for sensitivity and interference rejection. Discussion centered around the dynamic range requirement and it was determined that the limiting factor in systems with an 8-bit A/D converter was the dynamic range of the converter itself. A minimum of 10 bits in the A/D converter is recommended for all future systems, in order to take advantage of the dynamic range capability in a well-designed receiver.

Explored in a limited fashion during this session were the transmitter requirements for systems operating at higher frequencies such as 200 MHz and 400 MHz. Lumped components are still suitable at 200 MHz and possibly at 400 MHz, while cavities are probably more efficient, though more costly, at 400 MHz. Higher frequency operation is being considered to enable faster T/R switch recovery for lowering the minimum altitude at which data can be obtained and for reducing the size of the antennas so that portable systems may be built. It was generally felt that systems at the higher frequencies would not cost significantly more than systems at 50 MHz and that efforts should be made to develop transmitters at the higher frequencies as dictated by the scientific requirements.

RECOMMENDATIONS

1) Transmitter designs for operation at higher frequencies such as 200 MHz and 400 MHz should be investigated for use as portable ST systems and for faster recovery times for lowering the minimum altitude capabilities of MST systems.

2) A/D converters with a minimum of 10-bit resolution should be utilized in all future radar systems to optimize the dynamic range capabilities of new MST radars.

# 6.1A DESIGN CONSIDERATIONS FOR HIGH-POWER VHF RADAR TRANSCEIVERS: DISTRIBUTED VERSUS SINGLE LARGE TRANSMITTER

W. L. Ecklund and B. B. Balsley

Aeronomy Laboratory
National Oceanic and Atmospheric Administration
Boulder, CO 80303

Many factors enter into the choice of using a single large transmitter versus a number of smaller units in clear-air radar systems. Surprisingly, simple economic considerations seem not to be an important factor, since best current estimates of transmitter costs suggest a linear relationship in terms of watts/dollar in the kilowatt to megawatt peak power range. Feedline costs in large arrays have also been cited as favoring distributed over single transmitters. However, when all the extra costs of a distributed system are considered (transmitter shelters, phase controllers, etc.) the higher cost of high-power feedline is not a very significant factor. Feedline attenuation may be a consideration at frequencies of several hundred MHz and above for very large arrays (200 x 200 meters), however at 50 MHz the calculated loss for a simple branch feed driven by an 800 kW peak power transmitter located at one edge of a 200 x 200 meter array is only about 0.7 dB. When considering single transmitter/feedline economics, it is interesting to note that the average to peak power percentage rating for flexible low-loss foam and air dielectric cable is about 18% at 50 MHz and about 5% at 400 MHz. This suggests that at lower VHF transmitter duty factors of about 15% would best utilize the capacity of a given transmission line.

The above considerations do not apparently favor one approach over the other in choosing the number of transmitters for use in a clear-air radar system. However, other less obvious factors which involve operating strategy are important in the distributed/single transmitter question. It is very desirable from a number of scientific standpoints to obtain continuous data over extended periods (weeks to months). For most research installations this requires safe, reliable, unattended system operation. Most large transmitters with peak power ratings over several hundred kilowatts are not operated unattended, primarily because of potential catastrophic failure modes. Such failure might destroy an expensive transmitter tube or lead to a station fire without the intervention of on-site personnel. In contrast, if the same average transmitter power is divided between a number of smaller, distributed transmitters, catastrophic failure of one unit would be much less serious. In fact, if the number of distributed transmitters is fairly large (about 16 or more), loss of several units may not significantly reduce data quality. Thus, distributed transmitters should provide a safer, more reliable system with respect to one using a single large transmitter.

Ease of repair and the cost of spare parts also favors using multiple transmitters since entire transmitters can be replaced by a spare unit in a distributed system. Experience with 50 kW peak power transmitters has shown that one spare for about ten operating units is reasonable to ensure continuous operation. Spare parts thus constitute only about 10% of the total transmitter cost in this approach. For a single large transmitter another complete system (spare cost = 100%) would be required for equivalent back-up. Most large transmitters also require a certain amount of routine servicing which may seriously affect data continuity. In a distributed system newly serviced units can be swapped with units needing service with minimal data loss.

If the clear-air radar system uses a scanning antenna beam, distributed transmitters can be electronically phased at low power input levels whereas

branch feeding an array from a single large transmitter requires high power phase switching. The cost of high-power phase switches could be a major consideration in choosing between distributed and single transmitter systems. A final consideration involves the inherent modular structure of a distributed system. When building a large system this modular structure allows valuable early operation with a small part of the final system. Additional modules can be added over time until the system is complete.

## 6.1B DISTRIBUTED VS. SINGLE TRANSMITTER

J. Rottger

EISCAT Scientific Association
P.O. Box 705
S-98127 Kiruna, Sweden

Recently the requirements for an operational VHF radar system were discussed by ROTTGER (1981a,b) who proposed to apply the new spaced antenna drifts (SAD) method. Owing to the fact that diffuse partial reflection from horizontally stratified refractivity structures (viz., vertical temperature and humidity gradients in the troposphere) determines VHF radar echoes, the SAD method appears to be more appropriate and practical for measurements of wind and turbulence than the commonly used Doppler beam swinging method. The general scheme of such an improved SAD-VHF radar is shown in Figure 1.

Different from a common VHF radar operation, three transmitter (XMTR) and three receiver (RCVR) channels but only one antenna are used. The antenna is separated into three subarrays by three transmit/receive duplexers (ATR), allowing for parallel signal analysis (German patent P3026424.5, 1982). It is assumed that this is the most efficient way to operate a VHF radar (ROTTGER, 1981a). The signals received at the three subarrays, ANT 1, ANT 2 and ANT 3, are range multiplexed (RMUX) and converted into digital data (ADC), which are coherently preintegrated (INT) and cross correlated (CORR). The cross-correlation functions then can be analyzed (AN) to yield height profiles of three-dimensional velocities, turbulence and stability parameters. These can be stored on magnetic tape, evaluated by means of real-time display and transmitted via a telemetry link to allow a central acquisition for meteorological application (CAMA). This system may be extended into a remotely controlled radar network. While the sketched system is proposed for operational purposes, i.e., real-time access to meteorological information, the results presented in the paper by ROTTGER (1981b) were recorded with a more basic system, developed essentially for research purposes. The observations were carried out with the SOUSY-VHF-radar which is operated on 53.5 MHz with an average power $\bar{P}$ = 22 kW, using one transmitter antenna with gain G = 31 dB and three multiplexed receiving antennas, each with 22 dB gain. It is estimated that typical operational parameters of an SAD-VHF radar for tropospheric observations, such as depicted in Figure 1, could be: $\bar{P}$ = 4 kW and G = 30 dB (ROTTGER, 1981a). Such VHF radar systems could be established with reasonable costs. Since rather unattended operation will be possible, saving of operational expenses can compensate investment costs.

REFERENCES

Rottger, J. (1981a), Investigations of lower and middle atmosphere dynamics with spaced antenna drifts radars, J. Atmos. Terr. Phys., 43, 277-292.

Rottger, J. (1981b), The capabilities of VHF radars for meteorological observations, ESA SP-165, 143-148 (publ. by European Space Agency, Paris).

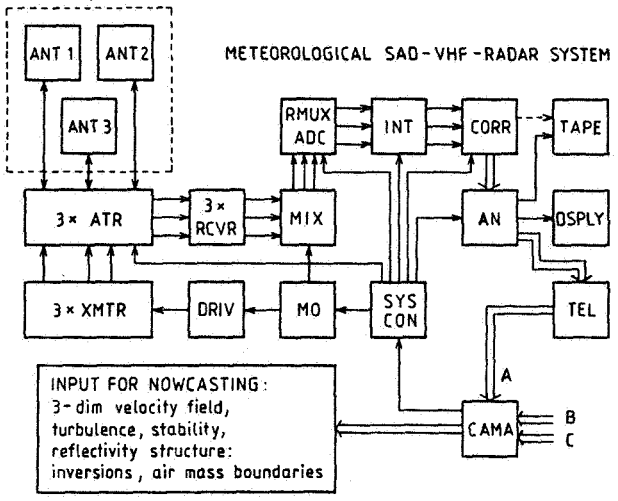


Figure 1. Spaced antenna drifts VHF radar.

# 6.2A PULSE COMPRESSION USING BINARY PHASE CODES

D. T. Farley

School of Electrical Engineering
Cornell University
Ithaca, NY 14853

## INTRODUCTION

In most MST applications pulsed radars are peak power limited and have excess average power capacity. Short pulses are required for good range resolution, but the problem of range ambiguity (signals received simultaneously from more than one altitude) sets a minimum limit on the interpulse period (IPP). Pulse compression is a technique which allows more of the transmitter average power capacity to be used without sacrificing range resolution. As the name implies, a pulse of power P and duration T is in a certain sense converted into one of power nP and duration T/n. In the frequency domain, compression involves manipulating the phases of the different frequency components of the pulse. A short pulse consists of contributions from a wide band of frequencies, all of which are in phase at one point in space-time. Changing the phase relations on transmission lengthens the pulse, but it can be reassembled into a short pulse upon reception by proper processing if the phases have not been perturbed in some unknown way in the meantime (i.e., by the scattering process). This is essentially the idea behind frequency 'chirping'.

Another way to compress a pulse is via phase coding, especially binary phase coding, a technique which is particularly amenable to digital processing techniques. This method has been used extensively in recent years in radar probing of the atmosphere and ionosphere, and it is the method we will discuss here. The general topic of pulse compression is dealt with in COOK and BERNFELD (1967), BARTON (1975), BROOKNER (1977), and other texts.

## BARKER CODES

A class of codes known as Barker codes (BARKER, 1953) has been used extensively in ionospheric incoherent-scatter measurements. The Barker coded pulse is considered to be made up of n 'bauds', each of duration T, so the total duration is nT, with the maximum value of n being 13. The phase of each baud is 0 or 180 degrees ($\pm 1$), in a sequence that depends on n. The pulse is decoded upon reception by passing it through a 'filter' whose impulse response is the reverse in time of the transmitted pulse (the pulse 'played backwards', so to speak). Such a filter is said to be 'matched' to the pulse. In practice these matched filters are usually specially designed acoustic surface wave devices or conventional filters plus digitizers, digital delay lines, and some add/subtract circuitry or equivalent software.

From another point of view, the decoding process consists of cross-correlating the received signal with a replica of the transmitted pulse; hence, when an undistorted coded pulse is passed through such a decoder, the output is the autocorrelation function (ACF) of the pulse. As an example, the phase coding sequence and the ACF of a 5-baud Barker coded pulse are listed below.

\+ + + − +

. . . 0 0 0 1 0 1 0 5 0 1 0 1 0 0 0 . . .

If the compression process were perfect, only the 5 would be present in the above ACF; the 1s represent undesired range 'sidelobes'. In Barker codes (n up to 13) the sidelobes are always unity and in the pattern above, and the central

peak is n. For ionospheric applications the sidelobes are generally not a problem since, for n equal 13, say, the power corresponding to the central peak is 169 times greater than that in each of the 12 sidelobes. (Note that the signal-to-noise ratio in the central peak is increased by the compression by a factor of 13, not 169, since the noise is the sum of 13 independent samples.)

The above discussion is valid for scatter probing of the atmosphere as long as the correlation time of the scattering medium is long compared to the total (uncompressed) duration of the coded pulse. In practice this is always the case for MST applications but may not be true for incoherent scatter from the ionosphere, for example. Detailed calculations of what happens in the latter case are given by GRAY and FARLEY (1973), and a general discussion of the 'ambiguity function' of a Barker coded pulse as a function of target-induced Doppler shift is given in COOK and BERNFELD (1967). GRAY and FARLEY also discuss the use of multiple coded pulse sequences in the measurement of the ACF of the scattering medium. The effect of the coding is usually minimal; in typical situations the 'true' ACF is convolved with a function whose width is about one baud. Finally, although 13 bauds is the longest possible Barker sequence (unity sidelobes), there are many longer sequences with sidelobes that are only slightly larger. As an example, a 28-baud sequence with a maximum sidelobe level in the ACF of 2 is listed by GRAY and FARLEY and has been used by WOODMAN et al. (1980) for observations with the SOUSY radar.

## COMPLEMENTARY CODE PAIRS

The codes discussed above have range sidelobes which are small, but which may still cause problems in MST applications. Ideally we wish to use high compression ratios (long codes) to get the best possible altitude resolution, but if we do so the 'wanted' signal from an altitude in the upper stratosphere, say, may be contaminated by range sidelobe returns from lower altitudes, since the scattered signal strength is a strong function of altitude, typically decreasing by 2-3 dB per kilometer. This problem can be completely eliminated, at least in principle, by the use of a special class of binary phase codes known as complementary codes.

The existence of complementary codes was first pointed out by GOLAY (1961) and has been mentioned in the radar literature (e.g., RABINER and GOLD, 1975), but the severe restriction on their use -- phase changes introduced by the target must vary only on a time scale much longer than the interpulse period (IPP) -- have prevented them from being utilized much in practice. The Doppler shifts encounted in military applications and in incoherent scatter from the ionosphere are much too large, for example, but the very small Doppler shifts associated with MST radar observations are entirely compatible with the use of such codes. The medium correlation time is typically tens or hundreds of times longer than the IPP.

Complementary codes are again binary phase codes and they come in pairs. They are decoded exactly as are Barker codes, by a 'matched' filter/delay line combination whose impulse response is the time reverse of the pulse. The range sidelobes of the resulting ACF output will generally be larger than for a Barker code of comparable length, but the two pulses in the complementary pair have the property that their sidelobes are equal in magnitude but opposite in sign, so that when the outputs are added the sidelobes exactly cancel, leaving only the central peak; i.e., the compression is perfect. As the simplest possible example, consider the 2-baud complementary pair below

```
Code:       +  +      (first pulse)
            +  -      (second pulse)

ACF:  0 +1 +2 +1 0    (first pulse)
```

```
0 -1 +2 -1 0    (second pulse)
0  0 +4  0 0    (sum)
```

Representing the above pair as (A, B) it is easy to show that the sequence (AB, $A\bar{B}$), where $\bar{B}$ is the complement of B, is also a complementary pair that is twice as long. Proceeding in this way one can obviously generate long n-baud code pairs, where n is any power of two. It turns out that n can also be ten, or ten times any power of two. Further properties of these sequencies are given by GOLAY (1961). In the first reported MST studies using these codes at SOUSY (SCHMIDT et al., 1979) and Arecibo (WOODMAN, 1980) n was 32 and the baud lengths were 2 μs and 1 μs, respectively (300 m and 150 m resolution).

There are two practical limitations on the maximum value of the compression rate n: (1) as n increases the effect of ground clutter extends to higher and higher altitudes; (2) the computing requirements for decoding increase with n. The first is the most serious limitation; the computing requirements can usually be handled one way or another. One process that often simplifies the computing is coherent integration (summing N successive voltage samples from a given altitude before doing any other processing). Since coherent integration and decoding linear operations they can be interchanged; e.g., samples from 100 pulses, say, can be coherently integrated and then decoded all at once. In dealing with the first limitation one must achieve some compromise between three competing goals: (1) the desire to confine strong ground clutter effects to the lowest possible range of altitudes (i.e., use short pulses); (2) the desire to avoid range ambiguity (use a long IPP); and (3) the desire to use the full average power capabilities of the transmitter to achieve maximum sensitivity.

## MORE COMPLEX COMPLEMENTARY CODING SCHEMES

More complicated schemes can partly alleviate the ground clutter/range ambiguity problem. The cross correlation function (XCF) of the basic complementary transmitted sequency A, B, A, B, ... with the decoding function A, B is periodic with a period 2T, where T is the interpulse period (between A and B), but there are also substantial non-zero values of the XCF in the vicinity of T. For example, for the 4-baud pair (+++−, ++−+) the XCF is

```
... 0008000 ... 0040400 ... 0008000 ...
```

At delays near T from the 'wanted' return, in other words, the range sidelobes of the individual pulses add rather than cancel, whereas the main peak does cancel. The 4s in the above represent the most important source of range ambiguity. These can be eliminated by transmitting the more complex sequence A, B, A, $\bar{B}$, A, B, A, $\bar{B}$, ... and decoding by cross correlating with A, B, A, $\bar{B}$. The XCF for this scheme consists of single identical spikes at intervals of 2T; i.e., the first range sidelobes is pushed out to twice the interpulse spacing. By extending this idea the first sidelobe can be pushed out to even higher multiples of T. In this way a substantial range of altitudes could be probed at a very high pulse repetition frequency (PRF). In actual practice, though, some altitudes would be lost because of the necessity of blanking the receiver during actual pulse transmission and because of receiver saturation by ground clutter. GONZALES and WOODMAN (1981) used such a scheme for HF partial-reflection studies of the mesosphere at Arecibo.

## QUASI-COMPLEMENTARY CODE SETS

The results presented so far have all been based on the assumption that the transmitted pulses were perfectly coded. In practice of course this won't be true; the phase shifts will require a finite amount of time and will not be exactly 180 degrees, etc. As a result, the range sidelobes for the complementary code pairs will not cancel exactly; the location of the sidelobes will de-

pend on what sort of error is made by the transmitter. SULZER and WOODMAN (unpublished manuscript, 1982) have developed a technique to minimize this problem. Rather than transmit just a pair of complementary 32-baud codes, they transmit a sequence of 48 different 32-baud pulses. Each is decoded individually and the results are combined coherently, so in a sense the whole sequence can be considered to be a single code. But from another point of view we can think of the sequence as 24 quasi-complementary pairs, each with a different set of small range sidelobes, due partly to errors in transmission and partly to the fact that the pairs are not perfectly complementary. Because the sidelobes produced by the individual pairs have a more or less random distribution, the resultant sidelobes of the entire sequence are lower and more uniform than those of a single (imperfect) complementary pair. This is no accident of course; the codes were chosen by an extensive computer search requiring about 350 hours (!) using a Harris computer and an FPS AP120B array processor. The major disadvantage of this technique is that no coherent integration before decoding is possible; at present only the Arecibo Observatory has the digital preprocessing equipment required for the extensive high-speed decoding.

A similar idea has been developed by the same authors for mesospheric observations at Arecibo. To achieve the desired resolution of 600 m (4 μs) and fully utilize the transmitter, one would ideally use a 52-baud Barker code, which unfortunately does not exist. A good approximation to this can be achieved by a pseudo-random sequence of pseudo-random 52-baud codes found by a 10 hour computer/array processor search.

## CYCLIC CODES

These codes (also called maximal length sequences) are a well-known class of periodic code which repeats at intervals of $N=2^n-1$ bauds and can be generated by an n-bit shift register. The ACFs of such sequences have periodic peaks of amplitude N at intervals of N times the baud length but are unity everywhere else. Hence if the periodic major range sidelobes cause no range ambiguity problems, very high compression ratios can be achieved. These codes are used widely in radar astronomy, since the interval between sidelobes can be made larger than the target size and ground clutter is unimportant. In MST work, however, such codes are useful only for bistatic radar systems.

## REFERENCES

Barker, R. H. (1953), Group synchronizing of binary digital systems, in Communications Theory, W. Jackson (ed.), 273-287, Academic Press, New York.

Barton, D. K. (ed.) (1975), Radars, Vol. 3, Pulse Compression, Artech House.

Brookner, E. (ed.) (1977), Radar Technology, Artech House. (See especially chapter 8 by C. E. Cook.)

Cook, C. E. and M. Bernfeld (1967), Radar Signals: An Introduction to Theory and Applications, Academic Press, New York.

Golay, M. J. E. (1961), Complementary series, IRE Trans. Info. Theory, IT-7, 82-87.

Gonzales, C. A. and R. F. Woodman (1981), A high power HF radar for probing the mesosphere (abstract), URSI General Assembly, Washington, D.C.

Gray, R. W. and D. T. Farley (1973), Theory of incoherent-scatter measurements using compressed pulses, Radio Sci., 8, 123-131.

Rabiner, L. R. and B. Gold (1975), Theory and Application of Digital Signal Processing, Prentice-Hall.

Schmidt, G., R. Ruster and P. Czechowsky (1979), Complementary code and digital filtering for detection of weak VHF radar signals from the mesosphere, IEEE Trans. Geosci. Electron., GE-17, 154-161.

Woodman, R. F. (1980), High-altitude resolution stratospheric measurements with the Arecibo 430-MHz radar, Radio Sci., 15, 417-422.

Woodman, R. F., R. P. Kugel and J. Rottger (1980), A coherent integrator-decoder preprocessor for the SOUSY-VHF radar, Radio Sci., 15, 233-242.

# 6.2B USE OF PULSE CODES

J. Rottger

EISCAT Scientific Association
P.O. Box 705
S-98127 Kiruna, Sweden

Pulse compression techniques are now more often applied in MST radar facilities. It was found that typical resolutions necessary to resolve some of the atmospheric phenomena must be about 150 m. The corresponding pulse length of 1 μs is still feasible for MST radars operating in the lower VHF band. It was recognized, however, that even a better resolution than 150 m should be used in some instances (e.g., to resolve thin turbulence layers). The upper range limit in the stratosphere of typical MST radars is between 20 km and 30 km. With single pulses, duty cycles of 0.5% then have to be used. However, present transmitter technology allows about an order of magnitude larger duty cycles of a few percent. The average power determines the sensitivity of MST radars, and one has to apply these long duty cycles, because higher peak powers are not feasible.

The only way to achieve a good height resolution at the maximum average power is to apply pulse coding. There are several ways to do this; which are briefly summarized and their feasibilities and limitations mentioned:

(1) Barker codes allow good pulse compression, fairly easy decoding but suffer from a fairly unacceptable sidelobe suppression.

(2) Polarization switching needs special preparation of antennas, two receiver channels and has a pulse compression factor of 2 only.

(3) Frequency stepping needs as many receiver channels, A/D converters and accumulators as frequencies are transmitted. Changing frequencies from pulse to pulse may allow to solve range ambiguity problems.

(4) Complementary codes yield optimum sidelobe suppression. The needed coherence of the scattering/reflecting target from pulse to pulse is guaranteed for MST radars. The shortcoming of long complementary codes, i.e., the unavoidable masking of short ranges, can be overcome by using a double series of complementary codes and single pulse.

It turns out, in summary, that the latter approach is most feasible for many MST radar applications.

# 6.2C DECODERS FOR MST RADARS

R. F. Woodman

Instituto Geofisico del Peru
Lima, Peru

## INTRODUCTION

Different coding schemes, their advantages, and the need for the use of phase coded pulses is discussed by Farley (page 410, this volume). Here we shall limit ourselves to describe decoding techniques and equipment which has been used by MST radars and briefly present some recommendations for new systems.

Decoding can be done either by software in special-purpose (array processors, etc.) or general-purpose computers or in specially designed digital decoders.

## SOFTWARE DECODING

Decoding, if done in a straightforward manner, would normally take several tens of operations per sec and would be out of the possibilities of moderately priced computers. Decoding is used to obtain optimum resolution, which in the case of MST radars is of the order of a few hundred meters, this corresponds to one complex sample per one or few μsec. If we take a 32 baud code with a baud-width of 1 μsec, as an example, straight decoding would take 64 adding or subtracting operations perμsec; certainly a requirement beyond the capabilities of even the fastest computers and a very demanding one even for specially built digital equipment. Fortunately, MST radars at VHF and lower UHF frequencies produce highly redundant information. Correlation times in the medium, and hence of the echo signals they produce, are of the order of a fraction of a second ($\simeq$ 0.5 to 2 sec for 50 MHz). This calls for coherent integration from pulse to pulse, which, when performed, reduces the amount of information by as much as two orders of magnitude.

Decoding and coherent integration are linear operations and, as pointed out by WOODMAN et al. (1980), they commute. One can perform the coherent integration first, and decode afterwards, with identical results. This possibility permits performing decoding operations in just about any mini- or micro-computer available in the market.

Coherent integration is so efficient in reducing the amount of information, that this can be put in a few tapes per day of observation. In this case, decoding, statistical processing and parameter estimation can then be performed off-line. This approach has been taken for the SOUSY radar -- using a hardware integrator -- (SCHMIDT et al., 1979) and by the same group at Arecibo with a portable 50-MHz transmitter.

Coherent integration usually requires special-purpose digital equipment, but can be done with fast array processors when used at the front end of the processing system. The M-mode at Millstone Hill uses this approach using an AP-120B for the integration and decoding (see p. 509, this volume, by Rastogi).

Jicamarca, at present, performs low resolution decoding off-line, by coherently integrating on line with a Harris/6 general-purpose computer.

## HARDWARE DECODERS

Coherent integration by general-purpose computers, usually takes most of the computer power to perform this task, leaving no CPU time to perform the

decoding and statistical processing. Therefore, is highly recommended to perform the coherent integration in a dedicated device. A device constructed to do this task can perform the decoding operation with very little added complexity.

A coherent integrator and decoder has been designed and built for the SOUSY radar (WOODMAN et al., 1980). To the author's knowledge, it is the only device specially designed for MST applications which has been built for this purpose. The device is described in some detailed in the cited reference. Here we shall limit ourselves to reproduce the block diagram (Figure 1) and discuss some of its features.

The W.K.R. decoder is a programmable device. It also performs the function of a radar controller. All the parameters which control the radar and data-taking sequence are programmed in 4 computer-addressable PROMS. The parameters include: transmitter IPP, baud length, code length, code sequence, sampling rate and groupings. For this purpose it interprets 16 program instructions which are accompanied by a number that specifies a time delay before next instruction is executed. Maximum sampling rate is 0.5 μsec, it can process 1024 altitudes (before decoding) with single codes, or 512 in the case of code pairs, like complementary codes.

Apart of the W.K.R. decoder, the only other hardware decoder that has been used for an MST radar is the Arecibo Planetary Decoder (schematic and some text in a maintenance document at the Arecibo Observatory). The device was built for planetary radar, a more demanding application. It is capable of performing 1000 additions or subtractions per μsec and has a maximum sampling rate of 1 μsec. It has been used for decoding at the front end of any previous processing, since it has sufficient computing power to perform decoding (as much as 256 x 1 μsec bauds) without any previous coherent integration.

The device is more powerful than required by MST applications, but it was already available. It has been used to decode and coherently integrate (in that order) 32 baud complementary code sequences in conjunction with the 430-MHz radar (WOODMAN, 1980b). Its speed allows the implementation of quasi-complementary sequences. These are long sequences of transmitter pulses, each coded with a different code which present advantages that have been discussed by SULZER and WOODMAN (unpublished manuscript, 1981) but which do not permit coherent integration before decoding.

The Arecibo Planetary Decoder consists, essentially, of four parallel cross correlators. Each cross correlator consists of a selectable number of lag-product integrators (2048 maximum). Each integrator register is associated with a given lag, and integrates the product of the present, 10-bit digitized analog signal, "multiplied" by the delayed value of a 2-bit (3 level, also called 1 1/2 bits sample of the other signal (code in our case). The delay for the delayed signal is produced by a 2-bit shift register. Each integrator is associated with one of the registers of the shift register and, therefore, to a given lag delay. The necessary multiplications and updating additions are performed by 64 parallel adders per cross correlator. Speed is achieved by parallel operations and by the fact that multiplying by 3 level signals involve only additions, subtractions and no-operations (1.-1.0).

## DECODING OF BISTATIC RADARS

Decoding of bistatic radars -- where the atmosphere is illuminated by a continuous, but coded, wave -- requires special discussion. The length of the code in this case is much larger than in the case of a pulsed radar. It has to be at least as long as the range of altitudes one expects to receive echoes, to prevent range folding of the echoes. This can put demands on the decoding

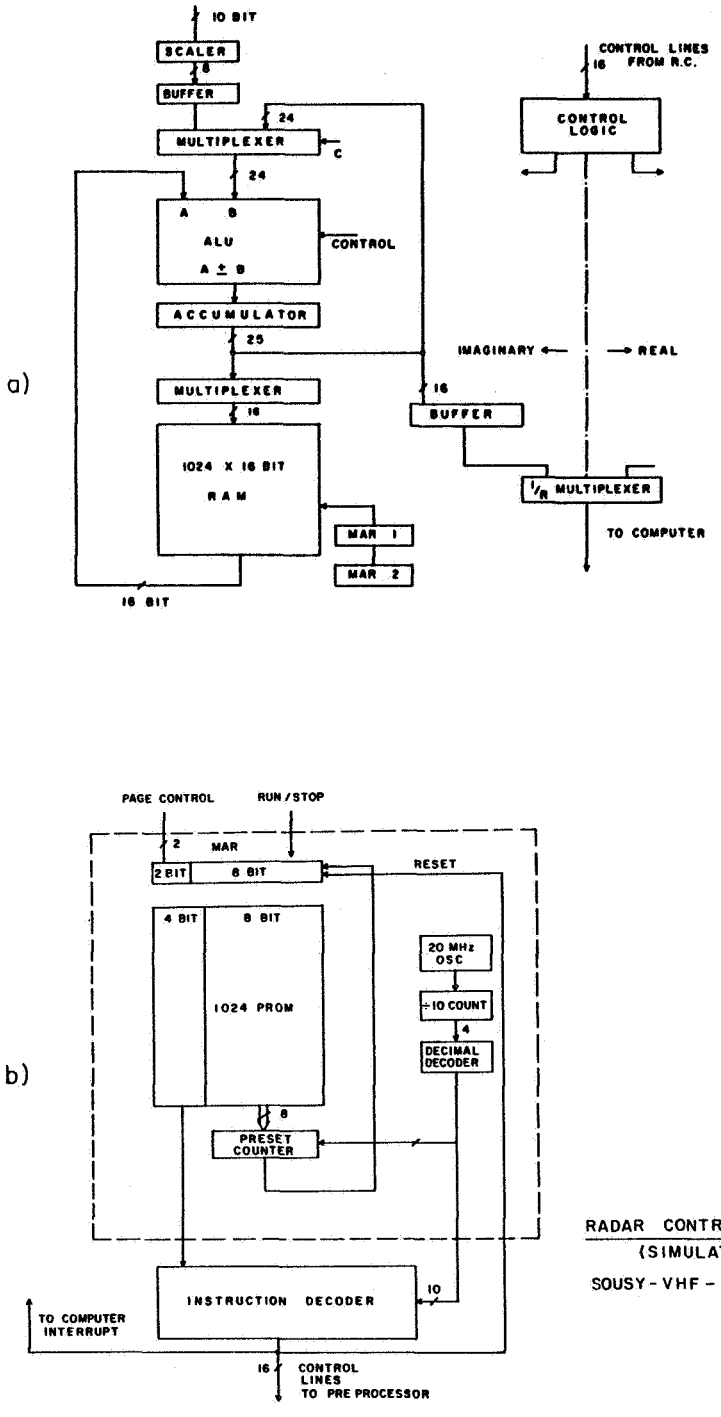


Figure 1. a. Integrator-decoder preprocessor block diagram.
b. Radar-controller and instruction-decoder block diagram.

operation which are many orders of magnitude higher than in pulsed MST radars.

So far, the only ST radar which works in a bistatic coded mode is the Arecibo 2380-MHz radar (WOODMAN, 1980a). In this case pseudo-random phase coded sequences with a baud length of 0.2 μsec and a period of 1024 bauds were used. This corresponds to a resolution of 30 meters with a range ambiguity of ∿ 30 km. Decoding at all ranges would involve ≃ 5000 operations per μsec, a formidable requirement, even when we reduce the number of ranges. Coherent integration does not help much in this case since the coherent time at 2380 MHz is nearly two orders of magnitude shorter than at 50 MHz. Nevertheless, decoding of these signals was accomplished by means of the Arecibo 1008-channel correlator (HAGEN, 1972).

Decoding becomes possible, because of the time stationarity of the radar returns, since the codes have constant amplitude and are transmitted continuously. This time stationarity permits the use of one-bit and three level (1 1/2 bit) cross correlators, which can be economically implemented by parallel integrations with a large numbers of lags at a high sampling rate. The Arecibo correlator has 1008 lags and a maximum sampling rate of 20 MHz. This represents 20,000 operations per μsec, which in this case involve simply the counting up or down of 1008 parallel counters.

The correlator at Arecibo was built for the spectral analysis of broadband (10 MHz) radio astronomy signals, by evaluating its autocorrelation function. It is divided in four identical units of 252 lags each. The scheme reported by WOODMAN (1980b) used two of them in parallel, one for the real and one for the imaginary, with 252 lags on each. This limits the range of observations to 7 1/2 kms, which is more than enough, since the range of altitudes of interest is from ≃ 14 to 19 km. The radar can illuminate below 14 km and there is no sensitivity beyond 19 km.

The Arecibo correlator has one limitation: it takes too long to dump the information. It takes so long that two consecutive decoded profiles do not have any correlation in between. This lack of correlation did not allow the determination of either the velocity or spectral width of the echoes. This limitation has been circumvented recently by using the other half of the correlator in what corresponds to a double scheme.

At present a new correlator is being built at Arecibo, which will have a buffered dump, with practically no dumping delay between decoded profiles. This should allow the evaluation of full spectral information in the future.

## CONCLUSIONS AND RECOMMENDATIONS

MST radars should include hardware coherent integrators. This reduces the decoding efforts by many orders of magnitude. Once the decision to include a hardware coherent integrator has been made, a decoding operation can be included with little additional money and effort. If coherent integration and decoding is performed with dedicated devices, the existing computing capacity can be used for statistical computations and parameter estimation.

Long sequences of codes, like the quasi-complementary sequences, cannot be implemented with simple coherent integrators and decoders. Straight decoders are required, but devices simpler than the Arecibo decoder would have to be implemented for these codes to be economical.

Bistatic CW radars should use continuous periodic pseudo-random codes. One-bit correlators can perform the decoding operation economically.

REFERENCES

Boriakoff, Planetary Decoder (1956), User and Maintainance Manual, still in preparation, Arecibo Observatory.

Hagen, J. (1972), The Arecibo 1008 lag correlator, User and Maintainance Manual, Arecibo Observatory.

Schmidt, G., R. Ruster and P. Czechowsky (1979), Complementary code and digital filtering for detection of weak VHF radar signals from the mesosphere, IEEE GE-17.

Woodman, R. F. (1980a), High-altitude resolution stratospheric measurements with the Arecibo 2300 MHz radar, Radio Sci., 15, 423-430.

Woodman, R. F. (1980b), High-altitude resolution stratospheric measurements with the Arecibo 430 MHz radar, Radio Sci., 15, 417-422.

Woodman, R. F., R. P. Kugel and J. Rottger (1980), A coherent integrator-decoder preprocessor for the SOUSY-VHF radar, Radio Sci., 15.

# 6.3A A TRANSCEIVER MODULE OF THE MU RADAR

S. Kato, T. Ogawa, T. Tsuda, and T. Sato

Radio Atmospheric Science Center, Kyoto University, Gokanosho, Uji 611, Japan

and

I. Kimura, and S. Fukao

Department of Electrical Engineering, Kyoto University, Sakyo-ku, Kyoto 606, Japan

A Japanese group working on radar remote sensing has been constructing the MU (Middle and Upper Atmosphere) radar since 1981, which is a pulse-modulated monostatic doppler radar operating at 46.5 MHz with a bandwidth of 1.65 MHz. It is situated at 34.85°N and 136.13°E, where the L value is 1.208 and the dip angle of the local magnetic field is 42.38°. The general design concept of the MU radar was studied by FUKAO et al. (1980), although several modifications were carried out in accordance with recent investigations. An updated block diagram is shown in Figure 1. One of the main characteristics is that the MU radar adopts an active array system in which each antenna is connected to a solid-state transceiver module (TR module).

The MU radar will attain a peak power of 1 MW with a duty factor of 0.05 by using 475 TR modules so as to observe three components of wind velocity in the altitude range 2-300 km with good height resolution. However, only 57 TR modules (3/25 of the whole system) have been installed up to now, so that the present peak transmitting power is 120 kW. In this report, we describe a block diagram of the TR module and a preliminary result of the power amplifier which is the main part of the TR module.

The TR module used in the MU radar is mainly composed of two units: a mixer (MIX unit) and a power amplifier (PA unit) whose block diagrams are shown in Figure 2a and b, respectively. The former generates the RF wave for transmission and converts the received echo to the IF signal. An arrow in the figure indicates a control signal from the radar controller. A 41.5-MHz local signal fed to mixers passes through a digitally controlled 8-bit phase shifter which can change its value up to 1,000 times in a second, so that the MU radar has the ability to steer its antenna direction quickly and flexibly. The MIX unit also contains a buffer amplifier and a gate for the transmitting signal and pre-amplifier for the received one whose noise figure is less than 5 dB.

The PA unit amplifies the RF signal supplied from the MIX unit up to 63.7 dBm (2350 W), and feeds it to the crossed Yagi antenna. The younger stage amplifier operates in A-class and gains 39.5 dB, while the final stage one is composed of four push-pull amplifiers whose gain is 12 dB. A TR switch attains an isolation of 100 dB between TX and RX signals by using high power PIN diodes. A band-pass-filter is inserted after the TR-switch and prevents unnecessary harmonics from transmitting. Phase and intensity of the transmitting signal and the value of VSWR are monitored by using a directional coupler. The output circuit can give linear, right and left circular polarizations. Signal level at three points and gain of both driver and final amplifiers are shown in Figure 2b. An over-all gain of the PA unit is about 50 dB.

Figure 3 shows input output characteristics of the PA unit. The output increases linearly up to 2350 W for the input signal in the range from 5 to 13 dBm, and satulates because of an action of the APC (automatic power control). Considering loss in connecting cables to the antenna, the final radiation power

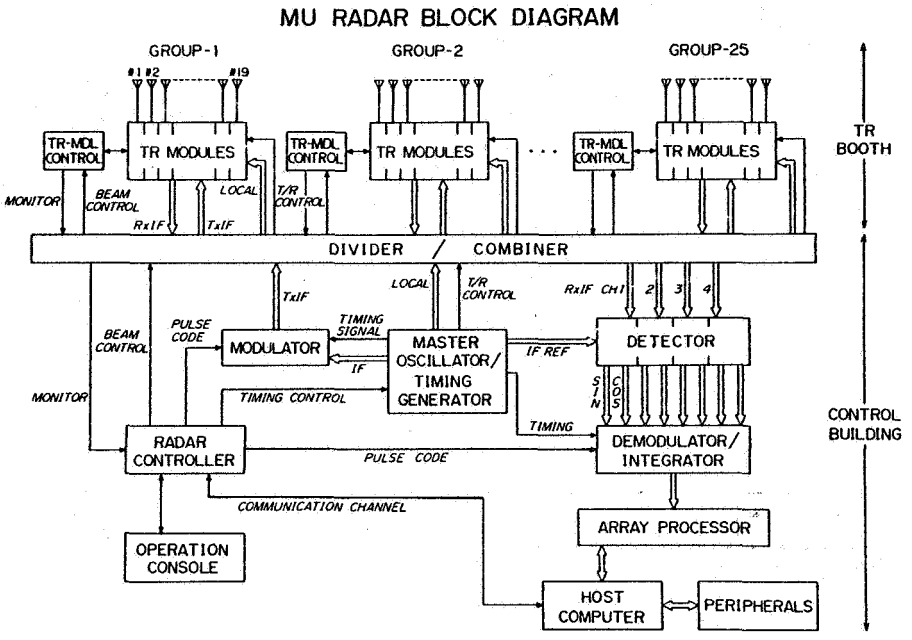


Figure 1. A block diagram of the MU radar.

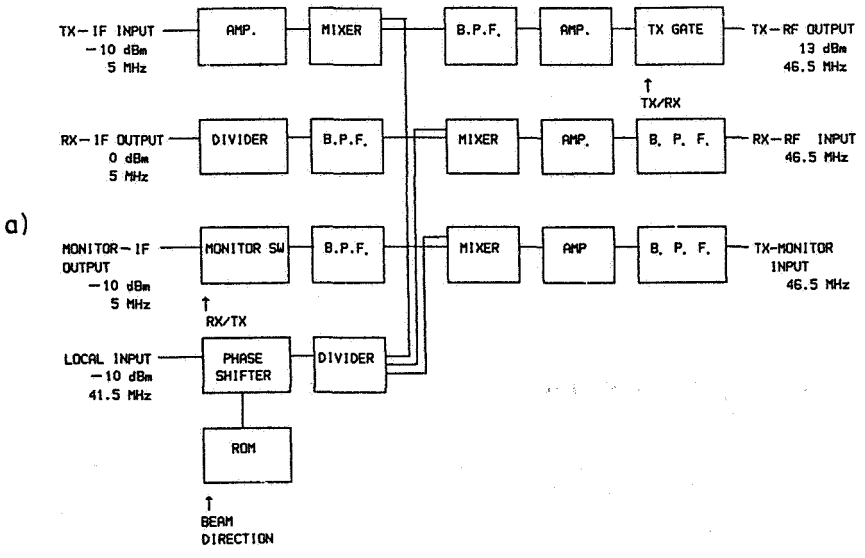


Figure 2(a). Block diagram of the MIX unit of the transceiver module used in the MU radar.

b)

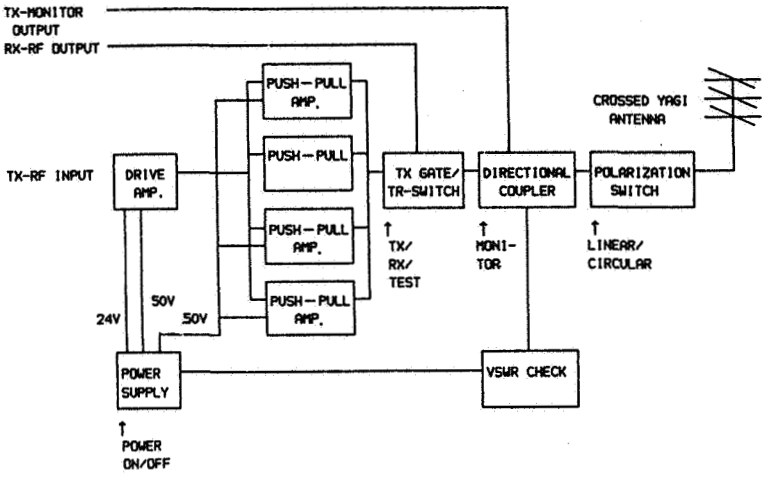


| | | | | | | |
|---|---|---|---|---|---|---|
| SIGANL LEVEL | 13 dBm | | 52.5 dBm | - | - | 63.7 dBm (2350 W) |
| GAIN | - | 39.5 dB | - | 12 dB | - 0.8 dB | |

Figure 2(b). Block diagram of the PA unit of the transceiver module used in the MU radar.

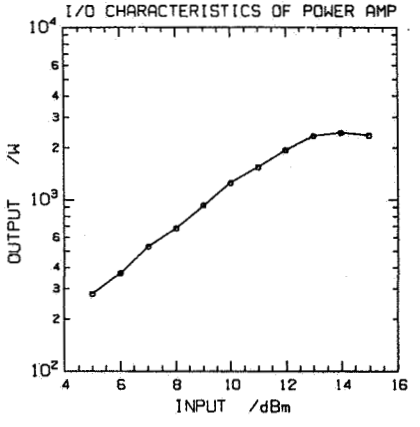


Figure 3. Input/output characteristics of the PA unit.

Considering loss in connecting cables to the antenna, the final radiation power will become 2050 W.

The TR module of the MU radar is manufactured by the Communication Equipment Works of Mitsubishi Electric Co.

REFERENCE

Fukao, S., S. Kato, T. Aso, M. Sasada and T. Mikihira (1980), Radio Sci., 15, 225-231.

# 6.3B DESIGN CONSIDERATIONS FOR HIGH-POWER VHF RADAR TRANSCEIVERS: THE POKER FLAT MST RADAR PHASE CONTROL SYSTEM

W. L. Ecklund and P. E. Johnston

Aeronomy Laboratory
National Oceanic and Atmospheric Administration
Boulder, CO 80303

Sixty-four separate 50-kW peak-power transmitters are distributed throughout the 200 x 200 meter Poker Flat MST radar antenna array. The relative phase of each transmitter is automatically controlled by a 64-channel unit located in the main building at the edge of the antenna. In this note we describe the phase control unit and present several photographs which show how the controller is constructed.

The Poker Flat antenna consists of 4, 100 x 100 meter coaxial dipole arrays with superimposed orthogonal elements. Each polarization/quarter consists of 32 strings of 48 dipoles each, and each set of 4 strings is driven by a separate transmitter. Thus 8 transmitters drive each polarization/quarter and the phase control unit described here consists of 8 sets of 8-channel rack-mounted modules all interconnected. One 8-channel module controls the 8 transmitters in a single polarization/quarter. The phase-control rack containing the modules is shown in Figure 1. Figure 2 shows an individual 8-channel controller with cover removed. The operation of a single channel will be described in the following paragraphs.

Figure 3 shows a simplified block diagram (within the dashed lines) of one channel of the phase controller. A sample of the RF outpulse pulse from a transmitter located in the antenna array is obtained from the built-in directional coupler and sent to the phase control unit via a phase-matched 256-meter coaxial cable (the "cable radar" used to phase match the cables from 64 transmitters is described in paper 6.3C, p. 427, this volume ). The RF pulse sample from each transmitter is brought to the top of the phase-controller rack. Carefully measured sections of RG-58 (0 cable in Figure 3) extend from the rack-top fittings to the channel inputs on the back of each 8-channel module. These sections determine the relative phase shifts of all the transmitters and determine the transmitted beam zenith angle. A phase reference pulse is derived from the transmitter master oscillator and is divided first in an 8-way power splitter which feeds each of the eight rack-mounted modules. The reference is again split 8-ways inside each module so that each channel obtains a phase-matched reference pulse (0 reference in Figure 3). The transmitter RF drive pulse is also split 64 ways and fed to the voltage controlled phase shifter in each channel.

In operation the RF pulse from a transmitter coupler is power divided (Figure 3) and compared with the phase reference in a mixer. The mixer output is low-pass filtered and sampled near the center of the resulting video pulse by an amplifying sample-and-hold integrated circuit. Phase control is effected by maintaining the mixer output pulse near zero volts by amplifying the sample-and-hold output which then drives the voltage-controlled phase shifter in the direction to null the mixer output. The voltage-controlled shifter achieves over 360° phase shift in the range from 0.7 to 24 volts. When the voltage into the shifter tracks to either voltage limit the wrap-around control resets the voltage so that the shifter is always operating within its control range.

Part of the RF pulse from the transmitter coupler is fed to a front panel connector where the phase and amplitude of each channel can be conveniently monitored for calibration. Part of the RF pulse is also fed to a peak detector so that the relative output of the transmitter can be monitored. This monitor-

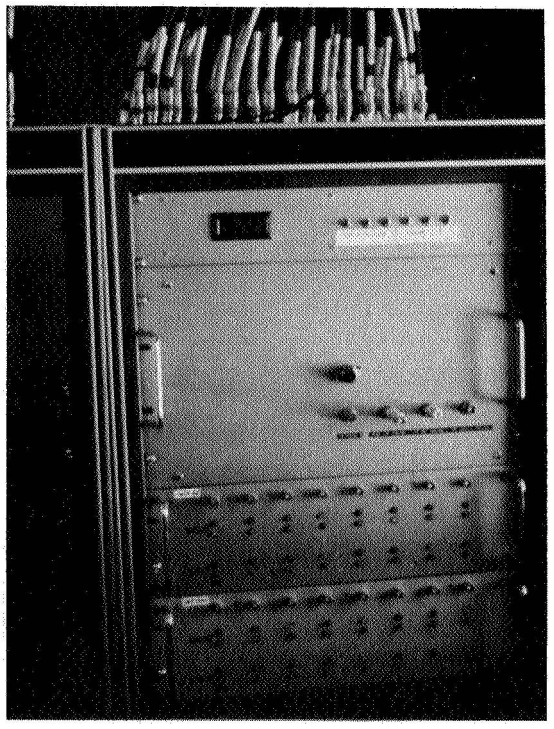

Figure 1.

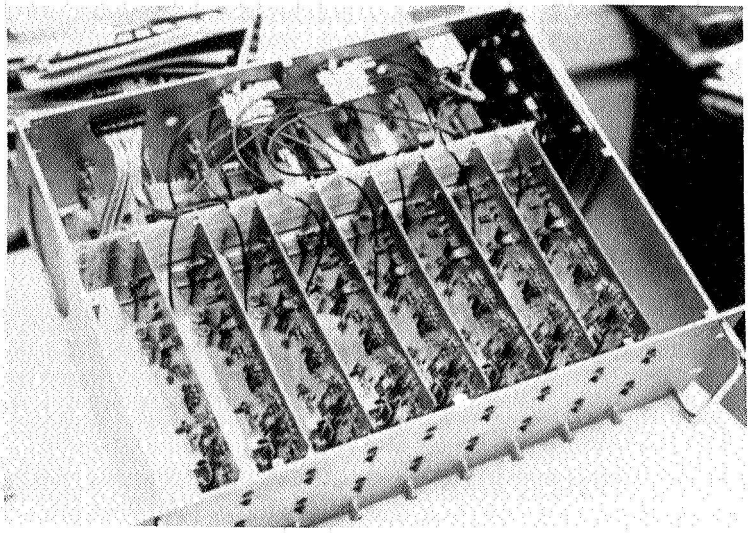

Figure 2.

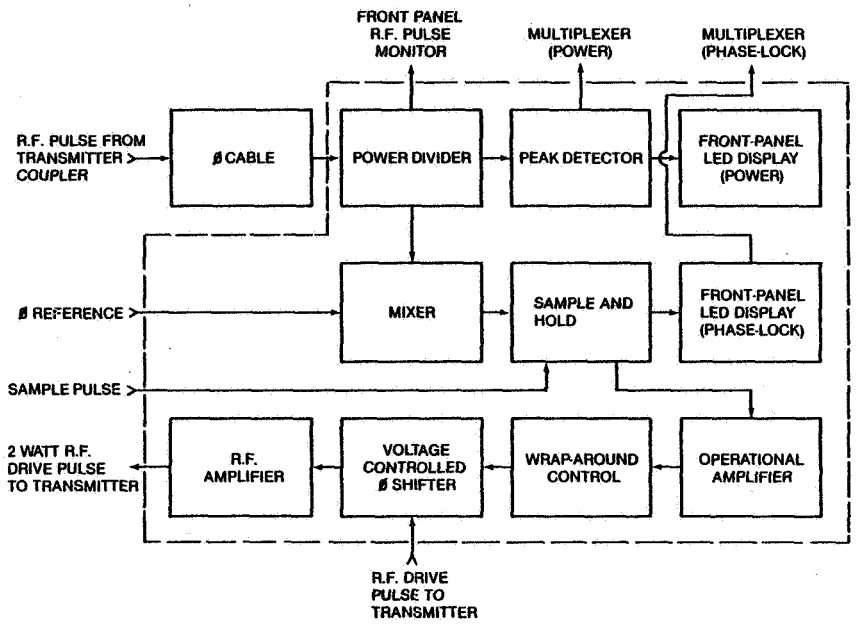


Figure 3.

ing takes place in two ways. For a quick-look determination of transmitter operation the signal is fed to a comparator which drives a pair of red/green LEDs (light emitting diodes) on the front-panel display (green indicates reasonable transmitter output, red indicates no or low output). The signal is also available at the input of a computer-controlled multiplexer so that individual transmitter outputs can be automatically logged. Individual outputs can also be manually addressed and read from a front-panel digital voltmeter. An additional pair of red/green LEDs on the front panel indicates proper phase locking. An error of a fraction of one degree causes a red light indication which is also available at another multiplexer input so that phase-lock can also be computer-logged. The LED indicator lights have proved to be very useful in providing a "quick-look" determination of system status.

The time constant of the phase-control feedback loop has been adjusted so that phase locking is achieved in about 1 second after transmitter turn-on. The phase is automatically controlled to within a fraction of a degree, and the relative phase of each unit can be adjusted by about 4° by a zero control on each sample and hold. Any channel can be quickly checked for proper operation by placing a 13-dB attenuator on the RF amplifier output and feeding the RF pulse back into the power divider input. The lengths of the RG-58 phase control cables could be changed in steps by low-power coaxial relays to obtain rapid scanning of the transmitted beam over a limited zenith angle.

# 6.3C DESIGN CONSIDERATIONS FOR HIGH-POWER VHF RADAR TRANSCEIVERS: PHASE MATCHING LONG COAXIAL CABLES USING A "CABLE RADAR"

P. E. Johnston and W. L. Ecklund

Aeronomy Laboratory
National Oceanic and Atmospheric Administration
Boulder, CO 80303

The Poker Flat 49.92—MHz MST radar uses 64 phase-controlled transmitters in individual shelters distributed throughout the antenna array. Phase control is accomplished by sampling the transmitted pulse at the directional coupler of each transmitter and sending the sample pulse back to a phase-control unit (described in paper 6.3B) located in the main building at the edge of the antenna array. This method requires phase matching 64 long (256 meter) coaxial cables (RG-213) to within several electrical degrees.

Preliminary measurements with a vector voltmeter showed that cables of this length changed electrical length by several tens of degrees due to mechanical flexing when being unspooled from cable reels. This result indicated that the cables would have to be installed in the cable troughs throughout the array before final cutting for phase match. Another set of preliminary measurements on two long RG-213 cables installed in cable troughs at Poker Flat showed that electrical length changed by about 60° for a temperature change of 20°C, but that the relative phase change between the two cables was essentially zero. Since only the relative phase is important in this system, a reference test cable was installed in the same cable trough system with the 64 phase sampling cables so that temperature effects would be same for all cables.

Tests with a time domain reflectometer showed that attenuation of high frequency components in the long RG-213 cable rounded the leading edge of the reflected pulse so that the cables could only be measured to within 50 cm (about 45° at 49.92 MHz). Another measurement technique using a vector voltmeter to compare forward and reflected phase required a directional coupler with unattainable directivity. Several other techniques were also found lacking, primarily because of loss in the long RG-213 cables. At this point we realized that what we needed was a simple version of the phase-coherent clear-air radar, i.e., a "cable radar". The only requirement was that the transmitted pulse be relatively short ($\sim$ 1 μsec) since the round-trip transit time in the cable was less than 3 μsec.

A block diagram of the cable radar is shown in Figure 1. The pulse generator puts out 0.6 sec pulses with an interpulse period of 4 μsec. The phase paths through the manual-select coaxial SPDT switch are matched for both the reference and unknown cable ports. There are two ports available for the unknown cable; one is a specially made coaxial fitting that makes good electrical contact with the square-cut end of RG-213 cable, the other is a type "N" jack. The special fitting allows rapid cable length adjustment by incremental cutting to achieve the desired phase.

In operation the reference cable is selected and the adjustable line is set for a null on the oscilloscope. A coaxial fitting of known electrical length is then inserted in the adjustable line path and the oscilloscope gain is set so that 1° phase change gives a 1-cm deflection on the oscilloscope. The fitting of known length is then removed and the unknown cable is selected and cut until the phase matches the reference. All unknown 256 meter cables were precut to within about 50 cm using the time domain reflectometer and the cable radar was used to trim each unknown cable to a 1° or better phase match with the reference cable. Type "N" plug connectors were then installed on each cable and a final

check of all 64 cables was carried out. Spot checks over a several year period at widely different outside temperatures show that the phases have remained the same to within a few degrees.

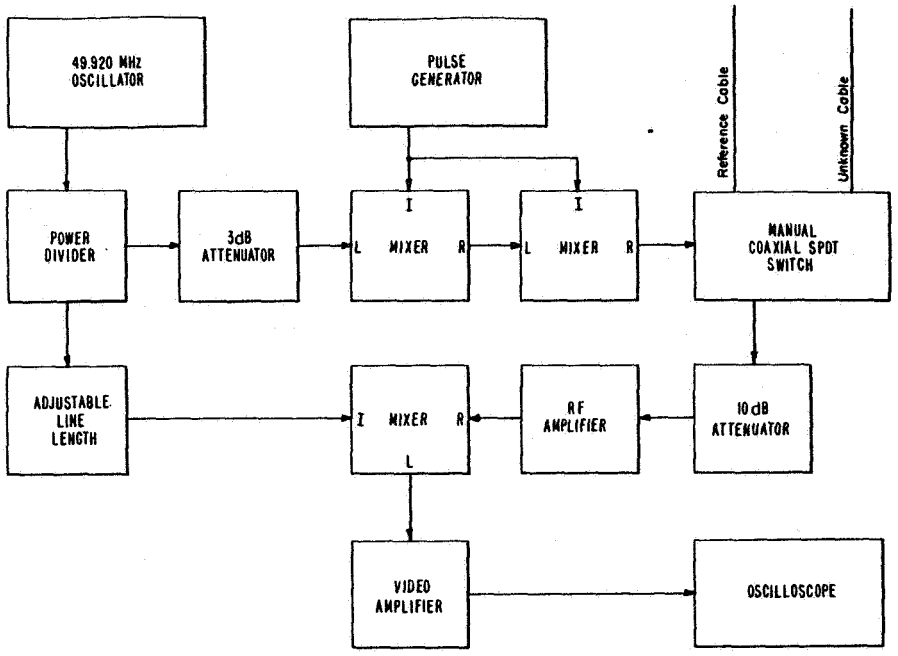


Figure 1.

# 6.3D MST RADAR TRANSMITTER CONTROL AND MONITOR SYSTEM

J. W. Brosnahan

Tycho Technology, Inc.
Boulder, CO 80306

As the MST radar technique proliferates, more applications-oriented facilities will be built. Typically an applications system, such as a wind profiler, will be operated in an unattended mode, or possibly with nontechnical operators. The next generation of transmitters will require microprocessor based, intelligent monitoring and control systems. Figure 1 shows a block diagram of the Tycho Technology, Inc. TX-3 transmitter system which is currently under development. To enhance the reliability of the system for attended operation, the low power tube stages of earlier designs have been replaced with a broadband FET amplifier. This also eliminates four tuned circuits and enhances phase stability. In addition, the new system provides for greatly enhanced monitoring and control functions of the RF and power supply circuitry with the addition of the controller module in the power supply.

In a typical MST radar transmitter, all dc voltage parameters should be monitored, as well as forward and reflected power, T/R switch current, air system operation, temperature, and safety interlocks. In addition, this monitor and control system provides all control functions and sequencing for normal operation, and provides for emergency shutdown during abnormal conditions, and automatic restart with proper sequencing in the event of a power outage. It also operates as a data logger for transmitter system parameters for the main computer system. If the host system computer has the requisite software, a limited amount of troubleshooting can be accomplished through the host system's modem via telephone should a transmitter failure occur.

A generalized control and monitor card has been developed using the Intel 8031 (8051 family) microprocessor. The design has been generalized so that this card can be utilized for virtually any control application with only firmware changes. The block diagram appears in Figure 2. The card provides for local control using a 16 key keypad (up to 64 keys are supported). The local display is four digits of 7 segment LEDs. (Up to 16 digits can be supported.) The display can indicate the status of all major system parameters and provide voltage readout for the analog signal inputs. The card can be populated with only the chips required for a given application.

Fully populated, the card has two RS-232 serial ports for computer communications. It has a total of 48 TTL parallel lines that can define as either inputs or outputs in groups of four. A total of 32 analog inputs with a 0-5 volt range are supported. In addition, a real-time clock/calendar is available if required. A total of 16 k bytes of ROM and 16 k bytes of RAM is available for programming. This card can be the basis of virtually any monitor or control system with appropriate software.

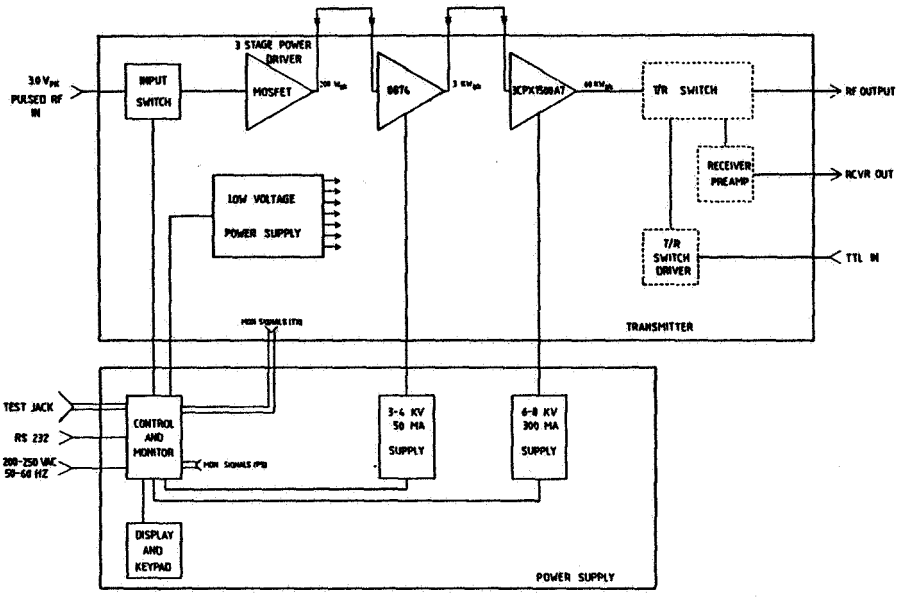


Figure 1.

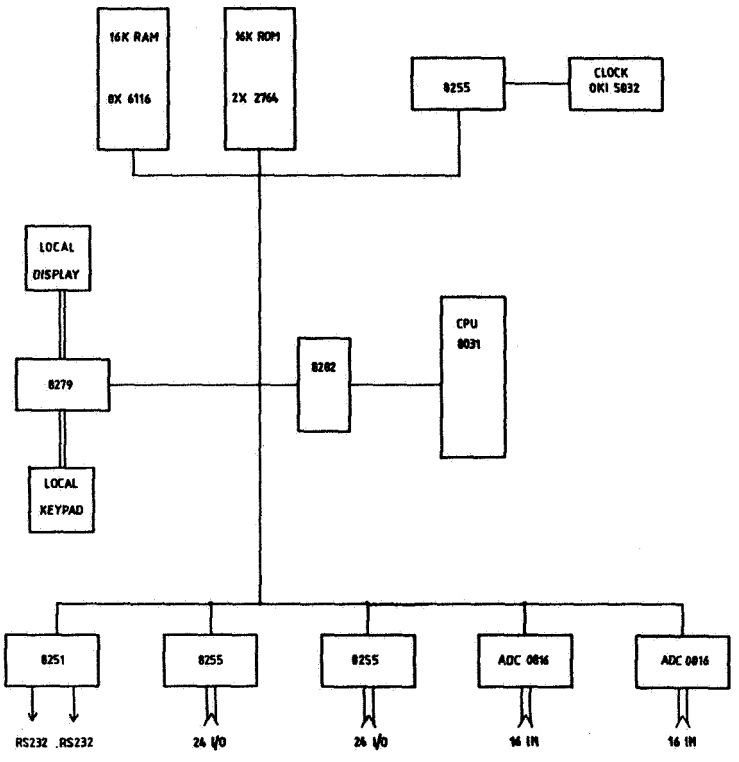


Figure 2.

# 6.4A DESIGN CONSIDERATIONS FOR HIGH-POWER VHF RADAR TRANSCEIVERS - T/R SWITCH DESIGN

W. L. Ecklund

Aeronomy Laboratory
National Oceanic and Atmospheric Administration
Boulder, CO 80303

This note describes the TR switch developed at NOAA's Aeronomy Laboratory for use in their 50 kW peak power, 50 MHz transmitter. A photograph of the switch with cover removed is shown in Figure 1. The switch mounts inside the transmitter chassis and has been designed to be compact while retaining the ability to handle well over 50 kW peak power at average power levels up to 2 kW. The TR switch is a conventional TR/ATR design with equivalent /4 transmission line sections constructed of lumped constant coils and transmitting capacitors in "Tee" sections as shown in Figure 2. Two TR sections are placed in series to achieve adequate receiver protection.

The switch is set into the "transmit" mode by forward biasing the 3 pin diodes (D1, D2, D3) to about 1.2 amperes each. The "receive" mode is achieved by back biasing the diodes to -15 volts. A directional coupler is also incorporated into the TR switch box to provide a convenient monitor point for forward and reflected transmitter power. The TR switch characteristics are listed in Table 1.

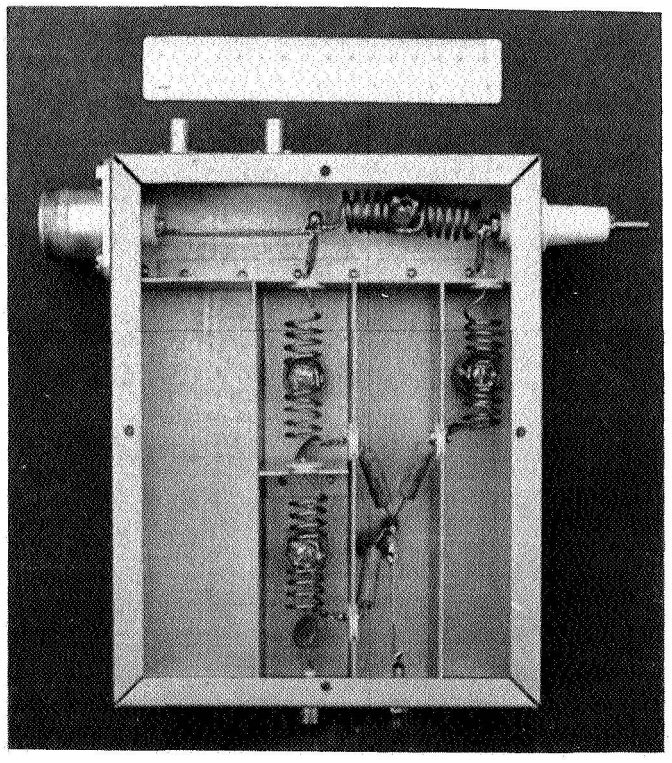

Figure 1.

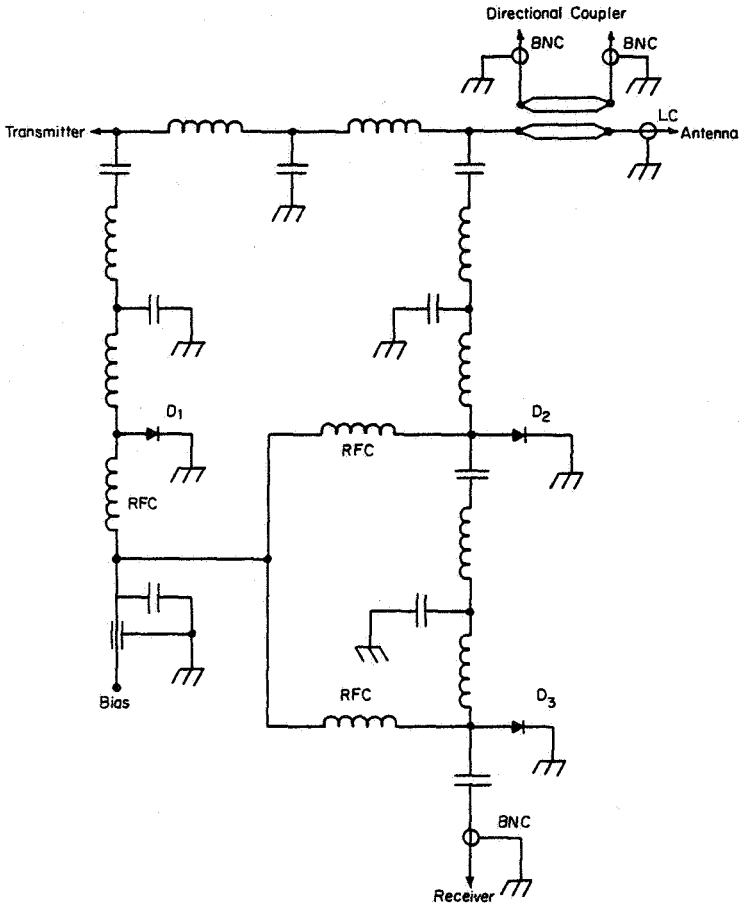


Figure 2.

Table 1. TR switch characteristics

| | |
|---|---|
| TRANSMIT INSERTION LOSS | ∿ .3 dB |
| RECEIVE INSERTION LOSS | ∿ .6 dB |
| RECEIVER ISOLATION | ∿ 50 dB |
| DIRECTIONAL COUPLER FACTOR | ∿ 46 dB |

# 6.4B THE MOBILE SOUSY-DOPPLER RADAR - TECHNICAL DESIGN AND FIRST RESULTS

P. Czechowsky, G. Schmidt and R. Ruster

Max-Planck-Institut fur Aeronomie
D-3411 Katlenburg-Lindau
Federal Republic of Germany

Based on the experience obtained with the stationary SOUSY radar in the Harz mountains, a mobile VHF Doppler system was developed during the last two years. The electronic part is installed in a 20-ft container and was tested for the first time during a joint experiment at the Arecibo Observatory (Puerto Rico) using a special log-periodic aerial to illuminate the 300-m dish. In 1982 this system was extended by designing a mobile phased antenna array with finally 576 Yagi elements. The grouping of the single Yagis, the system of transmission lines, the phase shifters, the power splitters and the T/R-switch are described. A summary of results obtained during the first two campaigns is presented as well as a survey of future programs demonstrating the flexibility of this mobile system.

## INTRODUCTION

During the last decade the development of the upcoming VHF-Doppler radars designed to study the structure and dynamics of the middle and lower atmosphere was mainly influenced by the demand to improve the efficiency of these systems. The power-aperture-product, therefore, was increased using larger antennas and transmitters and different pulse coding techniques (e.g., BALSLEY et al., 1979; CZECHOWSKY et al., 1979). The height and time resolution as well as the steerability of the phased antenna arrays were extended and other methods well known from ionospheric research, such as the spaced antenna drift technique, were applied to investigations of the middle atmosphere (ROTTGER and VINCENT, 1978).

At the same time the SOUSY radar facility was extended by a second system which is completely mobile, in order to increase the flexibility and to enable participation in other scientific programs studying geographical or orographical influences.

The purpose of this paper is to describe the technique and design of the SOUSY mobile radar in comparison to the stationary system, which has been in operation since 1977, and to discuss first results obtained during common experiments at the Arecibo Observatory and during the ALPEX campaign. Finally, a brief outline of future programs is presented.

## THE STATIONARY SYSTEM

The SOUSY radar was designed in 1975 and completed after successful test measurements in summer 1977. This system is located in a valley in the Harz mountains (lat. 51°42'N, long. 10°30'E) 26 km east of Lindau, in order to minimize interference with TV systems operating at the same frequency and to reduce ground clutter from distances behind the surrounding mountains. Since the radar has already been described in detail by SCHMIDT et al. (1978), only a brief summary of the most important technical parameters are presented in the block diagram of Figure 1a.

The minimum usable pulse length is 1 μs corresponding to a height resolution of 150 m. During some scientific programs, however, a special sampling technique was applied to improve the resolution to about 20-30 m (ROTTGER and SCHMIDT, 1979). The transmitter peak power is 600 kW with a maximum duty cycle

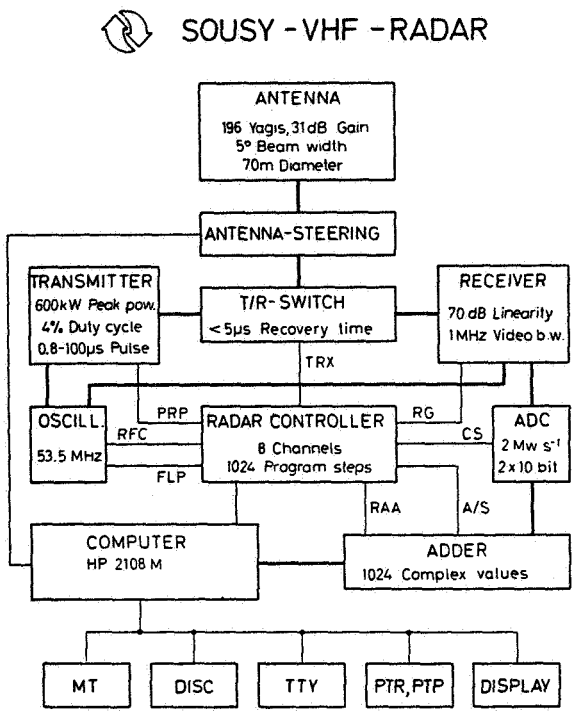


Figure 1a. Block diagram of the SOUSY stationary radar in the Harz mountains/Germany.

of 4%. The power supply is capable of handling a maximum length of 100 µs. The final amplifier -- a modified Philips TV transmitter -- operates in a push-pull mode using two water-cooled tetrodes. Phase coding was introduced to improve the signal-to-noise ratio especially for mesospheric observations. The radar transmitter and receiver is tunable in the frequency range from 48 to 67 MHz (Table 1). The receiver has a video bandwidth of 1 MHz and a linear amplification within a dynamic range of 70 dB to enable hardware coherent integration. The complex signals at the receiver quadrature output are digitized using a 10-bit ADC and coherently added by a hardware adder with a maximum

Table 1.

| | STATIONARY SYSTEM | MOBILE SYSTEM |
|---|---|---|
| Pulse peak power | 600 kW | 200 kW |
| Duty cycle | 4% | 4% |
| Number of elements | 196 | 576 |
| Single element | 4-element Yagi | 4-element Yagi |
| Polarization | linear | linear |
| Effective area | 3150 $m^2$ | 8880 $m^2$ |
| Gain | 31 dB | 35.5 dB |
| Steerability | continuously | 3 independent directions |
| Frequency | 53.5 MHz | 53.5 MHz |
| Tuning | 47-64 MHz | 45-58 MHz |
| Beam width | 5° | 3° |
| Pulse length | 1-100 µs | 1-100 µs |

storage for 1024 complex height values. The central unit is a radar controller which is programmed by a computer.

Pulse length, repetition frequency and coding are adjustable by software instructions based on the requirements of the scientific programs. Transmitter, receiver and antenna are connected to a high-speed transmit-receive-switch (TR-switch) with a recovery time of less than 8 μs. This corresponds to the near-far-field range R of the antenna which is about 1700 m ($R = 2d^2/\lambda$, d = diameter of the antenna and $\lambda$ = wavelength). This antenna is an extension of a first version of 76 Yagis which was in operation from April 1977 to June 1978. A detailed description of this phased array is given below in the following section, since both antennas are based on the same concept.

## THE MOBILE SYSTEM

The mobile SOUSY radar (Figure 1b) was developed to increase the flexibility and to enable participation in other scientific programs studying geographical or orographical influences. This system will be completed in summer 1983 and can be operated using different final amplifiers resulting in different average power-aperture-products from $1.4 \times 10^6$ to $7.1 \times 10^7$ $Wm^2$, the maximum of which is equal to the value of the stationary radar. The computer, the radar controller, the hardware adder and the AD converter are exchangable between both systems whereas the transmitter and the receiver are constructed in a compact version to be completely installed in a single 20-ft container.

The final power amplifier -- a modified Philips TV module - is aircooled and operates in a class-C push-pull mode with a peak pulse power exceeding

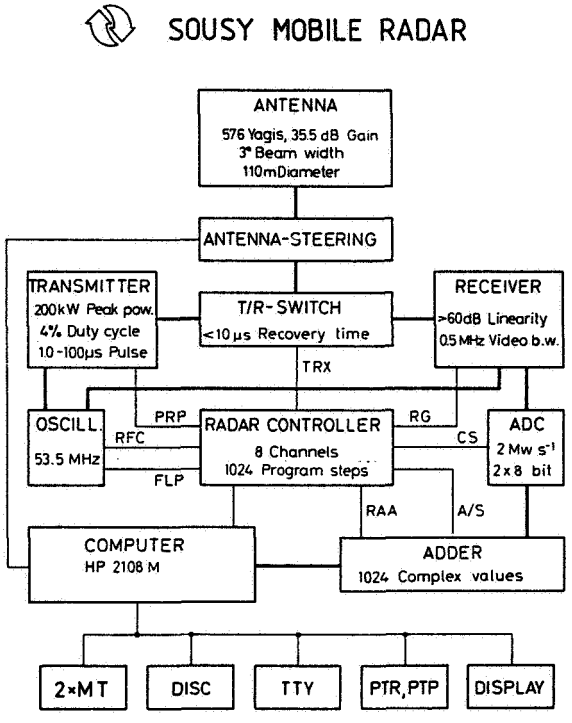


Figure 1b. Block diagram of the SOUSY mobile radar.

200 kW. Different drivers can be used separately with 4, 10 and 35 kW for low power operation. This system is continuously tunable from 45 to 56 MHz.

Between transmitter and antenna a bandpass filter with a bandwidth of 2 MHz and a low pass filter with a cut-off frequency at about 65 MHz is inserted to prevent harmonic signals and TV interference. Since the mobile system is to be used at different geographical locations with different orographic shielding, special efforts were necessary to develop an antenna array that satisfies the requirements of maximum sidelobe suppression especially at low elevation angles. Therefore the construction of the antenna, the calculation of the radiation pattern as well as the description of TR switch and phase shifters are main subjects of this paper. Results and experiences obtained with the stationary array are also discussed in some detail.

(a) Antenna Array

The design criteria of the mobile system are mainly derived from the concept of the existing stationary phased array antenna which is now in operation in its final version since 1978 (CZECHOWSKY and MEYER, 1980). This first completely steerable antenna was developed to increase the efficiency of the whole radar system by preventing clutter and interference with other users since the operation frequency band of $f = 53.5 \pm 1$ MHz fills the gap between colour and sound carrier of channel 2 of the German TV system. The frequency allocation therefore was coupled with the obligation to minimize the horizontally directed radiation. Consequently, the radar was located in a valley in the Harz mountains about 26-km east of the institute at Lindau. These mountains provide a considerable shielding up to elevation angles of 5° to 25° at different azimuths within a 2-km range. Since this distance is equal to that resulting from the near-far-field condition of the radiation pattern of the antenna the altitude of 2 km defines the lower limit of the SOUSY radar. Ground clutter from targets behind the shielding mountains was only detected during atmospheric conditions with strong ducting.

The second aspect to reduce interference can be achieved by the suppression of sidelobes which in turn requires an optimizing technique for calculating the antenna diagram. Operation in a TV channel has, of course, the advantage that several modules such as transmitter modules, the Yagi antennas, and power splitters could be bought from stock and were immediately ready for operation with slight modifications only. This advantage influenced the decision to use 4-element Yagis as single radiators instead of coaxial collinear dipoles of other systems.

The two phased arrays which are now in operation consist mainly of the same modules as e.g., 4-element Yagis, 3-dB power splitters, coaxial relays combined to phase shifters and different types of cables and connectors. The differences between the two systems lie in the size, the weighting of the Yagis, and the construction of the aerial masts. The technical parameters are summarized in Table 1.

The aperture of the first antenna array -- the stationary one -- is mechanically and electrically weighted in order to suppress the sidelobes by 25 dB at angles close to the zenith and by 40 dB at low elevation angles. This weighting is achieved by increasing the element spacing from 0.77 $\lambda$ to 1.17 $\lambda$ at the outermost positions and by feeding the antennas with different power, respectively.

The radiation pattern of n Yagis each fed with a current amplitude $J_\nu$ can be expressed by (HEILMANN, 1970):

$$E \approx F(\phi,\theta) \sum_{\nu=0}^{n-1} |J_\nu| e^{j\left(\frac{2\pi d_\nu}{\lambda} \sin\theta \cos(\phi-\phi_\nu)-\delta_\nu\right)},$$

where $d_\nu$ and $\phi_\nu$ are the polar coordinates of an individual Yagi. For a given direction $\phi_m$ and $\theta_m$ the field strength E has a maximum if $\delta_\nu = 2\pi d_\nu \cdot \sin\theta_m \cos(\phi_m-\phi_\nu)/\lambda$. The variables used for the optimization of the antenna pattern are: (1) the diagram $F(\phi,\theta)$ of the single element; (2) the number n of elements; (3) the polar coordinates $d_\nu$ and $\phi_\nu$; and (4) the current distribution $J_\nu = |j_\nu| \cdot e^{-j\delta_\nu}$.

The method which was applied for calculating the configuration of an array with an optimum radiation pattern is called "evolution strategy" and is based on the principle of "mutation" and "selection". As an initial condition a realistic configuration of the n elements is chosen to calculate a first diagram. Adding random variations to the original parameters a second diagram is computed and compared with the first one. If the second solution appears to be an improvement the new one is used as initial value for a further modification or "mutation". Otherwise the first "mutation" is cancelled and the original configuration is used for another "mutation". This latter procedure is called the "selection". Depending on the initial values up to twenty successive steps were necessary to find the optimum solution in calculating the radiation pattern of the first stationary antenna system. The coupling between the Yagi antennas as well as the reflection from the ground were neglected in the calculation since preliminary measurements have shown that the decoupling between the antennas -- independent of the polarization -- is above 25 dB and that the front-to-back-ratio is about 15 dB.

Because of the large number of elements in the mobile system, electrical weighting only was sufficient to assure a current distribution close to the Dolph-Chebychev distribution. The 576 Yagis of the mobile version, therefore, are located on straight lines with the same spacing.

For the mobile array Figure 2 shows the resulting current distribution (dots) in two planes at $\phi = 0°$ and $\phi = 45°$ to the dipole direction. The three solid lines represent the binominal (BI) and Dolph-Chebychev distributions with theoretical sidelobe suppression of 30 dB ($DT^1$) and 60 dB($DT^2$).

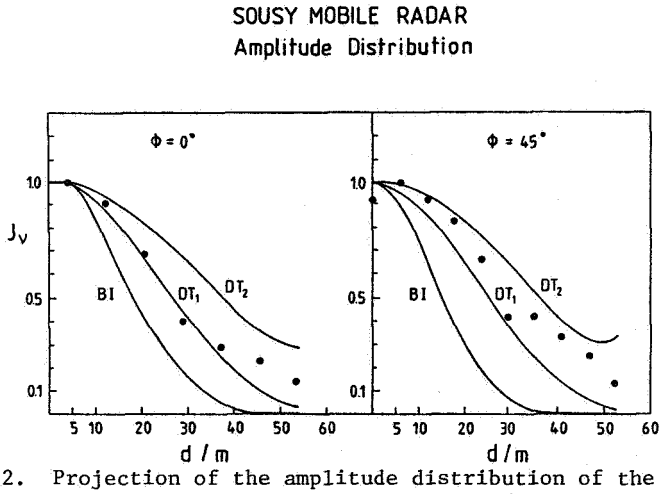


Figure 2. Projection of the amplitude distribution of the mobile SOUSY antenna compared with Dolph-Chebychev ($DT_1$: 30 dB sidelobe suppression and $DT_2$: 60 dB sidelobe suppression) and a binominal (BI) distribution.

Figure 3 presents the final diagram of the mobile antenna array for the plane 45° to the dipole direction indicating a sidelobe reduction of at least 25 dB close to the main lobe and of 40 dB for low elevation angles. The half power beam width is 3°.

The above-mentioned method for obtaining an optimum radiation pattern as well as all assumptions made have been tested by comparing the theoretical and measured antenna diagram. For this purpose the stationary array located in the Harz mountains which is continuously steerable within a cone of 30° vertex angle centered on the vertical has been used. This system was operated in the receiving mode only during the transit of Cassiopeia A, which is the most intense point source detectable for the SOUSY radar. The beam direction was tilted meridionally in steps of one degree from 12° north to 8° south within 1.5-min sweeps for a time interval of 3 hours on Oct. 25, 1981. Figure 4 presents in a three-dimensional plot the received noise power $P_N$ as a function of time and zenith distance. The power maximum was observed exactly at 7° north which agrees with the position of Cassiopeia A ($\theta$ = 58°35'N, SOUSY radar location 51°42'N), confirming the correct operation of the antenna steering. A detailed analysis (Figure 5) indicated that the measured half-power beam widths in the zonal and meridional planes for the tilted antenna deviate by $\pm$ 0.1° from the theoretical value of 5.6°. Unfortunately it was not possible to measure the suppression of the sidelobes applying that method since the level of the background noise was only 10-15 dB below those of the point source.

The final configuration of the mobile array is shown in Figure 6 consisting of 144 squared subsystems with 4 Yagis each. The antenna aperture has approximately an octogonal shape and is electrically weighted, indicated by the different symbols. The black subsystems in the center are fed with a power level "1", the white ones with "0.25" and only a few ones (grey) are fed with "0.5" to smooth the current distribution. At present the steerability of this system is limited to three independent beam directions only.

(b) Feeding Network

The feeding network for both antenna arrays is based on the same concept and consists of a system of broadband 3-dB directional couplers and quadruple power splitters arranged in a nine-level cascade. A quarter of the scheme of

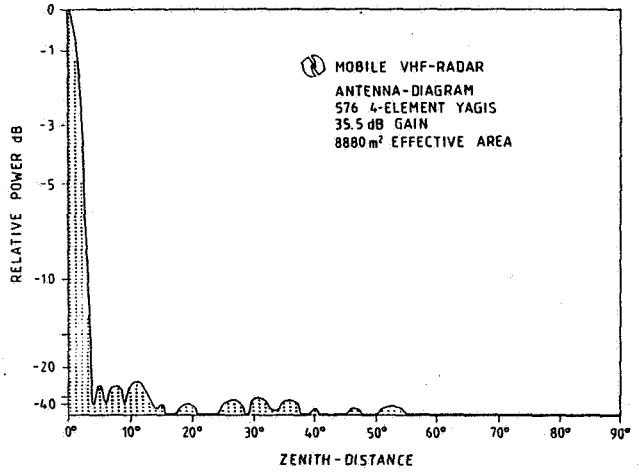


Figure 3. Diagram of the mobile SOUSY antenna.

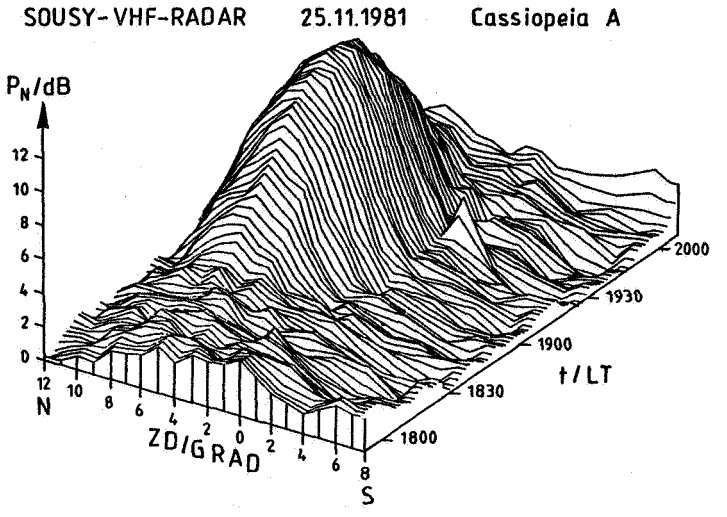


Figure 4. Received noise power $P_N$ of Cassiopeia A using the steerable stationary SOUSY antenna.

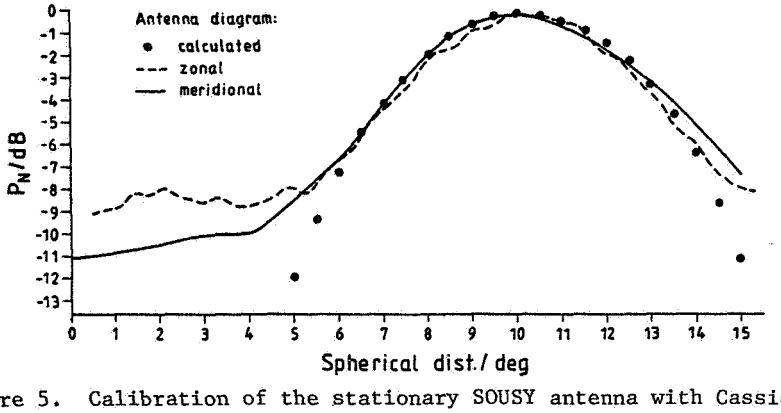


Figure 5. Calibration of the stationary SOUSY antenna with Cassiopeia A.

cables, power splitters, phase shifters and antennas is shown in Figure 7 starting at the third level of the cascade with an input power of 50 kW.

The decoupling between the two output ports of each directional coupler of about 35 dB prevents a direct connection between the single antennas. Consequently the main part of the reflected power caused by the VSWR is fed back to the transmitter or is absorbed in the terminating resistors at each hybrid (VSWR = 1.15) measured for the stationary antenna.

Due to the phase difference of 90° between the two output ports of each hybrid, four phase values (0°, 90°, 180°, 270°) occur at the last level of the cascade. To balance these differences, the phases of 90° and 270° are transformed to 180° and 0° by inserting additional 90° phase cables and the resulting displacement of 180° is compensated by two different antenna types with a direct and crossed connection to the driven dipole, which is indicated in this figure by the open and solid arrows.

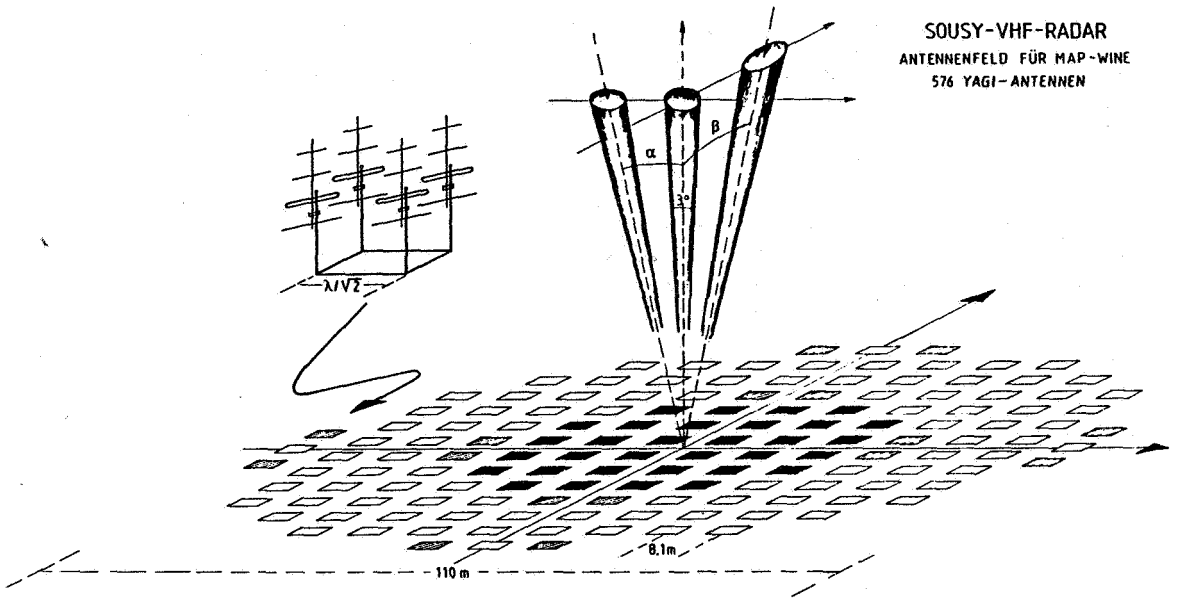


Figure 6. Configuration of the mobile SOUSY antenna. (Weighted subsystems: black - power level 1; grey - power level 0.5, white - power level 0.25.)

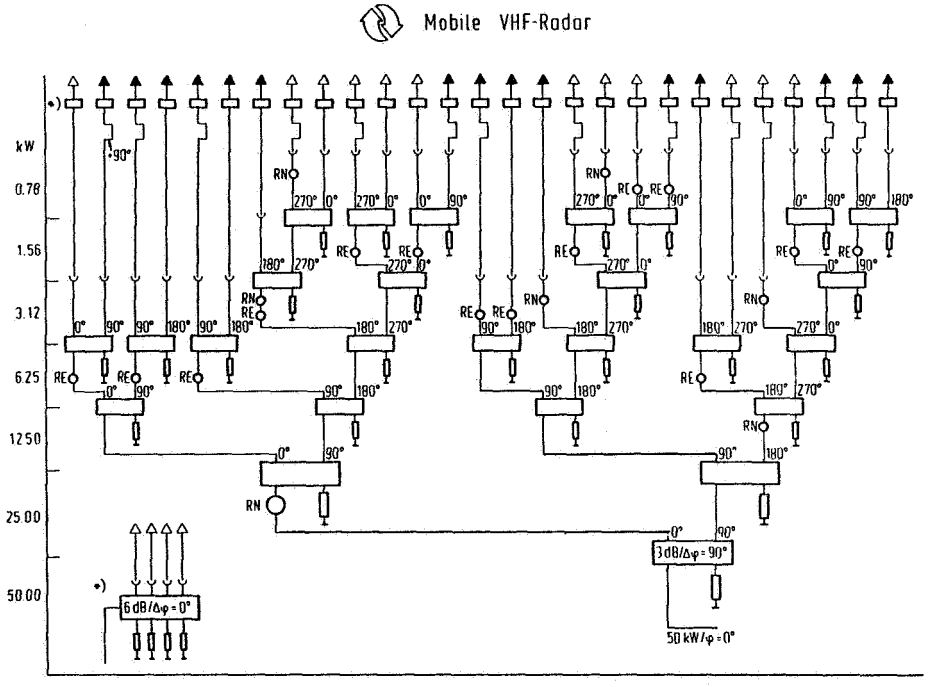


Figure 7. A quarter of the feeding system of the mobile antenna starting at the third level with 50 kW. The circles represent the position of the phase shifters.

The circles represent the position of the phase shifters which steer one or more subsystems each consisting of four antennas. This part of the antenna, the hybrids, and the phase shifters are the most expensive elements of the whole array.

(c) 4-Bit Phase Shifter

Figure 8 presents the principle of the 4-bit phase shifter, which is a combination of four 4-port coaxial switches. The phase can be changed in steps of $\lambda/16$ equal to 22.5° controlled by a computer program. In the "low" position all antennas are fed with equal phase and the beam is directed vertically. The switch-over-time of the relays is less than 50 ms.

(d) TR Switch

The transmit-receive switch which connects the antenna with the transmitter and receiver is a combination of two 3-dB directional couplers as shown in the Figure 9. This principle was first described by the Unitrode corporation (UNITRODE, 1968) in connection with the application of pin diodes in high-power duplexers.

The two hybrids are connected with a system of two cylindrical tubes where 2 x 6 high-power pin diodes are located on a circle between the inner and outer conductor. The switching pulse for the diodes is fed via a T-junction. The distance between the hybrid and the diodes is less than a quarter of a wavelength to reduce the high voltage of about 11 kV (stationary system) at the connector.

In the transmit position the output power is split by the first hybrid, transferred to the pin diode switches, then reflected at these diodes and fed back to the decoupled port, which is connected with the antenna. During the receiving phase -- with open diodes -- the signal from the antenna is split in the first hybrid, passes the tubes, is combined in the second hybrid, and fed into the receiver. This system is capable of handling 600 kW.

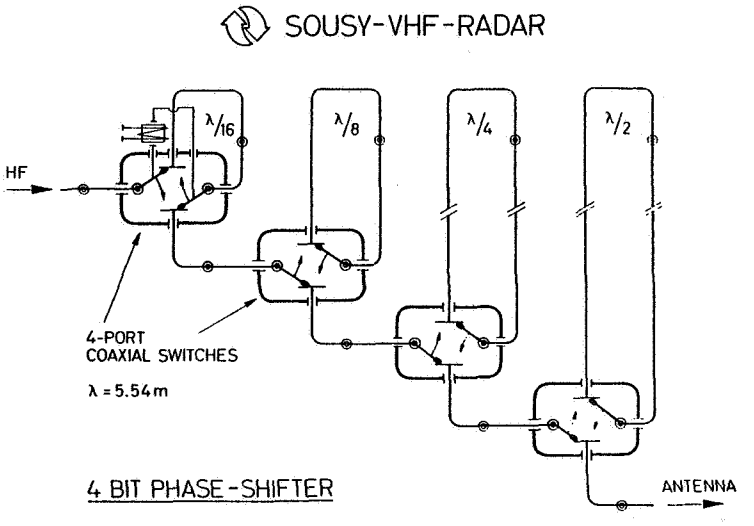


Figure 8. 4-bit phase shifter for the SOUSY radar antenna. Phase can be changed in multiples of 22.5°.

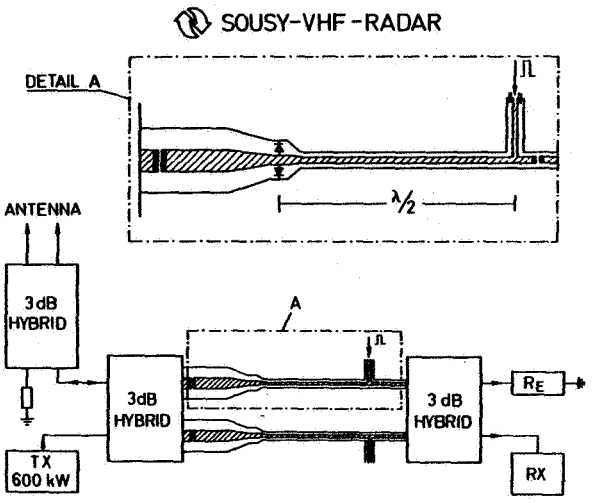


Figure 9. Scheme of the TR switch. Switching time is 8 μs.

The quality of the TR switch can be estimated by measuring the decoupling between the transmitter TX and the resistor $R_E$. For the stationary system the resulting voltage values were 5.5 kV at the transmitter and 11 V at the resistor, corresponding to 54 dB. With the additional decoupling of 30 dB of the second hybrid, a total decoupling of more than 80 dB to the receiver was proved.

The recovery time of the TR switch is less than 8 μs, enabling measurements from a lowest height level of about 1.2 km. The bandwidth of the TR switch is several MHz.

## OBSERVATIONAL RESULTS

In 1980 and 1981 the mobile SOUSY radar was operated for the first time at the Arecibo Observatory in Puerto Rico. The telescope at the Observatory is a unique instrument consisting of a large dish with a diameter of 300 m; line feeds and point-source feeds are installed on a platform 150 m above the base of the dish. This system can be steered within 12.5° off vertical. The SOUSY VHF transmitter and receiver were connected to a special log-periodic feed antenna, which was installed on the feed arm of the platform to illuminate the dish. This antenna configuration has a beam width of 1.6° with an antenna gain of 41 dB.

In 1981, observations were carried out sporadically at different times during the day in order to analyze short-term events (RUSTER and KLOSTERMEYER, 1983) and to investigate structures and scattering mechanisms (ROTTGER et al., 1983). In general, significant atmospheric radar echoes have been observed in the stratosphere up to 25 km and from 60 to 90 km in the mesosphere.

The most interesting results concern the characteristics of mesospheric structures indicating two different types of layers. The contour plot (Figure 10) presents details of the height and time variation of the echo occurrence for a period of about one hour. The structures above 80 km can be described as cloud-like whereas those below as thin laminated sheets. This distinct separation into two different echo regions is also clearly expressed by the different shapes of the observed Doppler spectra. In Figure 11 the profiles of

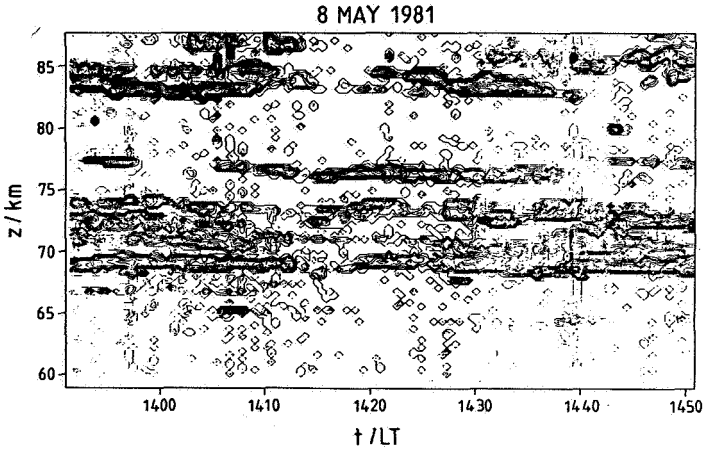


Figure 10. Mesospheric structures indicating two different types of layers measured in May 1981 with the mobile SOUSY radar in Arecibo, Puerto Rico.

the spectral intensity (grey scale) are plotted for the zonal and meridional component of the wind system. Below 80 km a strong directional shear is observed with a change of the wind direction of more than 90° within a height interval of 6 km. The spectra are extremely narrow in contrast to the broad spectra above 80 km.

On May 29, measurements were carried out to investigate further details of the scattering mechanism of these structures (Figure 12). For this purpose the beam direction was changed in steps of 1.7 degrees from the vertical to 6.8° off zenith. For five different examples the height integrated power was calculated

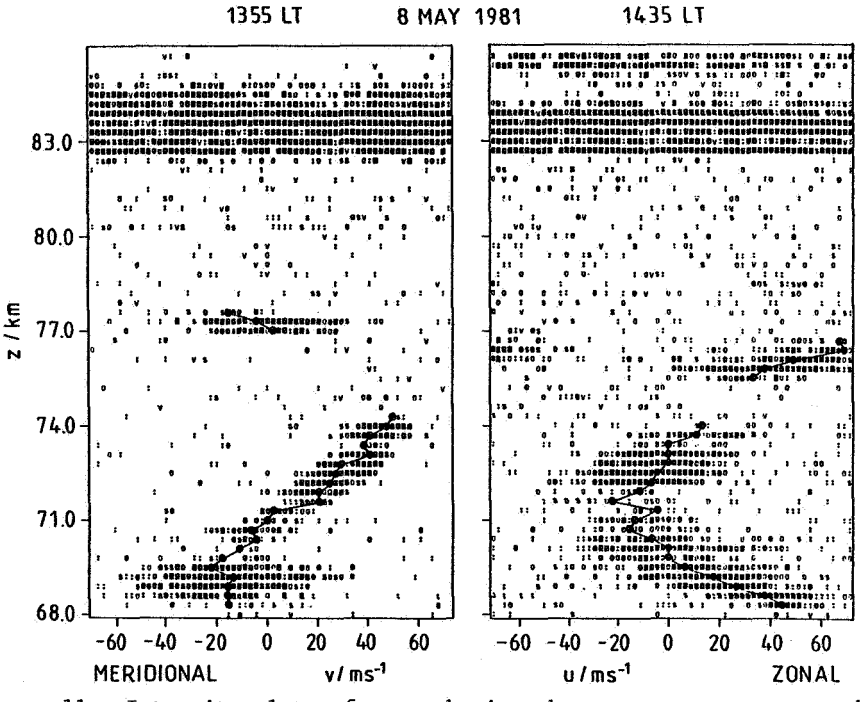


Figure 11. Intensity plots of mesospheric echo power spectra versus height measured in May 1981 with the mobile SOUSY radar in Arecibo, Puerto Rico.

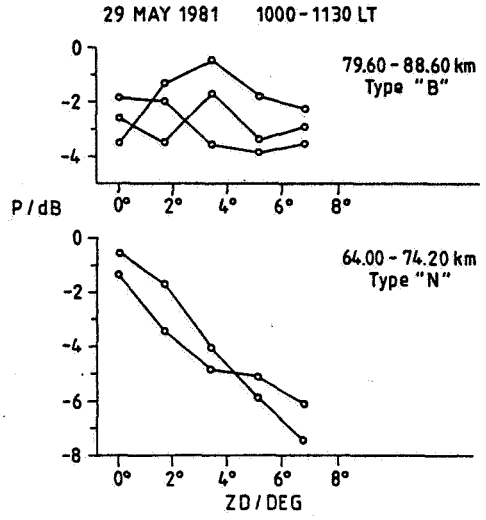


Figure 12. Aspect sensitivity of mesospheric signals measured in May 1981 with the mobile SOUSY radar in Arecibo, Puerto Rico.

for both height regions and plotted as a function of the antenna zenith distance. Within the altitude range from 64 to 74 km a strong aspect sensitivity of about 1 dB per degree was observed. Above 80 km, however, no significant variation in the echo power was measured during the change of the beam direction. The respective power spectra resulting from these echoes show the same significant differences as presented in Figure 11. In particular, the narrow spectra below 80 km and the broad ones above that height seem to indicate that turbulent structures are mainly present in the upper height interval giving rise to isotropic scatter. In the lower altitude range, however, laminated layers dominate causing partial reflections.

The airflow over and around mountains was one of the scientific problems selected for a major field study during the Global Atmospheric Research Program, which led to the Alpine Experiment (ALPEX) conducted in 1982 in Europe. Within the subprogram MERKUR designed for studying mesoscale phenomena, measurements have been carried out using the mobile SOUSY VHF-radar near Rosenheim in Bavaria, Germany (CZECHOWSKY et al., 1982; WEBER and RUSTER, 1982; WEBER et al., 1982). North and south of the radar site wind observations were performed by the German Weather Service and the Meteorological Institute of the University of Karlsruhe. During special observational periods additional in situ measurements by airplanes were carried out. These parallel measurements, therefore, offer the opportunity to compare the results obtained by the different techniques and to study the wind variation on a north-south baseline. Figure 13 shows the observed height profiles of the wind speed and wind direction. The solid line represents the VHF radar data, the dashed line the radiosonde data from Thalreit (5 km south), the crosses the radiosonde data from Munich (54 km northwest), the open and closed circles refer to the ascending and descending part of the flight measurements. This comparison shows a good agreement of the overall wind profile. The differences, in particular, result from the variations in time and location at which the data were taken. Differences of 1 hour and a few kilometers, respectively, can lead to variations in the wind field of up to 10 m $s^{-1}$.

## FUTURE PROGRAMS

The mobile radar is now prepared for operation during the MAP/WINE campaign

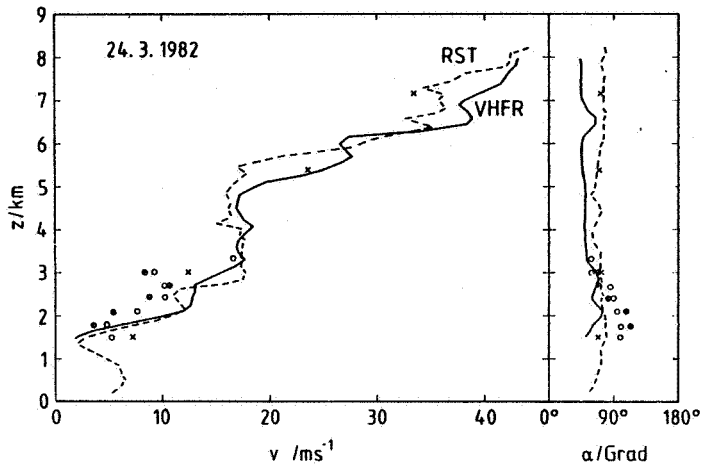


Figure 13. Height profiles of wind speed and direction compared with results from radiosondes from Munich and Thalreit measured with the mobile SOUSY radar system in March 1982 near Rosenheim, Bavaria during the Alpine Experiment (ALPEX).

and will be located on Andoya (Norway) during the winter season 1983/84. For the first time the final average power-aperture-product of 7.1 x 10 Wm (200 kW, 4% duty cycle, 35.5 dB gain) will be available during this program. The scientific goals can be summarized as follows:

(1) Investigation of the morphology of tidal waves, gravity waves and turbulent structures in the winter mesosphere.

(2) The study of sudden stratospheric warmings, their temporal and spatial developments and their effect on structural parameters and dynamics of the mesosphere.

Starting in 1985 joint experiments are planned together with the EISCAT and Heating facilities near Tromso (Norway).

REFERENCES

Balsley, B. B., W. L. Ecklund, D. A. Carter and P. E. Johnston (1979), The Poker Flat MST radar: First results, Geophys. Res. Lett., 6, 921-924.

Czechowsky, P. and K. Meyer (1980), Das Antennensystem des SOUSY VHF Radars, Report MPAE-T-00-80-19, Max-Planck-Institut fur Aeronomie, Katlenburg-Lindau.

Czechowsky, P., R. Ruster and G. Schmidt (1979), Variation of mesospheric structures in different seasons, Geophys. Res. Lett., 6, 459-462.

Czechowsky, P., R. Ruster and G. Schmidt (1982), VHF-Radarmessungen wahrend ALPEX, Annalen der Meteorologie, 19, 124-126.

Dolph, C. L. (1946), Proc. I.R.E., 34.

Heilmann, A. (1970), Antennen II, L-I-Hochschultaschenbucher 534/534a, Bibliographisches Institut, Mannheim/Wien/Zurich, 55-58.

Rottger, J., P. Czechowsky, R. Ruster and G. Schmidt (1983), VHF radar observations of wind velocities at the Arecibo Observatory, J. Geophys., 52, 34-39.

Rottger, J. and G. Schmidt (1979), High-resolution VHF radar sounding of the troposphere and stratosphere, IEEE Trans. Geosc. Electr., GE-17, 182-189.

Rottger, J. and R. A. Vincent (1978), VHF radar studies of tropospheric velocities and irregularities using spaced antenna techniques, Geophys. Res. Lett., 5, 917-920.

Ruster, R. and J. Klostermeyer (1983), VHF radar observations of Kelvin-Helmholtz instability in a subtropic jet stream, Geophys. Astrophys. Fluid Dynamics (in press).

Schmidt, G., R. Ruster and P. Czechowsky (1979), Complementary code and digital filtering for detection of weak VHF radar signals from the mesosphere, IEEE Trans. Geosc. Electr., GE-17, 154-161.

Unitrode (1968), Application of PIN-diodes in high power duplexers, Application Note M-139.

Weber, G. R. and R. Ruster (1982), Occurrence of a dry front over the Alpine region and Central Europe, Preliminary results of ALPEX (WMO).

Weber, G. R., R. Ruster and J. Klostermeyer (1982), VHF-Radarbeobachtungen im Voralpengebiet, Annalen der Meteorologie, 19, 99-101.

# 7. DESIGN CONSIDERATIONS FOR MST RADAR ANTENNAS (Keynote Paper)

S. A. Bowhill

Aeronomy Laboratory
Department of Electrical Engineering
University of Illinois
Urbana, IL 61801

## DESIGN REQUIREMENTS

This paper centers on the design of antenna systems for radar capable of probing the mesosphere. Since the spatial wavelength dependency of turbulently advected ionization cuts off rather rapidly below wavelengths of about 3 m, this implies that we are discussing frequencies of 100 MHz and below; most probably, in the range 40-60 MHz. Also, requirements of sensitivity call for a physical antenna aperture of $10^4$ $m^2$ or more. Taken together, the frequency and aperture requirements point to an array antenna of some kind as the most economical solution. Such an array could consist of dipoles or more directive elements; these elements can be either active or passive.

The use of an array implies severe limitations on steerability, so it is necessary to define carefully just how much steerability is required for the scientific goals of the facility. Is it sufficient to be able to point it vertically and at two fixed directions in the east-west and north-south planes? VINCENT (1982) has shown that momentum fluxes may be deduced if symmetrical pointing directions are available on either side of the zenith. So this represents an additional requirement. If more than one set of angles away from zenith is required (e.g., if different angles are required for stratospheric and mesospheric work) additional complexities result. Finally, one could suppose a capability of pointing at any direction within a limited portion of the sky.

Another requirement may be for modularity: the ability to split the antenna into two or more sections, each pointing at a different part of the sky, to permit simultaneous operation without beam switching. Again, different parts of the antenna may be required to be used for a spaced-antenna drift experiment.

The speed of the rapidity with which the antenna is required to be pointed in a new direction or reconfigured into a new modularity, is an important design consideration, as very rapid switching implies greater electronic complexities.

A final consideration is bandwidth for the antenna. Thin dipoles themselves have a finite bandwidth. If a long array is fed at the end, changing frequency results in swinging the direction of the beam. Impedance matching stubs may lead to a degradation of the VSWR if the design bandwidth is exceeded.

## COST CONSIDERATIONS AND DISTRIBUTED TRANSMITTERS

The signal-to-noise ratio S of an MST radar is given by:

$$S = K_1 PA$$

where P is the transmitter peak pulse power and A is the effective antenna area. The cost $C_T$ of the transmitter is given by

$$C_T = K_2 P + K_3$$

where $K_3$ represents the cost of the low-level drive stages. The antenna cost $C_A$ is

$$C_A = K_4 A$$

where A is the antenna area. Expressing the total cost in terms of a desired signal-to-noise ratio, we have

$$C = K_4 A + \frac{K_2 S}{K_1 A} + K_3$$

This cost is a minimum when

$$K_4 A = \frac{K_2 S}{K_1 A}$$

that is, when the antenna cost is equal to the variable portion of the transmitter cost. This principle is often violated in the construction of MST radar facilities; for example, the Urbana radar antenna cost about $30,000, while the transmitter cost was over $300,000. For the Jicamarca antenna, whose estimated cost was $800,000, the equality was probably nearly satisfied.

It is interesting to extend this simple calculation to the case of a distributed transmitter, consisting of N modules of area A and power P/N. The cost equation becomes:

$$C = K_4 A + \frac{K_2 S}{K_1 A} + K_3 N$$

and the criterion that the total antenna cost should equal the total variable portion of the transmitter cost still applies. The excess cost involved in using a distributed transmitter can be estimated by assuming $K_2$ = $3/watt, $K_3$ = $5000. This would make the fixed and variable transmitter costs equal for a peak transmitter power of 1700 watt, suggesting that the individual modules should be for at least that power in order to avoid paying an excessive price for modularity.

## MODULE SIZES

The attainment of phased-array steerability poses limitations on the design of modules for an MST radar antenna. Here, a module is defined as a subset of the array within which all radiating elements are fed in phase. For example, if unlimited steerability is required, the module must consist of no more than a single dipole. At the other extreme, one may consider the antenna at Jicamarca (Figure 1) which has 64 modules each 6 $\lambda$ x 6 $\lambda$, having a 1/2-power beamwidth of 8.24°. So it is possible to phase these modules to any direction within a circle of radius 4.12° (see Figure 2) without excessive degradation of overall gain, simply by rephasing the various modules. The Urbana array (Figure 3) is organized into modules (called "cells" here) also of dimension 6 $\lambda$ x 6 $\lambda$, though the feed system is somewhat different from that at Jicamarca.

The modular design of the Jicamarca antenna gives the possibility of having several simultaneous pointing directions. For example, it is common for mesospheric work to dedicate one polarization of the antenna to the vertical pointing direction, and to dedicate the two halves of the other polarization to an easterly and southerly direction, as shown on Figure 2; so that all three directions may be used simultaneously. Changing this arrangement, however, takes hours to accomplish.

Elements with increased directivity can be substituted for a module without changing the antenna performance. For example, the gain of each module of the

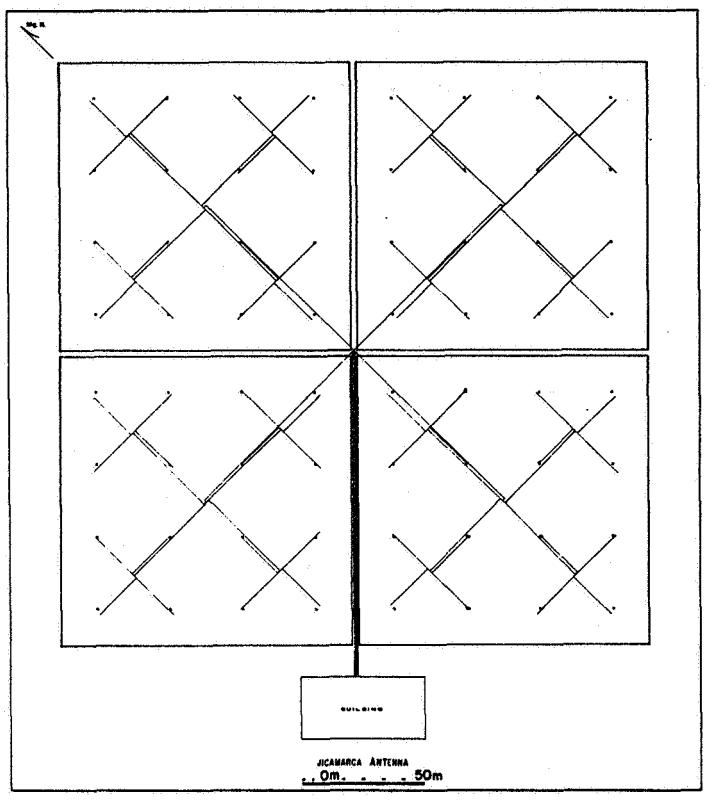


Figure 1. Configuration and the feed arrangement for the Jicamarca antenna (OCHS, 1965).

Jicamarca antenna is 21 dB over an isotropic radiator, so the 64 modules can be substituted by any directive elements with that gain, located at the center of each module. There would be no point in spacing them more closely, since the combined array would have the maximum gain achievable for a filled array. In the Japanese MU-radar, on the other hand, Yagi antennas are used for each module, but spaced only a one-half wavelength in each direction. The Yagi gain cannot contribute to the overall array gain, but additional protection against sidelobes is obtained.

## CHOICE OF POINTING DIRECTIONS

The size of module adopted is determined largely by the choice of pointing directions for the antenna. Given the 8.24° HPBW of the Jicamarca antenna, and its 1.5° tilt toward the southwest, pointing directions 3.5° towards the west and south were easily obtained. With the Urbana antenna, which coincidentally slopes also 1.5° from the vertical, but in this case towards the southeast, pointing directions at 2° to the south and east are obtainable. The modules of the Poker Flat antenna are fixed at 15° from vertical. What are the advantages of the relatively small (less than 5°) or relatively large ($\sim$15°) zenith angles?

Three considerations are important for this question. The first of these is the aspect sensitivity of the scattering irregularities. Where this is

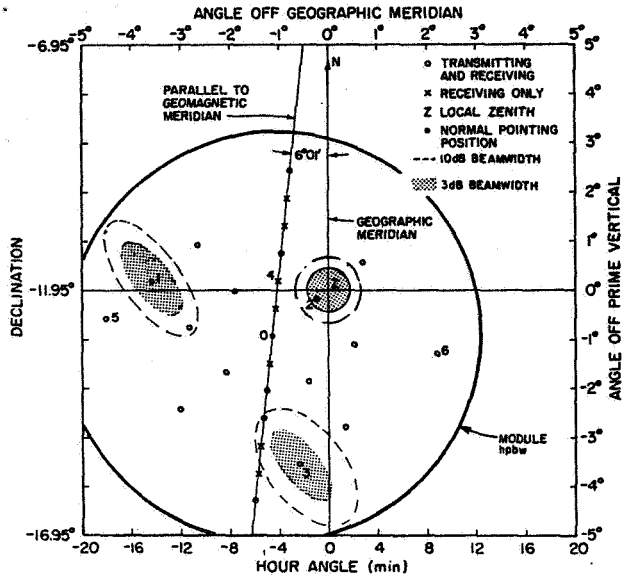


Figure 2. Antenna pointing directions used for mesospheric experiment. Horizontal (3 dB) dimensions of the off-vertical scattering volumes are 1 km by 2 km at 76 km altitude (adapted from RASTOGI and BOWHILL, 1975).

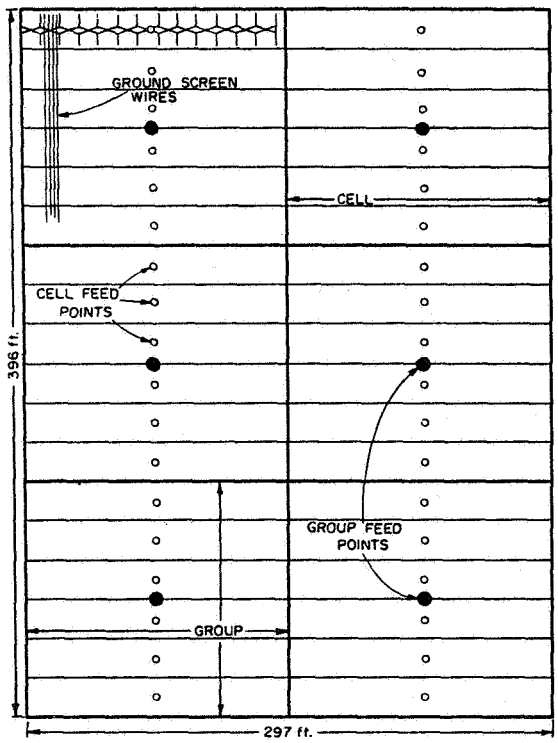


Figure 3. Schematic diagram of the Urbana MST radar antenna.

present, it may penalize the larger zenith angles by 10 dB or more. So one would like to avoid being wedded to a single choice of off-vertical pointing direction. The second consideration is the ability to measure horizontal winds and minimize the contamination from vertical gravity-wave velocities. In a separate paper (3.6-B) I discuss this effect, and show that pointing directions very close to vertical should be avoided, no matter how good the signal-to-noise of each individual measurement. Thirdly, the question arises as to the range of pointing angles which can be covered. Because of the need for symmetrical measurements either side of the zenith, the antenna beam should be centered vertically. The modules should then have polar diagrams such that the extreme pointing directions can be accommodated with no more than 3 dB loss in gain.

Bearing in mind these three compromises, it seems that pointing directions up to 5° away from vertical might be needed, implying a module size approximately the same as that at Jicamarca, namely, $6\lambda \times 6\lambda$.

## FEED SYSTEMS FOR PASSIVE ARRAYS

For feeding energy to the modules of an array, the corporate structure feed used by Jicamarca is attractive, maintaining good bandwidth without beam shifting. For the high voltages required, coaxial lines made from irrigation pipe were successfully used at Jicamarca and have proved successful at Urbana also. Their advantage lies in their large power-handling capability, extremely low loss, and excellent shielding. Open-wire lines are convenient for feeding dipoles within a module, depending whether the array uses end-fed full-wave dipoles (as in Bowles' original Havana array) center-fed full-wave dipoles (as in the Urbana array) or Franklin antennas (as at Jicamarca, Platteville, and Poker Flat). The exact choice depends on impedance-matching considerations.

The choice between these configurations is not particularly easy. The Franklin array has fewer feed lines, but has an awkward crossover at the junctions between the dipoles (Figure 4, OCHS, 1965). It is not clear that this type of coupling would survive anywhere but a very dry environment such as Jicamarca. The use of coaxial cable, as at Poker Flat, carries with it some questions of the ohmic loss in the thin conductor, particularly under conditions of high VSWR.

The question of ground conductor is one which needs careful thought. Wire mesh (as at Jicamarca) is a good solution for a dry climate. Multiple single conductors (as at Urbana) seem to be effective, though in a moist soil it is difficult to determine how much benefit is obtained. Single conductors under each dipole row are very inviting, but it is not clear how applicable this is under varying soil conditions.

## ACKNOWLEDGEMENTS

The work described was supported in part by the National Aeronautics and Space Administration under Grant NSG 7506 and in part by the National Science Foundation under Grant ATM 81-20371.

## REFERENCES

Ochs, G. R. (1965), The large 50 MC/S dipole array at Jicamarca Radar Observatory, NBS Report 8772.

Rastogi, P. K. and S. A. Bowhill (1975), Remote sensing of the mesosphere using the Jicamarca incoherent-scatter radar, Aeron. Rep. No. 68, Aeronomy Laboratory, Dep. Elec. Eng., Univ. Ill., Urbana-Champaign.

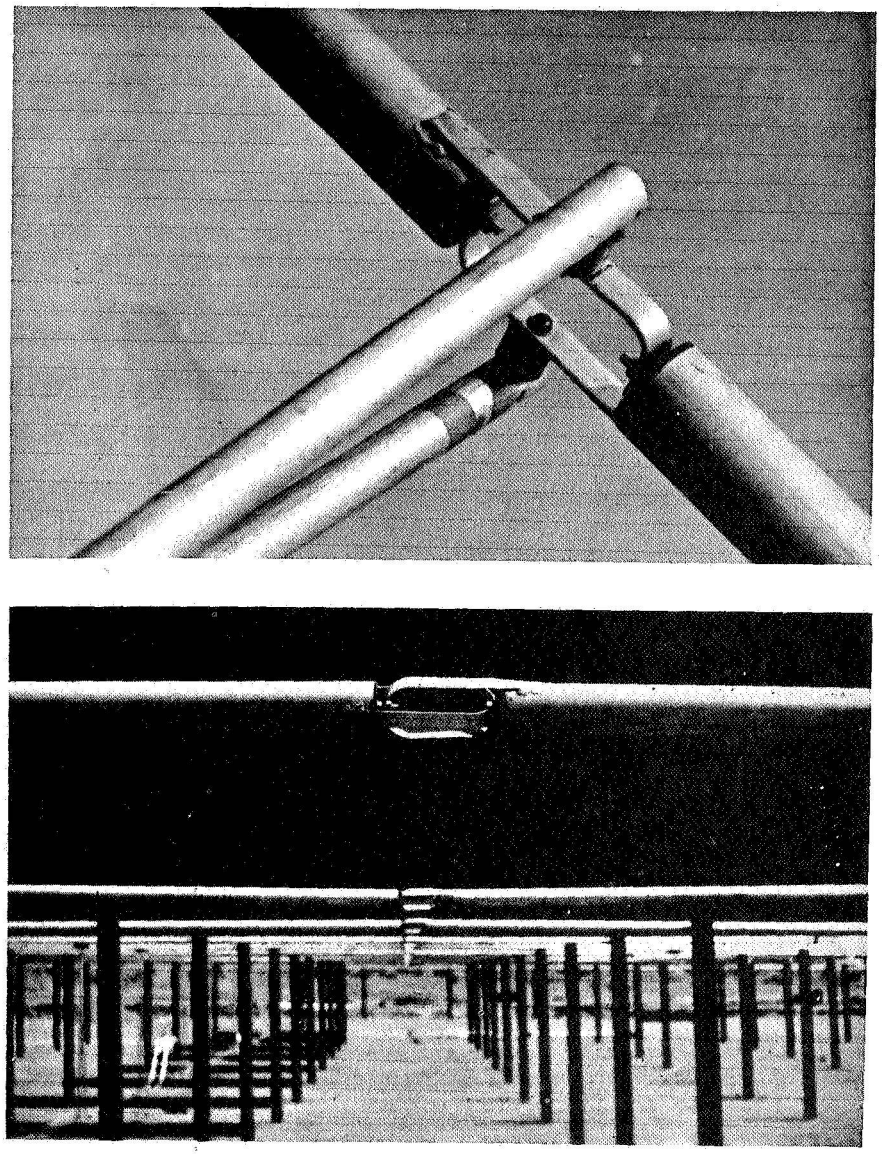

Figure 4. (top) Connection between dipoles (bottom) Central feed point of row of 12 dipoles (OCHS, 1965),

Vincent, R. A. (1982), The Adelaide Radar, Handbook for MAP, Vol. 7, edited by C. F. Sechrist, Jr., SCOSTEP Secretariat, Dep. Elec. Eng., Univ. Ill., Urbana, 133.

## SUMMARY OF ADDITIONAL TOPICS

Four topics were added to the list given in the tentative program: site selection, frequency allocation, absolute calibration, and polar diagram verification.

(a) Site Selection

Selection of a site for an MST radar system is subject to several constraints. The requirements of minimizing ground clutter suggests the placement either on very flat terrain (as at Urbana) or in a valley (Jicamarca) or sink hole (Arecibo). In heavy populated areas, the requirement of minimizing interference to other services requires extraordinary measures (as at SOUSY and Kyoto). Finally, it is desirable to select a site with as low a level as possible of natural and man-made noise.

Dr. Chao described noise surveys made for the MU radar in Japan. A vertically pointing Yagi and a field intensity meter monitored the 40-60 MHz band every 30 min for two months, and this formed the basis of the selected frequency band.

Dr. Crochet described the methods used to select the three sites for the ALPEX experiment. He cautioned that a small antenna can fail to see interference which later shows up in a large array located at the same place.

Dr. Rottger indicated that he had good experience using Yagi antennas for site selection. He also pointed out that geophysical reasons dictated that if wind measurements are important, the site should be located far away from mountains.

Dr. Strauch described his criteria for site selection, and prepared the following remarks:

"The general location of the site will usually be governed by the geophysical problem that is to be addressed and often this consideration, that cannot be compromised, places serious restrictions on the choice of the site. Usually, however, there are many local potential sites once the general locations has been determined. Some of the points to consider for site selection are the following:

1. Availability of power, telephone service, and other facilities. The quality of service must also be investigated.
2. The terrain at the site. How much effort will be required to modify the terrain for antenna installation?
3. The near-by terrain. Can it be a natural shield or will its clutter signal be at the same range as the atmospheric phenomena of interest?
4. Aircraft flight paths. Will the antenna pointing angles be close to directions where commercial aviation interference will be troublesome? Are there small airports nearby?
5. Protection. If the site will not be manned at all times, will it be secure? Can it be located on land that is already protected or already has restricted access.
6. Maintenance facilities. Will operations and maintenance people live close enough to the site?
7. Type of vegetation and soil. Is the drainage adequate enough to prevent flooding? Will natural vegetation interfere with the antenna? Is the ground suitable for easy antenna construction?
8. Man-made interference. Will automobile traffic cause a clutter or radiation interference? Will near-by residences cause interference from local oscillators on TV or radio bands? Are there near-by radio amateurs or commercial broadcasting stations?

"Although the actual interference problem will not be known until the antenna and receiver are installed, the prudent experimentor will conduct tests of interference before selecting a site. For large and expensive facilities these tests should be extensive and sensitive. A small directional antenna may be

suitable to simulate sidelobe sensitivity of radars, but it should be remembered that sophisticated data-processing methods make system sensitivity extremely good; therefore it would be advisable to use (if possible) the complete data system to look for interference. These measures would certainly be called for before installing expensive, fixed sites."

(b) Frequency Allocation

There was general agreement that two aspects of frequency allocation will become important as increasing numbers of ST or MST radars begin to operate in the low VHF band.

Firstly, there is the difficulty of allocation of frequencies -- almost continuous use by these radars will be made when the band 40-60 MHz is allocated to other services. It was agreed that URSI should be contacted to see if they can make overtures to CCIR concerning this question.

Secondly, there is the problem of interference of MST radars with each other. At the moment, the density of such radars is not sufficient to cause a problem, but some frequency allocation rationale must eventually be decided upon. In this connection, it seems clear that more attention should be paid to the problem of designing MST radar antennas with lower sidelobes which will help both transmitting and receiving.

(c) Absolute Calibration

Dr. Hocking described a technique for absolute calibration which he developed for the SOUSY radar and which is described in an MPI Report, "Absolute Calibration of the SOUSY VHF Stationary Radar". It uses a combination of noise measurement for the receiving system using a standard noise generator, and measurement of the diurnal variation of sky noise for each beam separately.

Dr. Balsley pointed out the difficulty of performing absolute calibrations for a multi-transceiver system, particularly because of the difficulty of estimating cable effects.

Dr. Schmidt described the method of calibration using the Cassiopeia source, and Dr. Bowhill described the Signus-A source.

Dr. Mathews suggested that all MST radars should permit determination of the absolute scattering cross section per unit volume for the given pulse widths used.

(d) Polar Diagram Verification

Several approaches were used for verifying the polar diagram of an MST radar antenna. Dr. Balsley described a method using a number of 1-m diameter spherical earth satellites whose ephemerides are accuately known. The number of these available is such that in a 10-day period as many as 8 passes may be made through a 1-deg-diameter beam. The updated ephemeris is accurate enough that they can be used to determine the direction of the antenna beam, as well as a calibration of the antenna by measurement of the absolute cross section.

Mr. Green described how a probe antenna can be moved through the antenna, accurately measuring the phase and amplitude of the field. The resulting field pattern can be used to synthesize the antenna pattern and to estimate the aperture efficiency.

Dr. Mathews described the use of an aircraft flying at 10,000 feet with a

calibrated dipole suspended on a weighted cable. The position of the aircraft was determined by multiple theodolites. When all the theodolites agreed, a time marker was used to calibrate the signal strength record from the receiver. Dr. Balsley used a similar arrangement by using a folded dipole made of RG-58, and using a Hewlett-Packard laser theodolite for position-finding. Dr. Bowhill described a piece of radio equipment using 3 ground-based transmitters which enables a suitably equipped airplane to fly along a known straight line path with about 1-ft accuracy. It is used for crop dusting and for surveying.

# 7.1A DIRECTIVITY AND SPACING FOR THE ANTENNA ELEMENTS

V. K. Koshy

Bharat Electronics Ltd
Bharatnagar P. O. - 201008
Ghaziabad (U.P.), India

While deciding on the optimum design choice for the MST radar antenna, the following factors are required to be considered: directivity and gain; beam width and its symmetry; sidelobe levels - near and wide angle; impedance matching; feeder network losses; polarisation diversity; steerability; cost-effectiveness; and maintainability.

The scope of this note will be restricted to the directivity and related beam-forming aspects of various antenna elements and also the directivity aspects when such elements are formed into an array. Array performance will be considered in regard to important variables, in particular, the spacing of the elements.

## ANTENNA CONFIGURATIONS

Alternative configurations possible for MST radar antenna are the following: coaxial collinear array; discrete dipole array; Yagi array; dish antenna; and short backfire array.

## COAXIAL COLLINEAR ARRAY

A collinear antenna (BALSLEY and ECKLUND, 1972) is constructed of a series of half wavelengths of coaxial cable that have been connected together by electrically interchanging the inner and outer conductors at each junction. A half-wave dipole has a length higher than $0.5\lambda$ to compensate for the propagation velocity of the cable ($0.67\lambda$ for RG-8 cable). The number of dipoles in a collinear antenna could be any even number and typical cases are 26-element, 16-element etc.

The collinear antenna (BALSLEY and ECKLUND, 1972), by virtue of its construction of large numbers of radiators, inherently has high directivity in the plane of the antenna. A 26-element collinear antenna has shown a theoretical beam width of 5.6° at 49.8 MHz. The directivity in the plane perpendicular to the collinear antenna is isotropic, as applicable in the case of any dipole.

The radiation pattern of a collinear antenna of n halfwave dipoles fed at the center summetrically (BALSLEY and ECKLUND, 1972) is expressed as

$$E_T = \frac{2\cos((\frac{\pi}{2})\sin\theta)}{\cos\theta} \sum_{K=0}^{K=(\frac{n-2}{2})} A_K \cos(\frac{2K+1}{2}\psi)$$

Where $\theta$ is the angle from the broadside axis, $A_K$ the amplitude of $K^{th}$ element from the center and $\psi = (\frac{2\pi}{\lambda})d\sin\theta$, d being distance between elements.

The collinear antenna when built into an array, as done in the case of Sunset (GREEN et al., 1981), Poker Flat radars (BALSLEY et al., 1981) of M X N elements produces a directive pattern on the broadside of the array. The array pattern is obtained from a product of the element pattern and the array space factor. The array space factor (ALLMAN and BOWHILL, 1976) is given by

$$S_{xy} = S_x S_y = \frac{1}{M}\left|\frac{\sin(M\psi_x/2)}{\sin(\psi_x/2)}\right| \cdot \frac{1}{N}\left|\frac{\sin(N\psi_y/2}{\sin(\psi_y/2)}\right|$$

The spacing elements in the plane of the collinear antenna does not provide much scope for adjustment. In the plane perpendicular to the antenna elements, the spacing should be decided from consideration of the following factors:

(1) A close spacing, say 0.5λ or less, would result in strong mutual coupling leading to large impedance variations. Also, the array area for a given number of elements and hence the directivity, would be reduced.

(2) A large spacing, say 1.0λ or higher causes generation of grating lobes and limits the angle of steerability.

A spacing between 0.5λ to 1.0λ is considered acceptable in practical situations and 0.6λ to 0.8λ may be deemed as optimum (KRAUS, 1950).

Further, spacing of the dipole from the ground influences the directivity and impedance. For a half-wave dipole, highest directivity (KRAUS, 1950) is realised for spacings between 0.1λ and 0.2λ, although the bandwidth will be narrow and the input impedance will be sensitive to ground variations, for such spacings. A spacing of λ/4 is considered optimum from considerations of good bandwidth, tolerance to ground undulations and minimum reflector losses. When wide-angle steerability is required, a spacing of 3λ/8 can ensure better gain performance at wide angles (OLINER and MALECH, 1966).

Directivity of an array of linear dipoles is also affected to some extent by mutual coupling. However, when the array is very large and dipoles are backed by a reflector, the effect of mutual coupling is negligible and the gain varies only by 0.1 dB from the value computed from the physical area of the array (DEVANE and DION, 1962).

The directivity of the array also depends on the amplitude illumination of the elements. While a uniform illumination gives maximum directivity of unity but poor sidelobe level (theoretically 13.2 dB), a tapered illumination (KOSHY et al., 1983) can improve the sidelobe level by 6 to 8 dB, at the expense of reduction in directivity of about 1 to 1.5 dB.

## DISCRETE DIPOLE ARRAY

Dipoles, half-wave or full-wave, fabricated out of aluminum tubes form the basic element. The beam is isotropic in the plane perpendicular to the dipole and moderately directive in the plane of the dipole. The 3-dB beam width for half-wave and full-wave dipoles are 78° and 47°, respectively.

An array of dipoles is constructed by arranging them collinear in columns and with several rows of such columns. Directivity of an array of dipoles is dependent on the number of elements in both planes, element directivity, spacing etc., the same way as in the case of the coaxial collinear antenna explained earlier. Excellent design details are provided by ALLMAN and BOWHILL (1976), BOWHILL and MAYES (1979), and MAYES and TANNER (1981) as part of their work on the Urbana MST radar.

Both the coaxial collinear and discrete dipole arrays require two independent orthogonal arrays to produce polarization in E-W and N-S directions. In respect of steering, while collinear coaxial array is capable of steering only in the plane perpendicular to the dipoles, the discrete dipole array can be made to steer in orthogonal planes by providing suitable progressive phase shifts in both planes (MAYES and TANNER, 1981).

YAGI ARRAY

Yagi antenna element is compact in hardware and provides a high directivity in both principal planes. A four-element Yagi antenna, as used in the SOUSY (CZECHOWSKY and MAYER, 1980) and MUR (FUKAO et al., 1980) gives a gain of 8.7 dB.

When formed into an array, the Yagi type requires a lesser number of elements in comparison to the dipole type, for realising a given directivity. The array directivity depends on the number of elements and is computed by the standard pattern multiplication method. The Yagi array, owing to the directive element pattern and discrete-element aperture available to illumination taper, can ensure low sidelobes (FUKAO et al., 1980).

The effect of spacing of elements on directivity of a Yagi array is governed by similar considerations as in dipole arrays. At close distances, where mutual coupling would be significant, the element factor generally sharpens so as to improve the directivity in low-elevation angles (FUKAO et al., 1980).

DISH ANTENNA

The dish antenna is a single element antenna consisting of a large parabolic reflector and a prime-focus or cassegranian feed system.

The directivity of the dish antenna depends primarily on the aperture area of the reflector (SILVER, 1949) and the gain is expressed by

$$g = K\left(\frac{4\pi A}{\lambda^2}\right)$$

where K is the antenna efficiency which is the product of a number of efficiency factors considering losses due to aperture illumination, spillover, blockage, surface error, VSWR, cross polarization, etc. By proper control of the feed illumination, very low sidelobe levels can be achieved in dish antennas with moderate loss of gain.

The only 'spacing' involved in dish antennas is that of the feed which is required to be at a unique position, namely, the focus of the reflector for optimum directivity. Movement of the feed in the focal plane perpendicular to the axis of the dish gives rise to steering of the beam.

SHORT BACKFIRE ANTENNA

The short backfire antenna (EHRENSPECK, 1965; EHRENSPECK and STROM, 1977) is a compact high-gain element, consisting of a slotted dipole feed, a reflector disc of diameter $0.5\lambda$ and a circular planar reflector with a rim of width $0.5\lambda$. For a planar reflector diameter of $2\lambda$, this antenna gives a gain of 15.1 dB.

In an array, the high element gain of the SBF antenna gives the advantage of high array directivity for a small number of elements. A 16 x 16 uniform array of 2 circular SBF antennas can realise a gain of 39 dB (PHYSICAL RESEARCH LABORATORY, 1981)

Nevertheless, the inter-element spacing of $2\lambda$ required in such an array would produce grating lobes at 30° and 90° from the array axis and hence would result in high sidelobe levels at these angles. Good sidelobe levels, better than 20 dB, can be achieved by reducing the element spacing to $1\lambda$ (EHRENSPECK and STROM, 1977). Consequent to this, the gain of the 16 x 16 element array

would, however, reduce to around 34 dB.

## CONCLUSION

In the foregoing sections, a brief recapitulation is given of the directivity and related features of the various elements available for realizing an optimum antenna for MST radar. The actual choice of a particular element and array configuration should, however, be based not only on directivity but also on a number of other considerations as mentioned in the first paragraph of this paper.

## REFERENCES

Allman, M. E. and S. A. Bowhill (1976), Feed system design for the Urbana incoherent scatter radar antenna, Aeron. Rep. No. 71, Aeron. Lab., Dep. Elec. Eng., Univ. Ill., Urbana-Champaign.

Balsley, B. B. and W. L. Ecklund (1972), A portable coaxial collinear antenna, IEE Trans. on Antennas and Prop., AP-20, 513-516.

Balsley, B. B., W. L. Ecklund, D. A. Carter, P. E. Johnston and A. C. Riddle (1981), The Poker Flat MST radar system: Current status and capabilities, 20th Conference on Radar Meteorology, Nov. 30 - Dec. 3.

Bowhill, S. A. and P. E. Mayes (1979), Proposal for engineering and cost study of a phased array antenna for Urbana coherent scatter radar, Aeron. Lab., Dep. Elec. Eng., Univ. Ill., Urbana-Champaign.

Czechowsky, P. and K. Mayer (1980), Antenna system for SOUSY VHF radars, Max-Planck Institut fur Aeronomie Report MPAE - T-00-80-19.

Devane, M. E. and A. R. Dion (1962), The El Campo solar radar antenna, MIT Lincoln Lab., Tech. Rep. No. 276.

Ehrenspeck, H. W. (1965), The short backfire antenna, Proc. IEEE, 53, 1138-1140.

Ehrenspeck, H. W. and J. A. Strom (1977), Short backfire antenna - a highly efficient array element, Microwave Journal, 20, 47-49.

Fukao, S., S. Kato, T. Aso, M. Sasada and T. Makihira (1980), Middle and upper atmosphere radar (MUR) under design in Japan, Radio Sci., 15, 225-231.

Green, J. L., J. M. Warnoch, W. L. Clark, F. J. Eggert and K. J. Ruth (1981), Modification to the sunset radar to provide antenna beam steering, 20th Conference on Radar Meteorology, Nov. 30 - Dec. 3.

Koshy, V. K., A. K. Majumdar and K. K. Gupta (1983), Non-uniform excitation of a coaxial collinear array (to be published).

Kraus, J. D. (1950), Antennas, Mc-Graw Hill, New York.

Mayes, P. E. and D. R. Tanner (1981), Preliminary draft on design studies of phased array for Urbana coherent scatter radar, Aeron. Lab., Dep. Elec. Eng., Univ. Ill., Urbana-Champaign.

Oliner, A. A. and R. G. Malech (1966), Microwave Scanning Antennas, (ed. R. C. Hansen), Academic Press, New York.

Physical Research Laboratory (1981), A proposal for atmospheric studies using high power VHF radar, Physical Research Laboratory, Ahmedabad, India.

Silver, S. (1949), Microwave Antenna - Theory and Design, Mc-Graw Hill, New York.

## APPENDIX

### COAXIAL COLLINEAR ANTENNA ARRAY

ELEMENT PATTERN

$$E_T = \frac{2\cos(\frac{\pi}{2}\sin\theta)}{\cos\theta} \sum_{k=0}^{\frac{n-2}{2}} A_k \cos(\frac{2k+1}{2}\psi)$$

where $\psi = \frac{2\pi}{\pi} d \sin\theta$

ARRAY FACTOR

$$S_{xy} = \frac{1}{M}\left|\frac{\sin(M\psi_x/2)}{\sin(\psi_x/2)}\right| \frac{1}{N}\left|\frac{\sin(N\psi_y/2)}{\sin(\psi_y/2)}\right|$$

MAXIMUM GAIN OR DIRECTIVITY OF ARRAY

$$G = \frac{4\pi \left|E_T(0,0)\, S_{xy}(0,0)\right|^2}{\int_o^{2\pi}\int_o^{\pi/2} \left|E_T(\theta,\phi)\, S_{xy}(\theta,\phi)\right|^2 \sin\theta\, d\theta\, d\phi}$$

Where there is no radiation below the ground plane.

### DISCRETE DIPOLE ANTENNA ARRAY

ELEMENT PATTERN

$$E_T = \frac{2\cos(\frac{\pi}{2}\sin\theta)}{\cos\theta}$$

ARRAY FACTOR

$$S_{xy} = \frac{1}{M}\left|\frac{\sin(M\psi_x/2)}{\sin(\psi_x/2)}\right| \frac{1}{N}\left|\frac{\sin(N\psi_y/2)}{\sin(\psi_y/2)}\right|$$

MAXIMUM GAIN OR DIRECTIVITY OF ARRAY

$$G = \frac{4\pi \left|E_T(0,0)\, S_{xy}(0,0)\right|^2}{\int_o^{2\pi}\int_o^{\pi/2} \left|E_T(\theta,\phi)\, S_{xy}(\theta,\phi)\right|^2 \sin\theta\, d\theta\, d\phi}$$

where there is no radiation below the ground plane.

## YAGI ARRAY

ELEMENT PATTERN

$$E(\theta) = \frac{\sin(kL/2)\ (\cos\theta - K)}{(kL/2)\ (\cos\theta - K)}$$

$$K = \frac{k_x}{k} = \frac{0{,}468 + L/\lambda}{L/\lambda}$$

Where L = length of the Yagi Element

$\cos k_x s = \cos ks - 1/2 e^{ksf(h,a)}$

$$f(h,a) = \frac{\cos kh\left(\frac{\sin kh}{kh}\right) - kh \cos kh \left(\frac{\cos ka}{ka}\right)}{\sin kh - kh \cos kh}$$

for $s >> a$, $h >> a$, $s >> \frac{a}{2}$

ARRAY FACTOR

$$S_{xy} = \frac{1}{M} \left|\frac{\sin(M\psi_x/2)}{\sin(\psi_x/2)}\right| \frac{1}{N} \left|\frac{\sin(N\psi_y/2)}{\sin(\psi_y/2)}\right|$$

MAXIMUM GAIN OR DIRECTIVITY OF ARRAY

$$G = \frac{4\pi \left|E_T(0,0)\ S_{xy}(0,0)\right|^2}{\int_o^{2\pi} \int_o^{\pi/2} \left|E_T(\theta,\phi)\ S_{xy}(\theta,\phi)\right|^2 \operatorname{Sin}\theta\ d\theta\ d\phi}$$

Where there is no radiation below the ground plane

## DISH ANTENNA

FIELD PATTERN

E plane:

$$E_\theta\Big|_{\phi=\pi/2} = \frac{j\omega\mu_0}{2\pi R} e^{-jk_o(R + 2f)} \left(\frac{1}{\zeta_o}\ \frac{P_t}{2\pi}\right)^{1/2} \cos\theta$$

$$\int_o^a \int_o^{2\pi} \frac{[G_f(\theta',\phi')]^{1/2}}{P} e_{ry} e^{jk_o r \sin\theta \sin\phi'} r\, d\phi'\, dr$$

H plane:

$$E_\phi\Big|_{\phi=0} = \frac{j\omega\mu_0}{2\pi R} e^{-jk_o(R + 2f)} \left(\frac{1}{\zeta_o}\ \frac{P_t}{2\pi}\right)^{1/2}$$

$$\int_o^a \int_o^{2\pi} \frac{[G_f(\theta',\phi')]^{1/2}}{P} e_{ry} e^{jk_o r \sin\theta \cos\phi'} r\, d\phi'\, dr$$

$\zeta$ = free space impedance.

$\theta' = 2 \tan - \frac{1r}{2f}$

$$P = \frac{4f^2 + r^2}{4f}$$

$$e_{ry} = \frac{(\sin^2\phi' \cos\theta' + \cos^2\phi')}{\sqrt{1 - \sin^2\phi' \sin^2\theta'}}$$

$$\text{Gain} = k\left[\frac{4\pi A}{\lambda^2}\right]$$

Where 'k' is efficiency.

## SHORT BACKFIRE ANTENNA ARRAY

ELEMENT PATTERN
E-plane

$$E_\theta = I_E(A,\theta) \sin\phi$$

H-plane

$$E_\phi = I_H(A,\theta') \cos\phi$$

$$I_E(A,\theta) = (1 + \cos\theta) \int_o^A \frac{\sqrt{A^2 - z^2}}{1 - \{4\sin\theta\sqrt{(A^2 - z^2)}\}^2} \cos\frac{\pi z}{2A} \cos(2\pi\sin\theta\sqrt{(A^2 - z^2)})dz$$

$$I_H(A,\theta') = (1 + \sin\theta') \int_o^A \sqrt{A^2 - z^2} \cos\frac{\pi z}{2A} \cos(2\pi z \cos\theta')dz$$

where $\theta' = \theta - 90°$

$A = \frac{D_M}{2}$ is the electrical aperture radius > physical aperture radius

ARRAY FACTOR

$$S_{xy} = \frac{1}{M}\left|\frac{\sin(M\psi_x/2)}{\sin(\psi_x/2)}\right| \frac{1}{N}\left|\frac{\sin(N\psi_y/2)}{\sin(\psi_y/2)}\right|$$

MAXIMUM GAIN OR DIRECTIVITY OF ARRAY

$$G = \frac{4\pi \left|E_T(0,0)\, S_{xy}(0,0)\right|^2}{\int_o^{2\pi} \int_o^{\pi/2} \left|E_T(\theta,\phi)\, S_{xy}(\theta,\phi)\right|^2 \sin\theta \, d\theta \, d\phi}$$

Where there is no radiation below the ground plane.

# 7.2A FULL VERSUS LIMITED VERSUS NO STEERABILITY

B. B. Balsley

Aeronomy Laboratory
National Oceanic and Atmospheric Administration
Boulder, CO 80303

There is no single definitive "optimum" configuration of antenna beam steerability for all purposes. As with every other design problem, specific requirements suggest specific configurations; in this case, however, the broad spectrum of specific requirements requires a correspondingly broad spectrum of "optimum" configurations.

A preliminary look at the range of phenomena to be studied by the MST radar technique suggests that it may be possible to divide the steerability versus non-steerability problem into two broad subsets, with a third subset (limited steerability) that lies between these two limits.

Basically, it seems reasonable to study processes that are spatially homogeneous on a horizontal scale comparable to the range of steerability of the probing beam by using fixed-beam systems. Alternatively, processes that do vary on a horizontal scale comparable to the area of the probing radar beam can best studied using fully steerable (insofar as possible) beams.

For example, one study that would be optimized using fixed-beam systems would be a long-term study of the mean wind field. On the other hand, orographic effects due to mountain ridges and/or land-sea interfaces demand steerable beams, particularly if the effects are three dimensional in character.

In view of their lack of moving "parts" (mechanical or electrical), fixed beam systems are inherently more reliable. Clearly, there are concomitant limitations that may well be unacceptable for many requirements. It is probably realistic to crudely assume that -- in the long term -- the reliability of a system is inversely proportioned to the number of moving parts. It is unreasonable to expect, for example, that a fully steerable dish can operate at a scan rate of one revolution/minute continuously for a number of years. This is not a problem, however, for fixed-beam systems.

In Table 1 a number of possible atmospheric study programs are listed, along with the most reasonable antenna steering configuration for each. The most reasonable configuration is labelled with three asterisks (***), the second-most reasonable with two asterisks (**), and the least reasonable with one asterisk (*). Note that this listing and comparison should be considered as preliminary and tentative.

In broad aspect, Table 1 shows a roughly equal division of the two extreme antenna configurations for the listed studies. Only two studies (frontal passages and average upward gravity-wave flux measurement) appear to be best served using partially steerable beams.

Finally, it should be stressed that while many of the studies appear to be best done using a fully steerable system, they may be done almost as well using less-than-fully steerable (i.e., partially steerable) beams. Clearly, the optimum configuration for a given study must be examined in terms of the availability of specific systems.

Table 1. Phenomenological study programs vs. antenna steerability

| TOPIC | FULLY STEERABLE | PARTIALLY STEERABLE | FIXED |
|---|---|---|---|
| Orographic studies | *** | ** | * |
| Cloud dynamics | *** | ** | * |
| Severe storms | *** | ** | * |
| Turbulent structure | *** | ** | * |
| Gravity-wave structure | *** | ** | * |
| Ageostrophic winds | *** | ** | * |
| Tropopause folding | *** | ** | * |
| Frontal passages | *** | *** | *** |
| Average upward GW flux | ** | *** | * |
| Mean winds | * | ** | *** |
| Tides | * | ** | *** |
| Planetary waves | * | ** | *** |
| Tropopause monitoring | * | ** | *** |
| Jet stream monitoring | * | ** | *** |
| Vertical winds | * | ** | *** |
| Stratospheric warmings | * | ** | *** |
| Rawinsonde replacement | * | ** | *** |
| Atmospheric turbulence | * | ** | *** |
| Spectral studies $3^m < T < 3^D$ | * | ** | *** |
| Seasonable variability | * | ** | *** |
| Stratospheric temperature | * | ** | *** |
| Sun-weather relationships | * | ** | *** |

# 7.3A ANTENNA SIZE FOR MST RADARS

D. T. Farley

School of Electrical Engineering
Cornell University
Ithaca, NY 14853

The purpose of this note is to point out that it is possible to make the antenna of an MST radar too large (unless some sort of focussing scheme is used). And it is not just that the signal ceases to become stronger beyond some critical antenna size; the received scattered signal actually becomes weaker as the antenna size is increased whenever the target is in the near field (Fresnel region) of the antenna. The Arecibo antenna is a case in point; for MST work it would be worthwhile to use a feed which illuminated only a portion of the dish, as we shall see.

The radar equation for a monostatic radar (single antenna for transmitting and receiving) can be written as

$$P_r = \frac{P_t G \Sigma A_{eff}}{(4\pi R^2)^2} \tag{1}$$

where $P_r$ and $P_t$ are the received and transmitted power, G is the antenna gain, $A_{eff}$ is the antenna effective area, $\Sigma$ is the total radar scattering cross section of the target, and R is the range to the target. (The radar equation should really be written as an integral over the antenna pattern, but we omit this complication here.) The gain and effective area of an antenna are related by the well-known relation

$$G = 4\pi A_{eff}/\lambda^2 \tag{2}$$

where $\lambda$ is the wavelength. It is important to note that this result follows directly from the reciprocity theorem for antennas (identical transmitting and receiving patterns) and that this theorem holds for any antenna separation (e.g., STUTZMAN and THIELE, 1981); i.e., it applies in the near field as well as the far field of an antenna. Next we assume that the target is 'soft' (fills the beam) and so

$$\Sigma = \sigma V_s \tag{3}$$

where $\sigma$ is the scattering cross section per unit volume and $V_s$ is the scattering volume defined by the pulse length and the beam, i.e.,

$$V_s \cong \Omega R^2 \Delta r \cong \frac{4\pi}{G} R^2 \Delta r \tag{4}$$

where $\Omega$ is the beam solid angle and $\Delta r$ is the pulse length. Combining (1)-(4) and dropping proportionality constants gives

$$P_r/P_t \sim \frac{\lambda^2 \sigma \Delta r}{R^2} G \sim \frac{\sigma \Delta r}{R^2} A_{eff} \tag{5}$$

Now all we need to do is express G in terms of the antenna size and the range. The relationship depends upon whether we are in the near or far field of the antenna (Fresnel or Fraunhofer region). As shown in the sketch below, the beam will be more or less cylindrical out to a distance of 1-2 x $D^2/\lambda$, where D is the diameter of a circular (say) aperture, and will spread out with a beam

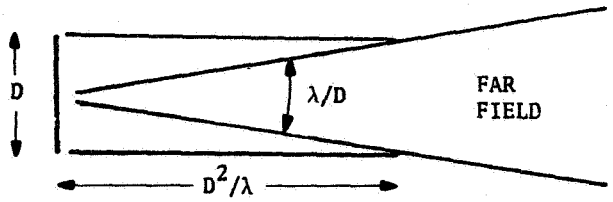


width of roughly $\lambda/D$ for larger distances (the far field). Hence we can write, very approximately,

$$\begin{aligned} G &= 4\pi R^2/(\text{Beam area}) \\ &\cong 4\pi R^2/A \qquad \text{(near field)} \\ &\cong 4\pi R^2/(\lambda R/D)^2 \cong 4\pi A/\lambda^2 \qquad \text{(far field)} \end{aligned} \tag{6}$$

Expressed in another way, using (2)

$$\begin{aligned} A_{eff} = \lambda^2 G/4\pi &\cong \lambda^2 R^2/A \qquad \text{(near field)} \\ &\cong A \qquad \text{(far field)} \end{aligned} \tag{7}$$

The optimum antenna size for receiving the scattered signal from a given range R would be very roughly $A \cong \lambda R$. Note that $A_{eff}$ and hence the received signal strength <u>decreases</u> with increasing antenna size A in the near field, and that this result has been obtained using only the most basic principles of antenna theory. Of course, in the near field (Fresnel region) the antenna could be focussed in some way to give a much stronger return, but in many cases focusing will not be practical.

As an example of how the numbers can work out, consider the Arecibo Observatory antenna, with a diameter D of 300 m and a wavelength of 0.7 m for the 430-MHz radar. The near field in this case extends beyond 100 km even though the dish is not uniformly fed (see SHEN and BRICE, 1973, for detailed calculations of the Arecibo case), and at a range of 20 km, say, (7) gives $A_{eff} \cong 3 \times 10^3$ m$^2$ vs $A \cong 7 \times 10^4$m$^2$. A feed which fed only a fraction of the dish should actually improve the signal-to-noise ratio for MST experiments at Arecibo. These effects are less important for VHF radars, but may still need to be considered for observations in the troposphere and lower stratosphere.

REFERENCES

Shen, J. S. and N. Brice (1973), Near-field gain calibration for large spherical antennas, <u>IEEE Trans. Antennas Propagat., AP-21</u>, 787-792.

Stutzman, W. L. and G. A. Thiele (1981), <u>Antenna Theory and Design</u>, John Wiley and Sons.

# 7.4A DELAY LINE AND MUTUAL COUPLING CONSIDERATIONS FOR MST RADAR ANTENNA ARRAYS

J. W. Brosnahan

Tycho Technology, Inc.
Boulder, CO 80306

Basic antenna theory states that the field radiated from an antenna array is equal to the sum of the currents flowing in each element of the array. The feedline distribution system must guarantee the proper amplitude and phase of the current for each element of an array. This sounds easy, just make sure that the difference in electrical lengths of the feedlines to the elements equals the desired phase angle. But this isn't necessarily correct. The current (or voltage) delay in a transmission line is equal to the transmission line electrical length in only a few special cases, when the transmission line is terminated in its characteristic impedance or when the transmission line's electrical length is a multiple of 90 degrees.

The impedance of any element in an array is dependent on the coupling between that element and the other elements. This mutual coupling is dependent on the phase relationship of the current in the element in question and the other elements. If the phase of the current is changed in one element, then the other elements can show a change in their input impedances, and therefore not terminate the transmission line properly, resulting in an additional change of phase in the other elements.

If an MST array is to be steered during operation by changing the delay line lengths, attention should be paid to this mutual impedance effect. Typical MST radar arrays consist of Yagis or coaxial-collinear (BALSLEY and ECKLUND, 1972) elements. To determine the mutual coupling effect with coaxial-collinear elements, an experiment was performed using two coaxial-collinear elements with 1/2 wavelength spacing between elements 1/4 wavelength above a ground plane.

The impedance of one 26-element coaxial-collinear antenna was measured while open circuiting and short circuiting a second 26-element antenna 1/2 wavelength away. Virtually no impedance change was noted. The second element was then completely removed and still no impedance change was noted. This lack of mutual coupling between coaxial-collinear antennas can be explained by the following. Elements 1/4 wavelength above ground with half wavelength spacing have relatively low mutual coupling. In addition, the input impedance of the element is so dominated by the 26 dipoles electrically connected together that mutual coupling effects at 1/2 wavelength spacing is minimal. A possible third factor is that the dipoles in a coaxial-collinear element are non-resonant because of the velocity factor of the coaxial cable used makes the dipoles 0.33 wavelength long.

It appears that coaxial-collinear arrays with 1/2 wavelength spacing and antennas 1/4 wavelength above ground are very forgiving because of the lack of the mutual coupling problem. Experience with Yagi elements indicates that they are not as forgiving to changing feedline lengths.

Yagi arrays require special attention to the array feedline system to minimize the mutual coupling problem. Figure 1 shows a beam-steering and power-divider scheme for the array of 64 Yagis as shown in Figure 2. This feed system utilizes delay lines of 1/4 wavelength multiples only. Figure 3 shows the required feedline phases for the various patterns. These delay lines will ensure proper current phase at each element, with changing feedline lengths. But current amplitude can vary because of the impedance changes with changing feed-

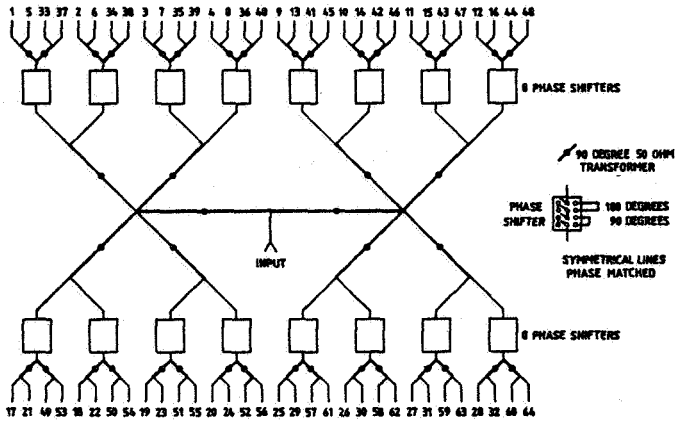


Figure 1. Power divider and beam steering delay system.

line lengths. With delay lines that are multiples of 1/4 wavelength, a spacing between elements of from 0.75 to 1.5 wavelengths provides a main beam lobe of between 19.5 degrees and 9.6 degrees. Antenna spacing is chosen to provide a null at the zenith, provide a main lobe at between 10 and 20 degrees and minimize sidelobes. In addition, spacing should be selected to minimize the mutual coupling effect.

Individual element feedlines are chosen to be odd multiples of 1/4 wavelength to utilize the constant current properties of quarter-wave transmission-line transformers. The constant current properties of a 1/4 wavelength line are such that the current in a load at the end of a 1/4 wavelength line is equal to the driving voltage divided by the characteristic impedance of the 1/4 wavelength line regardless of the load impedance (JASIK, 1961). This will provide proper current drive at each individual element in the subgroups of four elements, and will help minimize the mutual impedance problems of the array.

(Of course, a delay line system with only 90 degree and 270 degree delays is possible, but all array patterns will have a dual beam when the array elements are driven with currents having only 180 degree phase differences.)

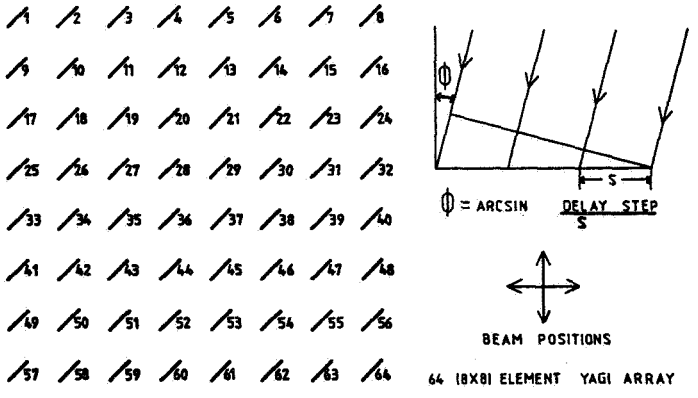


Figure 2. Yagi array orientation.

| | DELAY LINE PHASE LAG IN DEGREES | | | | | | |
|---|---|---|---|---|---|---|---|
| ELEMENT | VERT | NORTH | EAST | SOUTH | WEST | NORTH SOUTH DUAL | EAST WEST DUAL |
| 1, 5,33,37 | 0 | 270 | 0 | 0 | 270 | 0 | 0 |
| 2, 6,34,38 | 0 | 270 | 90 | 0 | 180 | 0 | 180 |
| 3, 7,35,39 | 0 | 270 | 180 | 0 | 90 | 0 | 0 |
| 4, 8,36,40 | 0 | 270 | 270 | 0 | 0 | 0 | 180 |
| 9,13,41,45 | 0 | 180 | 0 | 90 | 270 | 180 | 0 |
| 10,14,42,46 | 0 | 180 | 90 | 90 | 180 | 180 | 180 |
| 11,15,43,47 | 0 | 180 | 180 | 90 | 90 | 180 | 0 |
| 12,16,44,48 | 0 | 180 | 270 | 90 | 0 | 180 | 180 |
| 17,21,49,53 | 0 | 90 | 0 | 180 | 270 | 0 | 0 |
| 18,22,50,54 | 0 | 90 | 90 | 180 | 180 | 0 | 180 |
| 19,23,51,55 | 0 | 90 | 180 | 180 | 90 | 0 | 0 |
| 20,24,52,56 | 0 | 90 | 270 | 180 | 0 | 0 | 180 |
| 25,29,57,61 | 0 | 0 | 0 | 270 | 270 | 180 | 0 |
| 26,30,58,62 | 0 | 0 | 90 | 270 | 180 | 180 | 180 |
| 27,31,59,63 | 0 | 0 | 180 | 270 | 90 | 180 | 0 |
| 28,32,60,64 | 0 | 0 | 270 | 270 | 0 | 180 | 180 |

Figure 3. Beam steering element phasing.

Currently, computer analysis is being conducted to optimize element spacing for the best pattern under all phasing conditions. Element spacings in the 1.0 to 1.25 wavelength range appear most promising. At these spacings the mutual coupling effect should be relatively low for typical size Yagis. An array of three of these 64 Yagis systems will be used in the Chung-Li, Taiwan, R.O.C. radar planned for completion in the third quarter of 1984 (BROSNAHAN et al., 1982).

## REFERENCES

Balsley, B. B. and W. L. Ecklund (1972), A portable coaxial-collinear antenna, IEEE Trans. Ant. Prop. AP-20(4), 513-516.

Brosnahan, J., J. Chao and J. Rottger (1982), Chung-Li, Taiwan dual mode (doppler and spaced antenna) VHF radar: Preliminary specifications, Estes Park MST Radar Conference, May 1982.

Jasik, H. (1961), Antenna Engineering Handbook, McGraw-Hill.

# 7.5A REVIEW OF SPECIFIC ANTENNA CONFIGURATIONS: AN ESTIMATE OF COST AND PERFORMANCE VERSUS FREQUENCY FOR A SIMPLE $(10\lambda)^2$ CLEAR-AIR RADAR ANTENNA ARRAY

W. L. Ecklund

Aeronomy Laboratory
National Oceanic and Atmospheric Administration
Boulder, CO 80303

## INTRODUCTION

At the present time there is widespread interest in building operational clear-air radar wind profilers. The choice of operating frequency and antenna configuration for these profilers is currently under discussion. In this report we compare the cost and performance of a $(10\lambda)^2$ antenna array versus operating frequency over the range 30 to 400 MHz. To simplify the comparison the array beam will be fixed (no steering) and the array will be uniformly fed (no tapering). We consider both Yagi and coaxial collinear (COCO) cable antennas in this comparison, although other configurations (Franklin arrays, printed dipole arrays, fixed dish-type antennas, etc.) may be competitive. We assume that the array is driven by a typical 50 kW peak power, 1 kW average power transmitter located at the array edge when calculating feedline power-handling requirements and when comparing system performance. For this comparison we chose an array aperture of $(10\lambda)^2$ since a one-way beam width of 5° ($\sim$ 3.5° 2-way) or less is desirable to limit beam-spreading effects.

## YAGI ARRAY

The following table gives the gain (with respect to a dipole), effective aperture, and boom length for 3, 5, 6, 12 and 17 element Yagi antennas. These values were taken from NBS Technical Note 688 (VIEZBICKE, 1976). The table also gives the effective aperture of a coaxial cable dipole $\lambda/4$ above ground. The right-hand column of the table gives the number of antennas required to fill a $(10\lambda)^2$ aperture.

A survey of the cost of good quality Yagi antennas in the frequency range from 30 to 400 MHz shows that the cost to fill a $(10\lambda)^2$ aperture at a given frequency is about constant for 5- to 17-element Yagis (for example at 144 MHz 6-element Yagis cost \$50 x 71 (Table 1) = \$3,550 and 17-element Yagis cost \$100 x 35 (Table 1) = \$3,500). For cost comparison we take an 8 x 8 array of 6 to 7 element Yagis to fill the $(10\lambda)^2$ aperture. Boom lengths of 6 to 7 element Yagis are 1.2 to 1.5$\lambda$ long (12 to 15 meters at 30 MHz) and would cause mounting problems at frequencies below 50 MHz. The increased element height might also enhance ground clutter problems with respect to elements located closer to the ground. It is probably logical to use a larger number of shorter Yagis (fewer elements) in the lower VHF band although the cost of feedline and connectors would be higher than given in this report.

We have assumed a simple branch feed for the 8 x 8 Yagi array, with feedline extending to a building at the edge of the array. The curves in the upper part of Figure 1 show the array component costs versus frequency. Curve A gives the antenna costs only, curve B includes baluns at \$10 each and antenna mounts at \$20 each. Curve C gives the total array cost using feedline consisting of a combination of RG-213 and RG-218 polyethylene dielectric coaxial cable and connectors, and curve D gives the array cost when 1/2" and 7/8" foam dielectric cable (foamflex) is used for the feedline. The loss (in dB) versus frequency for the two types of feedlines are compared at the bottom of Figure 1. The relative performance of the arrays using the two feedline types is considered later in this report.

Table 1.

| NUMBER OF YAGI ELEMENTS | BOOM LENGTH | GAIN | AE | NUMBER TO FILL $(10\lambda)^2$ ARRAY |
|---|---|---|---|---|
| 3 | .4λ | 5.1 | $.67\lambda^2$ | 149 |
| 5 | .8λ | 8.3 | $1.1\lambda^2$ | 91 |
| 6 | 1.2λ | 10.5 | $1.4\lambda^2$ | 71 |
| 12 | 2.2λ | 17.0 | $2.2\lambda^2$ | 46 |
| 17 | 3.2λ | 21.9 | $2.9\lambda^2$ | 35 |
| Coaxial cable dipole 1/4λ above ground | | | $.17\lambda^2$ | 588 |

## COAXIAL CABLE DIPOLE ARRAY

The coaxial-collinear (COCO) antenna constructed of RG-213 cable has been described by BALSLEY and ECKLUND (1972) and has been used in a variety of antenna arrays since that time. The advantages of the COCO antenna include low cost, simplicity, portability, and a single feed point for up to 48 dipole elements. The major disadvantage seems to be antenna loss (2 dB for a 48-element RG-213 antenna at 50 MHz). For this comparison we take an array of 16 strings consisting of 36 dipoles each to fill the $(10\lambda)^2$ aperture. The COCO antennas are made from RG-213 cable and when comparing performance we assume 2 dB antenna loss at all frequencies even though the loss may be lower than 2 dB at frequencies above 50 MHz.

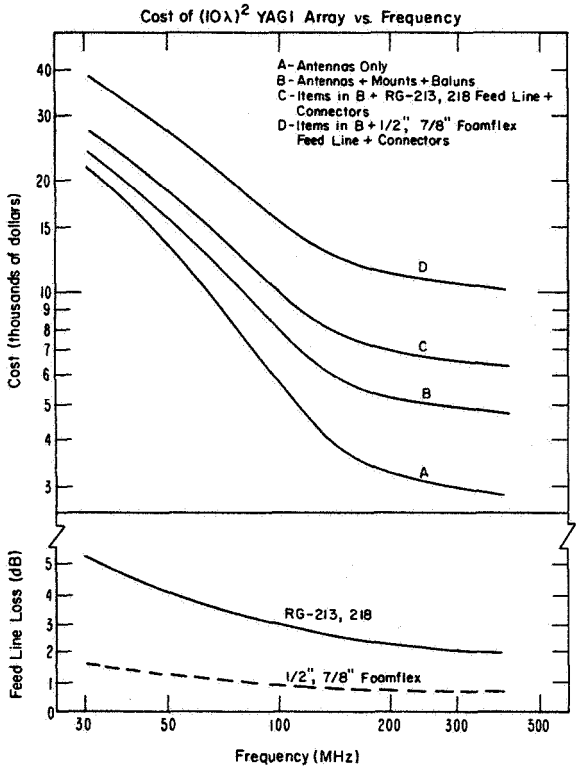


Figure 1.

The COCO antenna costs shown in Figure 2 include RG-213 cable, support rope, support posts, clips and ground wire at $2.15/meter. The interchange of inner and outer cable conductors between dipoles costs $1.50 for materials and $6.65 for labor. Baluns cost $10 each. Curve A shows the $(10\lambda)^2$ array cost versus frequency using RG-218, RG-213 feedline and curve B shows the cost for 1/2" and 7/8" foamflex feedline. Feedline loss (in dB) versus frequency for the two types of feedline are shown at the bottom of Figure 2. Curves AA and BB give the cost of $(10\lambda)^2$ arrays using RG-213, RG-218 feedline (AA) and foamflex feedline (BB) less the labor cost of $6.65/dipole for interchanging the inner and outer cable conductors. The antenna cost curves in Figure 2 are dashed above 200 MHz because manufacturing tolerance problems may increase costs at higher frequencies.

## ESTIMATED PERFORMANCE OF $(10\lambda)^2$ ARRAYS

The relative performance of the Yagi and COCO $(10\lambda)^2$ arrays using the two types of feedlines considered in the previous sections has been calculated by using the radar detectability equation given in BALSLEY and GAGE (1982). The equation has been modified by replacing the temperature term in the denominator by $[cbT_S + (1-b)\ T_C + b(1-c)\ T_A + T_R]$ where $T_S$ = sky temperature, $T_C$ = feedline temperature, $T_A$ = resistive antenna temperature, $T_R$ = receiver noise temperature, b = feedline transmission coefficient, c = antenna radiating efficiency. For these calculations $T_C$ and $T_A$ were set to 290°, $T_R$ was 120°K (1.5 dB noise figure) and maximum, minimum and typical values for $T_S$ were taken from KRAUS (1966). The 2-dB COCO antenna loss was accounted for by setting c = .63. Antenna loss of 0.5 dB (c = .89) was used for the Yagi array. Average transmitted power was set to 1 kW at all frequencies, height resolution was set to 1 km, and minimum detectability was set at 3 dB. The radio refractive turbulence structure constant ($C_n^2$) was taken as $10^{-(15.5+.2z)}$ where z = height in km. This value ($C_n^2 = 10^{-18}$ at 12.5 km) was found by NASTROM et al. (1982) to be typical of quieter conditions observed at Poker Flat, Alaska. The

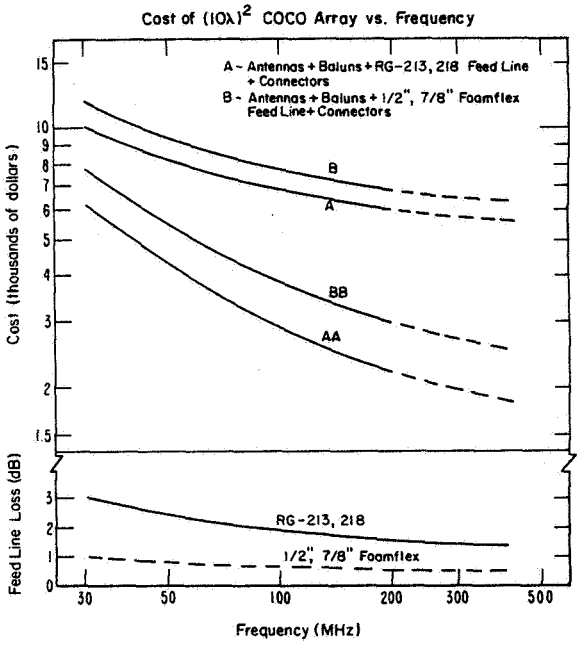


Figure 2.

lowest value of $C_n^2$ observed at 12.5 km was $\sim 3 \times 10^{-19}$ and ranged up to $3 \times 10^{-17}$ under strong wind conditions. The detectability equation was solved for maximum height for usable signal-to-noise for the $(10\lambda)^2$ arrays discussed in the previous sections. Figure 3 gives maximum height versus frequency for Yagi (solid curve) and COCO (dashed curve) arrays, calculated using foamflex feedline for maximum, minimum and typical sky temperatures for the Northen Hemisphere. Figure 4 shows the curves for both types of feedline for both antenna types using typical sky temperatures.

The data from Figures 1, 2 and 4 are combined in Figures 5 and 6 to show the cost/height relationship versus frequency for Yagi arrays (Figure 5) and COCO arrays (Figure 6). Each figure gives the relationship for both foamflex and RG-218, RG-213 feedline with frequency indicated at spot values near the thin lines that link the curves for the two types of feedlines. The curves for foamflex feedline in Figures 5 and 6 are combined in Figure 7 to give a more direct comparison of the Yagi and COCO cost/height relationship. At frequencies below about 100 MHz the COCO array has a large cost advantage over the Yagi array with only a 0.5 km loss in maximum observing height. Above 144 MHz all combinations cost $12,000 or less and the height difference is 1 km or more ($\sim$ 1.5 km at 420 MHz). The Yagi array curve is dashed from 30 to 50 MHz since boom length would be too long for the 8 x 8 array considered in this comparison. The COCO array curve is dashed above 200 MHz since it may be difficult to manufacture COCO elements with the required precision above this frequency. Although operating frequencies above 200 MHz seem at a disadvantage for either type of array, at 420 MHz it would be possible to nearly double the effective aperture by using 64 17-element Yagis with larger spacing. The $3.2\lambda$ boom length (2.25 meters) would be no problem from a height standpoint, increased antenna costs would be $2,500 and increased feedline costs would be minimal. The maximum observable height would increase to 13.5 km (indicated by the circled X in Figure 7).

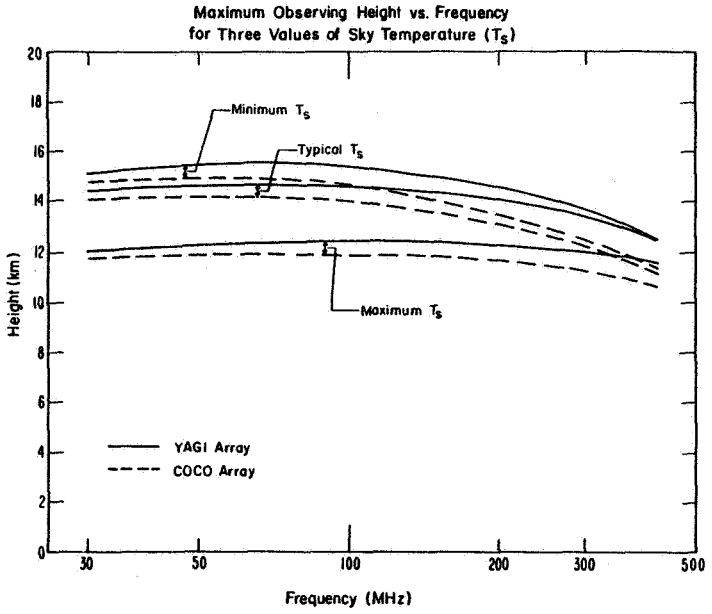


Figure 3.

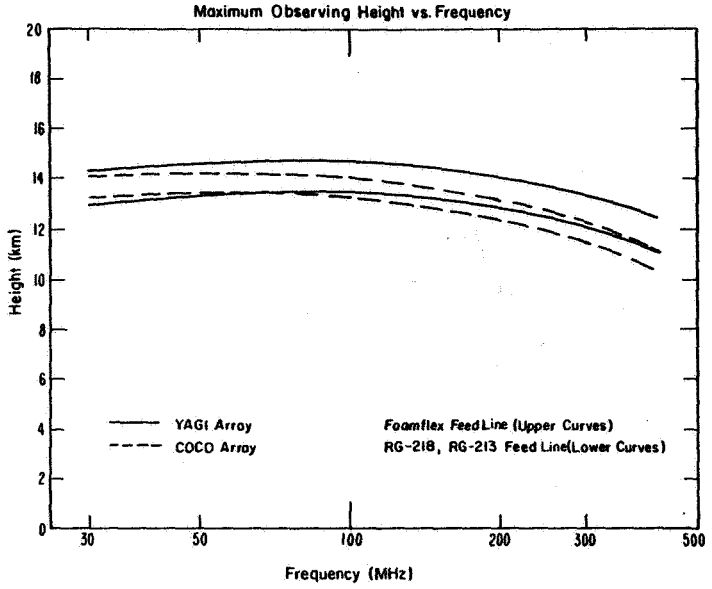


Figure 4.

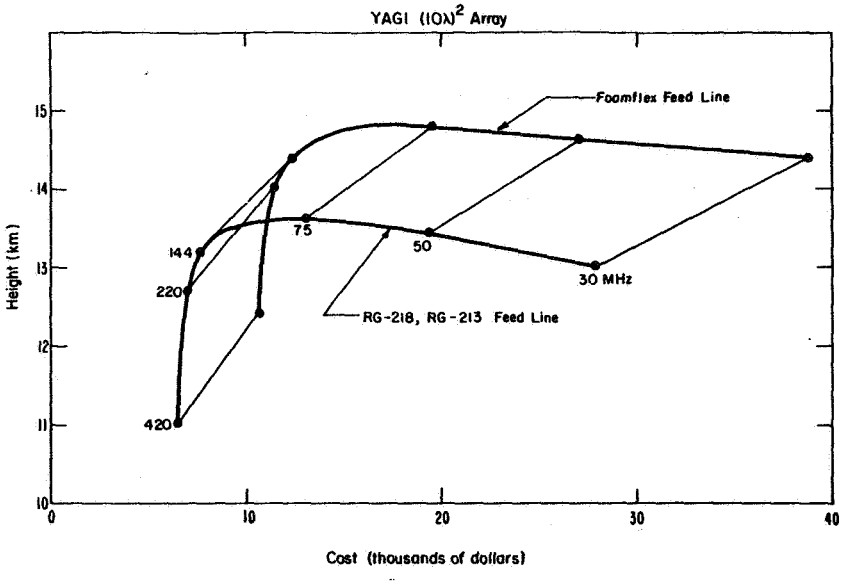


Figure 5.

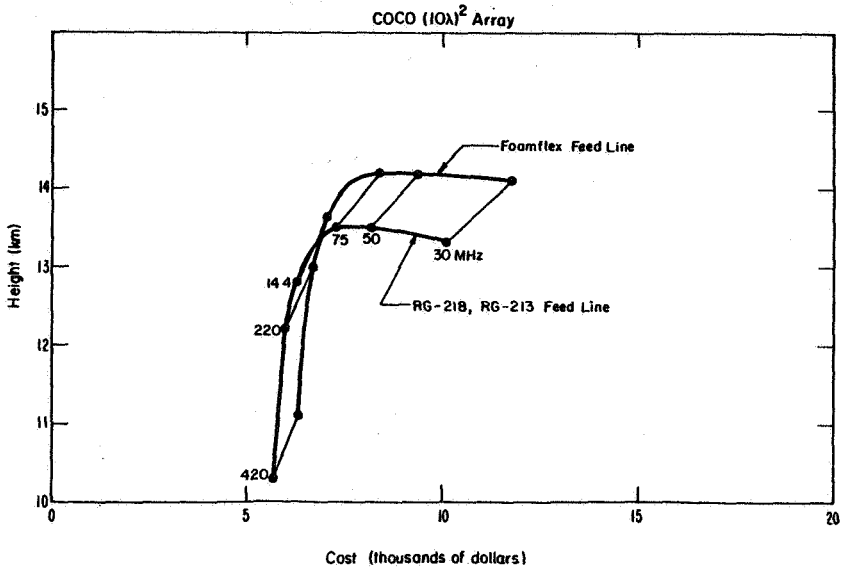


Figure 6.

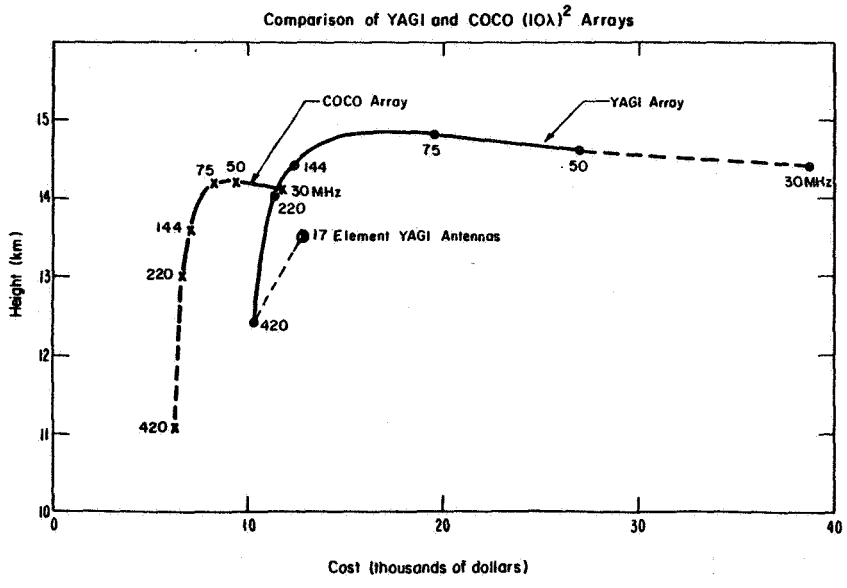


Figure 7.

## SUMMARY

In this report we have compared costs and performance for $(10\lambda)^2$ Yagi and COCO arrays suitable for use in clear-air radar systems. In general the COCO antennas seem to have a clear cost advantage below 100 MHz with only a slight corresponding loss in performance due to loss in the antenna elements. At frequencies above 150 MHz the YAGI arrays have a larger performance gain for somewhat higher costs. The curves presented in this report can be used to determine the relative performance gain for dollar cost when choosing operating frequency, antenna type and feedline type for a $(10\lambda)^2$ array. The maximum observing heights shown in Figures 3 through 7 were calculated using values of $C_n^2$ typical of relatively quiet conditions; under high wind conditions the heights could increase by over 5 km.

## REFERENCES

Balsley, B. B. and W. L. Ecklund (1972), A portable coaxial collinear antenna, IEEE Trans. on Antennas and Propagation, AP-20, 513-516.

Balsley, B. B. and K. S. Gage (1982), On the use of radars for operational wind profiling, Bull. Am. Meteorol. Soc., 63, 1009-1018.

Nastrom, G. D., K. S. Gage and B. B. Balsley (1982), Variability of $C_n^2$ at Poker Flat, Alaska, from mesosphere, stratosphere, troposphere (MST) Doppler radar observations, Optical Eng., 21, 347-351.

Viezbicke, P. P. (1976), Yagi Antenna Design, NBS Tech. Note 688, available NTIS, Springfield, VA 22151.

# 8. DATA PROCESSING TECHNIQUES USED WITH MST RADARS: A REVIEW (Keynote Paper)

P. K. Rastogi

Haystack Observatory
Massachusetts Institute of Technology
Westford, MA 01886

## ABSTRACT

The data-processing methods used in high-power radar probing of the middle atmosphere are examined in this paper. The radar acts as a spatial filter on the small-scale refractivity fluctuations in the medium. The characteristics of the received signals can be related to the statistical properties of these fluctuations. A functional outline of the components of a radar system is given. Most computation-intensive tasks are carried out by the processor. The processor computes a statistical function -- usually the power spectrum, or equivalently the autocovariance function -- of the received signals, simultaneously for a large number of ranges. The slow fading of atmospheric signals is used to reduce the data input rate to the processor by coherent integration. The inherent range resolution of the radar experiments can be improved significantly with the use of pseudo-noise phase codes to modulate the transmitted pulses and a corresponding decoding operation on the received signals. Commutability of the decoding and coherent-integration operations is used to obtain a significant reduction in computations. The limitations of the currently used processors are outlined. At the next level of data-reduction, the measured function is parameterized by a few spectral moments that can be related to physical processes in the medium. The problems encountered in estimating the spectral moments in the presence of strong ground clutter, external interference, and noise are discussed. Some salient steps involved in the subsequent (often ad hoc) graphical and statistical analysis of the inferred parameters are outlined. The requirements for special-purpose processors for MST radars are briefly discussed.

## INTRODUCTION

Over a decade has passed since the pioneering experiments at Jicamarca, Peru (WOODMAN and GUILLEN, 1974) and Millstone Hill (CRANE, 1980), that became the forerunners of the modern high-power radar studies of the middle atmosphere, were performed. These experiments established that powerful radars can detect clear-air turbulence at heights extending to well within the mesosphere and use it as a tracer for the larger scale motions -- winds and waves -- in the middle atmosphere. As a result, almost all the existing ionospheric incoherent-scatter radars also are used for studies of the mesosphere-stratosphere-troposphere (MST) region. Several new MST radars have been constructed within the last decade, and others are nearing completion or planned. The use of these radars for studies of the dynamics and turbulence in the middle atmosphere involved several levels of signal and data processing operations. It is the object of this paper to outline and review these operations.

The impact of the recent electronic data-processing innovations is clearly manifest in the amount of data handled in the currently used MST radar experiments, and especially in the rate at which it is processed. In the original single-altitude experiments at Jicamarca, 60,000 complex additions and 500 complex multiplications were performed each minute (GUILLEN, 1971). The number of operations in a typical S-T experiment at Arecibo, e.g., would be larger by four or perhaps five orders of magnitude (WOODMAN, 1980). Over 50 million spectra may already have been collected or analyzed in MST radar experiments during the past decade.

We begin with a functional description of the components of a radar system. Then following in respective order, a discussion of the advantages and limitations of coherent integration as a computation-saving intermediate step; the use of binary phase codes and decoding results in an improvement in spatial resolution; and the methods of computing the spectra or autocovariance functions of the received signals in the processor. The limitations of general-purpose processors in carrying out these computations in real time, and the need for special-purpose processors with larger memory, especially for UHF radars, also are discussed in this section. Next, the methods of reducing the spectra or the autocovariance functions to a few basic spectral moments, particularly in the presence of strong ground clutter, are reviewed; the use of statistical editing techniques and treatment of missing data in the analysis of derived parameters; and finally, a brief discussion of some possible future developments in MST radar data processing.

## FUNCTIONAL BLOCKS

A schematic block diagram of a typical MST radar system is shown in Figure 1. The functions of these blocks are outlined below.

The antenna is shared by the transmitter and the receiver system through a Duplexer. The transmitter is controlled by a modulator, and sends out narrow pulses, few tens of μs in width and about 1 MW peak power, at a typical pulse repetition interval (PRI) of 1-2 ms. In high altitude resolution experiments, the phase of the transmitted pulse can be modulated within the pulse in accordance with code(s) supplied by a code generator.

The receiver is connected to the antenna through the duplexer, shortly after the transmitter modulation is turned off. For UHF radars the front end of the receiver, usually a wide-band low-noise parametric amplifier, is mounted physically on the antenna. The receiver amplifies the RF signal and converts it to a lower intermediate frequency (IF). The IF signal is band-limited through a filter that is nominally matched either to the pulse length or, in experiments that use phase codes, to the baud length of the codes. The complex envelope of the IF signal is recovered through a pair of in-phase and quadrature phase detectors. The real and imaginary parts of this envelope are sampled in range and digitized with analog-to-digital converters. The duplexer must disconnect the receiver from the antenna after samples at all useful ranges have been obtained.

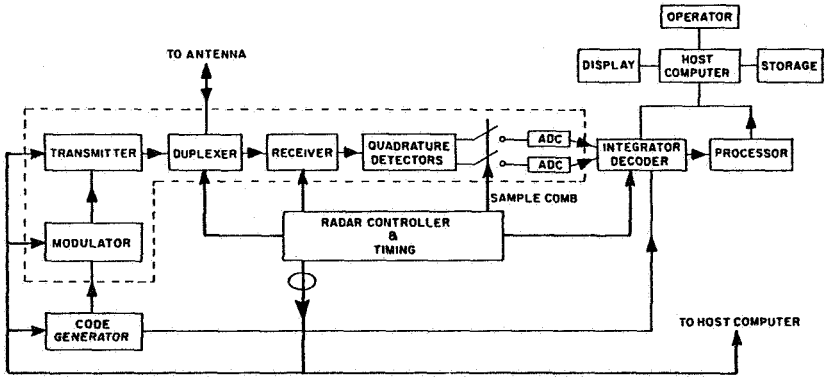


Figure 1. Block diagram for a typical MST radar. The signal flow is shown by thin lines, and the control flow by heavy lines. The control functions are not explicitly shown. The functions carried out in the blocks enclosed by the dotted lines are assumed to be linear.

The digitized signals are coherently integrated over several sweeps to reduce their bandwidth. If phase codes are used, the coherently integrated samples are correlated in range with the code pattern to effect decoding. It is, of course, necessary to temporarily store the integrated samples separately for each code.

From the integrated and decoded samples, the processor obtains time-averaged estimates of either the power spectrum, $S(f)$, or the autocovariance function, $R(\tau)$, of the received signal. The radar responds only to those components of the refractivity fluctuations within the scattering volume that have a spatial scale of $\lambda/2$ corresponding to the Bragg vector along the radar axis. Parameters inferred from the spectra or the autocovariance function of the received signal can be related to the statistical properties of the refractivity fluctuations at the Bragg scale under fairly general conditions as discussed, e.g., by TATARSKII (1971) and ISHIMARU (1978). The most widely used parameters are the low-order spectral moments of the received signal. The spectral-moment processing frequenty is carried out off-line.

Synchronization between the radar modules is effected through the radar controller. The overall transfer of digitized and processed data between the modules, and to the outside world for storage, display and further analysis, is exercised through an on-line host computer.

The signal-processing operations performed by the analog blocks (enclosed by dotted lines in Figure 1), and subsequently by the processor, assume linearity of the system. For this reason, it is crucial to avoid saturation of these modules.

## COHERENT INTEGRATION

A direct Fourier analysis of the signals received at the PRI, T is undesirable for two reasons: (1) the frequency band (-0.5T, +0.5T) is considerably wider than the expected Doppler shift of the signals, and (2) the processor can store only a finite number N of samples for each range and the available frequency resolution 1/TN may not adequately resolve the Doppler-shifted returns. It is, therefore, necessary to reduce the bandwidth of the signals by low-pass filtering. This also would result in a better overall signal-to-noise ratio (SNR), due mainly to the reduced bandwidth.

Coherent integration of the received signals, in which the signals are accumulated for a time MT and then fed to the processor at this reduced rate, provides a simple and computationally effective means of implementing a low-pass filter. The use of coherent integration was proposed first by WOODMAN and GUILLEN (1974), and is now standard in all MST radar experiments. The only exceptions to its use arise in UHF radar experiments, at low elevation angles and at mesospheric heights.

The coherent-integration method is equivalent to a convolution or moving average of the received signal with a rectangular window followed by coarse sampling at intervals of the window length. Since the coefficients of this window are all of unit weight, its implementation does not involve multiplications and needs only one storage location per range for the partial sums. The frequency response of the coherent-integration filter has been discussed by SCHMIDT et al. (1979). It approximates an ideal low-pass filter rather poorly. Its simple implementation, however, has strongly favored its use with MST radars.

Use of better low-pass filters is desirable for reducing external interference. Improved low-pass filters can be obtained through smoother and wider time windows (see e.g., OPPENHEIM and SCHAFER, 1975; RABINER and GOLD, 1975). The use of these improved filters involves, however, additional storage for the filter weights and for storing the partial product sums, and a large number of

extra multiplications. Their implementation would require a specially designed preprocessor. Alternatively, improved low-pass filters can be implemented directly in the frequency domain by bandlimiting, provided that the processor has adequate storage and Doppler resolution. Neither of these approaches appear to have been pursued with the existing MST radars.

## PHASE CODES AND DECODING TO IMPROVE THE RANGE RESOLUTION

The use of a narrow transmitted pulse and bandlimiting at the IF stage delineates for each sampled range a scattering volume in space. If the transmitted pulse shape is p(t), and the impulse response of the receiver system after correcting for a constant delay is h(t), then the shape of the scattering volume at a range delay t along the radar axis is given by the convolution (c/2) $p(t) \circledast h(t)$. In a direction orthogonal to the radar axis, the scattering volume is confined by the antenna beamwidth. A pulse width of 10 μs and a height resolution of 1.5 km is typical for MST radars, but it is inadequate for resolving the individual layers of turbulence that often are thinner than 100 m. The pulse width often can be reduced without an appreciable increase in the transmitter peak power. This would result in an improved resolution, but at the cost of decreased sensitivity at far ranges. The use of phase coding circumvents these limitations.

In coding schemes, a 0°/180° phase modulation is imposed on the transmitted pulses in accordance with a given code w(t). The receiver-system impulse response g(t), once again after correcting for a delay, should now be matched to baud rate [$\tau_b$] for the code w(t). In decoding, the received signal is correlated with w(t). The corresponding operation in range is now

$$(c/2)\Sigma_{t'} [w(t') \circledast g(t')] \times w(t+t')$$

For desirable codes, their autocovariance function

$$\Sigma_{t'} [w(t') \times w(t+t')]$$

should behave like noise, i.e., it should peak only in the vicinity of t=0. This results in a range resolution of the order of (c/2) x $\tau_b$.

The same argument can be extended for a linear system to sets of codes, e.g., to complementary code pairs, provided that the atmospheric signal may be regarded as coherent over the time required to cycle through the entire code set (WOODMAN et al., 1980). As discussed in the previous section, this often is the case. Complementary code pairs (RABINER and GOLD, 1975) have the nice property that the "sidelobes" in the autocovariance functions for the codes in the pair are equal and opposite and cancel on addition. In practice, this cancellation is not perfect. Implementation of complementary-code schemes for specific radar systems is discussed by SCHMIDT et al. (1979) and WOODMAN (1980). At present these codes are being used with the SOUSY, Arecibo, Millstone Hill and Poker Flat radars.

Since the codes are binary (i.e., have two levels of phase shift), the decoding operation involves only a one bit - multiple bit correlation of the code with the received signal. This correlation can be computed as a gated sum of the received signal, but still needs to be evaluated at the baud rate. For a 32-baud code and a 1 μs baud rate, decoding involves 32 logical operations and additions within the baud duration of 1 μs. For coherent signals, a remarkable reduction in the number of computations is possible by coherently integrating the signals before they are decoded (WOODMAN et al., 1980). For such signals, the dc bias in the system can be substantially reduced by successively sending the codes and their inverse, and correcting for the inverted codes by changing the sign of the received signals.

An extensive empirical search for "improved" practical code sets at specified sidelobe levels has been made by M. P. Sulzer. Practical implementation of such codes will require special hardware decoders, and is feasible with the available special purpose VLSI processors.

Complementary code pairs are not usable in mesospheric (incoherent-scatter) experiments with UHF radars, or in UHF experiments at low elevation angles. This is because the signals received in these experiments have a wide bandwidth and lack coherence from pulse to pulse. Barker codes are more practical in mesospheric incoherent-scatter experiments, and have been used for over a decade (IOANNIDIS and FARLEY, 1972).

## AUTOCOVARIANCE FUNCTION AND POWER SPECTRUM ANALYSIS

The principal function of the processor is to form the estimates of the power spectrum density (PSD) or the autocovariance function (ACF) of the received signals from the coherently integrated and decoded samples, simultaneously for a large number of range cells.

To carry out this function, the processor must have sufficient storage for the samples and the intermediate results, and adequate speed to keep up with the computations in real time and to avoid a backlog. Depending on the storage capacity and speed of the processor, it is configured to operate in either a single-buffer or a double-buffer mode. In the single-buffer mode, the radar operation must be halted to allow the processor to catch up with the processing of the stored data. In the double-buffer mode, sufficient memory must be available to maintain two data storage areas with one always free to receive data while the other is being processed, and the time to process the data in one area must be shorter than that required to replenish the other. When these conditions are met, the double-buffer mode allows uninterrupted radar operation. Both the modes are used in MST data processing, depending upon the installation.

It is perhaps relevant to point out that the data input rate to the processor depends upon the radar frequency. The operating frequency for VHF radars (50 MHz) is about ten times lower than for UHF radars (430 MHz). Under identical circumstances the UHF signals will have a Doppler shift and spread that is ten times that for VHF signals. The data input rate to the processor will therefore be faster by a factor of 10 for UHF radars. The computational requirements correspondingly are more stringent for UHF radars.

The ACF processing is most simply implemented by using the method of lagged products (BLACKMAN and TUKEY, 1959). For computing the ACF at m equispaced lags, the processor must maintain a history of m samples and must have a similar amount of storage for updating the lagged-product sums. For each new sample, the m complex product sums are updated. After processing a sufficient number (L) of samples, the product sums are normalized to obtain the ACF. The ACF processing requires approximately (m x L) complex multiplications and additions per range. The principal incentive for the use of ACF processing is the set of simple relations between the spectral moments and the derivatives of the ACF at zero lag (WOODMAN and GUILLEN, 1974; MILLER and ROCHWARGER, 1972). In principle, the most useful spectral moments can be estimated from the ACF values at just 3 or 4 suitable lags. For large values of m, the lagged product method becomes inefficient and is rarely used (see, however, HARPER and WOODMAN, 1977).

The PSD can be estimated directly from the coherently integrated and decoded samples using the method of averaged periodograms. The periodograms of an equispaced sequence is defined as the magnitude squared of its discrete Fourier transform (DFT). The DFT is efficiently implemented with fast Fourier transform (FFT) algorithms (OPPENHEIM and SCHAFER, 1975; RABINER and GOLD, 1975). A finite number ($m = 2^k$) of samples is stored in the processor memory,

and transformed in place with the FFT method. The transform involves usually $m \times \log_2 m$ complex multiplications. The periodogram is then computed as the square of the DFT, and averaged in time to obtain an estimate of the PSD. The method of averaged periodograms is now routinely used in MST radar experiments. It was used first at the Sunset radar by GREEN et al. (1975).

Statistical properties of the ACF and the PSD estimates have been discussed in detail in several texts (JENKINS and WATTS, 1969; KOOPMANS, 1976; PAPOULIS, 1977). The averaged periodogram P(f) gives a distorted estimate of the true PSD S(f), and its DFT also is a poor estimate for the ACF $R(\tau)$. This distortion is particularly significant in the presence of a strong, slowly fading ground clutter as discussed below.

The method of averaged periodogram for an m-point sequence is equivalent to applying a triangular window over a base (-m, +m) on the ACF. Because of the discrete nature of the sequences and their transforms, the windowed ACF is periodic and its components outside (-m, +m) are aliased. This aliasing is particularly significant if the ACF extends beyond -m/2, +m/2). The triangular window causes a smearing of discrete frequency components with a frequency window that decays slowly as $f^{-2}$.

A simple way of avoiding the distortion due to aliasing of the ACF is to append the m-point sequence with m or more zeros before the DFT operation. This is a well-known technique for estimating the ACF of a sequence with the DFT methods (RABINER and GOLD, 1975). It does, however, require extra storage capacity in the processor and perhaps for this reason has received scant attention for MST radar applications. The smearing of the discrete frequency components arises due to the finite length m of the sequences that are transformed. The only way to reduce this smearing is to increase m (i.e., the duration of the sequence), that is limited once again by the processor memory.

Two current developments in the field of digital signal processing (DSP) are worth mentioning as they are likely to have some impact on future MST radar processing.

The first development pertains to the parametric spectral analysis methods that increasingly are being used in signal-processing applications (CHILDERS, 1978; HAYKIN and CADZOV, 1982; DURRANI, 1983). The spectral analysis methods currently used with MST radars, e.g., the Blackman-Tukey method, are non-parametric in the sense that they do not use any specific model for the received signal. Parametric methods assume an underlying model for the process (received signal) being analyzed and, provided that the process adheres to this model, can provide excellent frequency resolution. A rather general class of these models assumes that the process is obtained by filtering white Gaussian noise through a pole-zero filter (MAKHOUL, 1975; GUTOWSKI et al., 1978), though the order of this filter needs to be determined empirically. An examination of MST radar spectra suggests that they can probably be characterized by an all-pole model. Exploratory spectral analysis of sequences of coherently integrated samples from VHF and UHF radars, with the methods outlines above, appears to be a very promising project.

The second development pertains to the declining cost of large addressable memory modules and the availability of special-purpose microcomputers (μCs) for DSP applications (MAGAR et al., 1982; ALLAN, 1982). A 16-bit 256-kiloword addressable memory module with 500 ns access time is currently priced at $2500. Programmable DSP μCs, that can compute a 64-point complex FFT in 2 ms, are also currently available. It appears that special-purpose processors for MST radar applications can be implemented inexpensively with a large addressable memory module and several DSP μCs.

SPECTRAL-MOMENT PROCESSING: GROUND-CLUTTER REMOVAL

At the next level of processing, the PSD or ACF estimates are used to obtain the basic spectral moments. The three lowest-order moments, defined below, are of special interest:

$$S_0 = \int_{-\infty}^{+\infty} S(f)\, df$$

$$S_1 = [\int_{-\infty}^{+\infty} f\, S(f)\, df]/S_0$$

$$S_2 = [\int_{-\infty}^{+\infty} (f-S_1)^2\, S(f)\, df]/S_0$$

These moments denote, respectively, the total power, Doppler shift and Doppler spread of the signals. The integrals in these definitions are over $|f| \leq \infty$. In practice the spectra are localized, and the moments must be evaluated over a limited frequency window F as discrete sums. In order than these sums converge to the true moments, a good frequency resolution is desirable. The definitions show that even for localized spectra, for the moment of order k to exist, the spectra must decay at least as fast as $f^{-k}$ away from $S_1$. To minimize the contribution of a constant (noise) part of the spectrum on the moments, and to reduce their dependence on the window function F, the constant part must be subtracted from S(f). Moreover, for localized spectra the definitions become nested. It therefore becomes necessary to determine these moments recursively, and to use several different windows F. The moments then should converge most rapidly for that window F that matches the shape of the spectrum best. Any prior information about $S_1$, e.g., from previous observations or from adjacent range cells, can be used for setting up the window F. This makes the estimates more robust and less susceptible to external interference.

The spectra estimated as averaged periodogram P(f) usually have a large variance (KOOPMANS, 1976) that hinders the task of spectral-moment estimation. Some prior smoothing of P(f), e.g., with a 3-point running window, is desirable. Smoothing also helps in forming an automatic initial guess for the location of the signal, e.g., as a local maximum, in the spectrum.

As already mentioned in the previous section, the spectral moments can be inferred efficiently from estimates of the ACF at small lags. This method is similar to that of obtaining the moments of a probability density from its characteristic function (PAPOULIS, 1977). $S_0$ is simply the value of the ACF at zero lag, $S_1$ is directly related to the phase of the ACF at a small lag, and $S_2$ is related inversely to the width of ACF (MILLER, 1974). The use of this method in atmospheric radar experiments is discussed by WOODMAN and GUILLEN (1974) and ZRNIC' (1979).

The ground clutter poses a serious problem in estimating the spectral moments. The contribution of ground clutter often is 10 to 30 dB stronger than the atmospheric signal and has a small but finite bandwidth. In the periodogram method of estimating the PSD, this contribution invariably is smeared in frequency. This smearing is more severe at UHF frequencies.

A simple method of removing the ground-clutter component in the PSD estimates is to assume that this component has no Doppler shift. The ground clutter contribution would then be symmetric about the zero Doppler shift and can be easily removed. This method generally works well for VHF radars, but for

UHF radars it requires the atmospheric signals to be sufficiently well-separated in frequency from the clutter.

SATO and WOODMAN (1982) describe a parametric method of estimating the spectral moments for UHF radar signals in the presence of fading ground clutter. The PSD is characterized as the sum of three components: a parabolic, Gaussian or Lorentzian function for the ground clutter, a Gaussian function for the signal, and a Gaussian function for the ocean returns or external interference. This composite spectrum is transformed to an ACF that is aliased and distorted as described in the previous section, and fitted to the DFT of the measured periodograms in a least-square-error sense. The processing time for obtaining the best fit can be reduced substantially if an initial guess for the parameters is supplied. The (nonparametric) spectral-moment estimation methods discussed earlier can be useful for obtaining the initial guess.

Special processing techniques that reduce the smearing of the fading ground clutter in the PSD estimates are obviously desirable from the point of view of spectral-moment estimation. One such technique is to increase the frequency resolution of the periodograms by transforming a very long sequence of samples (WAND et al., 1983). This technique is limited by the processor memory. The second technique is to use parametric spectral-estimation methods (HAYKIN et al., 1982). The application of these techniques to MST radar experiments deserves attention.

## DATA ANALYSIS: OUTLIERS AND MISSING DATA

Analysis of the MST radar data -- the spectral moments and physical parameters derived from these -- requires statistical, numerical and graphical techniques. Though the details of these analyses depend on the scientific objectives, some techniques that are useful in handling spurious points and missing data are worth mentioning.

Spurious data values or outliers frequently occur in physical data. Manual editing techniques to isolate and discard these values are impractical for large data sets. Techniques based on running statistics of data are effective in removing outliers. One such statistic is the median. A median filter examines a few points on either side of a data point and determines the local standard deviation and median. If the data value deviates too much from the median, it is classified as an outlier and replaced by the median. Properties of the median filters have been discussed by NODES and GALLAGHER (1982).

Runs of missing data can occur in a long sequence of radar observations for reasons such as equipment outage, interference or weak signal level. Spectral analysis of a sequence with missing data requires extra care. BLACKMAN and TUKEY (1959) suggest modifications of their averaged lagged-product method of spectral analysis to sequences with gaps. In the periodogram method, missing data introduce unknown frequency components. The periodogram of an indicator function (with a value 1 for data and 0 for gaps) is useful for identifying these frequency components. Interpolation techniques, with spline functions e.g., are useful for smooth sequences with short gaps. BOWLING and LAI (1979) describe an interesting technique based on parametric spectral estimation methods for interpolation and spectral analysis of a sequence with missing data.

Graphical techniques are particularly valuable for examination and succinct displays of large amounts of geophysical data. The use of color graphics appears well established in fields such as remote sensing and radar meteorology, and will undoubtedly be useful for MST radar data analysis.

## DISCUSSION

The techniques used in MST radar data processing appear to have become fairly well established. The processing of VHF radar signals follows the more standard procedures, due mainly to the large number of such radars (approaching ten) and the smaller data rate encountered at their operating frequencies. The number of UHF radars usable for ST studies is presently limited to two -- Arecibo and Millstone Hill -- though other incoherent-scatter radars in France, Greenland and Norway will probably soon be added to this list. The full steerability the smaller UHF radars gives them a unique capability, but they require more specialized data processing methods.

Phase codes and decoding to achieve a better altitude resolution (300 m or better) are already in use with a few MST radars. Fully automated processing of radar data in real time -- up to the level of spectral-moment estimation -- appears to be a desirable goal for obtaining long, unattended sequences of observations, with manageable output data rates. At present this goal has been reached only at the Poker Flat radar.

Special-purpose hardware processors for FFT analysis, and preprocessors for filtering and decoding, can now be inexpensively constructed. For VHF radars a 512 channel processor with 64 point FFTs can cover the entire MST region with a 150-m height resolution. A similar processor for UHF radars will require 256 channels with 512 point FFTs to cover the entire ST region. Special-purpose preprocessors to carry out low-pass filtering and decoding for 512 or 256 channels are required for better interference rejection and improved height resolution.

The use of parametric spectrum and spectral-moment estimation methods needs to be explored, especially for the UHF radars, to overcome the problems related to ground clutter.

## ACKNOWLEDGMENT

This material is based on work supported by the National Science Foundation under grant number ATM-8000060.

## REFERENCES

Allan, R. (1982), Signals processors enlist in a variety of advanced systems, Electronic Design, (Aug. 5), 75-86.

Blackman, R. B. and J. W. Tukey (1959), The Measurement of Power Spectra, Dover, New York, 190 pp.

Bowling, S. B. and S. T. Lai (1979), The use of linear prediction for the interpolation and extrapolation of missing data and data gaps prior to spectral analysis, Lincoln Lab. Rep., 1979-46, 19 pp., Lexington, Mass.

Childers, D. G. (1978), Modern Spectrum Analysis, (selected reprints), IEEE Press, New York, 334 pp.

Crane, R. K. (1980), A review of the radar observation of turbulence in the lower stratosphere, Radio Sci., 15, 177-193.

Durrani, T. S. (ed.) (1983), Special Issue on Spectral Analysis, IEE Proceedings, Part F, 180(3), April 1983.

Green, J. L., J. M. Warnock, R. H. Winkler and T. E. VanZandt (1975), Studies of winds in the upper troposphere with a sensitive VHF radar, Geophys. Res. Lett., 2, 19-21.

Guillen, A. (1971), Measurements of winds up to 85 km altitude using radar and electronic digital computer, Engineer thesis, Nat. Univ. Engg., Lima, Peru.

Gutowski, P. R., E. A. Robinson and S. Treitel (1978), Spectral estimation: Fact or fiction, IEEE Trans. Geosci. El., GE-16, 80-84.

Harper, R. M. and R. F. Woodman (1977), Radar observations of waves and winds in the mesosphere over Jicamarca, J. Atmos. Phys. Terr., 39, 959-963.

Haykin, S. and J. A. Cadzow (1982), Special issue on spectral estimation, Proc IEEE, 70(9), 883-1125.

Haykin, S., B. W. Currie and S. A. Kesler (1982), Maximum-entropy spectral analysis of radar clutter, Proc. IEEE, 70(9), 953-962.

Ioannidis, G. and D. T. Farley (1972), Incoherent scatter observations at Arecibo using compressed pulses, Radio Sci., 7, 763-766.

Ishimaru, A. (1978), Wave Propagation and Scattering in Random Media, Academic, New York, 572 pp.

Jenkins, G. M. and D. G. Watts (1969), Spectral Analysis and its Applications, Holden-Day, San Francisco, 525 pp.

Koopmans, L. H. (1976), The Spectral Analysis of Time Series, Academic, New York, 366 pp.

Magar, S., R. Hester and R. Simson (1982), Signal-processing μC builds FFT-based spectrum analyzer, Electronic Design (Aug. 19), 149-154.

Makhoul, J. (1975), Linear prediction: A tutorial review, Proc. IEEE, 63, 561-580 (also in Childers, 1978).

Miller, K. S. (1974), Complex Stochastic Processes, Addison-Wesley, Reading, 238 pp.

Miller, K. S. and M. M. Rochwarger (1972), A covariance approach to spectral moment estimation, IEEE Trans. Inf. Th., IT-18, 588-596.

Nodes, T. A. and N. C. Gallagher, Jr. (1982), Median filters: Some modifications and their properties, IEEE Trans. Ac. Ap. Sig. Proc., ASSP-30, 739-746

Oppenheim, A. V. and R. W. Schafer (1975), Digital Signal Processing, Prentice-Hall, Englewood Cliffs, NJ, 585 pp.

Papoulis, A. (1977), Signal Analysis, McGraw-Hill, New York, 431 pp.

Rabiner, L. R. and B. Gold (1975), Theory and Application of Digital Signal Processing, Prentice-Hall, Englewood Cliffs, NJ, 762 pp.

Sato, T. and R. F. Woodman (1982), Spectral parameter estimation of CAT radar echoes in the presence of fading clutter, Radio Sci., 17, 817-826.

Schmidt, G., R. Ruster and P. Czechowsky (1979), Complementary codes and digital filtering for detection of weak VHF radar signals from the mesosphere, IEEE Trans. Geosci. El., GE-17, 154-161.

Tatarskii, V. I. (1971), The effects of the turbulent atmosphere on wave propagation, Nat. Tech. Inf. Serv., Springfield, VA, 472 pp.

Wand, R. H., P. K. Rastogi, B. J. Watkins and G. B. Loriot (1983), Fine Doppler resolution observations of thin turbulence structures in the tropo-stratosphere at Millstone Hill, J. Geophys. Res., 88, 3851-3857.

Woodman, R. F. (1980), High-altitude resolution stratospheric measurements with the Arecibo 430-MHz radar at Arecibo, Radio Sci., 15, 417-422.

Woodman, R. F. and A. Guillen (1974), Radar observations of winds and turbulence in the stratosphere and mesosphere, J. Atmos. Sci., 31, 493-505.

Woodman, R. F., R. P. Kugel and J. Rottger (1980), A coherent integrator-decoder preprocessor for the SOUSY-VHF radar, Radio Sci., 15, 233-242.

Zrnic', D. (1979), Estimation of spectral moments for weather echoes, IEEE Trans. Geosci. El., GE-17, 113-128.

## REPORT AND RECOMMENDATION

This report on the data processing techniques currently in use with MST radars is based on the contributions that were presented in two workshop sessions, and on an open discussion following these presentations. The contributions addressed the current methods, problems and new developments in the use of coherent integration, autocovariance function (ACF) and power spectrum density (PSD) analysis, estimation of spectral moments, pseudo-noise phase codes and decoding, and special-purpose processors in the analysis of radar data.

Coherent integration is an intermediate computation-saving step that reduces the data rate before PSD or ACF analysis. In experiments that use phase codes, it is often possible to carry out decoding after coherent integration with a remarkable saving in computations. In the frequency domain, coherent integration approximates a poor low-pass filter that arises due to the use of a rectangular time window. Other time windows with better frequency response are known, but their implementation is deemed impractical as it requires considerable extra storage and a steep increase in computations. The simplicity of implementing coherent integration remains a strong point in its favor.

The ACFs can be evaluated for a small number of lags as the lagged-product sums. The number of lags is eventually limited by the processor speed. More efficient implementations are possible for an assumed ACF shape, or indirectly with the use of discrete Fourier transform (DFT) methods. The use of DFT methods for ACF computations has not been deemed favorable as it requires a null extension of the data, hence extra storage in the processor. The PSDs are estimated most frequently with the method of averaged periodograms. The periodogram is efficiently computed from the DFT of data samples, but provides a distorted estimate of the spectrum. This distortion is most serious in the presence of a strong, slowly fading ground clutter.

Spectral moments, that contain infomation about the physical and dynamical characteristics of the medium, can be estimated directly from the spectra, or indirectly and often more efficiently from the ACF at small lags. In VHF radar experiments both methods have been successfully used. The ACF method can be implemented even with processors of modest speed and storage. In UHF radar experiments, the estimated spectra invariably are contaminated with a strong, slowly fading ground clutter. At pointing directions far from the vertical, the signals have a sufficiently large Doppler shift and can be readily discriminated from the clutter. Under these conditions simple ad-hoc methods can be used effectively for finding the spectral moments. For signals with small Doppler

shifts, the contribution of ground clutter and other undesired components must also be estimated. Parametric spectral moment estimation using nonlinear least square fitting has been found to be a useful and perhaps the only effective technique in this case.

Phase codes and decoding are used to improve the range resolution without degrading the received signal-to-noise ratio. For slowly fading MST returns the use or complementary code pairs can routinely provide altitude resolution of 150-300 m, except for close ranges. The use or coherent integration before decoding results in a substantial saving in computational effort and is often actually required for carrying out decoding in real time. Special hardware processors are usually necessary for decoding. For small code sets and slowly fading returns, decoding can be implemented in software for a limited height range. For large code sets, decoding must be carried out on a pulse-by-pulse or code-by-code basis. A fast hardware decoder has recently been designed and is under construction at the Arecibo Observatory.

Due to rapid advances in the technology of storage and signal-processing devices and their declining costs, it is now feasible to develop large, high-speed processors for MST radar applications. One such processor is currently being developed at the University of Alaska with two relatively inexpensive array processors and a large external buffer memory. A fast pipe-lined radar signal processor, suitable for MST and other applications, is under development at Cornell University.

The nature of ground clutter observed with the existing MST radars was briefly discussed. Since the ground clutter returns are tens to thousands of times stronger than the atmospheric returns, it is necessary to provide a large dynamic range in their digitization. An eight-bit digitization is often sufficient for VHF radars, but UHF radars may require up to twelve bits. The ground clutter returns fade much more rapidly at UHF due to the shorter wavelength. This fading is usually not a serious problem at VHF frequencies, except for conditions of strong ground wind. The ground clutter fading is usually more severe during the daytime, in precipitation environment, and during boundary-layer inversions. Further empirical studies of the nature of ground clutter fading and its severity are deemed essential. Spectral analysis of longer data records, with a finer Doppler resolution, offers a reasonable alternative for reducing the smeared contribution of fading ground clutter, but requires the use or processors with large storage.

The need for software exchange between radar groups was considered. At present the data processing software is implemented in a rather ad-hoc way within each user group. As more radars with similar characteristics are constructed (e.g., VHF ST radars), there certainly will be a need for standardization and exchange of such software.

Further open discussions regarding the current and future data processing needs at the existing and planned MST radar facilities led to the following recommendation:

"The group, NOTING with concern that many MST observatories have inadequate data processing facilities, and with pleasure that major advances in developing powerful but low cost digital equipment have been made in recent years, RECOMMENDS that existing observatories investigate the cost effectiveness of upgrading their computing facilities and that adequate attention be given to this topic in planning new facilities".

# 8.1A DECODING: CODES AND HARDWARE IMPLEMENTATION

M. P. Sulzer* and R. F. Woodman**

*Arecibo Observatory, Box 995, Arecibo, Puerto Rico
**Instituto Geofisico del Peru, Apartado 3747, Lima, Peru

## INTRODUCTION

MST radars vary considerably from one installation to the next in the type of hardware, operating schedule, associated personnel, and amount of funding. Most such systems do not have the computing power to decode in software when the decoding must be performed for each received pulse, as is required for certain sets of phase codes. These sets allow one to obtain the best signal-to-sidelobe ratio when operating at the minimum baud length allowed by the bandwidth of the transmitter. We discuss here a number of realizations of the hardware phase decoder, and discuss the applicability of each to decoding MST radar signals. We present a new design for a decoder which is very inexpensive to build, easy to add to an existing system and is capable of decoding on each received pulse using codes with a baud length as short as one microsecond.

## CODES USED WITH MST RADARS

In nearly all MST radar sounding, the received signal is stationary over a time equal to at least several periods of the transmitter pulse sequence. This fact has a strong influence on the type of codes which can be used. The most-used codes have been the binary complementary codes as described in WOODMAN (1980). Because these codes have zero sidelobes, there has been no need to use multiphase codes which are much more difficult to implement. Recently however, binary code sets have been developed which use a different code for each transmitted pulse (SULZER and WOODMAN, 1982; 1983). In a perfect system, these codes offer no advantage over the complementary pair, since the latter has no sidelobes. In a real system, however, there are imperfections, especially in the transmitter, and the quasi-complementary codes offer significant advantages. The use of these new codes has one large disadvantage: decoding must be performed on each received pulse. On the other hand, the use of the complementary code pair means that the returns from each of the two codes can be added before decoding so that only two decodings are necessary for each of the two codes coherent interpretation period. Thus the new codes require a lot more computation.

## HARDWARE VERSUS SOFTWARE DECODING

The low computation rates associated with decoding the complementary pair when the coherent interpretation time is long allow the decoding to be performed in software in many systems. This is not the case if each pulse must be decoded. In this case a special purpose hardware device (DECODER) must be used. Decoders vary tremendously in their complexity, speed, the method used to perform the decoding and flexibility. As a consequence, they also vary tremendously in their cost.

The advantages of hardware decoding are the following:

(1) Much higher data rate than a general purpose computer, even higher than an array processor.

(2) Faster "programming" of code changes than in a computer. (Some types of decoders only.)

(3) On-line monitoring (at output of decoder) shows good height resolution.

The advantages of software decoding are the following:

(1) For low data rates, an already available general purpose computer may be used.

(2) Ease of implementation.

The next sections of this paper describe various types of hardware decodes, and present a new design for one which is well-suited for middle atmosphere work.

## THE DECODER: A TRANSVERSAL FILTER

A decoder perform a convolution

$$o(t) = i(t) * h_j(t) \tag{1}$$

where $i(t)$ is the input signal
$h_j(t)$ is the impulse response of the decoder programmed for code j

and $o(t)$ is the output signal.

The convolution may be written out as an integral

$$o(t) = \int_0^t i(q)\, h(t-q)dq \tag{2}$$

This integral becomes a summation for discrete samples. Figure 1 shows a block diagram of a decoder for a code N long. The present value and N-1 earlier values are stored in a delay line. In the case of a binary phase code the impulse response consists of +1 or -1 and so the multiplications are replaced with additions of either the signal or the inverted signal. The figure shows a digital implementation. This could be done with an analog delay line and analog inverter and adders.

If we wish to change the code quickly, we must add a shift register and selector switches. This is shown in Figure 2. Note that if the signal values

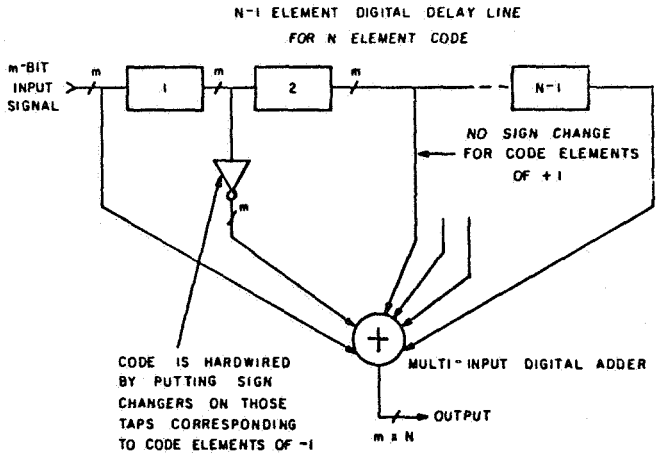


Figure 1. Transversal filter decoder for code length N.

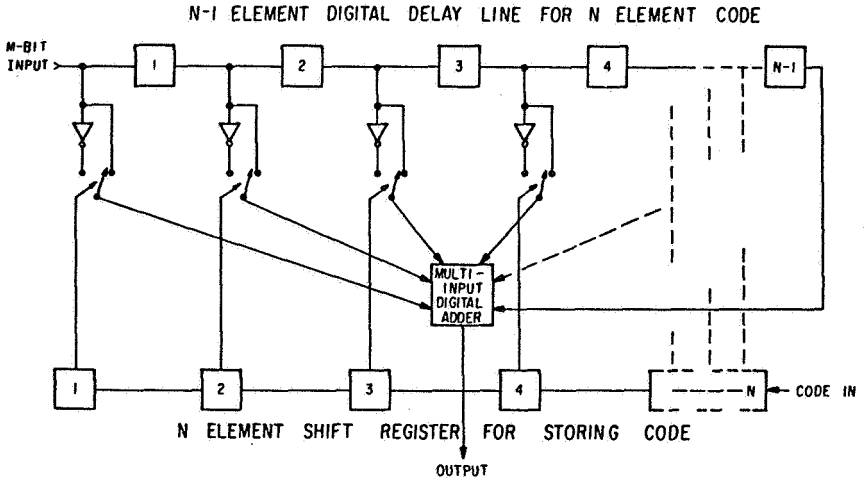


Figure 2. Transversal filter decoder for code length N allowing quick changes of code.

enter from the left, the code must fill the shift register from the right. This accomplishes the folding about the time axis which is indicated by the negative sign in equation 2.

For a practical decoder, we need one more shift register which is parallel to the one storing the phase code. This is the amplitude of the code and is '1' wherever the code is defined and '0' otherwise. It is also attached to the control lines on the switches and when it is '0' neither switch is connected. This makes it possible to use codes with the length less than N.

An example of the type of decoder described in Figure 1 is the Barker Decoder used at Arecibo Observatory. The device is completely analog and works at the 30 MHz IF frequency. The input signal is fed to a surface-wave delay line with taps. The appropriate taps are inverted and added. The device is good only for the 13 bit Barker code with 4 μsec baud.

The transversal filter decoder would probably not be built with a digital implementation because of the complexity of the multi-bit delay line. The next section describes a digital design which is much more efficient.

## THE DECODER: A CORRELATOR

The convolution described in the last section can be performed in a very different way which is particularly useful for digital implementation and has the advantage that the number of bits in the code may exceed the number of storage resistors. This implementation has the form of a correlator, where each lag corresponds to a different decoded range. Hence, the number of ranges, rather than the number of bits in the code, is limited.

Referring to Figure 3, we see that the code enters a shift register which is as long as the number of ranges. At the output of each flip flop in the shift register is an adder (or subtractor) which adds into the associated accumulator if the flip flop state is '1' or subtracts if '0'. The signal to be added (or subtracted) is in all cases the present value, the one just digitized. If the code has N bits, then after N cycles, the ith accumulator will contain

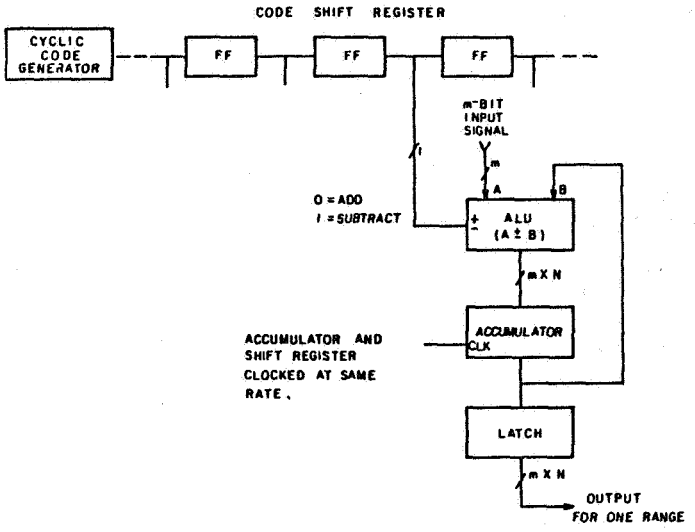


Figure 3. Decoder using correlator architecture uses one channel per range (one channel shown).

$$A_i = \sum_{n=0}^{n-1} (S_{i+1}) \cdot h_n$$

where $S_i$ is the m-bit input signal
$h_n$ is the code value (1 or -1)
$A_i$ is the accumulated signal.

We can see that there is no limitation to the length of the code, in principle, although the accumulator will eventually overflow. On the otherhand, if the code is shorter than this number of registers, there is no range limitation either since each accumulator may be dumped to the computer as it completes, and the code may be started into the shift register again.

Figure 3 is a simplified block diagram of the planetary radar decoder at the Arecibo Observatory; this decoder has been used for MST observations in additon to its intended purpose. The actual circuit does not have an ALU for each range, but rather time shares one ALU among as many as 32 ranges, thus reducing the amount of hardware.

## REQUIREMENTS OF AN MST RADAR DECODER

In the last section we have seen several ways to design a decoder. In designing a new decoder for MST work, the most important criterion for the instrument is that it fit into all, or nearly all, existing systems with a minimum of change. Since all, or nearly all such systems already have A/D converters and the ability to coherently add samples either in the general purpose computer for just before it, it is best not to interfere with this part of the system. This means that the model of the decoder as an analog filter is most appropriate. In this case, the decoder is placed after the baseband mixer, and before the A/D converter. Actually, the decoder could be digital inside; the important thing is that it be analog to analog and operate in real time. The requirement may seem unnecessary, but it should be remembered that the cost of any equipment must include the cost of altering the system of which it will be a part.

Other requirements are relatively simple. A length of 64 is adequate; we would like to use baud lengths of 1 μsec and keep errors better than 40 dB down if possible.

## THE ANALOG RING DECODER

When designing a filter which will have an analog input and output, we must consider the possibility that using analog circuitry inside may be the best approach. High-speed digital processors are very powerful machines, but they have some disadvantages. The most important disadvantage for our purpose is difficulty in maintenance. These machines are usually one, or few, of a kind and the trouble-shooting procedures are often not well-defined.

We present here a new analog design which is similar to the normal transversal filter design in that the output is the simultaneous sum of N stored samples but is like the correlator design in that only the code, a simple three-level signal, need be shifted.

Figure 4 is a block diagram showing the concept of the analog ring decoder. To understand its operation first look at the rotor of the central rotary switch which is connected to the input signal. This switch deposits samples on the capacitors which are stored until the switch completes a revolution and deposits a new sample. As long as the code is shorter than the number of capacitors, we have enough information stored to decode the signal. All we have to do is add the signals from N adjacent capacitors with the correct polarity. To do this, we place the code in a shift register, and the outputs of the shift register control switches in the amplifiers to give the proper gain (+1, -1, or 0) to the signal. Everytime the switch moves forward one step, so does the shift register, and the correct signs are given to the delayed signals, which are added through the resistors to the output buss.

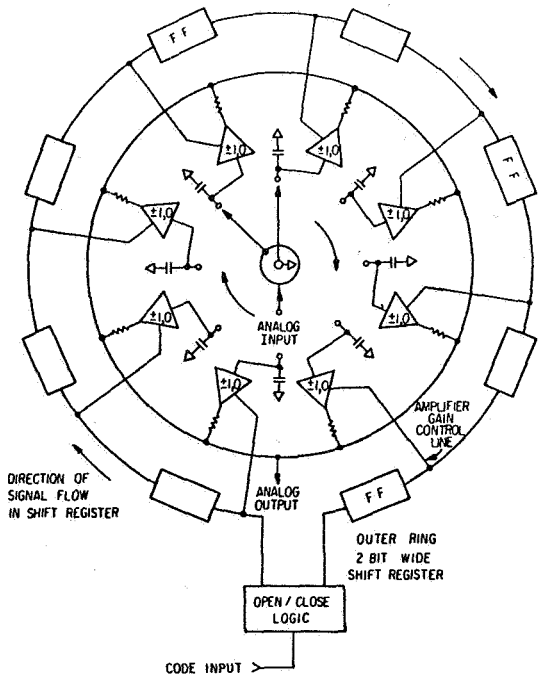


Figure 4. Block diagram of analog ring decoder.

This sample block diagram is very close to the way the actual machine operates. However, we can make a few simple additions which will allow the machine to run much faster with high accuracy. First let us make the number of capacitors and switch positions, M, somewhat larger than N, the length of the largest code we will use. Second, we arrange the phase of the switch rotor so that the code begins two positions after the switch pointer. This means that the present sample and the ones surrounding it will be connected to amplifiers with gain of 0. Third we add a second rotor to the switch which runs one step ahead of the other. This rotor is connected to the ground.

Figure 5 shows one section of the ring. Swintches A and B are each part of a CMOS analog multiplexer which acts like the rotary switch of Figure 4. The first step in taking a sample is to discharge the capacitor; the second step is to connect it to the input line so that a sample may be taken. This latter step also removes the previous signal, but it turns out that it is more important to discharge as nearly completely as possible the previous signal, than it is to fully charge it with the new signal. This is because keeping an old signal will cause a "ghost" and there is no way around this problem except to discharge the capacitor. On the other hand, if all of the capacitors and switch resistances had the same values it would not matter how many time constants of settling time were allowed since the relative values of the samples would be unaffected. Therefore, it is only the differences between these component values which set the necessary settling time for sampling. Allowing 2.5 time constants ($R = R_{switch} + R_{amp}$) and a maximum component value error of 10% give a maximum error of .8% in voltage, which is more than 40 dB down. Using an additional cycle to discharge the capacitor ($R = R_{switch}$ only) puts the ghost down over 80 dB. To achieve the same ghost level without the extra cycle would slow down the machine by more than a factor of two.

The two operational amplifiers and switches C and D in Figure 5 are equivalent to the gain-switched amplifier of Figure 4. After the sample is completed in step two, we wait one more clock cycle for the two amplifiers to settle. Once the outputs of the two amplifiers have settled, they will not change for M-3 clock cycles. The gain charge is "passive" in that it is achieved by switching between two unchanging signals. The addition of the various delayed signals is also passive in that it invokes only resistors and no operational amplifier. The output does contain "glitches" due to the finite switching time (∿50 nsecs) and pick up from the logic circuitry. Since all of the logic is synchronous, all the glitches occur on clock transitions and may be removed by using a sample and hold on the output which samples just before the clock transition.

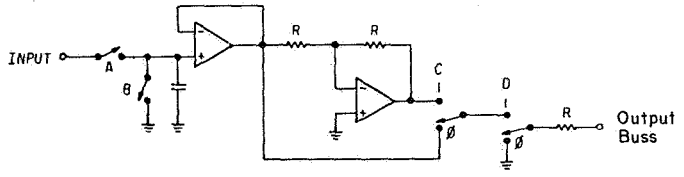


| | SWITCH | | | | |
|---|---|---|---|---|---|
| STEP | A | B | C | D | PURPOSE |
| 1 | 0 | C | X | Ø | CLEAR CAP. |
| 2 | C | 0 | X | Ø | SAMPLE |
| 3 | 0 | 0 | X | Ø | SETTLE |
| 4-N | 0 | 0 | Ø or 1 | 1 | ADD / SUB |

X = DON'T CARE
Ø or 1 DEPENDS UPON PHASE OF CODE

Figure 5. Sampling and switching.

A complete error analysis is not possible in a paper of this length, but a few comments will give a general idea of the sensitivity to errors. Assume that there will be a relative error in each of the N slices of the decoder given by $\Delta E_i$ for i = 1,N, where by relative error we mean the error in the sampled signal divided by the signal. When the N samples are added the N signals add directly but the N error add as random numbers since they are independent and so the relative error in the output signal voltage will be $\sqrt{N}$ times smaller than the typical relative error on a single sample or N times better in power. Furthermore, the error in the output signal is a function of the code; that is, some codes will give a positive error, others negative. Thus by using the Quasi-complementary codes which have a different code for each member of the sequence, we obtain a further reduction in the error in the decoder in the same manner errors in the transmitter are reduced.

REFERENCES

Sulzer, M. P. and R. F. Woodman (1982), Quasi-complementary codes, presented at the Workshop on Middle Atmosphere Measurements and Middle Atmosphere Radars (Cosponsored by SCOSTEP, COSPAR, IAGA, IAMAP, VRSI), May 10-12, Estes Park, Colorado.

Sulzer, M. P. and R. F. Woodman (1983), Quasi-complementary codes: A new technique for MST radar sounding, accepted for publication by Radio Science.

Woodman, R. F. (1980), High-altitude resolution stratospheric measurements with the Arecibo 430-MHz radar, Radio Sci., 15, 417-422.

# 8.2A DECODING: SOFTWARE IMPLEMENTATIONS

G. B. Loriot

Haystack Observatory
Massachusetts Institute of Technology
Westford, MA 01886

## ABSTRACT

The motivation to use phase-coded observations for the stratosphere-troposphere region is briefly discussed. Previous work using hardware correlators to decode the received signal is referenced. An alternative technique using software to decode the signal samples is described in detail, and results of this implementation are presented.

## INTRODUCTION

High-power sensitive Doppler radars have been shown to be feasible probes of clear air turbulence in the troposphere and stratosphere (BALSLEY, 1981; RASTOGI, 1981). Typically, a 10-20 μs pulse is transmitted with a peak power of 1-2 MW, and the backscattered signal is sampled at or near the pulse length. Several range gates are simultaneously sampled to cover a desired altitude span, and the samples are stored in a processor. Coherent integration (presuming) may be employed to narrow the bandwidth, and the range resolution is determined by half the pulse length (1.5-3.0 km). After a sufficient number of radar sweeps have been stored, power spectra are estimated from the time series of samples at each range gate. Spectral moments yield estimates of properties of turbulence in the medium as a function of range, with the spatial resolution as set by the pulse length. Routine observations of this type have been carried out by several groups during the past decade (WATKINS and WAND, 1981; ROTTGER, 1981). Observations of the development, organization, and decay of these structures may lead to an understanding of their role in the dissipation of short period motions and in their effect on vertical transport.

However, turbulent structures in the strato- troposphere (ST) are known to exist in layers as thin as tens of meters. Many of the details of these structures would be obscured if a resolution of 1-2 km were used (SATO and FUKAO, 1982). If short pulses (1-2 μs) were used to increase the resolution, the peak power limitations of ~1-2 MW would severely degrade the signal-to-noise ratio (SNR) of the received signals, and many regions of weak turbulence would not be observed. In order to resolve these structures with radar, pulse compression by phase coding has been employed by several investigators, and has proven to be effective in increasing the SNR while maintaining a fine range resolution (WOODMAN, 1980; WOODMAN et al., 1980; SCHMIDT et al., 1979; SATO and WOODMAN, 1982a).

The phase-coded method comprises transmitting a long pulse to obtain good SNR, but modulating the phase at the desired resolution (baud rate) according to a pseudo-random binary code. The backscattered signal is sampled at the baud rate and the samples are correlated (decoded) with a replica of the code. This yields pulse compressed samples with the resolution set by the baud length. For an arbitrary code, the zero lag correlation will always give a maximum value, but lags further along the pulse will also contain significant values. There are many finite length codes in which this effect may be minimized, that is, the correlation sidelobes will be much smaller than the zero lag peak; Barker codes and some codes due to Turyn are two such examples (see Table 1). Signals from one range will still contaminate another range within the code length, but at a much reduced level. For ST studies, where the atmospheric signal is phase coherent over more than one radar sweep, special codes called "complementary

Table 1 Phase codes available at Millstone Hill

| CODE | BIT PATTERN | DESCRIPTION |
|---|---|---|
| A | 11101101111000101110110100011101<br>11101101111000100001001011100010 | 32-bit complementary code pair |
| A1 | 11101101111000101110110100011101<br>11101101111000100001001011100010<br>00010010000111010001001011100010<br>00010010000111011110110100011101 | 32-bit complementary code pair, followed by pair of negatives |
| B | 1110110111100010<br>1110110100011101 | 16-bit complementary code pair |
| B1 | 1110110111100010<br>1110110100011101<br>0001001000011101<br>0001001011100010 | 16-bit complementary code pair, followed by pair of negatives |
| C | 1111100110101 | 13-bit Barker code |
| D | 11011010010001000100011111000 | 28-bit code (TURYN, 1968) |
| E | 11100111000000010101001001001 | 28-bit code (TURYN, 1968) |

NOTES: (A) and (B) autocorrelation sidelobes are equal and opposite in sign, yielding zero when summed. Requires coherence over 2 radar sweeps.

(A1) and (B1) are identical to (A) and (B) respectively, but their complements follow them in this sequence. Allows use of dc subtraction. Requires coherence over 4 radar sweeps.

(C) has low correlation sidelobes. Intended for D-region observations.

(D) and (E) have low correlation sidelobes.

codes" may be used to reduce this effect still further. Complementary codes are pairs of codes having very desirable sidelobe properties: the sidelobes of one code are complements of the other's, so that they cancel when summed together, leaving an enhanced contribution only at the zero lag peak. This is taken as the pulse compressed signal for a range cell with resolution set by the baud length.

In the studies referenced above, the raw samples from the radar receiver are decoded by a high-speed hardware digital correlator before transfer to either the processor or to magnetic tape for spectral processing. The radar facility at Millstone Hill has recently been modified to operate with phase coding (including complementary codes), but the implementation uses a programmable array processor to presume, decode, and spectrally process the raw samples in real time. No hardware correlator is required in this approach. The next section describes this system in more detail.

## IMPLEMENTATION AT MILLSTONE HILL

### (a) General Description

A phase-coded mode of operation for ST experiments has been implemented at the 440-MHz Millstone Hill radar using a Floating Point Systems AP-120B array processor to decode the samples and perform spectral calculations in real time. This mode has been implemented as an option for the real-time data-collection system recently developed (WAND et al., 1983; HOLT et al., 1983). Figure 1 is an overall diagram of this system, including antenna, transmitter, receiver and processors (see p. 357, this volume, by P. K. Rastogi). A control and formatting program runs in the Harris H100A host computer. The CAMAC interface controls and monitors radar timing, transmitter modulation, antenna selection and motion, and various ancillary functions. The array processor performs all signal processing tasks on the detected samples; all functions are under program control from the host computer. Rapid switching of experimental modes is easily

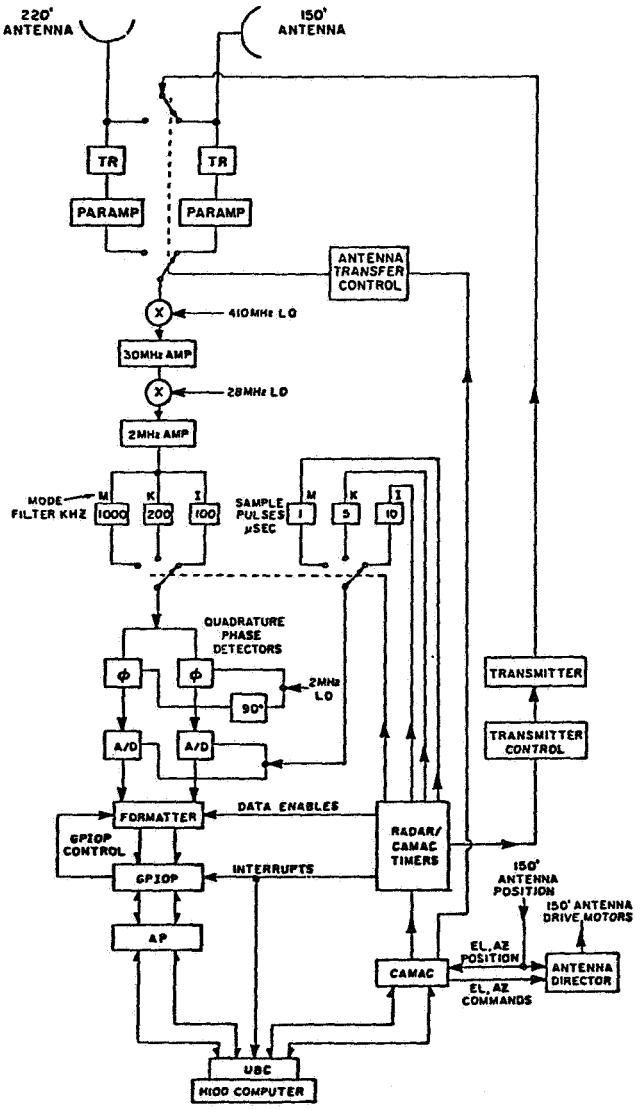


Figure 1. UHF radar system for ST observations at Millstone Hill.

achieved; a sequence of operations is specified at program initiation, and the Harris computer cycles through any mixture of coded or uncoded ST and/or incoherent scatter observations. This section concentrates on the special modes using complementary codes for ST observations.

Typically, a four-pulse sequence of 16- or 32-bit complementary codes has been used; the bit patterns are stored in PROMs and the specified code is selected under program control to modulate the transmitted pulse. The received signal is sampled at the baud rate (usually 2 μs), digitized, and transferred to the array processor (AP). Special purpose subroutines in the AP integrate the samples and decode them according to the transmitted code. Vendor-supplied routines estimate power spectra for each range gate from the time series of demodulated samples, and average these spectra for a specified integration period. At the end of this period, the time-averaged spectra are written to disc as formatted data records for real-time graphic display and subsequent off-line processing.

(b) Transmitter Modulation and Receiver Details

Table 1 lists the phase codes selectable for ST observations. Codes A, A1, B, and B1 are complementary codes having desirable sidelobe properties as described in the introduction. Codes C, D, and E have low correlation sidelobes. Selection of the code and its baud length is via computer control, through the CAMAC interface to the coded pulse generator (CPG). Each code's bit pattern is stored in PROMs in the CPG whose output is hardwired to the 30-MHz radar exciter. On initiation of the transmitted pulse, the selected code is clocked serially out to the exciter, where the 30-MHz phase is modulated. The clock rate (and thus the baud length) is determined by the CPG clock, which may have a period from 1.0 μs to 3.2 μs, in increments of 200 ns. The modulated 30-MHz signal is upconverted to 440 MHz and applied to the driver amplifier.

The complex envelope of the backscattered signal is received at a low-noise parametric amplifier, down converted to 30 MHz IF, bandlimited, and quadrature detected in a linear detector. The detected complex signal is digitized by a pair of 12-bit A/D converters, sampled at a programmable rate corresponding to the baud length, and transferred to the signal processor (array processor).

Figure 2 shows details of the Radar Timing Control. The CAMAC timers output 14 pulses for gating the transmitter, receiver and a calibrated noise source, and for data input to the array processor. Two banks of registers contain setpoints for the timers and the CPG; only one bank can control the radar at any one time, leaving the other free to receive new setpoints. After the new values are written and verified, the Bank Select Logic will switch register banks to select the new mode. All operations are under program control; to avoid timing errors, the setpoints are calculated in advance from input parameters during program initiation and verified for consistency.

(c) Signal Processing Details

All processing of the real and imaginary digitized radar samples is performed in the AP-120B array processor in real time. The inputs to the AP are raw digitized samples; one complex sample per range gate plus additional samples for decoding are input each radar sweep. The outputs of the AP to the host computer are time-averaged power spectra, (square of the complex DFT of a time series), one for each range gate. Processing in the AP may be subdivided into pre-processing (coherent integration and decoding) and spectral estimation (calculation of power spectra). Figure 3 is a diagram of the software implementation.

The AP contains a programmable I/O processor (GPIOP) which receives the

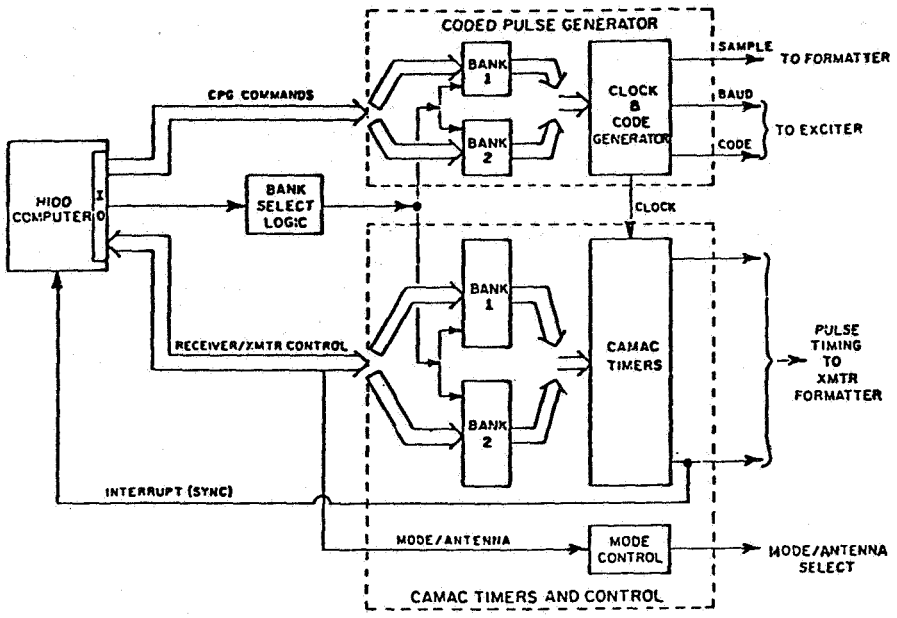


Figure 2. Radar control details showing control paths between H100 computer and radar transmitter and receiver. Clock rates for input samples and for baud length are output by CPG; timing pulses are output by CAMAC timers, and ancillary functions are selected by mode control.

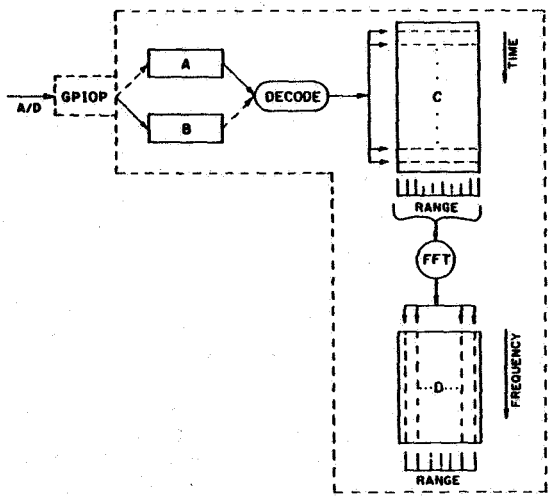


Figure 3. Signal processing.

digitized complex samples from a locally built "formatter" module in response to interrupts from the radar timers. As received, the 2 12-bit integers are packed into a 32-bit word. The GPIOP processor unpacks the samples and converts the integers to 38-bit AP floating point numbers. These are then transferred to input buffers in AP main memory; a separate processor in the GPIOP controls the word count and buffer addresses. Samples are pre-processed in blocks of 4 radar sweeps, in order to provide adequate time to decode. Two AP memory input buffers are defined (A and B in Figure 3), and pre-processing proceeds in parallel with input, in a double-buffered mode. The GPIOP fills one input buffer with samples from 4 consecutive radar sweeps. During this time, the AP: (1) integrates the samples in the other buffer, (2) decodes the resulting 2 sweeps of samples according to the appropriate complementary code, (3) adds the resulting decoded sweeps of samples to cancel their autocorrelation sidelobes, and (4) transfers the result to intermediate buffer C. This process presume and decodes 4 sweeps of data, with one set of samples as a result. If additional coherent integration (modulo 4) is specified, the transfer process ("4" above) sums the results to previous samples in buffer C. The pre-processing then switches to the other input buffer, and continues until buffer C has been filled.

Pre-processing in this manner requires considerable computation speed, and is beyond the capabilities of a general purpose computer. For this reason, previous phase-coded implementations have used a hardware correlator to decode the radar samples. The computational speed of the AP microcode has allowed us to eliminate the need for a hardware correlator; an additional benefit is the flexibility of the processor to operate in various modes of signal processing. The 6-MHz rate of computations and the fact that decoding is simply a one-bit-multi-bit correlation allows these processes to be carried out in real time for the codes used and for a sufficient number of signal heights. Although the AP cannot process as fast as hardware decoders, it is adequate for the number of heights required for typical ST observations. The typical interpulse period used at Millstone Hill is 2 ms, leaving 4x2 ms = 8 ms for the AP to complete its tasks. Table 2a gives some timing limitations of the pre-processor. These limits depend only on the specific code and the number of ranges specified, and are independent of the number of coherent integrations or the number of spectral points. These are timing limits for the pre-processor only. More stringent limits are imposed by the memory size (32 k at present) of the AP, and Table 2b gives some overall limits of the processor with this memory configuration. Efforts are presently underway to increase the memory size to 64 k, and the limits for this configuration are also listed in the table.

Following the pre-processing of a specified number of radar sweeps to fill buffer C, input is suspended and power spectra are estimated for each range. A vendor-supplied FFT routine computes a complex DFT, which is then squared and summed to previous spectra in output buffer D. Total power and dc levels are also calculated and stored in buffer D. Input of samples is then resumed, and the process repeats for a specified number of cycles. Note that although samples are input in a double buffered mode, the overall processor runs single buffered. This leads to a "dead time", when input is suspended, of ~1-2% of the total integration time for typical experimental parameters.

At the end of the integration period, the processor halts and the time-averaged spectra, power and dc levels are transferred to the host computer and written to disc as formatted data records for subsequent tape storage and off-line processing. If desired, the raw spectra and simply processed spectra may be displayed on a fast vector display in real time. The host computer downloads the next set of experimental parameters to the radar system, and processing resumes. The flexibility and rapid switching capabilities of the system allow one observation to differ in any or all aspects from the previous one. In particular, the start range can be changed to the last range observed in the

Table 2a. Pre-processing limits imposed by AP computation speed

| CODE | NUMBER OF RANGES |
|---|---|
| 16-bit complementary | 450 |
| 32-bit complementary | 250 |

Table 2b. Processing limits imposed by AP memory size

| SPECTRUM LENGTH | NUMBER OF RANGES 32k Memory | 64k Memory |
|---|---|---|
| 32 | 340 | 681* |
| 256 | 38 | 84 |
| 512 | 18 | 42 |
| 4096 | 1 | 5 |

*Although this exceeds the number of ranges given in Table 2a, a minor software change can permit such operation. In this case, the number of coherent integration must be a multiple of 8 rather than 4.

previous record, to compensate for the height limitation imposed by AP memory size. At a sacrifice in time resolution, heights from ~8 to 30 km can be scanned in short order, typically 3-4 minutes. As explained in the next section, the smearing of FFT processing can be reduced by increasing the time series, and spectra with 512 FFT points are typically used at Millstone Hill. The 32-k memory size of the AP restricts the number of ranges to 17 (plus 1 noise range). Using 300 m resolution, about 5 km of range can be observed simultaneously, and a radial velocity resolution of ~4 cm/sec is obtained. To cover the total range of ~20 km (from 8 to 28 km) four successive records will suffice. An integration time of ~40 sec per record provides a good SNR, yielding a cycle time of ~3.5 minutes.

(d) System Tests

A series of tests were conducted to estimate the overall system performance for the complementary code mode of observations. The method employed was to inject a coded 440-MHz signal into the receiver, and then run the data collection program as in an actual experiment. The code was synchronized with the radar sweep interrupt (TO) and repeated continuously along the time base. A complementary code and its partner were interchanged as in an actual experiment. This technique exercises all receiver and processing components: IF mixing, sampling, bandlimiting, signal processing, formatting, range tags, etc. In the absence of noise, and with complete sidelobe cancellation, a strong power peak will appear at zero frequency every N-th range gate for an N-element code. The first peak will occur at an integral multiple of (NxBaud) microseconds after TO. For a perfectly matched input filter, no spillover of power to adjoining range gates will occur. Furthermore, the peak at zero frequency will be very narrow in frequency, and no signal will be present in other frequency bins.

In practice, the sharpness of the peak and its amplitude above the noise will give a measure of system performance. Figure 4 is an example of such a

test. Here, a 16-bit complementary code was used; eight coherent integrations were employed, yielding a frequency bandwidth of 60 Hz (18 m/s), and 512-point power spectra were estimated at 18 range gates (the top spectrum is the noise gate). The log of the raw spectra is shown on the left; the right plot is a log plot of the relative power at each range. Frequency resolution here is ~.11 Hz (velocity resolution ~3.3 cm/sec). The sharp peak at one range gate, with an amplitude ~25 dB above the noise, indicates good performance. This peak reappears every 16 range gates as the receiver window is moved along the time base.

## OBSERVATIONS USING COMPLEMENTARY CODES

The received signal from ST observations at Millstone Hill comprises ground clutter, system noise, interference, and atmospheric signal. The ranges of interest are severely contaminated by ground clutter, with power levels often 60 dB above the signal. If this clutter were confined to a single (zero) frequency, it could easily be removed and spectral moments estimated after filtering interference and noise. However, the clutter is fading clutter, with a finite width about zero frequency. This effect is exacerbated by the "spill-over" effect of FFT processing, and complicates spectral moment estimation, especially when the atmospheric signal has a small Doppler shift. At Arecibo Observatory (SATO and WOODMAN, 1982b) this effect is handled by a nonlinear least squares fit of a parameterized function which includes the clutter. At Millstone, the clutter is much more intense than at Arecibo, due to the lack of natural sheilding. Although a fitting technique will be employed to estimate moments, this task is simplified by computing spectra from long time series, thus collapsing the clutter to nearly its intrinsic width. If the number of spectral points is increased to 2048 or 4096, the clutter width is extremely narrow, and signals with very small Doppler shifts can be clearly identified (WAND et al., 1983). However, due to limited AP memory size, a compromise must be made, since the number of range gates that may be observed decreases with increased in spectral length (see Table 2b). A spectral length of 512 points yields a fairly narrow clutter width, and 17 signal ranges plus 1 noise range may be observed at present (32k AP memory). With a baud length of 2 μs (300 m

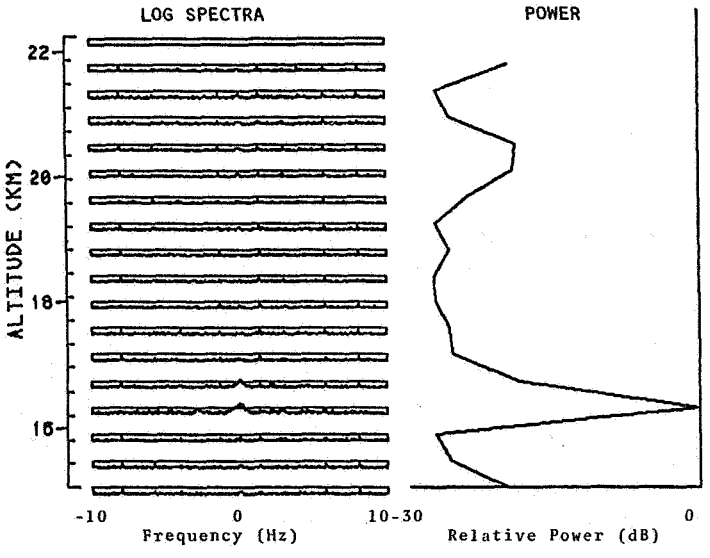


Figure 4. Test signal. (See text for details.)

resolution), a total range of ~5 km is covered at once. This alone is insufficient for ST observations, which should cover the altitude range of ~8-~30 km. This can be rectified, at a sacrifice in time resolution, by moving the start range to successively higher altitudes for 3 to 4 successive records. (Alternatively, the AP memory size may be increased to 128k, giving adequate storage for the full ST range.)

Figure 5 shows the raw spectra for such an experiment. Here, 3 successive records are merged, with altitude coverage from 12 to 29 km and altitude resolution of 300 m. Twelve of the 51 signal ranges are shown. Each spectral plot is a superposition of 6 observations, so that a total of 18 integration periods is represented. The variance of the signal seen in these plots is a measure of the variability of turbulence at each height over this period of ~1 hour. The frequency bandwidth is 20 Hz, velocity bandwidth 6 m/s, and velocity resolution ~1.5 cm/sec. Signals can clearly be seen up to 20 km, and again at 24-25 km altitude. The clutter still has a wide frequency spread, even with a 512-point power spectra, but is manageable and appears to be a good candidate for removal using fitting techniques.

Figure 6 shows a 30-hour time series of 2 selected heights from a similar experiment. These spectra were gathered on the steerable antenna at 5.8 deg from the zenith. The frequency bandwidth was increased to 60 Hz (18 m/s), and velocity resolution ~3 cm/sec. Atmospheric returns are seen with varying intensity and frequency (radial velocity) throughout this period.

## SUMMARY

A phase-coded mode of ST observations has been successfully implemented at Millstone Hill, using a programmable array processor to perform signal processing in real time. Its capabilities are sufficient to gather spectral observations over an altitude range of 20 km in some 3-4 minutes, with a spatial resolution of 300 m and radial velocity resolution of ~2 cm/sec. Atmospheric returns from the UHF radar are observed up to 25 km.

## ACKNOWLEDGEMENTS

The author gratefully acknowledges many useful discussions with, and suggestions from Dr. P. K. Rastogi. His conceptual advice was essential to the many modifications required for this implementation. The efforts of Messrs. P. M. Chizinski, W. A. Reid, R. Murcek, E. U. Gallardo, and R. R. Norander were essential to the successful implementation of all necessary hardware interfaces, and their work is greatly appreciated and acknowledged. The overall guidance by Dr. J. V. Evans was invaluable to the completion of this work. This work was supported by the National Science Foundation under grant ATM-80-00060.

## REFERENCES

Balsley, B. B. (1981), MST techniques - A brief review, J. Atmos. Terr. Phys., 43, 495-509.

Holt, J. M., J. V. Evans, W. L. Oliver and R. H. Wand (1980), The upgraded Millstone Hill radar, Radio Science (in press).

Rastogi, P. K. (1981), Radar studies of gravity waves and tides in the middle atmosphere: A review, J. Atmos. Terr. Phys., 43, 511-524.

Rottger, J. (1981), Investigations of lower and middle atmosphere dynamics with spaced antenna drifts radars, J. Atmos. Terr. Phys., 43, 277-292.

Sato, T. and S. Fukao (1982), Altitude smearing due to instrumental resolution

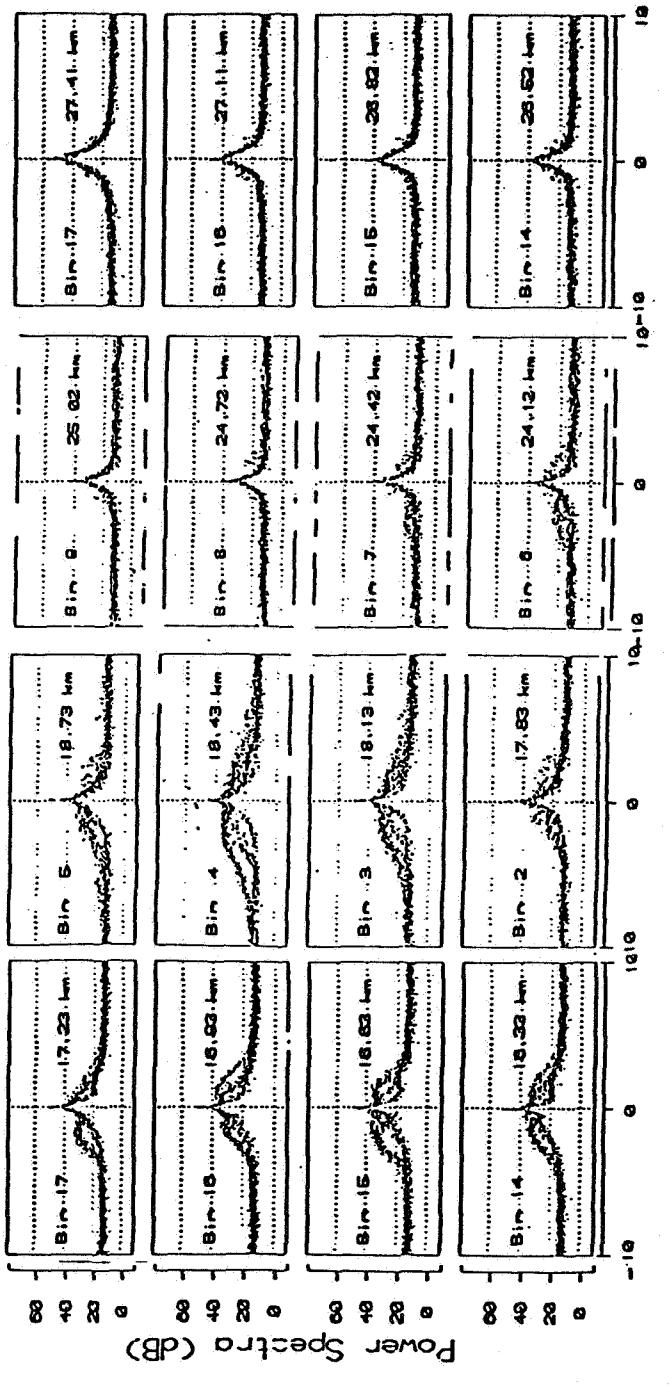


Figure 5. Raw spectra observed using complementary codes. Altitude coverage was 12 to 29 km, 300 m resolution. About 1/4 of the ranges are shown.

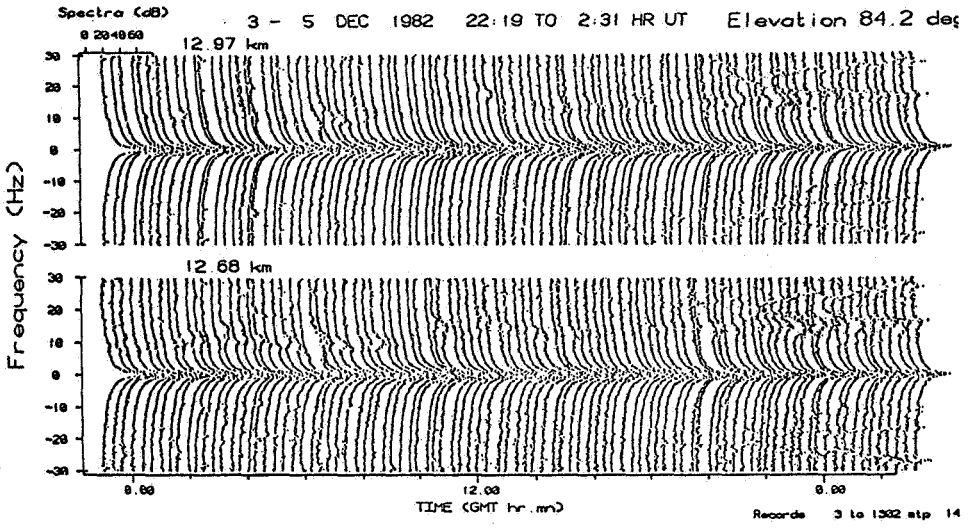


Figure 6. Time series of spectra. A 30-hour time series of phase-coded observations. Spectra at 2 heights are shown. Height resolution is 300 m, velocity resolution is 1.5 cm/sec.

in MST radar measurements, Geophys. Res. Lett., 9, 72-75.

Sato, T. and R. F. Woodman (1982a), Fine altitude resolution observations of stratospheric turbulent layers by the Arecibo 430 MHz radar, J. Atmos. Sci., 39, 2546-2552.

Sato, T. and R. F. Woodman (1982b), Spectral parameter estimation of CAT radar echoes in the presence of fading clutter, Radio Sci., 17, 817-826.

Schmidt, G., R. Ruster and P. Czechowsky (1979), Complementary codes and digital filtering for detection of weak UHF radar signals from the mesosphere, IEEE Trans. Geosci. El., GE-17, 154-161.

Turyn, R. (1968), Sequences with small correlation, in Error Correcting Codes, ed. H. Mann, 195-228, J. Wiley, New York.

Wand, R. H., P. K. Rastogi, B. J. Watkins and G. B. Loriot (1983), Fine Doppler-resolution observations of thin turbulence structures in the tropo-stratosphere at Millstone Hill, J. Geophys. Res. (in press).

Watkins, B. J. and R. H. Wand (1981), Observations of clear air turbulence and winds with the Millstone Hill radar, J. Geophys. Res., 86, 9605-9611.

Woodman, R. F. (1980), High-altitude-resolution stratospheric measurements with the Arecibo 430 MHz radar, Radio Sci., 15, 417-422.

Woodman, R. F., R. P. Kugel and J. Rottger (1980), A coherent integrator-decoder for the SOUSY-VHF radar, Radio Sci., 15, 233-242.

# 8.3A COHERENT INTEGRATION

D. T. Farley

School of Electrical Engineering
Cornell University
Ithaca, NY 14853

Coherent integration is essentially a digital filtering process and was first applied to MST radar observations by WOODMAN and GUILLEN (1974). It is simple to implement with either hardware or software and is appropriate for the very narrow band (in a sense; see below) signals usually received by MST radars. By filtering the signal before performing spectral processing, the computations required for FFT or similar analysis are greatly reduced. Coherent integration does not increase the signal-to-noise ratio per unit bandwidth in the signal band; it simply filters out much of the wideband noise, something that could also be done (slightly better, in fact, but at far greater cost) by full FFT processing of the raw signal.

A pulsed MST radar samples many altitudes at the interpulse period (IPP), giving a matrix (say) of sample voltages $V(h_i,t_j)$. The samples from differing $h_i$'s are uncorrelated, but those from the same $h_i$ but different $t_j$'s are correlated; the correlation time of the fluctuations in the atmosphere responsible for the scattering may be as long as a substantial fraction of a second. In contrast, the bandwidth of the raw signal entering the receiver is large (e.g. about 1 MHz for the 1 μs pulse required to achieve an altitude resolution of 150 m). It is this mismatch between the 1-MHz-wide raw signal and the few Hz-wide scattering process (i.e., the signal bandwidth that would be measured by a bistatic CW radar) that the coherent integration (digital filtering) process partially corrects.

In the MST radar literature, at least, coherent integration has come to mean replacing N consecutive voltage samples from a given altitude with their sum, i.e.,

$$W(h_i,t_k) = \sum_{j=k}^{k+N} V(h_i,t_j)$$

Subsequent analysis is done on the Ws. The number of samples which need to be processed and/or stored is thereby reduced by the factor N, a number which is typically between ten and a few hundred. In other words, most of the operations required in full FFT processing are replaced by simple additions, which can be done very rapidly by special purpose hardware if desired.

To analyze what coherent integration actually does to the signal, it is simplest to consider it to be made up of two separate operations: (1) filtering via a running average (a filter with a unit impulse response of duration T), followed by (2) sampling at intervals T, where T is N times the IPP. This interval represents a drastic undersampling of the original wideband signal.

The first operation multiples the voltage spectrum of the original signal by sinX/X, where $X = \pi fT$ and f is the frequency in Hz. The second operation leads to frequency aliasing with a window $-1/2T \leq f \leq 1/2T$; i.e., signals at the frequencies f and $f + n/T$, where n is any integer, are summed together. (This aliasing is in addition to the aliasing introduced by the initial sampling at the IPP.) The combination of these two processes has a few features which may be worth noting here.

(1) Since the filtering function has nulls at $f = \pm n/T$, the zero frequency (dc) point in the final aliased spectrum is the true dc component, with no aliased contributions.

(2) The square of the filter function falls to 0.5 for $f = \pm 0.44/T$.

(3) The first two 'sidelobe' maxima in the filter function at $f = \pm 1.5/T$, $\pm 2.5/T$ are at -13.5 dB and -17.9 dB, respectively.

(4) The combined filtering and aliasing process is such that a spectrum which is flat before coherent integration will still be flat afterwards; i.e., white noise emerges as still white.

In practice, the desired signal in the time series usually changes quite slowly, with a maximum frequency component, say, of $f_{max}$, and N is chosen so that $f_{max} << 1/T$. Then coherent integration increases the apparent signal-to-noise ratio by a factor N, essentially because all but one Nth of the original wideband noise is filtered out. And, to reiterate, exactly the same result would be achieved (but at greater cost) by Fourier transforming the original unintegrated signal, retaining only the interesting part.

One final point: Since coherent integration preserves phase information, it can be interchanged with pulse decoding. So when phase coding is used for pulse compression, the decoding can be done after integration, reducing the number of operations required by a factor of N.

REFERENCE

Woodman, R. F. and A. Guillen (1974), Radar observations of winds and turbulence in the stratosphere and mesosphere, J. Atmos. Sci., 31, 493-505.

# 8.3B A NOTE ON THE USE OF COHERENT INTEGRATION IN PERIODOGRAM ANALYSIS OF MST RADAR SIGNALS

P. K. Rastogi

Haystack Observatory
Massachusetts Institute of Technology
Westford, MA 01886

## ABSTRACT

The effect of coherent-integration on the periodogram method of estimating the power spectra of MST radar signals is examined. The spectrum estimate usually is biased, even when care is taken to reduce the aliasing effects. Due to this bias, the signal power for Doppler shifted signals is underestimated by as much as 4 dB. The use of coherent integration in reducing the effect of aliased power-line harmonics is pointed out.

## INTRODUCTION

In experiments used to probe the atmosphere with sensitive high power radars, the autocovariance functions (ACF) or power spectra of atmospheric returns are estimated by a processor. Coherent integration is a technique that reduces the data input rate to the processor without unduly distorting the information-bearing part of the returns. In experiments that use phase codes and decoding to obtain a fine range resolution, it is possible to cut down on computations in the processor by relegating the decoding operation till after coherent integration. The use of coherent integration has been discussed for ACF processing by WOODMAN and GUILLEN (1974), and SCHMIDT et al. (1979). Discrete Fourier transform (DFT) methods, especially for estimation of power spectra as time-averaged periodograms (OPPENHEIM and SCHAFER, 1975; COOLEY et al., 1979), increasingly are being used in atmospheric radar experiments (GAGE and BALSLEY, 1978; WOODMAN, 1980; BALSLEY, 1981). In this note, the use of coherent integration in periodogram analysis of MST radar signals is examined.

## SPECTRAL WINDOW AND ALIASING

Let $z(t)$ be the complex signal after coherent demodulation for a given range. Samples of $z(t)$ are input at discrete intervals T, usually the pulse repetition interval (PRI), to the processor. The processor can handle only a finite number N of samples for each range. For these samples the processor obtains first their N-point DFT $Z(f)$, and then estimates the power spectrum $S(f)$ of the atmospheric returns as the time-averaged periodogram

$$P(f) = \langle Z(f)\, Z^*(f) \rangle \tag{1}$$

The periodogram estimate is obtained over the frequency range (-F,F), where $F = 1/2T$, at N points with a frequency resolution $1/TN$. At each point in the above range $P(f)$ is obtained as a discrete convolution of $S(f)$ with the standard periodogram window $H(f)$ (COOLEY et al., 1979).

$$H(f) = \frac{1}{N} \{\sin(\pi fN)/\sin(\pi f)\}^2 \tag{2}$$

For large N, $H(f)$ approximates a delta function. For modest values of N, however, smearing of a strong undesirable feature such as the ground clutter can mask the atmospheric signal. Components of $S(f)$ outside the range (-F,F) are aliased or folded-in. For most MST radar experiments, this range is considerably wider than a baseband containing features of interest in $S(f)$. With coherent integration of $z(t)$ over several radar sweeps, it is possible to reduce the frequency range and to improve the frequency resolution.

With coherent integration, M successive samples of z(t) are accumulated and it is these accumulated samples that are fed to the processor. Thus coherent integration is equivalent to first obtaining a process g(t) that is the moving average of z(t).

$$g(kT) = \frac{1}{M} \sum_{m=0}^{m=M-1} z(kT - mT) \tag{3}$$

and then coarsely sampling g(t) at multiples of MT. The processor now obtains the time-averaged periodogram from N-point sequences of samples of g(t), in the way outlined above for z(t).

The effect of the moving average operation in (3) is to weight S(f) with a frequency window

$$G(f) = \frac{\sin^2 (\pi\ f\ T\ M)}{M^2 \sin^2 (\pi\ f\ T)} \tag{4}$$

This window is a comb function (SCHMIDT et al., 1979) with maxima at multiples of 1/T. Between any two maxima there are M-1 minima with zero weight at multiples of 1/MT. Due to sample time MT, the basic frequency range is now (-F/M, F/M), sampled at N points with a frequency resolution 2F/MN. Th components outside this range are weighted by G(f) and aliased. To reduce undesired effects of this aliasing it is necessary to ensure that the expected Doppler shifts of the atmospheric returns remain smaller than F/M.

## DISCUSSION

The behavior of the frequency window G and the folded parts is illustrated for two values of M in Figure 1. The frequency axis is normalized as fTM. The parts of S(f) outside the normalized range (-0.5,+0.5) are aliased.

When care is taken to avoid the aliasing effect discussed above, the averaged periodogram provides a reasonable estimate of the signal spectrum S(f). Over the basic window (-F/M, F/M), these estimates are still biased by the window G(f). Usually the Doppler-shifted returns have a bandwidth small compared to the folding frequency F/M. The effect of frequency weighting is therefore negligible on the estimates of Doppler shift and spectral width. The signal power, however, depends on the Doppler shift. Figure 2 shows the bias in signal power as a function of the normalized frequency fTM. For unaliased signals this bias may cause the signal power to be underestimated by as much as 4 dB. For signals that are aliased only once, a Doppler profile can usually be constructed, but the signal power is underestimated by an even larger amount.

In most radar experiments, the computational advantage with the use of coherent integration outweighs the small bias in the spectrum estimates. In some experiments, however, this bias can be critical. This is especially true of the aspect-sensitivity experiments (GAGE and GREEN, 1978; FUKAO et al., 1980) that have been used to detect enhanced specular reflection at quasi-vertical incidence. Unless the Doppler shifts are small compared to F/M, a 2-4 dB reduction of signal power estimates for off-vertical echoes is expected as a result of this bias alone.

The occurrence of nulls in the part of the spectrum that is folded can be used to reduce the contribution of the aliased power-line harmonics. When the number M of coherently integrated samples is large, both M and the PRI T can be adjusted to ensure that the power-line harmonic frequencies coincide with (or are close to) the nulls in G(f).

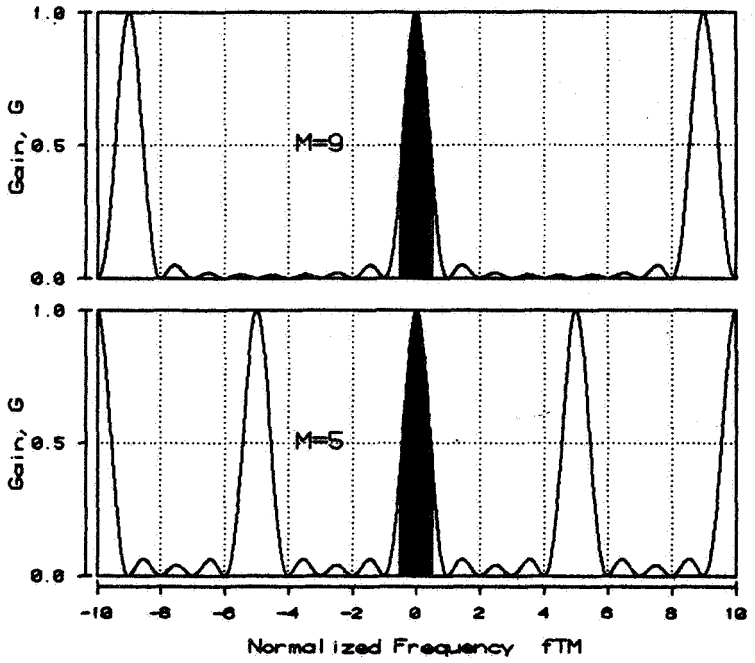


Figure 1. Gain of the frequency window G due to coherent integration over M samples as a function of the normalized frequency fMT, where T is the sampling rate. The frequency components outside (-0.5,+0.5) are folded in.

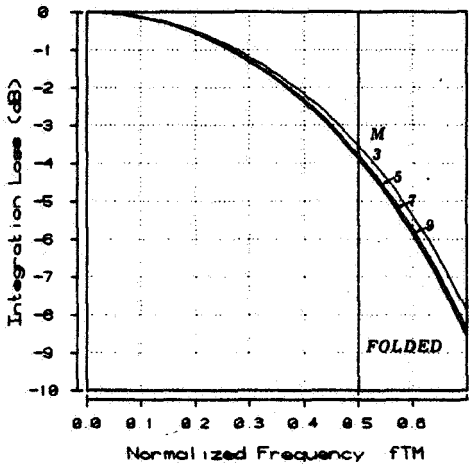


Figure 2. Periodogram bias due to coherent integration as a function of the normalized frequency fMT for different values of M.

ACKNOWLEDGEMENT

This material is based on work supported by the National Science Foundation under grant number ATM-8000060.

REFERENCES

Balsley, B. (1981), The MST technique - A brief review, J. Atmos. Terr. Phys., 43, 495-509.

Cooley, J. W., P. A. W. Lewis and P. D. Welch (1977), The fast Fourier transform and its application to time series analysis, in Statistical Methods for Digital Computers, Ed. by K. Enslein, A. Ralston and H. S. Wilf, J. Wiley and Sons, New York, 377-423.

Fukao, S., T. Sato, R. M. Harper and S. Kato (1980), Radio wave scattering from the tropical mesosphere observed with the Jicamarca radar, Radio Sci., 15, 447-457.

Gage, K. S. and B. Balsley (1978), Doppler radar probing of the clear atmosphere, Bull. Am. Meteorol. Soc., 59, 1074-1093.

Gage, K. S. and J. L. Green (1978), Evidence for specular reflection from monostatic VHF radar observations of the stratosphere, Radio Sci., 6, 991-1001.

Oppenheim, A. V. and R. S. Schafer (1975), Digital Signal Processing, Prentice-Hall, Englewood Cliffs, 585.

Schmidt, G., R. Ruster and P. Czechowsky (1979), Complementary code and digital filtering for detection of weak VHF radar signals from the mesosphere, IEEE Trans. Geosci. El., GE-17, 154-161.

Woodman, R. F. (1980), High altitude resolution stratospheric measurements with the Arecibo 430 MHz radar, Radio Sci., 15, 417-422.

Woodman, R. F. and A. Guillen (1974), Radar observations of winds and turbulence in the stratosphere and mesosphere, J. Atmos. Sci., 31, 493-505.

# 8.3C SIGNAL PROCESSOR ARCHITECTURE FOR BACKSCATTER RADARS

W. E. Swartz and P. Johnston*

*School of Electrical Engineering, Cornell University, Ithaca, NY 14843
**NOAA, Poker Flat MST Radar, P. O. Box 80128, College, AK 99708-0128

## ABSTRACT

Real-time signal processing for backscatter radars requires enormous computational throughput and I/O rates; however, the operations that are usually performed in real time are highly repetitive simple accumulations of samples or of products of samples. Furthermore, since the control logic does not depend on the values of the data, general-purpose computers are not required for the initial high-speed processing. The implications of these facts on the architectures of preprocessors for backscatter radars are explored and applied to the design of the Radar Signal Compender.

The Radar Signal Compender is a programmable high-speed pipelined real-time multiprocessor machine intended for coherent and incoherent backscatter radars. Its architecture lends itself to time-critical processing where the operations performed are only the direct accumulations of samples or the accumulations of products of the original samples. The programmability of this machine allows it to be adapted to a wide range of experiments, yet without the difficulty usually found with more general-purpose array processors. The Compender is composed of several Functional Modules which parallel process multiple data streams, a Master Control Module which provides for timing and communication between the host computer and each of the Functional Modules, and an Analog-to-Digital Conversion Module which feeds samples directly into the input memories of the Functional Modules under the control of external timing logic. Each of the Functional Modules can be individually programmed under the control of the Host Computer and the Master Control Module. Control of each of the data-processing pipelines is nearly transparent to the user, in that, control operands are tagged to the sample address operands and then follow the processing through a control pipeline for use at the proper stage. Input and output memories are fully double buffered for most usual configurations, and all memories are 2 k words deep. The four input memories of each Functional Module are 16 bits wide, while the four output memories are each 32 bits wide and can be configured as two 64-bit wide memories.

Programming the device consists of the loading of the configuration registers and the address control RAMs of each Functional Module using simple directives to the Master Control. The configuration registers establish the data flow paths that are uniquely determined for a given experiment. The address control RAMs consist of BASE plus DISPLACEMENT operands with flexible incrementing and looping control.

A Compender with 10 Functional Modules and high-speed memories should be capable of a throughput of 100 MHz for multiply-replace-add sequences. The more modest version for the Poker Flat MST radar with 6 Functional Modules and slower memories achieves a 30-MHz throughput.

## INTRODUCTION

Since the signals received from backscatter radars are noise like, the basic requirement of the processing hardware is to average as many samples as possible in as short a time as possible. For some experiments, the computational limitations restrict only the amount or quality of the real-time displays that can be generated. For others the limitations is a trade-off between what can be done in real-time versus what must be done off-line. Yet

for many experiments, the actual science in terms of height resolution, time resolution, number of heights, bias corrections, or dynamic interaction is limited by insuggicient compute power.

The most popular atmospheric backscatter radar experiments can be split between four major headings, as shown in Table 1. Since the correlation times of the medium being probed under each of the headings differ from one another, various transmitter pulse and receiver sampling schemes are used to optimize a given experiment. However, in every case the initial real-time fast processing is a highly redundant sequence of additions of samples or of products of samples. The bottom two lines give a comparison of the computational requirements in terms of the rate of multiply-replace-add operations. It is obvious that even state-of-art general-purpose array processors with single multipiliers and adders cannot keep up for experiments requiring rates of more than just a few Megahertz. Remember too that commercial array processors use floating-point formats, yet integer arithmetic is sufficient provided the data paths are wide enough to avoid truncation of the summations. Floating-point formats can lead to subtle biases and just the conversion from the integer outputs of the analog-to-digital converters can be a bottleneck within the processor. Integer logic is simpler and faster; hence, it should be preferred for the preprocessors used with backscatter radars.

Table 1. Signal processing requirements

| | MST | E REGION | F REGION | PROTONOSPHERE |
|---|---|---|---|---|
| Interpulse period (msec) | 0.5-1.0 | 2-10 | 10-15 | 40 |
| Pulse Width (μsec) | 0.1-4.0 | 2-4 | 4-300 | 1000 |
| Number of Pulses per IPP | 1 | 1-7 | 1-7 | 1 |
| Coding | Various | Possibly Barker | Not Usually | No |
| Number of Bauds | 1-256 | 7-13 | 13 | |
| Sampling Rate (MHz) | 1-20 | 0.25-0.5 | 0.05-0.5 | 0.5 |
| Number of Complex Products per Sample (1) | 1 | 1 | 1-50 | 400 |
| Number of Lags | | 10-20 | 10-100 | 30 (60 if ACF is formed at IF) |
| Number of Heights | 200-2000 | 20-600 | 20-1000 | 20 minimum |
| Rate for Multiply-Replace-Adds (MHz) | 100-1000(2)<br>0.2-100 (2) | 4-50<br>0.04-1.3 | 100<br>0.06-3 | 200 (3)<br>20 (4) |

NOTES: (1) Multiple products are independent only when signal to noise is low. The number of real products is four times the number of complex products given.
(2) Rate for additions only -- multiplies not required at this level.
(3) Rate for unbuffered case.
(4) Rate for double buffered case.

The order (i.e., addressing) of the samples sent to the processor and the ordering of the processed data output to the host computer can be very simple. In fact, there is never any need for the addressing of these two transfers to be anything but sequential. For experiments requiring pulse decoding or multiple lag products, the addresses of samples being supplied to the processing stages are still highly repetitive, but not completely sequential; more will be said about this later.

## FUNCTIONAL OVERVIEW

With these ideas in mind, one can easily write a block diagram showing the data flow for a simple signal processing example where the samples are simply accumulated before being passed on to the host computer. This has been done in Figure 1. The addressing of the Output Memory at this level can be assumed to be as flexible as required by a given experiment. Since there is no input buffer to temporarily store the samples, each accumulation must be accomplished within the sample interval. If the same sample is used for several accumulations (a very typical situation), then the time needed for multiple fetches and stores to the memory, plus the time for the accumulations, soon exceed the sample interval time, even for the fastest logic available. Many such units could be paralleled together, but one immediately realizes that typical radar applications have a significant amount of time between the end of one sample raster and the start of the next raster. The addition of a buffer memory between the ADC and the accumulator would then allow this extra time to be utilized, at least partially.

With a single memory between the ADCs and the accumulator, the next bottleneck arises when the ADC wants to write a sample to the memory at the same time as the accumulator wants to read some other sample. This would be the situation in general-purpose processors even with double buffering. (All that double buffering alleviates is the problem of guaranteeing the validity of the data before it is over-written with the next sampling sequence, assuming that the processing keeps up.) This bottleneck can only be eliminated by the use of two independent input buffers, where one can be written, while the other is being read. This configuration is illustrated in Figure 2. If the addressing of the two buffers is also independent, then sampling can proceed at the maximum rate allowed by the memory with no need to wait for the multiple memory accesses that may be required for processing.

Finally, Figure 3 illustrates the data paths required for maximum throughput when a multiplier is inserted within the data process stream. Note that this case shows four Data Input Buffers. Four buffers are needed, even for the case where the samples loaded into each memory are the same, but where the multiplications are formed between samples taken at different times (e.g., for a lag product of an autocorrelation function). These four buffers should be considered as two independent double buffers, each supplying one of the multiplicands. In this way, only one memory fetch is needed from each of two memories for each multiplication. Of course, this assumes that the memory fetch time is comparable to the multiply time, which, in practice with current technology, turns out to be true. (If the memories were twice as fast as the multiplier, so that a double fetch could be accomplished in one cycle, then only two memories would be needed.)

The Radar Signal Compender is composed of several Functional Modules (FMs), a Master Controller (MC), an Analog to Digital Conversion module (ADC), and suitable interfacing to a host computer, as shown in Figure 4. Data from the ADC is fed directly to the FMs which perform the data processing. In order to provide flexibility, the host computer can separately program each FM. Programming includes the setting of the Configuration Register (which specifies which data processing paths are to be used, thereby, determining the data word

BLOCK DIAGRAM FOR BASIC SIGNAL PROCESSING

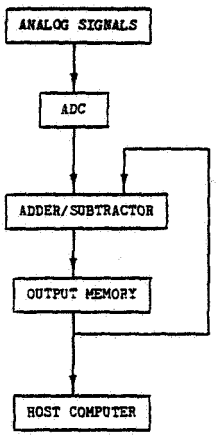


Figure 1.

BLOCK DIAGRAM FOR IMPROVED SIGNAL PROCESSING SPEED

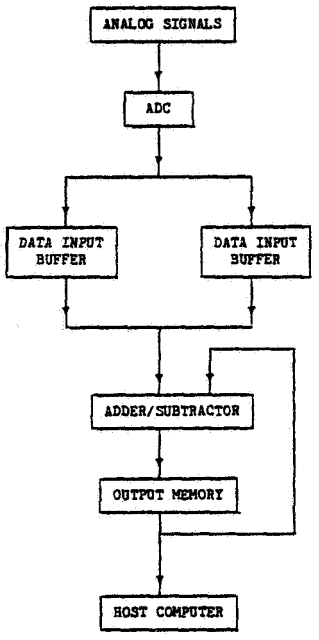


Figure 2.

size and whether or not the multiplier is to be by-passed) and includes the loading of the operands that control the addressing of the Data Input Buffers on the FMs. The latter is described, in detail, in a later section.

Data flow within one of the FMs is generally as illustrated in Figure 2 or 3 where each block may represent several stages in the pipeline. The processing pipeline is actually 9 or 7 stages long and uses either 23 or 18 cycles of the master clock, depending on whether the multiplier is used or by-passed, respectively. New data can be stuffed into the pipeline every 5 cycles of the master clock. The data paths can be up to 64 bits wide, or split up into as many as four 16-bit-wide paths for multiple independent parallel processing within each Functional Module. This feature is particularly useful in MST work where the extra guard bits are not needed. The Poker Flat MST radar will use the dual 32-bit-wide path configuration, while the incoherent-scatter applications use either the 48-bit or 64-bit configurations. For each configuration, the carry bits are appropriately propagated and any overflow conditions flagged.

The Functional Modules have been wired on 11" x 16" boards using a semi-automatic wire-wrapping service. Most of the 200-plus ICs on each FM either carry data or are part of one of the address busses. Since little space was left, much of the combinational logic required to control the FMs was placed in various PAL (Programmable Array Logic) circuits that must be specially programmed for the RSC.

An additional feature that had high priority in the design was the provision for automatic test features. Each of the memories (including the Data Input Buffers, the Base and Displacement Operand Memories, and the Output Data

BLOCK DIAGRAM FOR MORE GENERALIZED SIGNAL PROCESSING

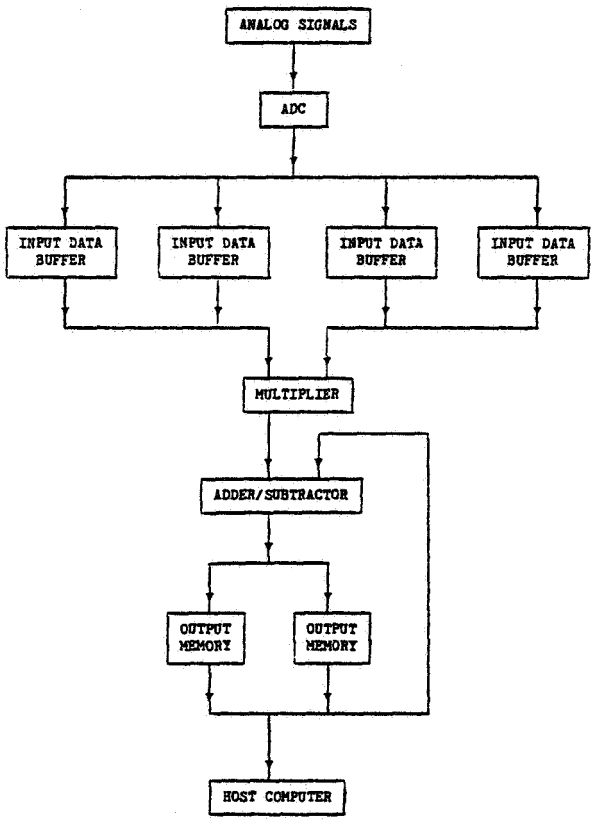


Figure 3.

Memories) can be loaded with test data from the host or MC and then read back out again to check memory and data buss integrity. Also, the multiphase clock can be single stepped to allow probing each stage of the pipeline.

The Master Control modules are somewhat dependent on the host to be used with the system. Differences arise from different I/O buss widths, handshaking, and the number formats (particularly in the integer to floating-point converters that are included). Control functions are generated and controlled by an on-board Z80 microprocessor.

## ADDRESSING OF THE PROCESSOR INPUT BUFFERS

Although sequential addressing of the Data Input Memories is possible during raw data input from the ADCs, a random addressing scheme must be provided for reading the data back out for sample processing. For both pulse decoding and lag produce calculations (which are the most complicated cases) the addresses can be formed as the sum of two operands -- one based on a given sample referenced to a specific range, and the other determined as a relative displacement to the other samples that contribute to the calculation of the desired quantity for that range. This is simply a nested loop structure where the outer loop indexes the range and where the inner loop indexes the terms that

BLOCK DIAGRAM FOR A SYSTEM USING THE RADAR SIGNAL COMPENDER ANALOG SIGNALS

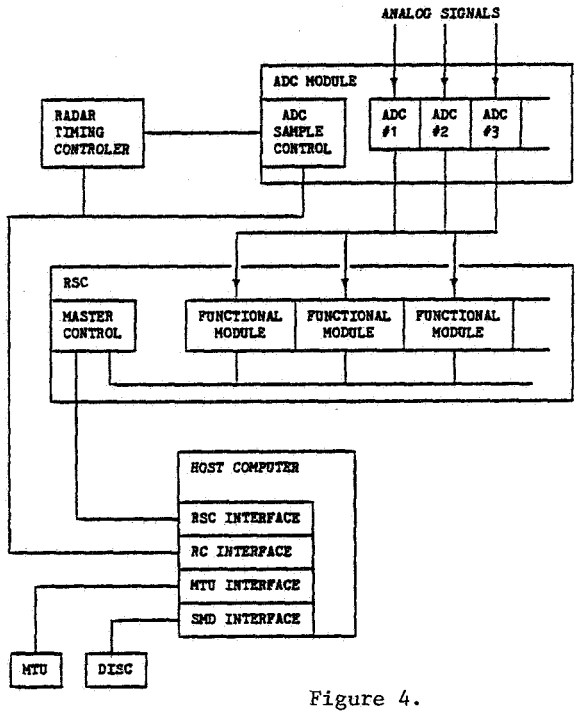


Figure 4.

contribute to that range. The Radar Signal Compender obtains such Base and Displacement operands for the Data Input Buffers from sequential locations in three operand memories. Figure 5 diagrams how this addressing scheme is accomplished.

Each stage in the address computations is also pipelined to maximize the speed. (Other more general address schemes were not fast enough.) Address generation using the Base and Displacement operands is applied to one buffer of each Data Input Buffer pair for data processing while a separate counter provides sequential addresses to the remaining buffers for data input from the ADCs. Since the I/O busses, the Data Input Buffers and their addresses are all independent, no memory cycles are lost from the processing for the I/O transfers. Selection of the opposite buffer requires only a change in the state of a control line, a change that takes only a fraction of one microsecond to accomplish. Hence, the entire time is available for processing the data. This is a tremendous advantage over the situation in general-purpose processors which must give up memory cycles even for double buffered I/O. Separate Displacement operands are provided for the left and right Data Input Memories so that samples taken at different times can be selected for the multiplier to create the lag products of an autocorrelation function (ACF). Only the lower 11 bits of the Base and the two Displacement RAMs (which are 2 k words deep) are used for address generation; the remaining 5-bits are used for process and address counter control. Note that the Base Address Computer generates the address for the Base Operand Memory, while the Displacement Address Counter generates a common address for both Displacement Operand Memories.

## CONCLUSIONS

The basic architecture of the Radar Signal Compender has been illustrated with respect to the very specific high-speed real-time signal processing

BLOCK DIAGRAM FOR ADDRESSING INPUT DATA
FOR SIGNAL PROCESSING

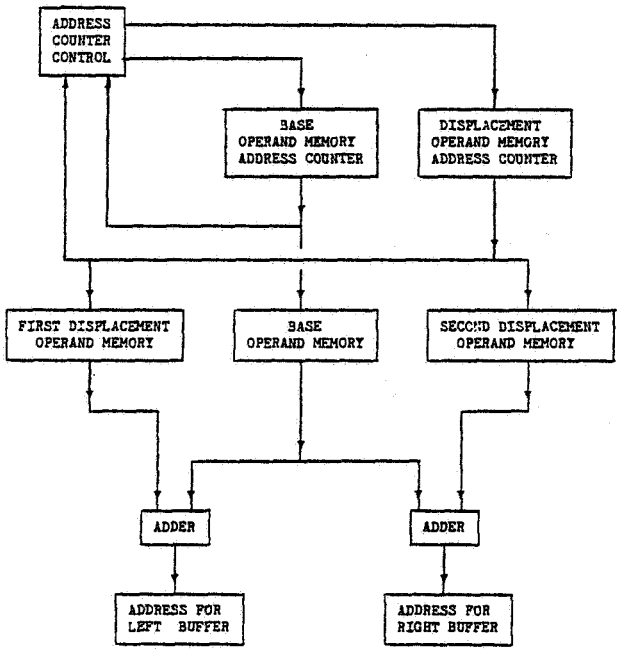


Figure 5.

requirements of backscatter radars. A full technical description will be available in the RSC users manual. The major features of the RSC are listed below

(1) Multiple Functional Modules provide many parallel data-processing streams, each of which is fully pipelined and programmable for maximum throughput and flexibility.

(2) Multiple Independent Data Input Buffers allow processing to be completely independent of I/O.

(3) Addressing is sequential for I/O with the RSC, but is flexible for processing within the RSC.

(4) Integer processing is used with user selectable data path widths. Sufficient guard bits can be chosen to avoid overflows for even very long integrations; even so, error checking for overflows is provided.

(5) Full multibit multiplications reduce biases and simplify the computation of weighting factors for off-line analysis.

Other uses of the RSC are envisioned. For example, since the Input Data Memories can be loaded directly from the host computer as well as from the ADCs, the device can also be used as an integer array processor for off-line analysis of much of our work that begins with Fourier transforms of large amounts of raw data. (This direct data load feature was originally developed for automatic testing of the RSC.) Other possible configurations have been considered where the output of one RSC was fed into another RSC for two-stage processing of the data. Eventually it may be desirable to substitute floating-point arithmetic units for the integer units where greater dynamic range is necessary for array manipulations. Note, however, that there is no reason to go to floating-point arithmetic for just the initial real-time processing of backscatter radar data.

# 8.3D REAL-TIME MST RADAR SIGNAL PROCESSING USING A MICROCOMPUTER RUNNING UNDER FORTH

S. A. Bowhill

Aeronomy Laboratory
Department of Electrical Engineering
University of Illinois
Urbana, IL 61801

Since January 1983, data on power, correlation time, and velocity have been obtained at the Urbana radar using an Apple II microcomputer and a single floppy disk drive. This system includes the following features:

(1) Measurement of the real and imaginary components of the received signal at 20 altitudes spaced by 1.5 km;
(2) Coherent integration of these components over a 1/8-s time period;
(3) Continuous real-time display of the height profiles of the two coherently integrated components;
(4) Real-time calculation of the one-minute averages of the power and autocovariance function up to 6 lags (namely, 0.75 s);
(5) Output of these data to floppy disk once every 2 minutes;
(6) Display of the 1-minute power profiles while the data are being stored to the disk;
(7) Visual prompting for the operator to change disks when required at the end of each hour of data; and
(8) Continuous audible indication of the status of the interrupt service routine.

Accomplishment of this goal was made possible by two developments: first, the use of a new correlation algorithm (see paper 8.4-A); and second, the use of the FORTH language to manage the various low-level and high-level procedures involved.

Sixty minutes of binary data can be stored on each side of an Apple floppy disk, so the storage requirements are not excessive. Subsequent analysis programs, written in BASIC and compiled, permit the velocity, correlation and power values to be stored on a single disk for a typical 6-hour sequence of data.

Advantages of this approach over our previous use of a minicomputer include:

(1) Greater convenience of using a small, easily handled microcomputer.
(2) Compactness and ease of access of floppy disks compared to magnetic tape.
(3) Ease of maintenance since the system involves only 1% of the complexity of the minicomputer.
(4) Availability of directly addressable screen memory, enabling updating eight times per second.
(5) Compatibility of the output format with numerous data analysis programs written for the Apple.

The details of this program will be described in a forthcoming University of Illinois Aeronomy Report. The software is available on floppy disk from the author.

ACKNOWLEDGEMENTS

The work described was supported in part by the National Aeronautics and Space Administration under Grant NSG 7506 and in part by the National Science Foundation under Grant ATM 81-20371.

# 8.4A REVIEW OF CORRELATION TECHNIQUES

S. A. Bowhill

Aeronomy Laboratory
Department of Electrical Engineering
University of Illinois
Urbana, IL 61801

The problem of correlation analysis in MST radar is to determine the scattered power, Doppler frequency and correlation time for a noisy signal. It is assumed that coherent detection has been employed, with two accurately balanced quadrature receiving channels. It is further assumed that coherent integration has been performed with a window length significantly less than the correlation time of the signal.

The analysis problem may be looked at from the point of view either of Fourier analysis or of correlation analysis, and it must be emphasized that the two approaches, if used properly, give identical results. Why, then, use correlation analysis at all? The reason can be seen from the spectrum and correlation function shown in Figure 1. In each case 1 min of data is represented, for example (with 1/8 sec coherent integration time) 480 pairs of data points (real and imaginary). Ordinary discrete Fourier analysis requires about $2 \times 10^5$ floating-point multiplications, all involving transcendentals.

In fact, however, only the area P under the echo spectrum, its position $f_1$ and its width $f_2$ are required; these quantities have to be calculated from the spectrum by separate algorithms.

It can easily be shown that the quantities P, $f_1$ and $f_2$ can be determined from the first few values of the complex autocovariance functions, shown on the lower part of Figure 1. This function can be calculated out to a number of lags approaching the length of the sample, but almost no additional information is contained in the part of the function beyond the first few lags. In examining such a function, it is necessary to make an assumption; namely, that the curve for lags other than zero can be extrapolated back to zero to give the signal power P and the noise power N as shown; this is possible because the noise power is uncorrelated from one coherently integrated sample to the next, while the coherent integration time has, as indicated above, been chosen so as to make the correlation between one sample and the next very good.

The correlation time (or time to correlation equals .5) is estimated as shown after the noise power has been removed. The spectral width $f_2$ is the reciprocal of the correlation time. The Doppler frequency $f_1$ is found from the slope of the imaginary part of the correlation function at the origin, care being taken to eliminate the unwanted variance N.

In principle, only 3 points on the complex autocorrelation function need to be calculated, which would require about 6000 multiplications, many fewer than the number required for the spectral approach. In fact, a larger number of lags (up to 12) is often calculated with the idea of improving the analysis. As described by COUNTRYMAN and BOWHILL (1979), the values of the argument of the complex covariance for the various lags can be weighted to give a more accurate value. A maximum likelihood analysis of the estimation problem is given in Appendix 1. This method of analysis has not yet been applied to experimental data.

The calculations of autocorrelation functions, however, need not necessarily use multiplication at all. BOWHILL (1955) described a method of

finding autocorrelations using the mean difference of separate samples rather than their mean product. Appendix 2 gives a description of the algorithms used. This technique has been successfully applied in a microcomputer operating system for the real-time processing of MST data (see paper 8.3-D).

There are other ways in which the correlation process can be speeded up. HAGEN and FARLEY (1973) describe 11 methods. Table 1 illustrates several of these algorithms, together with the efficiency in terms of use of the input data. It should be emphasized that the technique of Appendix 2 has an efficiency in excess of 95%. The question arises as to whether a hardware correlator is worthwhile for MST radar. It is my opinion that the use of coherent integration, which reduces the number of input data by about 2 orders of magnitude, makes a special hardware device unnecessary, particularly with the use of algorithms such as those described in this paper.

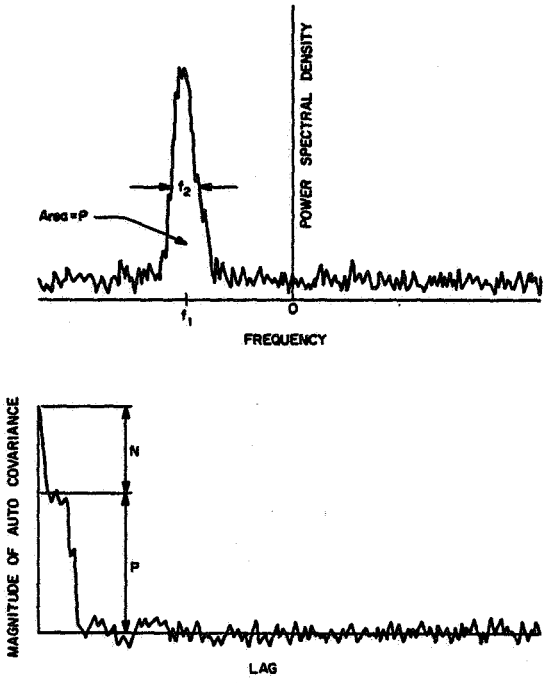


Figure 1. Power spectrum and autocovariance function corresponding to a coherently scattered signal plus noise.

Table 1

| Type of Correlation | Output | Efficiency (%) |
|---|---|---|
| Multibit | $\sigma^2\rho$ | 100 |
| One-bit x multibit | $(2/\pi)^{1/2}\sigma\rho$ | 64 |
| One-bit | $(2/\pi)\ \sin^{-1}\rho$ | 41 |

ACKNOWLEDGEMENTS

The work described was supported in part by the National Aeronautics and Space Administration under Grant NSG 7506 and in part by the National Science Foundation under Grant ATM 81-20371.

REFERENCES

Bowhill, S. A. (1955), Ph. D. Thesis, Cambridge University, Appendix 8.1-A.

Countryman, I. D. and S. A. Bowhill (1979), Wind and wave observations in the mesosphere using coherent-scatter radar, Aeron. Rep. No. 89, Aeron. Lab., Dep. Elec. Eng., Univ. Ill., Urbana-Champaign.

Hagen, J. B. and D. T. Farley (1973), Digital-correlation techniques in radio science, Radio Sci., 8, 775-784.

## APPENDIX 1. Maximum-Likelihood Estimation of C-S Parameters.

Suppose that the real part of the complex autocorrelation function is given by

$$r(\tau) = r_o \exp(-a\tau^2) \cos\omega\tau + \varepsilon_o(\tau)$$

where $\varepsilon_o(\tau) = 1 - r_o \quad (\tau = 0)$
$= 0 \quad (\tau > 0)$

and $\tau = 0, 1, 2 \ldots n.$

Now let the observed autocorrelation function have real part $R(\tau)$. For the imaginary part, $i(\tau) = r_o \exp(-a\tau^2) \sin\omega\tau + \varepsilon_o(\tau)$ if the r and i channels have equal sensitivity.

Now let the noise n on the r and i channels have a Gaussian distribution $\exp(-bn^2)$ then the likelihood of a given set of $I(\tau)$ and $R(\tau)$ is

$$L = \exp[-b \sum_o^n \{R(\tau) - r(\tau)\}^2 - b \sum_o^n \{I(\tau) - i(\tau)\}]$$

and $$-\frac{1}{b} \ln L = \sum_o^n [R(\tau) - r(\tau)]^2 + \sum_o^n [I(\tau) - i(\tau)]^2$$

and maximum likelihood amounts to a least squares fit of $R(\tau)$ and $I(\tau)$ by $r(\tau)$ and $i(\tau)$.

Substituting for $r(\tau)$ and $i(\tau)$, and neglecting $\tau = 0$,

$$-\frac{1}{b} \ln L = \sum_1^n [R(\tau) - r_o \exp(-a\tau^2) \cos\omega\tau]^2 + \sum_1^n I(\tau) - r_o \exp(-a\tau^2) \sin\omega\tau]^2$$

$$= \sum_1^n [R^2(\tau) + I^2(\tau) + r_o^2 \exp(-2a\tau^2) - 2r_o^2 \exp(-a\tau^2) (R(\tau) \cos\omega\tau + I(\tau) \sin\omega\tau)]$$

Differentiating with respect to $r_o$, a and $\omega$, and equating to 0, we get the following equations which must be satisfied simultaneously:

$$r_o \sum_1^n \exp(-2a\tau^2) - \sum_1^n \exp(-a\tau^2)\,[R(\tau)\cos\omega\tau + I(\tau)\sin\omega\tau] = 0$$

$$r_o \sum_1^n \tau^2 \exp(-2a\tau^2) - \sum_1^n \tau^2 \exp(-a\tau^2)\,[R(\tau)\cos\omega\tau + I(\tau)\sin\omega\tau] = 0$$

$$\sum_1^n \exp(-a\tau^2)\,[R(\tau)\sin\omega\tau - I(\tau)\cos\omega\tau] = 0$$

or $$\omega = \frac{\Sigma\, I(\tau)\ \exp(-a\tau^2)}{\Sigma\, R(\tau)\tau\, \exp(-a\tau^2)} \qquad \text{for } \omega\tau \ll 1.$$

---

## APPENDIX 2. Rapid Pseudocorrelation Technique.

Consider two voltages R(t) and I(t), nominally the real and imaginary parts of the phasor of a radar return signal. The problem is to determine the center frequency and power, and correlation time, of an embedded signal of frequency $\omega$.

### REPRESENTATION OF R(t) AND I(t)

The signal of frequency $\omega$ can be represented by a phasor $S(\tau)$ at that frequency, giving $S_R(t)\cos\omega t$ and $S_I(t)\cos(\omega t+\phi)$ in the voltages R(t) and I(t), respectively. $S_R(t)$ and $S_I(t)$ are random variables, such that $S_R(t)/S_I(t)$ = constant. The phase shift $\phi$ is nominally $\pi/2$. A noise voltage n(t) will also appear in R(t) and I(t), which is supposed to be completely uncorrelated from one pulse to the next.

We therefore have

$$R(t) = S_R(t)\cos\omega t + n_R(t)$$

$$I(t) = S_I(t)\cos(\omega t+\phi) + n_I(t)$$

### MEAN SQUARE DIFFERENCE DEFINITIONS

Let $$RO^2 = \langle R^2(t)\rangle$$

$$IO^2 = \langle I^2(t)\rangle$$

$$RR^2(\tau) = \langle [R(t) - R(t+\tau)]^2\rangle$$

$$II^2(\tau) = \langle [I(t) - I(t+\tau)]^2\rangle$$

$$RI^2(\tau) = \langle [R(t) - I(t+\tau)]^2\rangle$$

$$IR^2(\tau) = \langle [I(t) - R(t+\tau)]^2\rangle$$

Now all these quantities may be related to the mean absolute values of the squared quantities by the relation:

$$\langle X^2(t) \rangle = k[\langle |X(t)| \rangle]^2$$

where k is a constant for a given waveform.

EVALUATION OF DIFFERENCES

From the expression for R(t),

$$\langle R^2(t) \rangle = \frac{1}{2} \langle S_R^{\,2}(t) \rangle + \langle n_R^{\,2}(t) \rangle$$

since $S_R(t)$ and $n_R(t)$ are independent random variables. Further, we define

$$S_R^{\,2} = \langle S_R^{\,2}(t) \rangle, \quad N_R^{\,2} = \langle n_R^{\,2}(t) \rangle,$$

$$RO^2 = \frac{1}{2} S_R^{\,2} + N_R^{\,2}$$

$$IO^2 = \frac{1}{2} S_R^{\,2} + N_R^{\,2}$$

$$RR^2(\tau) = \langle [S_R(t) \cos\omega t + n_R(t) - S_R(t + \tau) \cos(\omega t + \omega\tau) - n_R(t + \tau)]^2 \rangle$$

$$= \frac{1}{2} S_R^{\,2} + N_R^{\,2} + \frac{1}{2} S_R^{\,2} + N_R^{\,2} - 2\langle S_R(t) S_R(t + \tau) \cos\omega\tau \cos(\omega t + \omega\tau) \rangle$$

$$= S_R^{\,2} + 2N_R^{\,2} - \langle S_R(t) S_R(\tau) \rangle \cos\omega\tau$$

and defining

$$\rho(\tau) = \langle S_R(t) S_R(t + \tau) \rangle / S_R^{\,2}$$

$$RR^2(\tau) = S_R^{\,2}[1 - \rho(\tau) \cos\omega\tau] + 2N_R^{\,2}$$

$$II^2(\tau) = S_I^{\,2}[1 - \rho(\tau) \cos\omega\tau] + 2N_I^{\,2}$$

Similarly,

$$RI^2(\tau) = \langle [S_R(t) \cos\omega t + n_R(t) - S_I(t + \tau) \cos(\omega t + \omega\tau + \phi) - n_I(t + \tau)]^2 \rangle$$

$$= \frac{1}{2} S_R^{\,2} + N_R^{\,2} + \frac{1}{2} S_I^{\,2} + N_I^{\,2}$$

$$+ 2 \langle S_R(t) S_I(t + \tau) \cos\omega t \cos(\omega t + \omega\tau + \phi) \rangle$$

$$+ 2 \langle n_R(t) n_I(t + \tau) \rangle$$

and the latter term is always zero. So

$$RI^2(\tau) = \frac{1}{2} S_R^{\,2} + \frac{1}{2} S_I^{\,2} + N_R^{\,2} + N_I^{\,2}$$

$$+ 2 \langle S_R(t) S_R(t + \tau) \frac{1}{2} \cos(\omega t + \phi) \rangle$$

$$= \frac{1}{2} S_R^{\,2} + \frac{1}{2} S_I^{\,2} + N_R^{\,2} + N_I^{\,2} + S_R S_I \rho(\tau) \cos(+\omega\tau + \phi)$$

Similarly,

$$IR^2(\tau) = \frac{1}{2} S_R^{\,2} + \frac{1}{2} S_I^{\,2} + N_R^{\,2} + N_I^{\,2} + S_R S_I \rho(\tau) \cos(-\omega\tau + \phi)$$

POWER AND FREQUENCY CALCULATIONS

From the above relations,

$$2RO^2 - RR^2 = S_R^2\,\rho(\tau)\cos\omega\tau$$

$$2IO^2 - II^2 = S_I^2\,\rho(\tau)\cos\omega\tau$$

$$RI^2 - RO^2 - IO^2 = S_R S_I\,\rho(\tau)\cos(\omega\tau + \phi)$$

$$IR^2 - RO^2 - IO^2 = S_R S_I\,\rho(\tau)\cos(-\omega\tau + \phi)$$

and

$$[(2RO^2 - RR^2)(2IO^2 - II^2)]^{1/2} = S_R S_I \rho(\tau)\cos\omega\tau$$

$$IR^2 - RI^2 = 2\,S_R S_I \rho(\tau)\sin\omega\tau \cdot \sin\phi$$

$$RI^2 + IR^2 - 2(RO^2 + IO^2) = 2\,S_R S_I \rho(\tau)\cos\omega\tau \cdot \cos\phi$$

Normally, $\phi$ is set to $\pi/2$, so the first two equations become

$$[(2RO^2 - RR^2)\,(2IO^2 - II^2)]^{1/2} = S_R S_I \rho(\tau)\cos\omega\tau$$

$$IR^2 - RI^2 = 2\,S_R S_I \rho(\tau)\sin\omega\tau$$

and $S_R S_I$ and $\omega\tau$ may be found trigonometrically. $S_R S_I$ may be adopted as the measure of scattered power. The third equation may be used as a check upon the accuracy with which the phase-quadrature channels have been adjusted.

# 8.4B CORRELATION METHODS

J. Rottger

EISCAT Scientific Association
P.O. Box 705
S-98127 Kiruna, Sweden

Both the Doppler and the spaced antenna method make use of complex data processing. This can be done in the temporal domain by processing correlation functions or in the frequency domain by processing spectra. The original approach of the spaced-antenna analysis made use only of the correlation analysis, but can be extended also to the spectrum and cross-spectrum analysis for interferometer applications.

In known MST radar schemes, raw data are either dumped directly on tape, are preintegrated and then dumped or Fourier analysed, or the spectra are averaged and then dumped on tape. An alternative approach would be the following:

After suitable hardware preintegration (and decoding) of complex data taken at three receiving antennas, complex autocorrelation functions $c_{11}$, $c_{22}$, and $c_{33}$ as well as complex cross-correlation functions $c_{12}$, $c_{13}$ and $c_{23}$ are calculated in a hardware correlator from a times series of Ndata. Since the shorter lags of the correlation functions contain the significant information, it is sufficient to store only a fraction of the entire correlation functions, say N/6 of the integration time interval. Owing to the fact that 6 correlation functions have to be stored, the amount of data is not reduced. This, however, can be done by accumulating (postintegration) many correlation functions. After a suitable postintegration time, these can be transferred into the computer memory for real-time analysis and tape dump.

An example:

| | |
|---|---|
| interpulse period | 1 ms, |
| preintegration time | 100 ms, |
| integration time (corr. function) | 60 s, |

yields N=600 complex data points per antenna and range gate. This reduces to 100 complex data points of the 6 correlation functions, corresponding to a maximum lag of 10 s (frequency resolution 0.1 Hz). Transfer to the overhead computer takes place once per minute, and this time will be suitable for most on-line analyses. Even further postintegration of the correlation functions can be done in the computer or in a hardware postintegrator.

Since complex auto- and cross-correlation functions are calculated and stored, almost no information is lost, since Doppler spectra and cross spectra (for interferometer applications) can be directly obtained by Fourier transformation of the correlation functions. These also can be analysed in terms of the full correlation analysis of the spaced-antenna-drifts technique. The proposed approach therefore appears to be very feasible to suit most MST radar applications.

# 8.5A DATA ANALYSIS TECHNIQUES: SPECTRAL PROCESSING

R. G. Strauch

NOAA/ERL/Wave Propagation Laboratory
Boulder, CO 80303

Most radars used for wind sounding use a data-processing scheme similar to that illustrated in Figure 1. The processing method shown uses spectral analysis and assumes a pulse Doppler radar. Radial profiles of the first three moments of the Doppler spectra are estimated: signal power P, mean radial velocity $V_r$, and spectrum width W. The input signal is the backscattered signal for each radar resolution cell after translation to a convenient frequency. The receiver limits the bandwidth with a filter that is (usually) matched to the transmitted pulse. Complex video is obtained by baseband mixing with a reference voltage. Samples of video are generated for each pulse repetition period T and for each range resolution cell centered along the antenna axis; these voltage samples represent the composite amplitude and phase of the scattering process in the resolution volume. The averaging that occurs in each step of the data processing is examined in this paper.

The signal-to-noise ratio SNR can be improved for some radars by summing the complex video samples from a number J of consecutive received pulses. Since the noise bandwidth is determined by the radar pulse width, noise samples taken at the pulse repetition period will be uncorrelated; therefore the noise power increases linearly with the number of samples added. The signal, however, remains well correlated for approximately 0.2 $\lambda/W$ seconds (NATHANSON, 1969) where $\lambda$ is the radar wavelength. Typically W is about 1 m/s, so the correlation time is milliseconds with microwave radars and seconds with VHF radars. If, in addition to being correlated, the phase of the signal samples changes very little between samples, then signal samples can be added so that signal power increases with the square of the number of samples added. This occurs for radars whose unambiguous velocity $\lambda/(4T)$ is much greater than the radial velocity of the scatterers. The SNR improves by the number J of samples averaged, and the unambiguous velocity will decrease to $\lambda/(4JT)$. Two points should be noted. (1) It is not necessary to use time domain averaging to improve detection. The SNR improvement can be obtained in later processing, but time domain averaging minimizes the calculation burden in succeeding processing stages without sacrificing sensitivity. (2) Time domain averaging filters the input signal so that signal components with velocity greater than $\lambda/(4JT)$ will be aliased and may be greatly attenuated (SCHMIDT et al., 1979). Without time domain averaging when signal components are aliased they are not attenuated. We select J as large as possible such that $\lambda/(4JT)$ is greater than the maximum expected mean radial velocity and such that the signal is correlated for much longer than JT.

The next step in signal processing is to compute the power spectrum of K (averaged) signal samples. K is selected such that the available coherent integration is realized. If K is too small, sensitivity is reduced; if K is too large, the calculation burden is increased without improving sensitivity or retrieving additional information. Figure 2 shows how the SNR in the spectral domain improves as dwell time $T_D = JKT$ increases. The improvement factor is given by

$$K \left[ \operatorname{erf} \frac{\Delta V}{2\sqrt{2}W} \right]$$

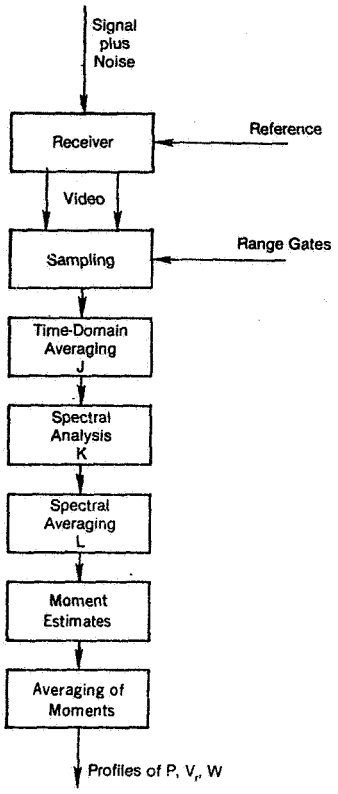


Figure 1. Data processing sequence. Spectral processing for a pulse Doppler radar is illustrated.

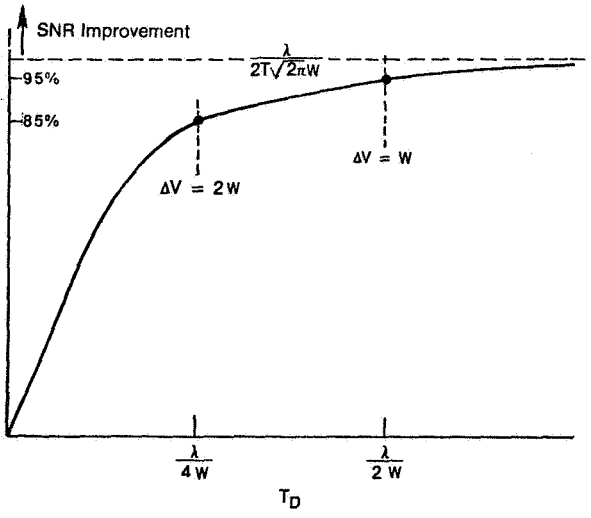


Figure 2. Signal-to-noise ratio improvement by spectral processing. The limiting value is $\lambda/(2T\sqrt{2\pi}\ W)$. Dwell times longer than $\lambda/2W$ improve spectral resolution but yield little SNR improvement.

where $\Delta V$ is the velocity resolution of the spectral processor $\lambda/(2T_D)$. For small K the improvement factor increases linearly with K; spectral resolution is so poor that all the signal power remains in one velocity resolution element. As observation time increases, the noise power in each velocity resolution element decreases, while signal power remains constant. When the dwell time is increased such that signal power starts to occupy more than one spectral point, SNR improvement no longer increases linearly with dwell time. When the dwell time is $\lambda/(2W)$ or $K = \lambda/(2JTW)$, 95% of the available coherent integration is achieved. Longer dwell times yield little SNR improvement because both noise power and signal power decrease in the velocity resolution element that contains maximum signal. Note, however, that for large K, spectral points can be averaged and the spectrum will still be resolved. If this is done, SNR improves as $T_D^{1/2}$ as expected for incoherent integration. Thus, to minimize calculations we choose $K = \lambda/(2JTW)$ and use any additional observation time to measure new spectra.

The next processing step is the averaging of L spectra, each obtained from JK radar pulses. The L power estimates for each frequency or velocity will be exponentially distributed with a standard deviation equal to the mean (HILDEBRAND and SEKHON, 1974). We expect averaging to improve the spectral domain SNR by $\sqrt{L}$; however, this improvement will occur only if the mean wind is the same for each dwell time. If the mean wind is not the same, then the width of the averaged spectrum increases during the averaging and the SNR improvement will be less than $\sqrt{L}$. It is readily seen that if the mean wind changes abruptly by more than W, then the SNR can actually decrease with averaging time. The dependence of spectral width on averaging time can be deduced by examining the dependence of spectral width on averaging distance as studied by FRISCH and CLIFFORD (1974) and LABITT (1981). They derive the relationship $W \propto d^{1/3}$ where d is the maximum dimension of the observation volume (beamwidth or range resolution, whichever is greater) and d is less than the outer scale of turbulence $L_o$. If we average for time $T_o$ such that $d < \bar{v}\, T_o < L_o$, then, using Taylor's hypothesis, $W \propto (\bar{v}\, T_o)^{1/3}$ where $\bar{v}$ is the mean wind speed. Therefore, if the averaging time is less than $d/\bar{v}$, then the width of the averaged spectrum is about the same as the width of the individual spectra; for greater averaging time, the width of the averaged spectrum increases as $T_o^{1/3}$. To take full advantage of $\sqrt{L}$ improvement in SNR by averaging spectra, L should be limited to about $d/(JKT\bar{v})$.

The next data-processing step is the estimation of the important spectral moments from the averaged Doppler velocity spectrum. The signal spectrum must be isolated from the measured signal-plus-noise spectrum before the moments can be found. The methods used to do this (and to remove undesired spectral components such as ground clutter near zero velocity) are usually empirical. The average value of the complex time series is usually removed prior to calculating the power spectrum. Noise rejection is accomplished by applying a threshold, either a specified amount above the mean noise level or below the peak level. Another method to locate the signal is to find the maximum power in a velocity window of width equal to the expected signal width. The method used with the 6-m radar at Platteville, Colorado (the Platteville radar is operated cooperatively by NOAA's Aeronomy Laboratory and Wave Propagation Laboratory) is as follows (CARTER, 1982). The mean value of the complex time series is removed prior to calculating the individual power spectra. This filtering is sufficient to remove any clutter. The noise spectra are white (except when interfering transmission is detected), and the mean noise level is found by applying an objective technique (HILDEBRAND and SEKHON, 1974) for each spectrum. A fixed noise level cannot be assumed because the noise is governed by cosmic background. The signal spectrum is isolated by locating the peak value of the averaged spectrum and including all those contiguous spectral points that exceed the noise level. The classic definition of the moments is then applied to the isolated signal spectrum after subtracting the mean noise level from each of the

selected spectral points. In very weak signals, or if the input consists of noise only, the algorithm selects the peak and one or two additional spectral points; it therefore becomes a maximum-likelihood estimator of the mean velocity (WHALEN, 1971). It is an unbiased estimator of the mean (in noise it selects a random value between ($\pm\lambda/(4JT)$) for the mean velocity). Since it selects that portion of the noise in the isolated spectral points that exceeds the mean noise as "signal", both power and width estimates are slightly biased by the noise. This method appears to work well for a wide variety of conditions.

Finally, estimates of spectral moments can be averaged. The averaging time depends on the type of information sought and the temporal evolution of the scattering phenomena. For example, the Platteville radar is used primarily to obtain hourly estimates of tropospheric winds; during an hour M radial profiles of mean velocity are measured. At the upper heights the mean velocities are random because of low SNR. Some of the profiles are also contaminated by interference from other transmitters or by scattering from aircraft. The profiles are averaged by applying a simple version of Random Sample Consensus (FISCHLER and BOLLES, 1981). The set of M data points at each measurement height are examined to find the largest subset of points within X m/s of each other. If the subset includes fewer than Y data points, the data are rejected for that height; otherwise the subset is averaged to obtain the mean radial wind. This algorithm rejects data when the SNR is too low and also rejects random points caused by interference. In practice X is 1 m/s (where the maximum radial velocity is $\pm$19 m/s), and the smallest subset allowed is 4 of 12 measurement points.

REFERENCES

Carter, D. A. (1982), Private communication, Aeronomy Laboratory, NOAA.

Fischler, M. A. and R. C. Bolles (1981), Random sample consensus: A paradigm for model fitting with applications to image analysis and automated cartography, Commun. Assoc. Comput. Mach., 24, 381-395.

Frisch, A. S. and S. F. Clifford (1974), A study of convection capped by a stable layer using Doppler radar and acoustic echo sounders, J. Atmos. Sci. 31, 1622-1628.

Hildebrand, P. H. and R. S. Sekhon (1974), Objective determination of the noise level in Doppler spectra, J. Appl. Meteorol., 13, 808-811.

Labitt, M. (1981), Coordinated radar and aircraft observations of turbulence, Project Report ATC 108, MIT Lincoln Laboratory. 39 pp.

Nathanson, F. E. (1969), Radar Design Principles, McGraw-Hill, New York, 626 pp.

Schmidt, G., R. Ruster and P. Czechowsky (1979), Complementary code and digital filtering for detection of weak VHF radar signals from the mesosphere, IEEE Trans. Geosci. Elec., GE-17, 154-161.

Whalen, A. D. (1971), Detection of Signals in Noise, Academic Press, New York, 411 pp.

# 8.5B SIGNAL PROCESSING AT THE POKER FLAT MST RADAR

D. A. Carter

Aeronomy Laboratory
National Oceanic and Atmospheric Administration
Boulder, CO 80303

Signal processing at the Poker Flat MST radar is carried out by a combination of hardware in high-speed special-purpose devices and software in a general-purpose minicomputer/array processor. Figure 1 is a block diagram of the signal processing system.

The received signals from three antennas (one directed vertically and two directed obliquely) are detected by three receivers. The six receiver quadrature outputs are sampled simultaneously by six 8-bit analog-to-digital converters. With the current ADCs, the minimum sampling period is 2 μsec. Each conversion is triggered by a pulse from the Radar Pulse Box which also contains the system clock and creates the transmitter and TR switch pulses.

Because of the low atmospheric Doppler shifts (less than 10 Hz) and the high radar pulse rate (about 1 kHz), coherent integration of the received signals can greatly simplify the signal processing. Currently the digitized data points from the ADC box are transferred directly to the minicomputer. On the computer/ADC interface board is a simple circuit to add the incoming values one by one to the corresponding coherent integration sum in computer memory. This simple coherent integrator is much faster than software algorithms used previously.

Even greater coherent integration speed will be attained in the near future when the digitized ADC samples will be passed to a high-speed preprocessor, called the Radar Signal Compender (RSC), which can process the six channels in parallel. This box, designed by Wesley Swartz (Cornell) and Paul Johnston (NOAA), is currently being assembled and will be capable of performing coherent integration and decoding. The RSC consists of six function modules (FMs), each of which can process a pair of quadrature channels, and a master control module. Each function module contains four 2 k by 16-bit double-buffered input memories, four 2 k by 32-bit double-buffered output memories, and two high-speed 32-bit wide adders. Each function module can be individually programmed by the host computer via the master control module. In the anticipated operating mode at Poker Flat, each pair of quadrature channels will feed two function modules so that a different number of coherent integrations can be performed on two height ranges from each receiver. Pulse coding/decoding will be implemented in the system at a later date.

After coherent integration, the data (one 32-bit floating point value per range gate per channel) will be transferred from the RSC to the host computer. The computer is a Data General AP/130 which contains a 128 k by 16-bit main memory and an integral floating-point array processor with its own high-speed 2 k by 32-bit local memory. After all coherently integrated points (typically 64 for each range gate) are stored in the computer, the following operations are performed by the array processor on the data from each range gate:

(1) The values are normalized by dividing by the number of coherent integrations,

(2) The mean value of each quadrature component is computed and subtracted from the data.

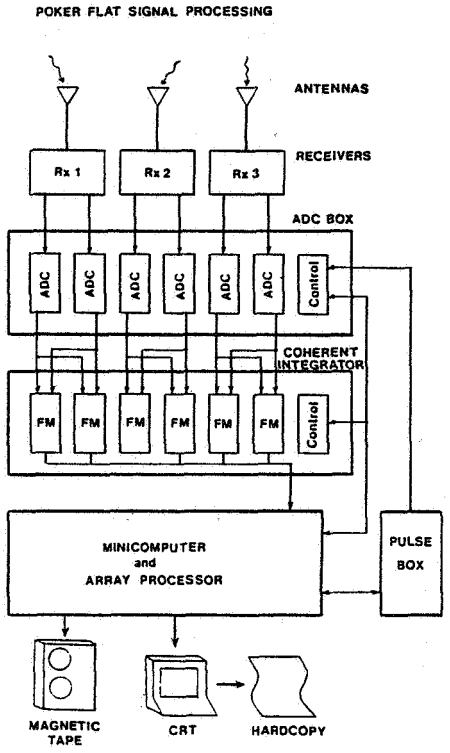


Figure 1.

(3) A Hanning window is applied,

(4) The fast Fourier transform is computed,

(5) The power spectrum is computed from the squared magnitude of the transform, and

(6) The spectrum is added to the spectral sum for that range gate.

The array processor performs the above operations much faster than possible using the standard minicomputer. A 1024-point complex floating-point FFT takes about 9 msec and a 64-point FFT about 0.3 msec in the AP, which is at least 50 times faster than an integer FFT algorithm used previously on a standard minicomputer. The entire analysis time for 45 heights on each of 3 receivers using 64-point spectra takes about 0.2 sec, which is much shorter than the 3-30 sec required to acquire the coherently integrated data set. Thus, many more heights can be sampled before data are lost due to processing overhead.

After about a minute of spectral averaging, the moments of the Doppler power spectra are calculated and the signal power, mean Doppler shift, spectral width, and noise power for each range gate are written to magnetic tape (see Riddle, p. 863, this volume). Long-term averages of the Doppler power spectra are accumulated for a longer period (typically about 10 min) and also written to tape when complete. By not writing the complete spectra to tape for every short-term average, a standard 2400 ft 1600 BPI tape of 1-minute averages for about 135 total range gates will last for at least 50 hours. The availability

of the Doppler spectra on tape allows additional off-line processing of the spectra, a good quality control check of the system, and possible further averaging to detect signals at ranges where no echoes were apparent in the 1-minute data.

The Doppler spectra can also be displayed on a graphics CRT terminal. Hardcopies of the spectra are routinely printed out every hour, providing a good, quick overview of the data taken during the normal unattended operation of the radar.

# 8.6A PARAMETERIZATION OF SPECTRA

C. R. Cornish

School of Electrical Engineering
Cornell University
Ithaca, NY 14853

Following reception and A/D conversion, atmospheric radar backscatter echoes need to be processed so as to obtain desired information about atmospheric processes and to eliminate or minimize contaminating contributions from other sources. Various signal processing techniques have been implemented at various MST facilities to estimate parameters of interest from received spectra. Such estimation techniques need to be both accurate and sufficiently efficient to be within the capabilities of the particular data-processing system. This paper will review and compare the various techniques used to parameterize the spectra of received signals.

## SIGNAL CONSTITUENTS

The received signal consists of one or more of the following;

(1) Backscattered signal. Generally one is interested in quantifying the signal power, Doppler shift (velocity) and Doppler width of the signal spectrum. There may be one or more signal peaks in a given spectrum.

(2) Noise. While anything other than the desired signal can be considered noise, we will exclude clutter and interference from specific sources from our definition and consider only atmospheric, cosmic and receiver noise.

(3) Contribution to zero frequency power due to obstacles such as mountains and ocean waves. In the case of ground clutter there may be a non-fading dc component and a fading component with non-zero Doppler shift and width, the latter due to multiple phase paths from index of refraction variations and the rustling of leaves on trees. The magnitude and frequency spread of ground clutter is dependent on radar wavelength and antenna configuration. For 50-MHz systems, clutter is usually non-fading; higher frequency systems have a broader clutter spectrum. In the cases of Millstone Hill and Arecibo, antenna geometry introduces severe ground clutter contamination from antenna sidelobes. Distant ocean waves and moving vehicles can produce apparent signals of significant power and Doppler shift.

(4) Interference from electromagnetic sources. Other transmitters with operating frequencies or harmonics at the radar frequency can produce spurious peaks or an increase in the spectral noise level. Electromagnetic interference may originate from near sources and propagate line-of-sight, or from far sources and propagate via ionospheric reflections or along atmospheric ducts.

(5) Interference, i.e., echoes from airplanes and other scatterers of an intermittent, short period nature. Airplanes produce a characteristic dragontail-like spectrum, while rain produces a broadband spectrum which is dependent on radar wavelength. Depending on system operating parameters such as IPP, code and coherent integration time, echoes from ionospheric layers can produce spurious peaks and raise the noise level.

(6) 60 Hz and power line harmonics. This quasi-stationary electromagnetic interference may enter the radar system at various points of transmission and reception.

(7) Signal processing effects and artifacts, i.e., pulse coding, coherent integration, finite time series. Truncations of time series and frequency domain sampling cause a spillover of clutter into other frequency bins across the spectrum (SATO and WOODMAN, 1982). Coherent integration has a sin X/X transfer function which distorts the power and width of the signal spectrum. Imperfect implementation of complementary codes can produce ghost echoes.

(8) Instrumental effects, i.e., beam and shear broadening. A finite antenna beam width results in a broadening of the spectrum. Spectral broadening due to wind shear is a function of available height resolution which depends on pulse width and coding.

(9) Ducting, i.e., multiple ray propagation from main or sidelobes along atmospheric waveguides such as temperature inversions.

Figure 1 taken from SATO and WOODMAN (1982) illustrates some of the spectral characteristics discussed above. One will note a strong dc component as well as a fading clutter component which is symmetric about zero frequency and spreads over the lowest frequencies. The secondary peak at 10.1 km is a ghost peak due to code imperfections; a similar peak occurs at higher altitudes due to ocean clutter. Figure 2, courtesy of P. K. Rastogi, is a Doppler profile taken at Millstone Hill. Two interesting features of this profile besides the signal are power line spikes at 60 Hz and harmonics and a tropospheric duct which emulates the signal profile.

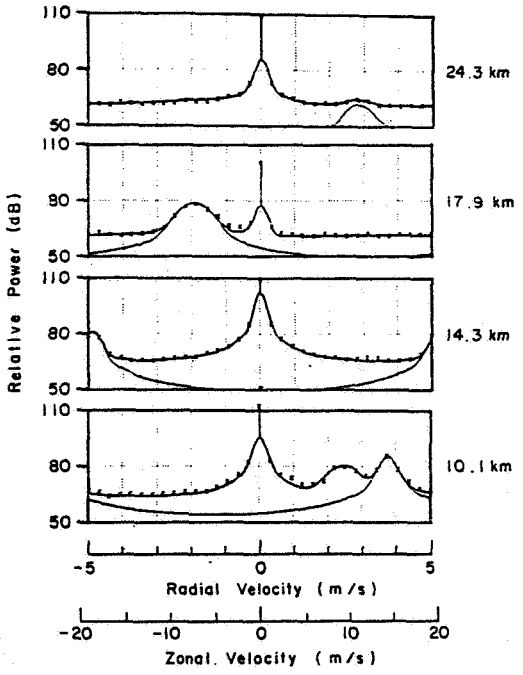


Figure 1. Examples of theoretical curves fitted at four different altitudes. The dotted, the thick and the thin line stand for the data, the fitted spectra, and the CAT contribution, respectively. The vertical line at zero Doppler shift shows the unfading clutter component (from SATO and WOODMAN, 1982).

## SPECTRAL CALCULATION AND PREPARATION

At most MST radar facilities, either the power spectrum or the corresponding autocorrelation funtion (ACF) of the returned signal is computed. ACF calculations have been performed historically at incoherent-scatter and meteor-scatter radar facilities due to their computational ease with limited digital hardware and are to be discussed elsewhere. Power spectra of the returned signal are generally computed via fast Fourier transform (FFT) algorithms either on-line or during off-line processing.

Before taking the FFT of the sampled signal, the dc component of the time series may be filtered out by subtracting the mean value, and an appropriate weighting function, e.g., Hanning (cosine) window, can be applied to minimize truncation effects; both of these are performed at Poker Flat. Additionally, phase errors in quadrature demodulation and differential amplification of the two (i.e., complex) channels of the signal can be compensated by calculation of a covariance matrix based upon the statistical independence and the equipartition of average power over a long-term interval of the two channels; this scheme has been implemented at SOUSY (SCHMIDT et al., 1979).

After taking the FFT of the time series and computing power spectra, spectra may be smoothed by taking a running mean over the spectra to minimize fluctuations. The averaging (incoherent) of several time contiguous spectra yields a similar result. At Millstone Hill, a recursive despiking and notching routine is applied to the spectra before a recursive smoothing (running mean) routine is used. Despiking consists of replacing a spike in the spectrum by the average of its two adjacent points, followed by a notching and filling in from adjacent frequency bins of certain interfering frequencies (e.g., 60 Hz).

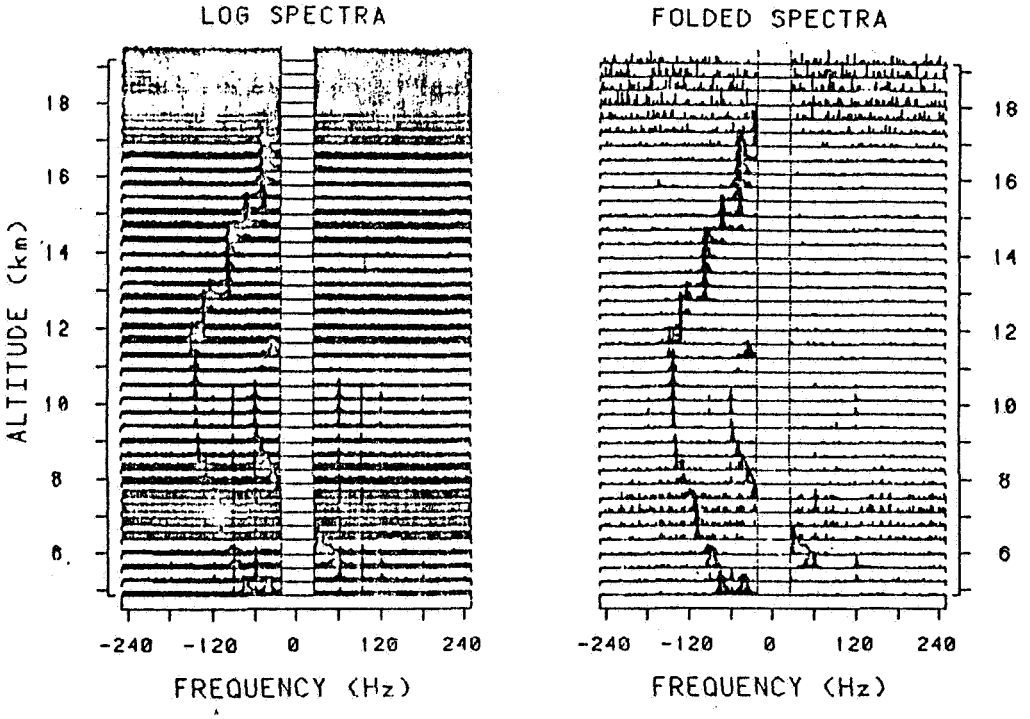


Figure 2. Profile of spectra from Millstone Hill (courtesy P. K. Rastogi).

## PARAMETER ESTIMATION

In the following section we will discuss the variety of techniques used to eliminate undesirable interference and clutter and to estimate the desired signal parameters.

Contributions to the dc or zero frequency of the power spectrum originate from ground clutter, system biases, noise and possibly signal. During transmission and reception, system dc can be eliminated by a 180° flip from pulse-to-pulse and subsequent coherent integration. During spectral parameterization any one of the following schemes is useful for eliminating dc contributions from non-fading clutter and system biases:

(1) Notching out the zero frequency and averaging the two adjacent bins to interpolate a new zero frequency value;

(2) Before FFT, subtracting the long term mean from the time series of returned echoes;

(3) After FFT, subtracting the coherent average (phase preserved) at zero frequency from the incoherent average of several power spectra.

The second and third techniques are equivalent and yield information (i.e., values of signal and noise at zero frequency) that may be lost by the first in the presence of fading clutter.

Treatment of non-fading clutter has been discussed above. Fading clutter is either non-existent or minimal at 50 MHz. At higher frequencies and for particular antenna geometries, fading clutter is significant, rivaling or surpassing the signal in power. At Millstone Hill long FFTs (256 or 512 pts) are computed to separate clutter from signal, with the zero and nearby frequencies subsequently notched out. Non-fading clutter is generally symmetric; a symmetric part subtraction of the spectrum can eliminate most all of it. However, fading clutter can have a slight Doppler shift resulting in a slight asymmetry. At Arecibo a sophisticated approach of using a nonlinear (N-L) least squares fit to the fading clutter (power, Doppler shift, width, form: Gaussian or Lorenzian) and ocean clutter (power, Doppler shift, width) as well as to the signal has been implemented. The forementioned symmetric subtraction scheme is used at Arecibo to obtain initial values for the N-L least squares fit.

Interference, both electromagnetic and from other sources, introduces spurious peaks or spikes and raises the noise level of the spectrum. Spikes can be removed by notching the spike and averaging over adjacent values and/or filtered out by taking a running mean across the spectrum. Depending on the parameters of the interfering source, e.g., duration bandwidth, and the sampling parameters, e.g., IPP and coherent integration time, interference can be smeared across the spectrum. Interference from othe transmitters is generally non-synchronized with the pulse repetition frequency (PRF) of the probing system and not much energy is contained within their transmissions unless the interfering transmitter is strong or nearby. During the ALPEX experiment in 1982, signals from most altitudes were contaminated by an interfering harmonic of a distant transmitter in Canada; the interference was eliminated by an appropriate high pass filter in the front end of the 50-MHz receiver (W. Ecklund, personal communication, 1983). Airplanes have a characteristic dragontail-like spectral signature spreading across many frequency bins which varies in time as the airplane orientation and position changes. A scheme implemented at Poker Flat to eliminate airplane interference checks the total power in the spectrum with previous total power values for that height. Should the total power exceed the previous value by a threshold factor, that spectrum and following ones are

skipped until the power returns to the uncontaminated value (CLARK and CARTER, 1980).

Power line interference at 60 Hz and its harmonics can be eliminated during transmission by an alternating 180° phase flip of the transmitted pulses and subsequent summation/subtraction of the samples. Proper selection of PRF and coherent integration time can cause 60-Hz interference to fall at a null of the coherent integration filter transfer function or to be folded back into a given point of the spectrum, e.g., near zero frequency. Should the above tactics be inapplicable at the time of spectral sampling, power line harmonics, which occur at known points in the spectrum, can be notched and filled in as done at Millstone Hill.

Spectral broadening due to signal processing and instrumental effects can be represented by transfer functions, which differ from an ideal delta sampling function. Coherent integration, for example, has a sin X/X transfer function, where $X = \pi fT$ and f is the frequency in Hz. Attenuation of the power at a given spectral point can be compensated for by applying a spectral weighting function as proposed by CLARK and CARTER (1980). Recently, HOCKING (1983) has determined the spectral broadening effects due to finite beam width and wind shear and has deconvolved measured spectra from the mesosphere with the calculated transfer functions so as to determine signal spectral widths due to turbulence. At Arecibo, SATO and WOODMAN (1982) have applied an N-L least-squares fit of a measured spectrum to a theoretical one. To compensate for signal processing effects on the measured spectrum due to coherent integration, finite time series and frequency domain sampling, the theoretical spectrum is similarly distorted. This procedure, similarly done in fitting incoherent scatter ACFs at mesospheric heights and higher, frees the estimated parameters from processing biases.

Having recognized and eliminated or compensated for undesirable contributions to a given spectrum, we proceed to a discussion of estimation of noise and signal in a given spectrum calculation. While backscattered echoes are being collected, a noise profile can be made without the transmitter or a "noise" height can be sampled during each IPP. The former technique, while measuring cosmic and receiver noise, does not include noise contributions by the transmitter. The latter procedure, while including transmitter noise effects, assumes there is no measurable signal at a given range of altitude. This procedure requires additional data acquisition and storage of samples from the noise heights, and, like the first, does not give a value of the atmospheric noise at a given height.

Noise estimation from a given spectrum is based on the assumption that the signal is confined to the narrow part of the spectrum and the noise power is evenly distributed across the spectrum. Noise power unit frequency cell is estimated from either:

(1) The lowest value of spectrum;

(2) The average from outer wings of spectrum, where no signal is assumed to be present;

(3) Dividing the spectrum into segments and using the average power from those segments which have the lowest average values.

Subsequently, the noise power is estimated by multiplying this noise per cell value by the number of frequency cells. All three methods are subject to biases of insufficient sampling.

A novel and perhaps more objective noise estimation technique first

described by HILDEBRAND and SEKHON (1974) and used at Poker Flat is based on the statistics of a Gaussian random variable. Specifically, the ratio of the variance to the square of the mean of the spectrum is computed.

$$R_n = \{ \sum_{i=1}^{n} S_i^2 - 1/n( \sum_{i=1}^{n} S_i)^2 \} / \{ 1/n( \sum_{i=1}^{n} S_i)^2 \, 1/M \}$$

where $S_i$, i = 1, n are the n smallest values of a spectrum obtained from the average of M sequential spectra (A. C. Riddle, private communication, 1983). An estimate of the noise level is determined from the mean value of the N smallest values of the spectrum for which $R_n > 1$, $n > N$. In any procedure of noise estimation from the spectrum, spectral leakage of signal and clutter to other frequencies must be compensated for in order to obtain an unbiased noise estimate. Noise estimation from the spectrum includes all contributions (cosmic, atmospheric, system, interference) and provides a suitable value for signal/noise (S/N) determination.

Following determination of the noise level, one can proceed to estimate the signal parameters of interest, usually power, Doppler shift, and width. A simple but crude approach to signal estimation is to attribute the largest peak to the signal, using the peak value as the signal power and its frequency as the Doppler shift. This method, while fast and computationally simple, is subject to biases with the frequency resolution as good as the spectrum's. Furthermore, one must ascertain that peaks from non-signal sources have been eliminated or recognized and compensated for.

The most common method of estimation of signal parameters is the calculation of the first 3 spectral moments. In general the noise level is calculated and subtracted out. Some signal-to-noise criterion is used to discard weak and uncertain signals; if the peak-to-noise ratio is below some threshold level, that spectrum is eliminated before the moment calculations. Then the spectral moments are calculated for some frequency band centered about the peak of the spectrum. The signal power, velocity and width are characterized by the zeroth, first and second moments of the band limited spectrum, respectively. At Poker Flat, a window centered at the largest peak in the spectrum is set for moment calculations; starting at the center peak, all contiguous points with values greater than the noise level are attributed to the signal. At Millstone Hill the peak of the spectrum is found and some window is chosen; then the 1st moment is recursively calculated, with a window centered at the value of the 1st moment of the previous iteration. The number of iterations and window width may be fixed or may be varied so that the window size converges to a width where signal is present. Subsequent to the choice of a window the first 3 spectral moments are calculated. In general, estimation of signal parameters by moment calculations is a straightforward method, can be performed on-line in real time, and provides unbiased estimates over the ensemble average. In cases when true signal widths are narrower than the frequency resolution of the spectrum, or when signal strength is weak and comparable to noise power fluctuations, the signal velocity is biased towards the nearest frequency bin.

A powerful but computationally intensive technique for parameter estimation of the signal is to fit the measured spectrum to a theoretical one using an N-L (nonlinear) least squares fitting routine. Such a method has been implemented at Arecibo by SATO and WOODMAN (1982), where computed spectra of atmospheric echoes are Fourier transformed into ACFs and subsequently fitted to a theoretical ACF. Time domain fitting has certain computational advantages over spectral domain fitting. Either eight or eleven parameters are fitted to the ACF:

| | |
|---|---|
| 1 | zero frequency (dc) component, i.e., non-fading clutter; |
| 2-5 | power, width, Doppler shift, form of fading clutter; |
| 6-8 | power, width, Doppler shift of signal; |

9-11 power, width, Doppler shift of secondary peak due to ghost echo, ocean clutter, or secondary signal.

An N-L squares fitting method in the spectral domain has been used to fit three signal parameters (power, velocity, width) to measured spectra from Jicamarca by CORNISH et al. (1982). The N-L least squares approach offers the advantages of a frequency resolution which is better than the sampling interval of the spectrum, the estimation of spectral widths even as narrow as a frequency cell, and the inclusion of contaminating effects, e.g., clutter, in the actual fitting and estimation of signal parameters. The biggest drawback of the N-L least squares approach is that it is computationally intensive; at Arecibo a profile of 150 heights collected over a minute's duration requires one minute of post-collection processing with an array processor. Furthermore, the nonlinear fitting necessitates constraints and initial values; the former may be unduly restrictive at times, the latter requires prefitting guesses obtained by visual inspection, computer algorithms such as moment calculations, or comparison to other wind measurements such as radiosonde data.

So far we have considered parameter estimation of the signal and clutter and interference elimination only for a single spectrum. There exist temporal and spatial continuities in a time series of spectral profiles which can be employed. Certain a priori information such as the occurrence of power line radiation at 60 Hz and harmonics or the characteristics of fading clutter (e.g., magnitude, persistence in time and diminution with height) is useful in minimizing contaminating effects. Echoes backscattered from the atmosphere exhibit continuity in time and height that can restrict the search of signal peaks to a certain part of the spectrum. Doppler tracking from height to height uses continuity arguments for establishing a window to search for a signal within based on Doppler shift of an adjacent height; such schemes are employed at Arecibo and Millstone Hill. Furthermore, aliased spectra can be unwrapped if height continuity arguments show that they are indeed aliased. A full profile of spectra can provide additional information about the spectra such as the occurrence of ducts as seen in Figure 2; without such continuity arguments and confusion over two signal-like peaks would arise.

Temporal continuity provides initial guesses for the estimation of signal values. At Arecibo initial guesses to the N-L least squares routine are computed from a weighted average of previous fitted values at a given height. Temporal and height continuity restrictions are dependent on the temporal and height resolution of the probing radar system in relation to the temporal and height variations of the scattering atmosphere. While temporal and height continuities confine a signal window to a part of the spectrum, it is still possible for the algorithm used for parameter estimation of the signal to lock onto some spurious peak or interference. Such "wandering" effects can be checked and minimized. One proposed algorithm checks minima between peaks, attributes minima above the noise level to a multi-peaked signal, and combines these above-noise-level peaks and valleys in subsequent moment calculations (A. C. Riddle, private communication, 1983). In the future, image processing techniques may be helpful in tracing backscatter echoes in height and time.

The selection of a particular parameter estimation technique is determined by the information desired and the capabilities of the particular radar and processing systems to obtain it. On the one hand, one may want highly accurate and precise estimates of spectral widths from atmospheric backscatter to study atmospheric turbulence. On the other hand, precision may be sacrificed in order to obtain a continuous long term series of the 3-D wind vector over many heights for studies of planetary waves and longer period oscillations. The need and availability of on-line and post-collection processing, limitations of computer memory and speed, availability of array processors and special devices and development of general use and special use software are considerations in the

selection and implementation of a parameter estimation technique.

ACKNOWLEDGEMENTS

The author gratefully acknowledges the useful discussions with D. A. Carter and W. L. Ecklund about the Poker Flat MST radar and with P. K. Rastogi about the Millstone Hill radar.

REFERENCES

Clark, W. L. and D. A. Carter (1980), Real-time scaling of atmospheric parameters from radars using the MST technique, Preprint Vol. AMS 19th Conf. on Radar Meteorology, AMS, Boston.

Cornish, C. R., B. B. Balsley, D. T. Farley and R. F. Woodman (1982), Observations of radar scatter from entire altitude region to 97.5 km above Jicamarca, Abstracts, National Radio Meeting (Boulder), Jan. 1982.

Hildebrand, P. H. and R. S. Sekhon (1974), Objective determination of the noise level in Doppler spectra, J. Appl. Meteor., 13, 808-811.

Hocking, W. K. (1983), Mesospheric turbulence intensities measured with a HF radar at 35°S - II, J. Atmos. Terr. Phys., 45, 103-114.

Sato, T. and R. F. Woodman (1982), Spectral parametr estimation of CAT radar echoes in the presence of fading clutter, Radio Sci., 17, 817-826.

Schmidt, G., R. Ruster and P. Czechowsky (1979), Complementary code digital filtering for detection of weak VHF signals from the mesosphere, IEEE Trans. Geosci. Elec., GE-17, 154-161.

# 8.6B PROPERTIES OF ECHO SPECTRA OBSERVED BY MST RADARS

K. Wakasugi

Kyoto Institute of Technology
Matsugasaki, Kyoto 606
Japan

## INTRODUCTION

Turbulent scatter and Fresnel reflection are the fundamental echoing mechanisms to interpret the signals observed by MST radars (HARPER and GORDON, 1980). Turbulent scattered echoes provide information about the turbulence structure and mean flow of the atmosphere. Observational results with VHF MST radars, however, show the importance of Fresnel reflection due to the infinite gradient of reflectivity at the edges of a scattering layer. This condition is excluded for the weak fluctuation models but it is still possible to include the observed aspect sensitivity by assuming an anisotropic structure of fluctuations. This paper tries to give another explanation of the aspect sensitivity observed by MST radars. Spectral estimates by the widely used periodogram are related to a four-dimensional spectrum of atmospheric fluctuations with anisotropic structure. Effects of radar system such as antenna beam width, beam direction and FFT data length are discussed for anisotropic turbulent atmosphere. Echo parameters are also estimated.

## PERIODOGRAM ESTIMATION

The Fourier transform of scattered echo, $Q(\omega)$, is defined as follows;

$$Q(\omega) = \int w(t)q(t)\exp[-j\omega t]dt \qquad (1)$$

where $q(t)$ and $w(t)$ are the sampled data at pertinent altitude and the FFT window function, respectively. The periodogram of $q(t)$ is defined as the ensemble average of $QQ^*$.

$$\langle |Q(\Omega)|^2 \rangle = \iint \Phi(K,\omega)|H(K,\omega-\Omega)|^2 dKd \qquad (2)$$

where $\Phi$ is a four-dimensional (space-time) spectral density which we have expressed as the product of a power-law spatial spectrum and a Gaussian temporal spectrum (ISHIMARU, 1978).

H represents the effects of the radar used for the observations. Radar frequency, antenna beam width, pulse waveform and data length of the FFT window determine the properties of H. LIU and YEH (1980) showed that the classical Booker-Gordon formula is valid when the condition $D/\lambda_F << \lambda/Lo$ is satisfied, where D and $\lambda_F$ are the antenna beam extent and the Fresnel radius at altitude z, respectively. For anisotropic fluctuations, the effective horizontal length scale becomes comparable to the Fresnel radius, thus $H(K, \omega-\Omega)$ is computed to include the phase difference of incident waves in the scattering region.

Figure 1 shows an example of the calculated periodograms. Parameters for the calculation are given in the figure. The dotted line represents the temporal spectrum of $\Phi(K, \omega)$. It shows that the observed spectral width does not always agree with that of the temporal fluctuation.

## PARAMETER ESTIMATION

We now discuss a moment dependence of periodograms on the beam width, beam direction and FFT data length.

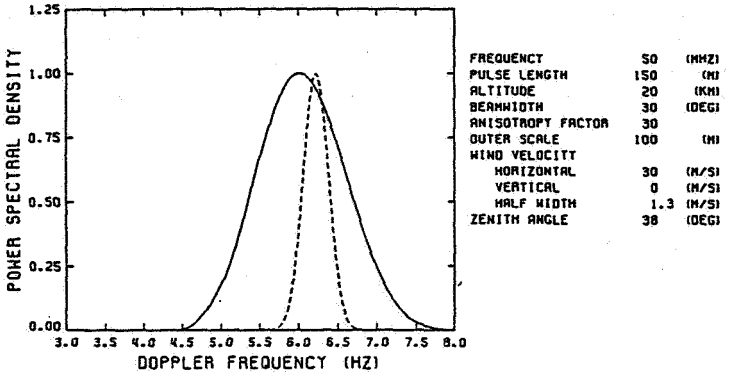


Figure 1. An example of estimated periodograms.

Figure 2 shows the zeroth moment (echo power) dependence on the zenith angle. When the anisotropy of fluctuations is relatively small, the angle of coherence cone is much wider than the antenna beam width, resulting in the echo power slightly dependent on the zenith angle. Results observed by the Jicamarca radar conclude, however, that the difference of echo power between the vertical and off-vertical (3 degrees from the zenith) beams is about several decibels (FUKAO et al., 1980). Our calculation suggests that the horizontal length scale of fluctuations is about a few tens times larger than that of the vertical direction.

For the first moment of periodograms, the estimation error increases for larger values of anisotropy with wider antenna beams. But the relative error is very small, thus it could be concluded that the effects of the radar system on thw Doppler velocity estimations are virtually neglected.

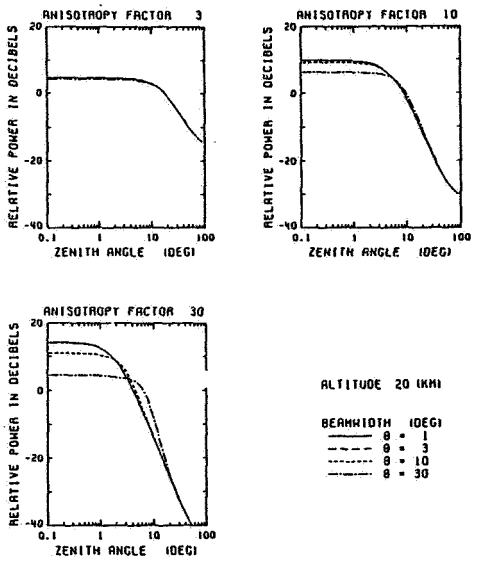


Figure 2. Echo power versus antenna zenith angle.

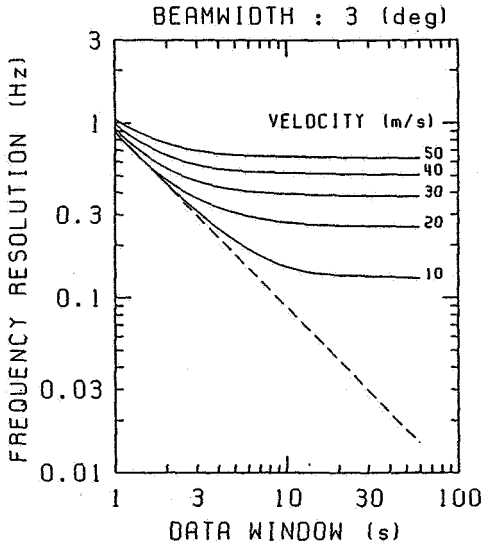


Figure 3. Frequency resolution versus FFT window length.

The bandwidth of H in the frequency direction determines the frequency resolution of periodograms, which then affects the estimations of the second moment. Figure 3 shows the relation between the spectral resolution and the time duration of FFT window. When the horizontal velocity of fluctuations is relatively small, the resolution is inversely proportional to the FFT duration. The resolution converges to a certain value that is determined by the beam width and/or wind velocity. This is due to the finite extents of scattering volume.

## CONCLUSIONS

The effect of finite space-time extents is examined for spectral estimations or MST radar observations. An aspect sensitivity of scattered echo can take place in the case of a weak refractive index fluctuations with anisotropic structure.

## ACKNOWLEDGEMENTS

The author wishes to thank Prof. S. Kato and Dr. S. Fukao for interesting suggestions and constructive comments.

## REFERENCES

Fukao, S., T. Sato, R. M. Harper and S. Kato (1980), Radio wave scattering from the tropical mesosphere observed with the Jicamarca radar, Radio Sci., 15, 447-457.

Harper, R. M. and W. E. Gordon (1980), A review of radar studies of the middle atmosphere, Radio Sci., 15, 195-212.

Ishimaru, A. (1978), Wave Propagation and Scattering in Random Media, Vols. 1 and 2, Academic Press, New York.

Liu, C. H. and K. C. Yeh (1980), Scattering of VHF and UHF radar signals from the turbulent air, Radio Sci., 15, 277-282.

# 8.6C PARAMETERIZATION OF SPECTRUM

A. C. Riddle

CIRES/NOAA Aeronomy Laboratory
Boulder, CO 80303

Typical of many radars used for wind sounding, the Poker Flat, Alaska, radar generates Doppler power spectra as output. For compact data archiving purposes, as well as for data analysis, it is desirable to produce a few parameters to characterize each spectrum. The parameters chosen are noise level, echo signal strength, velocity and width. Both because this is an experimental radar and because the derived parameters may be the only quantities available for future analysis, it is important that the parameters do not contain biases imposed by the derivation techniques. This consideration has led to a processing scheme in which the parameters are derived independently for each spectrum.

The parameterization scheme adopted for use at Poker Flat (D. A. Carter, NOAA) commences with a noise level determination based on the HILDEBRAND and SEKHON (1974) method. The Hildebrand and Sekhon method utilized the expected relationship between mean and variance for the spectrum of white noise source. In the Carter implementation the quantity

$$R_n = \{\sum^{n} S_i^2 - \frac{1}{n}(\sum^{n} S_i)^2\} \Big/ \{\frac{1}{n}(\sum^{n} S_i)^2 \cdot \frac{1}{M}\} \qquad (1)$$

(where the $S_i$, i = 1, n, are the n lowest values of all the spectral points evaluated and M is the number of independent transforms used to generate the spectrum) is evaluated over all values of n. The noise level is chosen to be the mean value of the N lowest points for which $R_n > 1$ for all $n > N$. Although Hildebrand and Sekhon developed this objective method for determination of noise levels on spectra with many hundreds of points, this implementation has been found to work surprisingly well on spectra with as few as 32 points.

Once the noise level has been determined, the normal method used to identify the signal is to look for the largest value in the spectrum and assign to the echo all those contiguous points with values that are above the noise level and include the peak. The zeroth, first and second moments of the components of the selected points above the noise level are taken to be the signal strength, velocity and half-width parameters characterizing this spectrum. Over an ensemble average these parameters are unbiased. However, for an echo whose width is comparable to the spacing between points, or whose power is comparable with the noise power fluctuations, the strength and width are underestimated and the velocity is biased towards the nearest spectral point.

The parameterization above is maximally unbiased by considerations of past values, expected echo profiles or other expectations. However, in our subsequent analysis the spectral parameters are routinely checked against expectations and past values in order to cull out erroneous data. It is found that this post-parameterization selection process is usually effective.

However, we have experienced a class of interference that puts a false echo on the spectrum. Typically, this false echo increases slowly in strength and then weakens. This causes the derived velocity to slowly transfer from the true echo velocity to the false one and back. Under these circumstances the post-parameterization selection processes often fail. We are experimenting with another method of signal selection to eliminate this problem. The newer method

uses expectations of the genuine echo shape. In particular, the method makes use of the fact that genuine echoes are generally compact and without extreme multiple peaks. The technique initially selects as potential echoes those regions between minima in the spectrum. Adjacent regions are then examined and are combined only if the minimum between them is significantly above the noise when compared with the peak values in each region. This process often separates genuine and false echoes when the earlier method would have combined them. Although it is still possible to "lock-on" to the false echo the transition from true to false echo selection is likely to be abrupt and hence more obvious to the post-parameterization selection criteria. Further investigation of this process is in progress.

REFERENCE

Hildebrand, P. H. and R. S. Sekhon (1974), Objective determination of the noise level in Doppler spectra, J. Appl. Meteorol., 13, 808-811.

# 8.7A SPECTRAL MOMENT ESTIMATION IN MST RADARS

R. F. Woodman

Instituto Geofisico del Peru
Aportado 3747
Lima, Peru

## INTRODUCTION

Due to the random nature of turbulence, radar returns from turbulence-induced fluctuations are stochastic processes and have to be characterized statistically. The returns from any one height form a random time series which, for the purpose of this work, we will consider quasi-stationary (stationary within an integration time) and Gaussian. Both assumptions are fair and very close to reality; one can always adjust the integration time so that the first assumption is true; the second is a consequence of the multiscattering nature of the radar return.

A Gaussian and stationary process is fully characterized by its autocorrelation function, $\rho(\tau)$, or equivalently by its Fourier transform, the frequency power spectrum, $F(\omega)$. Because of the Gaussian distribution of velocities in the turbulent scatter volume, we know the shape of these functions: they are also Gaussians. Thus, the processes we will be discussing are Gaussian stationary processes with a Gaussian shaped power spectrum. The first qualifier refers to the multivariant amplitude distribution of the signal proper and the second to the distribution of the power at different frequencies, i.e., its spectral shape. They should not be confused. The autocorrelation function has also a (complex) Gaussian shape, since the Fourier transform of a Gaussian is also Gaussian.

A Gaussian power spectrum has the form

$$S(\omega) = \frac{P}{\sqrt{2\pi W^2}} \exp[-(\omega - \Omega)^2/2W^2] \qquad (1)$$

It is fully defined by the value of three parameters: P, $\Omega$, W. They correspond to the total power, the frequency shift and the spectral width, respectively. They contain all the information we can obtain from the radar echoes, and they are all we need to know to characterize the process. They are a measure of three important physical properties of the medium: turbulence intensity, mean radial velocity and velocity dispersion (turbulent velocity variance, $\langle \mu^2 \rangle^{\frac{1}{2}}$, under certain conditions).

These three parameters correspond, also, to the three first moments of $S(\omega)$, defined as

$$P = \int s(\omega)\, d\omega \qquad (2)$$

$$\Omega = \frac{1}{P} \int \omega\, S(\omega)\, d\omega \qquad (3)$$

$$W^2 = \frac{1}{P} \int (\omega - \Omega)^2\, S(\omega)\, d\omega \qquad (4)$$

It is preferable to take (2), (3) and (4) as the definition of the three parameters of interest, P, $\Omega$ and W, since they are always well defined, even in the case when there are deviations from our assumptions and expectations about the nature of the process.

The scope of the present paper is to review signal processing techniques which have been used, or should be used, in MST radars, i.e., techniques which lead to a good estimation of the three first moments of the spectrum.

The number of possible estimators for P, $\Omega$ and $W^2$ is unlimited. Therefore, we can not be exhaustive. In order to reduce the scope of the paper to bounds, we shall limit ourself to "good" estimators and to estimators that are presently in use.

We would like to talk about "best" estimators, but we have a problem, since there are two criteria for goodness one would like to satisfy: the estimator should be good from an statistical point of view, i.e., the variances of the estimated values should be as close to minimum as possible, but at the same time they should be practical. These two criteria are usually not compatible. As one improves the goodness of an estimator one increases the complexity of the procedure. It is possible to talk about best estimators from an statistical point, as we will see when we talk about the Maximum-Likelihood (M-L) estimators, but they are very difficult if not impossible to implement. In general one would like a procedure which one can use in real time. This requirement can be very limiting, not so much because of the time scale of the processes, which are relatively slow, but for the large number of parallel channels one has to process. The demands are very large if one is after the whole MST region with high altitude resolution.

We can limit the scope of our paper, if we limit ourself to representative techniques which have been actually implemented in MST radars. We shall do this, but include also some discussion about M-L estimators since they give us a limit in performance with which we can compare other techniques.

Recently ZRNIC'(1979) has reviewed the subject of spectral moment estimation. Although the paper was motivated by weather radar applications and needs, it is fully applicable for MST radars. We shall take advantage of this review, avoiding repetition, unless we want to stress important conclusions. This includes the references; the reader will find a very extensive list of references in Zrnic's review.

In the next section we shall describe straightforward power spectrum approaches, we shall then describe and discuss a correlation or covariance approach and finally the M-L estimator concept and discuss the limits of performance they define.

## MOMENT ESTIMATORS VIA POWER SPECTRUM

The most straightforward estimators of the three parameters of interest is suggested by their definition, through (2), (3) and (4). We should remember, though, that we cannot obtain in practice $S(\omega)$; we obtain instead statistically estimated values of it, $S'(\omega_i)$ at a finite discrete number, N, of points of frequencies.

The definitions suggest the following estimators, P', i' and W', for P, $\Omega$ and W:

$$P' = \sum_{i=1}^{N} S'(\omega_i) \tag{5}$$

$$\Omega' = \frac{1}{P'} \sum_{i=1}^{N} \omega_i \, S'(\omega_i) \tag{6}$$

$$W'^2 = \frac{1}{P'} \sum_{i=1}^{N} (\omega_i - \Omega')^2 \, S'(\omega_i) \tag{7}$$

We need then, procedures, hopefully optimum, to find good estimated values of the power spectra. This is a very old and general problem for which there is extensive literature. The reader is referred to the book by BLACKMAN and TUKEY (1958) for an introduction, and to the section on spectral estimation in the IEEE book on signal processing for more modern approaches (RABINER and RADAR, 1976).

We would like to point out, that unless the sampling frequency, $1/T_s$, is larger than the mean frequency plus a few spectral widths, $2\Pi(\Omega + 2W)$ , $\Omega'$ and $W^2$ as given by (6) to (7) would be biased because of aliasing. This bias can be reduced if we assume periodicity and calculate the moments centered around a good guess of $\Omega$. Let $\omega_j$ be a good guess of the actual value of $\Omega$, then we evaluate a correction $\omega_\varepsilon^j$ such that $\Omega' = \omega_j + \omega_\varepsilon$, $\omega_\varepsilon$ is evaluated from

$$\omega_\varepsilon = \frac{1}{N} \sum_{i=j-N/2}^{i=j+N/2} (\omega_i - \omega_j) \, S'(\omega_i) \tag{8}$$

the spectral width is better estimated from

$$W' = \frac{1}{P} \sum_{i=j-N/2}^{i=j+N/2} (\omega_i - \omega_j + \omega_\varepsilon) \, S'(\omega_i) \tag{9}$$

In practice the problem is complicated by the fact that the signal is contaminated with noise and echoes from efficient targets on the ground (ground clutter). If we have an independent way of evaluating the noise power spectrum, $N(\omega)$, the algorithms presented in (5) to (9) are still valid provided we replace $S'(\omega)$ by $S''(\omega) - N$, where $S''(\omega)$ is the power spectrum estimate including noise. Here the noise spectra have been taken as constant independent of frequency since usually the receiver bandwidth is much narrower than the PRF, and there is no correlation between noise at two different sample pulses. The noise level can be estimated from an altitude where there is practically no signal, for instance from 45 km or from ionospheric altitudes, or from a few pulses with the transmitter off. The last approach requires a fraction, but fortunately small, of the observing time, since the noise level is independent of altitude and one can use an average of the estimates from all the different altitudes.

The presence of ground clutter presents a source of bias and an additional problem. Different techniques have been used to cancel or minimize its effect. Ground clutter signals have a spectral signature which consist essentially of a single spectral line at the origin with a strength which depends on the ground shielding of the radar. At tropo- and stratospheric heights, it is at least comparable to the signal, and often many orders of magnitude larger. When the clutter is strong enough, it presents, in addition, a component of the spectrum with a spectral width comparable to the signal strength width. This results from the slight propagation fading of the clutter. As in the case of noise, one should subtract the contribution of this interference before evaluating the moments. This contribution can be easily estimated in the case of non-fading clutter. The clutter adds a constant value to the signal, i.e., a spectral line, and can be estimated by integrating the returns for as long as the spectral estimation time (usually one or two minutes). One can, then, subtract the theoretical contribution of this constant component.

The fading component is difficult to estimate independently. One way to eliminate its biasing effect is to ignore the frequencies around zero (dc) frequency. This is only possible when the signal is frequency shifted by a magnitude larger than its width. This occurs frequently and presents difficulties only when one is looking too close to vertical, or the medium velocity is too slow (of the order of 1 m/sec or less). Another technique takes advantage of the symmetry of the ground clutter component. It consists of evaluating the antisymmetric component of the spectrum, replace the negative powers by zero, and evaluate the moments of what is obtained (SATO and WOODMAN, 1982). This technique also has difficulties when the signal is too close to the center or to the Nyquist frequency.

In using the spectral moment technique the observer has some freedom in selecting the frequency spectrum estimating algorithm, the sampling frequency (or size of the spectral window) and the frequency resolution. This freedom has direct implications on the processing speed.

As far as the estimating algorithm, most modern procedures use a Fast Fourier Transform. This is an efficient way of doing it and should always be pursued, unless one has a hardwired autocorrelator. One should always use algorithms especially designed for $2^n$ samples, and if possible, specially designed for the particular exponent, n, selected. There can be considerable savings in time this way.

As far as the sampling frequency and maximum (Nyquist) frequency are concerned, the MST signals deserve some special considerations. The maximum duty cycle and maximum range of interest permit, in MST radars, pulse repetition frequencies which can be more than two orders of magnitude higher than the maximum frequency content of the signals. This produces high redundance in the sampling and calls for some signal filtering; not so much to increase the system sensitivity -- as one sometime reads or hears -- as for reducing the information input into the spectrum system and the amount of signal processing. As it is well known, an FFT evaluation takes, N ln N additions and computations. A reduction, of let us say, a factor of 256 in the number of points, speeds up processing by a factor of 2000.

The simplest and easiest filter to implement digitally is a boxcar integrator (coherent integration). This simply integrates N number of samples from a given altitude, takes the integrated value as a sample of the filtered output and resets the integrator register to zero, ready for the next integration. The integration time should not be much larger nor shorter than half the period of the expected maximum Doppler frequency shift plus the expected spectral width. The integration time defines the sampling rate. Some undersampling and consequent aliasing can be allowed, if (8) and (9) is used for the evaluation of $\Omega'$ and $\sigma$; but, any oversampling is a waste of effort.

Another processing parameter that the observer has some freedom to choose is the frequency resolution. It is inversely proportional to the size of the time span taken in evaluating the DFT or the time width of the weighting function (Hanning window, etc.). The latter should not be much longer than the correlation width, say 2 or 4 times the half correlation time, since this will give us 4 or 8 points to sample the spectral function shape, more than enough to determine the three parameters that define it. Higher resolution increases the processing effort without much gain in parameter accuracy.

In order to discuss the goodness of the spectral moment estimators we need to know the variances $\sigma^2$, $\sigma^2$, $\sigma^2$ of the estimated values with respect to their expectations. $\sigma_{Pi}^2 = \xi(P_i - \langle P_i \rangle)^2$. This in general depends on the algorithm used for the evaluation of $S'(\bar{\omega})$. We will quote here the results obtained by MILLER (1974).

He gives us a simple expression for the variances for the case of a Gaussian-shaped spectrum with no additive noise. The derivation was made assuming a continuous time series weighted with a Gaussian window of width $T/2\pi$. The variances, using our notation, are given by

$$\sigma_{\Omega}^{2} = \frac{W^{2}}{2N[1 + (WT)^{2}]^{\frac{1}{2}}} \tag{10}$$

$$\sigma_{\omega} = \frac{3W^{2}}{16N[1 + (WT)^{2}]^{\frac{1}{2}}} \tag{11}$$

Usually $WT > 1$, since it is a good practice. Also we have that for a given observation time $T_o$, the number of DTFs is given approximately by $T_o/2T$. In terms of $T_o$ we can then write

$$F_{\Omega} \equiv \frac{\sigma_{\Omega}\sqrt{T_o W}}{W} \approx 1 \tag{12}$$

$$F_{W} \equiv \frac{\sigma_{\omega}\sqrt{T_o W}}{W} \approx \frac{3}{8} \tag{13}$$

which are figures of merit, that serve to compare different techniques. They normalize the variances with respect to the width of the spectra and include the dependence on the square root of the number of degrees of freedom (number of independent samples) which should be common to any estimator.

One can improve on the estimators 5, 8 and 9 with additional effort. Following a rule that one should not use data that carries no information, one should use only those points in the spectrum, $W_i'$ for which there is a significant value for $S'(\omega_i)$, especially when the signal is contaminated with noise. This can be achieved with very little additional processing time, once we have a reasonable estimate for the mean frequency and its width.

We can, in general, say that the spectral moment approach provides good estimators of the desired parameters. It involves the real-time evaluation of DFTs for every altitude. This is a time-consuming operation, but fortunately MST echoes are slow, specially at 50 MHz. With proper filtering (coherent integration) and the use of FFT processors, it should be possible to perform the necessary operations in real time, even in the case of high resolution radars. The processing system at the Arecibo radar, for instance, is capable of processing in real time 32-point spectra, at 256 heights (WOODMAN, 1980). It is actually capable of processing at least 4 times more information, being limited at present by the memory capacity of an array processor. It should be pointed out that the frequency of the Arecibo radar is 430 MHz, producing time series close to ten times faster than a 50-MHz radar and, therefore, ten times more demanding. The coherent integration is performed by a special purpose preprocessor (a decoder). On the other hand, with the present state of the art, real-time full-spectral processing of high-resolution radars is not possible with a simple minicomputer. One needs the help of a special purpose coherent integrator and an FFT processor.

## PARAMETER ESTIMATION BY NONLINEAR CURVE FITTING TECHNIQUES

The processing scheme described and discussed above implements the defining equations (2), (3) and (4) and does not take advantage of the knowledge about the spectral shape. There is a golden rule in detection theory that one should make use ot as much information as one has and ask only what one ignores. Equation (1) suggests another technique for evaluating the moments, or more properly -- in this approach -- the parameters P, $\Omega$ and $W^2$. We can ask for a set of parameters such that $S(\omega) = S(\omega; P, \Omega, W)$ best approaches, in a least-squares sense, the experimentally determined set $\{S'(\omega_i)\}$, for all i's. This is a standard parameter estimation problem. This approach is more time demanding, but should produce better estimates of P, $\Omega$ and W. In fact we shall see later that, with proper weighting, parameters obtained in this way are maximum likelihood estimates for a given set of experimental estimates $\{S'(\omega_i)\}$.

The technique consists in minimizing an expression of the form

$$\varepsilon^2 = \sum_{i=1}^{N} A_i \left[S'(\omega_i) - S(\omega_i; P, \Omega, W)\right]^2 \qquad (14)$$

The problem is nonlinear in the unknowns, P, $\Omega$, W and involve special techniques. The reader is referred to the text by BARD (1974) for a comprehensive treatment.

This approach has been taken by SATO and WOODMAN (1982) to process ST spectra obtained with the 430 MHz. In fact, they used the technique to estimate up to 8 additional parameters which define the noise, N, ground clutter interference, and if necessary, possible interference from strong turbulent layers from lower altitudes which leak to higher altitudes through code sidelobes. The technique includes instrumental and signal processing sources of distortion and biases in the theoretical function. In this way, the parameters of interest are evaluated free of all sources of biasing. Notice that an estimation of noise level and clutter characteristics are obtained simultaneously with the signal parameters. This approach involves first the estimation of $S'(\omega)$, as in the previous case. The parameter information is obtained at the cost of additional processing.

Nonlinear automatic least square parameter estimation involves nontrivial procedures. In the case of Arecibo, the additional processing is performed off line (SATO and WOODMAN, 1982). This takes -- making use of a floating-point array processor (AP-120) -- a time equivalent to the time it took to obtain the data. It is feasible to perform this additional processing in real time by doubling the processing capacity. Although, for many applications, it would not be necessary to perform the nonlinear estimation in real time.

## THE AUTOCOVARIANCE OR AUTOCORRELATION APPROACH

One of the most efficient techniques from the point of view of processing requirements is the single delay autocorrelation approach. In this approach the signal power and the autocovariance at a single delay is evaluated through the classical estimators

$$P' = \rho'(o) = \frac{1}{N} \sum_{i=1}^{N} x_i x_i^* \qquad (15)$$

$$\rho'(\tau) = \frac{1}{N-\tau} \sum_{i=1}^{N-\tau} x_i x_{i+\tau}^* \qquad (16)$$

where $x_i$ is the ith complex sample corresponding to a given altitude. The mean frequency shift and the velocity spread $\Omega'$ and $W'$, are then obtained from

$$\Omega' = \frac{\phi(\tau_1)}{\tau_1} \tag{17}$$

$$W^2 = 2\,\frac{1 - |\rho'(\tau_1)|/(\rho(o) - \text{Noise}}{\tau_1^2} \tag{18}$$

The technique takes advantage of the relationship that exists between the nth derivation of the correlation function evaluated at the origin and the nth moment of the frequency spectrum.

The technique was first used in 1968 by WOODMAN and HAGFORS (1969) for estimating the electromagnetic drift of ionospheric plasmas at Jicamarca, and it was first used in 1972 by WOODMAN and GUILLEN (1974) for stratospheric and mesospheric applications. The technique is in much use today by the weather radar community, but, apparently, as a consequence of some independent work by RUMMLER (1968) and by MILLER and ROCHWARGER (1972) and has been subjected to much discussion and evaluation in the literature.

This technique involves only two complex multiplications and additions per altitude sample, as compared to lnN in the case of spectral moment estimation (where N is the number of spectral points). The variance of this approach, seemly surprising, is comparable to the one obtained by integrating the moments of the frequency spectrum (RUMMLER, 1968; WOODMAN and HAGFORS, 1969). But, this should not come as a surprise. After all, it is easily accepted that evaluating the power via the average of the square of the magnitudes (equation 12) yields the same value as the one evaluated by integrating the area of the frequency spectrum (equation 5). This is only a particular case, corresponding to the zeroeth moment of a more general rule.

Woodman and Hagfors give us a simple expression for the variance of the mean angular frequency shift, valid for large Ns and small resultant values of $\tau^2\sigma_\Omega^2$(<<1 radians):

$$\sigma_\Omega^2 = \frac{\rho(o) - \rho^2(\tau)}{2\tau^2 N\,\rho^2(\tau)} \tag{19}$$

It is interesting to compare the figure of merit of this approach as with that of 12. For large S/N ratios and Gaussian-shaped autocorrelation functions, 18 takes its best values at small $\tau$s.

$$\sigma_\Omega^2 = \frac{W^2}{2N} \tag{20}$$

For a given observation time $T_o$, the number of (sufficiently) independent estimates is $N \simeq T_o W$. Hence,

$$F_\Omega \simeq 1/\sqrt{2} \tag{21}$$

comparable to the spectral moment approach.

Later on, when we consider the case of using autocorrelation values at multiple delays, we shall see that the variances of the estimate using the single delay technique is close to optimum only when the signal-to-noise ratio

is high. This relative good performance deteriorates as the signal-to-noise ratio goes down. But, it should be mentioned that the same happens with the spectrum moment approach represented by equations (5), (6) and (7), but not of the more sophisticated algorithm which includes weighting the spectral density by zero in the regions where there is no signal (match filter approach), or with the parameter estimation technique we have previously discussed.

Another limitation of this technique is the difficulty in discriminating against fading ground clutter or any other kind of interference. Fortunately, in many MST installations, there is only nonfading clutter and white noise to worry about, and the biasing effect they produce can be eliminated by subtracting independent estimates of their contributions to $\rho(o)$ and $\rho(\tau)$. These estimates can be obtained by the same methods described before for the spectral moment approach.

Going from (3) and (4) to (17) and (18) involves approximating the derivative of $\rho(\tau)$ by finite differences between $\rho(o)$ and $\rho(\tau)$. This presents a bias which could become significant for relatively large $\tau$s (MILLER, 1972). Fortunately, in the case of symmetric spectrum, equation (17) is an equality and the bias disappears. This is important since optimum values of $\tau$, for noisy signals, are not close to the origin.

We are reproducing here, two graphs (Figures 1 and 2) from MILLER (1972) which depict the performance of the single delay, autocorrelation technique, by plotting the standard deviation of the estimates for $\Omega$ and W as a function of the sample separation $\tau(\equiv h$, in their notation).

From Figures 1 and 2 we can see that the best separation for $\tau$ is that around a characteristic width of the correlation function 1/W and that, for noisy signals, the standard deviations of the estimates $\Omega_i'$ and $W_i'$ are inversely proportional to the S/N ratio. Similar plots were produced by WOODMAN and HAGFORS (1969) but for a typical incoherent-scatter autocorrelation function shape.

It should be mentioned that the single delay autocorrelation approach, in contrast to the frequency spectrum approach, is very sensitive to the pre-filtering of the time series. Filtering of the signal in this case does improve the signal-to-noise ratio and hence reduces the variance of the estimates. As it is to be expected, optimum results are obtained using a matched filter, matched to the shape of the signal spectrum. But, a boxcar integator (coherent integration) produces similar results and it is much easier to implement. It should be kept in mind, in any case, that filtering could be a source of $\Omega$ and W biasing. This bias can be computed theoretically and should be corrected.

## COVARIANCE APPROACH AT MULTIPLE DELAYS

If the covariance approach was so efficient at a single delay, it is natural to ask how much improvement can be obtained using more than one delay, $\tau$. Let $\Omega_i$ and $\sigma_i$ be estimates of $\Omega$ and $\sigma_i$ obtained on the basis of equations (17) and (18) for different values $\tau_i$ of $\tau$. We can always obtain a new estimate $\Omega_a$, $W_a$ through

$$\Omega_a = \sum_{i=1}^{M} C_i \Omega_i \tag{22}$$

$$W_a = \sum_{j=1}^{M} C_j W_j \tag{23}$$

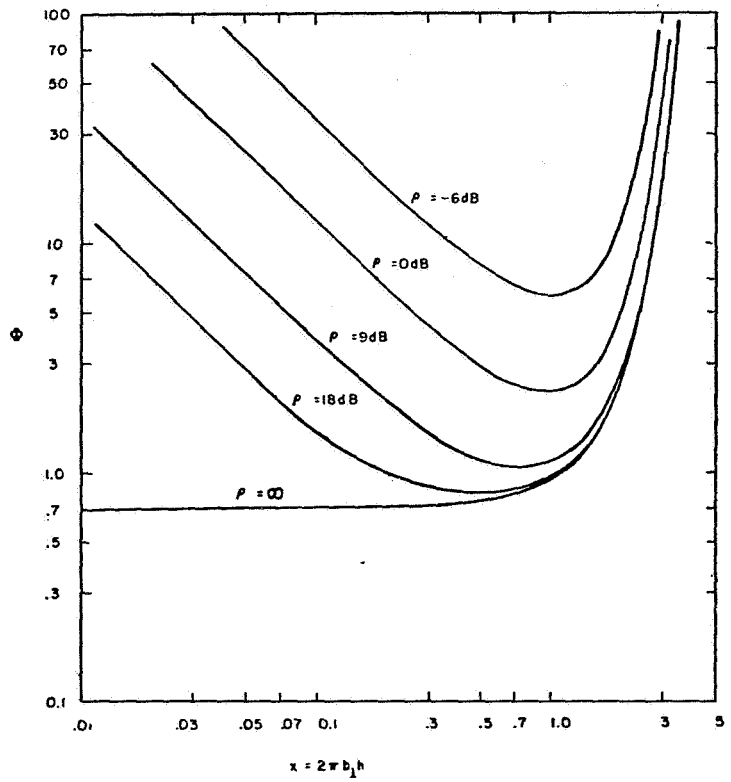


Figure 1. Normalized standard deviation of mean-frequency estimator versus pulse-pair spacing.

where $C_i$ and $C_j$ are weights properly selected to minimize the variances of $\Omega_a$ and $W_a$, and normalized such that $\Sigma C_i = \Sigma C_j = 1$. WOODMAN (1975) has treated the problem for the frequency shift $\Omega_a$. He found an optimum set of values $C_i$, such that $\langle \Omega_a - \Omega^2 \rangle$ is a minimum and discussed numerically the effect of averaging for different signal-to-noise ratios, sampling spacing, number of points M and correlation function shapes. Figure 3 depicts the optimum set of weights for two S/N ratios, for a Gaussian-shaped autocorrelation function sampled at 32 points with a spacing of 0.1 (of the typical width). The set for low signal-to-noise is as expected; it corresponds to the normalized inverse of the variances of $\Omega_i$ a well-known result for optimum averaging of independent samples. The resultant set for high S/N ratio is somewhat surprising; it has negative as well as positive signs, with absolute values which are larger than unity. This is a consequence of the fact that the difference estimates are not independent of one another.

Figure 4, shows the variance of $\Omega_a$ as a function of the coordinate of the last sample (in typical width units). There are two groups corresponding to different S/N ratios. In each group there are 6 curves corresponding to 1, 2, 4 ... 32 samples. The first conclusion we can draw from these results is that, indeed, for high signal-to-noise ratios there is not much difference between the variance with 32 points at optimum delay and a single point close to the origin. There is a 60% difference (30% for the standard deviation) in going from 1 to 2 points, and an additional 50% (25% for the sd) in going from 2 to 32. This last improvement, is certainly not worth the effort. The increase from 1 to 2

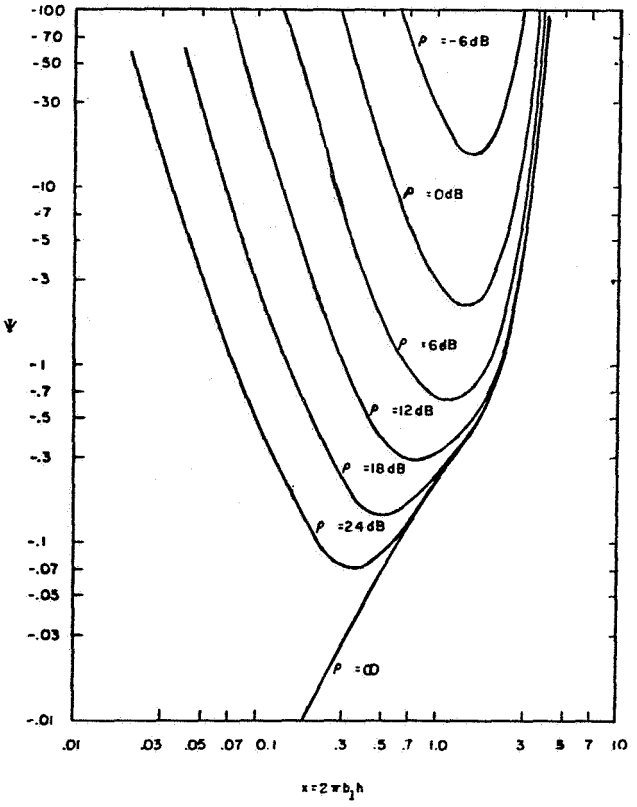


Figure 2. Normalized standard deviation of the estimate of frequency spread versus pulse-pair spacing.

could be justified if the redundancy is used to check the existence of unexpected interference.

On the other hand, we see that, for high S/N ratios, the variance is roughly inversely proportional to the number of sample points. This is not surprising since the estimates $\{\Omega_i\}$ have statistically independent errors with respect to the real $\Omega$.

We can conclude then that $\Omega$, as defined in (17), is a good estimator from a statistical as well as from a practical point of view when the S/N is better than one, but it is far from optimum when the signal-to-noise ratio is low.

Notice that the above discussion assumes that the sampling in the time series is such that the spacing for 32 points is optimum, i.e., that approximately 32 or N points can be fit in approximately a correlation time. Otherwise, a gain proportional to the number of samples cannot be achieved. Correlation samples which fall at points where the correlation is low do not contribute to improve the accuracy of the estimate.

It should be mentioned that the deterioration of the single delay covariance approach should not be held as an argument in favour of the sampled spectral moment approach. Unless some more sophisticated processing is performed with the spectra, the single delay autocorrelation approach yields the same performance as the straight spectral moment approach, including the case of noise signals, as it was quoted before (RUMMLER, 1968).

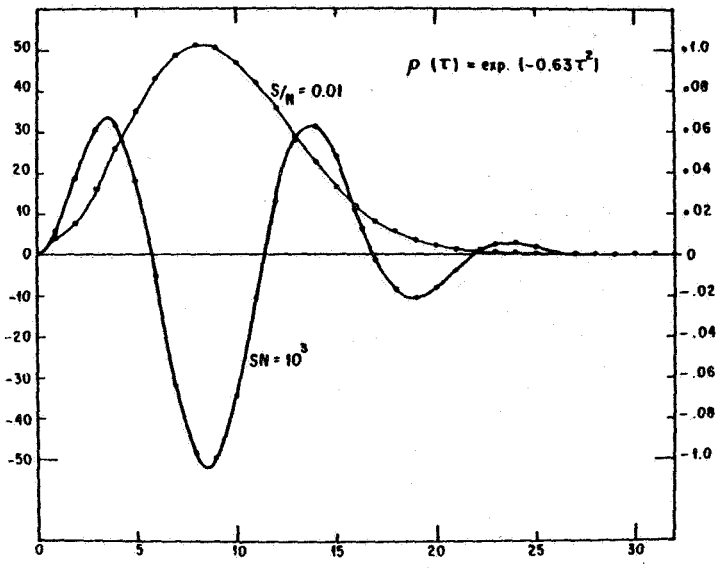


Figure 3. Optimum weighting coefficients $c_i$, to minimize $(\Omega_a - \Omega)^2$, where $\Omega_a = \sum_{i=1}^{M} c_i \Omega_i$. Two cases, one for low and the other for high S/N ratio, are considered.

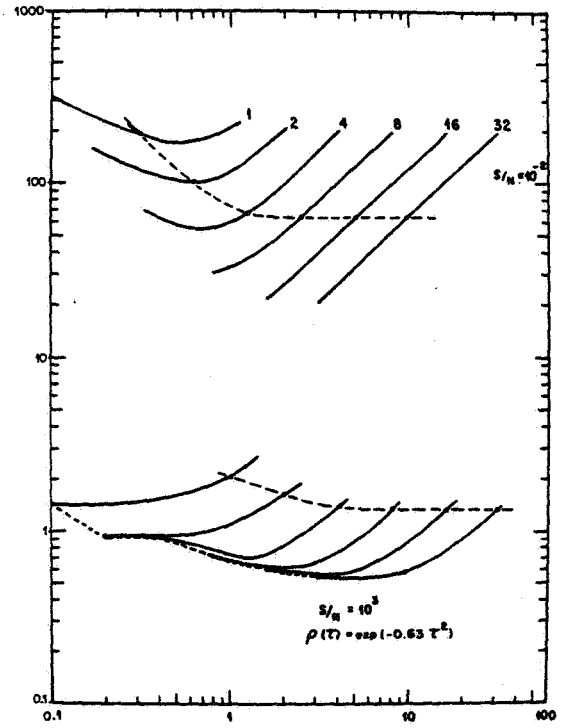


Figure 4. Variances of $\Omega_a$, when evaluated in accordance to the weight coefficients shown on Figure 3. Labels correspond to the number of $\Omega_i$'s, and the absisa shows the delay of the last point, i = M.

Similar computations have not been performed for the variance of the spectral width estimate, but we can expect that, qualitatively at least, the same conclusions will hold.

## MAXIMUM LIKELIHOOD ESTIMATORS AND BOUNDS

Given a set or sequence (random process) of N observables $x_i$ with an N joint probability function $F(\underset{\sim}{X};\{A\})$ such that $F(\underset{\sim}{X};\{A\}) = g(\underset{\sim}{X}<\underset{\sim}{X}<\underset{\sim}{X}+d^n\underset{\sim}{X}/\{A\})$ where $\{A\}$ is a set of parameters. It is possible to find practically an innumerable number of estimators of $\{A\}$ and estimates of $\{A_i\}$ as a function of the observables. For these estimates to be of practical use they must meet the condition that $\langle A_i' \rangle = A_i$ and that the variances $\sigma_a^2 = \langle (A_i' - A_i)^2 \rangle$ be small. For a given sample $\underset{\sim}{x}$ of the process, we can form a function $F(\underset{\sim}{x};\{A\})$ and let $\{A\}$ vary. There will be a value of $\{A\}$ for which $F(\underset{\sim}{x};\{A\})$ is a maximum in $\{A\}$ space. This value is called the maximum likelihood estimate of $\{A\}$. It can be shown that such an estimate produces minimum variance among all possible estimators (CRAMER, 1946).

Usually it is not possible to find explicit solutions or practical algorithms for the ML etimators, on the other hand, the theory gives us formal expression for the ML variances, which can be used to compare the "efficiency" of a given estimator. It is possible, in the case of large N processes with a Gaussian-shaped spectrum plus white noise, and using justifiable approximations, to obtain explicit expressions for these bounds. Zrnic, for instance, using a ML approach, finds the following lower bounds.

$$\sigma_\Omega^2 \geq \frac{W^2 (WT_s/2\pi)^2}{M(1 - (WT_s/2\pi)^2)^{\frac{1}{2}}} \tag{24}$$

when the noise level is zero, and

$$\sigma_\Omega^2 \geq \frac{W^2}{M} 4\sqrt{\pi}\, (WT_s/2\pi)\, (N/S)^2 \tag{25}$$

when the $S/N \ll 1$ and $WT_s/2\pi \ll 1$. He assumes a continuous sequence of N complex, samples spaced by $T_s$.

We should state, though, that we find equation (24) disturbing, since for a given observation time $T_o = T_s M$, we can make the variance arbitrarily small by making $T_s$ as small as possible. This is contrary to our expectations, since, for a given W and no noise, sampling times smaller than $W^{-1}$ gives redundant information, and should not improve the variance of any estimator. There is no explicit indication on the reference for the expression not to be valid for small $WT_s$.

If the sequence of observables $\{x_i\}$ is given by M pairs of independent complex values $(x_{1i}, x_{2i})$ but correlated in between. The ML estimator can be found explicitly for large Ns (MILLER, 1972). It turns out to be the same as the covariance approach heuristically described by RUMMLER (1968) and WOODMAN and HAGFORS (1969) and discussed previously.

It is also possible to use an M-L approach starting with sample estimates of, $\rho'(\tau_i)$ or $S'(\omega_i)$, of either the autocovariance function, $\rho(\tau)$, or the spectrum $S(\omega)$, as the set of random variables to be used in an M-L estimate of the parameters P, $\Omega$, W and N, we are interested in. The procedure, then, starts with the set of observables $\{x_i\}$, from which we obtained an estimate, $\rho'(\tau_i)$ or $S'(\omega_i)$, of $\rho(\tau_i)$ or $S(\omega_i)$, using any of the available algorithms. These estimates, which hopefully contains all the desired information about the

process, are then used in an M-L approach to obtain the desired parameters. LEVINE (1965) has taken this approach starting with an estimate $S(\omega)$ of the frequency spectrum. We refer the reader to the original reference, or to Zrnic's review for the solution algorithm. There is no explicit formula for the estimates. They involve the solution of some nonlinear simultaneous equations. The lower bounds for the variances are given by

$$\sigma_\rho^2 \geq \frac{P^2}{M}\left(2.25 - \frac{30}{(2\pi)^2}(WT_s)^2 + \frac{180}{(2\pi)^4}(WT_s)^4\right) \tag{26}$$

$$\sigma_\Omega^2 \geq \frac{3}{\pi^2}\frac{W^2}{M}(WT_s)^2 \tag{27}$$

$$\sigma_w^2 \geq \frac{45}{4\pi^4}\frac{W^2}{M}(WT_s)^4 \tag{28}$$

These bounds are valid for large signal-to-noise ratios.

We should notice that (27) gives about the same lower bounds as (24), which means that, at least for the frequency shift variance, this approach can be as good as the M-L approach which starts with the observational time series $\underset{\sim}{x}_i$. In terms of our figures of merit we can write

$$F_\Omega = \frac{\sqrt{3}}{\pi}(WT_s)^{3/2} \tag{29}$$

$$F_W = \sqrt{45}\,\frac{1}{2\pi^2}(WT_s)^2 \tag{30}$$

We can see that for sampling times comparable to a correlation time, i.e., for $WT_s \simeq 1$. The performance of the spectrum and the signal delay frequency shift estimators is comparable to both M-L estimators. According to (29) and (30) both estimators improve as we reduce the sampling time spacings eventually becoming much better than the simple estimators we have mentioned. Again, we find this behavior in the limit -- as $T_s \to 0$ -- disturbing, since (high sampling) rates redundant should eventually produce oversampling, which should not decrease the variance of our estimates. Figure 3, for instance, despite its sophistication, definitely does not show this improvement; it shows instead some leveling off, as we expect.

The corresponding variances for the case of small S/N ratios are:

$$\sigma_\rho^2 = \frac{3}{2\sqrt{\pi}}(WT_s)\frac{N^2}{M} \tag{31}$$

$$\sigma_\Omega^2 = \frac{2W^2}{\sqrt{\pi}M}(WT_s)\left(\frac{N}{S}\right)^2 \tag{32}$$

$$\sigma_\omega^2 = \frac{2}{\sqrt{\pi}}\frac{W^2}{M}(WT_s)\left(\frac{N}{S}\right)^2 \tag{33}$$

The corresponding figure of merit for the first moment is:

$$F_\Omega = \frac{2}{\sqrt{\pi}}(WT_s)\left(\frac{N}{S}\right), \tag{34}$$

which behaves in the same way as far as its dependence on $T_s$ and $(\frac{N}{S})$, as the multiple delay autocovariance approach we have discussed previously (Figure 2).

We have mentioned before, that parameter estimation by a least square fitting of the theoretical shape of the spectrum is an M-L technique. It is indeed an M-L estimator which starts with the frequency spectrum estimates $s(\omega_i) \equiv s_i$ as the original set of random variables. Let $F(\underset{\sim}{S};\{P_i\})$ be the multivariance distribution function, where $\underset{\sim}{S}$ is the set of spectral values $S(\omega_i) \equiv S_i$ in vector form. If $s(\omega_i)$ is obtained by averaging a sufficiently large number $M_a$ of DFTs of weighted sections of the original time series, $F(\underset{\sim}{S}, \{P_i\})$ is a Gaussian joint probability distribution function and the logarithm of the likelihood function is given by

$$L(\{P_i\};s_i) = -\ln |Q|^{-1} - \sum_{i,j} (s_i - S_i)\,(Q_{ij})^{-1}\,(s_j - S_j) + \text{const.}$$

where $S_i = S(\omega_i;\{P_k\})$ is a known function of the unknown parameters $P_k$. We shall consider the covariance matrix Q known. Maximizing the likelihood function L is equivalent to minimizing the quadratic expression, namely to solve the set

$$\frac{\partial}{\partial P_k} \sum_{i,j} (s_i - S_i)\,(Q)^{-1}_{ij}(s_j - S_j) = 0 \qquad \text{for all ks} \tag{35}$$

It is known that, if the size of the time window in the DFT is large with respect to the correlation time, the variances of $(S_i - s_i)$ are independent, and $Q_{ij}$ is diagonal with elements $\sigma^2_{sii}$. The problem is then reduced to solve the set

$$\frac{\partial}{\partial P_k} \sum_{i} (s_i - S_i(\{P_m\}))^2 \cdot \frac{1}{\sigma^2_{ii}} = 0 \qquad \text{for all ks} \tag{36}$$

But this is exactly the starting point of a least squared estimation technique provided that each element $(s_i - S_i)^2$ in the quadratic expression is weighted by the inverse of their expected variance.

Note that the set of parameters is not limited to P, $\omega$, W. The parameter estimation procedure used for the Arecibo ST data, (SATO and WOODMAN, 1982), for instance, fits up to eleven parameters.

## CONCLUSIONS

The single delay autocorrelation approach is a very simple and statistical efficient estimator for MST radars and should be used for real-time processing of MST radar signals, whenever the complexity and cost of the installation is to be kept low. A coherent integrator is indispensable, since this reduces the processing capacity requirements and improves the (S/N) and final estimated variances. Nonfading clutter and noise should be estimated concurrently and accounted for. The technique does not allow for correcting other sources of interference.

If the complexity of the installation allows for the inclusion of an FFT processor, the full spectrum or correlation function should be evaluated and the parameters evaluated using existing sophisticated algorithms. Parameters can be evaluated in this way with much improvement over the single delay correlation technique specially under conditions of low S/N ratio and existence of sources of interference like fading ground, ocean or self clutter. Normally only the

estimation of the spectrum or correlation needs to be evaluated in real time.

REFERENCES

Bard, Y. (1974), Nonlinear Parameter Estimation, Academic Press, New York.

Blackman, R. B. and J. W. Tukey (1958), The Measurement of Power Spectra, Dover Publications, Inc., New York.

Cramer, H. (1946), Mathematical Methods of Statistics, Princeton University Press, Princeton.

Levine, M. J. (1965), Power spectrum parameter estimation, IEEE Trans. Inform. Theory, IT-11, 100-107.

Miller, K. S. (1974), Complex Gaussian Processes: An Introduction to Theory and Application, Addison-Wesley Publishing Co., Inc., Reading, Mass.

Miller, K. S. and M. M. Rochwarger (1972), A covariance approach to spectral moment estimation, IEEE Trans. Inform. Theory, IT-18, 588-596.

Rabiner, L. R. and N. Radar (editors) (1976), Digital signal processing, Selection of papers edited by the Digital Signal Processing Committee of the IEEE.

Rummler, W. D. (1968), Introduction of a new estimator for velocity spectral parameters, Bell Telephonse Labs., Whippany, NJ, Tech. Memo MM-68.

Sato, T. and R. F. Woodman (1982), Spectral parameter estimation of CAT radar echoes in the presence of fading clutter, Radio Sci., 17, 817-826.

Woodman, R. F. (1975), Error analysis of multiple delay correlation function velocity estimates, Abstracts of URSI, General Assembly, Lima, Peru.

Woodman, R. F. (1980), High-altitude resolution stratospheric measurements with the Arecibo 430-MHz radar, Radio Sci., 15, 417-422.

Woodman, R. F. and A. Guillen (1974), Radar observations of winds and turbulence in the stratosphere and mesosphere, J. Atmos. Sci., 31, 493-505.

Woodman, R. F. and T. Hagfors (1969), Methods for the measurements of vertical ionospheric motions near the magnetic equator by incohering scattering, J. Geophys. Res., 75, 1205-1212.

Zrnic', D. S. (1979), Estimation of spectral moments for weather echoes, IEEE Trans. Geosci. Elec., GE-17, 113-128.

# 8.8A THE DISCRETE PROLATE SPHERIODAL FILTER AS A DIGITAL SIGNAL PROCESSING TOOL

J. D. Mathews*, J. K. Breakall**, and G. K. Karawas*

*Department of Electrical Engineering and Applied Physics,
Case Institute of Technology, Case Western Reserve University,
Cleveland, OH 44106

**Lawrence Livermore National Laboratories, P.O.B. 808, Livermore, CA 94550

## ABSTRACT

The discrete prolate spheriodal (DPS) filter is one of the class of non-recursive finite impulse response (FIR) filters. The DPS filter, first introduced by TUFTS and FRANCIS (1970), is superior to other filters in this class in that it has maximum energy concentration in the frequency passband and minimum ringing in the time domain. We give a mathematical development of the DPS filter properties, provide information required to construct the filter, and compare the properties of this filter with those of the more commonly used filters of the same class. We note that use of the DPS filter allows for particularly useful statements of data time/frequency resolution "cell" values and that overall it forms an especially useful tool for digital signal processing.

## INTRODUCTION

The reduction of digitized data to final form usually involves what is broadly described as digital filtering. This process may be applied in either the domain in which sampling occurs (e.g., time or space) or in the corresponding transform domain (e.g., frequency or spatial frequency). The net result of digital filtering is always to "smooth" or restrict the frequency content of the data. However, it is often very important that this smoothing or filtering process be done with minimum and well-understood distortion to the results in both domains. An example of an often misused filter is the equal weight ("square") running average which "smooths" in the domain of application but results in a $(\sin x/x)^2$ like passband shape in the transform domain. The $(\sin x/x)^2$ behavior may have unacceptable sidelobe levels and/or spacing.

The difficulty of minimizing distortion due to filtering starts with a statement of the criterion for judging when a filter is most satisfactory. We will follow the approach of TUFTS and FRANCIS (1970), PAPOULIS and BERTRAN (1972), and SLEPIAN (1978) in which an optimum finite (length) impulse response (FIR) non-recursive filter is derived on the basis of maximum energy concentration in the passband of the filter relative to energy in the total bandpass up to the Nyquist frequency $\omega_N(=2\pi/2\tau$ with $\tau$ the sampling interval). Choice of this energy concentration criterion leads to filters described in terms of discrete prolate spheriodal sequences and wave functions. These sequences and wave functions have many desirable properties which were first investigated in the continuous case by SLEPIAN and POLLAK (1961), LANDAU and POLLAK (1961, 1962), and SLEPIAN (1964).

This paper is basically tutorial in that our major goals are to demonstrate the usefulness of FIR filters based on maximum passband energy concentration and to supply the information necessary for the "construction" of these filters. We do however introduce several apparently new results which prove useful in numerically solving the matrix equations which describe the filter. In the following section we develop the general equations for symmetric FIR digital filters and then obtain solutions based on the energy concentration criterion. Next we demonstrate that these filters have features which are desirable

especially when compared with more traditional filters, and finally, we present a summary and conclusions.

## MATHEMATICAL DERIVATIONS

### (a) A General Non-Recursive FIR Filter

Using the time and frequency domains, a tapped delay line implementation of a non-recursive FIR filter acting on analog signal x(t) is shown schematically in Figure 1. The resultant output signal has the form

$$y(t) = \sum_{n=-K}^{K} a_n x(t-n\tau) \tag{1}$$

where the coefficients $a_n$ are real and where the time reference is, for later convenience, at the center of the delay line. Assuming that the Fourier transform of $x(t) \leftrightarrow X(\omega)$ exists we Fourier transform (1) and find

$$Y(\omega) = H(\omega) \cdot X(\omega) \tag{2}$$

where

$$H(\omega) = \sum_{n=-K}^{K} a_n e^{-jn\omega\tau} \tag{3}$$

is the "voltage" transfer function and $j = \sqrt{-1}$. The corresponding "power" transfer function is

$$S(\omega) = H(\omega) \cdot H^*(\omega) = \sum_{n,m=-K}^{K} a_n a_m e^{-j(n-m)\omega\tau}$$

$$= \sum_{n=-K}^{K} \left[ a_n^2 + 2 \sum_{m=-K}^{n-1} a_n a_m \cos(n-m)\omega\tau \right] \tag{4}$$

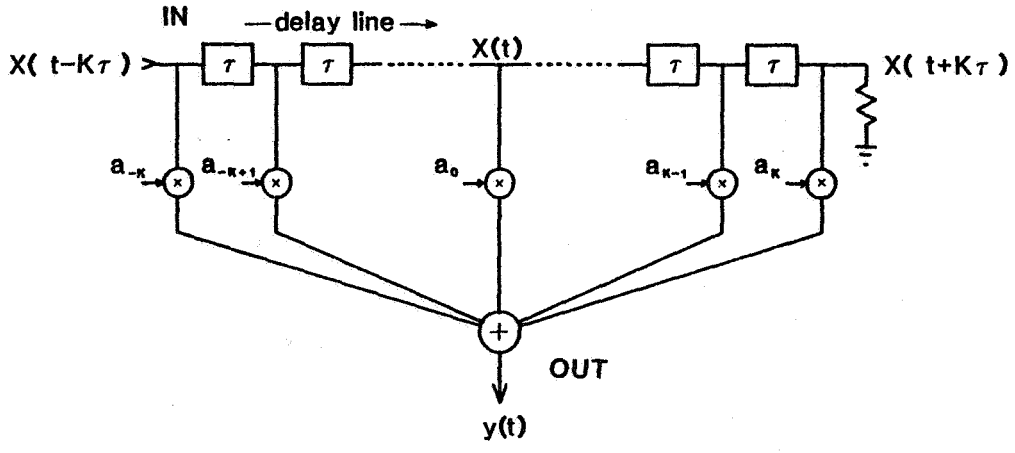


Figure 1. Block diagram of the non-recursive FIR filter described by Equation 1.

while the inverse Fourier transform of (3) is

$$h(t) = \sum_{n=-K}^{K} a_n \delta(t-n\tau) \tag{5}$$

the filter impulse response with $\delta(t')$ the unit impulse. Note that h(t) convolved with x(t) yields equation (1).

The filter described by (3) or (5) becomes a digital filter if we uniformly and instantaneously sample y(t) at intervals of $\tau$ time. Then (1) becomes

$$y_j = \sum_{n=-K}^{K} a_n x_{j-n} \tag{6}$$

where the index j refers to consecutive members of the set of sampled signals. If we restrict x(t) to be bandlimited to the Nyquist frequency ($2\pi/2\tau$) or less, then the sampling/filtering process occurs without aliasing.

(b) Choice of Coefficients

Equations (3) or (5) describe the effects of the filter on an input signal given a particular set of coefficients $\{a_n\}$. These coefficients are often chosen such that the digital filter characteristics are similar to one of various common analog filters (e.g., the "ideal" filter). The process of synthesizing these filter characteristics often involves smoothing (windowing) of the resultant coefficient sequence to suppress ringing (BLACKMAN and TUKEY, 1958; HAMMING, 1977).

As mentioned in the introduction, we propose to choose the sequence $\{a_n\}$ by maximizing the energy concentration of S(ω) (equation (4)) in some interval $[-\omega_c,\omega_c]$ on $[-\omega_n,\omega_n]$ where $\omega_c$ is the filter "cutoff" frequency. Thus let

$$\alpha = \int_{-\omega_c}^{\omega_c} S(\omega)\, d\omega \Big/ \int_{-\omega_n}^{\omega_n} S(\omega)\, d\omega \tag{7}$$

and find $\{a_n\}$ such that α is maximized. Substituting equation (4) for S(ω) in (7) and performing the integrations yield

$$\alpha = \frac{\sum_{n,m=-K}^{K} a_n a_m \frac{\sin (n-m)\pi\varepsilon}{(n-m)\pi}}{\sum_{n=-K}^{K} a_n^2} \tag{8}$$

where $\varepsilon = \omega_c/\omega_n$. If we define $\{a_n\}$ as elements of vector $\underline{a}$ then (8) becomes

$$\underline{a}^T \cdot \underline{\underline{E}}_K \cdot \underline{a} - \alpha \underline{a}^T \cdot \underline{a} = 0 \tag{9}$$

where each $\underline{a}$ has (2K + 1) elements and the elements of matrix $\underline{\underline{E}}_K$ are

$$e_{mn} = \frac{\sin (n-m)\pi\varepsilon}{(n-m)\pi} \tag{10}$$

$$-K \leq m,\ n \leq K$$

We are thus searching for $\underline{a}$ such that α is maximum. From Lagrange

multiplier theory, it is clear that (9) is satisfied by the set of (2K + 1) orthonormal eigenvectors $\underline{a}^{(i)}$ and the corresponding eigenvalues $\lambda_i$ of the system

$$(\underline{\underline{E}} - \lambda_i \underline{\underline{I}}) \cdot \underline{a}^{(i)} = 0 \tag{11}$$

where $\underline{\underline{I}}$ is the identity matrix. We choose the elements of $\underline{a}^{(o)}$ the eigenvector associated with $\lambda_o$, the largest eigenvalue, as coefficients of our "optimum" filter. That is, $\underline{a}^{(o)}$ maximizes equation (8) with $\alpha = \lambda_o$ for the K and $\varepsilon$ (i.e., $\omega_c$) values in question.

SLEPIAN (1978) refers to these eigenvectors and corresponding H(ω)'s as discrete prolate spheriodal sequences and wave functions, respectively. He demonstrates that if we order the eigenvalues according to magnitude,

$$1 > \lambda_o > \lambda_1 > \ldots > \lambda_{2K} > 0$$

and if $a_n^{(i)}$ is the n'th element of the eigenvector corresponding to $\lambda_i$ then

$$\sum_{n=-K}^{K} a_n^{(i)} a_n^{(j)} = \delta_{ij} = \begin{cases} 1 & i = j \\ 0 & i \neq j \end{cases}$$

Letting $b_n^{(j)}$ be the n'th element of the eigenvector corresponding to eigenvalue $\lambda_j'$ calculated for $\omega_c' = \omega_N - \omega_c$ then (SLEPIAN, 1978; section 2.2)

$$\left.\begin{aligned} a_{-n}^{(i)} &= (-1)^i a_n^{(i)} \\ a_n^{(i)} &= (-1)^{|n|} b_n^{(2K-i)} \\ |n| &\leq K \end{aligned}\right\} \tag{12}$$

Slepian also notes that the discrete prolate spheroidal wave functions U(ω) satisfy a Sturm-Liouville equation of the form

$$\frac{d}{d\omega}\left[\cos\omega\tau - \cos\pi\varepsilon\right]\frac{dU}{d\omega} + \tau^2\left[K(K+1)\cos\omega\tau - \theta\right]U = 0 \tag{13}$$

where θ is the eigenvalue (different from λ) corresponding to a particular wave function and all other parameters are as before. Substituting H(ω) (=U) from (3) into (12) we find

$$(\underline{\underline{E}}_K' - \theta_i \underline{\underline{I}}) \cdot \underline{a}^{(i)} = 0 \tag{14}$$

where for $|n| \leq K$

$$e_{mn}' = \begin{cases} \frac{1}{2}(K+m)(K-m+1) & m = n - 1 \geq 0 \\ m^2 \cos\pi\varepsilon & m = n \\ \frac{1}{2}(K-m)(K+m+1) & m = n + 1 \leq K \\ 0 \quad \text{otherwise} \end{cases} \tag{15}$$

or equivalently

$$\frac{1}{2}(K+n)(K-n+1)a_{n-1} + (n^2\cos\pi\varepsilon - \theta_i)a_n + \frac{1}{2}(K-n)(K+n+1)a_{n+1} = 0 \tag{16}$$

The matrix $\underline{\underline{E}}'$ is tridiagonal and thus equation (14) is much easier to solve numerically than equation (11). Equation (14) yields the same normalized eigenvectors as (11) however the corresponding eigenvalues are different although we still seek the eigenvector corresponding to the largest eigenvalue $\theta_0$. Since we are interested only in $\underline{a}(0)$ which is symmetric we can essentially halve the size of $\underline{\underline{E}}'$ by invoking symmetry (see equation (12)) which yields

$$-\theta_i\, a_0 + K(K+1)a_1 = 0$$

plus equation (16) with $1 \leq n \leq K$. The compact form of (14) yields only eigenvalues corresponding to "even" eigenvectors and the resultant $\underline{a}$'s may be normalized such that $\underline{a}^T \cdot \underline{a} = 1$.

From equation (14) we find that for $\omega_c = 0$, $\theta_0 = K(K+1)$, and $a_n(|n| < K) = 1$ while for $\omega_c = \omega_N$ (i.e., $\varepsilon = 1$) we find (using the $\omega_c = 0$ case and (12)) that $\theta_0 = K^2$ and

$$a_n = a_{n-1}\,\frac{[K - (n-1)]}{K + n}$$

$$1 \leq n \leq K$$

We observe experimentally that $K(K+1) \geq \theta_0 \geq K^2$ for all $0 \leq \omega_c \leq \omega_N$ and that

$$a_0^{(0)} > a_1^{(0)} > a_2^{(0)} > \ldots > a_K^{(0)} \geq 0$$

$$1 \geq a_i^{(0)}(\omega_c) \geq a_i^{(0)}(\omega_c = \omega_N)$$

where $a_i^{(0)}(\omega_c)$ refers to the i'th component of the eigenvector corresponding to the largest eigenvalue for $0 \leq \omega_c \leq \omega_N$. The range constraints on the value of $\theta_0$ may be used in finding $\theta_0$ from (14).

## COMPARISON OF FILTER PROPERTIES

In the previous section we showed that FIR filters with discrete prolate spheriodal sequences as coefficients (see equation (1)) have maximum energy concentration in the passband. These filters are known as discrete prolate spheriodal (DPS) filters and in this section we compare their properties with those of more traditional FIR filters.

These "traditional" filters are all based on various windowing (weighting) functions applied to the coefficients of the infinite Fourier series representation of the ideal low-pass filter. The coefficients of this series are

$$C_n = \frac{\sin n\pi\varepsilon}{n\pi}$$
$$n = 0, \pm 1, \pm 2, \ldots \qquad (17)$$
$$\varepsilon = \omega_c/\omega_n$$

and the windowing function W(n) is such that $W(n) = 0$ for $|n| \geq K$ thus truncating the series so that the resultant transfer function becomes

$$H_W(\omega) = \sum_{n=-K}^{K} W(n)C_n e^{-jn\omega\tau} \qquad (18)$$

The W(n) ($-K \leq n \leq K$) are chosen to minimize in some sense the ringing (Gibb's phenomena) which results from truncation of the series representation of the ideal lowpass filter (HAMMING, 1977; Chap. 5, or RABINER and GOLD, 1975; Chap. 3). In this discussion, we compare the DPS filter with the $H_W(\omega)$ (equation (18)) of same length using rectangular, Kaiser, Von Hann, Dolph-Chebyshev, and Hamming windows. The W(n) corresponding to these windows are given or referenced in Table 1 and are discussed in more detail by HAMMING (1977) and RABINER et al. (1979).

Figures 2 and 3 compare the frequency response (in dB) plotted versus normalized frequency f (Nyquist frequency $f_N = 0.5$) and impulse response envelope plotted versus time in samples for all six filters. For this comparison we choose K = 15 (total length 31) and adjust filter parameters such that the -3 dB level of each filter occurs near f = 0.05. The filters appear in order of, in our opinion, acceptability with the rectangular windowed filter least acceptable and DPS filter most acceptable.

The frequency domain distortion of a signal spectrum is just the filter frequency response as shown in Figures 2 and 3. However, the time domain distortions due to the impulse responses are not so obvious. In Figure 4, we show the effects of these filters in the time domain on a square wave plus Gaussian distributed noise. As expected, all filters except the DPS filter "ring". The DPS filter "smooths" the input signal while retaining a "smooth" frequency domain behavior.

To aid in understanding the "evolution" of the DPS filter, we show in Figure 5 the DPS filter frequency response characteristics for normalized cutoff frequency $f_c = 0.2$ as K is increased from 1 (3 coefficients) to 8 (17 coefficients). Recall that in each case energy concentration in the passband ($f \leq 0.2$) is the maximum possible for the number of coefficients used.

## SUMMARY AND CONCLUSION

We have investigated the properties of the discrete prolate spheroidal filter relative to other common FIR filters. To accomplish this comparison we first derive the general properties of FIR filters and then specialize these

Table 1. Weighting coefficients of various windows
($W(|n| > K) = 0$ for all windows

---

RECTANGULAR WINDOW: $W(n) = 1$

KAISER WINDOW:

$$W(n) = \frac{I_o(\alpha\sqrt{1 - (n/K)^2})}{I_o(\alpha)}$$

where $I_o(x) = 1 + \sum_{n=1}^{\infty} [\frac{(x/2)^n}{n!}]^2$

and we use $\alpha = 3.395$ (40 dB minimum stopband attenuation)

VON HANN WINDOW: $W(n) = \frac{1 + \cos \pi n/K}{2}$

DOLPH-CHEBYSHEV WINDOW: See HELMS (1968) and RABINER et al.(1979)

HAMMING WINDOW: $W(n) = 0.54 + 0.46 \cos (2\pi n/(K-1))$

---

properties to the case of maximum energy concentration in the filter passband. The condition of maximum energy concentration gives rise to an eigenvalue problem which has the discrete prolate spheroidal sequences (SLEPIAN, 1978) as eigenvector solutions. The eigenvector corresponding to the largest eigenvalue is used as the coefficient sequence in the DPS filter.

SLEPIAN (1978) also points out that the prolate spheroidal wave functions satisfy a form of the Sturm-Liouville equation. This fact leads to a second eigenvalue/eigenvector problem which is much simpler to solve numerically than the first problem. We note that the elements of the eigenvector ($\underline{a}^{(0)}$) corresponding to the largest eigenvalue ($\theta_0$ or $\lambda_0$) are symmetric around the center value ($a_0$) and that

$$a_{n-1}^{(0)} \geq a_n^{(0)} \geq 0 \quad (1 \leq n \leq K).$$

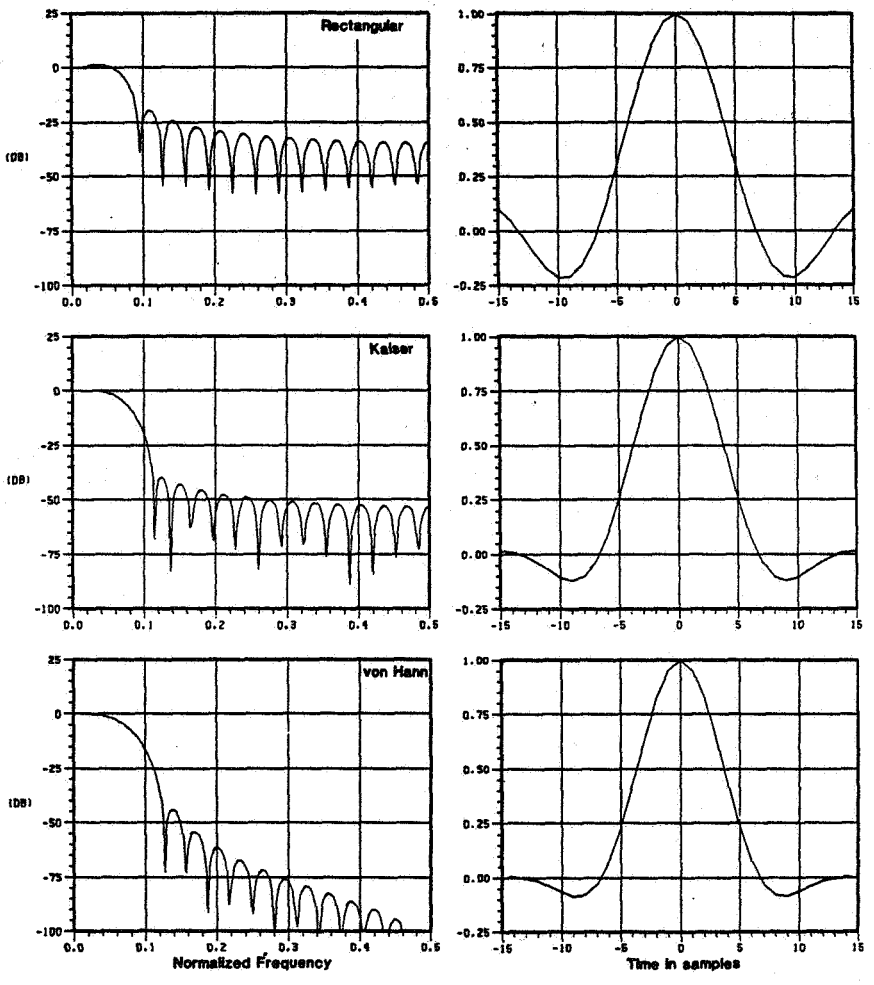


Figure 2. Filter frequency response (dB) plotted versus normalized frequency (Nyquist frequency $f_N$+).5) and corresponding impulse response envelope plotted versus time in samples for rectangular, Kaiser and von Hann windows of length 31 (see Equation 18 and Table 1). In all cases the normalized 3 dB frequency is about 0.05.

When used, DPS filters have several features which we feel make them superior to more standard FIR filters. Specifically, the DPS filter is "smooth" in both domains and thus distortion of the signal is minimal and easily described in both domains. Thus for example, after removing high frequency noise, a time domain feature may be more easily "restored" by deconvolving the DPS impulse response than by deconvolving the other sin x/x like impulse responses. Another useful feature of DPS filters is that descriptions of time and frequency resolutions of published data can be more readily appreciated and used by the reader. In fact, we suggest that the DPS filter might form a basis for standardization of information concerning the "resolution cells" of data.

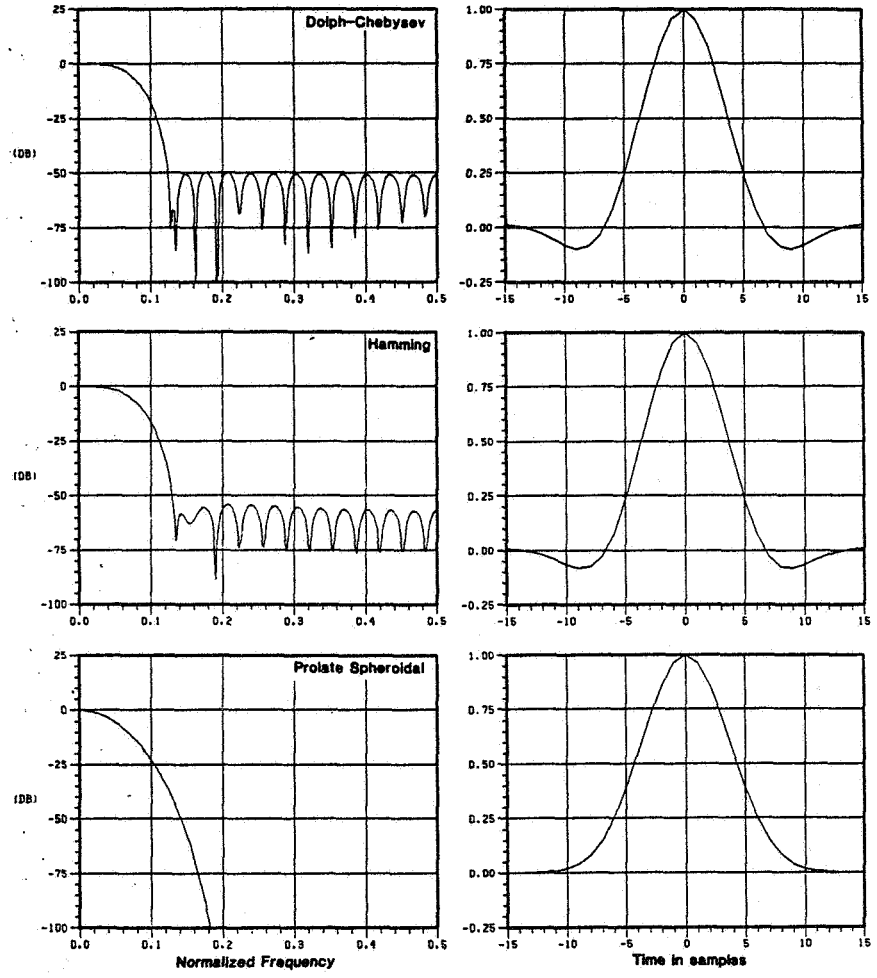


Figure 3. Similar to Figure 2, but for Dolph-Chebysev and Hamming windows and the prolate spheroidal filter. The normalized cutoff frequency of the prolate spheroidal filter is 0.2. The filters in Figures 2 and 3 are ordered according to overall quality with, in our opinion, the rectangular window filter worst and prolate spheroidal filter best.

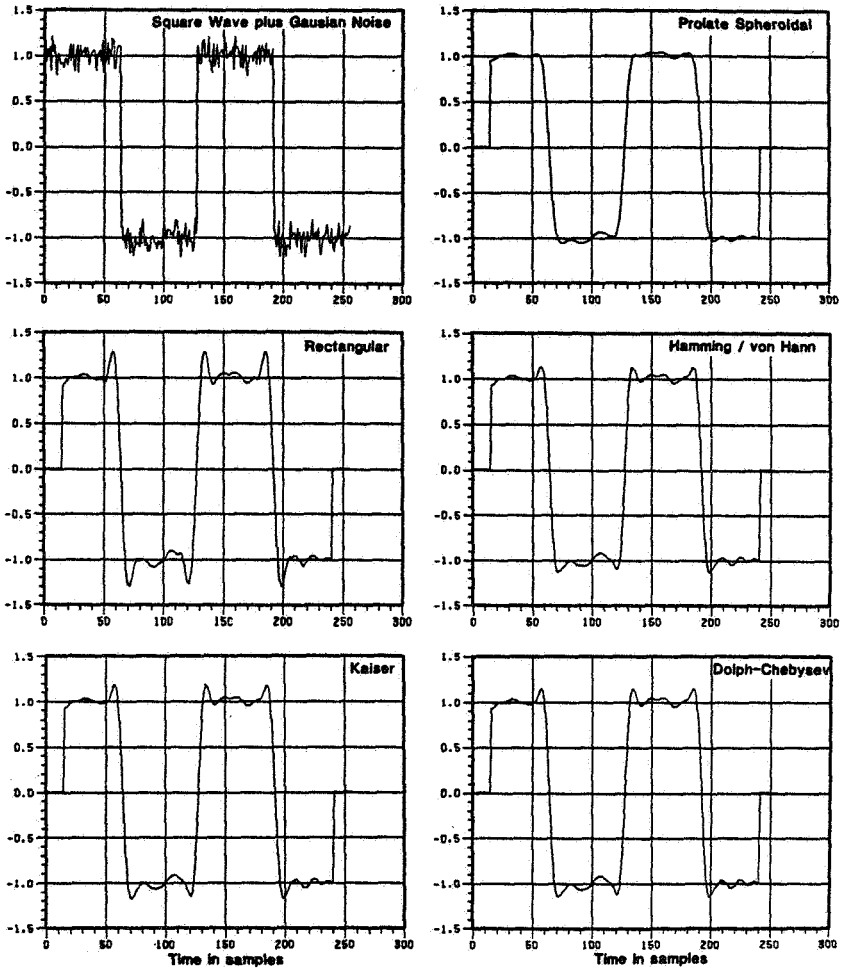


Figure 4. We compare the time domain effects of the various filters on a square wave plus Gaussian distributed noise. Note that all filters except the prolate spheroidal filter "ring" and that the rectangular window filter rings most with the Kaiser window next while the Dolph-Chebysev, Hamming, and von Hann windows are similar in this case.

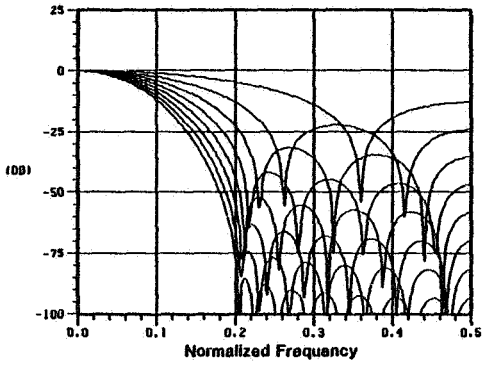


Figure 5. The evolution of the prolate spheroidal filter frequency response as K increases from 1 through 8 for a normalized cutoff frequency of 0.2.

ACKNOWLEDGEMENTS

This work has been supported by the National Science Foundation Atmospheric Sciences Division under grant ATM 79-18379 to the Case Western Reserve University.

REFERENCES

Blackman, R. B. and J. W. Tukey (1958), The Measurement of Power Spectra, Dover Publications, New York.

Hamming, R. W. (1977), Digital Filters, Prentice-Hall Signal Processing Series, Prentice-Hall, Englewood Cliffs, New Jersey.

Helms, H. D. (1968), Non-recursive digital filters: Design methods for achieving specifications on frequency response, IEEE Trans. Audio Electroacoust., AU-16, 336-342.

Landau, H. J. and H. O. Pollak (1961), Prolate spheroidal wave functions, Fourier analysis and uncertainty-II, Bell. Sys. Tech. J., 40, 65-84.

Landau, H. J. and H. O. Pollak (1962), Prolate spheroidal wave functions, Fourier analysis, and uncertainty-III, Bell. Sys. Tech. J., 41, 1295-1336.

Papoulis, A. and M. S. Bertran (1972), Digital filtering and prolate functions, IEEE Trans. Circuit Theory, CT-19, 674-681.

Rabiner, L. R. and B. Gold (1975), Theory and Application of Digital Signal Processing, Prentice-Hall, Inc., Englewood Cliffs, New Jersey.

Rabiner, L. R., C. A. McGonegal and C. Paul (1979), FIR windowed filter design program - WINDOW, section 5.2, Programs for Digital Signal Processing, IEEE Press, The Institute for Electrical and Electronics Engineers, Inc., New York.

Slepian, D. (1964), Prolate spheroidal wave functions, Fourier analysis, and uncertainty-IV, Bell Sys. Tech. J., 43, 3009-3058.

Slepian, D. (1978), Prolate spheroidal wave functions, Fourier analysis, and uncertainty-V: Discrete case, Bell Sys. Tech. J., 57, 1371-1430.

Slepian, D. and H. O. Pollak (1961), Prolate spheroidal wave functions, Fourier analysis, and uncertainty-I, Bell Sys. Tech. J., 40, 43-64.

Tufts, D. W. and J. T. Francis (1970), Designing digital low-pass filters - comparison or some methods and criteria, IEEE Trans. Audio and Electroacoustics, AU-18, 487-494.

# 9. MST RADAR DATA-BASE MANAGEMENT
(Keynote Paper)

V. B. Wickwar

SRI International
Menlo Park, CA 94025

The management of data is an important topic and one that has had considerable attention during the last few years (e.g., CODMAC, 1982; LIDE, 1981; JENNE, 1981; ROEDERER, 1981; USRA, 1978). Indeed, for MST radars, there are several reasons for considering it. The first is a very practical consideration, the large amount of data that are acquired by an MST radar, whether operating continuously or in campaign mode. Another is the desire to exchange data among scientists at the several radars located around the world. Now that the MST technique is maturing, there is also a growing desire by researchers using other techniques to acquire correlative radar data and a desire by theoreticians to compare theory and observation. Thus I believe that this is an appropriate time to discuss the management of MST data.

However, I do not want to step forward as an expert in the area of data management. I was, nevertheless, greatly involved as a catalyst in setting up an incoherent-scatter radar data base at NCAR. Let me emphasize the word "catalyst" because setting up such a data base has to be a collective effort of scientists involved in obtaining and using the data in question.

What I would like to do in this article is review some ot the questions and concerns that were involved in setting up that data base. That experience should be relevant to the present concerns because of the similarity of the techniques and the overlap in the scientific community interested in data from the two techniques.

The first question is the purpose of the data base. Is it to bring together all the data from one type of instrument, or is to bring together all the data from any source that pertains to a given scientific problem? The solution we chose was a blend of both, but it tended to emphasize the former. We felt that certain portions of the radar data could make particularly valuable contributions to the scientific field, and therefore we recommended including them. But for the data to be useful, we felt certain geophysical parameters should also be included. While we did not recommend the inclusion of other major data sets, we did recommend that that option be left open and, similarly, that the option to obtain data from other data bases not be precluded.

The rationale was that keeping the data base limited addid to the likelihood of having a responsive facility and one that would greatly complement the radars over the years. We even hoped that the facility would become a center of excellence for using the radar data. In another direction, we believed that this type of data base could contribute easily and greatly to short-term CDAWS-like exercises where many varieties of data are brought together to study a particular event or problem.

The next question we considered was the nature of the data base. Should it be a distributed system or a centralized one? In this age of networking and decentralization, we chose a centralized facility. This came about because of two realities: (1) the present cost of having a network linking radars in different countries or, even worse, on different continents, and (2) the expense of having all the data on line all of the time or even portions of the data shifted around on a fixed schedule. It also came about for positive reasons. We felt there would be more uniform quality control if all the data passed

through a common gateway. We felt that a central facility would be in a better position to train and help data-base users, to be able to assemble catalogs of observations, etc.

Another aspect of the nature of the data base is whether it should be on line or not. While having the data on line would be very nice, it is expensive; and it was not clear that it was necessary. The data could be kept on magnetic tape and then promoted to disks when requested. It could then be left on disk for a few days in case it was looked at again. The delay in promoting a tape would not affect most users. However, it was felt that something small and very useful for selecting data, such as a catalog, should be kept on line for easy browsing.

Yet another aspect of the nature of the data base was the nature of the data-base management system. Almost all computer systems have data-base management systems. However, while they may be excellent for keeping track of mailing lists, inventory control, or customer accounts in financial institutions, they are not well adapted to scientific data. Among other reasons, the data formatting may vary very greatly from radar to radar, or even for a single radar from one experiment to the next. Another is that relationships may exist with a series of points instead of on a one-to-one basis. However, the data can be handled simply with a far simpler file management system.

Having examined the nature of the data base, the next question was what data to include. This had two major aspects. The first was the level of the data. For example, there are the raw data that are recorded on tape for subsequent reduction. They are very radar-specific and comprise the bulk of the data. However, these data can only be reduced to geophysical parameters at the radar site. Thus, we felt that they should be kept at the radar location and not, at least initially, made part of the data base. However, magnetic tapes do deteriorate with time, and so it seems advisable that those tapes should be copied on to new tapes or into new storage media in the future if they are to be saved. The next level of data consists of geophysical parameters derived directly from the power and spectral shape as well as from combining line-of-sight velocities into vectors. Because at this level the parameters are independent of the radars and are used directly in scientific studies or used to derive a higher level of parameter, they are the ones submitted to the data base. Finally, the next higher level of data could then be derived in a uniform manner from data from any of the radars. They would be best derived by the users with their own programs or those available at the central facility. So, essentially, our rationale in deciding how to treat the various levels of data was based on what could best be done at the most appropriate location.

The second aspect of what data to include had to do with whether the data base should include data from all experiments or from only a subset. The decision was to include all long experiments that observed standard ionospheric parameters. The rationale was that these longer experiments would be the most usable by those other than the original observers. Similarly, it was felt not appropriate to include studies of special parameters or of new altitude regions. Often such studies are experimental in nature, i.e., aimed at extending the technique, or are of limited interest to the wider scientific community.

Having decided on what data to include, our next area of concern was with what tape format to use for transferring data. The aim was to adopt a format that was well specified yet versatile, one that would handle any type of radar data -- present or future -- plus other types of correlative data. To do that the format also had to be largely self-documented. The result was a format with three types of records. The first is a protocol record that uses ASCII characters to describe the experiment and data. The second is a header record that identifies the radar, date, time, pointing directions, etc. Following the

header is the third type, a data matrix of values and identifiers. The second and third records are written in twos-complement 16-bit integers. While the machinery was moving forward to establish the data base, the three radars involved in Project MITHRAS (Chatanika, Millstone Hill, and EISCAT) implemented the tape format and used it for exchanging data.

Although the foregoing considerations have largely been concerned with technical aspects of the data base, there are some very important human considerations that must not be forgotten. For the data base to be useful, the users must have confidence in the quality of the data or have a mechanism for assuring themselves of that quality. Similarly, if they do not understand how some of the geophysical parameters were derived or what their limitations are, they need a mechanism for finding that out. Analogously, the scientists working with the radars need a compelling reason for reformatting their data and submitting it in a timely fashion to the data base. Although data acquired with public funds usually have to be made available, it was not felt that coercion was the best method to ensure data quality. Instead, in recognition of the effort put in by the scientists working with the radars, it was felt that the "carrot" was the best approach. A set of "Rules of the Road", such as those pioneered by the Atmospheric Explorer team, was developed to set out the responsibilities of the providers and the users. The critical point was that, in exchange for providing the data in a timely fashion and for answering questions about quality and derivation, the appropriate scientist working with the radar could be offered coauthorship on resulting papers and reports.

While it is implied in the foregoing paragraphs that there would be appropriate people at the facility housing the data base who would be entering the data, the committee felt that for the data base to prosper and evolve, there had to be at least one scientist associated with it who would, among other things, use the data. He or she would therefore be intimately aware of the programs to access the data, plot, derive higher level parameters, and compare them to advanced models. He or she would also participate in the development of those types of software. The efforts of this person would be supplemented by outside scientists and visitors contributing additional software.

The deliberations that led to the establishment of the data base were conducted by a committee carefully selected to include representatives of each radar, the user community, and experts in data-base systems. It was strongly felt that some such committee had to be established on a permanent basis to assess how the data base was developing and to guide its evolution.

In conclusion, the management of data is exceedingly important, particularly in those disciplines that have to rely on extensive observations instead of controlled experiments. The solution of putting data in a "data base" is a very appealing one. However, I hope my descriptions of some of the issues that came up during the meeting on the formation of an incoherent-scatter data base have convinced you that the doctor cannot write a simple prescription for "one data base". Considerable thought, discussion, and active involvement are required of the whole community. Let us continue to think, discuss, and become involved during the remainder of this workshop and beyond.

## ACKNOWLEDGMENTS

The other participants in the Incoherent-Scatter Radar Data Base Workshop were D. Alcayde, J. Baron, R. A. Behnke, O. de la Beaujardiere, B. A. Emery, C. Gonzales, T. Hagfors, J. M. Holt, R. L. Jenne, D. H. Joseph, M. C. Kelly, L. A. Lee, W. M. MacIntyre, E. S. Oran, A. D. Richmond, R. G. Roble, R. W. Schunk, P. Shames, J. Silen, W. Swartz, and R. F. Woodman. Support for participation in this workshop was provided by SRI International.

REFERENCES

CODMAC (Committee on Management and Computation) (1982), Data Management and Computation, Volume 1: Issues and Recommendations, Space Science Board, National Academy Press, Washington.

Jenne, R. L. (1981), Strategies to develop and access large sets of scientific data, In report of conference on "Frontiers in Data Storage Retrieval and Display", National Geophysics and Solar-Terrestrial Data Center, EDIS/NOAA, Boulder.

Lide, D. R., Jr. (1981), Critical data for critical needs, Science, 212, 1343-1349.

Roederer, J. G. (1981), Considerations in the development of a national geophysical data policy, EOS, 62, 569-570.

USRA (Universities Space Research Association) (1978), Proposal for a national data center to promote data analysis and theoretical research in solar terrestrial physics, Final Report, USRA Data Analysis Panel, Houston.

# AUTHOR INDEX

ATTENDEES

B. Ackerman, University of Illinois, Urbana, IL
S. K. Avery, CIRES, Boulder, CO
B. B. Balsley, NOAA, Boulder, CO
S. A. Bowhill, University of Illinois, Urbana, IL
J. W. Brosnahan, Tycho Technology, Inc., Boulder, CO
D. A. Carter, NOAA, Boulder, CO
J. K. Chao, National Central University, Chung-Li, Taiwan
F. Chen, University of Illinois, Urbana, IL
Y. H. Chen, National Central University, Chung-Li, Taiwan
W. Clark, NOAA, Boulder, CO
C. R. Cornish, Cornell University, Ithaca, NY
M. Crochet, University of Toulon, France
R. J. Doviak, National Severe Storms Laboratory, Norman, OK
W. L. Ecklund, NOAA, Boulder, CO
C. Fairall, The Pennslyvania State University, University Park, PA
D. T. Farley, Cornell University, Ithaca, NY
J. M. Forbes, Boston, College, Chestnut Hill, MA
K. S. Gage, NOAA, Boulder, CO
M. A. Geller, NASA Goddard Space Flight Center, Greenbelt, MD
M. Glass, CRPE/PAB, Issy-les-Moulineaux, France
L. D. Goss, University of Illinois, Urbana, IL
J. L. Green, NOAA, Boulder, CO
A. J. Hall, Rutherford Appleton Laboratory, Chilton, UK
W. K. Hocking, Max Planck Institut fur Aeronomie, Katlenburg-Lindau, FRG
M. Ierkic, Arecibo Observatory, Puerto Rico
E. C. Jordan, University of Illinois, Urbana, IL
V. K. Koshy, Bharat Electronics Ltd., Ghaziabad, India
F. S. Kuo, National Central University, Taiwan
P. Lagos, Instituto Geofisico del Peru, Lima, Peru
M. F. Larsen, Cornell University, Ithaca, NY
C. H. Liu, University of Illinois, Urbana, IL
J. D. Mathews, Case Western Reserve University, Cleveland, OH
C. E. Meek, University of Saskatchewan, Saskatoon, Canada
E. A. Mueller, Illinois State Water Survey, Champaign, IL
R. Peters, The Pennsylvania State University, University Park, PA
P. K. Rastogi, Massachusetts Institute of Technology, Westford, MA
A. C. Riddle, NOAA, Boulder, CO
R. G. Roper, Georgia Institute of Technology, Atlanta, GA
J. Rottger, EISCAT Scientific Association, Kiruna, Sweden
O. Royrvik, University of Illinois, Urbana, IL
T. Sasamori, University of Illinois, Urbana, IL
G. Schmidt, Max Planck Institut fur Aeronomie, Katlenburg-Lindau, FRG
C. F. Sechrist, University of Illinois, Urbana, IL
L. G. Smith, University of Illinois, Urbana, IL
G. Stitt, University of Illinois, Urbana, IL
D. Staggs, Illinois State Water Survey, Champaign, IL
R. G. Strauch, NOAA, Boulder, CO
M. P. Sulzer, Arecibo Observatory, Arecibo, Puerto Rico
W. E. Swartz, Cornell University, Ithaca, NY
D. Tetenbaum, University of Illinois, Urbana, IL
T. Tsuda, Kyoto University, Kyoto, Japan
T. E. VanZandt, NOAA, Boulder, CO
K. Wakasugi, Kyoto Institute of Technology, Kyoto, Japan
C. Wang, University of Illinois, Urbana, IL
B. J. Watkins, University of Alaska, Fairbanks, Alaska
V. B. Wickwar, SRI International, Menlo Park, CA
R. F. Woodman, Instituto Geofisico del Peru, Lima, Peru
W. P. Ying, Case Western Reserve University, Cleveland, OH
B. Yu, University of Illinois, Urbana, IL
K. S. Zhang, University of Illinois, Urbana, IL

*U.S. GOVERNMENT PRINTING OFFICE : 1984 0-434-005/607

CUMULATIVE LISTING FOR THE MAP HANDBOOK

| Volume | Contents | Date of Publication |
|---|---|---|
| 1 | National Plans, PMP-1 Report; PMP-2 Report, PMP-3 Report, MSG-4 Report, Approved MAP Projects | June 1981 |
| 2 | Symposium on Middle Atmosphere Dynamics and Transport (extended abstracts) | June 1981 |
| 3 | PMP-5 Report, MSG-1 Report, MSG-2 Report, MSG-3 Report, Antarctic Middle Atmosphere Project (AMA), EXOS-C Scientific Observations, WMO Report No. 5, Updated Chapter 2 of MAP Planning Document, Condensed Minutes of MAPSC Meetings | November 1981 |
| 4 | Proceedings of MAP Assembly held in Edinburgh, 14-15 August 1981, Condensed Minutes of MAP Steering Committee Meetings held in Edinburgh, Proceedings of MAP Open Meeting held in Hamburg, 19 August 1981 | April 1982 |
| 5 | A Catalogue of Dynamic Parameters Describing the Variability of the Middle Stratosphere during the Northern Winters | May 1982 |
| 6 | MAP Directory | November 1982 |
| 7 | Acronyms, Condensed Minutes of MAP Steering Committee Meetings, Ottawa, May 1982, MAP Project Reports, National Reports, Committee Reports, PMP and MSG Reports, Workshop Reports, Announcements and Corrigendum | December 1982 |
| 8 | MAP Project Reports: DYNAMICS, GLOBUS, and SSIM, MSG-7 Report, National Reports: Czechoslovakia, USA | July 1983 |
| 9 | Papers presented at the URSI/SCOSTEP Workshop on Technical Aspects of MST Radar, May 23-27, 1983, Urbana | December 1983 |

WORKSHOP ON TECHNICAL ASPECTS OF MST RADAR
SESSION TOPICS